U.S. Department
of Transportation
**National Highway
Traffic Safety
Administration**

Design and Development of an Advanced ATD Thorax System for Frontal Crash Environments

---

Final Report

Volume 1:
Primary Concept Development

Trauma Assessment Device Development Program

Technical Report Documentation Page

1. Report No.	2. Government Accession No.	3. Recipient's Catalog No.
DOT HS 808 138		

4. Title and Subtitle	5. Report Date
DESIGN AND DEVELOPMENT OF AN ADVANCED ATD THORAX SYSTEM FOR FRONTAL CRASH ENVIRONMENTS, VOLUME 1: PRIMARY CONCEPT DEVELOPMENT	June 1992
	6. Performing Organization Code

7. Authors	8. Performing Organization Report No.
Lawrence W. Schneider, Leda L. Ricci, Michael J. Salloum,* Michael S. Beebe,* Albert I. King,** Stephen W. Rouhana,† Raymond F. Neathery††	UMTRI-92-22-1

9. Performing Organization Name and Address	10. Work Unit No.
University of Michigan Transportation Research Institute 2901 Baxter Road Ann Arbor, Michigan 48109	11. Contract or Grant No. DTNH22-83-C-07005

12. Sponsoring Agency Name and Address	13. Type of Report and Period Covered
U.S. Department of Transportation National Highway Traffic Safety Administration 400 Seventh Street S.W. Washington, D.C. 20590	Final Report
	14. Sponsoring Agency Code

15. Supplementary Notes

* First Technology Safety Systems, Plymouth, Michigan
** Wayne State University, Detroit, Michigan
† GM Research Laboratories, Warren, Michigan
†† Oklahoma State University, Stillwater, Oklahoma

Mark P. Haffner, NHTSA COTR

16. Abstract

This report documents a research and development effort to design and test a new thorax assembly that will improve performance with regard to restraint-system interaction and injury-sensing capability for the chest and abdomen. The new features include a ribcage with more humanlike geometry, an articulated thoracic spine, shoulders with load-bearing clavicles connected to the sternum and enhanced front/back range of motion, a biofidelic frangible abdomen, and a chest deflection measurement system capable of monitoring three-dimensional displacements of the ribcage at the sternum and at the left and right regions of the lower ribcage.

Volume 1 of this report describes the development, design, and performance of the prototype assembly and its components. Volume 2 documents an exploratory effort to develop an alternative approach to damped steel ribs for achieving the desired biofidelity in the chest and abdomen regions. Volume 3 describes the chest deflection instrumentation system developed in the project and provides a user's guide for a subprogram DEFLECT that computes three-dimensional displacements at four regions of the thorax.

17. Key Words	18. Distribution Statement
Anthropomorphic Test Device, Crash Dummy, Dummy Design, Thorax, Abdomen, Shoulder, Spine	Document is available to the public from the National Technical Information Service, Springfield, Virginia 22161

19. Security Classif. (of this report)	20. Security Classif. (of this page)	21. No. of Pages	22. Price
NONE	NONE	344	

ACKNOWLEDGEMENTS

The research and development work described in Volume I of this report is the result of the combined efforts of a great number of talented and knowledgeable individuals who, over the period of three years, contributed their time and energy to resolving the many biomechanical and design challenges encountered in this project. In particular, the authors wish to acknowledge the contributions of Mark Haffner and Rolf Eppinger of the National Highway Traffic Safety Administration, who worked closely with the project staff throughout the program and who played key roles in the development of the design approaches used in the Prototype-50M.

Throughout the design and development process, the project staff sought to work closely with the Frontal Impact Dummy Enhancement (FIDE) Task Force and the Chest Deflection Task Force of the Mechanical Simulation Subcommittee of the Human Biomechanics Simulation and Standards Committee of the SAE. Appreciation is expressed to all members and attendees of these meetings who listened and offered constructive input to the design process. Special thanks is due to Roger Daniel of Ford Motor Company, who chaired the FIDE Task Force, and who offered strong support and encouragement for the development effort.

In addition, the project benefited from the valuable input of numerous consultants who gave generously of their time, and who reviewed design specifications and offered valuable insight and suggestions on dummy design and enhancement needs. These include David Viano, John Melvin, Harold Mertz, and John Horsch of the General Motors Research Labs (GMRL), Charles Kroell, now retired from GMRL, Priya Prasad of Ford Motor Company, and Richard Chandler, now retired from the Federal Aviation Administration.

Particular recognition is due to First Technology Safety Systems who participated in the design effort, fabricated many of the components used in the prototype, and who provided general support to the R&D effort. Special thanks go to Joseph Smrcka who fabricated the modified pelvis.

The authors also wish to gratefully acknowledge and thank the following persons and organizations who assisted with the many technical aspects of this project.

UMTRI

Bruce Bowman, who provided modeling and analytical support,

Brian Eby, who fabricated most of the components for the Prototype-50M, contributed to the design and fabrication of the double-gimballed string potentiometers, and fabricated all of the fixtures used in testing the assembly and its separate components,

R. Jeff Lehman, who developed software for collection, analysis, and plotting of test data and results,

Lloyd Dunlap and Marvin Dunlap, who assisted with much of the testing and calibration of test transducers,

Eric Olson, who provided photographic support and documentation of the development process, and

Kathleen Crockett Richards, who produced most of the artwork and graphical input for project reports and program presentations.

Wayne State University

John Cavanaugh, Paul Begeman, Warren Hardy, Tim Walilko, and S. Ruan, who provided technical, analytical design, and testing support throughout the project.

R.A. Denton, Inc.

Craig Morgan, who provided expertise for the design and dimensions of new load cells.

Space Age Controls, Inc.

John Gates, who served as a resource and provided support to the instrumentation design effort.

CONTENTS

LIST OF TABLES

LIST OF FIGURES

EXECUTIVE SUMMARY

INTRODUCTION

A primary concern for crash testing of today's vehicles equipped with various designs and geometries of passive and active restraint systems is the ability of a crash dummy to provide realistic response and injury assessment for both concentrated and distributed types of loading. This three-volume report documents a research and development project to upgrade the Hybrid III crash dummy toward improved assessment of restraint-system effectiveness through more humanlike interaction of the dummy's chest and abdomen with restraint systems and steering wheels, and improved assessment of injuries to these body regions from belt, airbag, and steering-wheel loading.

In the initial phases, attention was directed toward expansion and refinement of the thorax and abdomen design goals and performance specifications documented in Phase I of the Advanced Dummy Program. The results are contained in a report entitled *Design Requirements and Specifications: Thorax-Abdomen Development Task* (Schneider et al. 1990). Since the design and performance of the spine and shoulder components are thought to influence how the thorax and abdomen interact with vehicle components and restraint systems, redesign of these Hybrid III components was included in the study. Also, preliminary modifications to the neck, pelvic, and lumbar regions of Hybrid III were required to interface the new components with the existing Hybrid III architecture.

Throughout this report, the term Prototype-50M is used to refer to the advanced or upgraded 50th-percentile-male dummy (i.e., the upgraded Hybrid III) while AATD-50M refers to the anthropometric specifications of future 50th-percentile ATDs. Also, the terms *thorax system* and *thorax assembly* are used to refer to the set of dummy components targeted for redesign in this study, which primarily include the chest, abdomen, spine, and shoulders.

In addition to designing dummy components for durability, repeatability, reproducibility, and insensitivity of response to temperature variations, it was desired that the prototype thorax system should:

- interface with the existing Hybrid III head/neck, pelvis, and extremity components until these components can be upgraded;
- perform for vehicle, sled, or component impacts within thirty degrees of frontal;
- provide humanlike interaction with, and response to, distributed and concentrated types of loading from airbags, belts, and steering wheels;
- incorporate improved anthropometry, posture, and geometry in accordance with the AATD-50M anthropometric specifications;
- have more humanlike ribcage geometry, including representation of the lower ribcage in the liver and spleen areas, and with biofidelity and injury-sensing capability in these regions;
- have improved biofidelity in response at the sternal region for impacts with a rigid 152-mm (6-in) diameter, 23-kg (51.5-lb) mass in accordance with available force-deflection corridors with the highest priority given to the low-velocity or 4.3-m/s corridor;

- have impact biofidelity in the lower ribcage region in accordance with preliminary force-deflection response corridors developed in the study;
- have more humanlike quasi-static stiffness properties;
- have more humanlike regional and interregional stiffness and coupling;
- allow lateral movement of the sternum and ribcage similar in magnitude to that currently provided in the Hybrid III chest (between 25 and 50 mm, or 1 and 2 in) until new human response data suggest otherwise;
- provide response biofidelity for impact severities ranging from AIS-2 to AIS-4;
- incorporate an abdomen with response biofidelity capable of measuring abdominal intrusion from lap belts and vehicle components;
- include shoulders that incorporate humanlike compliance, mobility, mass, and mass distribution including a clavicle like structure connecting between the sternum and the shoulder/arm complex;
- incorporate a nonrigid thoracic spine with at least one articulation providing at least ten degrees of flexion and extension from the initial seated posture;
- provide for measurement of three-dimensional displacements of the chest at the sternum and left- and right-lower ribcage;
- include measurement of triaxial spinal accelerations close to the center of gravity of the thorax;
- measure shear and compressive loads to the spine that may be induced by direct lap-belt loading through the abdomen, by shoulder-belt and steering-assembly loading through the chest and shoulders, and/or by inertial loading from the head, neck, arms, and thorax;
- include instrumentation to measure relative flexion and extension of the thoracic spine and the pelvis.

One of the initial development tasks was to explore the feasibility of using an alternative design approach, other than the damped-steel-rib concept used in Hybrid III, to achieve the desired impact response and performance characteristics of the human thorax and abdomen. Numerous approaches to achieving an internal response element for incorporation into the dummy chest were pursued, including various configurations of fluid-filled inextensible "bags" with different orifice patterns, gas-filled "bags" inside of fluid-filled "bags" with venting of the gas, fluid-filled bellows or rolling diaphragms with multiholed orifice plates between the fluid compartment and gas-filled accumulator, energy-absorbing and fluid-filled foams, and special designs and configurations of linear and rotary dampers. Details of these exploratory efforts are contained in Volume 2 of this report (Schneider et al. 1993). While some progress toward achieving the desired response biofidelity was made, none of the approaches offered a solution with the desired rate sensitivity. All had problems with space, durability, user friendliness, and/or compatibility with potential deflection instrumentation that could not be resolved within the time and funding of the current program. Therefore, the internal-response-element approach to thorax/abdomen design was ultimately set aside in favor of a highly-modified damped-steel-rib model of the chest.

DESIGN

Using both analytical and physical modeling to guide the design process, and an iterative approach to prototype development and testing, the Prototype-50M thorax system was developed. The key features of this new thorax system include:

- a new ribcage with more humanlike geometry and response to quasi-static and low-velocity impacts;

- a new spine with more humanlike curvature from the pelvis to the neck and a flexible link in the thoracic spine;
- new shoulders with increased front/back mobility and clavicles connecting between the sternum and the lateral aspect of the shoulders;
- a modified version of the GM frangible abdomen to provide biofidelity for lap-belt loading and to monitor intrusion due to lap-belt submarining;
- a pelvis with modified Hybrid III pelvic bone and preliminary design changes to accommodate the new ribcage and abdomen;
- an enhanced chest deflection instrumentation system that measures three-dimensional displacements of the chest at four potential injury sites, including the left and right midsternum and the left- and right-lower ribcage;
- provision for a six-axis pelvic/lumbar load cell to quantify forces and moments at the spine due to restraint and vehicle component interactions.

RIBCAGE

The new ribcage consists of seven damped, 1.6-mm (0.063-in) thick steel ribs that slant downward relative to the torso line. From the side view, the ribcage was shaped to follow the anterior contour of the human ribcage as represented in the AATD-50M drawings. From the front view, the breadth of the ribcage widens incrementally from the top or first rib through the sixth rib. Also, the ribcage mimics the human geometry anteriorly near the midline so that the distances between the anterior ends of ribs two through four are constant at about 64 mm (2.5 in) with the sternum in between, while the distances between the anterior rib ends increase from rib five through rib seven to form the central abdominal cavity, which is unprotected by the ribcage in the human.

At the back of the ribcage, heavy-duty rib stiffeners or "helpers" have been included and shaped to reduce rib bending at the spinal interface where damping material is not present. Also, to reduce the tendency for downward displacement of the ribcage, Teflon-surfaced steel shelves were added to the upper thoracic spine to limit downward movement of the first rib and, through the bib coupling to the other ribs, increase resistance to downward movement for the whole ribcage.

The sternum consists of two pieces of mild steel—an upper part to which the clavicles and top rib attach, and a lower rectangular plate that is positioned between the two sides of ribs two through four and is connected to the anterior ends of the ribs by a triple-layered, weighted urethane bib. In order to provide a smooth contour for attaching the chest bib to the ends of the ribs at the front of the chest, the ends of the steel ribs were twisted prior to heat treating. The bib extends to the seventh rib on each side and the outer layer of urethane sheet extends over the clavicles and attaches to the upper thoracic spine behind the neck.

A weighted pad is loosely attached to the inside of the lower sternum by means of a small-diameter steel cable through the bib and a large band of neoprene rubber looped around the sternal portion of the bib and fastened at both ends to the upper sternum. Addition of this compliant 140-g mass was found to improve the dynamic response at the sternum during pendulum testing and also offers overload protection for severe impacts that may exceed the stroke distances of the chest-deflection transducers.

A 19-mm (0.75-in) thick Ensolite pad has been shaped to cover the area of the bib and is sewn into a lining or pocket on the inside of the prototype jacket. This pad replaces the 25-mm (1-in) pad used in Hybrid III and is tapered at the sides to improve the cross-

sectional geometry of the chest and at the top so that the pad does not extend over the clavicles.

SPINE

The spine of the Prototype-50M thorax system consists of upper and lower rigid segments separated by a flexible rubber segment. In the current Prototype-50M, a rectangular block of durometer-70 Shore A natural rubber was designed and molded with steel end plates. In addition, bilateral steel cables were incorporated into the assembly to provide durability and lateral stability. The location of the spinal articulation in the current Prototype-50M corresponds approximately to the level of T7 in the human.

The upper thoracic spine segment consists of two side plates with two steel shelves welded inside for mounting the modified neck bracket (or load cell) at the top and the thoracic spine articulation at the bottom. The front of the upper thoracic spine is open for access to fasteners and the back is enclosed with a stair-step plate designed to orient and fasten the top four ribs at their specified angles.

The lower thoracic spine was similarly designed but is longer to allow for mounting of the four chest deflection instrumentation transducers and is not as deep as the upper thoracic spine segment in order to allow maximum inward rotation of the transducer units. The front of the lower thoracic spine segment is fitted with a triangular-shaped and padded lead ballast that is fastened by four modified screws and that also serves as an overload "stop" and protective cover for the chest deflection instrumentation housed within the spine.

The back of the lower spine segment was designed for attaching the bottom three ribs at the specified nine-degree angle and is fitted with a second lead ballast to increase the torso mass and to lower the thorax center-of-gravity closer to the specified level near the top of the lower thoracic spine segment. This ballast also serves as a protection for instrumentation cables that exit through a hole in the back of the lower thoracic spine.

A mounting plate for the accelerometer block is provided at the top front of the lower spine segment close to the center of gravity of the AATD-50M thorax. Both upper and lower thoracic spine segments also provide for mounting of magnetohydrodynamic angular motion sensors (MHD AMS) to monitor relative movement at the thoracic spine articulation. A third MHD transducer is mounted to the pelvic block to provide kinematic information of relative rotation between the thoracic spine and the pelvis.

The new lumbar spine that is required to interface the new thoracic spine with the modified Hybrid III pelvic block consists of steel plates molded into the ends of a block of durometer-70, Shore A natural rubber with holes provided for two bilaterally-positioned steel cables. In designing this lumbar segment, provision was made for a new six-axis load cell between the lumbar spine and the pelvic ballast block to replace and compensate for the necessary removal of the lower thoracic load cell used in Hybrid III.

The neck mounting bracket and lower neck load cell were redesigned and configured so that the Hybrid III neck mounts directly above the neck bracket or load cell and in line with the upper thoracic spine. In order for the top of the neck and the head to retain their original orientations and positions relative to the pelvis in the pretest posture, the neck was angled forward nine degrees from its previous orientation in Hybrid III and the top surface of the nodding block was beveled to compensate for this neck angle. The overall result is a more humanlike spinal contour with a continuous, uninterrupted curvature from the lumbar spine to the top of the neck.

SHOULDERS

Each shoulder of the prototype thorax assembly consists of a main shoulder support that pivots in an aluminum bushing block mounted to the side of the upper thoracic spine segment. An aluminum mounting bracket for attachment of the arm clevis is connected to the lateral end of this main support by a second pin joint, and a steel "clavicle" connects between the forward portion of this mounting bracket and the top of the sternum with rod-end bearings at each end.

While this design does not explicitly include lateral compliance, the rearward mobility and initial rearward angulation of the main shoulder support provides energy absorption during contact of the shoulder with a vehicle door structure in frontal-oblique barrier tests. In addition, the arm clevis joints of the small female dummy have been used in the current Prototype-50M to reduce the size of this component and allow greater deflection of the arm flesh before contact with the clevis joint.

Resistance to forward and rearward movement of each shoulder assembly is provided by a steel "finger" that extends down from the back edge of the main support between blocks of compressible rubber captured by the spine box on one side (rearward motion) and a steel bar attached to the shoulder bushing block on the other (forward motion). This joint-stop mechanism serves to limit shoulder movement to about 35 mm (1.4 in) forward or rearward of the initial position measured at the distal end of the clavicle.

PELVIS AND ABDOMEN

Although the pelvis of the Hybrid III was not included in the original project scope, it was necessary to make preliminary modifications to this component to accommodate the new ribcage and abdomen. The pelvic crests of the Hybrid III bone were cut down 25 mm (1 in) and back 25 mm to match the AATD-50M drawings, and the contours of the ASISs were shaped to provide anatomical similarity to the human pelvis. The modified pelvic bone was positioned in the Hybrid III pelvic mold approximately 25 mm forward of its usual position. This had the effect of moving the back line of the buttock flesh approximately 25 mm rearward to improve its position relative to the spine of the new thorax assembly.

The current project has used a modified version of the GM frangible abdomen, which consists of a Styrofoam insert and a reaction plate that is fastened to the top of the pelvic block that has been cut back to make room for the abdominal insert. The most significant modification to the Styrofoam insert from the previous model developed for Hybrid III is a change from five points to two points that was necessary to accommodate the insert to the new ribcage and to reduce the potential for interference with the ribs and the telescoping string potentiometers. The abdomen "flesh" that extends up from the front of the Hybrid III pelvis between the left and right ASIS has been cut away to provide for installation and positioning of the modified GM frangible abdomen. By removing this abdominal portion of the Hybrid III pelvic flesh, more humanlike and independent inward deflection of the abdomen is allowed.

The frangible abdomen is held in place against the reaction plate by a screw through a wedge of hard urethane positioned at the bottom of the V between the two Styrofoam points, and by a steel "finger" at the top of the support bracket. In addition, the prototype chest jacket was designed to cover the pelvis as well as the chest and abdomen and thereby hold the abdomen against the reaction plate. Access to the abdomen is possible without completely removing the jacket by unfastening the Velcro attachments on a crotch strap and the leg fittings.

Overall, the thoracic and pelvic masses of the Prototype-50M agree well with the AATD-50M, except for differences in distribution of mass between the pelvis and the thighs due to differences in segmentation planes and corresponding assignments of segment masses. The CG is located within 25 mm of (above) the desired CG specified on the AATD-50M drawings, which is also the approximate location for the chest accelerometers attached to the lower thoracic spine.

CHEST DEFLECTION INSTRUMENTATION

Throughout the process of developing and testing prototype models for the new thorax assembly, efforts were simultaneously underway to find and/or develop a measurement system to quantify the thoracic deflection-time and/or velocity-time histories at critical response and injury regions at the sternum and the left- and right-lower ribcage. Numerous measurement concepts were considered and explored throughout the development process, including two types of sonic-based transducers, light-based transducers, and various configurations of linear and string potentiometers. The best and most reasonable solution to the measurement problem was determined to be a combination of a string potentiometer threaded through a telescoping joy stick to measure inward compression, and two rotary potentiometers to measure the changing orientation of the cable within the chest due to upward and downward movement. The resulting transducer system is referred to as a double-gimballed string potentiometer with telescoping joy stick (DGSP).

Four DGSP transducers are mounted to the lower thoracic spine of the Prototype-50M assembly with the joy sticks of the two top units connected to the ends of rib three on each side of the sternum by means of small universal joints and the two lower units attached to the ends of rib six in a similar manner. The DGSP transducer system was evaluated in a controlled impact test on the pneumatic pendulum at Wayne State University. The results show excellent agreement between the displacements predicted from the output of the linear potentiometer and results calculated from the gimbal and string-potentiometer output.

In order to perform the necessary deflection calculations, a subroutine called DEFLECT was developed to compute compressive, lateral, and up/down motion of the ribcage at each of the four measurement sites from the digitized output of the DGSPs during crash testing. Sternal compression is computed in the direction of the spinal X-axis, but deflections can also be calculated in any other axis system that the user wishes to define relative to the spinal axis system. For the lower ribcage, there is currently no precedent for a compression direction and the direction of the X-axis of the spinal coordinate system seems inappropriate. Thus, in addition to calculating deflections in the spinal axis system, DEFLECT also computes deflections in an alternate compression axis system defined by the user.

PENDULUM TESTS

Kroell-type pendulum tests to the sternal region were conducted at both 4.3 m/s and 6.7 m/s with 19 mm (0.75 in) of Ensolite padding attached to either the impactor plate or the sternal region of the dummy. The low-velocity response of the Prototype-50M thorax falls within the 4.3-m/s corridor better than the Hybrid III response, and the 6.7-m/s response matches the corridor equally as well as the Hybrid III. Lateral displacements during sternal impacts were quite small, but downward movement of the ribcage was more than 20 mm (0.78 in).

For pendulum-type impacts to the lower ribcage, the dummy was rotated so that the impactor was aimed at the lower thoracic spine and so that the surface of the impactor plate was parallel to the surface of the ribcage in the impacted area. The low-velocity force-deflection responses of the lower ribcage were constructed using the inward deflection computed for the alternate compression axes and were found to be somewhat stiffer than desired based on a preliminary corridor developed in the study.

QUASI-STATIC LOADING TESTS

The new thorax assembly was tested under quasi-static loading conditions on the Instron machine using a 152-mm (6-in) diameter rigid plate to compress the chest at midsternum. The sternal region of the Prototype-50M was found to be considerably more compliant than that of the Hybrid III dummy, but somewhat stiffer than results reported for tensed humans.

Quasi-static loading tests were also performed using a 50-mm by 100-mm (2-in by 4-in) rigid loading plate employed previously in tests on cadavers and Hybrid III. The plate was placed in direct contact with the prototype ribcage (i.e., the bib) at different regions of the chest. In addition to obtaining quasi-static stiffness data from this smaller loading plate, the relative deflections produced at other regions of the chest were manually measured to determine the degree of ribcage coupling.

The most important difference between the two dummies for these loading conditions was in the relative stiffness between the sternum and the lower and lateral regions of the ribcage. With Hybrid III, the stiffness lateral to the midline at the bottom of the ribcage is seen to be significantly greater than it is at the sternum. For the Prototype-50M, the stiffness of the lower ribcage is significantly lower than at the sternum, as it is in the human. There is also generally good agreement between the actual and desired ribcage coupling under these quasi-static loading conditions, as measured by relative chest deflections away from the loaded site.

BELT-RESTRAINED SLED TESTS

Several 30-mph, 20-G, driver-side sled tests were conducted with the Prototype-50M thorax assembly installed in the Hybrid III dummy using a three-point belt restraint system. The dummy was seated on a simulated automotive seat with a flat, rigid, and horizontal seat surface and a flat, rigid seatback reclined to produce a 24-degree back angle. Instrumentation for these tests included the four DGSP chest displacement assemblies, three chest accelerometers located at the top of the lower thoracic spine, three angular velocity sensors attached to the upper and lower thoracic spine and pelvis, respectively, and belt load cells.

The Prototype-50M thorax assembly demonstrated excellent durability in these tests with no structural damage occurring to any of the hardware or chest deflection instrumentation. Also, the results of calculated AP, RL, and IS displacements show significant differences in chest displacements at different regions of the thorax. Maximum AP compression at the sternum was greatest on the right side (i.e., on the side opposite the shoulder loaded by the belt), due to routing of the shoulder belt on this region. RL displacements were primarily leftward and were greatest for the right sternal area where maximum AP compression occurred. IS displacements were primarily upward and were largest for the lower ribcage.

SUMMARY

The research conducted during this program has resulted in the development of a promising torso for incorporation into a next-generation crash test dummy. The essential features of this new assembly include:

- anthropometry based on the AATD-50M specifications of Robbins (1985a),
- a ribcage with more humanlike geometry including representation of the lower ribs over the regions of the liver and spleen,
- a new thoracic spine with a flexible link at level T7,
- a new shoulder design with humanlike clavicle connecting between the sternum and lateral aspects of the shoulders and greater mobility (than Hybrid III) in the anterior and posterior directions,
- a modified version of the GM frangible abdomen,
- enhanced chest deflection instrumentation for three-dimensional measurement of chest displacements at the sternal and left- and right-lower ribcage regions.

In addition, the neck mounting bracket, lumbar spine, and pelvis of Hybrid III have been modified to accommodate the new thorax system and associated anthropometry.

The Prototype-50M thorax has been designed using a slanted, damped-steel-rib model and with lower stiffness to quasi-static and low-velocity loading than that in Hybrid III. The first priority in thorax biofidelity at the sternum was for impact velocities of 4.3 m/s and test results indicate excellent fit of the Prototype-50M sternal response to the low-velocity corridors. To date, sled tests have been conducted using three-point-belt restraints at UMTRI and both belt and airbag restraint systems at the Transportation Research Center, with positive indications for durability and performance.

Following a period of additional testing and evaluation of this prototype hardware by the NHTSA and other organizations, it is expected that further refinement and upgrading of these components will occur. Specific provision for this refinement effort has been made by the NHTSA in announced plans for continuation of frontal dummy development activity.

1. INTRODUCTION, BACKGROUND, AND SCOPE

This project was a continuation of the Advanced Anthropomorphic Test Device (AATD) Development Program initiated by the NHTSA in the early 1980s. In the initial project, the anthropometric specifications for a family of future anthropometric test devices (ATDs) were determined based on experimental measurements of driver position, posture, and anthropometry in the automotive seating environment. The results of that study are contained in a three-volume final report by Schneider et al. (1985) and Robbins (1985a, 1985b) and a set of eleven full-size engineering drawings (DOT-HS-806–715, 716, 717 available from NTIS, accession no. PB-86–105046), as well as three full-size fiberglass epoxy shells of the three dummy sizes. In the second part of the program, which has been referred to as Phase I, the most recent biomechanical data on human response to impact and patterns of motor vehicle injuries were studied, analyzed, and compiled into a series of task reports (Carsten and O'Day 1988, Melvin and Weber, ed. 1988, Arendt et al. 1988, Melvin et al. 1988a, Melvin et al. 1988b) that are published in a single bound volume (DOT-HS-807–224 available from NTIS, accession no. PB-88–174495). This document provides the basis for design and engineering of the next generation of ATDs.

The focus of the current effort was to design and develop new components for the thorax and abdomen regions of the Hybrid III ATD. It has been well established that motor-vehicle-related injuries to the thorax and abdomen comprise a major portion of the total injury problem. Measured by percent of HARM, Malliaris et al. (1982) have determined that injuries to the chest of unrestrained front-seat occupants comprise 26.7 percent of total body Harm, second only to that of the head. Using the Injury Priority Rating (IPR) system developed in Phase I of the AATD study, the percent IPR for chest injuries to unrestrained occupants was found by Carsten and O'Day (1988) to be 21.0 percent. Similarly, injuries to the abdomen comprise 18.2 percent of the Harm and 7.9 percent of the total IPR. The lower percents for IPR compared to Harm are due to the fact that persons suffering injuries to the thorax and abdomen tend to experience total recovery more frequently than for injuries of similar severities to the head. Combined, injuries to the thorax and abdomen of unrestrained occupants comprise 44.9 percent of the Harm and 28.9 percent of the IPR.

For front-seat occupants restrained by two- and three-point belt systems, there is a significant reduction in internal injuries to the chest (Dalmotas 1980, Rutherford et al. 1985, Haffner 1987). However, there are clearly limits in human tolerance to concentrated loading of the thorax from belt- and belt-airbag-type restraint systems, especially for elderly persons. Restraint system effectiveness can also vary with differences in restraint system geometry and levels of preimpact belt tension that can affect occupant kinematics in a frontal crash. Thus, a primary concern for crash testing of vehicles equipped with different designs and geometries of passive and active restraint systems is the ability of the crash dummy to provide realistic response and injury assessment for both concentrated and distributed types of loading.

The R&D effort documented in this report has been motivated by concerns that the thorax and abdomen subcomponents of the Hybrid III crash dummy lack essential design and instrumentation features required to accurately access injuries to these body regions, particularly those injuries that may be due to interaction with different types of restraint systems. Since the spine and shoulder components play important roles in the interaction of the thorax and abdomen with vehicle components and restraint systems, design goals and specifications and redesign of these dummy components were incorporated into the scope of the project. For convenience, however, the terms *thorax assembly* and *thorax system* will be

used throughout this report to refer to the prototype hardware developed in this project, with the understanding that the abdomen, spine, and shoulders are included.

In the initial phases of this project, attention was directed toward expansion and refinement of the design goals and performance specifications for the thorax and abdomen documented by Melvin et al. (1988a) in the Phase I task reports. The results are contained in a separate report entitled *Design Requirements and Specifications: Thorax-Abdomen Development Task* by Schneider et al. (1990) and are supplemented in Appendix A of this report. Subsequent to completion of the initial draft of this document, the primary effort was directed toward exploring new design concepts and deflection instrumentation technologies that would offer the improved response and injury-assessment capabilities desired.

Early work was aimed at developing a new design approach for the thorax and abdomen that would better meet the defined goals and specifications. This work focused on development of an internal response element that would provide a means for controlling and differentially tuning regional chest impact response characteristics, including both viscous damping (i.e., rate sensitivity and energy absorption) and nonlinear elastic stiffness, which characterize the human chest during blunt impact loading. Exploration of internal response elements began with the concept of inextensible fluid-filled bags vented through an orifice plate to a gas-filled accumulator, as proposed by Melvin et al. (1988a) in the Task E-F report from Phase I of the AATD study. Numerous variations of this design approach were explored, but all were eventually set aside in favor of a significantly modified damped-rib design due to limitations in time and funding. Because a significant amount of effort went into the experimental and analytical exploration of alternative design approaches, it is felt that documentation of these efforts and their results is important to future ATD design efforts, even though the internal-response-element approach was not applied in the hardware ultimately developed in this project. Accordingly, these activities are documented in Volume 2 of this report.

The remaining sections of this volume address the activities and results involved with the development of a first and second prototype of the new thorax assembly using a modified damped-rib thorax design concept. Section 2, which follows, provides a brief summary of the design goals and performance specifications that guided the design effort, while Section 3 describes the research performed in developing the new damped-rib chest model. Section 4 describes the exploration, development, and evaluation of new three-dimensional chest deflection instrumentation, while Section 5 describes the design features of the prototype components and assembly, and the application of the new chest deflection instrumentation to this new design. Section 5 is supplemented by Volume 3 of this report, which contains a more detailed discussion of the chest deflection instrumentation and a user guide to a computer subprogram, DEFLECT, that calculates three-dimensional rib displacements for the four instrumented regions of the chest. Also, a set of detailed engineering drawings of the individual hardware components and thorax assembly is available as a supplement to this final report. Section 6 of this volume presents results from mechanical tests of the prototype hardware, including quasi-static compression tests with two different loading plates, pendulum-type impacts at low and medium velocities, and 48-km/h sled tests with three-point restraint systems. Section 7 provides a brief summary of the development process and the results achieved, and offers a few comments on potential needs for future development and upgrading.

For purposes of this report, the two prototypes developed and described in this volume will be referred to as the First Prototype-50M and the Second Prototype-50M, where 50M refers to 50th-percentile or average male. Due to the large number of figures referenced in the text, these are all included at the end of each section.

2. SUMMARY OF DESIGN GOALS AND SPECIFICATIONS

As previously noted, design goals and performance specifications for the new thorax/ abdomen components have been set forth in a separate document (Schneider et al. 1990) and in Appendix A of this report. For reader convenience and perspective in reviewing the design approaches described in this report, these design requirements and specifications are summarized in Section 2.2 below. First, however, a review of the enhancement needs of the Hybrid III crash dummy relative to the scope of the current project is presented. While these design specifications and Hybrid III enhancement needs served as the basis for the design and development work described in Volume 2 of this report and in Sections 3 through 7 that follow, not all of these requirements have been fully achieved within the time and cost frame of the present study.

2.1 SUMMARY OF HYBRID III ENHANCEMENT NEEDS

While the chest of the Hybrid III AATD has improved biofidelity compared to that of the Hybrid II or Part 572 thorax, and also includes chest deflection measurement capability, there has been an increasing recognition of the need for additional improvements in the design and performance of the thorax as well as in the shoulder, spine, and abdomen components. Among the needs noted within the user community and the Mechanical Human Simulation Subcommittee of the Human Biomechanics and Simulation Standards Committee (HBSS) are the following.

2.1.1 Durability

Compared to the Hybrid II, the ribcage of Hybrid III is less durable. The primary problem lies in the damping material that is bonded with epoxy to the steel ribs. Although improvements in bonding have been made in the past couple of years, separation of the damping material from the steel bands and breakdown (i.e., cracking) of the damping material still occur after approximately thirty calibration-level tests. Cost of rib replacement and the need for frequent calibrations and inspections to detect material failure continue to present problems to users.

2.1.2 Temperature Sensitivity

Because damping and rate sensitivity of the Hybrid III ribcage under dynamic compressive loading are derived from material properties (i.e., from the material bonded to the steel ribs), the thorax exhibits undesirable sensitivity in response variability with different ambient temperatures. While equations for adjusting measured peak chest deflections as a function of temperature are available, application of these equations to adjustment of the deflection- and velocity-time histories required for calculating the viscous criterion is not feasible and the need to make such adjustments for peak deflection values is an additional burden and source of error to the user. A design with reduced temperature sensitivity would therefore be extremely desirable.

2.1.3 Biofidelity in Lower Ribcage

The Hybrid III thorax was designed to provide dynamic force-deflection response characteristics within the adjusted corridors developed by Neathery (1974) only at the sternum. It is becoming increasingly evident that an ATD must also have biofidelity and deflection-time measurement capability at the lower ribcage over the liver and spleen, where potentially serious injuries can result from concentrated loading of belt and steering wheel systems. In addition to the absence of ribs in the region corresponding to the eighth, ninth, and tenth ribs of the human chest, it has been shown that the Hybrid III ribcage is statically stiffer at the sixth rib lateral to the midline than it is at midsternum on the midline. In the human, the ribcage has been shown to be less stiff in this region, both statically (Cavanaugh et al. 1988) and dynamically (Viano 1989). It would seem important that this limitation of Hybrid III be improved for proper injury assessment in frontal crashes.

2.1.4 Humanlike Ribcage Geometry

The Hybrid III ribcage consists of six pairs of ribs that comprise an essentially barrel-shaped thorax. As indicated above, this ribcage does not adequately represent the shape or length of the human ribcage. Of particular concern is the lack of ribs at the levels of ribs eight through ten and the abrupt discontinuity that results as the nonslanted Hybrid III ribs terminate at the sixth rib. The latter, combined with the high static stiffness noted previously, has been shown to cause a response sensitivity problem (Toyota Comments to Docket No. 74–14, Matsuoka et al. 1989) when testing with two-point shoulder belts. A difference in belt positioning of about 25 mm (1 in) as it crosses the bottom rib can result in a significant difference in chest compression from otherwise identical tests. If the belt is positioned slightly high, it will ride up on the side of the ribcage and cause relatively little chest compression. If it is positioned slightly lower, the belt will catch under the ribcage and thereby cause significant compression of the chest.

2.1.5 Inappropriately High Coupling Between Thoracic Regions

The Hybrid III ribcage has been "tuned" to provide humanlike dynamic response characteristics to Kroell et al. (1974) impact conditions at the sternum (i.e., for human impacts centered at or just above the xiphoid process). As noted above, this is accomplished by six pairs of damped steel ribs that are fairly rigidly coupled from side to side by a nearly rigid Delrin sternum, a narrow span of urethane bib on each side of the Delrin, and two stiff steel bars that connect the ends of the ribs up and down on each side. A consequence of this design is that the sternum behaves nearly like a rigid structure and the load coupling between different regions of the chest, particularly up and down, is too stiff. This has been demonstrated in static tests by L'Abbe et al. (1982) and Kallieris (1987), and more recently by Cavanaugh et al. (1988). Clearly, this aspect of biofidelity (i.e., ribcage coupling) is important to achieving realistic interactions and injury assessments with the concentrated loading patterns imposed by shoulder belts and steering rims, and should be an important consideration in an improved ATD thorax.

2.1.6 High Static Stiffness

It is well recognized that the Hybrid III ribcage has a very high static stiffness at the sternum compared to a tensed human (approximately 61 N/mm compared to 24 N/mm). Furthermore, and as previously indicated, the Hybrid III ribcage has been shown to be stiffer lateral to the midline, whereas the human ribcage has been shown to be less stiff lateral to the midline, particularly in the region of the lower ribcage. While concerns for biofidelity in static stiffness have not been a primary concern for unrestrained dummy

testing, this is not the case in belt-restrained dummy tests where the loading rates can be quite low and in the range of 1 to 3 m/s.

2.1.7 Shoulder

The Hybrid III shoulder has limited mobility compared to that of the Hybrid II and, more importantly, compared to the human. While the Hybrid III shoulder design offers high durability, there is concern that the shoulder may not interact appropriately with shoulder belts, particularly with regard to the percentage of load taken by the shoulder compared to the load on the chest. For this reason, as well as the influence of shoulder mobility and coupling on dummy kinematics (Robbins in Melvin et al. 1988b), the shoulder design should be modified to provide greater mobility if it can be done without significant sacrifice in durability and repeatability.

2.1.8 Clavicle

Associated with the absence of shoulder mobility in Hybrid III is the lack of a claviclelike structure by which shoulder loads can be transmitted to both the ribcage (i.e., to the sternum) and the spine via the chest. A claviclelike structure is needed in Hybrid III with representative mass, mobility, and coupling to the spine and sternum to ensure proper interaction of shoulder belt loads with the chest and shoulder structure.

2.1.9 Rigid Thoracic Spine

As with its predecessors, the Hybrid III ATD uses a rigid steel box to represent the thoracic spine. While most spinal mobility in the human spine is in the cervical and lumbar regions, the thoracic spine is not absolutely rigid, especially during dynamic loading to the chest. The importance of this flexibility is not entirely understood, but it may contribute to the manner in which the chest interacts with, and is loaded by, steering wheels and shoulder belts. It could also significantly affect kinematics of the cervical spine and neck which will, in turn, affect the likelihood and severity of head contacts. The addition of some degree of thoracic spine flexibility is therefore considered important to the new thorax design.

2.1.10 Biofidelic, Injury-Sensing Abdomen

The standard Hybrid III has only a soft, foam-filled, vinyl abdominal insert that has neither biofidelity in response nor injury-sensing capability. With the increasing use of belt restraint systems, the concern for detecting submarining of the pelvis along with the ability to assess the probability and severity of resulting injuries has become increasingly important. Recently, engineers at General Motors Research Laboratories have developed a replaceable, Styrofoam abdominal insert for the Hybrid III (Rouhana et al. 1989) that has biofidelity to lap belt loading and enables estimation of potential injuries through measurement of the depth of belt intrusion into the foam. While this replaceable insert is a significant step forward in abdominal injury measurement capability, it lacks humanlike mass properties and has other shortcomings with regard to measurement of abdominal deflections. The development of a reusable, permanently-installed abdomen with deflection-time measurement capability would be a significant contribution to the ATD thorax system.

2.2 SUMMARY OF DESIGN REQUIREMENTS AND PERFORMANCE SPECIFICATIONS

A detailed description of the design goals and performance specifications for the advanced thoracic system is provided in a separate document (Schneider et al. 1990). The following summarizes these requirements in light of the Hybrid III needs outlined in the previous section, and thereby provides a focus for the exploratory and design work described subsequently and in Volume 2 of this report. These requirements or goals have been prioritized into two categories, *primary* and *secondary*, based on their estimated importance and/or likelihood of implementation in the next generation of a new thorax/spine/shoulder system. As previously noted, not all of these goals have been achieved in the Prototype-50M thorax described in Section 5 of this report, and some remain as incentives for future ATD development efforts.

2.2.1 Primary Priorities

General Requirements

- The new thorax should be designed to interface with the Hybrid III head/neck, pelvis, and extremity components until these can be upgraded.
- The new thorax should be designed to perform for vehicle, sled, and component impacts within thirty degrees of frontal.

Anthropometry

- The new thorax should incorporate improved anthropometry, posture, and geometry of the human thorax, abdomen, shoulder, and spine in accordance with the dimensions given in Sections B3.1 and B3.2 of the thorax design goals and specifications (Schneider et al. 1990) and the anthropometric specifications described in Schneider et al. (1985) and Robbins (1985a, 1985b).

Response Biofidelity

- The new thorax should provide biofidelity in impact response to a rigid 152-mm (6-in) diameter, 23-kg (51.5-lb) impactor at the mid/lower sternum in accordance with the force-deflection corridors developed by Neathery (1974) and shown in Figures 2–1a and 2–1b.
- The ribcage of the new thorax should extend over the region of the liver and spleen and have impact biofidelity in accordance with preliminary force-deflection response corridors described in Appendix A.
- The new thorax should have humanlike quasi-static stiffness properties as described by Lobdell (1974) and illustrated in Figure 2–2 for tensed volunteers.
- Given that it may not be possible to achieve equal biofidelity for all loading velocities, the order of priority should be: (1) 4.3 m/s; (2) quasi-static; and (3) 6.7 m/s.
- The new thorax should allow lateral movement of the sternum and ribcage during asymmetric shoulder belt loading similar in magnitude to that currently provided in the Hybrid III chest (between 25 mm and 50 mm or between 1 in and 2 in) until new response data suggest otherwise.
- The new thorax should be designed to provide humanlike interaction with different types of restraint systems including two- and three-point shoulder belt systems and airbags, as well as with vehicle components such as the steering wheel and instrument panel. This implies more humanlike regional

- and interregional stiffness and coupling such that localized loading at one region of the chest results in more humanlike deflections at other regions of the chest based on results from L'Abbe et al. (1982) and Kallieris (1987) as described in Schneider et al. (1990), Cesari and Bouquet (1990), and analysis of the Cavanaugh data as presented in Schneider et al. (1990) and Appendix A of this report.
- The new thorax should provide response biofidelity for impact severities associated with AIS-2 to AIS-4 injuries. For low-velocity loading (i.e., below 3 m/s), this implies response biofidelity up to deflections of about 75 mm (3 in) at the sternum and about 90 mm (3.5 in) at the lower ribcage.
- The new thorax should incorporate an abdomen with response biofidelity as described in Sections B1.2.1 through B1.2.3 of the specifications document (Schneider et al. 1990).

Shoulder/Spine

- The new thorax should include a shoulder design that incorporates improved compliance, mobility, mass, and mass distribution in accordance with Sections B3.3 through B3.5 of the specifications document (Schneider et al. 1990). This implies a claviclelike structure with improved anatomy, compliance, mobility, and more humanlike connection to and interaction with the sternum and shoulder/arm complex.
- In order to improve overall kinematics and interaction with restraint systems and steering assemblies, the new thorax should incorporate a thoracic spine having some flexibility (i.e., at least one articulation) providing at least ten degrees of flexion and extension from the initial seated posture.

Instrumentation

- The new thorax should be designed to provide reliable measurements of injury criteria based on deflection- and velocity-time histories at critical regions of the thorax and abdomen including the sternum and left- and right-lower ribcage.
- The new thorax should provide for measurement of lateral and vertical displacements of the chest.
- The new abdomen should be capable of measuring intrusion from lap belts and vehicle components and would ideally include deflection-time or velocity-time measurement capability.
- The new thorax should include measurement of triaxial accelerations at the thoracic spine as close to the center of gravity of the thorax as possible, located according to the specifications given by Robbins (1985a).
- The new thorax should include the ability to measure impact loads to the chest that exceed the desired range of injury assessment (i.e., that exceed AIS-2 through AIS-4 injuries).
- The new thorax should include instrumentation to measure the kinematics of the spine and pelvis relative to inertial coordinates and with respect to adjacent ATD segments.
- The new thorax should have provision for measuring shear and compressive loads to the spine that may be induced by direct lap-belt loading through the abdomen, by loads transmitted through the femurs via knee contact, by shoulder belt and steering assembly loading through the chest and shoulders, and/or by inertial loading from the head, neck, arms, and thorax.

Repeatability and Durability

- The new thorax should be durable for crash severities that produce impact forces, accelerations, and deflections beyond the range of desired injury assessment. In terms of vehicle impact velocities, the new thorax should be able to survive impact forces generated in restrained- and unrestrained-occupant tests for 56-km/h (35-mph) barrier frontal impact tests and 48-km/h (30-mph) barrier impact tests at 30 degrees to frontal.
- The new thorax should be capable of surviving 50 to 100 rigid-impactor calibration tests without the need for replacement or recalibration of parts.
- The new thorax should perform with less than ten percent variability in deflection- and velocity-based injury criteria over the temperature range of 18 to 27 degrees Centigrade (65 to 80 degrees Fahrenheit). It should also withstand shipping and storage temperatures from –29 to 60 degrees Centigrade (–20 degrees Fahrenheit to 140 degrees Fahrenheit) without deterioration or change in structure and performance.
- The new thorax should provide test repeatability (within dummy variability) and reproducibility (between dummy variability) in response and injury criteria values with five percent or less variability.
- The new thorax should provide for overload protection for impact conditions that produce chest deflections exceeding the range of biofidelic response or the operating range of chest deflection instrumentation.

2.2.2 Secondary Priorities

General Requirements

- The new thorax should have potential application as a subcomponent test device.
- The new thorax should have potential for implementation into lateral and omnidirectional test devices.

Response Biofidelity

- For improved assessment of injury to out-of-position occupants from airbag deployments, the new thorax should offer biofidelity for loading rates of 9 m/s and higher.
- The quasi-static elastic stiffness of the new thorax should demonstrate the nonlinear stiffness (i.e., increasing stiffness with increasing deflection) described by Melvin et al. (1988a).
- To the extent possible, the new thorax should offer response biofidelity for chest deflections beyond the 75-mm (3-in) and 90-mm (3.5-in) general requirements stated above.

Instrumentation

- The new thorax should be designed to provide reliable measurements of injury risk directly without the need for human input as to the structures and/or surfaces contacted.
- The new thorax should have appropriate instrumentation to sense for injury potential from low-deflection, high-velocity impact events due to airbag loading (i.e., low-mass loading) into out-of-position occupants.

- The new thorax should include instrumentation to measure the kinematics of the spine and pelvis relative to inertial coordinates and with respect to adjacent ATD segments.
- The new thorax should measure the load applied to the clavicles to assess and compare the shoulder load delivered by different restraint system designs.

2.3 FIGURES

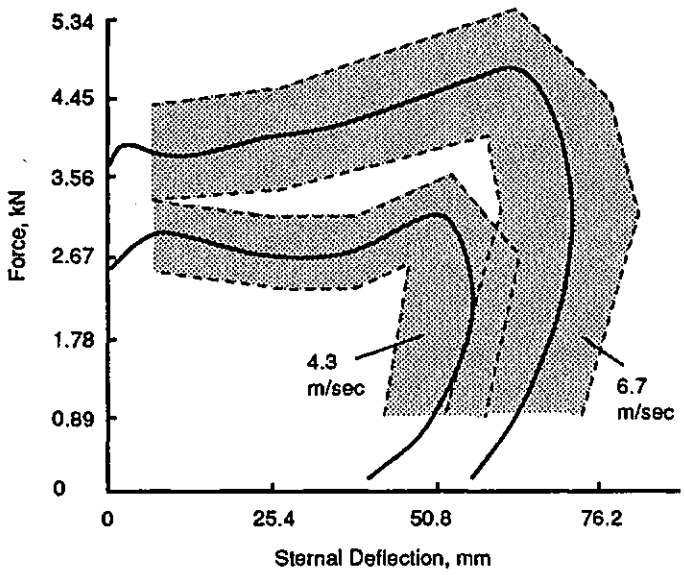

FIGURE 2–1a. Averaged adjusted skeletal force-deflection corridors for 4.3- and 6.7-m/s impacts to the sternum (Neathery 1974).

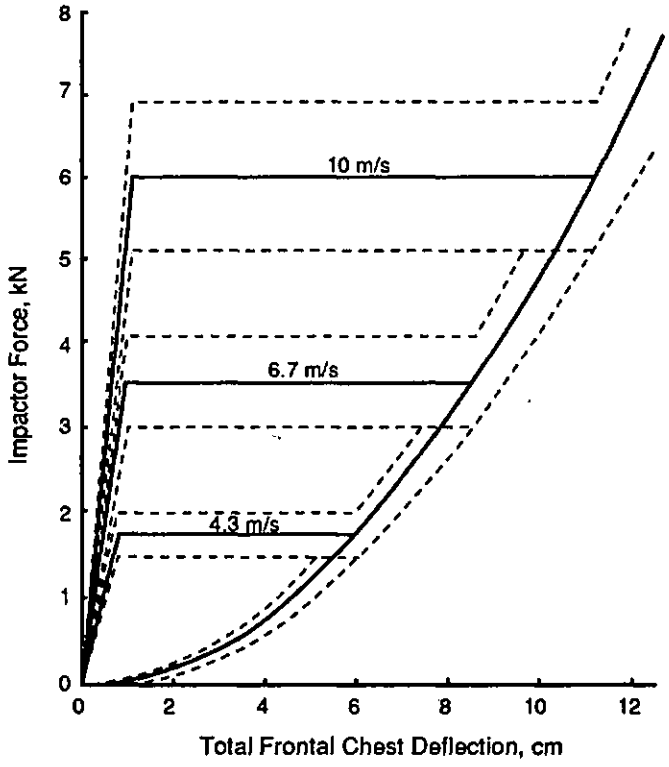

FIGURE 2–1b. AATD frontal thoracic impact response, loading only (Melvin et al. 1988a) using 152-mm (6-in) rigid disc, 23.4-kg (51.5-lb) impact mass.

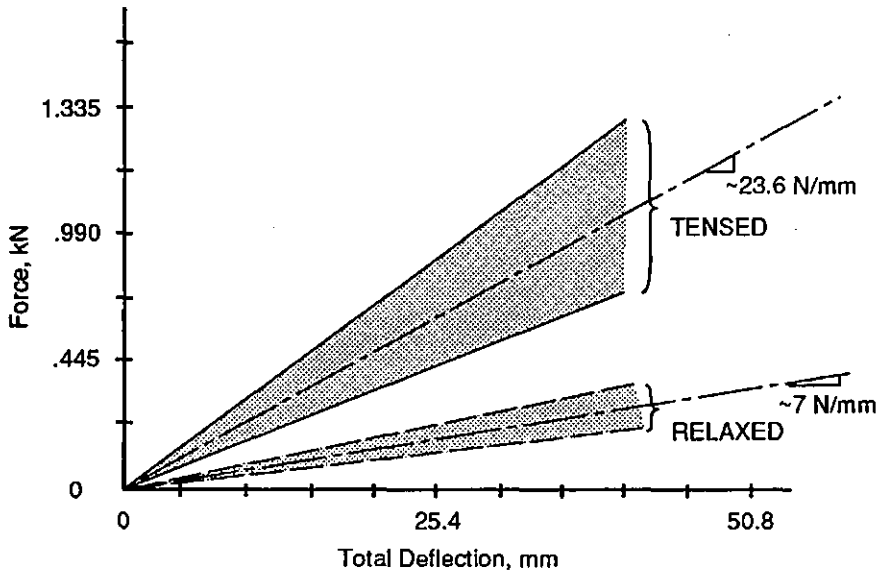

FIGURE 2–2. Static loading corridors for relaxed and tensed volunteers—back fully supported (Lobdell et al. 1973).

3. EXPLORATION OF MODIFIED DAMPED-RIB MODEL

A wide variety of fluid-filled internal response elements were explored and tested, as described in Volume 2 of this report. While some progress toward achieving the desired response biofidelity was made, none of the approaches offered a solution with the desired rate sensitivity, and all had problems with space, durability, user friendliness, and/or compatibility with potential deflection instrumentation that could not be resolved within the time and funding of the current program. Therefore, the internal-response-element approach to the thorax/abdomen design was set aside in favor of a highly modified, damped-steel-rib model of the chest that would include the following enhancements to the Hybrid III thorax/abdomen:

- improvement (i.e., lowering) of the static or quasi-static stiffness of the Hybrid III chest while maintaining and improving dynamic response biofidelity,
- improvement in the coupling (or decoupling) between chest regions,
- improvement and tuning to the low-velocity (i.e., 4.3-m/s) response corridor,
- removal of the barrel-shaped ribcage and general improvement of the ribcage geometry, including addition of a lower ribcage (R7 through R10) as well as upper ribs (R1 through R3),
- improvement in chest deflection measurement capability,
- improvement of the shoulder design relative to belt/shoulder interaction and transfer of shoulder loads to the chest and spine, and
- improvement of dummy kinematics and interaction with shoulder belts and steering wheels through improved shoulder (i.e., clavicle) mobility and the addition of thoracic spine flexibility.

3.1 BELT LOADING RATES AND BIOFIDELITY IN QUASI-STATIC STIFFNESS

Ideally, an ATD chest would have response biofidelity for all potential loading conditions and velocities. Given that this is not achievable, the design must be targeted to the most important loading velocities for the intended ATD use. For example, the Hybrid III chest was tuned to the midrange loading corridor defined by the 6.7-m/s (15-mph) Kroell et al. (1974) impact tests based on expected loading rates of unrestrained occupants interacting with vehicle interior components during 40- to 48-km/h (25- to 30-mph) vehicle impacts. However, as the loading rate decreases, the Hybrid III chest becomes inappropriately stiff.

Because a belt restraint system is essentially in contact with the occupant prior to a crash, the loading velocity of a shoulder belt on the occupant's chest and shoulder are considerably lower than loading rates for unrestrained occupants interacting with other vehicle interior components. Consequently, low-velocity and quasi-static response corridors become higher priorities than mid- and high-velocity response corridors for a crash dummy designed for improved performance and injury assessment under restrained-occupant test conditions.

While it was not possible to conduct a thorough study regarding occupant loading rates imposed by belt restraint systems, a preliminary investigation into this issue, using both CVS modeling (i.e., the MVMA 2-D model) and analysis of high-speed films from belted cadaver tests, has indicated that chest loading rates for belt-restrained occupants can range from 1 to 5 m/s, depending on the degree of slack present in the shoulder belt prior to the onset of impact. A loading rate of 6.7 m/s was therefore considered high for belt loading rates and tuning to the 4.3-m/s Kroell et al. corridor was considered to be a more appropriate goal for the new thorax. (See update on thorax design specifications in Appendix A of this document.) It can also be expected (and was demonstrated in some preliminary modeling work) that, at these lower loading rates, the quasi-static stiffness of the ribcage will have a greater influence on peak chest deflection and, therefore, achieving quasi-static loading biofidelity was also considered of greater importance for the new thorax than was biofidelity for the mid-velocity (i.e., 6.7-m/s) loading rates.

3.2 QUASI-STATIC LOADING OF HYBRID III CHEST

As illustrated in Figure 3–1, quasi-static loading of the Hybrid III chest was conducted using a 152-mm-diameter (6-in) plate positioned at midsternum. Tests were conducted with and without the chest pad and vinyl skin in place, and with the spine supported so that the ribcage was free to deflect rearward at the spine. Chest deflection was measured internally using the chest potentiometer installed in Hybrid III as well as externally using the displacement of the Instron table as a measure of chest compression.

Figures 3–2a and 3–2b show the force-time, deflection-time, and force-deflection loading and unloading curves for the tests without padding and vinyl skin, while Figures 3–2c and 3–2d show similar plots for testing with the padding and skin in place. For the test without padding, the peak internal and external deflections were essentially the same at about 50 mm (2-in). For the test with padding, the peak external deflection was about 63 mm (2.5 in), while the peak internal deflection was about 45 mm (1.8 in). The different stiffness values measured at these deflections are shown in Table 3–1.

TABLE 3–1

QUASI-STATIC STIFFNESS OF HYBRID III CHEST USING A 152-MM (6-in) DIAMETER RIGID LOADING PLATE

Test and Deflection Conditions	Chest Stiffness	
	N/mm	lb/in
Without padding and skin	56.7	323
With padding and skin—external deflection	35.2	201
With padding and skin—internal deflection	49.4	282

As shown in Figure 2–2, Lobdell et al. (1973) have determined the average sternal stiffness of the tensed human chest to be about 23.6 N/mm (135 lb/in) using a similar loading plate. For the dummy, the most meaningful stiffness measure for comparison is that based on internal deflection since this is the response measured during testing and since the flesh of the dummy is significantly thicker than that of the human, especially over the sternum.

From Table 3–1, it is seen that the tensed human chest stiffness measured by Lobdell et al. is significantly less than either the Hybrid III sternal stiffness without padding and skin or the internal sternal stiffness when tested with padding and skin. An explanation of the lower sternal stiffness based on internal deflection when tested with padding and skin compared to the stiffness based on external deflection when tested without padding and skin is not apparent, but may have to do with differences in internally and externally measured deflections due to the manner in which the ends of the ribs deflect inward during compression of the chest.

3.3 FINITE ELEMENT MODELING AND STATIC TESTING OF THE HYBRID III RIBS

Since the Hybrid III ribcage without padding is considerably stiffer under anterior-superior (AP) quasi-static loading than the tensed human chest, it was desired to determine the changes in material dimensions required to obtain a more humanlike static stiffness, and the consequences of making such a change on the lateral stiffness of the chest. Both quasi-static loading of damped and undamped Hybrid III ribs as well as finite element modeling of different rib configurations, were used to investigate this and other issues regarding rib and ribcage design. The results of initial tests and modeling were used to estimate the thickness of steel for the ribs of the first hardware prototype thorax.

Initially, the finite element model (FEM) ANSYS was used for static loading simulations but this was subsequently changed to MARC. Initial modeling was of Hybrid-III-shaped undamped steel ribs oriented so that the direction of loading was in the plane of the ribs. Figure 3–3 shows the FEM configuration of a three-rib system modeled for the following conditions:

Rib hoop widths	=	329 mm	(12.95 in)
Rib hoop depths	=	215 mm	(8.45 in)
Width of rib steel	=	19 mm	(0.75 in)
Thickness of rib steel	=	2 mm	(0.08 in)

The model used 160 quadrilateral shell elements with six degrees of freedom allowed at each element node. Young's modulus was set at 20.9 kPa (3.0×10^6 psi) and Poisson's ratio was set to 0.3. The ribs were assumed to be fixed at the spine but were unconnected at the sternum for these initial simulations. Figure 3–4 shows a six-rib model in the loaded and unloaded conditions.

To validate the FEM results, experiments were carried out in which undamped, Hybrid III ribs were loaded in the AP direction with a 152-mm-diameter (6-in-diameter) rigid plate. Figure 3–5 shows a schematic of the test setup, while Figures 3–6a through 3–6c show the ribs in preloaded and loaded conditions. As shown, the ribs were clamped between two metal plates and the dimensions of the bottom plate allowed the ribs to bend downward at this mounting. As shown in the simulations, the ribs were unconnected at the sternum.

Figure 3–7 compares the force-deflection results obtained from the FEM analysis with those obtained experimentally for a three-rib configuration. It will be noted that there was good agreement between the model and experiment, indicating that the model results were reasonable for these loading conditions.

Subsequent to these initial tests and modeling runs, additional tests and simulations were carried out using both three and six undamped-rib configurations and for both AP and lateral loading. For lateral loading tests, the ribs were connected at the sternum by a piece of plastic material to allow the loads to be transmitted to the ribs on the unloaded side. Figures 3–8a through 3–8c show the test setup and loading conditions for lateral tests in

effects of friction on rib deformation. As indicated in the figures, this resulted in a change in location of the loading surface on the ribs as loading progressed. For modeling, Young's modulus and Poisson's ratio for the plastic material were set to 30.2×10^6 kPa (4.35×10^6 psi) and 0.45, respectively. Figure 3–9 shows the FEM after simulation of lateral loading.

Table 3–2 summarizes and compares the stiffness values obtained from the model simulations and experiments for these conditions. In each case, axial stiffness corresponds to the stiffness in the direction of loading. Note that the model results for lateral loading are expressed in two ways. One is the stiffness for load versus displacement of the ribs at the point of loading, which is about halfway between the back and front of the rib hoops. The second is called the torsional stiffness and is based on the load versus the rotation angle of the ribs. The most important observation is the good agreement between results for the model and the experiment.

TABLE 3–2

COMPARISON OF RIB STIFFNESS FOR FEM MODEL AND EXPERIMENTS

Stiffness	AP LOADING				LATERAL LOADING			
	Three Ribs		Six Ribs		Three Ribs		Six Ribs	
	Model	Exper.	Model	Exper.	Model	Exper.	Model	Exper.
Axial* (N/mm)	15.36	15.29	33.94 to 36.07	33.80 to 39.84	29.59 to 39.05	30.42 to 39.59	45.53 to 66.35	52.54 to 63.48
Torsional (N·m/deg)	N.A.	N.A.	N.A.	N.A.	147.4 to 266.9	N.A.	311.4 to 532.9	N.A.

*Note that axial stiffness is the stiffness in the direction of the applied load.

Subsequent to these additional validations, the FEM was used to determine differences in AP and lateral stiffness values that might be expected for different thicknesses of rib steel and different thicknesses of damping material. Properties of the damping material under static loading conditions were obtained from EAR, Inc.

To validate the FEM model with damping material included, AP and lateral loading tests were conducted as previously described for a single Hybrid III rib, first without damping material and then with damping material about 13-mm (0.5-in) thick. The results are summarized in Table 3–3. In each case, a stroke distance of 50 mm (2 in) was used. As shown, the quasi-static AP loading stiffness of a single rib increased nearly 50 percent when the damping material was added, but the lateral loading stiffness increased only about 20 percent.

Figure 3–10 compares simulation and test results for AP loading of a single damped rib while Figures 3–11a and 3–11b show results obtained for simulations using different thicknesses of damping material and steel. From these plots it can be seen that changes in the thickness of the steel have a much greater influence on AP quasi-static loading stiffness than do changes in the thickness of the damping material.

TABLE 3–3

COMPARISON OF STIFFNESS VALUES FOR DAMPED AND UNDAMPED SINGLE HYBRID III RIB

Condition	Stiffness			
	AP		Lateral	
	N/mm	lb/in	N/m	lb/in
Rib *without* damping material	7.07	40.4	9.3	53.0
Rib *with* damping material	10.04	59.6	10.8	61.6

*Steel thickness=2.032 mm (0.081 in); damping material thickness=15.8 mm (0.625 in); stroke distance=50 mm (1.9 in).

3.4 QUASI-STATIC AND DYNAMIC TESTS OF THIN-STEEL DAMPED RIBS

As a result of the quasi-static testing and finite element modeling described above, a decision was made to produce the first prototype chest using 1.37-mm-thick (0.054-in) steel instead of 2.03-mm-thick (0.08-in) steel in order to reduce the static stiffness closer to that of the tensed-volunteer corridor determined by Lobdell et al. (1973). Before building the first set of prototype ribs, however, a set of Hybrid III ribs was fabricated using the thinner steel and static and dynamic tests were conducted. The damping material used in constructing these ribs was approximately 15.9 mm (0.625 in) thick.

3.4.1 Quasi-Static Stiffness Tests and Results

Quasi-static loading tests of the damped and undamped thin-steel (1.37-mm-thick or 0.054-in-thick) Hybrid III ribcage were carried out using a 152-mm-diameter (6-in-diameter) rigid plate. Figures 3–12a through 3–12c show the ribcage without the damping material in various stages of compression. In these tests, ribcage compression was measured by a single string potentiometer by Space Age Controls, Inc. installed on the side of the spine box and connected to the end of the third rib. (Note that the Hybrid III potentiometer was not activated in these tests.) This is illustrated in Figure 3–13.

Figure 3–14 compares the force-deflection results to the tensed-volunteer corridor and the Hybrid III ribcage without padding material or jacket in place. The stiffness of the thin-steel ribcage is much closer to the desired corridor for these loading conditions than is the Hybrid III ribcage. However, it was noted upon unloading of the thin-steel ribcage that the ribs took a considerable length of time to return to their original geometry.

3.4.2 Dynamic Pendulum Tests and Results

The thin-steel, Hybrid III ribcage was tested on a pendulum impactor as shown in Figure 3–15. Initial tests were conducted with the chest fixed rigidly to the test structure, with a 13.6-kg (30-lb) impactor, and with the standard Hybrid III sternum. Impact force was measured using a Denton uniaxial load cell (Model 2089) and chest deflection was measured using a single string potentiometer attached to the spine and connected to the end of the third rib.

Figure 3–16 shows the force-deflection responses obtained from this thin-steel ribcage with 16-mm (0.625-in) damping material when tested in the fixed-back (i.e., not in dummy) condition using a 152-mm (6-in) diameter rigid impacting surface. The tests were conducted at 4.3 m/s (14.1 ft/s or 9.6 mph) and 6.7 m/s (22 ft/s or 15 mph), respectively, with a 25-mm (1-in) thick Ensolite pad placed on the front of the sternum. In both cases, the peak deflections are within the appropriate shaded corridor (note that both the 4.3- and 6.7-m/s corridor are shown on each plot), but the force does not reach the desired plateau levels, except for the higher velocity case where it rises to this level at the end of chest compression.

It should also be noted that the total energy under each loading curve is not equal to the total energy delivered by the impactor based on the mass of the impactor and the initial impact velocity. At 4.3 m/s, the energy delivered is about 135 N·m (1200 in·lb) while at 6.7 m/s the energy delivered is about 305 N·m (2700 in·lb). The loading energies from the force-deflection curves are only 89.1 N·m (788.6 in·lb) and 237.3 N·m (2100.3 in·lb) for the two tests, respectively. The reason for the differences between observed and expected loading energies is not clear but contributing factors include the following:

- Measured force is approximately 5% low due to uncompensated inertial mass at the end of the load cell.
- Energy involved in compressing the padding is not included since deflection of the padding was not measured.
- There may be errors in deflection measurements due to curling of rib ends.

3.4.2.1 Effect of Padding and Mass. Figure 3–17 shows force-deflection plots for the same conditions as described above except that the 25-mm (1-in) Ensolite pad was replaced with a thinner, 6- to 7-mm (0.24- to 0.28-in) thick pad. The primary effect of the thin pad was to increase the initial force spike due to sternal mass. However, the initial peak in force rebounds to a lower level than occurred with the thicker pad in place. Also, the measured peak deflections were not increased as one might have expected if, as hypothesized above, a significant amount of energy goes into compression of the thick pad. Again, for each test, the total loading energy is less than the energy delivered but, in this case, the padding cannot be considered a significant source of the difference.

Figures 3–18a through 3–18c show additional test results for the fixed-back, thin-steel Hybrid-III ribcage with different conditions of sternal mass and sternal padding. By adding additional mass in the form of flexible lead sheets to the front of the chest, it was possible to increase the magnitude of the early peak in force, but this force decreased rapidly to a level which is inversely proportional to the magnitude of the peak. The addition of a 25-mm (1-in) thick Ensolite pad diminished this mass effect, especially at the lower impact velocity.

3.4.2.2 Effect of Rib Support at Spine. Upon examining these test results in conjunction with top-view, high-speed films (i.e., looking down on the top rib), it was noted that a significant amount of rib deflection occurred where the ribs attach to the back of the spine, even with the Hybrid III rib helpers (i.e., rib stiffeners) in place. It was reasoned that bending of the ribs at the spine would contribute to chest deflection but, since there is no damping material in this region, the forces might be low and not rate sensitive. It was therefore hypothesized that bending of the ribs at the spine might explain the low force levels during the first 25 mm (1 in) in the force-deflection plots, since the damping material on the sides of the ribs would not necessarily be deforming during this time.

In order to examine this hypothesis further, a rib-support structure was fabricated to provide "full support" for the ribs lateral to and behind the spine, thereby preventing rib bending at the spine/rib junctions (see Figure 3–22b). Figures 3–19a through 3–19e show the force-deflection plots from fixed-back tests at 4.3 and 6.7 m/s for different conditions of sternal mass and padding. Comparing these plots to those shown previously for the "normally-supported" ribs, it is seen that elimination of rib bending at the spine had a

significant effect on the response. Most notably, the peak deflection was reduced significantly and the force increased more quickly (i.e., with less deflection) to a somewhat higher value. The effect at 4.3 m/s was particularly dramatic and the peak deflections were considerably less than the desired values. At 6.7 m/s, the peak deflections were close to the lower edge of the corridor whereas, with the normally-supported ribs, the peak deflections were near the upper edge of the corridor. The effects of mass and padding are similar but less dramatic with the fully-supported ribs.

3.4.2.3 Effect of Adding Damping Material to Ribs at Spine. In addition to evaluating the effects of fully supporting the ribs at the spine, it was also desired to find out the effect of adding damping material to the ribs at their attachment to the spine. While this would not prevent bending at the spine, it would, in theory, add rate sensitivity to rib deformation occurring at the spine and might thereby enhance the early response of the chest.

Figure 3–20 shows the pendulum impact test setup of the thin-steel ribcage with about 10 mm (0.375 in) thickness of damping material epoxied to the back of the ribs across the spine. The chest was impacted in the fixed-back setup at both 4.3 m/s and 6.7 m/s in this condition using the 13.6-kg (30-lb) impactor. The results are shown in Figures 3–21a through 3–21d for different conditions of sternal padding and mass. Comparing these plots to those shown previously for the normally-supported ribcage (Figures 3–18a through 4–18c), it is seen that the damping material had little effect on the response. The reason was not immediately apparent but may have been a result of the thinness of the damping material used.

3.4.2.4 Quasi–Static Loading of Fully-Supported, Thin–Steel Hybrid III Ribcage. Additional quasi–static loading tests were performed on the damped, thin-steel Hybrid III ribcage with the ribs in both the normally-supported and fully-supported conditions. Figures 3–22a and 3–22b illustrate the test setup. Force-deflection results are compared in Figure 3–23, where the corridors are a consequence of measuring chest deflections with both the internal string potentiometer and the stroke distance of the Instron head, which provided somewhat different values due to curvature of the rib ends where the string potentiometer cable was attached. As shown, the stiffness increased from about 23.3 N/mm (133 lb/in) to 35 N/mm (200 lb/in) when the ribcage was changed from the normally-supported condition to the fully-supported condition.

3.5 DAMPED-BEAM VIBRATION TESTS

In order to better understand the relationship between thickness of the damping material and the extent of damping provided to the spring steel ribs, beam vibration tests were conducted using various configurations of damping materials and steel. Strips of Hybrid-III-type damping material (NAVY DAMP 1000) obtained from EAR, Inc. were cut from tiles to different thicknesses and bonded with 3M 2216 epoxy adhesive to straight 305-mm (12-in) lengths of 1.4-mm (0.054-in) and 2-mm (0.080-in) thick by 19-mm (0.75-in) wide, 1075 steel that had been heat treated to a Rockwell hardness of 43 (the same hardness as Hybrid III ribs). The beam configurations included the case with no damping material as well as damping material thicknesses of 4.7 mm (0.187 in), 9.5 mm (0.375 in), and 15.9 mm (0.625 in) epoxied to one side of the steel strips. In addition, each thickness of steel was tested for the cases of 4.7-mm (0.187-in) thick and 9.5-mm (0.375-in) thick damping material epoxied to both sides.

The test setup is shown in Figure 3–24. One end of the composite beam was clamped to a rigid surface while the other end was free and about 276 mm (10.5 in) from the edge of the clamped surface. A single-axis Endevco accelerometer was fastened to the free end to monitor amplitude and frequency of the oscillations resulting from manually bending the free end to a predetermined deflection of 25 to 50 mm (1 to 2 in) and suddenly releasing it.

Tests were conducted with the fixed end clamped in two ways. In the initial series of tests, only the steel was clamped and the damping material ended at the edge of the mounting block. In a second series of tests, the damping material was extended to the end of the steel strip and was clamped along with the steel rib. In this latter series of tests, the effective damping was significantly greater and it was necessary to add a 0.9-kg (2-lb) mass to the free end of the beam in order to achieve multiple oscillations.

Figures 3–25a and 3–25b show typical output signals from the accelerometer for vibrations of two damping configurations. It can be shown (Church 1963, p. 85) that the degree of damping of a second-order mechanical system consisting of mass, spring, and damper is indicated by the log decrement, δ, of the amplitudes of successive peaks of the free-vibration acceleration signals. This can be expressed as:

$$\delta \equiv \ln \frac{P_1}{P_2}$$

where P_1 is the peak of acceleration immediately preceding the peak, P_2.

Using this general relationship and the accelerometer output signals from the damped-beam free-vibration tests, the following observations were made:

- There is a direct relationship between thickness of damping material and damping ratio.
- The same total thickness of damping material divided in two and placed on both sides of the steel beam does not provide nearly the same damping as a single thickness of material placed only on one side.
- The damping appears to be the same for both compression and tension of the damping material (i.e., up or down movement of the beam).
- There is a very significant increase in effective damping when the damping material is clamped compared to when only the steel is clamped.

While these observations were made for low-frequency vibration tests, it is expected that they would also be relevant to higher frequencies and to the conditions of rib deflections during dummy loading, especially for the lower velocity loadings imposed by restraint systems.

3.6 SLANT VS. NONSLANT RIBS

Throughout the process of designing the ribcage, there was debate on the question of whether the ribs should slant with respect to the longitudinal axis of the thorax or be positioned essentially perpendicular to the spine axis as they are in Hybrid III.[1] The primary argument for slanting the ribs is related to achieving geometric similarity to the human ribcage, particularly with regard to the position of the anterior portion of the lower ribcage, while maintaining attachment of these ribs at reasonable locations on the lower thoracic spine. The primary arguments against slanting the ribs are the added complexity of rib design and fabrication and the uncertainty of the response of slanted ribs. While an additional advantage is increased resistance to upward movement of the ribcage, which has been a concern with Hybrid III, a potentially compensating disadvantage is the probability of a significant amount of downward movement of the ribs and the potential problems that this

[1]The Hybrid III ribs are, in fact, inclined upward from the horizontal with the sternum vertical when the dummy is tilted forward for calibration testing.

out-of-plane deflection would present, both with regard to interaction with the abdomen and pelvis and with regard to measurement and interpretation of chest compression.

The geometry of the human ribcage has been studied and described by Dansereau and Stokes (1988). As shown in Figure 3–26 and Table 3–4, the human ribs slant downward when viewed from both the front and the side, with the latter (frontal) angles in excess of 35 degrees.

TABLE 3–4

HUMAN RIB GEOMETRY:
MEANS AND STANDARD DEVIATIONS OF RIB SHAPE
AND ORIENTATION MEASUREMENTS (Dansereau and Stokes 1988)

Rib	Intrinsic Measures			Extrinsic Measures		
	Rib Length (mm)	Enclosed Area (mm^2)	Max. Curvature (mm^{-1})	Chord Length (mm)	Frontal Angle (deg)	Lateral Angle (deg)
T2	203.0 ±28.5	6001 ±1491	0.0331 ±0.0074	113.9 ±16.2	19.5 ±9.2	35.2 ±10.3
T3	254.8 ±25.6	9686 ±1763	0.0286 ±0.0034	142.6 ±16.1	16.9 ±8.4	34.5 ±9.1
T4	289.1 ±24.8	12543 ±2036	0.0253 ±0.0037	168.2 ±19.7	13.6 ±7.0	35.2 ±8.8
T5	304.8 ±28.9	14380 ±2372	0.0242 ±0.0043	190.0 ±19.9	12.1 ±6.5	36.1 ±7.8
T6	313.8 ±31.7	14732 ±3083	0.0239 ±0.0044	202.6 ±17.7	10.4 ±6.0	37.2 ±7.7
T7	307.9 ±37.6	13992 ±3724	0.0236 ±0.0032	212.4 ±21.4	10.9 ±6.2	39.0 ±6.6
T8	297.0 ±32.0	12878 ±3294	0.0225 ±0.0031	212.4 ±17.2	12.7 ±6.4	41.3 ±7.5
T9	297.7 ±29.6	11586 ±2914	0.0207 ±0.0025	200.0 ±15.7	19.7 ±5.8	40.0 ±6.8
T10	250.9 ±22.8	9271 ±2028	0.0184 ±0.0031	186.8 ±13.5	30.0 ±6.1	37.2 ±6.3
T11	195.3 ±27.7	5353 ±1719	0.0170 ±0.0028	154.8 ±18.3	39.5 ±4.9	32.4 ±6.1

An equally important question, however, is how the ribs move when loaded and impacted in the AP direction (i.e., essentially perpendicular to the sternum). The only evidence in this regard is a single test conducted by Kroell et al. (1974) in which a 23-kg (51.5-lb) impactor was used on a denuded cadaver chest where the ribs were visible during loading. The results indicated that the human ribs moved primarily in the AP direction and deflected downward very little. While this seems somewhat counter-intuitive, it is possibly related to the unitized structure of the human ribcage and the fact that the resistance to downward torsion of the unitized ribcage is greater than the inward resistance to compression. It may also be that much of the resistance to compression in the human chest

is generated by the soft tissues rather than the ribcage, and/or that friction between the impactor and the chest helped to prevent downward movement of the ribs and caused them to follow the horizontal trajectory of the impactor.

Preliminary finite element modeling of damped ribs (1.37-mm- or 0.05-in-thick steel with 15.9-mm- or 0.63-in-thick damping material) slanted at 10, 20, and 30 degrees to the AP loading direction suggested that very little (1 to 2 mm or 0.04 to 0.08 in) vertical deflection would take place for up to 75 mm (3 in) of AP deflection. These results were subsequently found to be in error, however, upon conducting some additional experiments.

Figures 3–27a and 3–27b show a test setup in which a single damped rib was oriented at both 10 and 30 degrees to the vertical and then loaded by hanging a mass at the center of the sternal piece. As shown in Figures 3–28a and 3–28b, the rib did not simply compress within the plane of the rib, but demonstrated considerable twisting and deflection out of the plane (i.e., downward deflection). The results are, of course, exaggerated for the case of a single rib where no torsional stability from interrib coupling is involved.

Additional tests were carried out under dynamic loading conditions using a set of Hybrid III ribs (2.3-mm- or 0.08-in-thick spring steel and approximately 16-mm- or 0.63-in-thick damping material) that was fastened to a rigidly mounted pseudospine in both slanted and nonslanted modes. Figure 3–29a shows the nonslant configuration that used the Hybrid III rib spacing and sternum and a sheet of urethane to couple the rib ends at the front. Figure 3–29b shows the slanted configuration in which the rib angles were set at 25 degrees to the horizontal (i.e., to the impactor direction) and the spacing between the ribs was reduced to maintain the same total vertical height of the ribcage at the sternum as in the nonslant or Hybrid III configuration. For this slant-rib configuration, it was necessary to add wedge-shaped pieces of urethane to the rib ends in order to couple the ribs with the same Hybrid III sternum and urethane bib.

High-speed films of these slant and nonslant ribcage configurations were taken during impact tests with a 23-kg (51.5-lb) impactor and 25 mm (1.0 in) of Hybrid III Ensolite padding on the front chest. Most important to the purpose of these tests, which were conducted at relatively low velocities due to use of a 23-kg (51.5-lb) impactor in the fixed-back test condition, was the observation that the slanted ribs deflected downward approximately 40 mm (1.6 in) as evidenced by the high-speed films and by indentations in soft clay positioned at the base of the spine (see Figure 3–29b).

3.7 PROTOTYPE RIBCAGE DESIGN

While test results described above confirmed that some torsion and downward deflection of the ribs could be expected from the slanted, damped-steel-rib approach, there was a general consensus that the optimal, long-term solution to an improved ribcage required significant geometric improvement over Hybrid III and that solutions to potential response problems of slanted ribs (i.e., downward movement and changes in chest compliance) could ultimately be resolved with equally positive results. A decision was therefore made to use a slant-rib design to the extent that slanted ribs would be compatible with the designs of the spine/shoulder and chest assembly.

ss values from AP quasi-sta
, steel was the best choice fo
and observations from the thin-steel Hybrid III tests (Section 3.4) argued for use of a thicker steel. Among these considerations were the following:

- The stiffness of the damping material tended to dominate the thin-steel rib resulting in an unacceptably long time period for the ribcage to fully recover from a compressed state,

- The relatively low lateral stiffness of the thin-steel ribcage resulted in a laterally "floppy" ribcage, and
- The dynamic stiffness (i.e., force load) achieved with 1.37-mm (0.05-in) thick Hybrid III ribs was too low.

As a result of these observations, a decision was made to fabricate the first set of prototype ribs using 1.63-mm-thick (0.064-in) 1075 spring steel. It was also decided to keep the widths of the ribs at 19 mm (0.75 in) as in Hybrid III, but to improve the length and shape of the ribcage to match the AATD 50th-percentile drawings as closely as possible. After several iterations overlaying prototype drawings on the AATD-50M drawings with skeletal rendering, and several iterations with acrylic and cardboard models of the shoulder/spine/chest assembly, an eight-rib configuration was established for the first prototype chest. This design, as well as subsequent modifications, are described in Section 5 of this report.

3.8 FIGURES

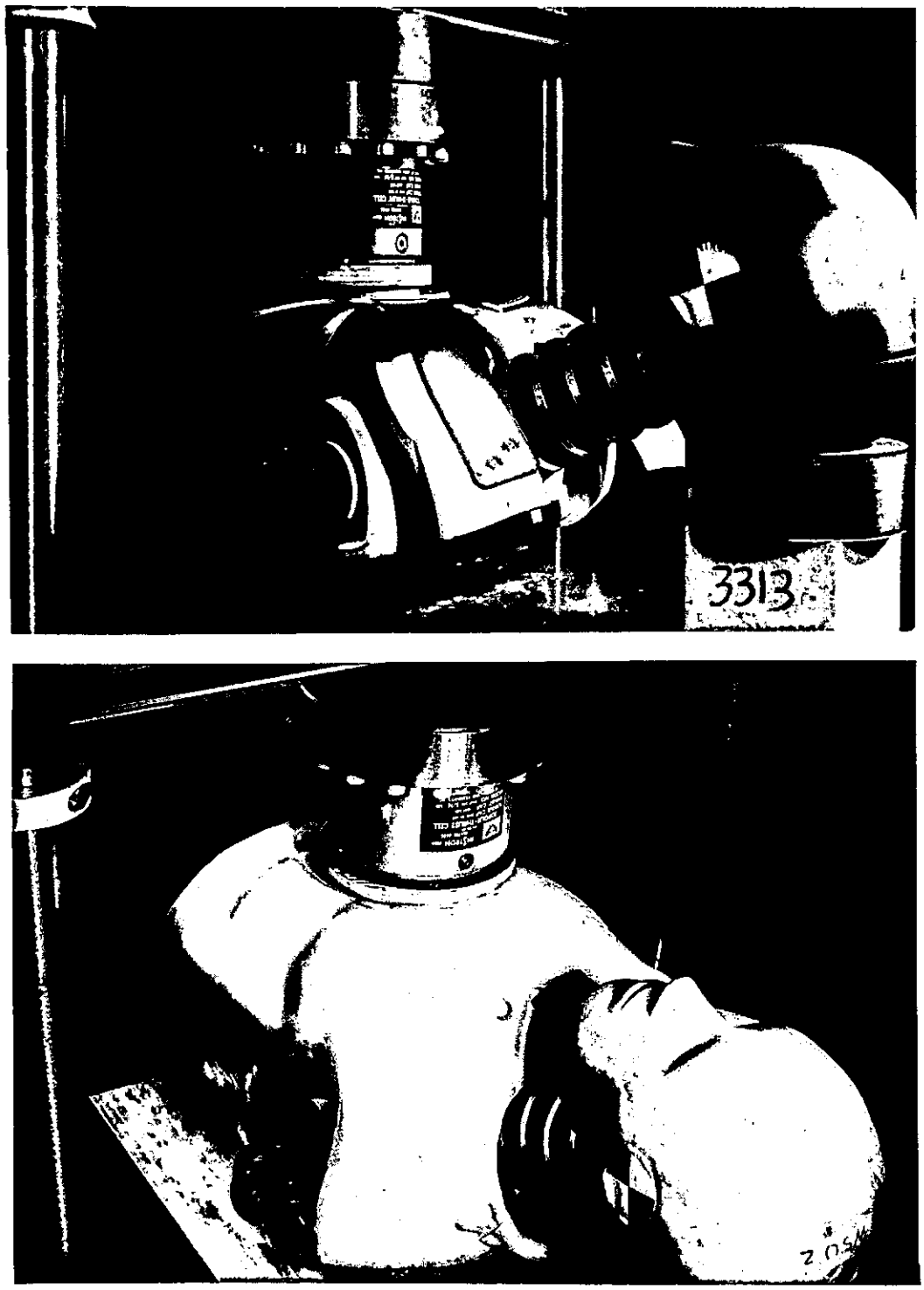

FIGURE 3–1. Quasi-static loading of Hybrid III chest *without* (top) and *with* (bottom) padding and vinyl skin.

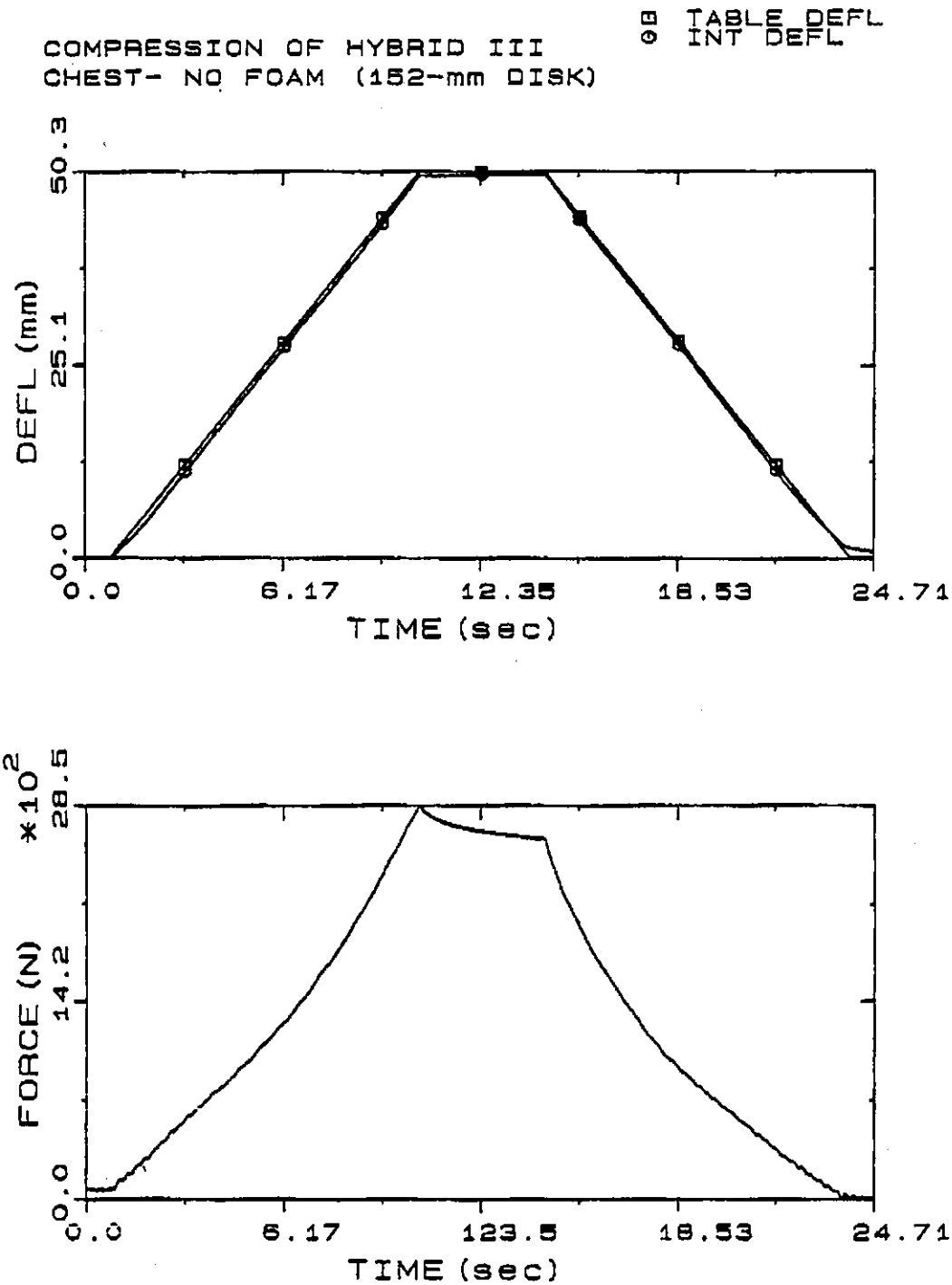

FIGURE 3–2a. Force-time and deflection-time histories for quasi-static loading and unloading of *unpadded* Hybrid III chest with 152-mm (6-in) diameter rigid plate. Deflection is measured by internal chest potentiometer as well as externally by displacement of Instron table.

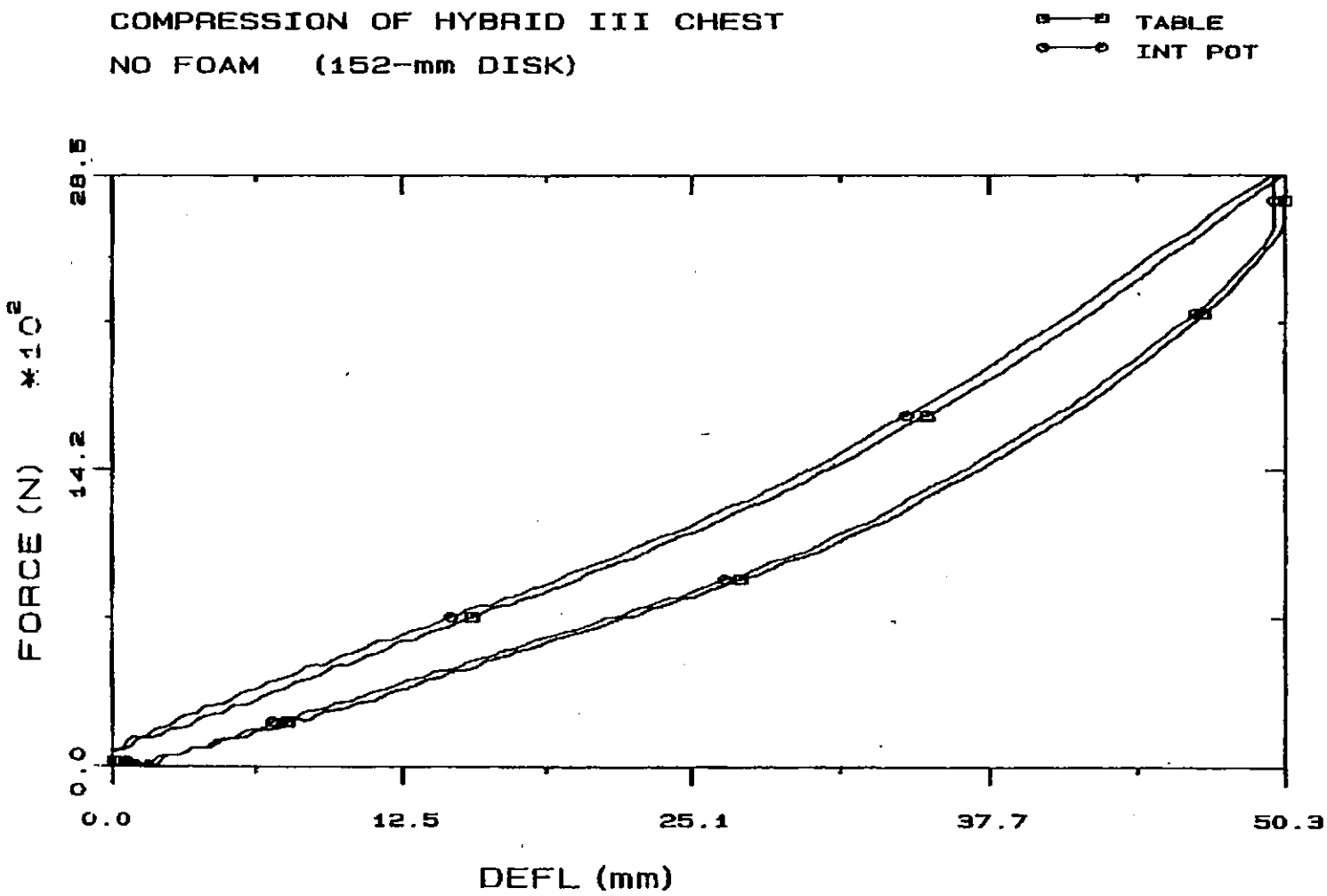

FIGURE 3–2b. Force-deflection plots for quasi-static loading and unloading of *unpadded* Hybrid III chest with 152-mm (6-in) diameter rigid plate. Deflection is measured by internal chest potentiometer as well as externally by displacement of Instron table.

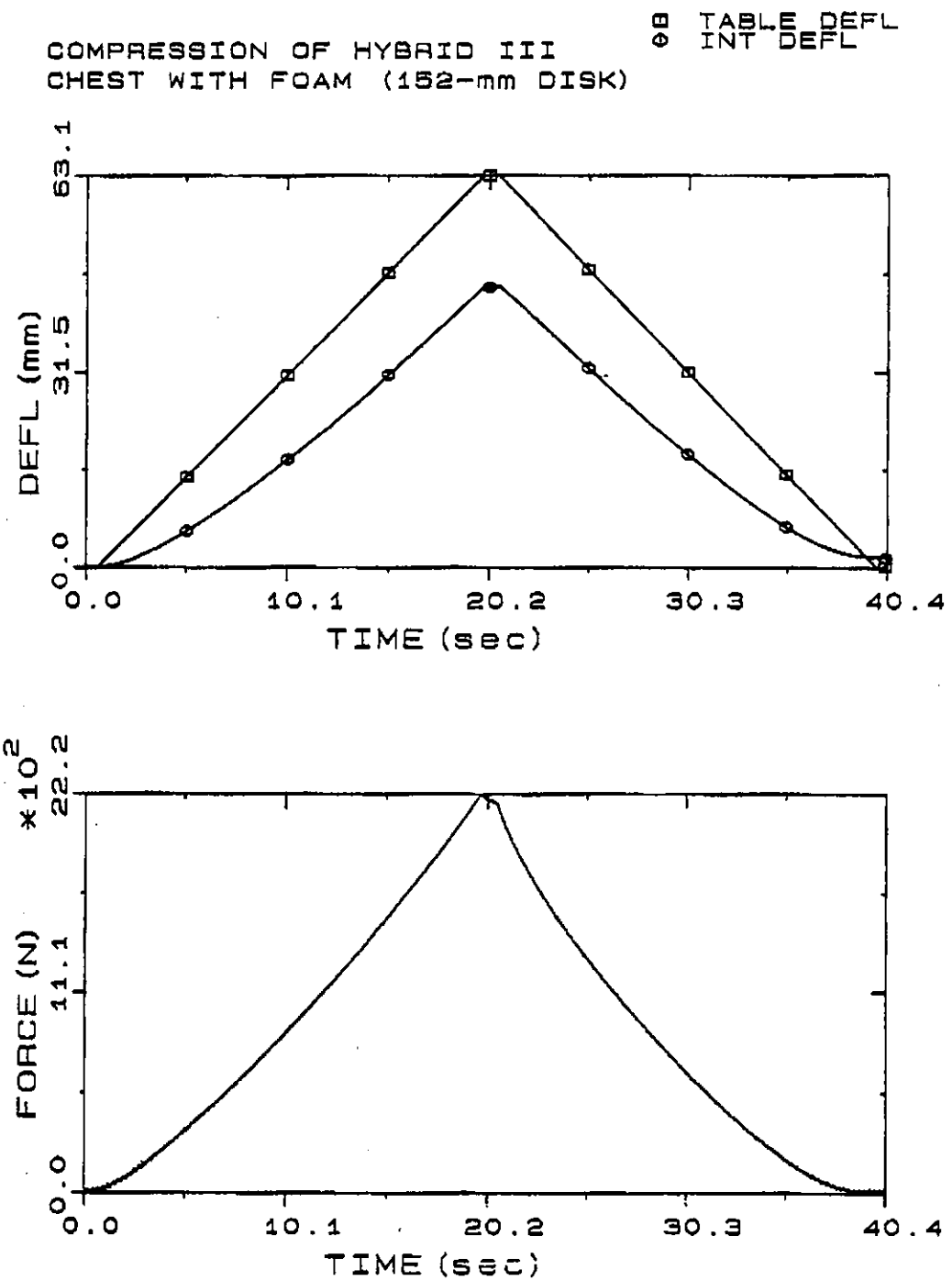

FIGURE 3–2c. Force-time and displacement-time histories for quasi-static loading and unloading of *padded* Hybrid III chest with 152-mm (6-in) diameter rigid plate. Deflection is measured by internal chest potentiometer as well as externally by displacement of Instron table.

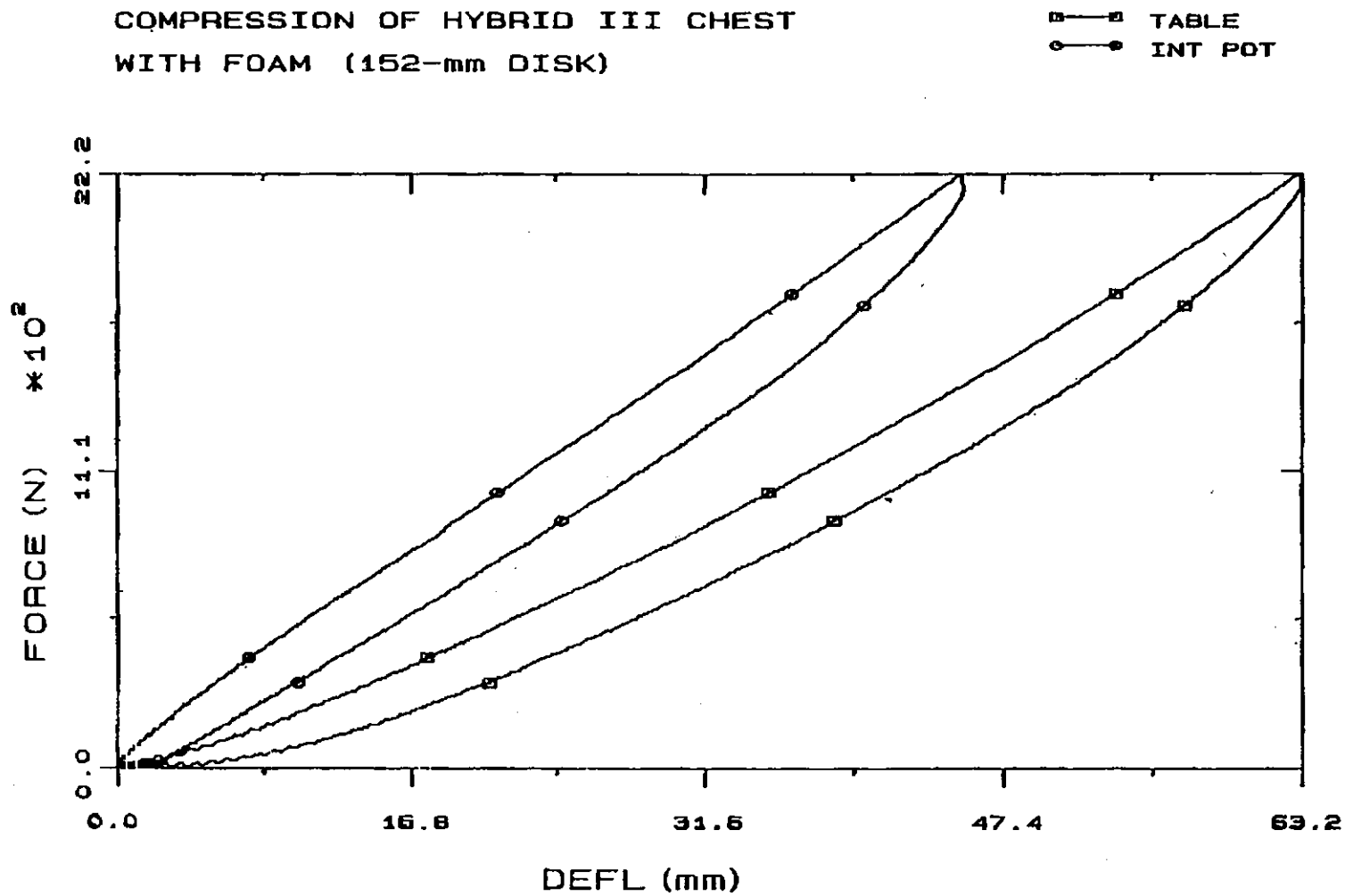

FIGURE 3–2d. Force-deflection plots for quasi-static loading and unloading of *padded* Hybrid III chest with 152-mm (6-in) diameter rigid plate. One plot is for internal deflection measured by chest potentiometer. Second plot is for external deflection measured by displacement of Instron table.

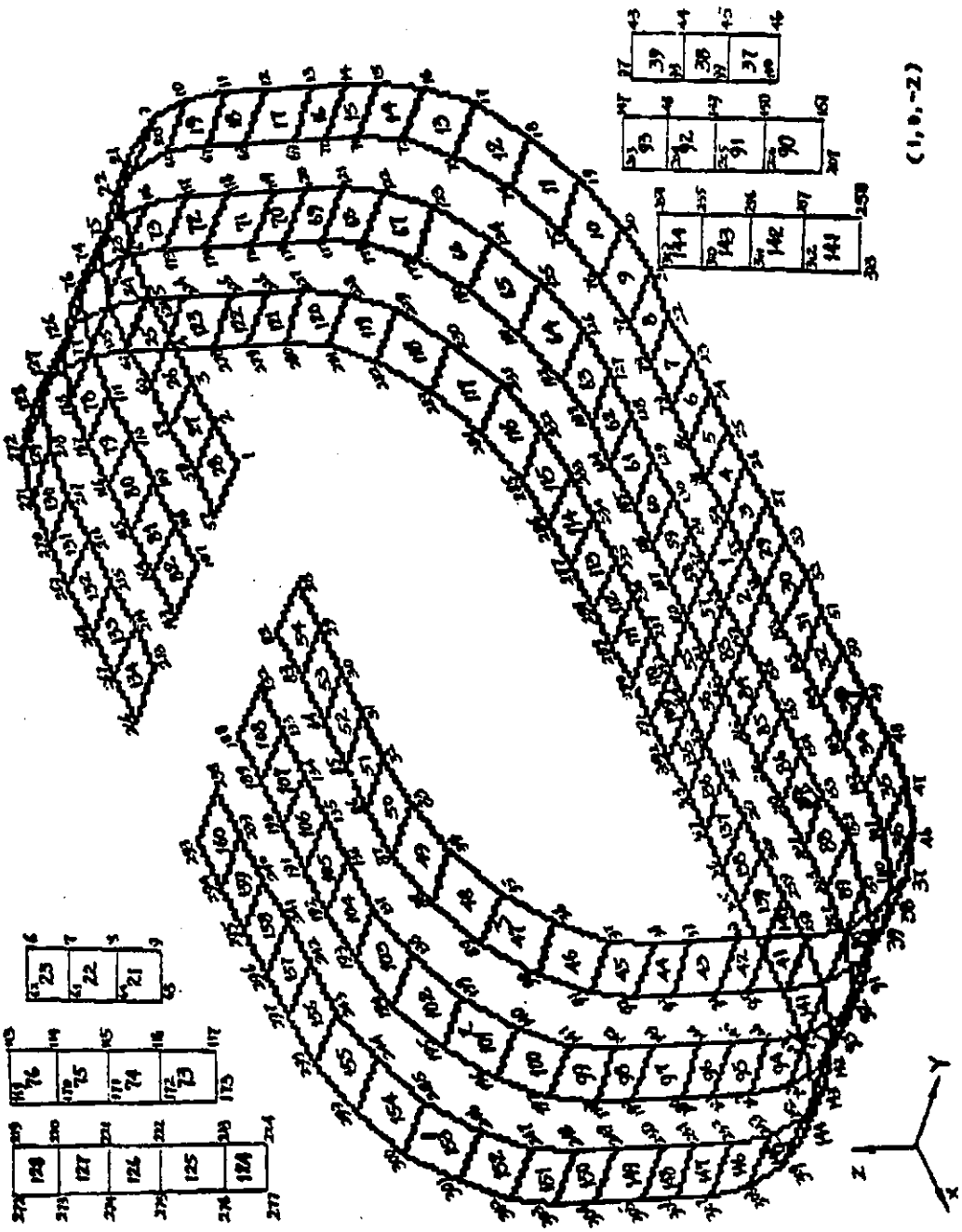

FIGURE 3–3. Three-rib FEM model configuration using MARC.

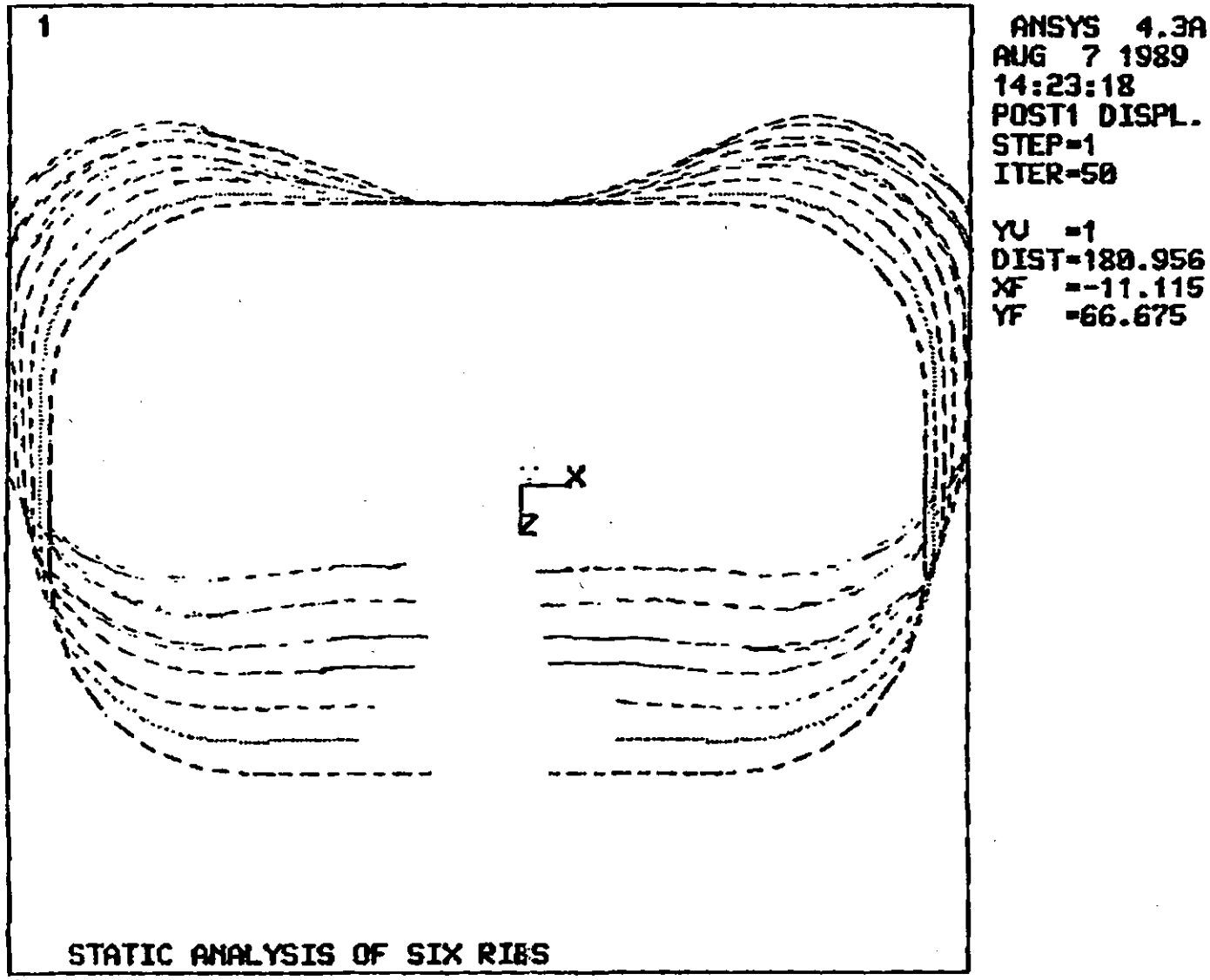

FIGURE 3–4. Six-rib FEM model undergoing AP loading.

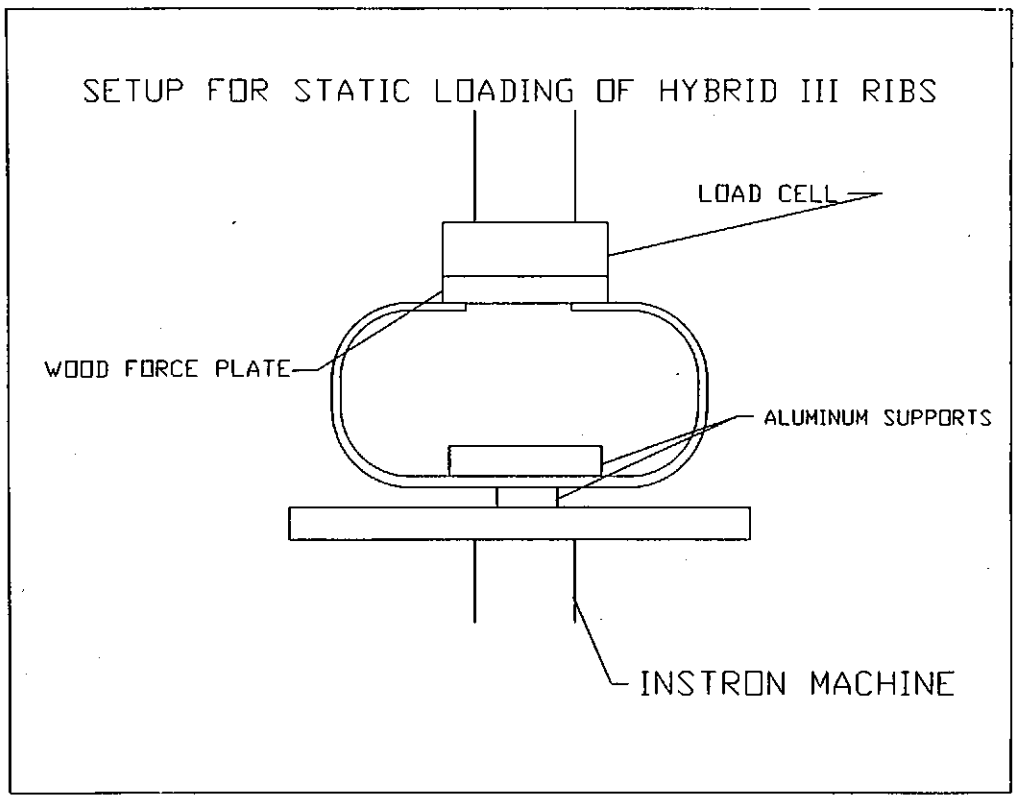

FIGURE 3–5. Schematic of Instron testing setup for quasi-static loading of undamped Hybrid III ribcage.

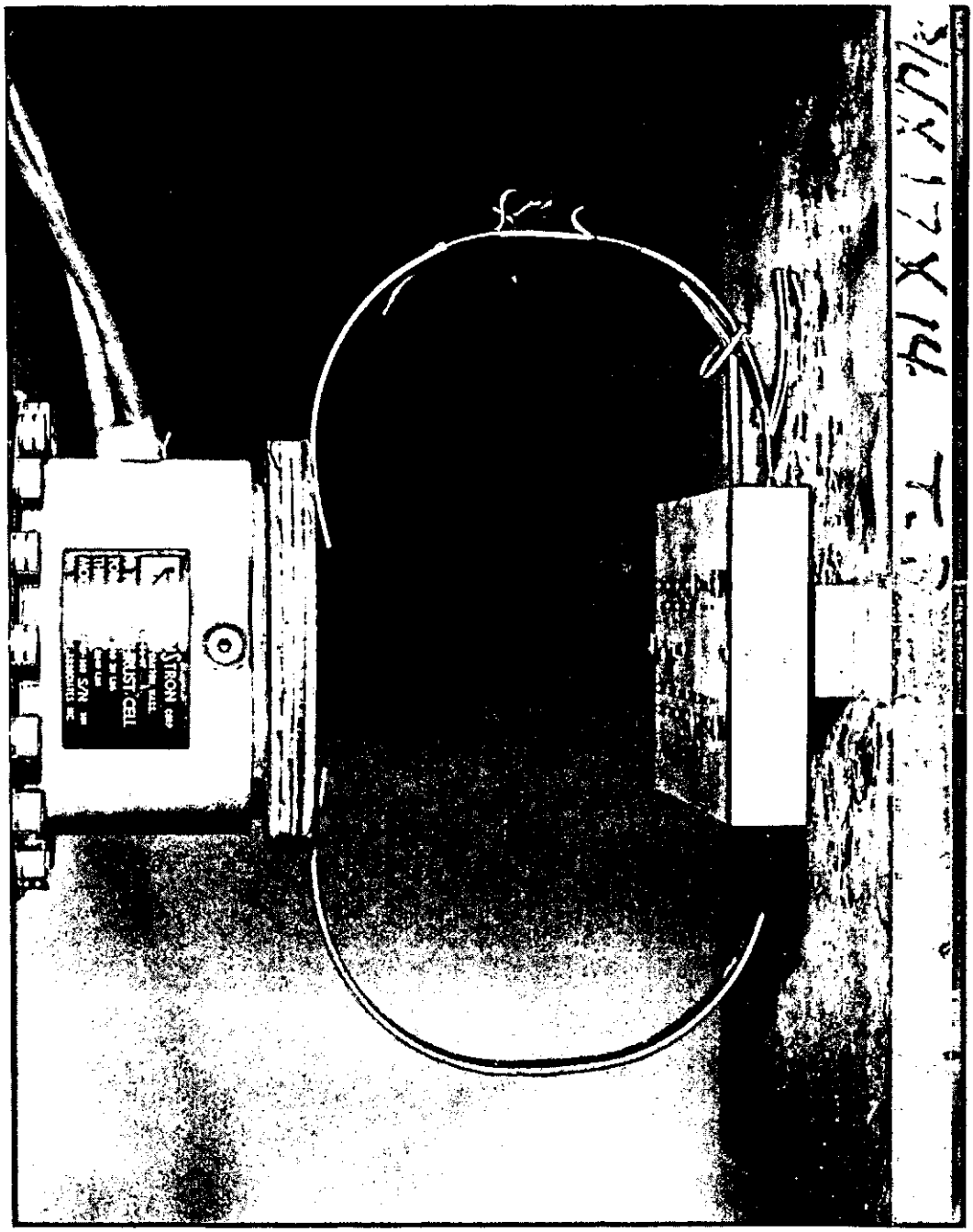

FIGURE 3–6a. Instron testing of undamped Hybrid III ribs—preload condition.

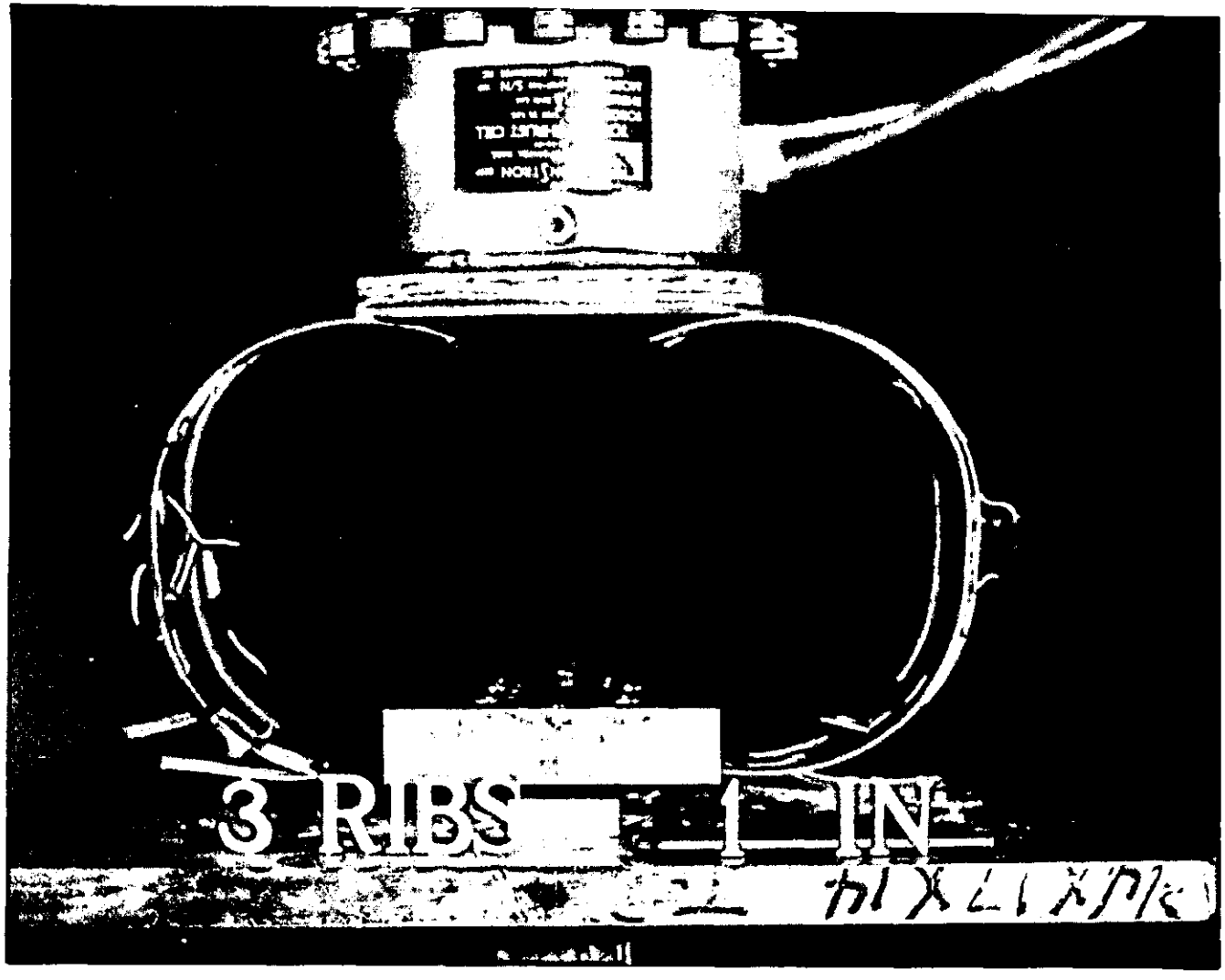

FIGURE 3–6b. Instron testing of undamped Hybrid III ribs—loading at 25-mm (1-in) deflection.

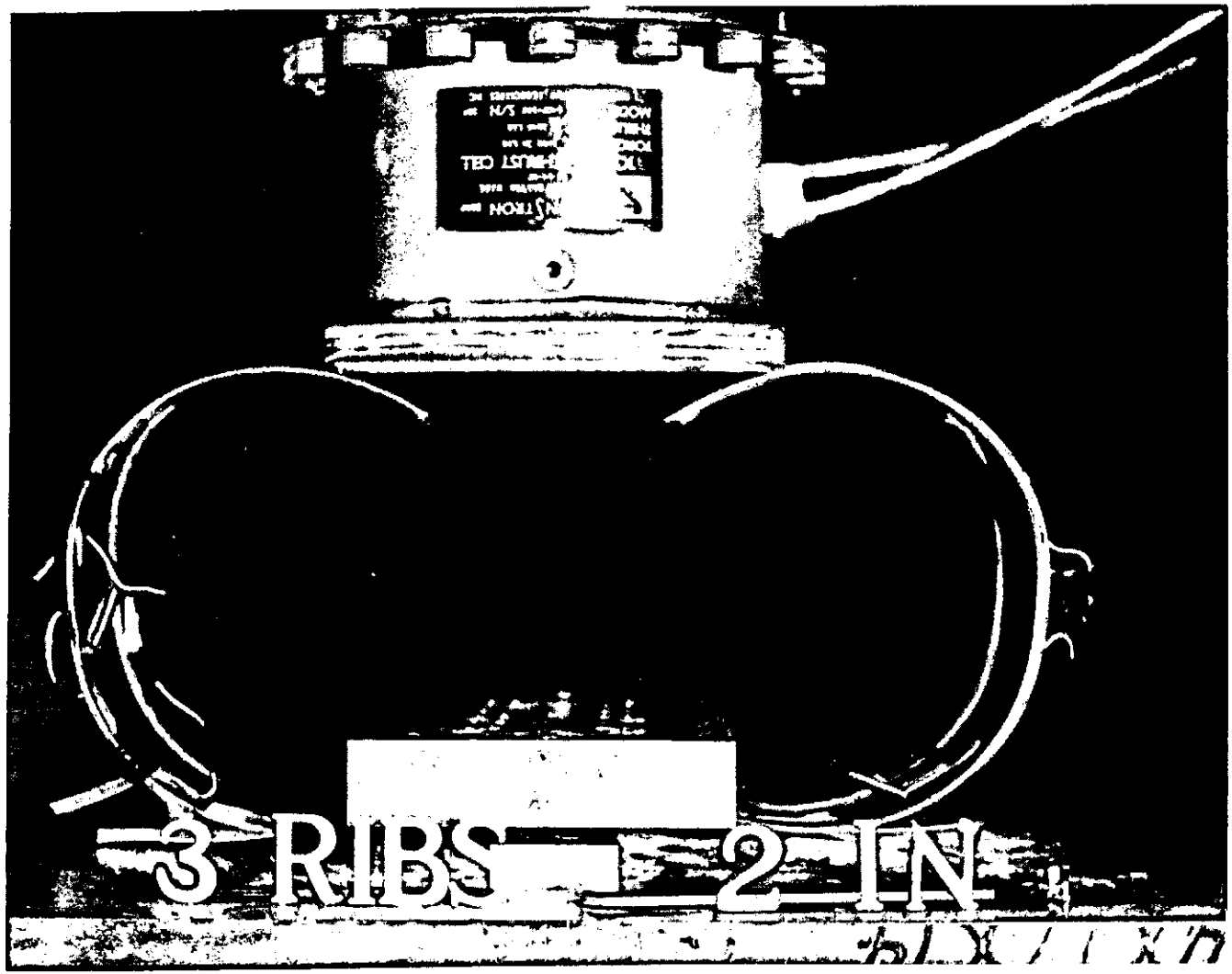

FIGURE 3–6c. Instron testing of undamped Hybrid III ribs—loading at 50-mm (2-in) deflection.

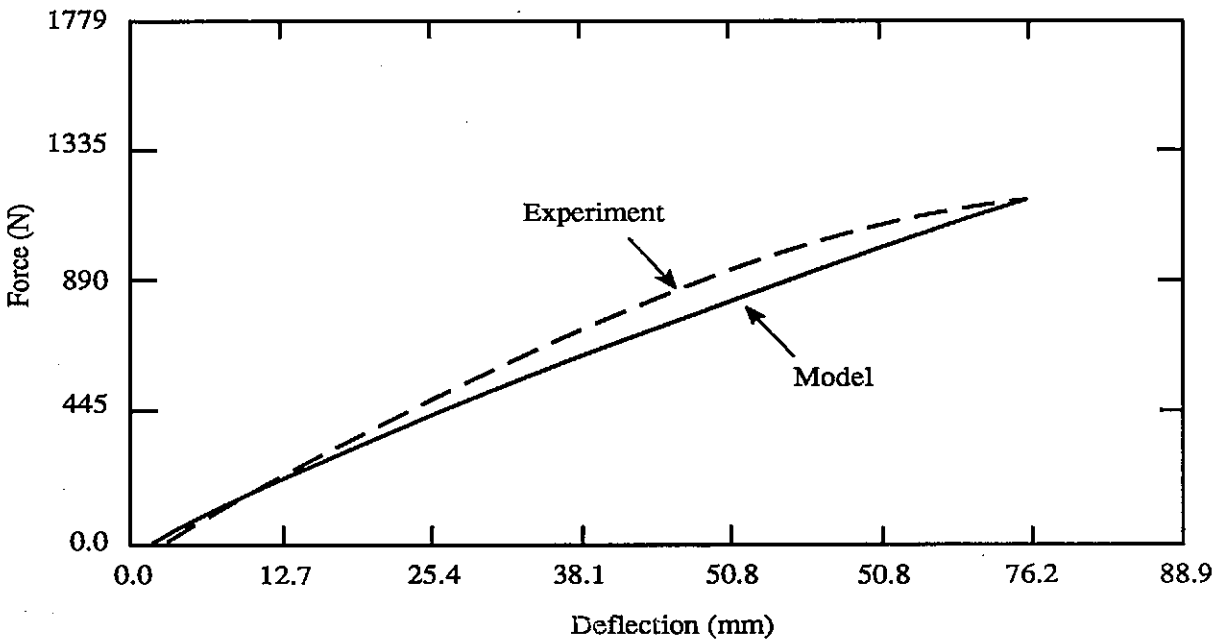

FIGURE 3–7. Comparison of F-δ quasi-static loading results for FEM simulation and experimental testing of undamped three-rib model.

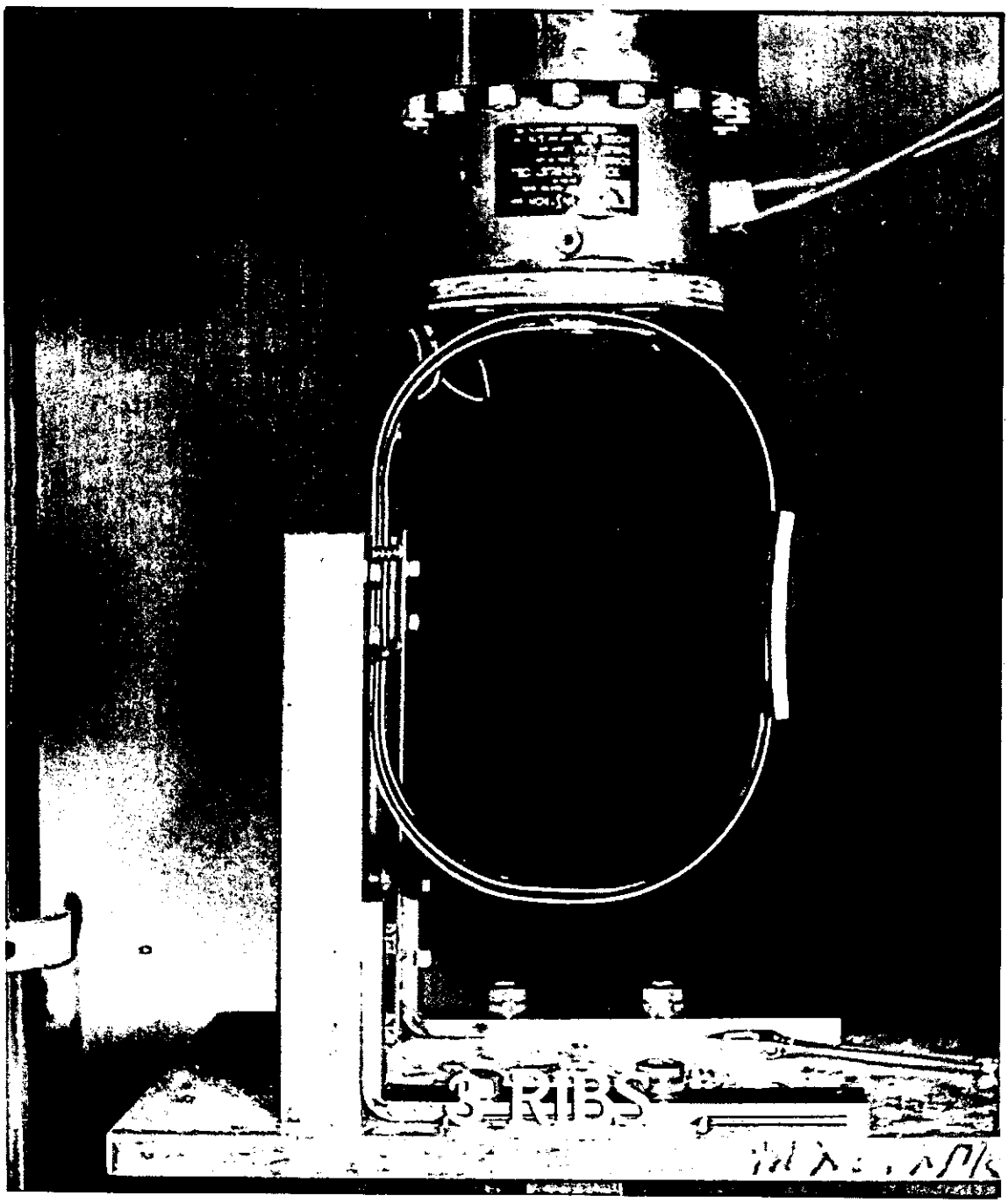

FIGURE 3–8a. Test setup for quasi-static lateral loading of undamped ribs—preload condition.

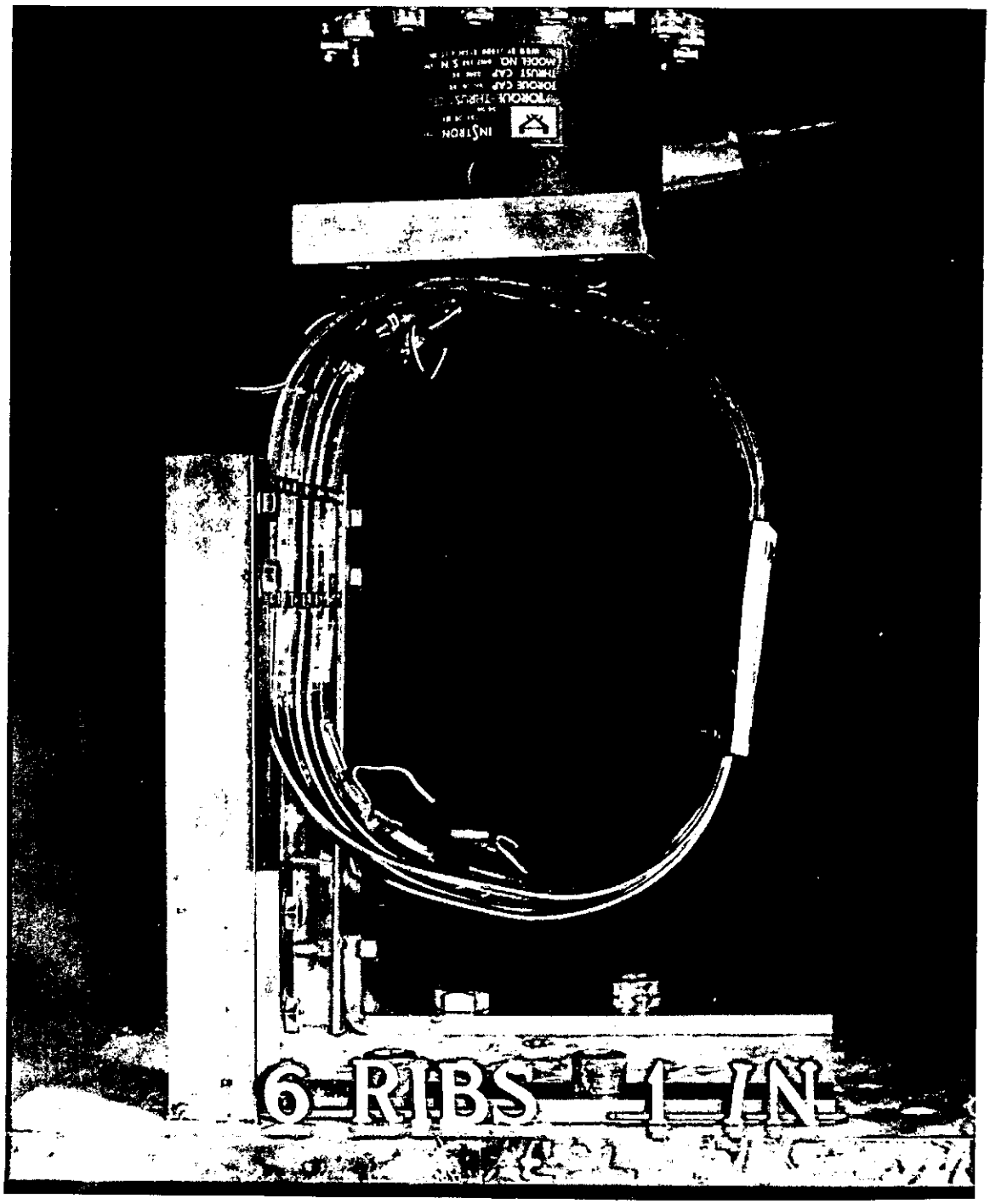

FIGURE 3–8b. Test setup for quasi-static lateral loading of undamped ribs—partially loaded condition.

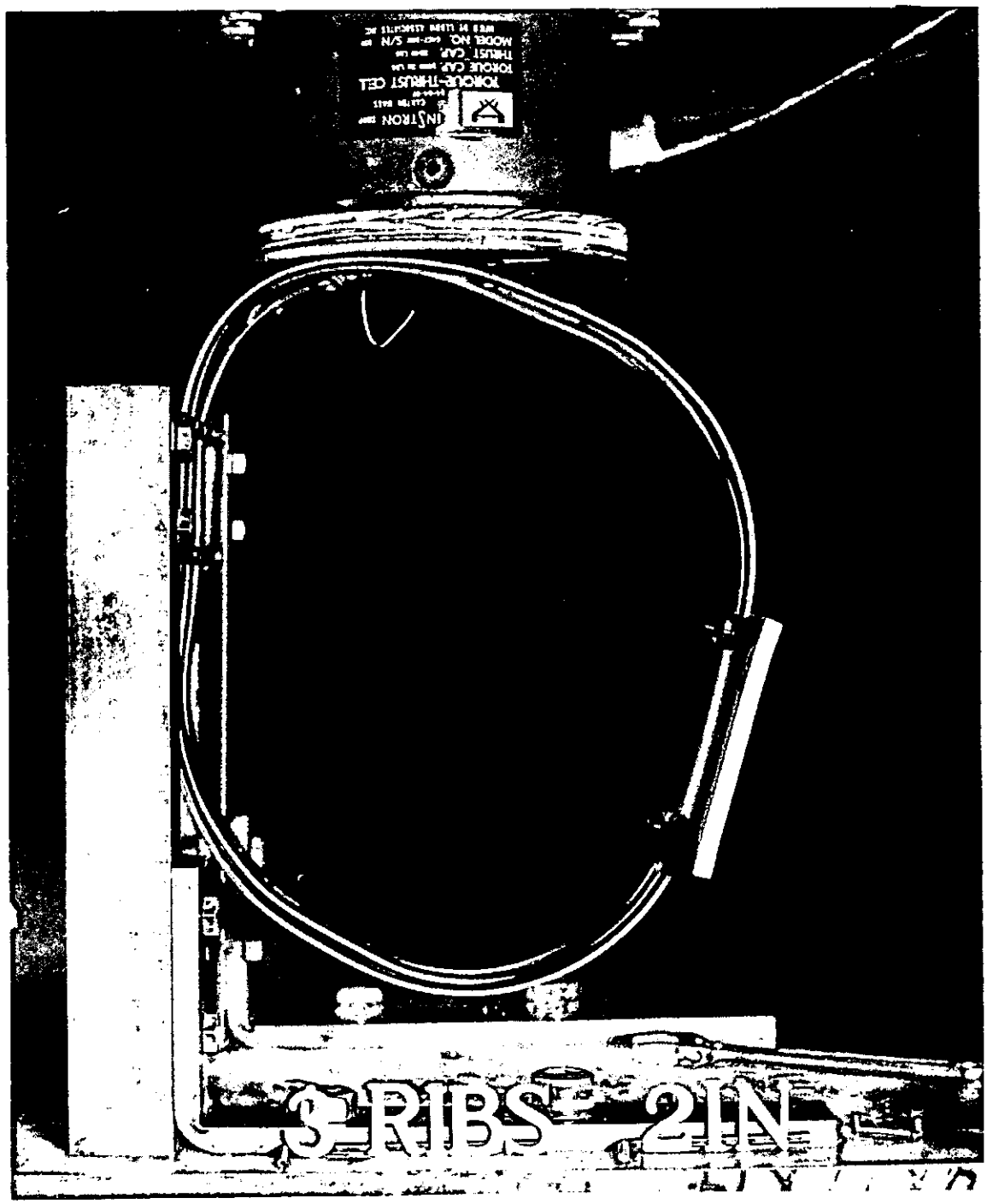

FIGURE 3–8c. Test setup for quasi-static lateral loading of undamped ribs—peak loaded condition.

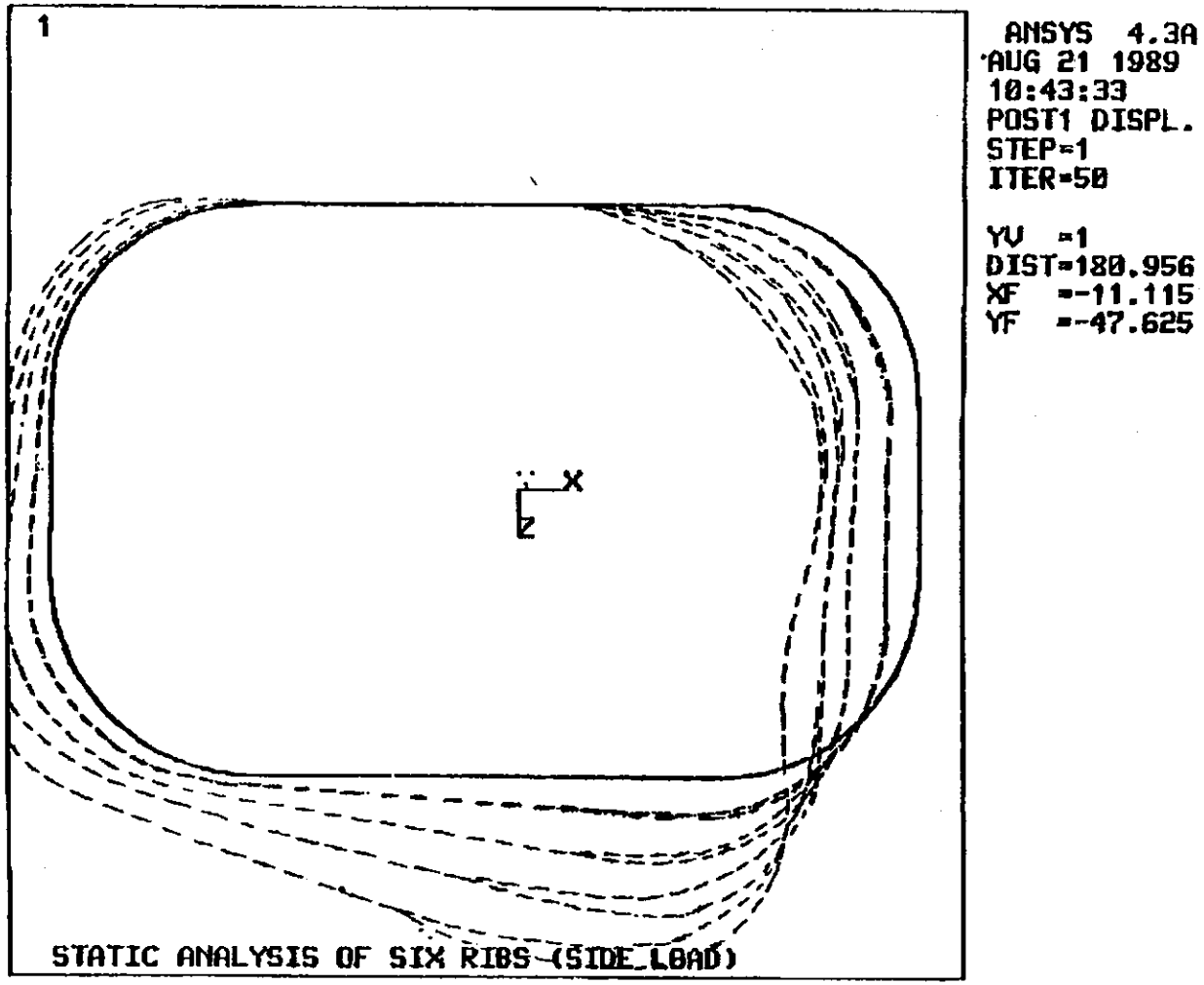

FIGURE 3–9. FEM model simulation of lateral loading of undamped ribs.

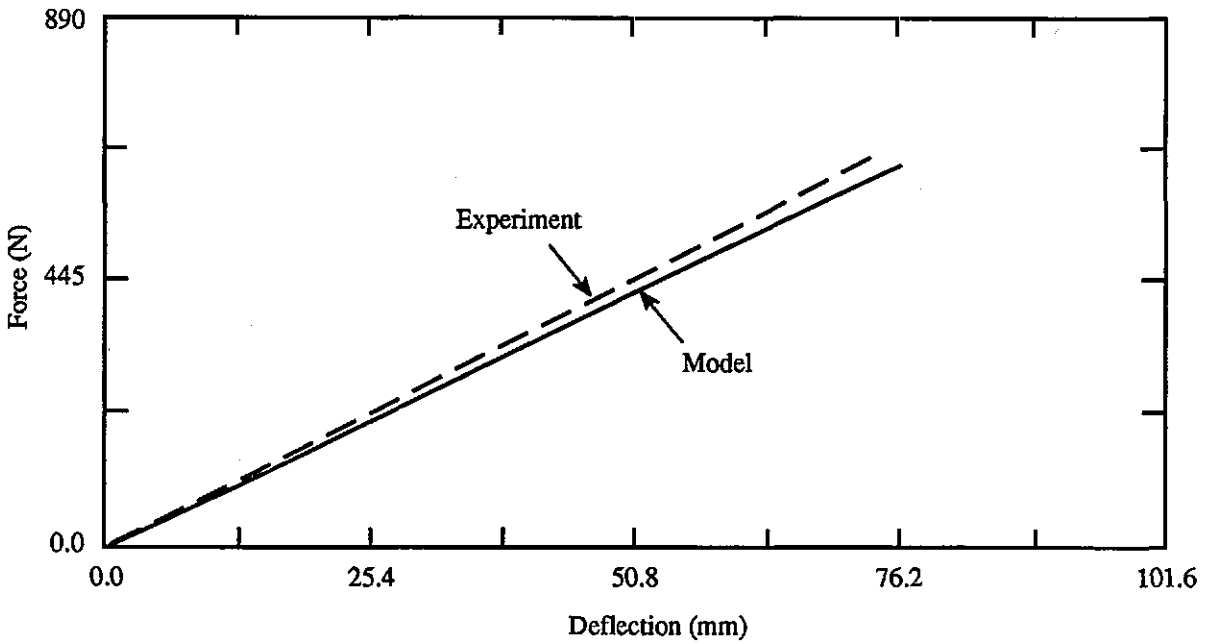

FIGURE 3–10. Comparison of FEM model and experimental F-δ for AP loading of a single damped rib. Steel thickness=2.03 mm (0.08 in), damping material thickness=16 mm (0.625 in).

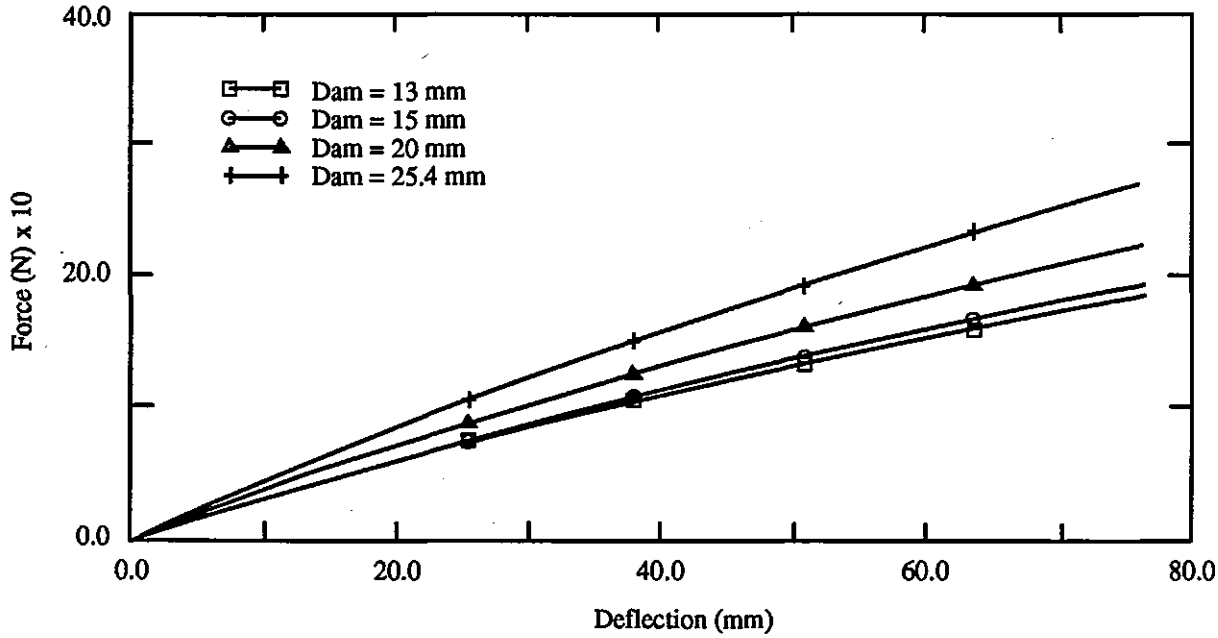

FIGURE 3–11a. Comparison of FEM model prediction for quasi-static F-δ properties of a single damped rib with different thicknesses of damping material. Steel thickness=1.27 mm (0.05 in).

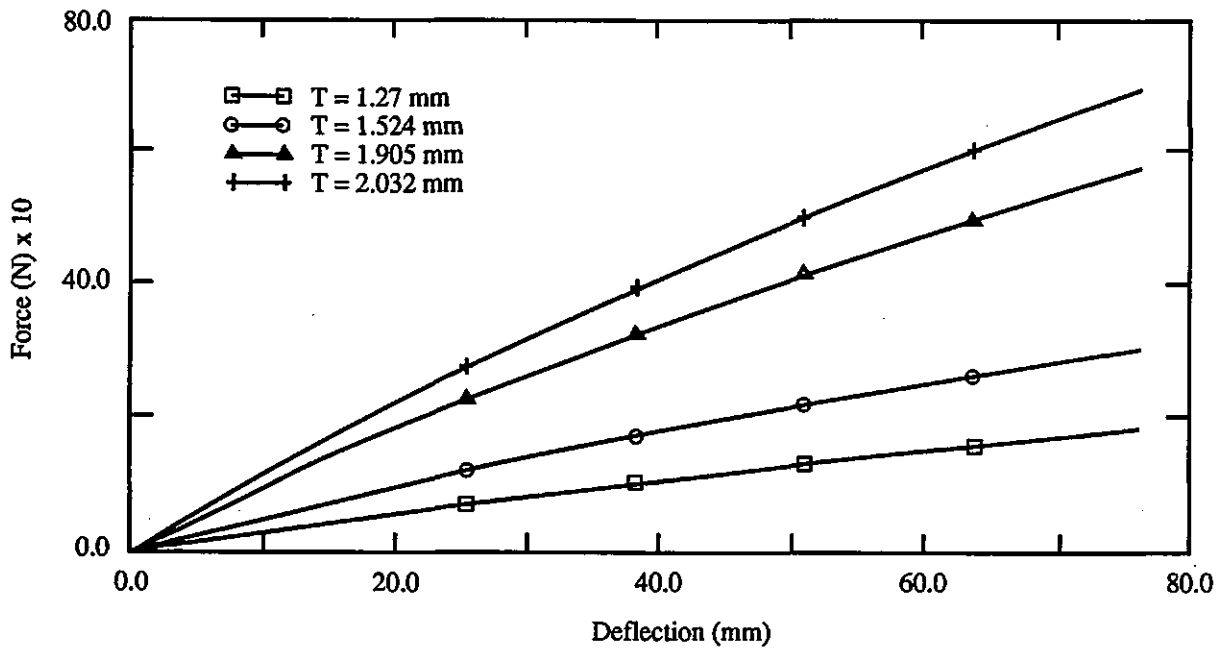

FIGURE 3–11b. Comparison of FEM model prediction for quasi-static F-δ properties of a single damped rib with different thicknesses of steel. Damping material thickness=13 mm (0.5 in).

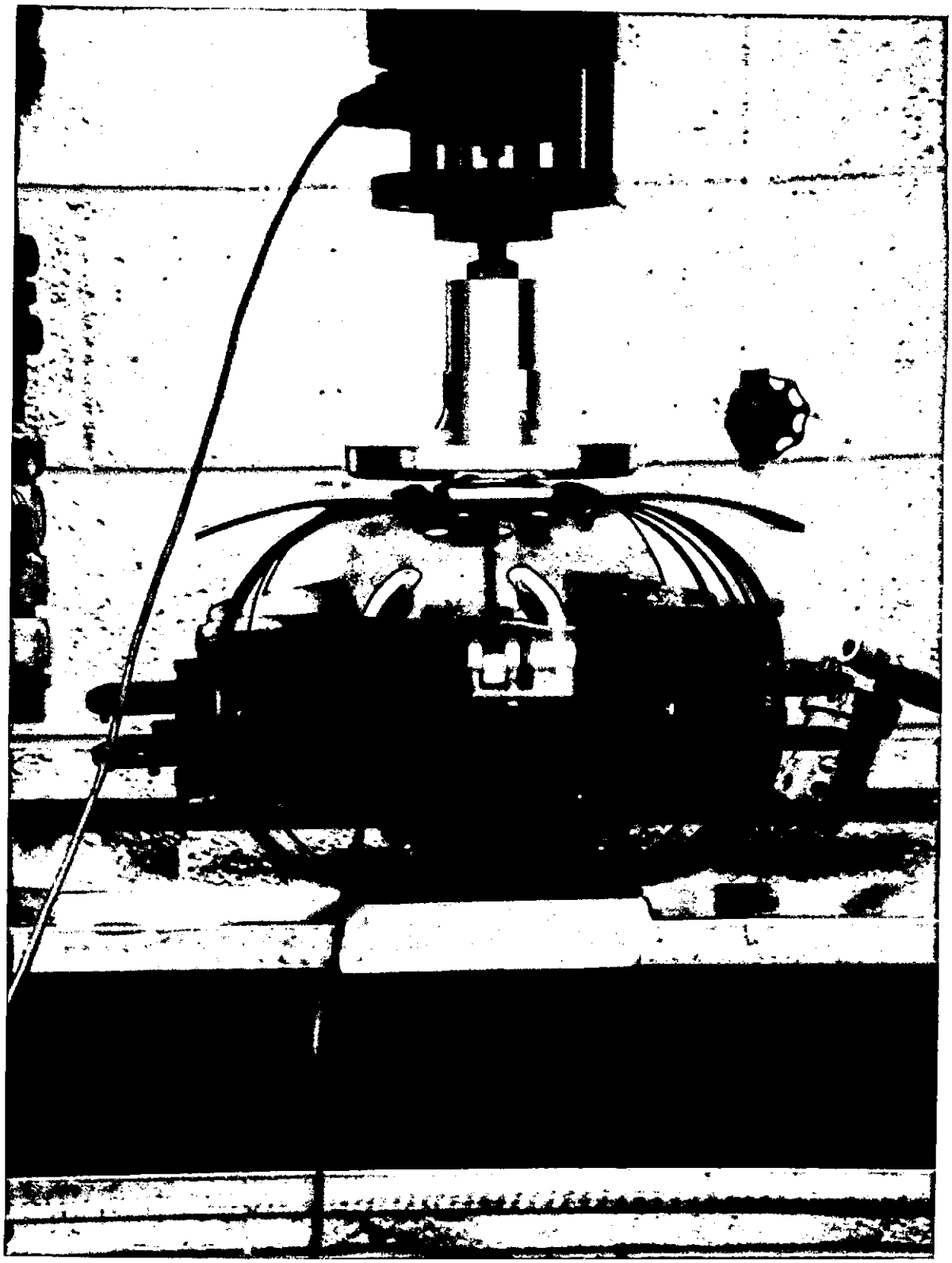

FIGURE 3–12a. Instron testing of undamped thin-steel Hybrid III ribcage—preload condition.

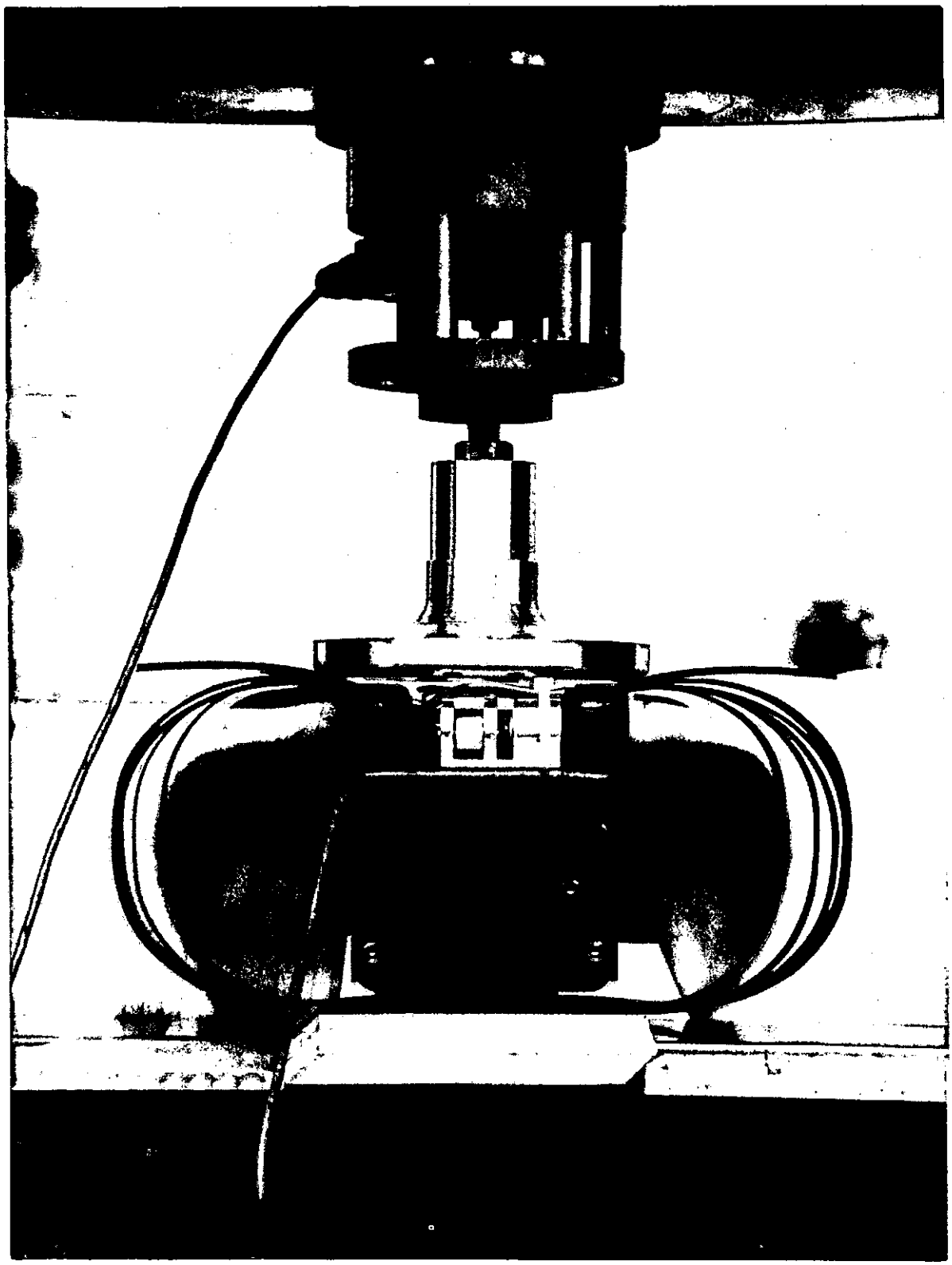

FIGURE 3–12b. Instron testing of undamped thin-steel Hybrid III ribcage loaded to 25 mm (1 in) of AP deflection.

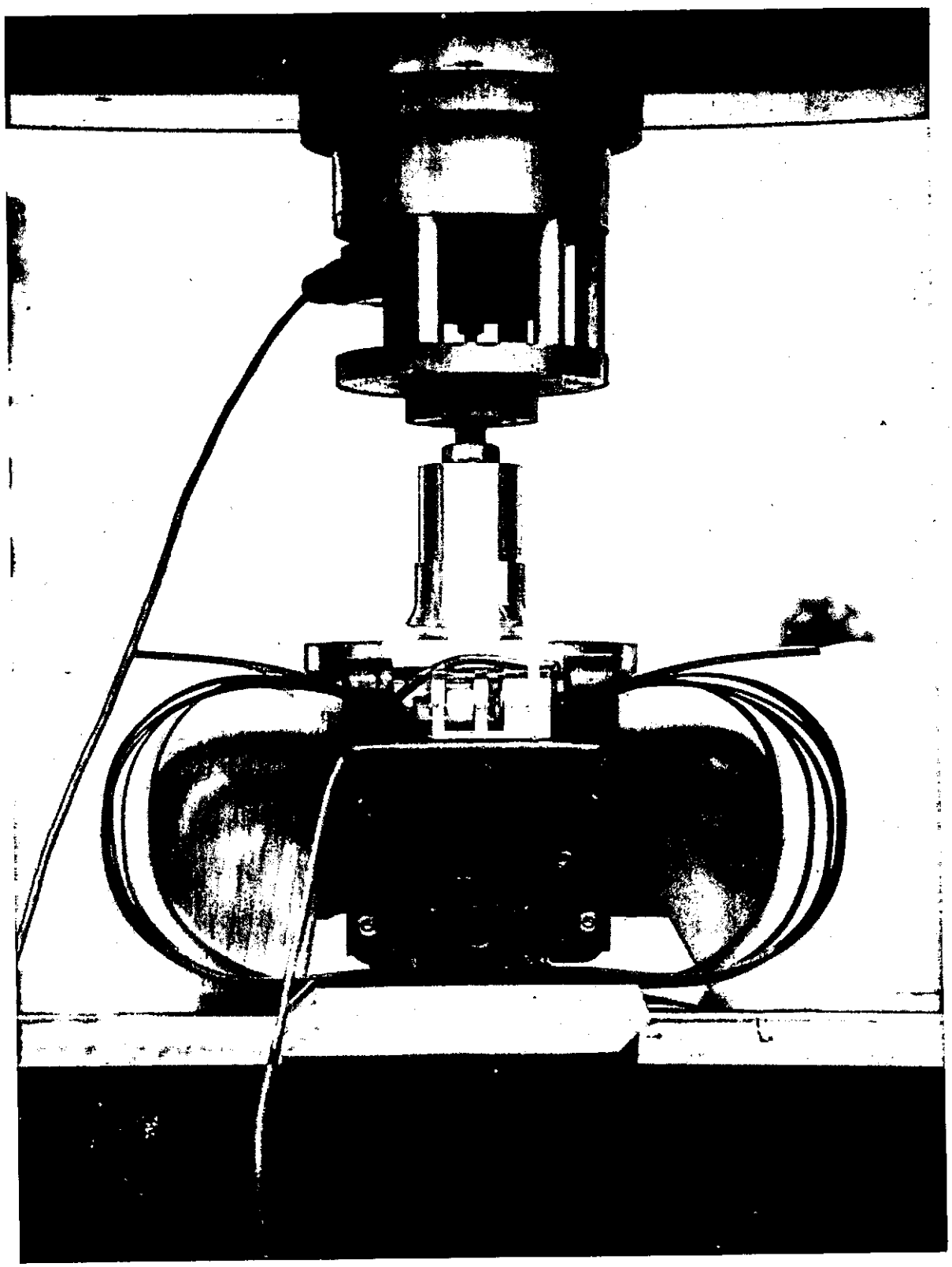

FIGURE 3–12c. Instron testing of undamped thin-steel Hybrid III ribcage loaded to 50 mm (2 in) of AP deflection.

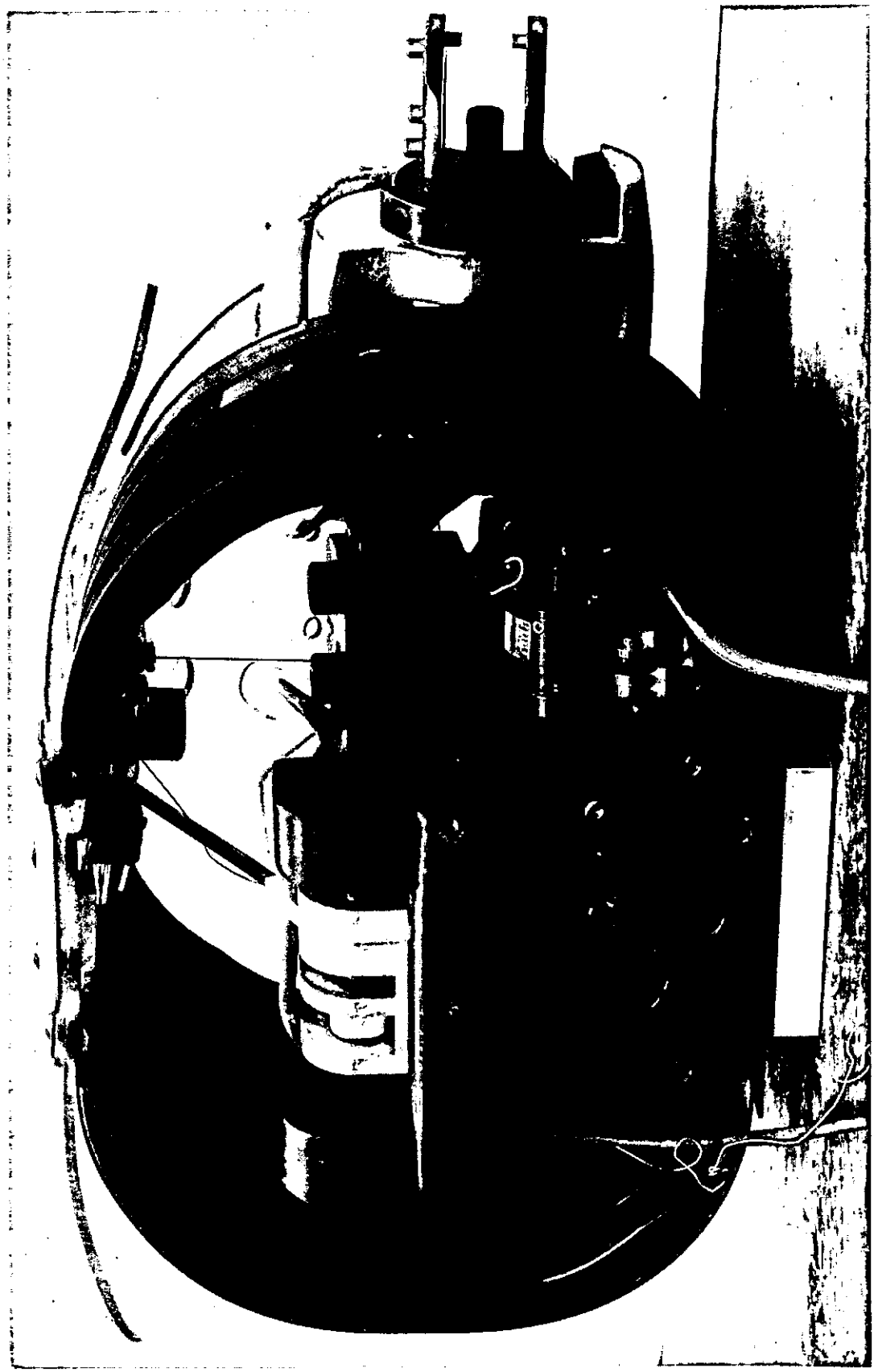

FIGURE 3–13. Thin-steel Hybrid III ribcage with damping material in place and string potentiometer from spine to end of third rib.

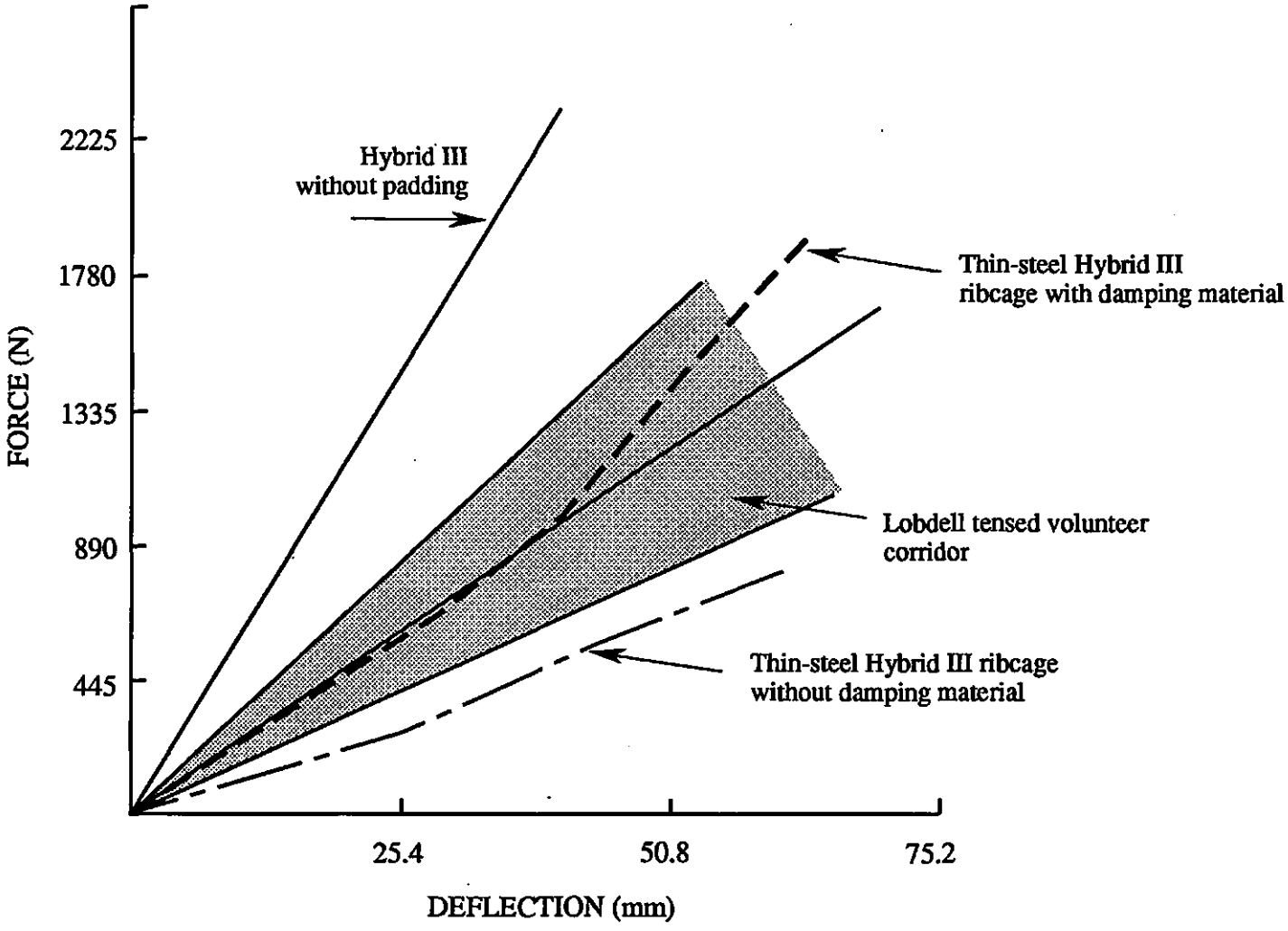

FIGURE 3–14. Comparison of quasi-static stiffness results for AP loading of damped and undamped thin-steel ribcage with tensed volunteer corridor from Lobdell et al. (1973) and quadratic stiffness curve by Melvin et al. (1988a).

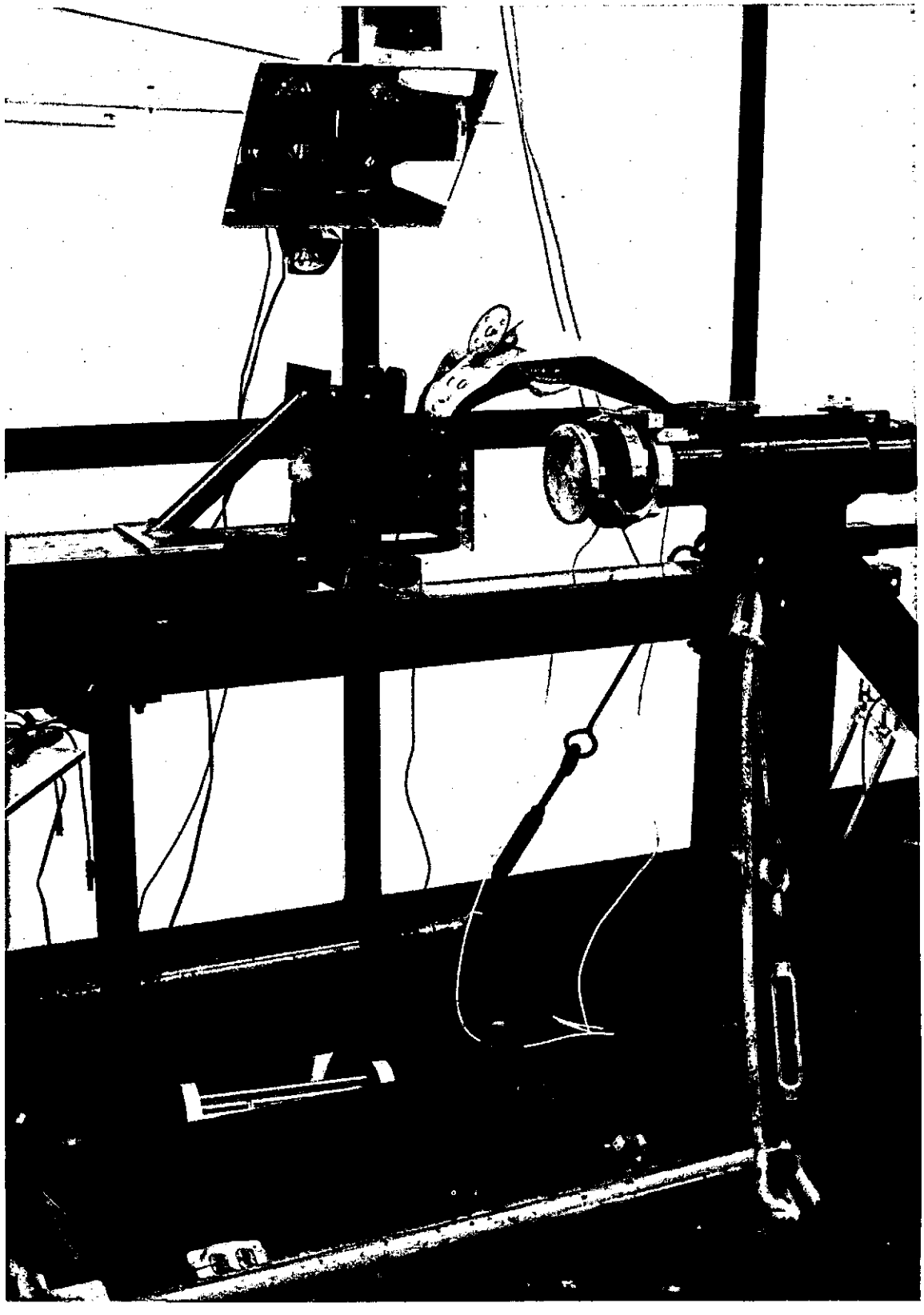

FIGURE 3–15. Impact testing of thin-steel Hybrid III ribcage on UMTRI pendulum facility.

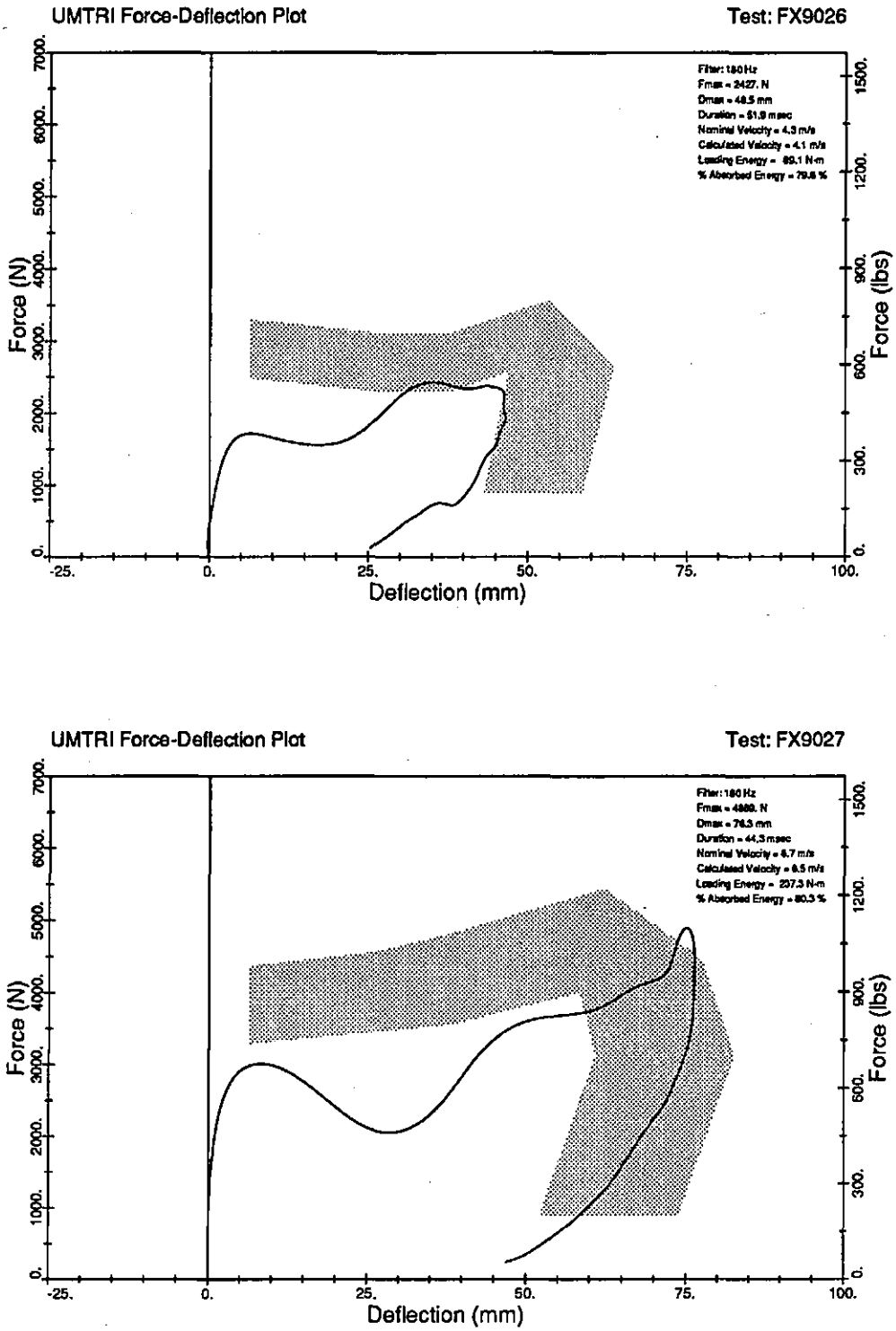

FIGURE 3–16. Force-deflection plots for nominal 4.3-m/s (top) and 6.7-m/s (bottom) impacts of restrained-spine, thin-steel (1.4-mm) Hybrid III ribcage with *25-mm-thick Ensolite pad in front of sternum*. Impactor mass=13.6 kg (30 lb).

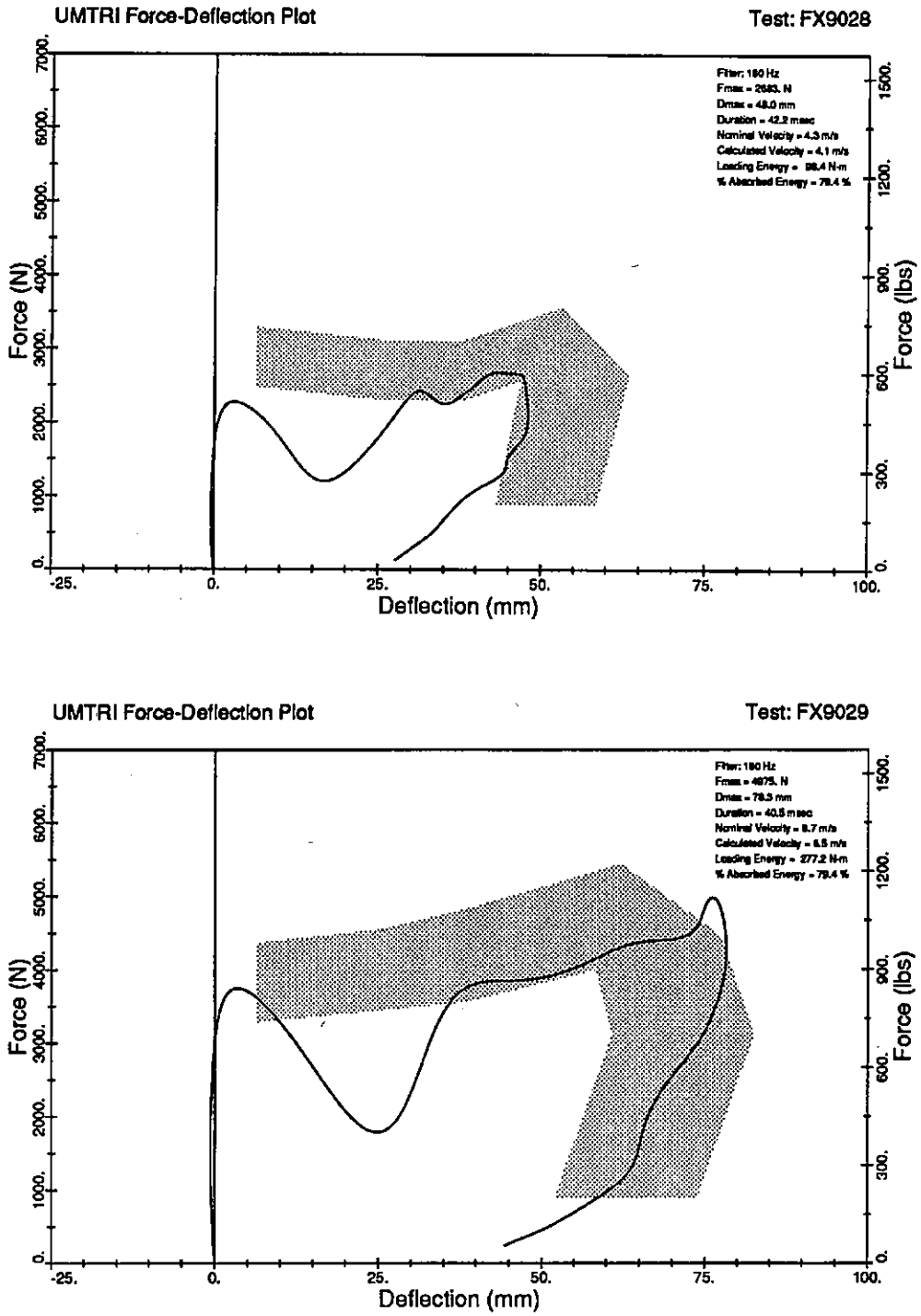

FIGURE 3–17. Force-deflection plots for nominal 4.3-m/s (top) and 6.7-m/s (bottom) impacts of restrained-spine, thin-steel (1.4-mm) Hybrid III ribcage with *thin (6-mm-thick) pad in front of sternum*. Impactor mass=13.6 kg (30 lb).

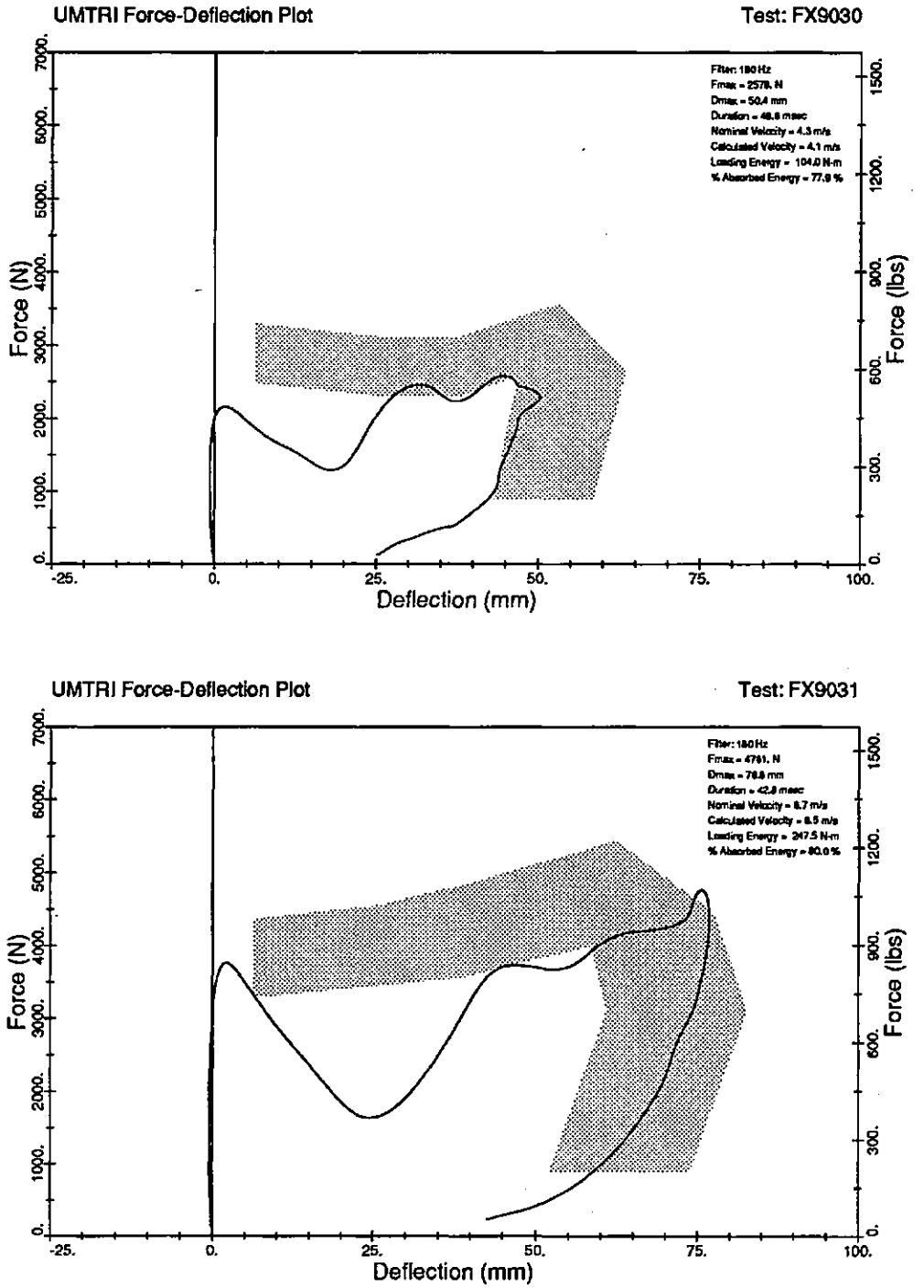

FIGURE 3–18a. Force-deflection plots for nominal 4.3-m/s (top) and 6.7-m/s (bottom) impacts of restrained-spine, thin-steel (1.4-mm) Hybrid III ribcage with *thin (6-mm-thick) pad and 0.45-kg (1-lb) mass in front of sternum.* Impactor mass=13.6 kg (30 lb).

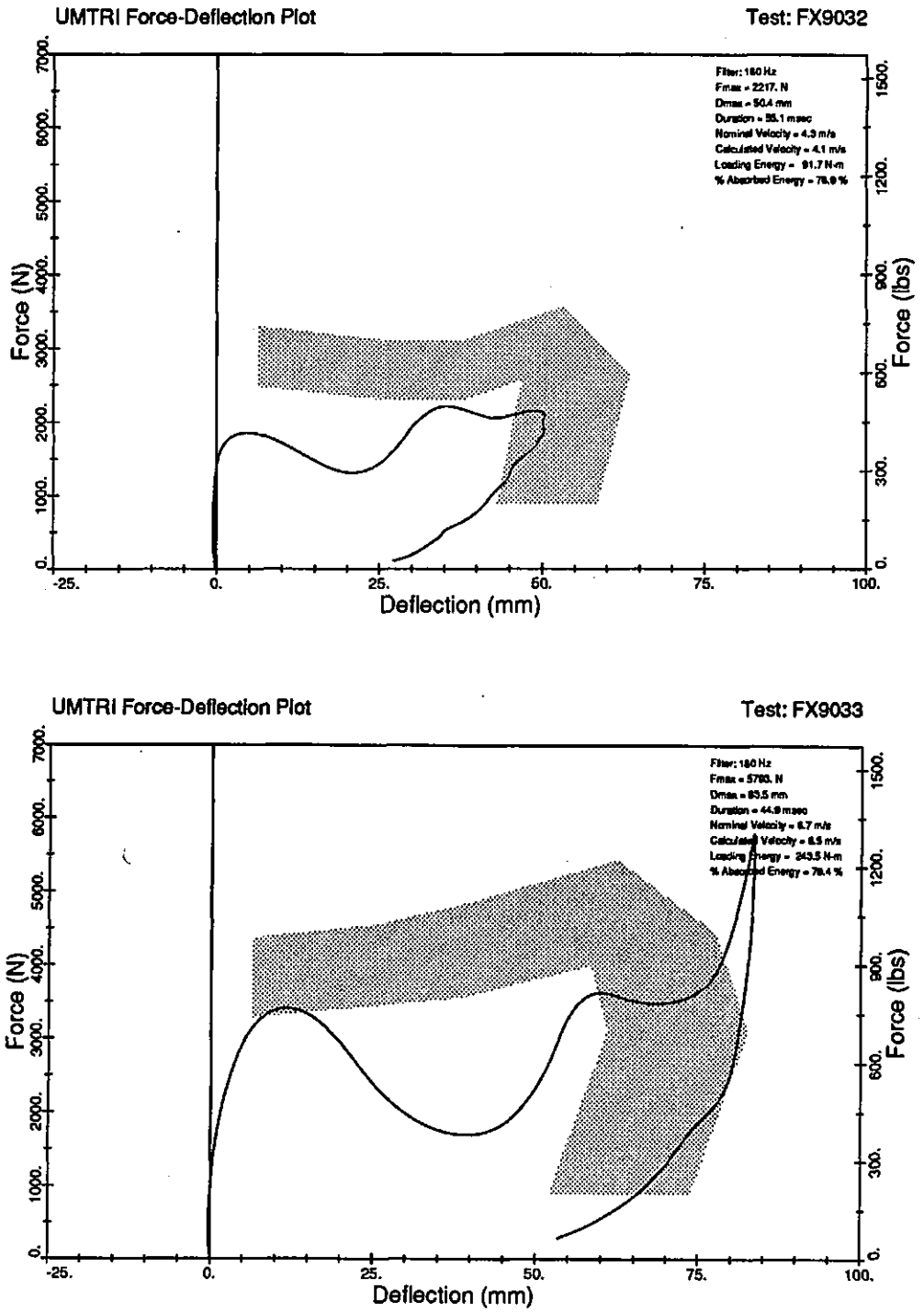

FIGURE 3–18b. Force-deflection plots for 4.3-m/s (top) and 6.7-m/s (bottom) impacts of restrained-spine, thin-steel (1.4-mm) Hybrid III ribcage with *25-mm-thick Ensolite pad and 0.45-kg (1-lb) mass in front of sternum*. Impactor mass=13.6 kg (30 lb).

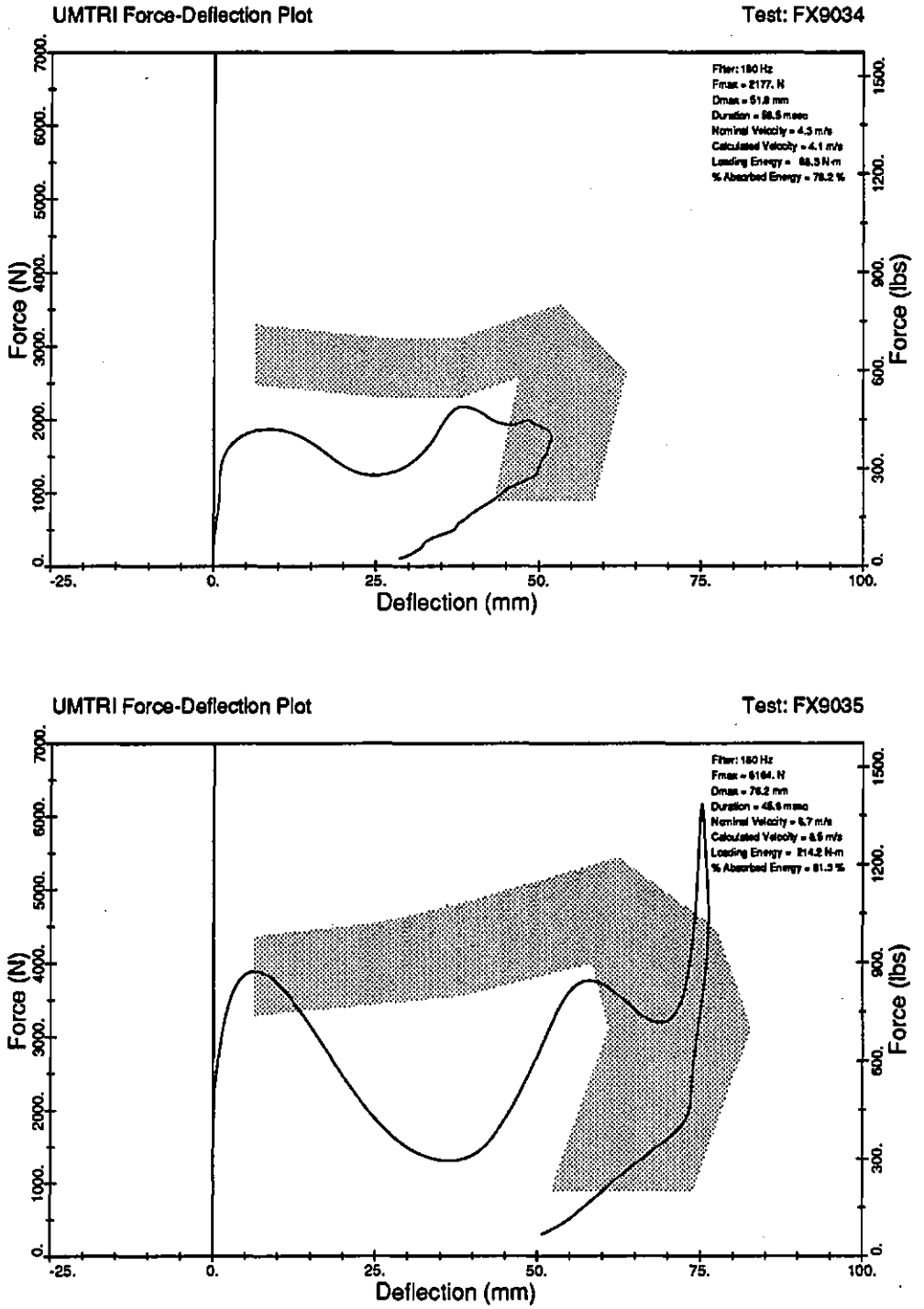

FIGURE 3–18c. Force-deflection plots for nominal 4.3-m/s (top) and 6.7-m/s (bottom) impacts of restrained-spine, thin-steel (1.4-mm) Hybrid III ribcage with *25-mm-thick Ensolite pad and 0.9-kg (2-lb) mass in front of sternum*. Impactor mass=13.6 kg (30 lb).

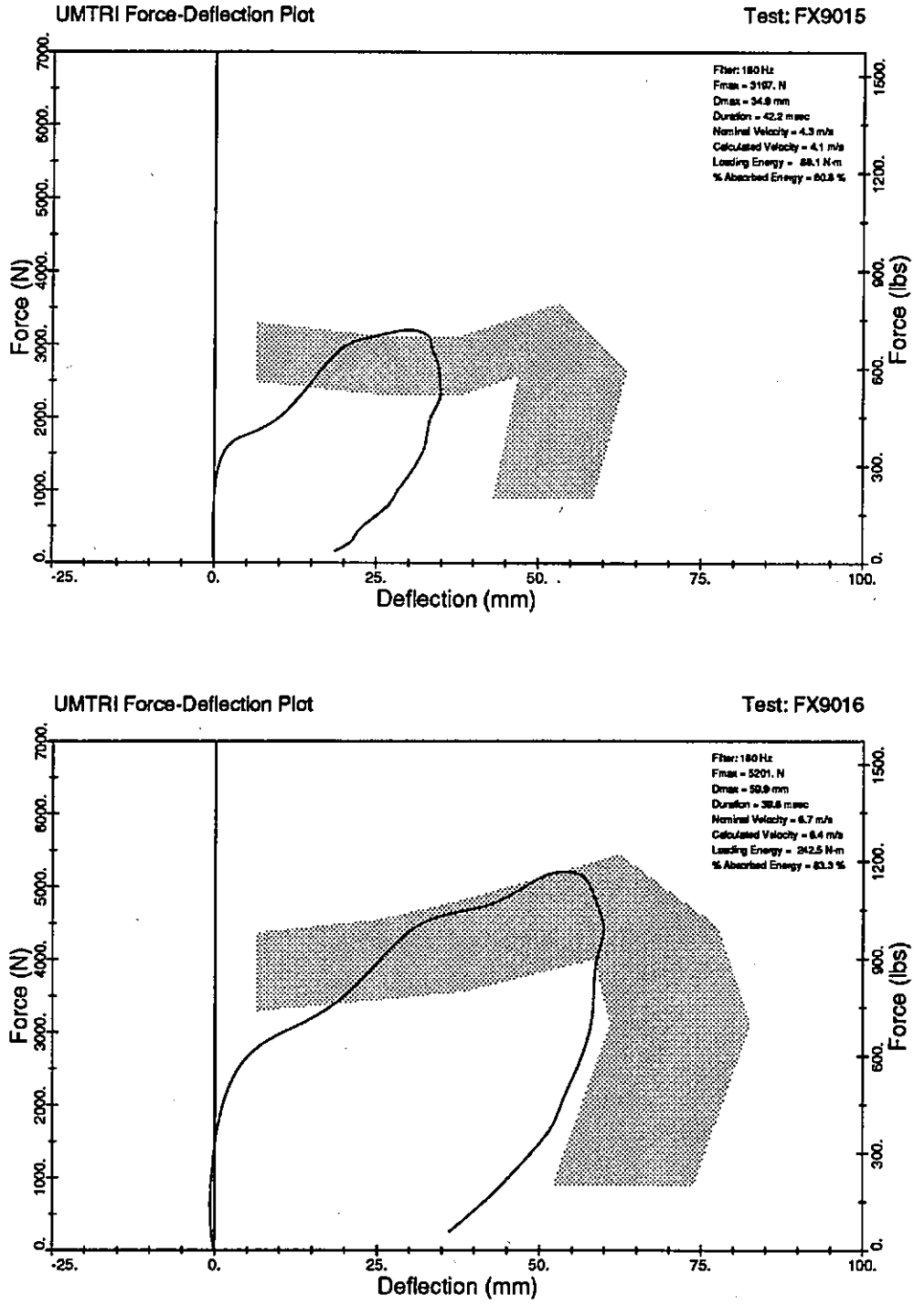

FIGURE 3–19a. Force-deflection plots for nominal 4.3-m/s (top) and 6.7-m/s (bottom) impacts of restrained-spine, thin-steel (1.4-mm) Hybrid III ribcage with 25-mm-thick Ensolite pad in front of sternum and *full support for ribs at spine*. Impactor mass=13.6 kg (30 lb).

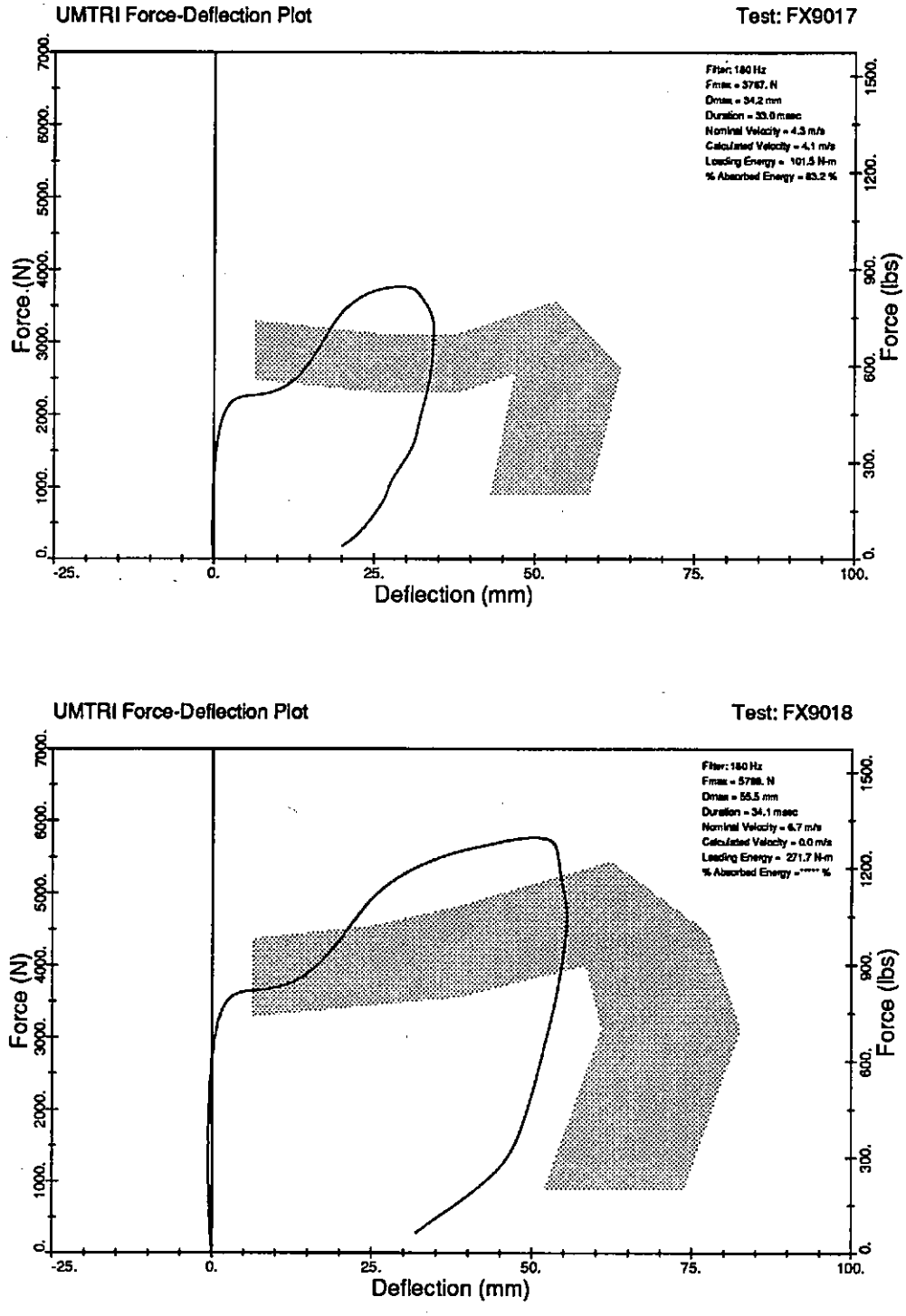

FIGURE 3–19b. Force-deflection plots for nominal 4.3-m/s (top) and 6.7-m/s (bottom) impacts of restrained-spine, thin-steel (1.4-mm) Hybrid III ribcage with thin (6-mm-thick) pad in front of sternum and *full support for ribs at spine*. Impactor mass=13.6 kg (30 lb).

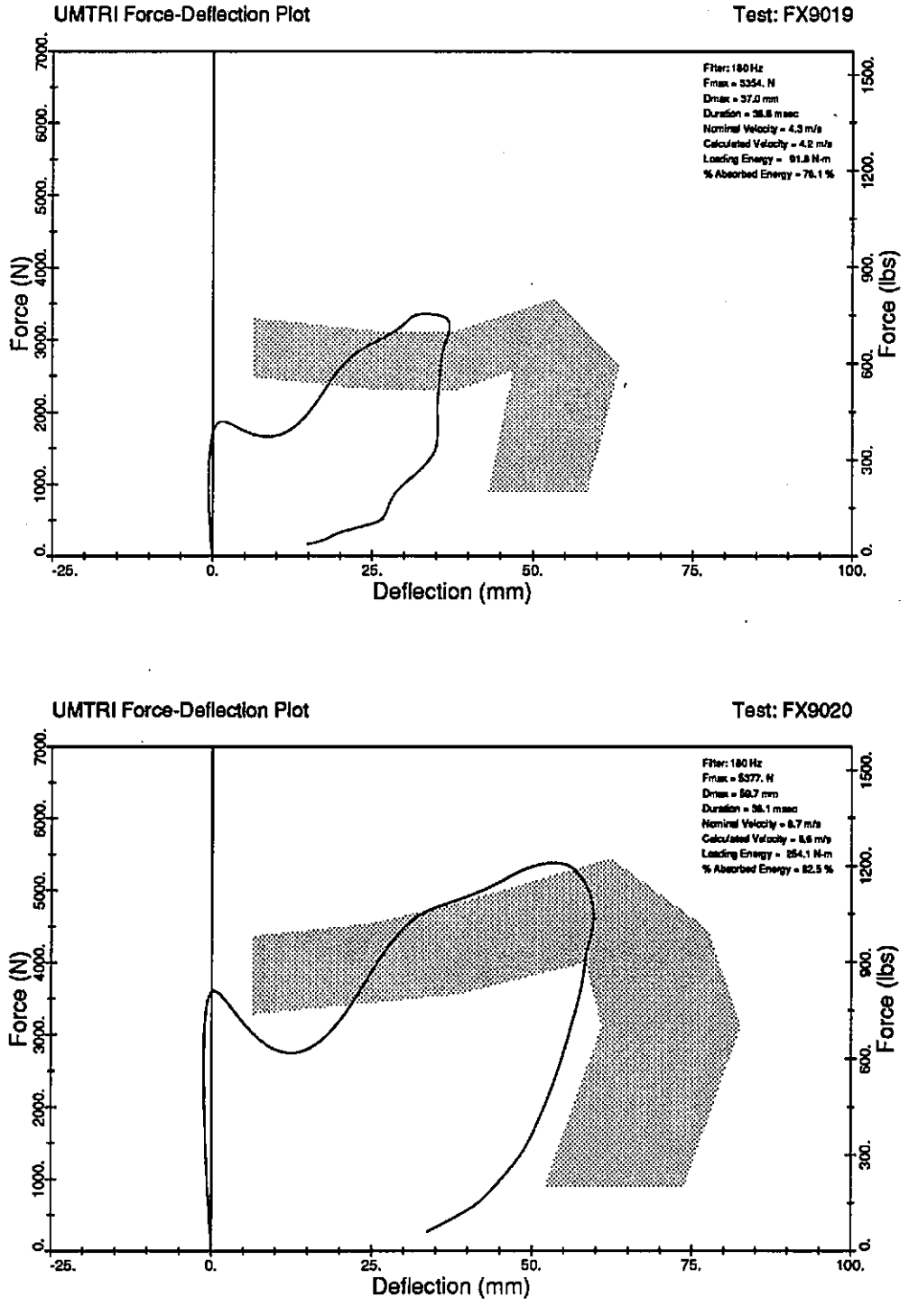

FIGURE 3–19c. Force-deflection plots for nominal 4.3-m/s (top) and 6.7-m/s (bottom) impacts of restrained-spine, thin-steel (1.4-mm) Hybrid III ribcage with thin (6-mm-thick) pad and 0.45-kg (1-lb) mass in front of sternum and *full support for ribs at spine*. Impactor mass=13.6 kg (30 lb).

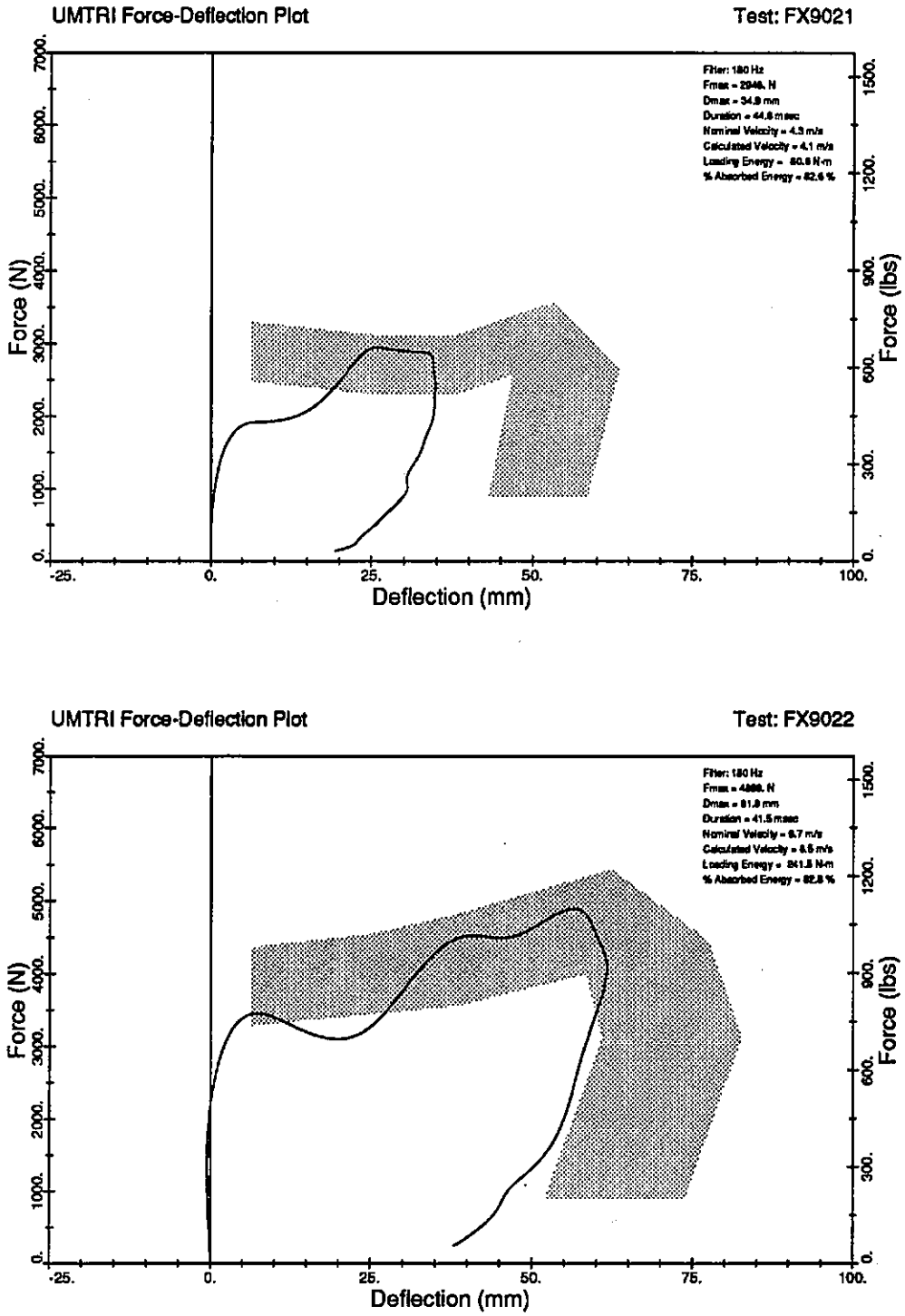

FIGURE 3–19d. Force-deflection plots for nominal 4.3-m/s (top) and 6.7-m/s (bottom) impacts of restrained-spine, thin-steel (1.4-mm) Hybrid III ribcage with 25-mm-thick Ensolite pad and 0.45-kg (1-lb) mass in front of sternum and *full support for ribs at spine*. Impactor mass=13.6 kg (30 lb).

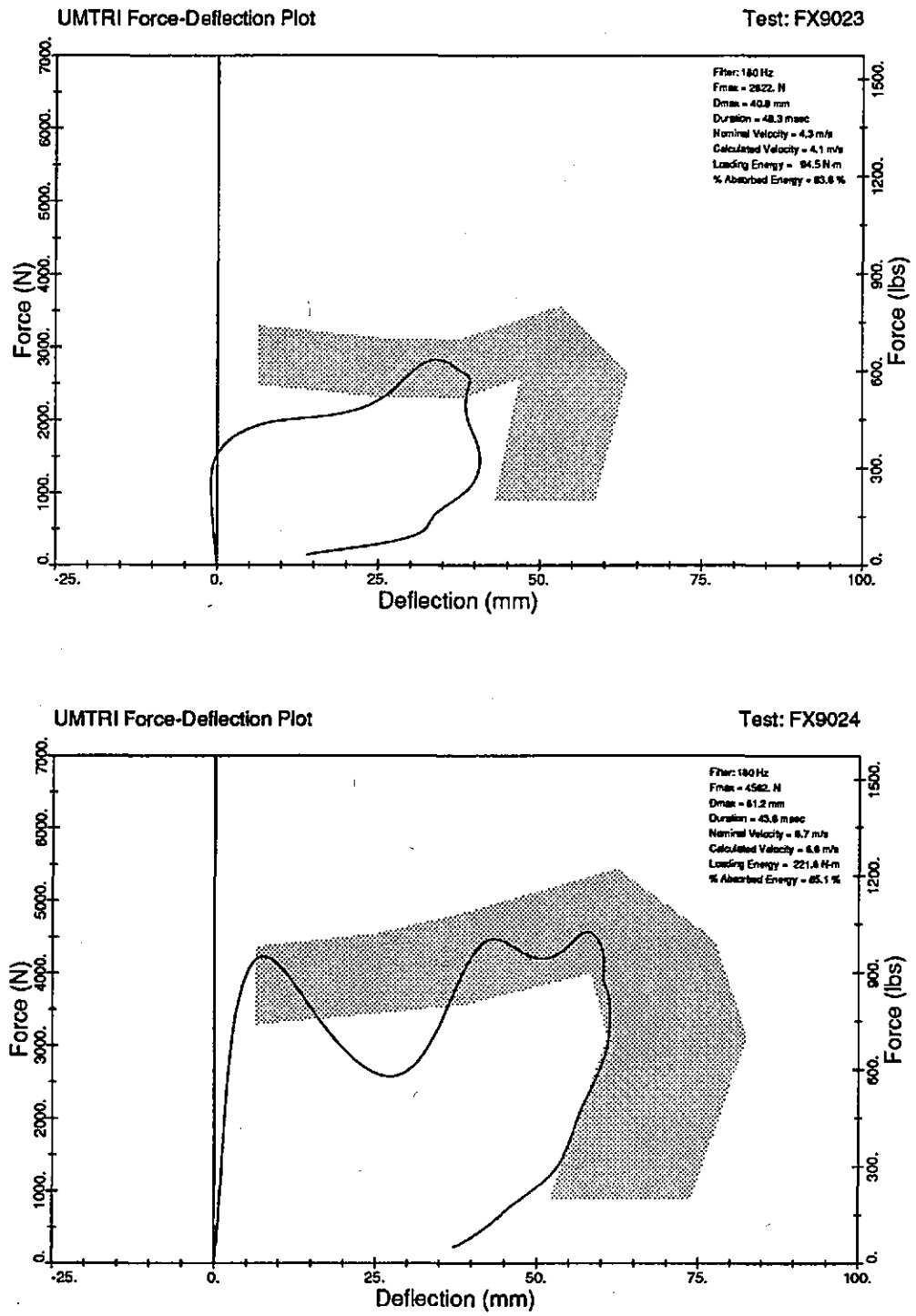

FIGURE 3–19e. Force-deflection plots for nominal 4.3-m/s (top) and 6.7-m/s (bottom) impacts of restrained-spine, thin-steel (1.4-mm) Hybrid III ribcage with 25-mm-thick Ensolite pad and 0.9-kg (2-lb) mass in front of sternum and *full support for ribs at spine*. Impactor mass=13.6 kg (30 lb).

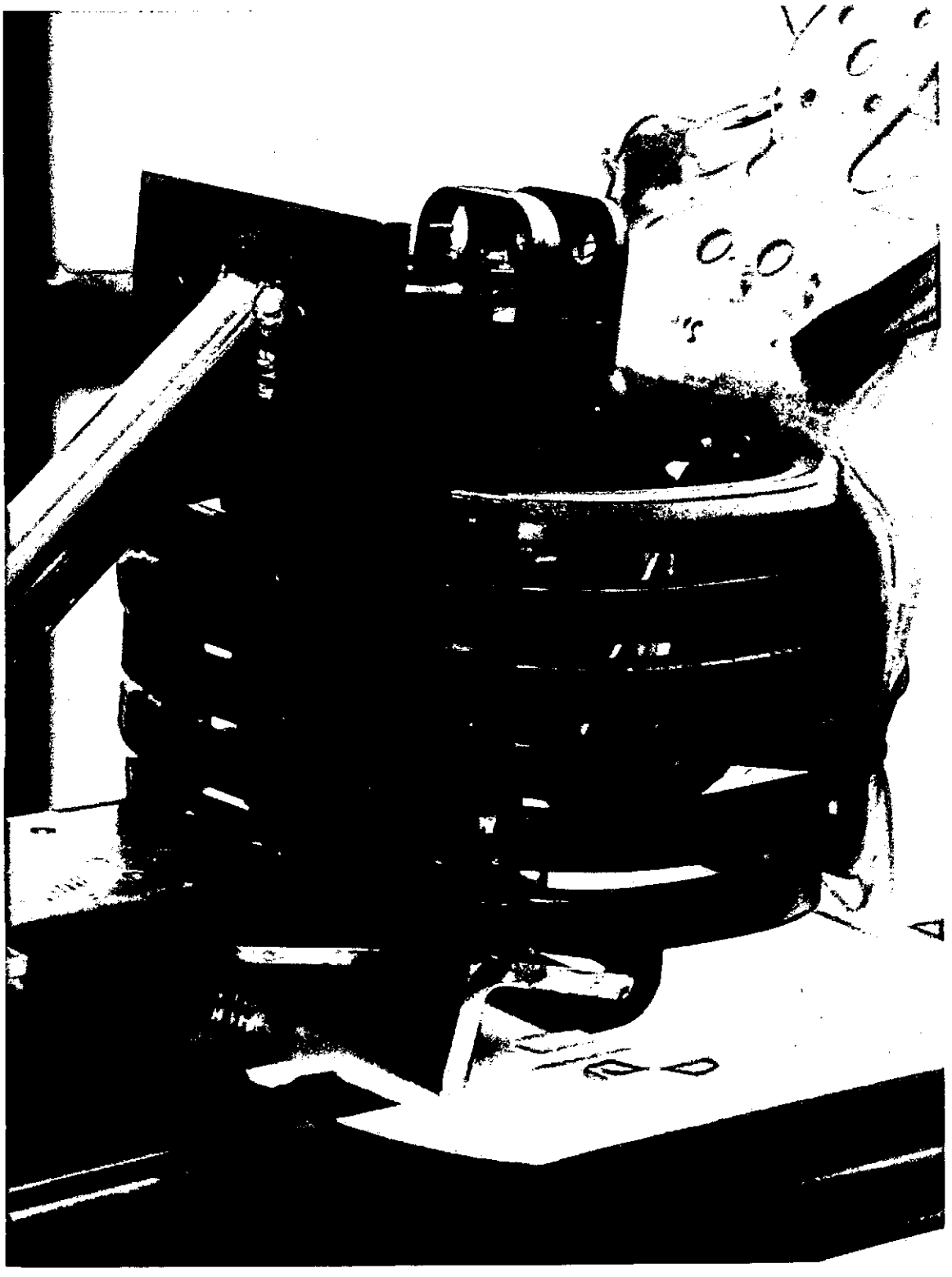

FIGURE 3–20. Setup for impact testing of thin-steel Hybrid III ribcage with 10-mm (0.40-in) thick damping material bonded to outsides of ribs across the back of the spine.

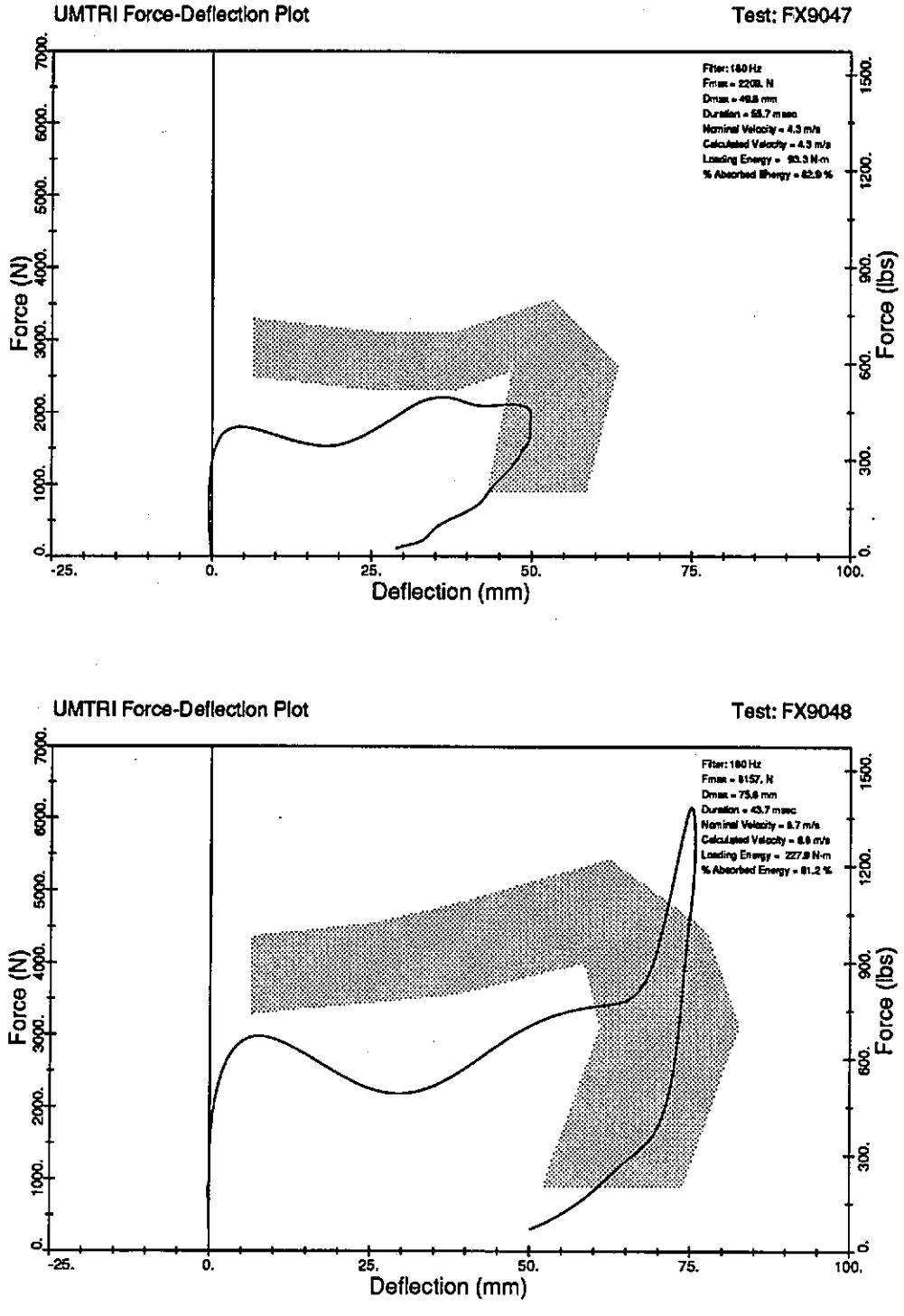

FIGURE 3–21a. Force-deflection plots for nominal 4.3-m/s (top) and 6.7-m/s (bottom) impacts of restrained-spine, thin-steel (1.4-mm) Hybrid III ribcage with 25-mm-thick Ensolite pad in front of sternum and extra damping material on ribs at spine in place of rib helpers. Impactor mass=13.6 kg (30 lb).

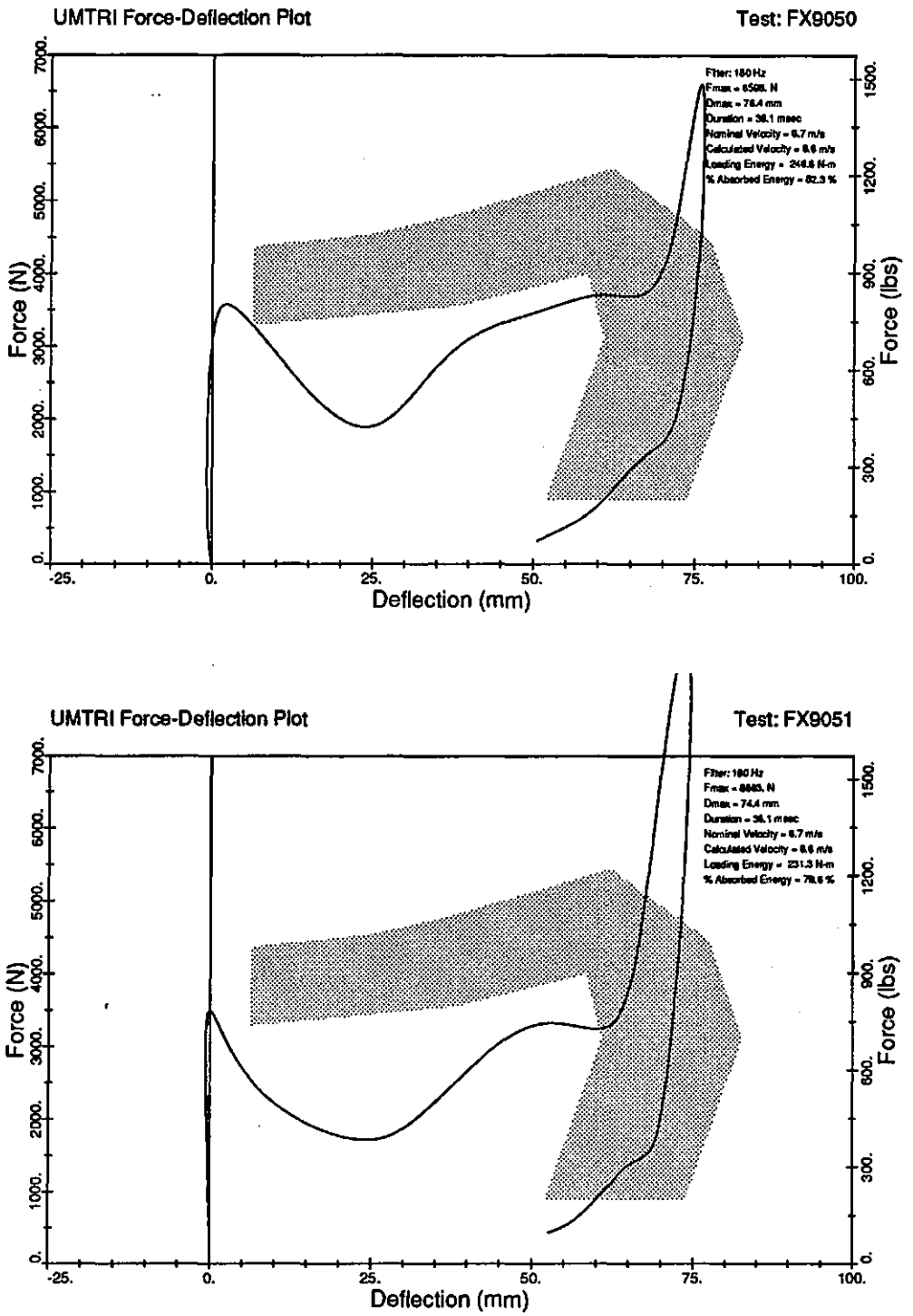

FIGURE 3–21b. Force-deflection plots for nominal 6.7-m/s impacts of restrained-spine, thin-steel (1.4-mm) Hybrid III ribcage with thin (6-mm-thick) pad in front of sternum and extra damping material on ribs at spine in place of rib helpers. Impactor mass=13.6 kg (30 lb). Bottom plot is for 0.45-kg (1-lb) mass added in front of sternum.

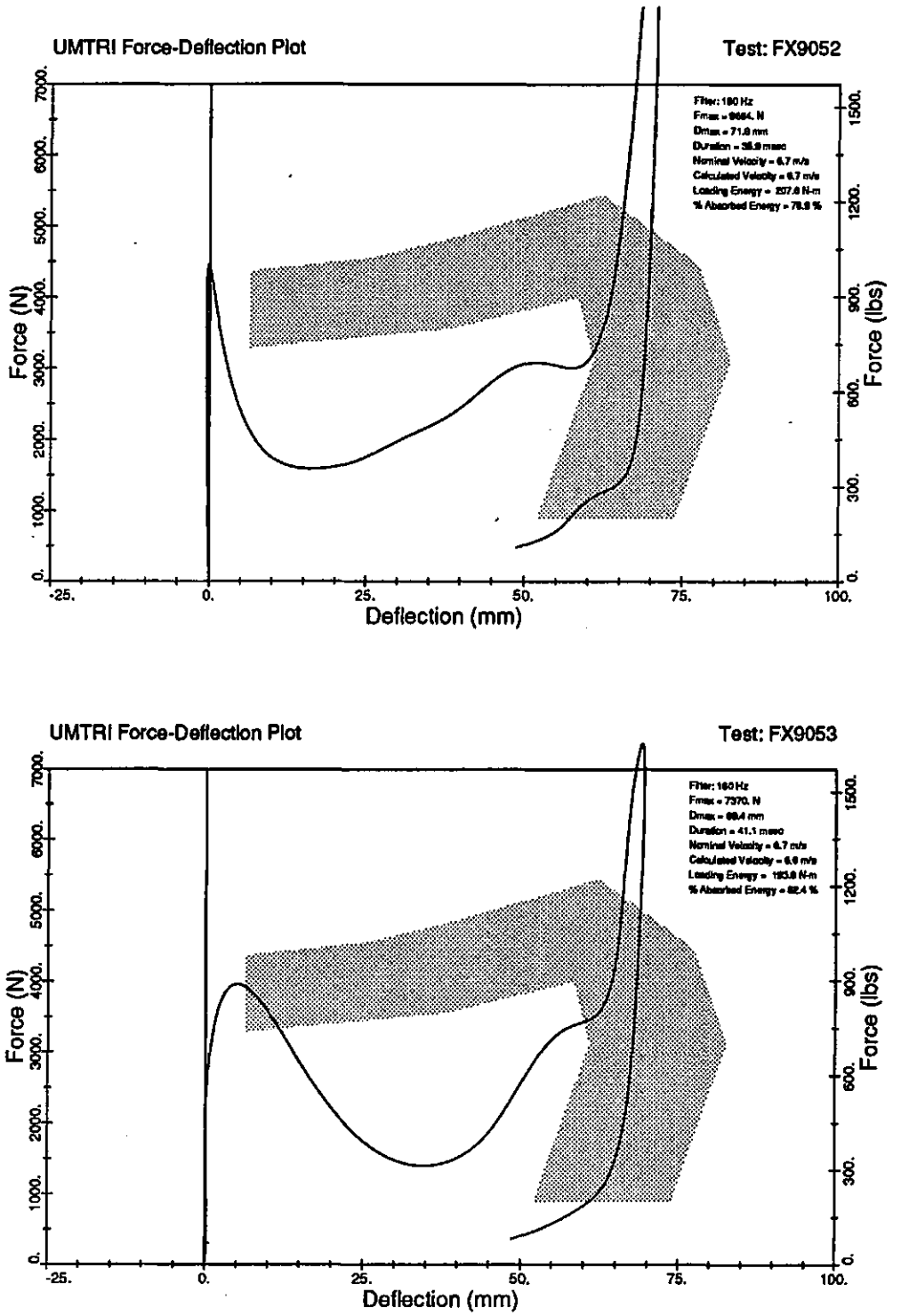

FIGURE 3–21c. Force-deflection plots for nominal 6.7-m/s impacts of restrained-spine, thin-steel (1.4-mm) Hybrid III ribcage with 0.9-kg (2-lb) mass in front of sternum and extra damping material on ribs at spine in place of rib helpers. Impactor mass=13.6 kg (30 lb). Top plot is for thin (6-mm-thick) padding over sternum. Bottom plot is for 25-mm-thick Ensolite pad over sternum.

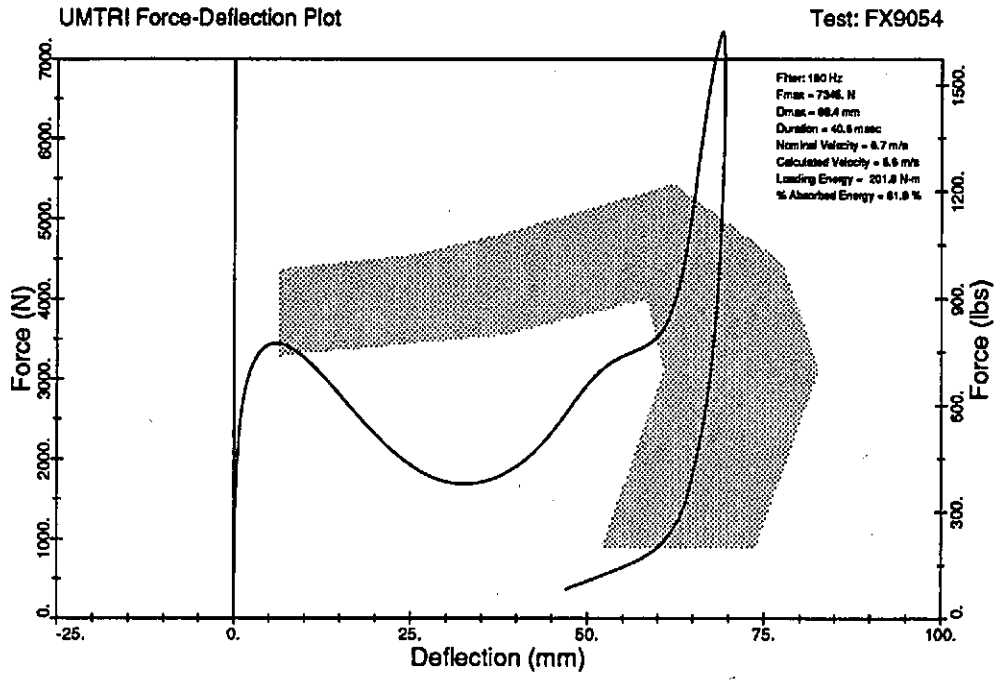

FIGURE 3–21d. Force-deflection plot for nominal 6.7-m/s impact of restrained-spine, thin-steel (1.4-mm) Hybrid III ribcage with 25-mm-thick Ensolite pad and 0.45-kg (1-lb) mass in front of sternum and extra damping material on ribs at spine in place of rib helpers. Impactor mass=13.6 kg (30 lb).

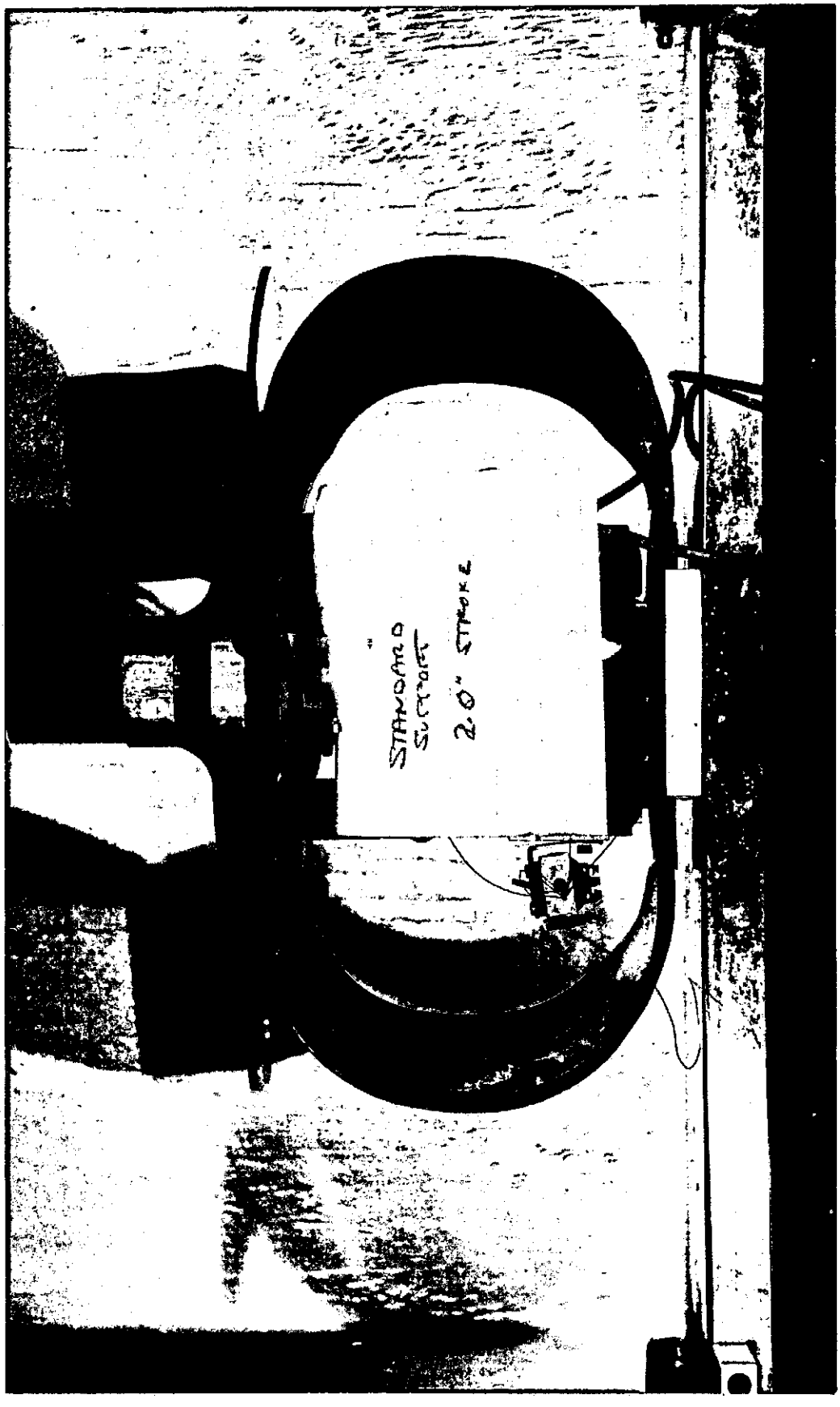

FIGURE 3–22a. Instron testing of damped thin-steel Hybrid III ribcage with *normally-supported ribs* at the spine. Loading is with a 152-mm (6-in) diameter rigid plate.

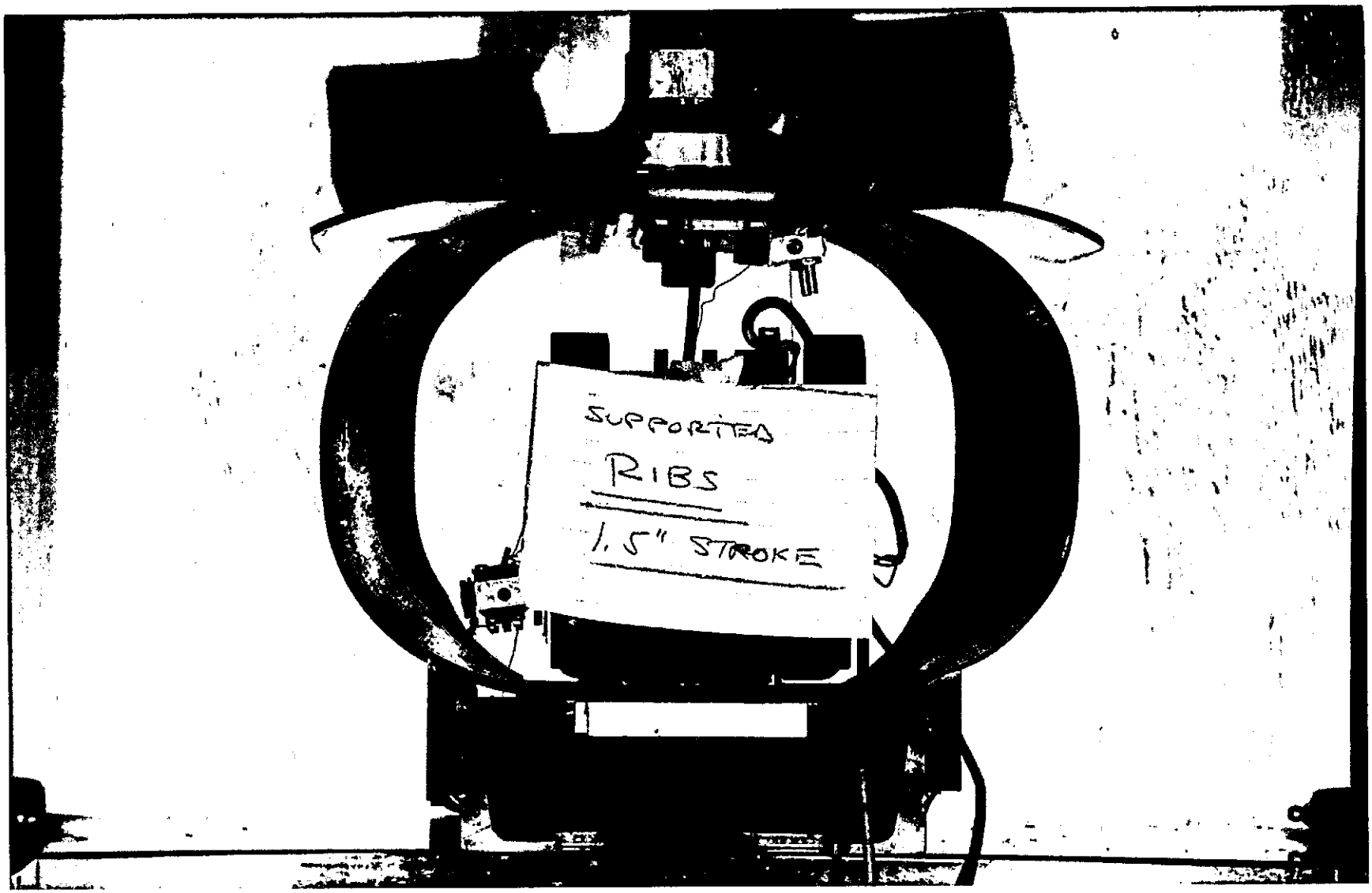

FIGURE 3–22b. Instron testing of damped thin-steel Hybrid III ribcage with *fully-supported ribs* at the spine.

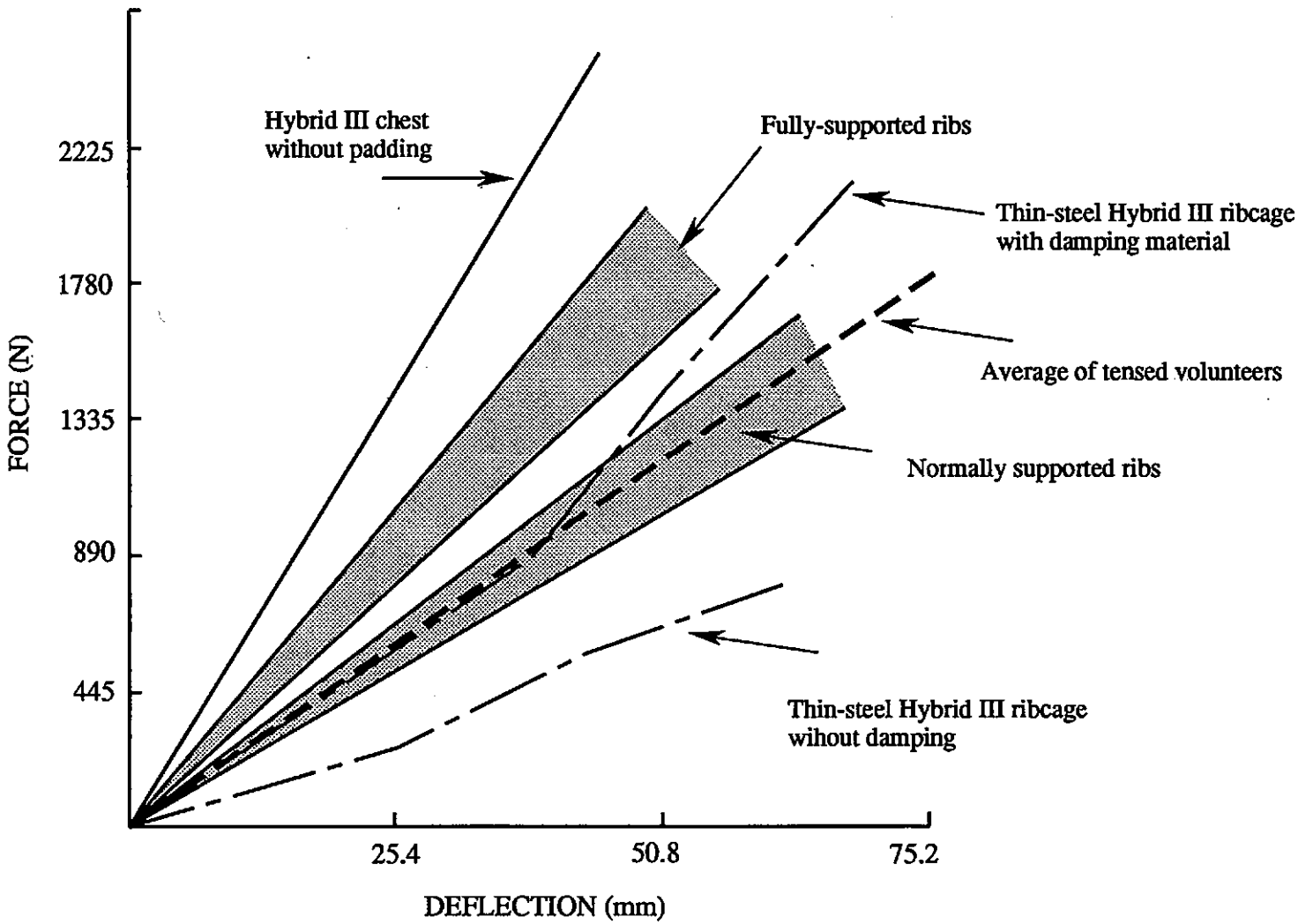

FIGURE 3–23. Comparison of quasi-static F-δ results for normally- and fully-supported damped thin-steel Hybrid III ribs.

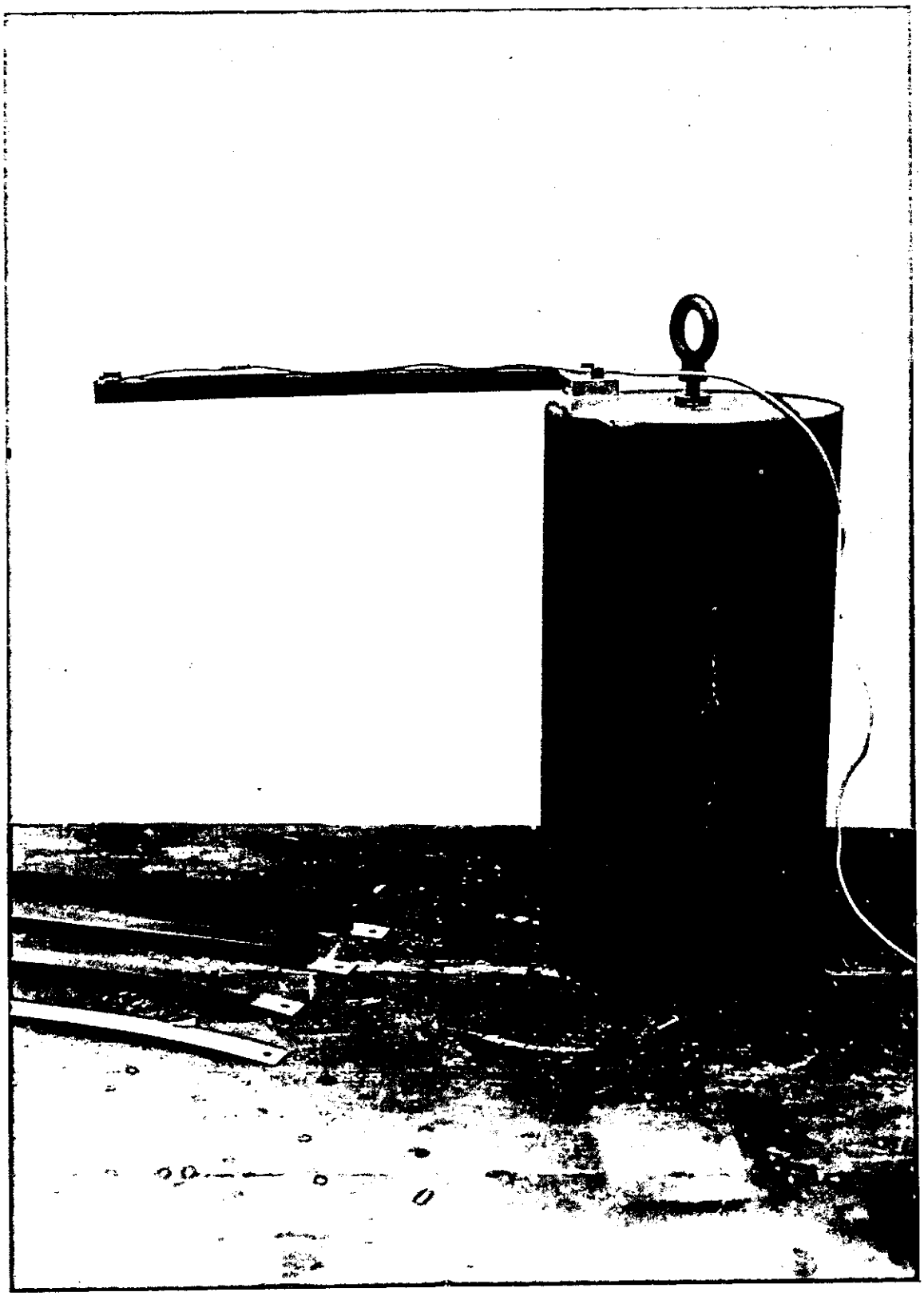

FIGURE 3–24. Test setup for damped beam vibration tests.

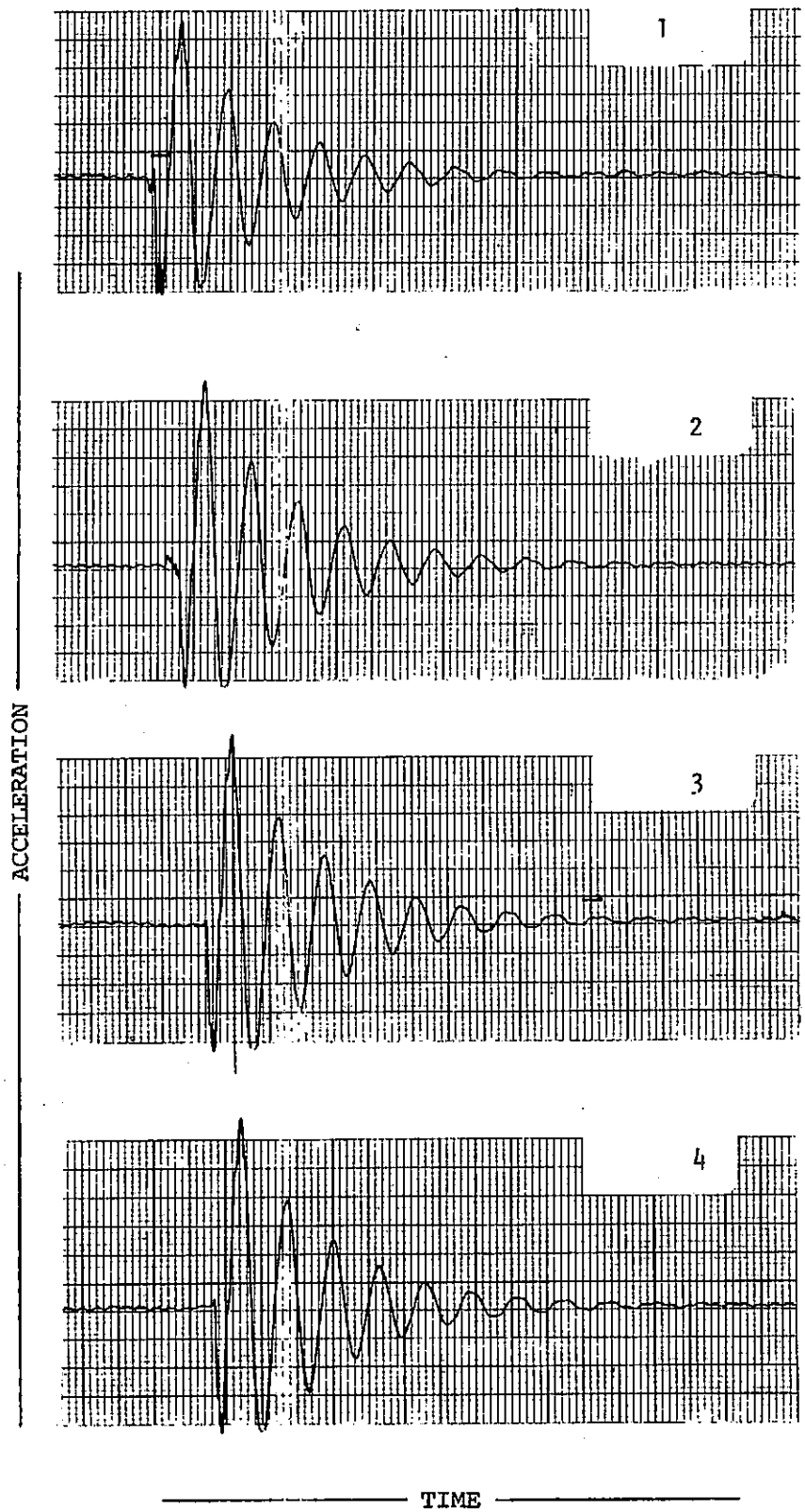

FIGURE 3–25a. Acceleration-time histories from damped-beam vibration tests using a beam with 2-mm (0.08-in) thick steel and 4.8-mm (0.19-in) thick damping material. Damping material *not* clamped.

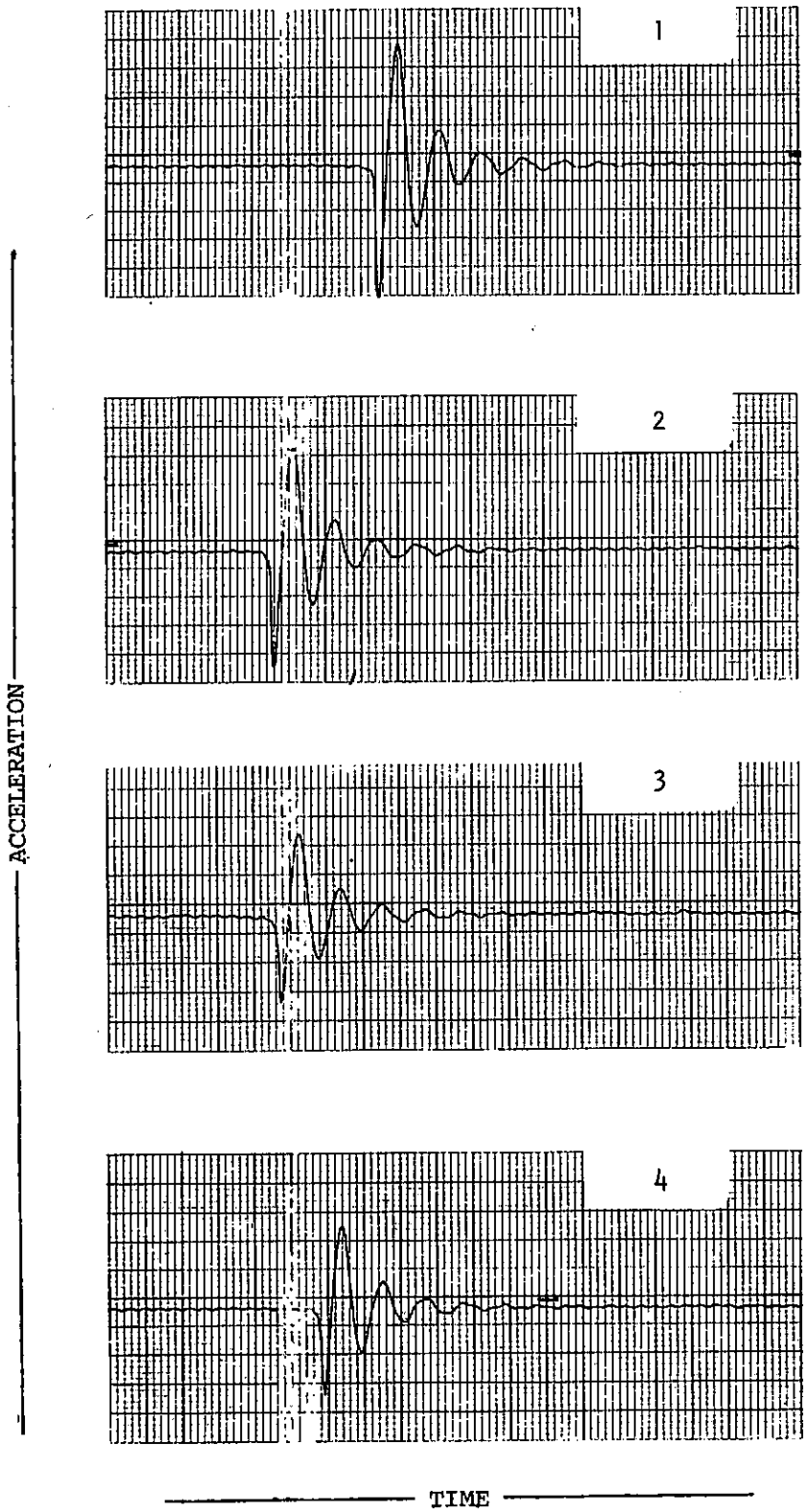

FIGURE 3–25b. Acceleration-time histories from damped-beam vibration tests using a beam of 2-mm (0.08-in) thick steel and 16-mm (0.63-in) thick damping material. Damping material *not* clamped.

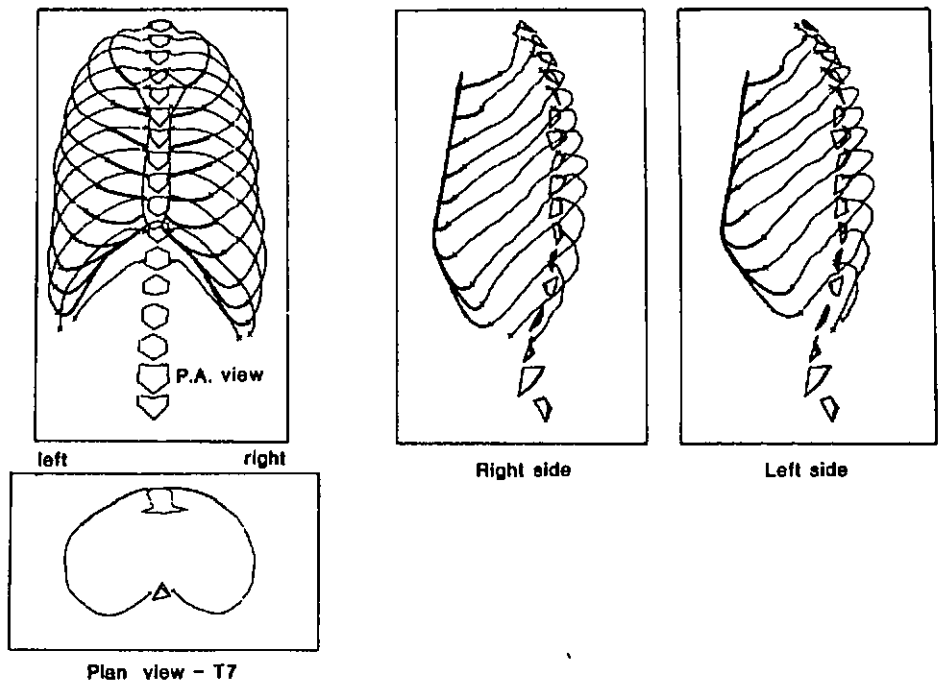

Frontal and lateral views of a reconstructed rib cage and spine and a plan view of ribs a T7 of a normal volunteer. Rib midline reconstruction was made by the iterative method; points on the spine and sternum were reconstructed by conventional stereoradiographic methods. Points on each vertebra and on the sternum have been joined by straight lines. In each of the lateral views the ribs on one side only of the skeleton are shown and both lateral projections are viewed from the left side of the subject.

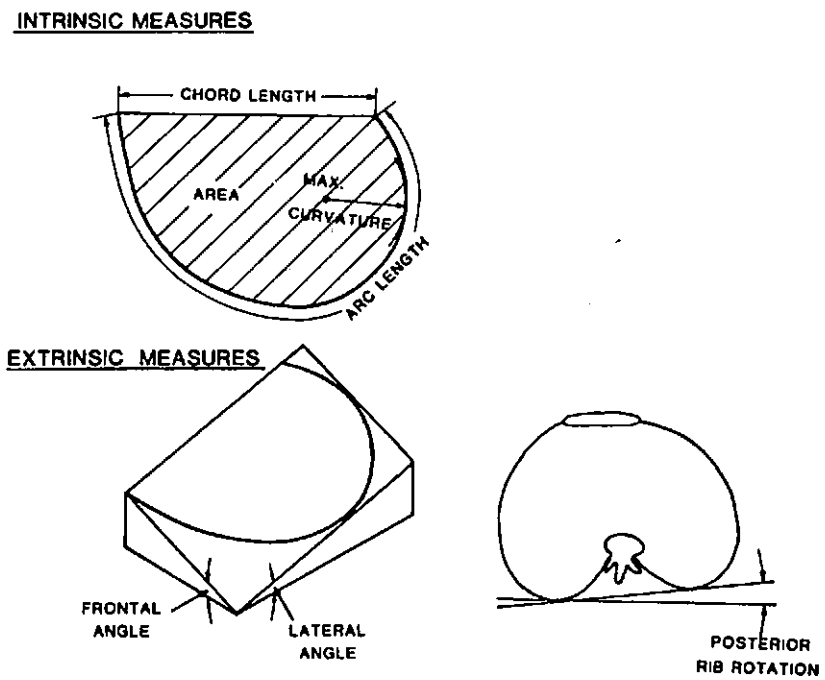

Intrinsic and extrinsic rib shape measures. Intrinsic measures were made in the 'best fit plane'. The angulation of this plane to the horizontal was measured by a 'frontal angle' and 'lateral angle'. Rotation of a pair of ribs in the plan view was measured by the 'posterior rib rotation'.

FIGURE 3–26. Human rib geometry (Dansereau and Stokes 1988).

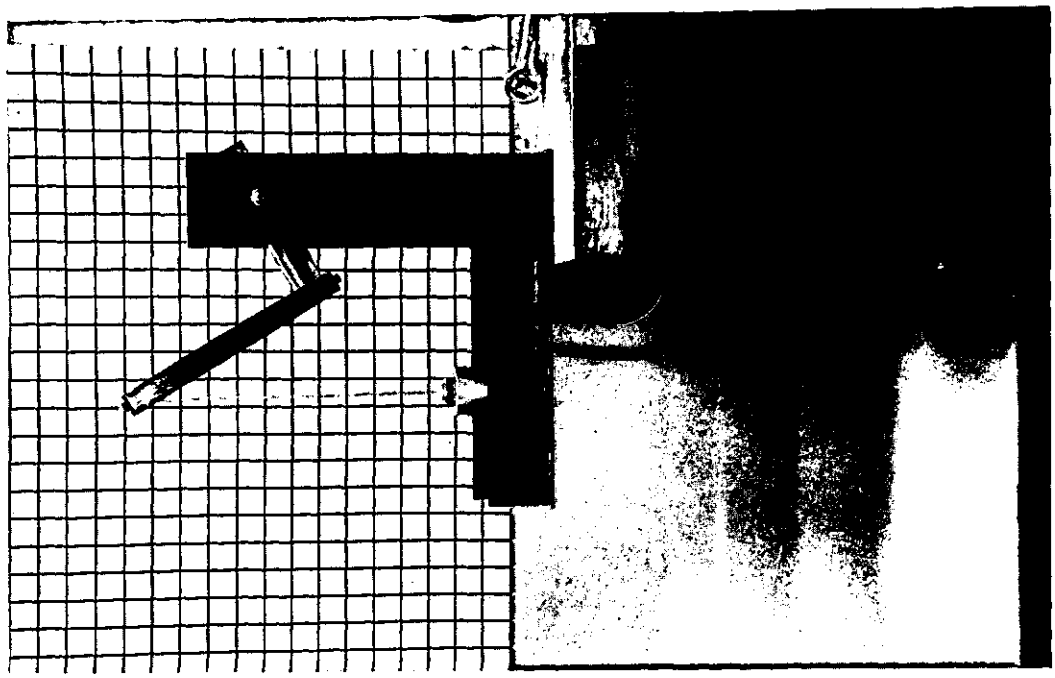

FIGURE 3–27b. Preload condition of rib at 30 degrees to vertical.

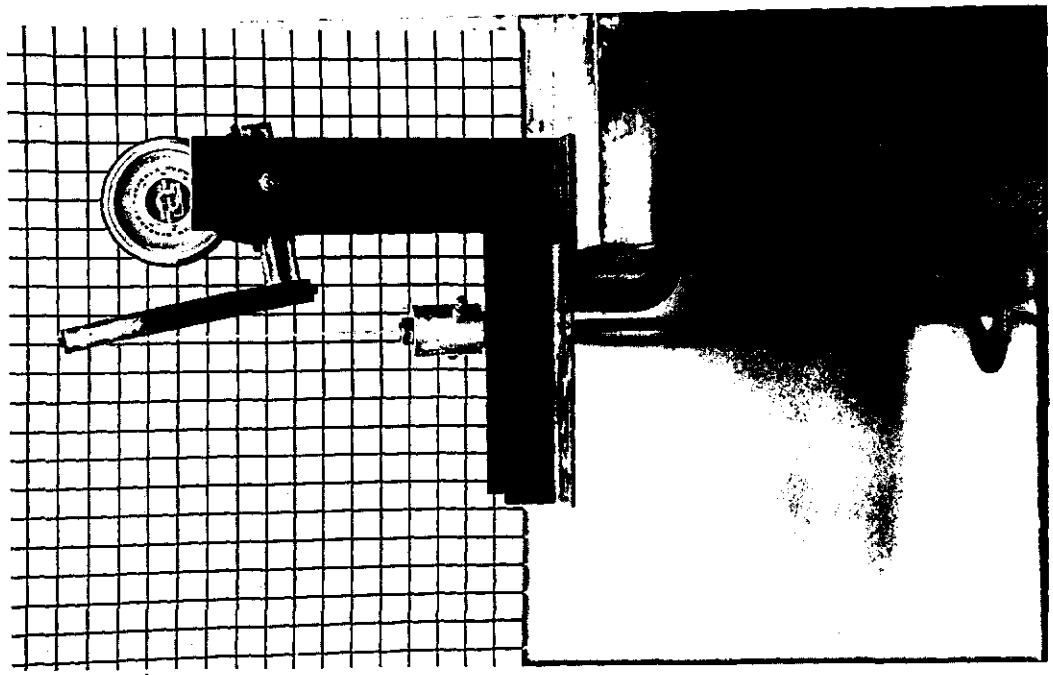

FIGURE 3–27a. Preload condition of rib at 10 degrees to vertical.

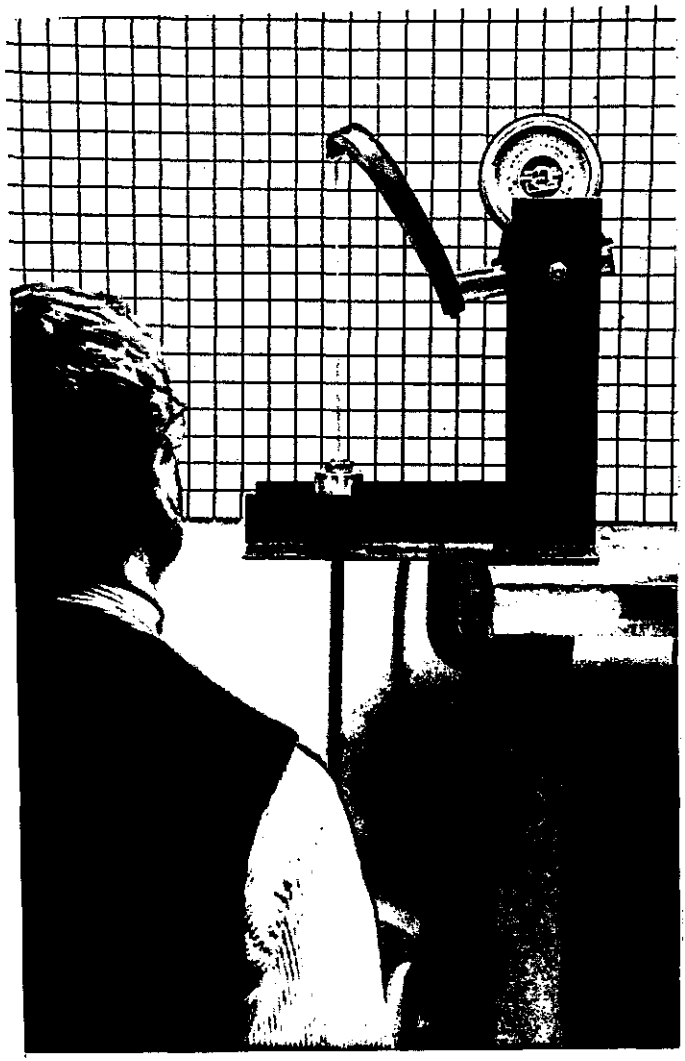

FIGURE 3–28a. Rib at initial angle of 10 degrees loaded with 6.8-kg (15-lb) mass in vertical direction.

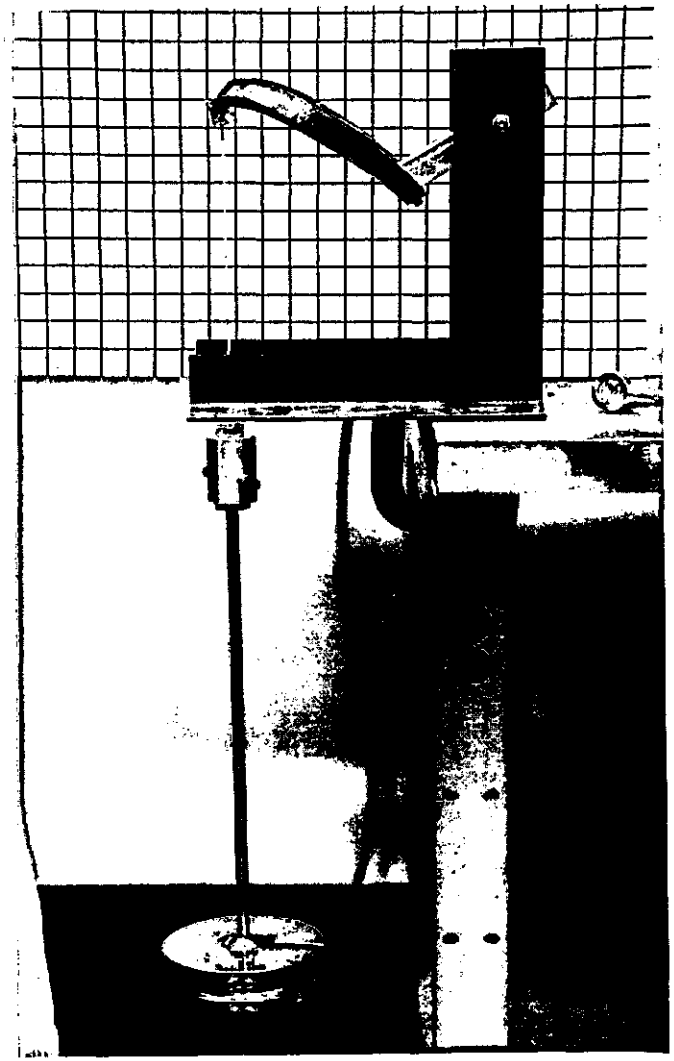

FIGURE 3–28b. Rib at initial angle of 30 degrees loaded with 4.5-kg (10-lb) mass in vertical direction.

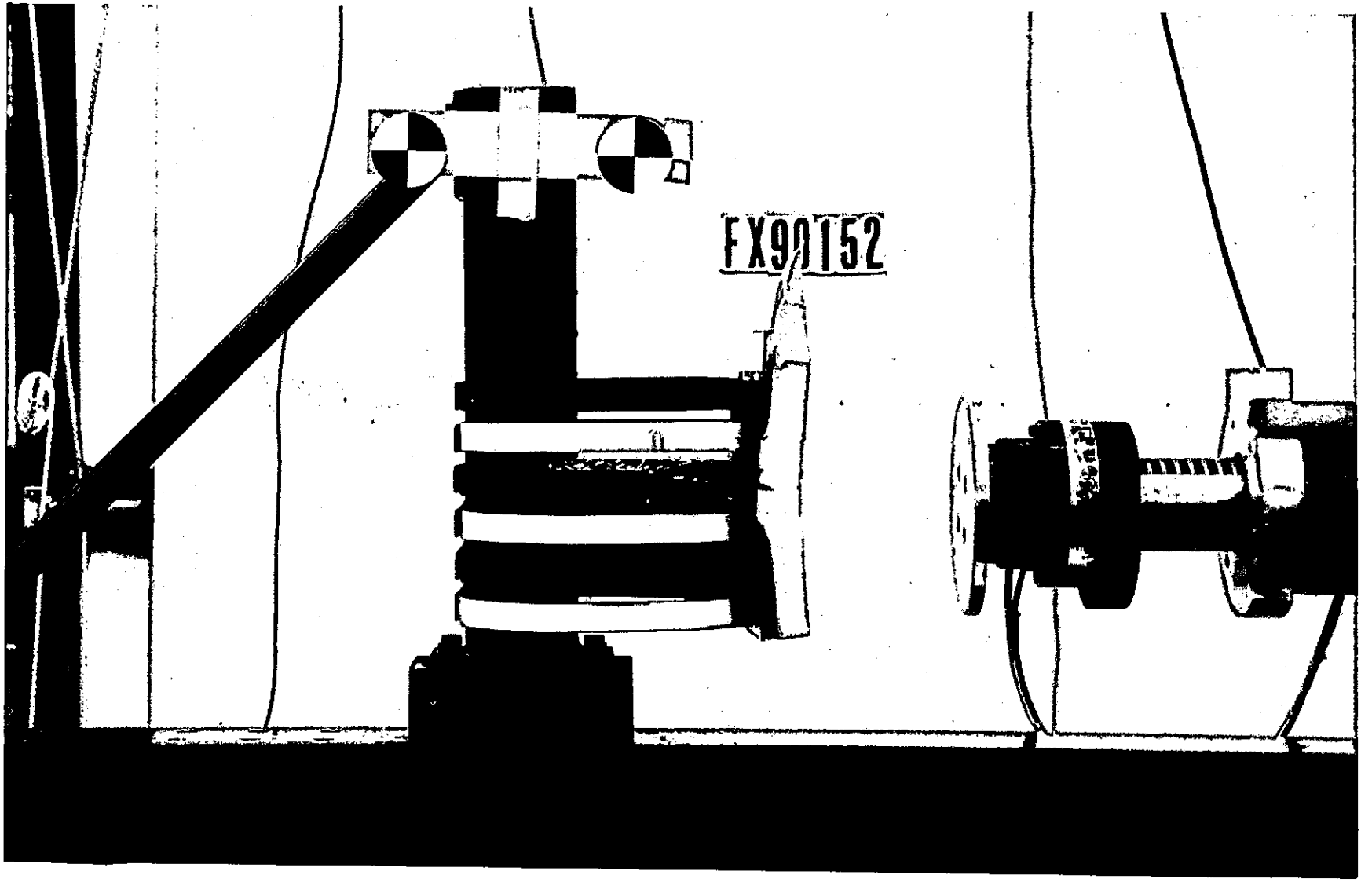

FIGURE 3–29a. Nonslant rib configuration for dynamic testing.

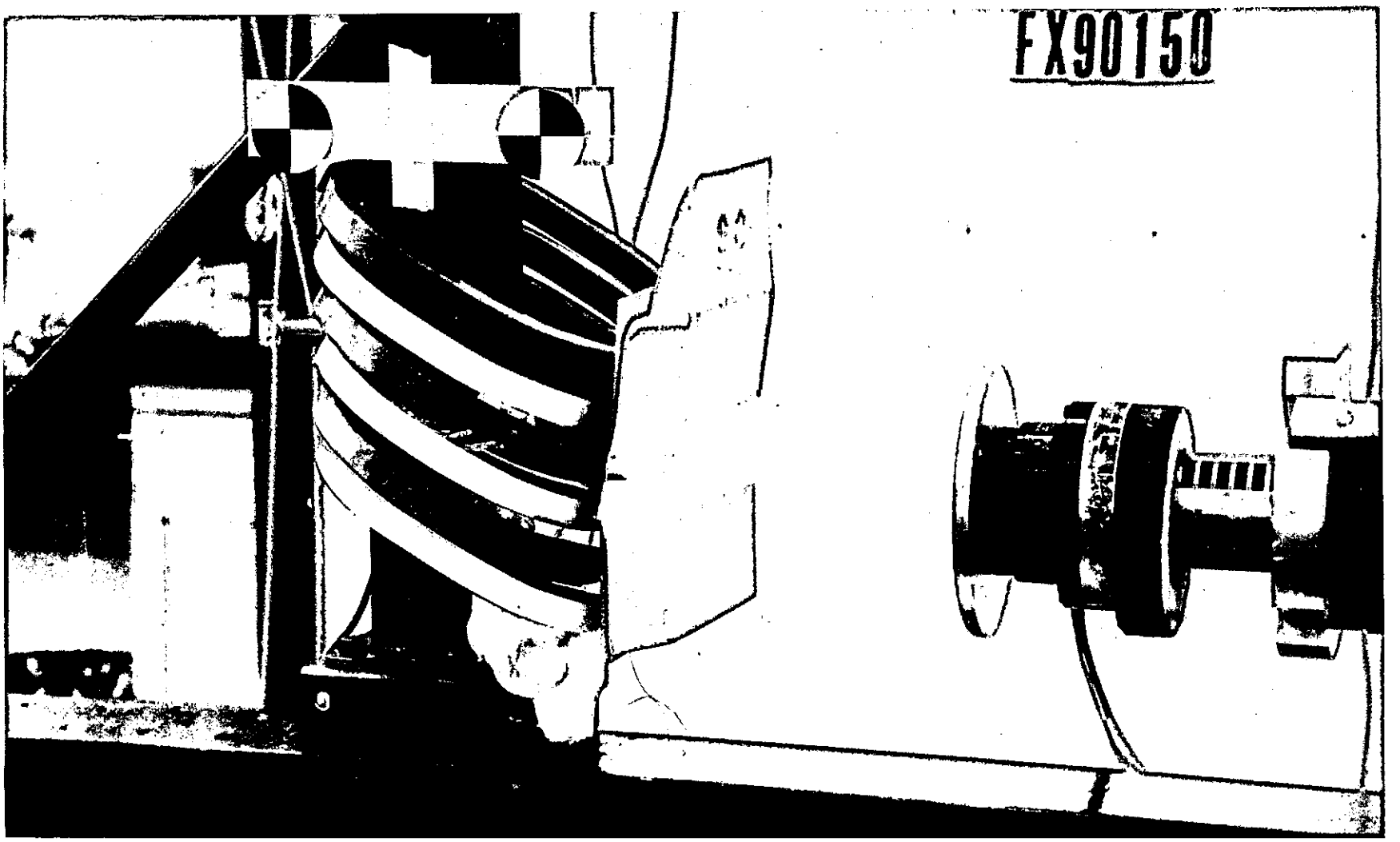

FIGURE 3–29b. Rib configuration for evaluation of slanted ribs under dynamic AP loading. Ribs are slanted at approximately 25 degrees to longitudinal axis of spine.

4. CHEST DEFLECTION INSTRUMENTATION

Throughout the process of developing and testing prototype models for the thorax/abdomen design concept, simultaneous efforts were underway to find and/or develop a reliable and accurate measurement system for quantifying the thorax and abdomen deflection- and/or velocity-time histories at critical response and injury regions (e.g., sternal area, and the lower ribcage). This pursuit of solutions to chest deflection instrumentation was carried out simultaneously with separate but similar efforts within the SAE Human Biomechanics and Simulation Standards Committee (HBSS) and at NHTSA's Vehicle Research and Test Center (VRTC) to develop an improved and more comprehensive chest deflection measurement capability for the Hybrid III chest.

In addition to measuring chest compression (defined as the inward displacement of a point on the chest relative to the spine) at each of the four identified injury and response regions, it was also considered necessary to measure the lateral and upward or downward movement of the chest. Within the SAE Hybrid III Chest Deflection Task Group of HBSS, the goal has been to quantify the two-dimensional motion of the rigid sternum (or the end of the four ribs at the corners of the sternum) and thereby provide information as to the X- and Y-deflections of any point on the sternum. After exploring a number of alternative approaches, the task group settled on the use of an array of eight high-tension string potentiometers manufactured by Space Age Controls, Inc. (SAC), with two each triangulating from the left and right sides of the spine to each corner of the sternum. Figure 4–1 shows the Space Age Controls string potentiometer that has been used for this application. This approach assumed that the ribcage would not move out of the plane of the ribs. Given that this assumption of planar motion may not be valid, consideration has also been given to adding a ninth string potentiometer to one of the sternal corners to measure the up/down movement of the ribcage at one location.

For the advanced dummy chest, however, triangulation with multiple string potentiometers was not feasible. The goal of improving (i.e., decreasing) the coupling between different regions of the thorax (e.g., left to right, and up/down) necessitates a different approach to characterization of chest deflection. Since each region responds relatively independent of other regions and with three-dimensional motion, it would be necessary to triangulate three string potentiometers to each measurement site, for a total of twelve string potentiometers in the chest. This is clearly prohibitive in the space available. Furthermore, the inclusion of a flexible thoracic spine, accomplished by means of a discrete flexible link (see Section 5), presents additional space constraints with regard to mounting instrumentation, as well as a somewhat different definition and interpretation of thoracic chest compression (i.e., relative to the upper or lower thoracic spine segment).

Ideally one could devise a measurement capability that would quantify the three-dimensional motion of all points of the surface of the dummy chest and abdomen. Given that this was not yet possible with current technology, it was necessary to consider measurement systems that would quantify the three-dimensional deflections at each of the four critical response regions. The primary challenge was to find a transducer technology capable of measuring the expected linear inward (i.e., AP) displacement of the chest of 75 to 100 mm (3 to 4 in) and capable of fitting within the limited space of the chest depth of 232 mm (9 in) at the sternum. Such a system would also need to measure the lateral and up/down movements, even if the only concern was for measurement of chest compression, since accurate measurement of compression (i.e., the length between the point on the ribcage and

spine) will both increase and decrease with lateral and up/down movement of the ribcage and therefore be in error if corrections for these out-of-plane movements are not made.

4.1 SONIC TRANSDUCERS

Since one of the primary problems was to find a transducer device capable of measuring the required displacements under nonaxial loading conditions, the possibility of using a noncontact measurement system was very appealing. Exploration of light-based measurement systems (i.e., infrared) did not reveal any device that could measure over the distance range of interest (i.e., 50 to 200 mm from the transducer) and that could fit inside the dummy chest. Investigations did, however, lead to two sonic-based devices that seemed potentially applicable to the crash dummy situation. These instruments were purchased and evaluated under dynamic test conditions.

4.1.1 Sona-Gage

One system, known as Sona-Gage and manufactured by EASI, Inc. of Milford, Michigan, utilizes small cylindrical sending and receiving units as illustrated in Figures 4–2a through 4–2c (both can be contained in the same module or separated), and transmits a continuous wave of sound at a frequency of about 40,000 Hz. The system was tested with the transmitter at opposite ends of a plexiglass telescoping tube since it was being considered for use with the internal response elements, and maintaining free space between the transmitter and receiver was an important consideration.

Figure 4–3 compares the output of the Sona-Gage with the output of a linear potentiometer positioned in parallel. A 15-kg (33-lb), 152-mm (6-in) diameter impactor was used to impact a block of Hexcell at about 10 m/s. As indicated, the Sona-Gage followed the shape of the position signal from the linear potentiometer, except during unloading when the signal dropped out momentarily. However, the magnitudes of the response were somewhat different, even though the two measurement systems were statically calibrated.

Subsequent to this test, further attempts to statically calibrate the Sona-Gage revealed significant variability over repeated trials. Because of these calibration problems and a high sensitivity to signal loss with very small misalignments and angle changes, the Sona-Gage was not considered a viable candidate for measurement at this time.

4.1.2 Pulsonic

The second sound-based transducer system investigated is called Pulsonic and is manufactured by Cleveland Machine Control of Cleveland, Ohio. This device transmits a pulse of sound and waits to receive the echo back before sending another pulse. As a consequence, the frequency response is limited by the speed of sound and the distance of transmission. In the 50- to 125-mm (2- to 5-in) range, the device could theoretically operate at 900 Hz, which is probably adequate for restrained-dummy testing.

Figures 4–4a and 4–4b show a test setup for this device mounted inside one end of an aluminum telescoping tube (again the immediate application was for use with internal response elements) installed inside a block of high-density foam. Figures 4–5a and 4–5b show output signals from the Pulsonic transducer for tests at 3 and 6 m/s and compare these signals to those from a linear potentiometer mounted in parallel with the Pulsonic system. As with the Sona-Gage, the Pulsonic signal follows the general shape of the linear potentiometer signal but lags the potentiometer signal during loading by 1 to 3 m/s. At 6 m/s, there is also disagreement in the peak displacement values between the Pulsonic and linear potentiometer signals, with the Pulsonic signal reading less than the linear potentiometer by about 7 mm (0.25 in). Not shown in the plots is the fact that, like the

Sona-Gage, the Pulsonic signal demonstrated periods of signal dropout during unloading, perhaps due to misalignment problems.

As with the Sona-Gage, the conclusion of these tests was that the Pulsonic system has potential for application to the dummy measurement problem but significant modifications to the system, beyond the scope of the present effort, are required. The system tested was quite large and expensive and required a special signal processor. While the device seemed durable under impact conditions, it was very sensitive to signal loss with small misalignments and, while the manufacturer indicated that the size could be reduced somewhat, there were significant limitations in this regard.

4.2 NESTED POTENTIOMETERS

Another approach that was considered and explored for chest deflection measurements is illustrated conceptually in Figure 5–6 and involves the use of several linear potentiometers nested in series to provide the 75- to 100-mm (3- to 4-in) stroke length required. As with the sonic devices, the potentiometers must be protected by a system of telescoping tubes that would also serve to provide stability and strength to the device. By connecting the wiper arm of each potentiometer to the adjacent cylinder section and mounting each potentiometer to the inside wall of a cylinder, the collective output of the potentiometers would be proportional to the total compression of the collapsing cylinders regardless of the order in which the collapsing of the cylinders takes place. As shown in Figure 4–7, a simple plexiglass model of this concept was built and successfully tested under quasi-static loading conditions. However, concerns about size (i.e., diameter) and durability of such a device resulted in a decision not to continue development.

4.3 INSTRUMENTATION TEST FACILITY

In order to test potential instrumentation concepts and prototypes for durability and accuracy under typical and expected thorax loading conditions, the test fixture shown in Figures 4–8a and 4–8b was developed. This facility uses a pneumatic impactor to deliver the impact loads to a block of Hexcell, which has been cut to an appropriate size to produce a Kroell-like force-deflection response to a 6.7-m/s impact velocity, as shown in Figure 4–9. The Hexcell is supported by a rigid backing plate, behind which is a sliding carriage assembly that connects to a thin metal plate at the front of the Hexcell by means of a steel rod inserted through the center of the Hexcell. Thus, the movement of the carriage is the same as the crush of the Hexcell.

Displacement of the carriage during impact loading is monitored directly by a linear potentiometer mounted behind the carriage. The instrumentation to be tested is mounted to a platform off to the side of the carriage and linear potentiometer, and can be oriented so that stroking of the carriage produces either two- or three-dimensional motion. In this way, the instrumentation can be tested for durability under worst-case, off-axis loading conditions of up to 50 mm (2 in) of lateral and/or up/down displacement for 75 mm (3 in) of AP compression. In addition, because the initial geometry is known, the actual AP lateral, and up/down displacements at any point in time can be determined from the displacement of the linear potentiometer, and the accuracy of the transducer system can be determined and compared.

4.4 STRING POTENTIOMETERS

The use of string potentiometers for displacement measurement in impact biomechanics has been a common practice for many years. In general, however, the experience has been that these devices are reliable only in the pulling direction, where the

string or cable is pulled against the spring tension, and not in the pushing direction, where the string or cable is reeled in as a result of impact loading. In the latter case, the tension in the string is generally not sufficient to allow the potentiometer rotation to follow the motion of the cable end, resulting in slack in the cable and a lag in the displacement measurement. Since a string potentiometer would need to work in a push mode inside a dummy chest, the idea of using string potentiometers was initially considered, but rejected.

As a result of efforts by the SAE Task Force to improve the Hybrid III chest displacement measurement capability, however, a high-tension string potentiometer manufactured by Space Age Controls, Inc. and shown in Figure 4–1 was evaluated and improved (i.e., reduced inertia, reduced size) to the extent that it provides accurate and reliable measurement capability for crash dummy loading conditions, particularly for the lower velocities of loading expected for belt-restrained occupants. As previously noted, an eight- or nine-array system of string potentiometers has been evaluated for application to the Hybrid III chest, and string potentiometers are now used for rib deflection measurements in the side-impact dummies. While triangulation with string potentiometers was not considered feasible in the advanced dummy chest, for reasons previously noted, the use of double-gimballed string potentiometers was considered feasible for installation in the prototype chest at the four critical response sites, as described in the following section.

4.5 TELESCOPING JOY STICK WITH DOUBLE-GIMBALLED STRING POTENTIOMETER

An alternative procedure to triangulation of string potentiometers for measuring two- or three-dimensional motion of the dummy chest is to use rotary potentiometers to measure the angles of movement of the point on the chest of interest relative to its original position with respect to a reference point on the spine. As illustrated in Figure 4–10, by gimballing a string potentiometer with its cable connected to the ribcage, the potential exists to simultaneously measure the distance to the ribcage (i.e., along the cable length) as well as the angular movement of that point relative to the spine. The accuracy of the angle measurement depends, however, on the ability of the cable to follow the lateral and up/down displacements of the ribcage. Given that the cable is "pushed" during chest compression, resulting in reduced tension and potentially a moment of slack, the ability of the cable to move the pivoting string potentiometer on its gimbals in phase with the off-axis chest movement must be seriously questioned.

A potential solution to this problem is the use of a collapsing joy stick made of multiple nested cylinders through which the cable can be threaded, and which would add stability and stiffness to the cable for tracking off-axis motion. An initial prototype was constructed from telescoping brass tubing and fastened to a double-pivot, aluminum-joy-stick controller used for radio-control airplanes. The system, which is shown in Figures 4–11a and 4–11b, does not include a string potentiometer but was installed in a Hybrid III chest for endurance testing of the gimbals and joy stick under AP loading as shown in Figure 4–12.

After numerous tests, no damage was noted and the system was subsequently tested using the facility described in the previous section for combined AP and lateral loading. Figure 4–13 shows the prototype unit mounted in position for testing. The unit again demonstrated that it could survive the expected impact environment including off-axis loading. Furthermore, while the model tested was found to have a loose attachment at the base of the collapsing joy-stick, the results were also encouraging with regard to system accuracy.

As a result of the success of this initial prototype device, the collapsing joy-stick system was further developed to enable the cable of the string potentiometer to be threaded down the center of the collapsing joy stick. Figure 4–14 shows a schematic of the new design and Figure 4–15 shows the new prototype. A special, heavy-duty, six-segment joy stick was

machined from solid stainless-steel rod and attached to an SAC string potentiometer. The housing of the string potentiometer was modified to provide for gimballing about an axis perpendicular to the axis of pulley rotation, and the support structure for this gimbal was designed for pivoting at the spine of the dummy. The string potentiometer cable is inserted down the center of the collapsing rod and is captured by a special fitting at a small U-joint that connects the joy stick to the ribcage. As indicated in Figure 4–14, an idler pulley, installed in the string-potentiometer housing, aligns the extended cable through the intersecting axes of the two gimbals.

An earlier version of this device (in which the axes and the cable were not aligned) was tested on the facility described above for simultaneous AP and lateral displacement using one gimbal at a time. Figure 4–16 shows a schematic of the two-dimensional test setup, while Figure 4–17 compares the results with expected AP and lateral displacements based on the output of the linear potentiometer and the known geometry. While the unit tested had a noisy potentiometer (a wafer potentiometer was used in this initial version) and some "play" in one segment of the telescoping joy stick, the results were extremely encouraging, in terms of both system accuracy and durability.

Additional three-dimensional testing was conducted on the latest version of the DGSP where the centers of the two gimbals and cable direction were aligned at a common point. The DGSP was mounted on the platform to the side of the carriage so that movement of the carriage in the direction of impact produced inward displacement of the telescoping joy stick and rotation in each of the gimbals according to the geometry shown in Figure 4–18. Figure 4–19 shows the setup for these tests in which the AP direction was assumed to be colinear with the initial orientation of the cable or joy stick. Figure 4–20 compares expected and measured results for front-to-back (AP), lateral (RL), and up/down (SI) displacements. The small oscillations observed in the lateral and SI signals calculated from the DGSP output signals may be due to flexure of the telescoping segments of the joy stick.

4.6 LINEAR POTENTIOMETERS

Initially, the idea of using linear displacement transducers was not considered, especially when the design focus was aimed at a system using fluid-filled internal elements. In addition to concerns about durability under loading conditions that produce combined lateral, up/down, and compressive movements of the chest, limitations of stroke distance to overall length appeared to be a major problem with these devices inside a dummy chest. However, after exploring the alternatives, and after deciding to use a damped-rib approach to the thorax design, the possibility of using simple linear displacement transducers mounted to the spine through a double-gimbal system similar to that described above for the string potentiometer was reconsidered.

As a result of further investigations into potential off-the-shelf systems, two types of transducers appeared promising. One is a high-frequency-response linear displacement transducer (FVDT) marketed by Data Instruments, Inc., and shown in Figure 4–21. Like a standard LVDT, the device consists of an outer cylindrical coil through which a metal shaft moves. Unlike most LVDTs, this inner core or shaft is tubular and needs to be inserted only a small distance into the cylindrical coil for the transducer to function in the linear range. Thus, with this device, it is possible to provide a 75-mm (3-in) stroke distance with a cylindrical coil that is just longer than 75 mm (3 in). It is therefore possible to obtain a much higher stroke-to-length ratio than with conventional LVDTs where operation in the linear range requires the metal core to be inserted some distance into the cylinder.

By attaching a nonmetallic end to the tubular core of the FVDT, one could design a device with sufficient initial overlap (i.e., enough bearing surface) to prevent binding of the shaft in the cylinder. However, to realize a minimal cylinder length (i.e., just greater than the maximum stroke distance), one would need to provide for the nonmetallic end to

protrude through the opposite end of the cylinder at maximum stroke. A disadvantage to this device is the need for a special signal processing module, although the cost of this hardware is only about $200.

The second linear potentiometer considered is currently used in dummy neck calibration testing and is a simple, lightweight linear potentiometer with a cylindrical body and a rod down the center. Manufactured by both Bourns, Inc. and Instrument Controls, Inc., this unit has a 75-mm (3-in) stroke with a 100-mm (4-in) body length. Figure 4–22 shows a unit as purchased from the manufacturer. While this stroke-to-overall length ratio is somewhat less than the ratio potential of the Data Instrument device and the units appear to be less durable than the FVDTs, their small diameter, lightweight, and low cost (about $150) make them attractive for dummy chest instrumentation.

To further evaluate this linear potentiometer, a unit was mounted in a double gimbal as illustrated in Figure 4–23 and tested for two-dimensional motion using the geometry of Figure 4–15. Figure 4–24 shows the transducer in the test setup. Figure 4–25 shows sample results from these tests. As indicated, results for AP and lateral movement calculated from the outputs of the rotary potentiometer and linear potentiometer are in excellent agreement with calculated AP and lateral movements calculated from the linear potentiometer of the test fixture. Of equal importance was the fact that the unit survived the impacts with no apparent changes in mechanical or electrical condition and function.

4.7 FIGURES

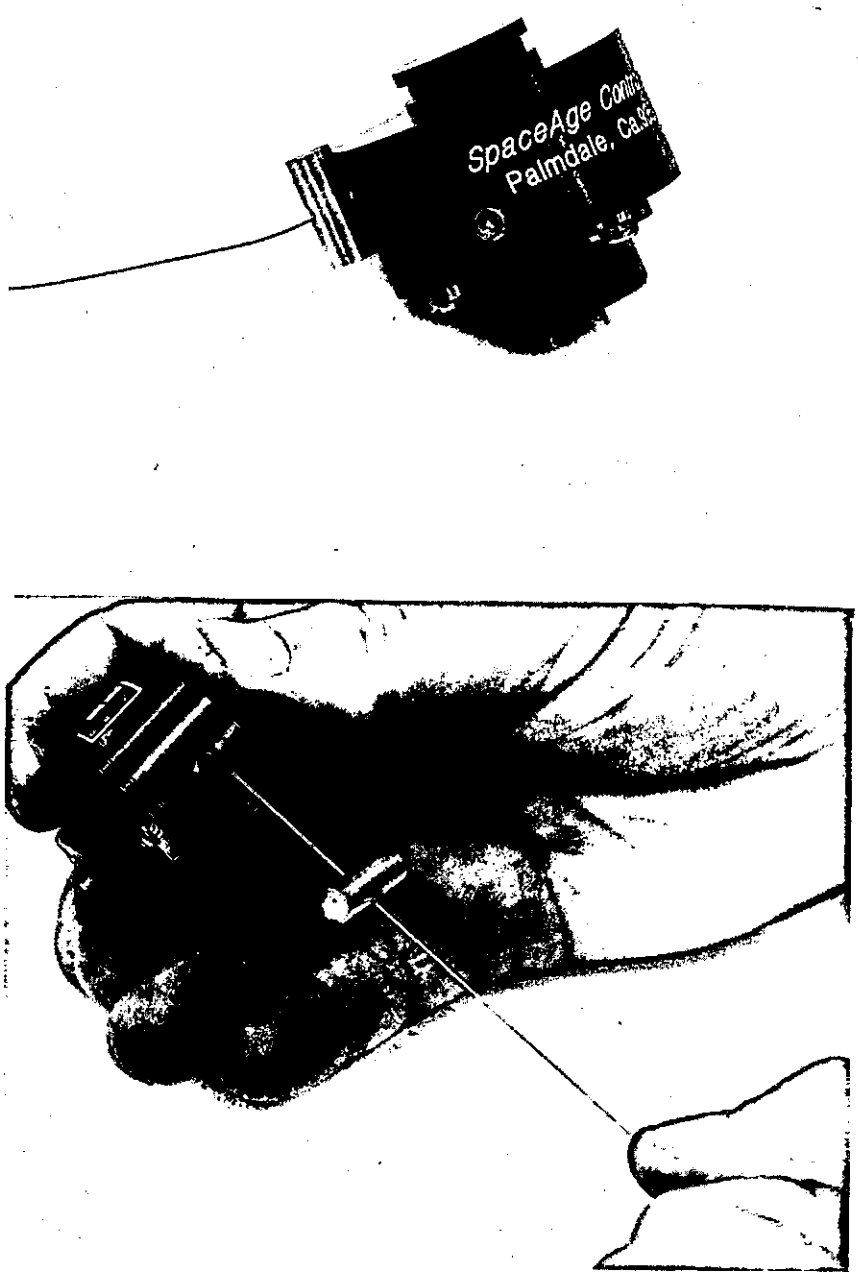

FIGURE 4–1. Space Age Controls, Inc. (SAC) string potentiometer used for dummy chest compression measurements.

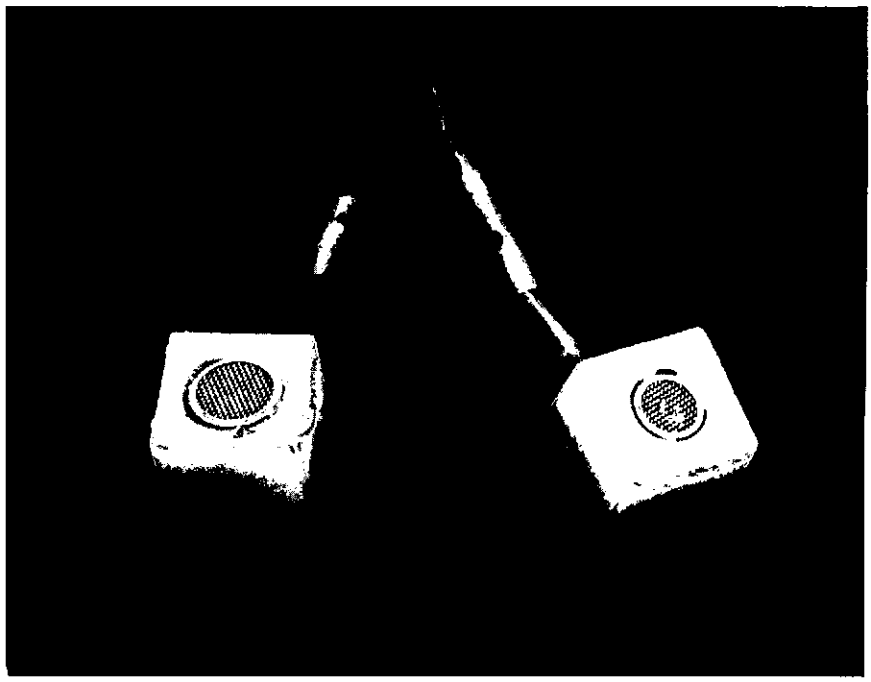

FIGURE 4–2a. Sona-Gage transducer: transmitting and receiving units.

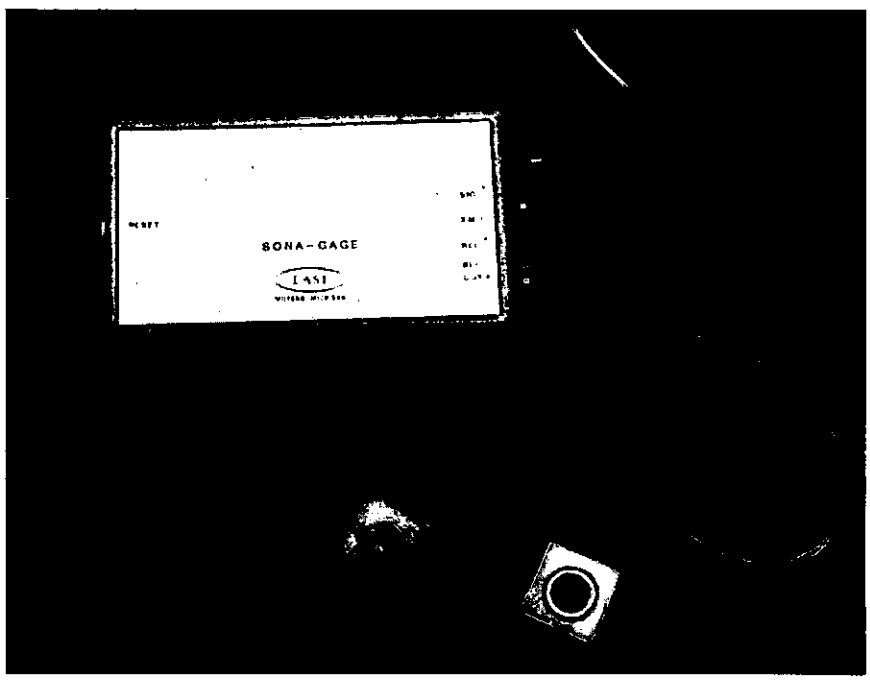

FIGURE 4–2b. Sona-Gage transducers and portable signal processing unit.

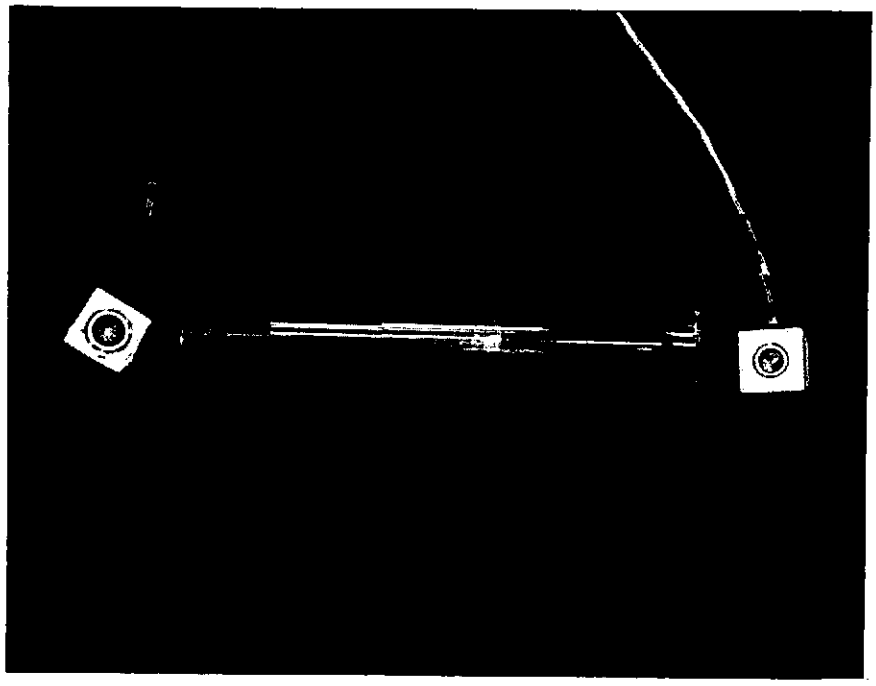

FIGURE 4–2c. Sona-Gage transducers and telescoping plexiglass cylinders used for impact testing.

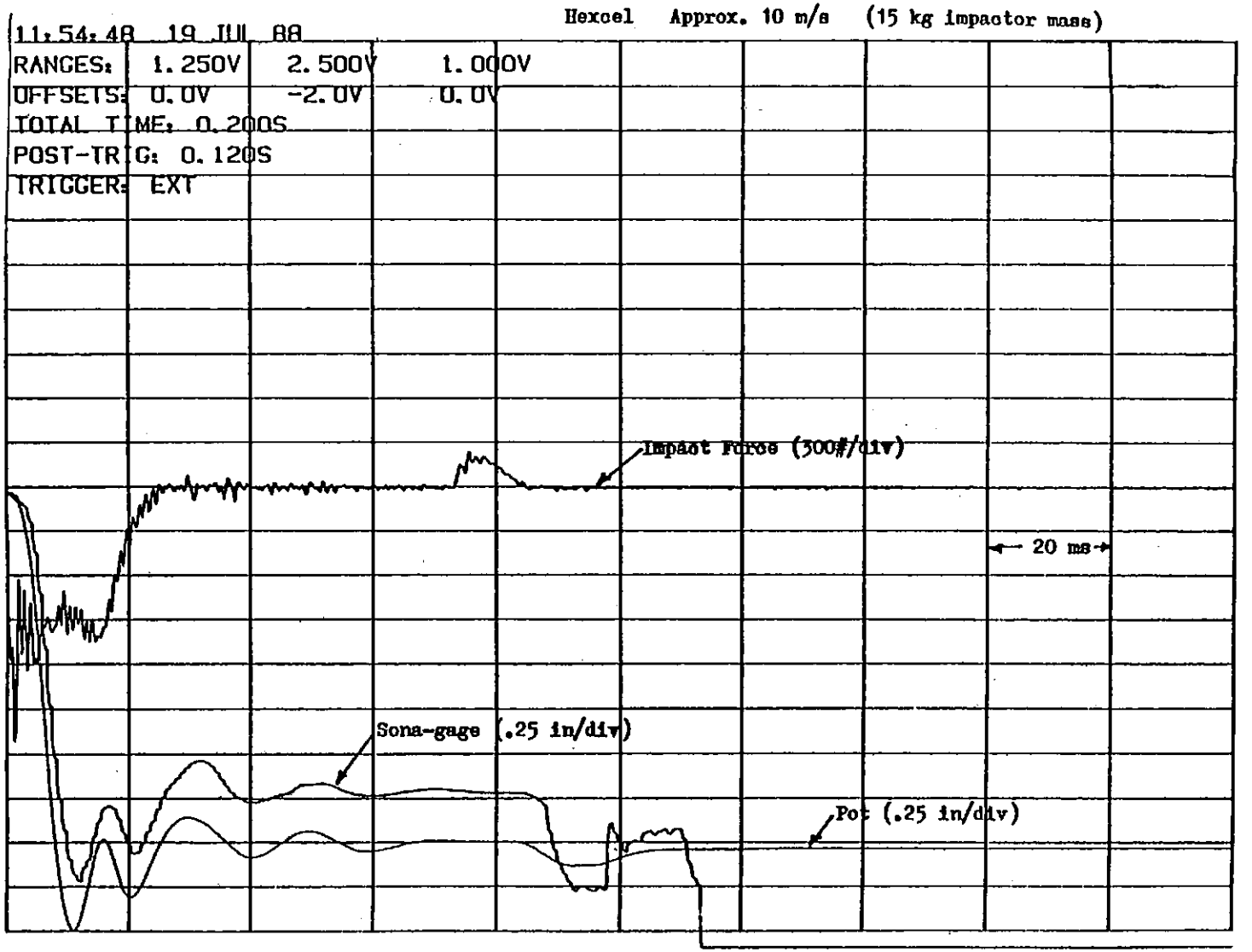

FIGURE 4–3. Comparison of Sona-Gage and linear potentiometer output for 10-m/s impact into Hexcell.

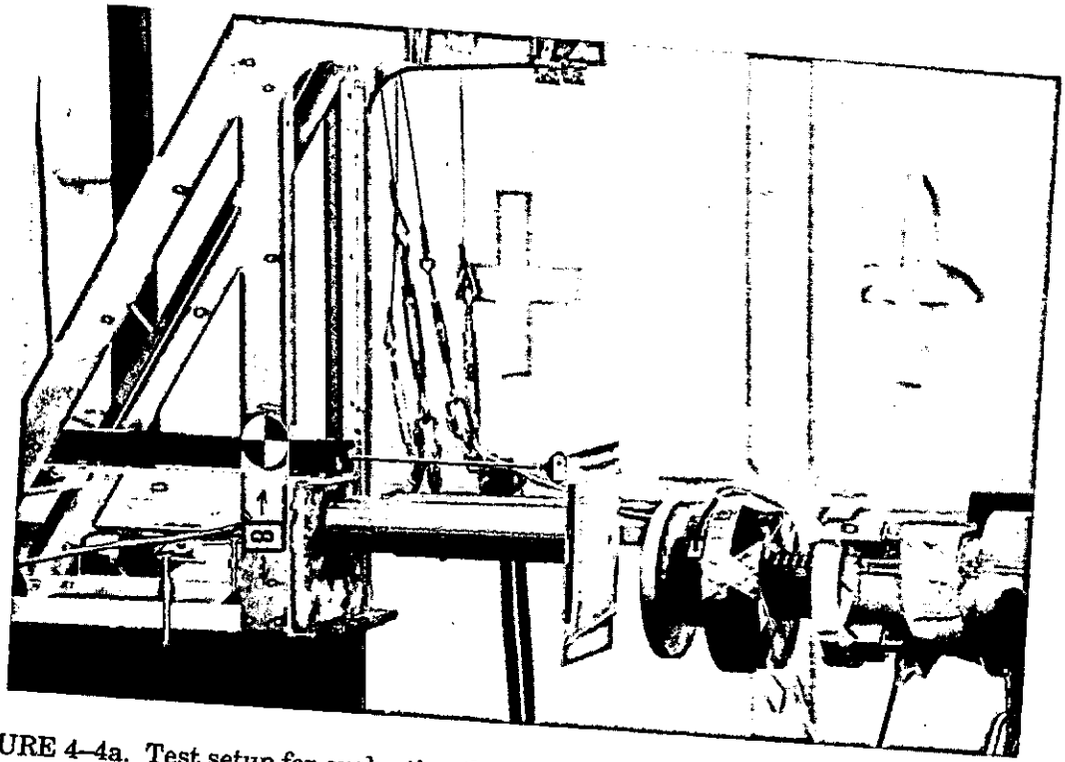

FIGURE 4–4a. Test setup for evaluating the pulsonic pulse-sound displacement measurement transducer inside a telescoping cylinder.

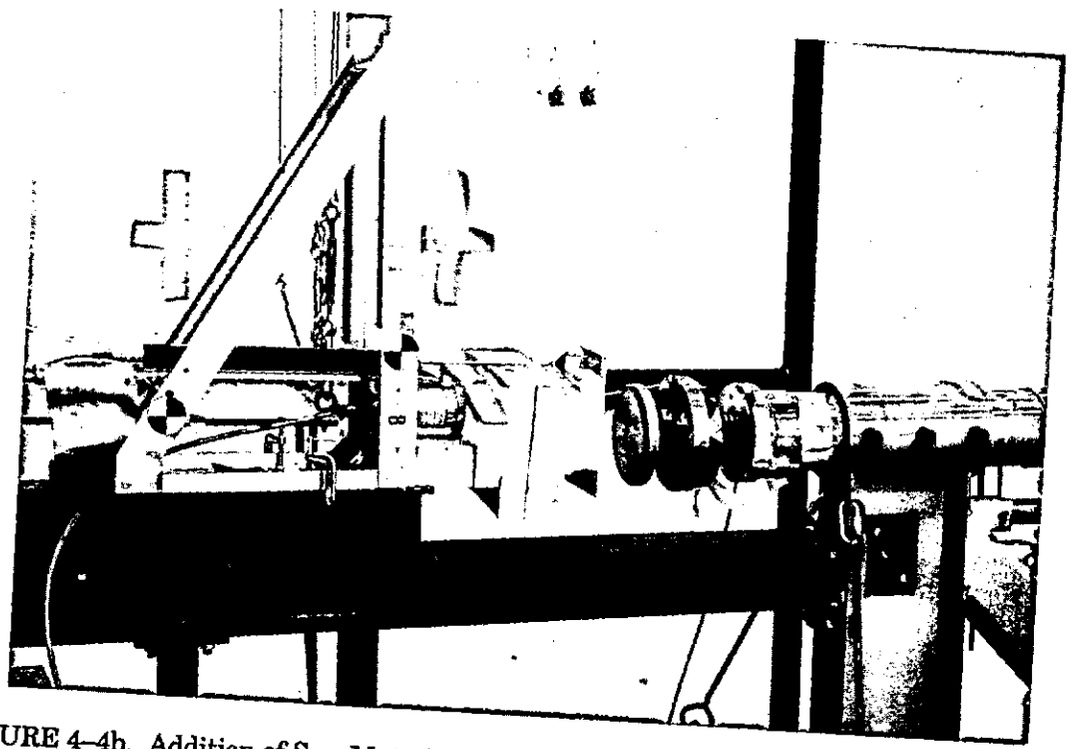

FIGURE 4–4b. Addition of Sun-Mate foam to test setup to provide resistance to impact loading during evaluation of Pulsonic transducer.

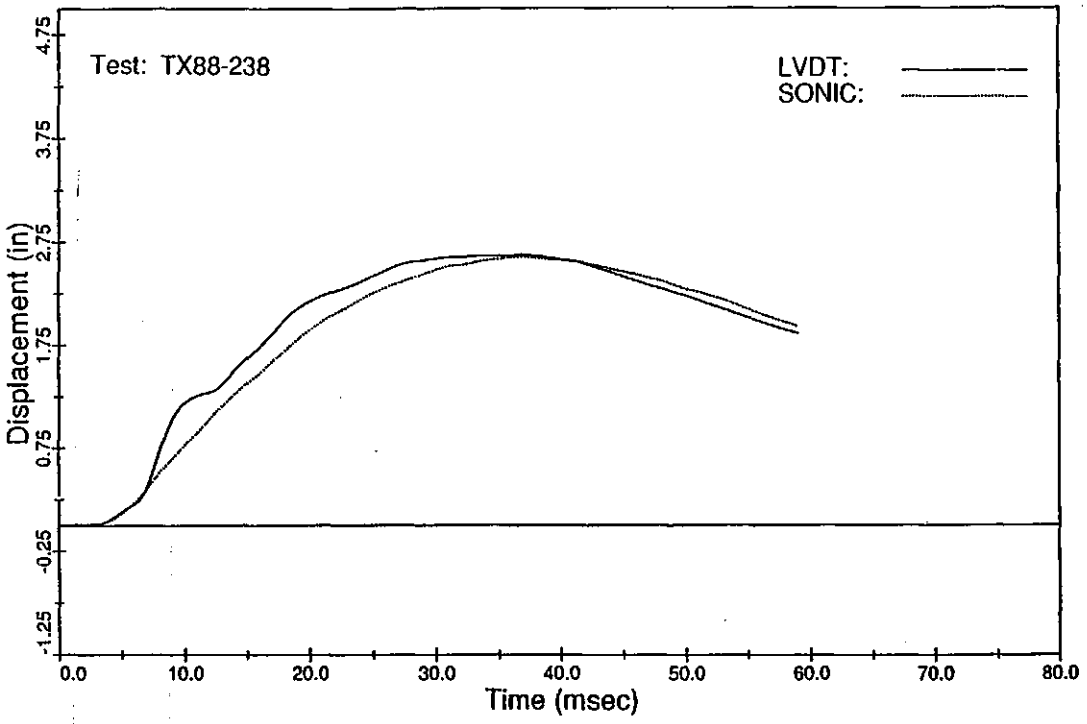

FIGURE 4–5a. Comparison of Pulsonic and linear potentiometer outputs for 3-m/s impact.

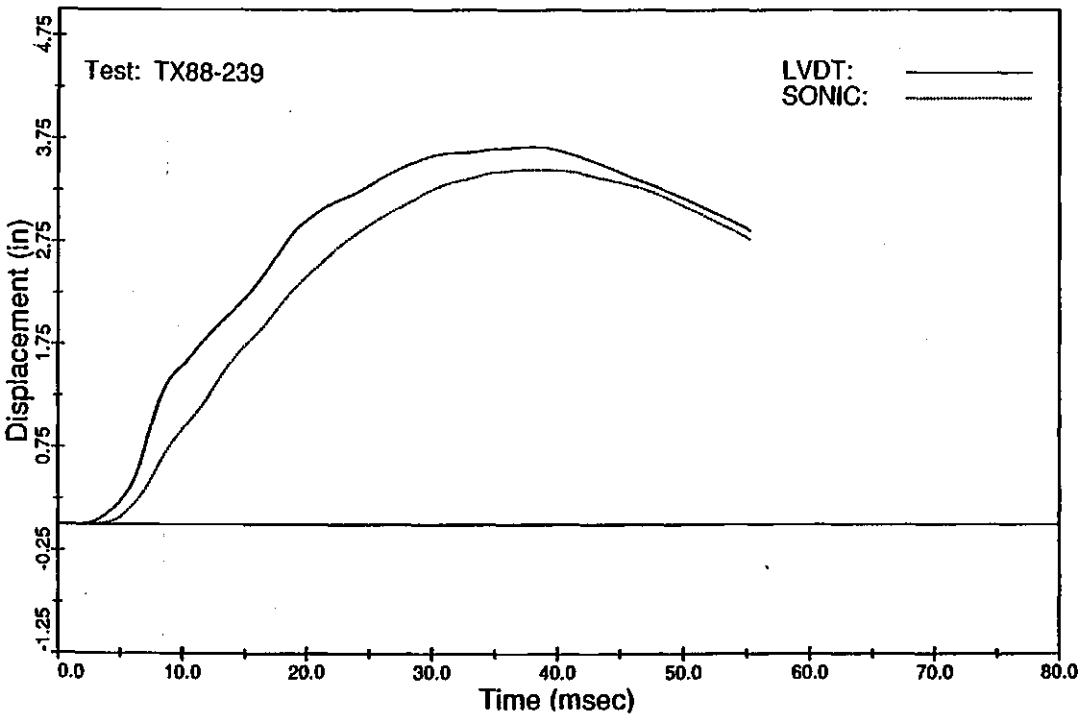

FIGURE 4–5b. Comparison of Pulsonic and linear potentiometer outputs for 6-m/s impact.

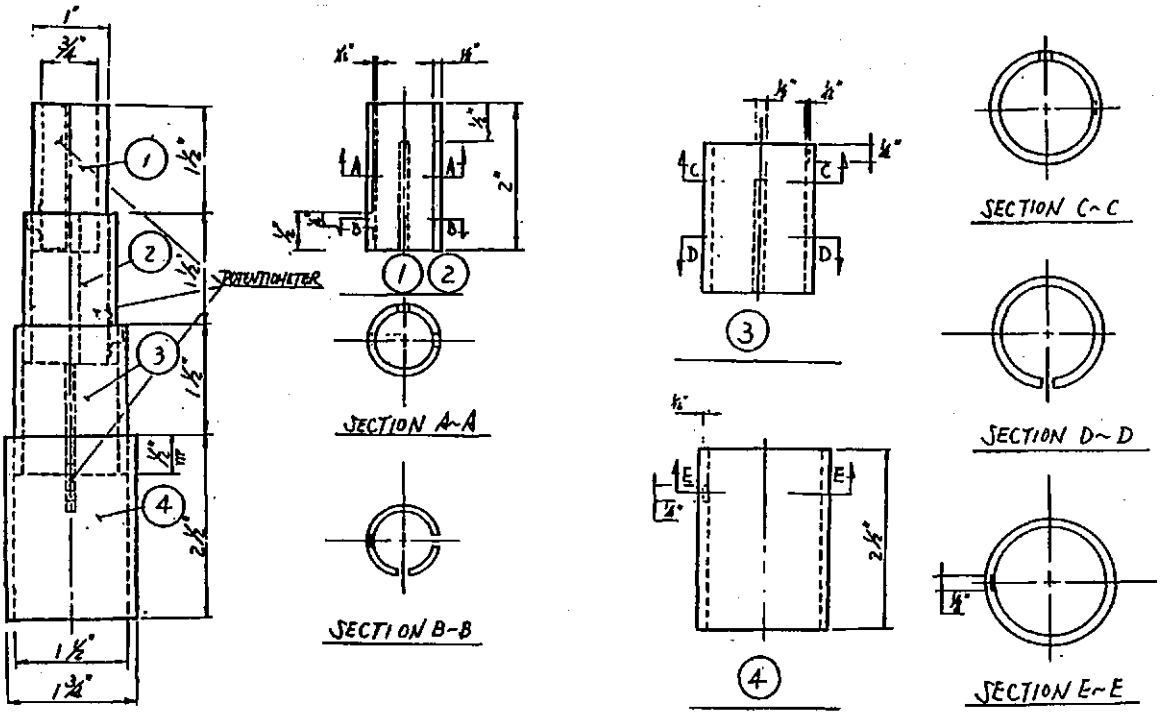

FIGURE 4–6. Schematic of nested potentiometers operating in telescoping tubing.

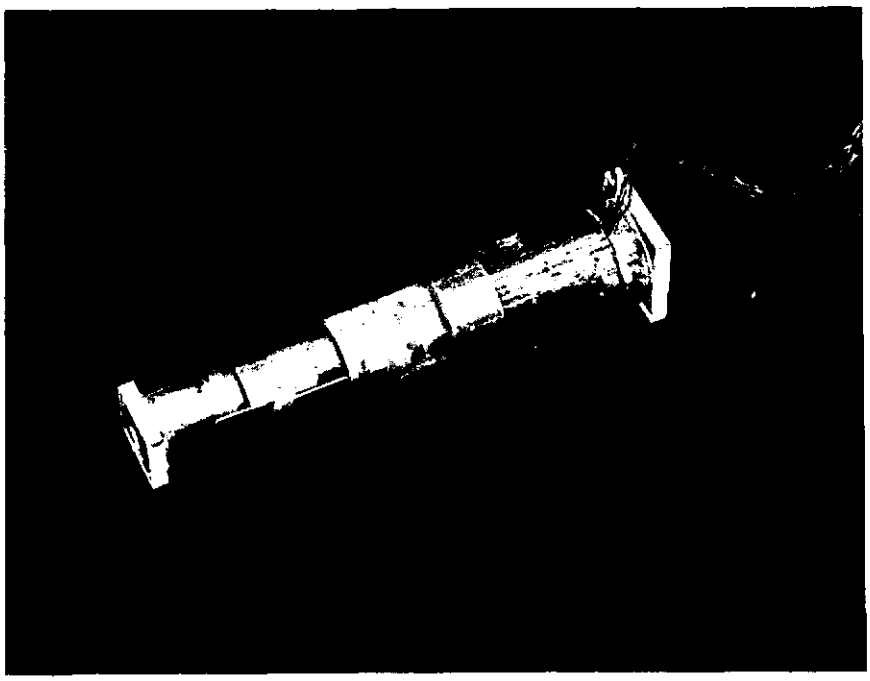

FIGURE 4–7. Plexiglass prototype of nested potentiometer displacement transducer system.

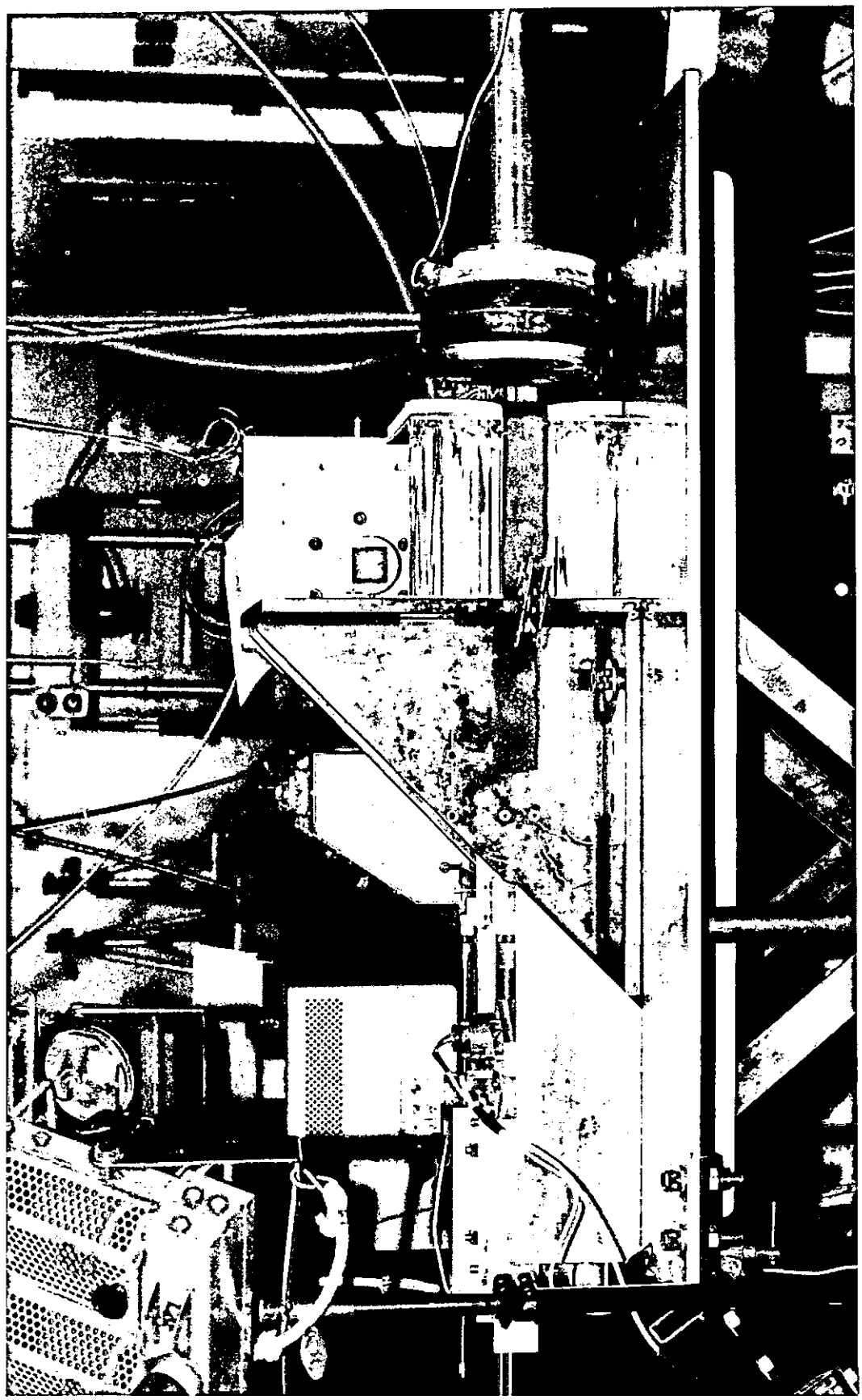

FIGURE 4–8a. Side view of test facility for evaluating chest deflection instrumentation under combined AP and lateral loading.

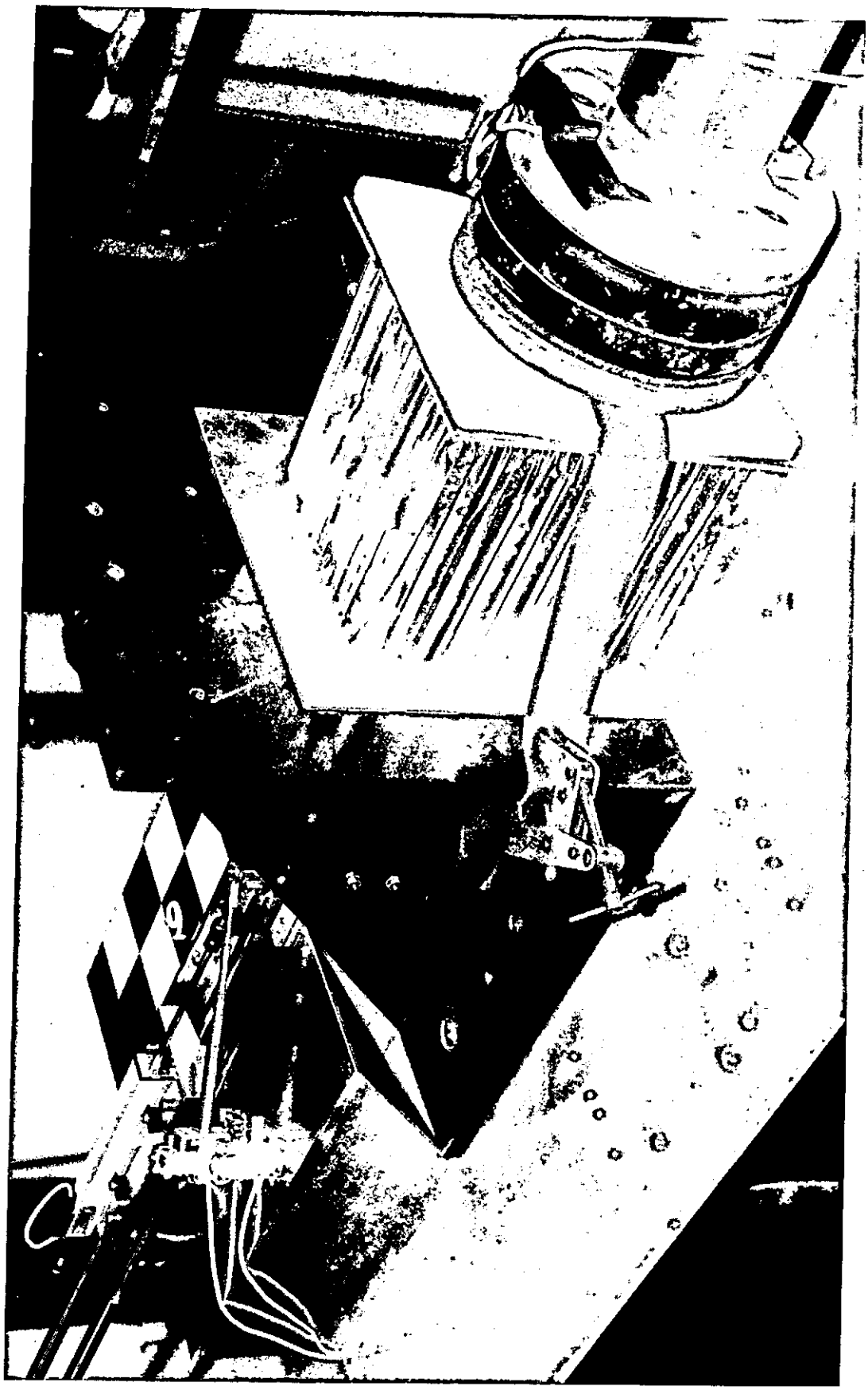

FIGURE 4–8b. Test facility for evaluating chest deflection instrumentation under combined AP and lateral loading. View showing Hexcell and impactor on right and linear potentiometer and transducer to be tested at upper left.

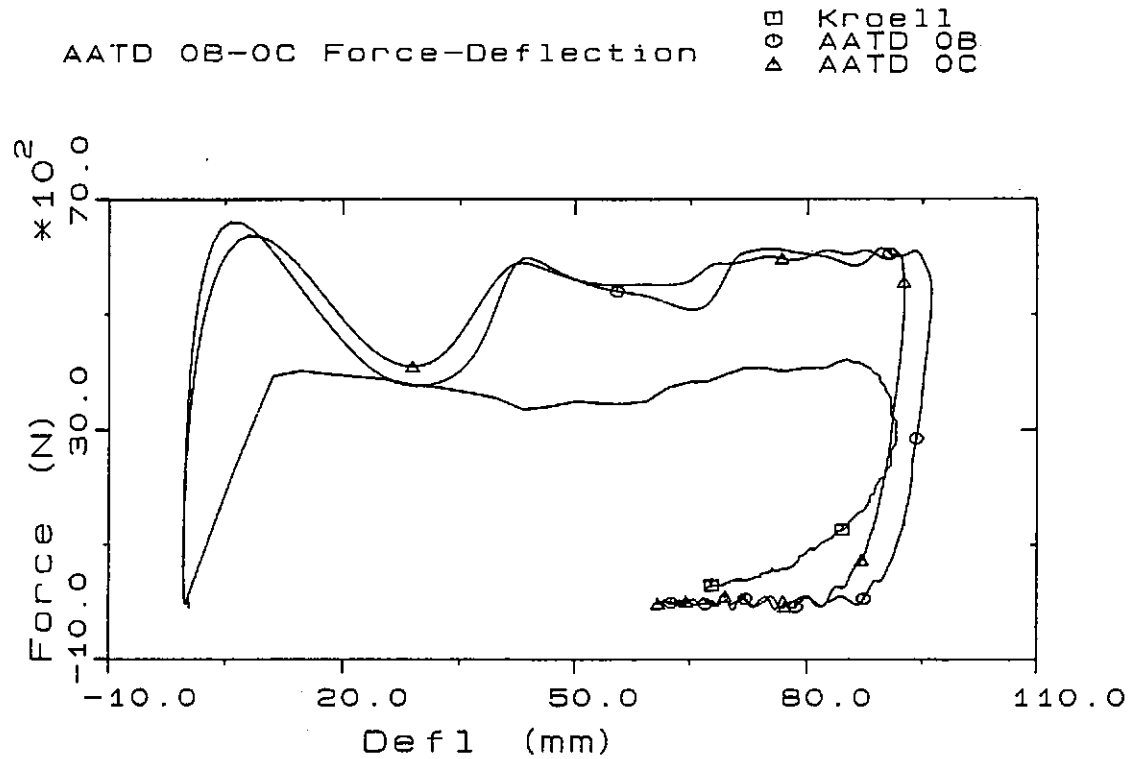

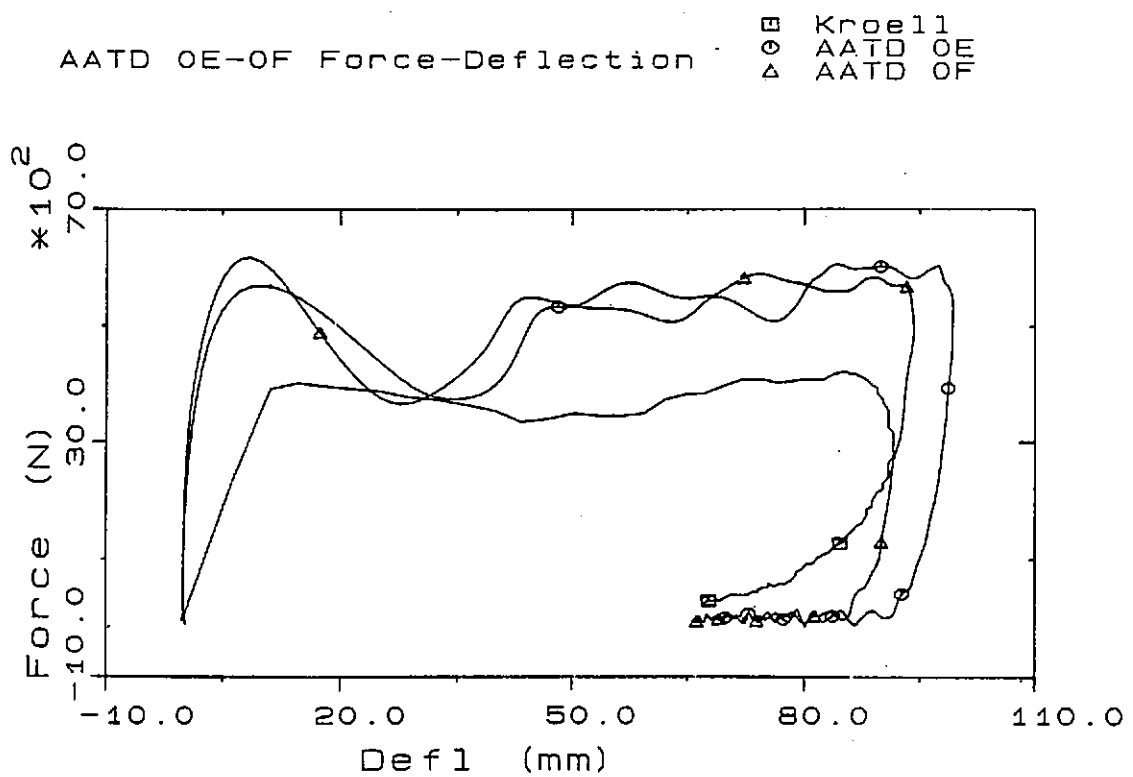

FIGURE 4–9. Comparison of Hexcell F-δ response to Kroell et al. (1974) impact F-δ curve at 6.7 m/s.

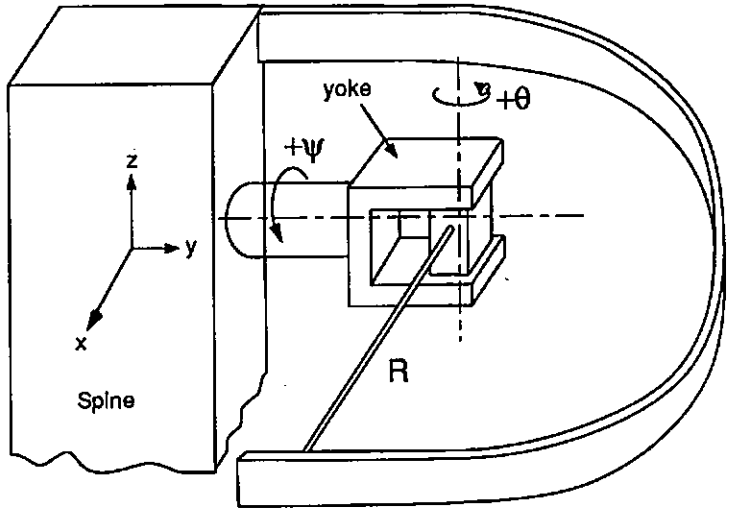

FIGURE 4–10. Measurement of three-dimensional rib displacement using two angles and a length.

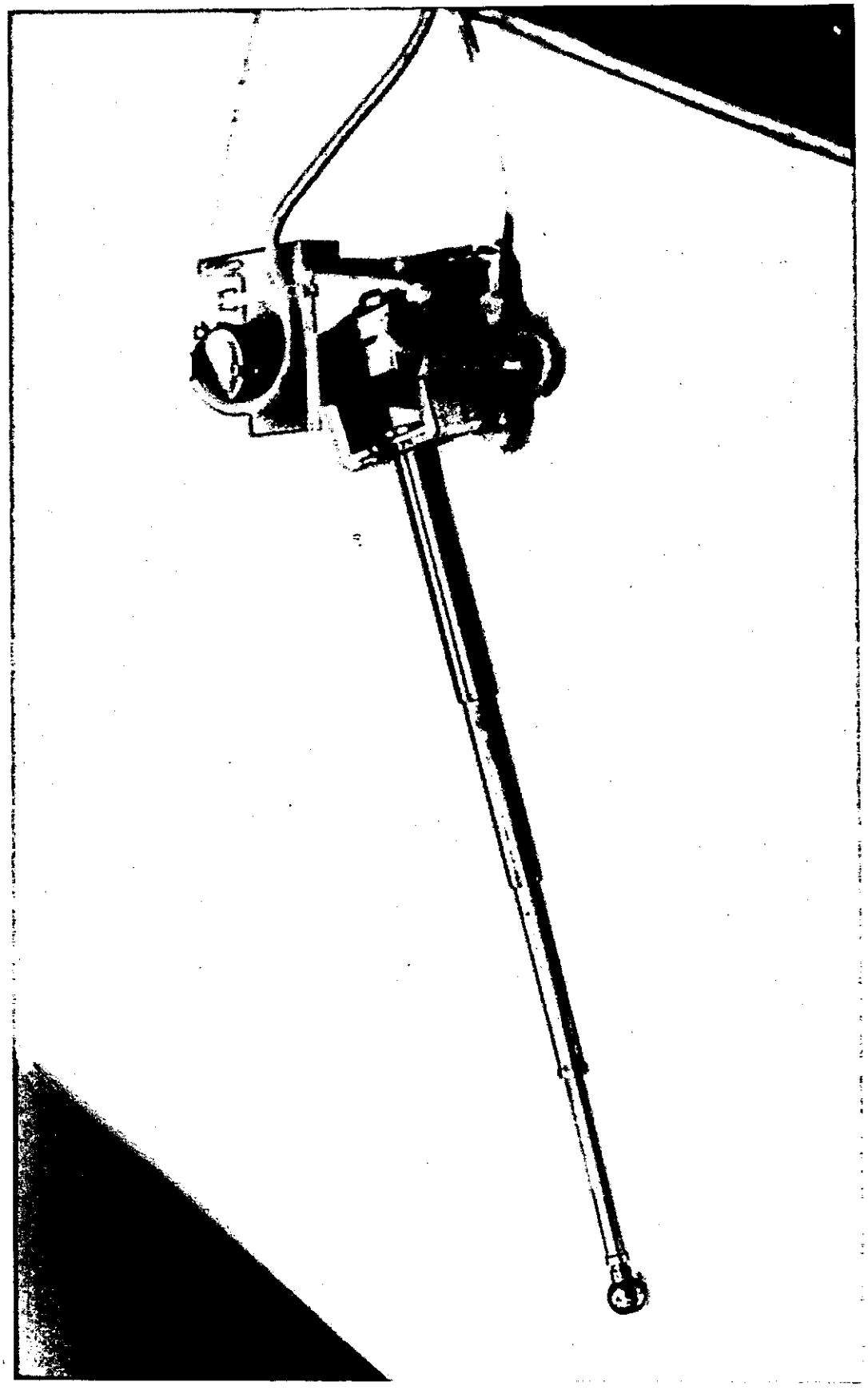

FIGURE 4–11a. Prototype of double-gimballed collapsing joy stick in fully extended mode.

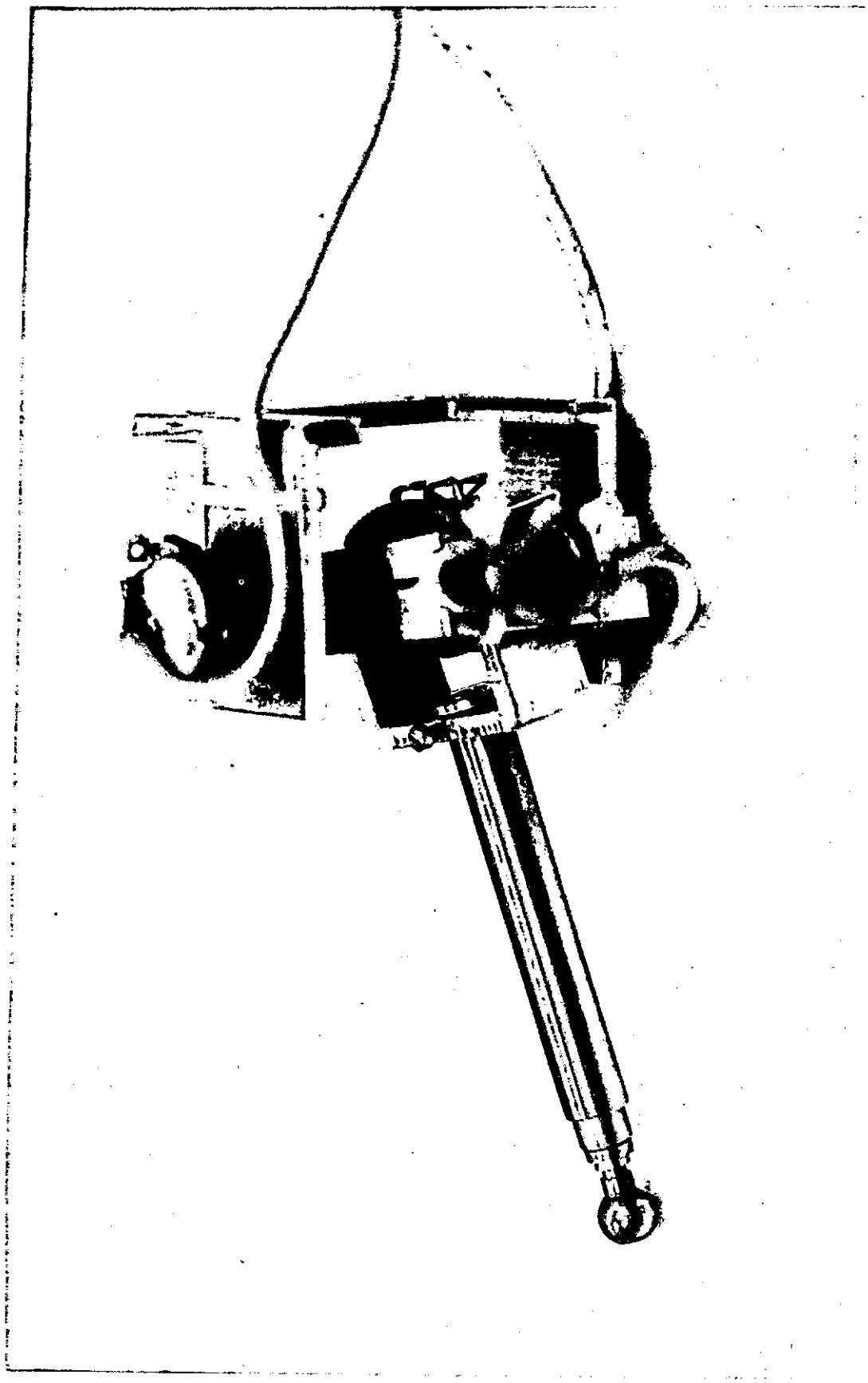

FIGURE 4–11b. Prototype of double-gimballed collapsing joy stick in fully collapsed mode.

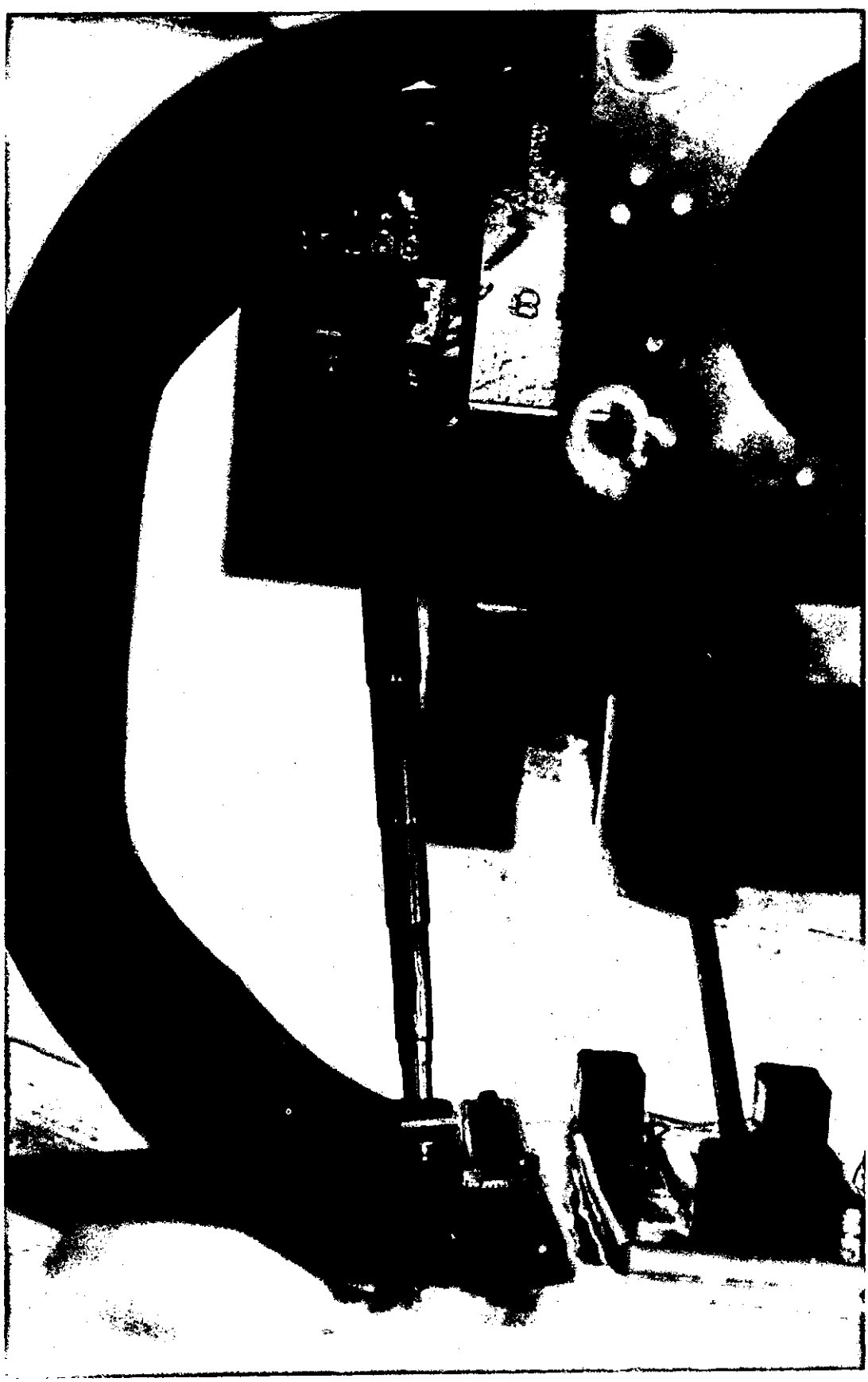

FIGURE 4–12. Prototype of double-gimballed, collapsing joy stick installed in Hybrid III chest.

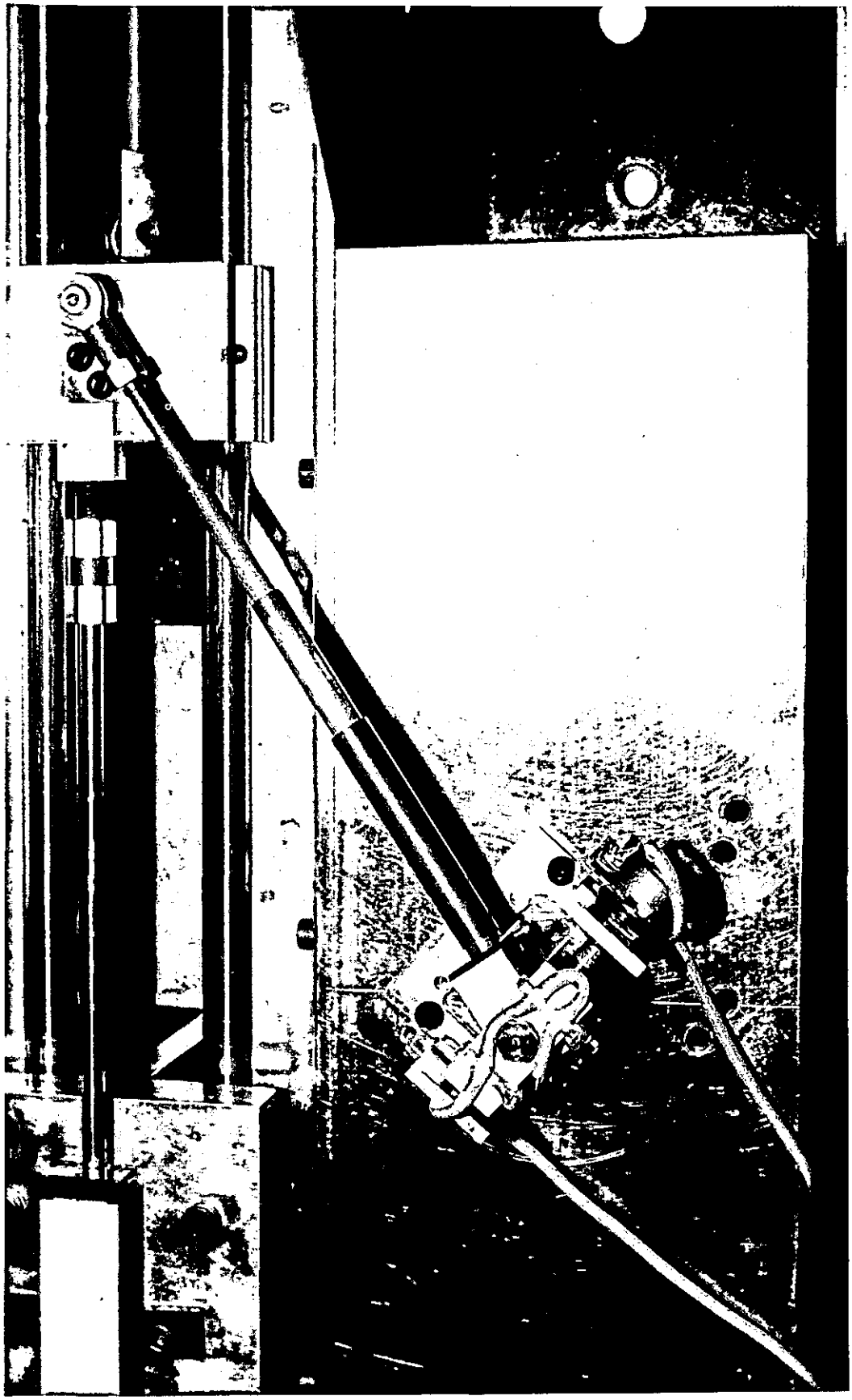

FIGURE 4–13. Top view of test setup for evaluating prototype of double-gimballed collapsing joy stick under combined AP and lateral loading.

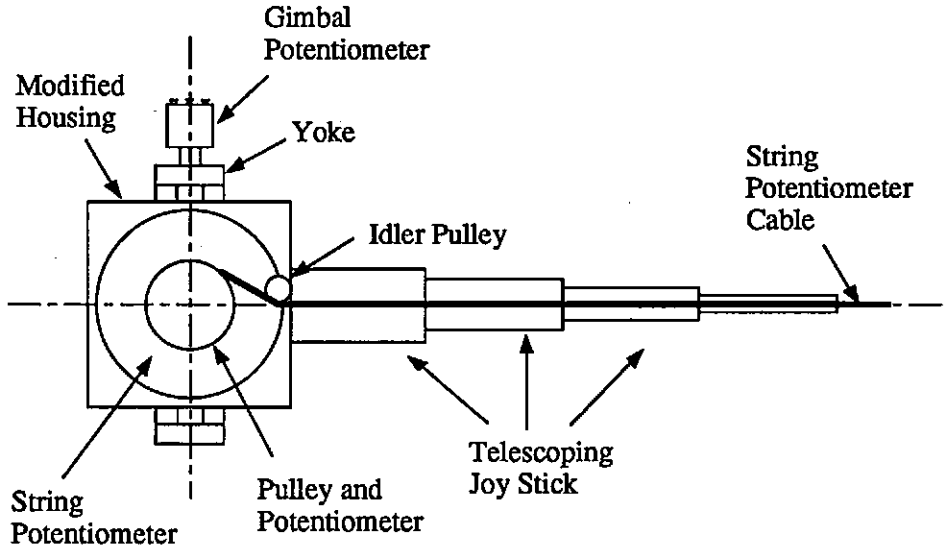

FIGURE 4–14. Schematic drawing of double-gimbal string potentiometer (DGSP) with cable running down the center and in line with the center of gimbal rotation.

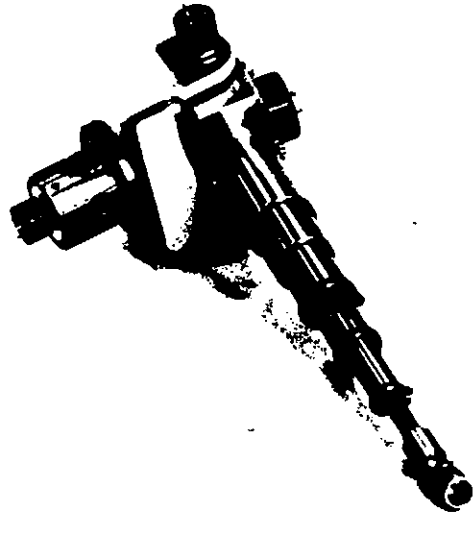

FIGURE 4–15. Double-gimballed string potentiometer with collapsing joy stick.

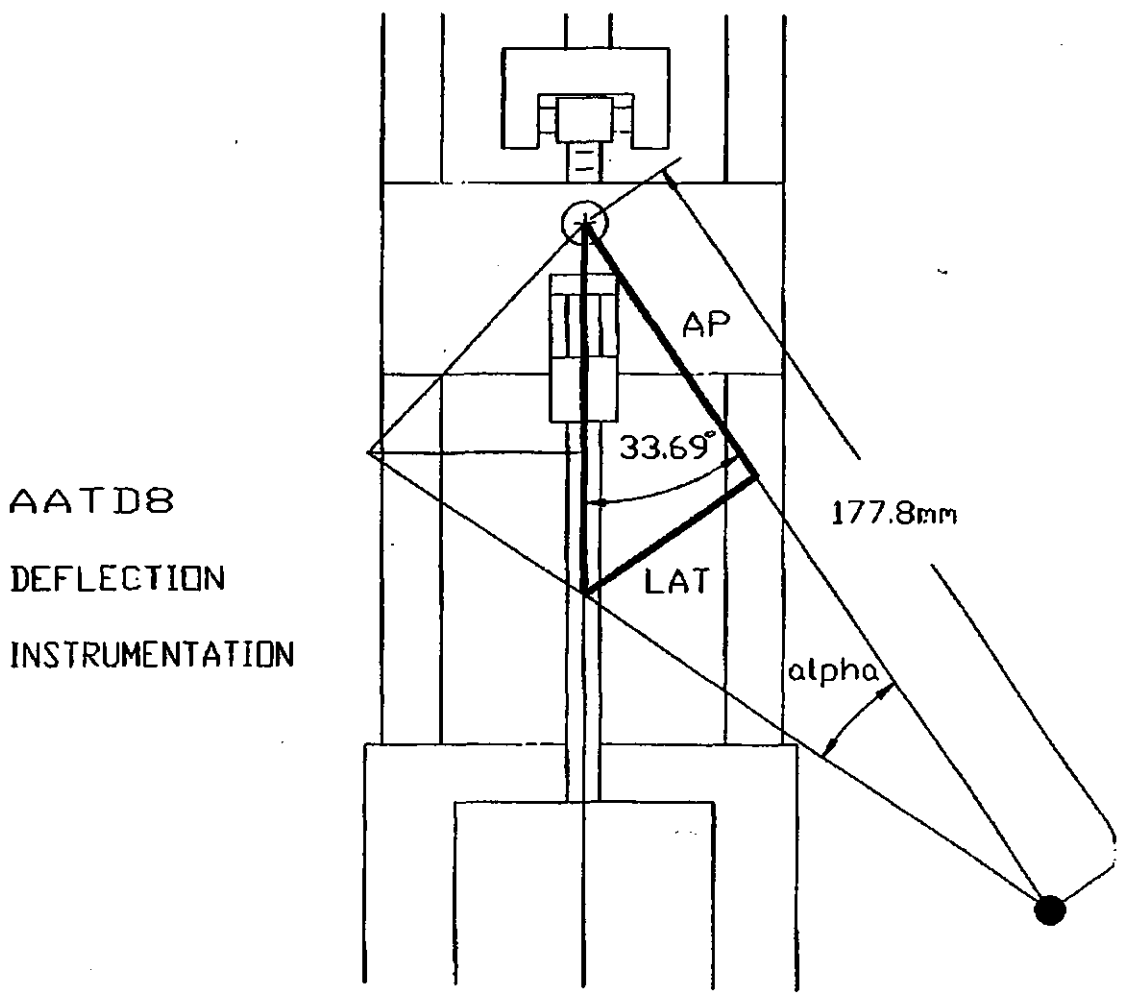

FIGURE 4–16. Schematic drawing of instrumentation test facility showing relationships of input direction to defined AP and lateral directions.

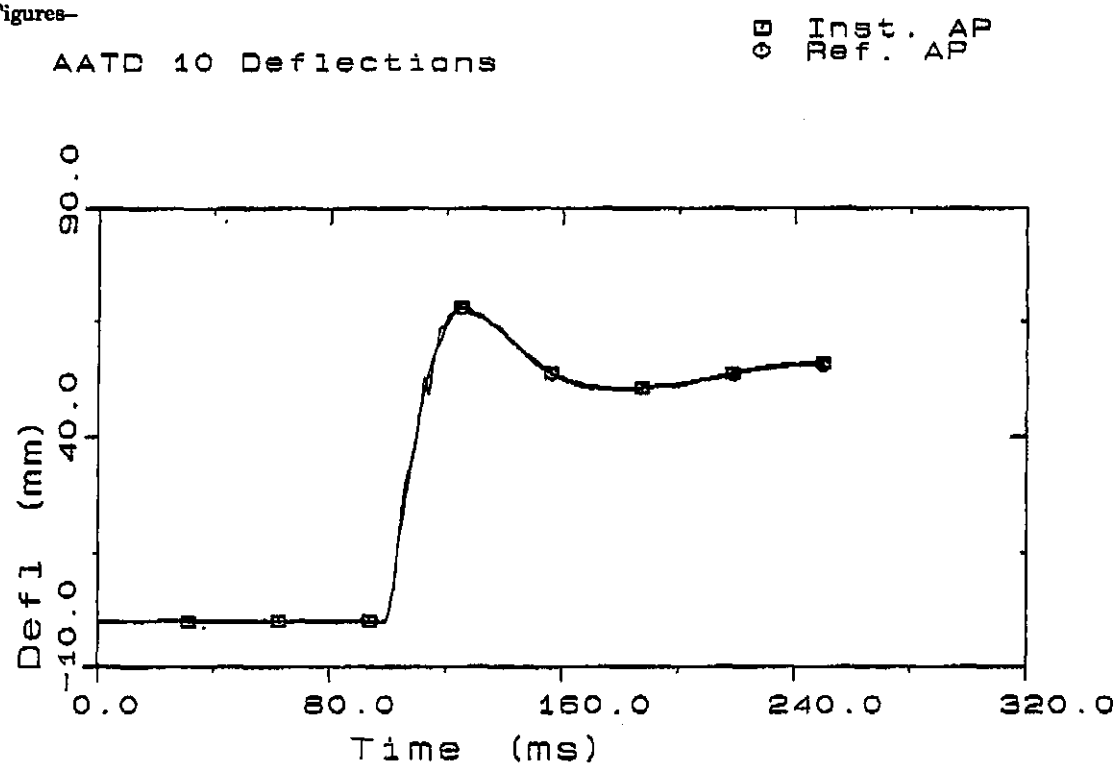

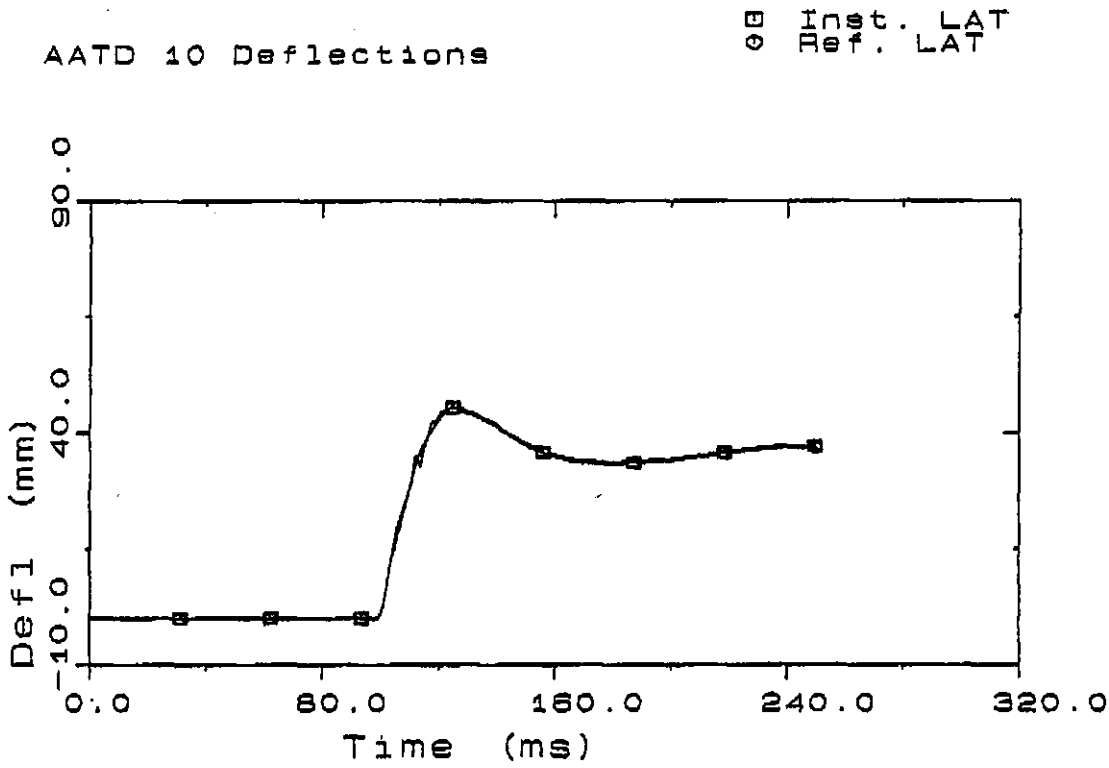

FIGURE 4–17. Comparison of AP and lateral deflection measurements from double-gimballed string potentiometer with telescoping joy stick to results from linear potentiometer installed on test facility. Top: AP deflections; Bottom: lateral deflections.

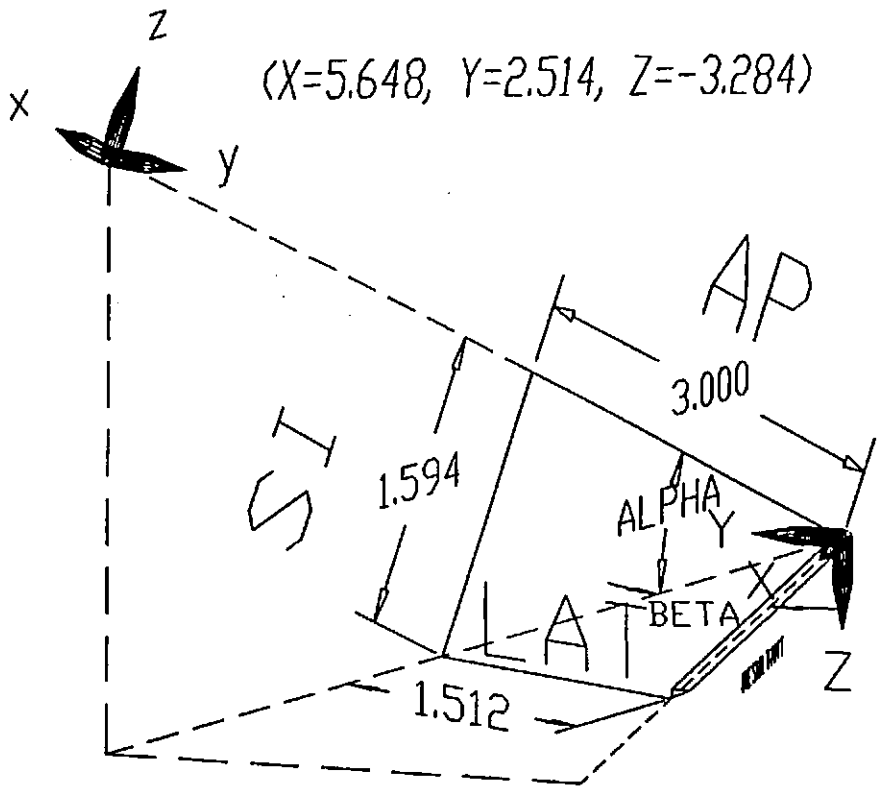

FIGURE 4–18. Three-dimensional test geometry for evaluating DGSP.

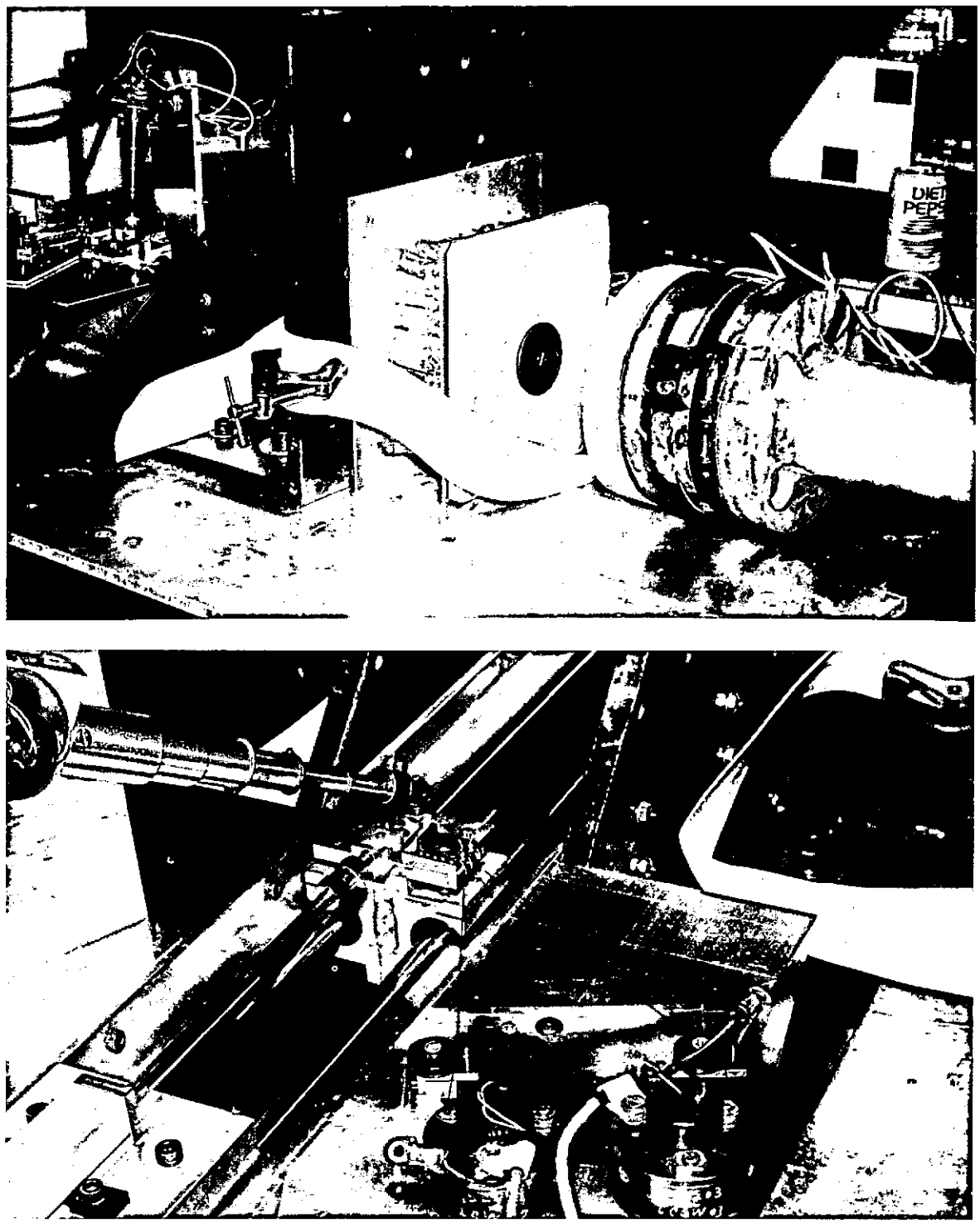

FIGURE 4–19. Setup for three-dimensional testing of DGSP along with two-dimensional testing of triangulated string potentiometers.

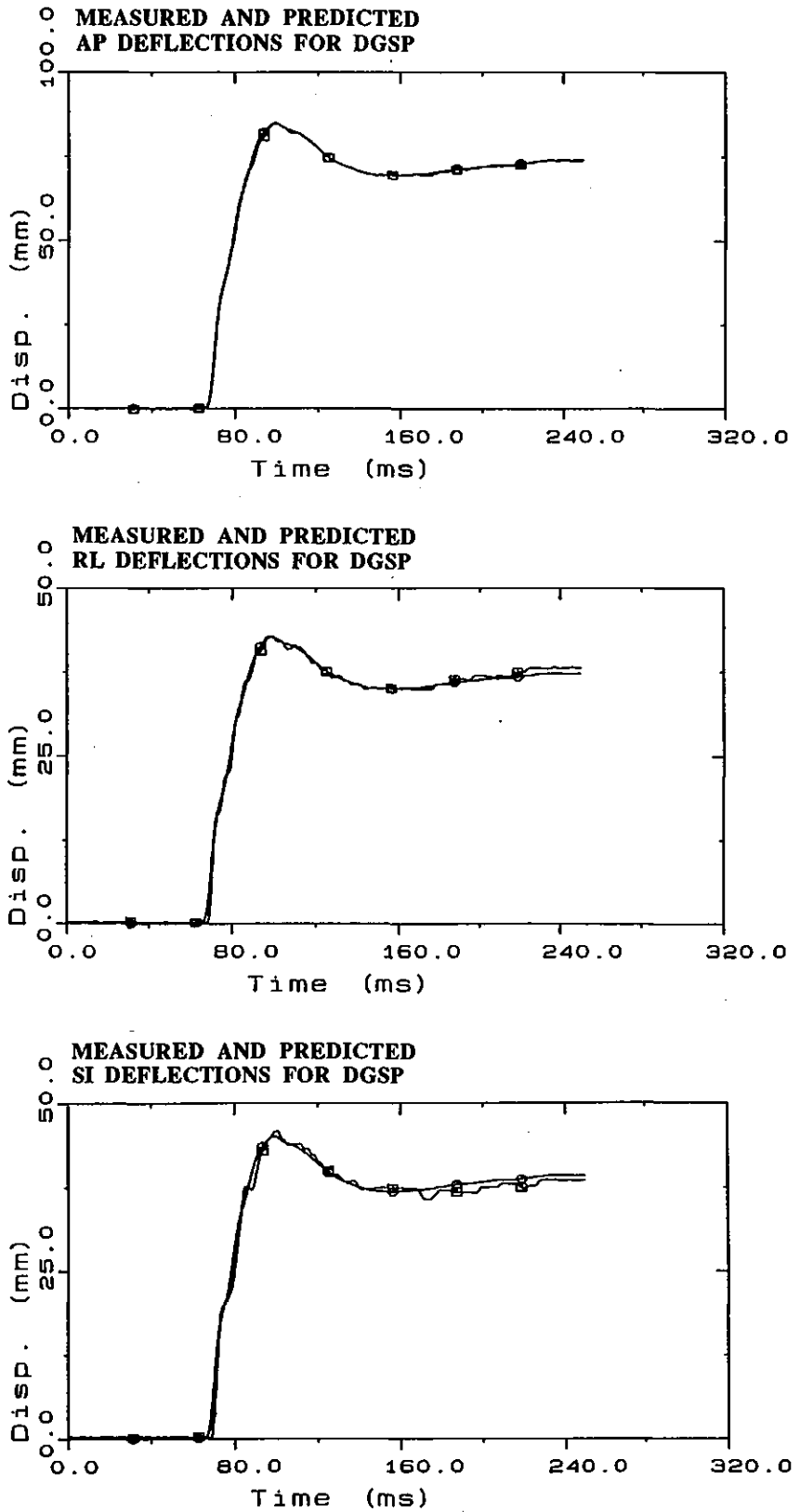

FIGURE 4–20. Comparison of measured and expected AP, RL, and SI deflection for DGSP.

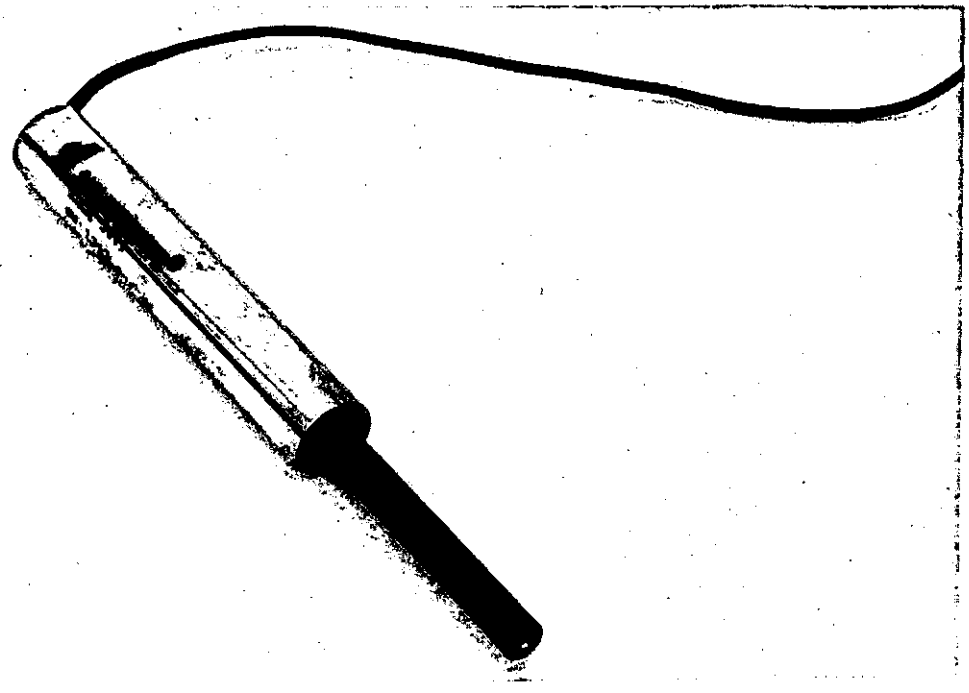

FIGURE 4–21. Data Instruments' linear displacement transducer.

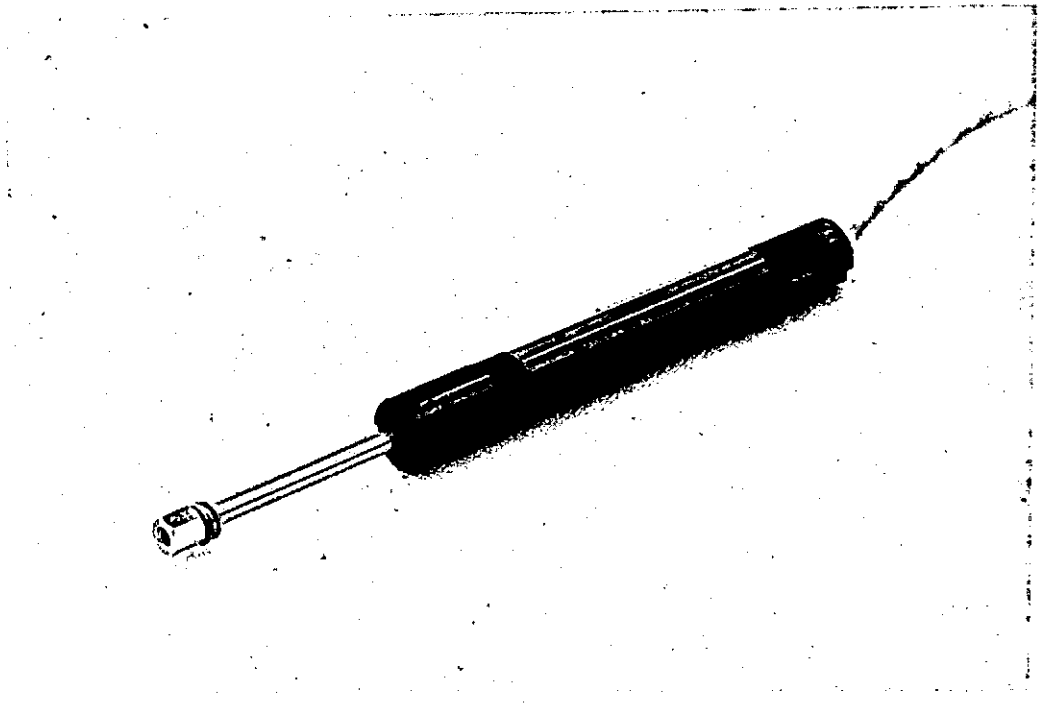

FIGURE 4–22. Linear potentiometer with 75-mm (3-in) stroke and 100-mm (4-in) body length.

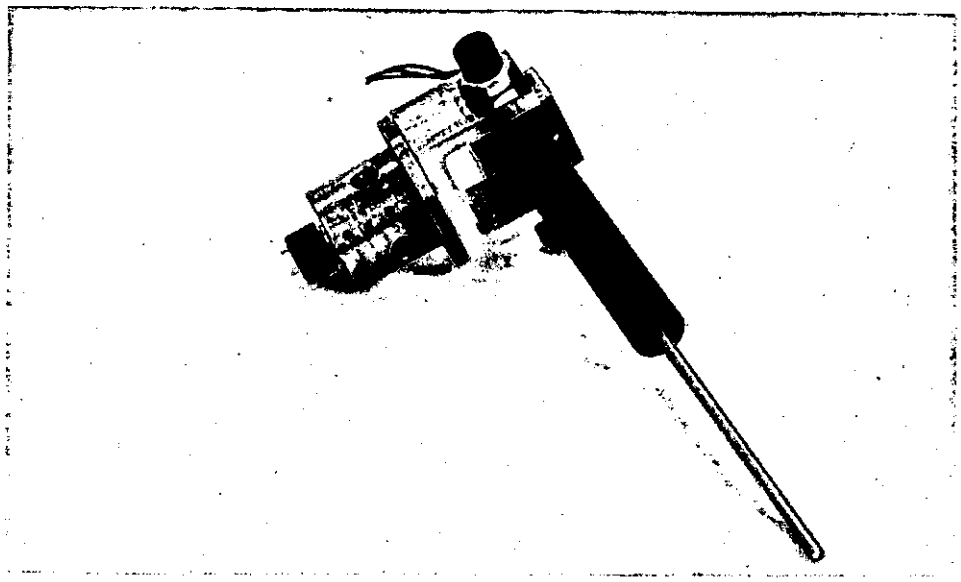

FIGURE 4–23. Double-gimballed linear potentiometer.

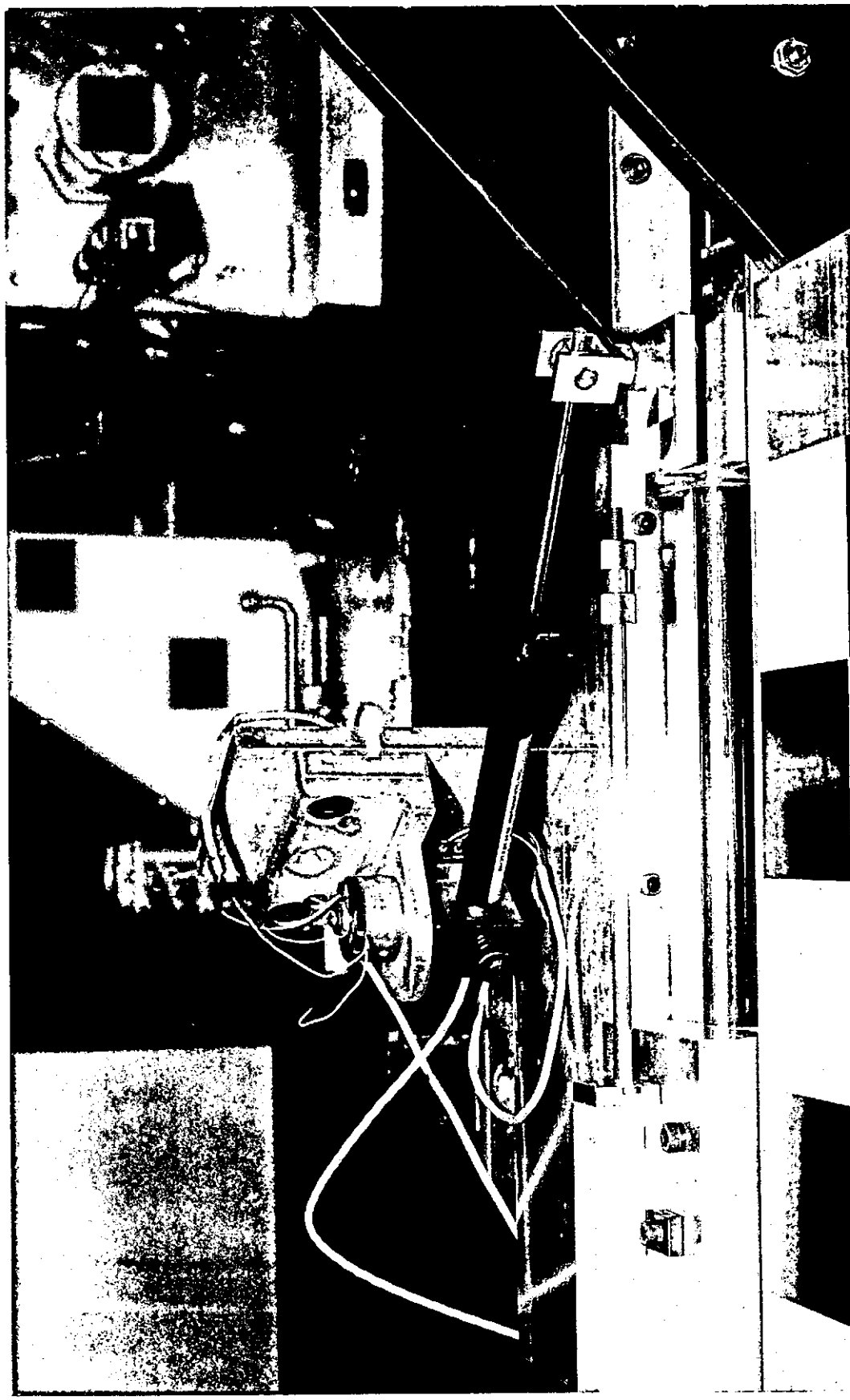

FIGURE 4–24. Double-gimballed linear potentiometer mounted on test facility.

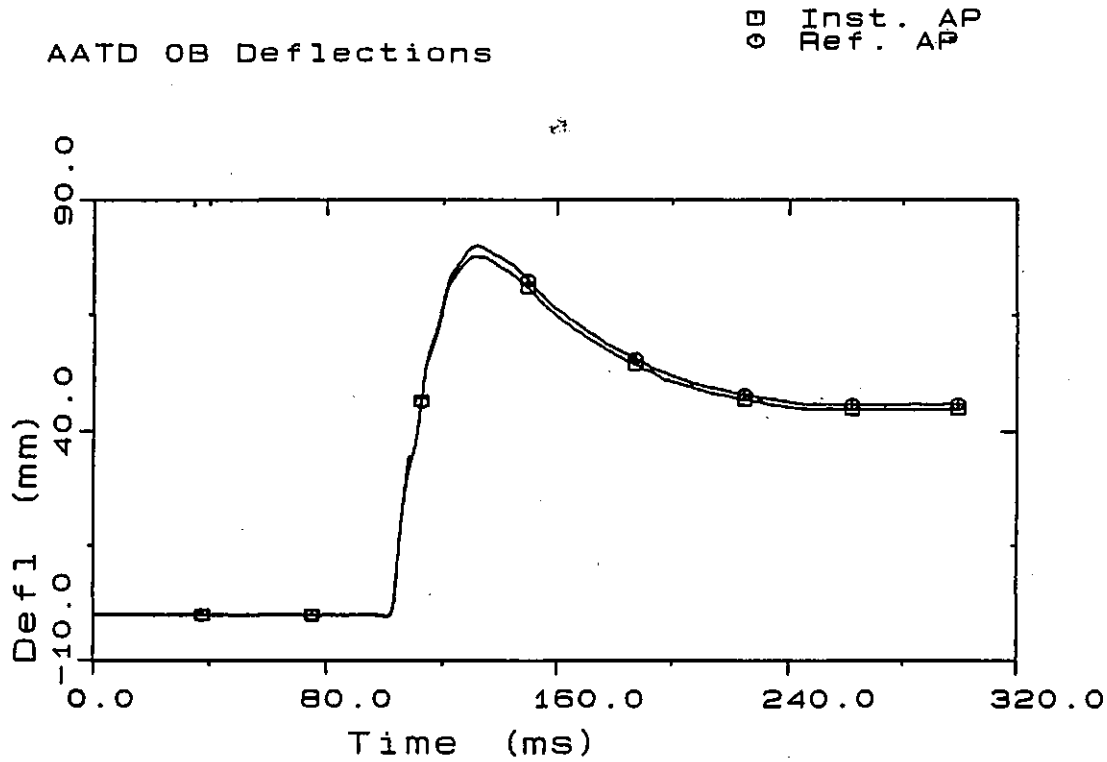

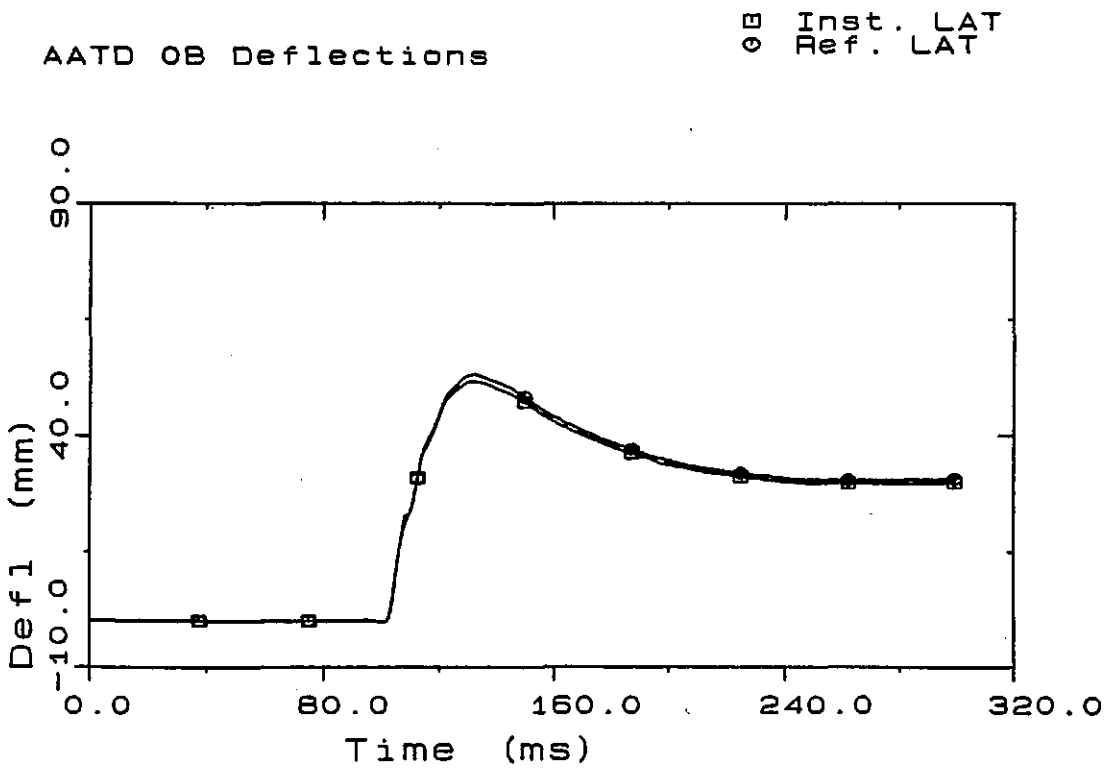

FIGURE 4–25. Comparison of AP and lateral deflection measurements obtained from gimballed linear potentiometer with calculated values from fixture linear potentiometer and known geometry. Top: AP deflections; Bottom: lateral deflections.

5. DESIGN OF FIRST AND SECOND PROTOTYPE-50M THORAX ASSEMBLIES

5.1 OVERALL DESIGN

In designing the new thorax system, an effort was made to follow the anthropometry and posture of the 50th-percentile-male AATD-50M drawings within the constraints imposed by the need to interface with existing Hybrid III components. To do this, a transparent mylar, full-size, side-view drawing of the AATD-50M with skeletal components was superimposed on a full-size, side-view drawing of Hybrid III with the H-points aligned and the C7/T1 articulation of the AATD-50M aligned to the approximate center of the base of the Hybrid III neck. As shown in Figure 5–1, when this is done the following relevant differences between the two drawings can be noted.

- The chest line of Hybrid III is approximately 25 mm forward of the chest line of the AATD-50M from the base of the neck to the abdomen where it intersects with the bulging abdomen line of the AATD-50M.
- The back line of AATD-50M is about 25 mm rearward of the back line of Hybrid III from the level of about T6 to L6, but the line merges with the Hybrid III pelvis at the bottom of the buttock.
- The C7/T1 articulation in the AATD-50M aligns with the level of the base of the Hybrid III neck (i.e., the bottom of the lowest rubber disk).
- The head and face of Hybrid III are approximately 25 mm higher than for AATD-50M, but the two align at approximately the same position front to back.
- The anterior-superior iliac spines (ASISs) and pelvic crests of Hybrid III are significantly more forward than for AATD-50M.
- The spine box of Hybrid III lies significantly forward of the vertebral bodies of AATD-50M.
- The ribs of Hybrid III are inclined upward at about 17 degrees to the horizontal with the dummy in the normal seated posture, while the ribs of the AATD (i.e., the human skeleton) are sloped downward at about 20 degrees to the horizontal for a difference of about 37 degrees between the angle of the human ribs and the angle of the Hybrid III ribs.
- The top Hybrid III rib corresponds to the level of the third human rib at the front of the chest and the level of the sixth or seventh rib at the spine.
- The bottom or sixth Hybrid III rib corresponds to the level of the seventh or eighth human rib at the front of the chest and to the level of the eleventh or twelfth human rib at the spine.

It will be noted that the top of the head of the Hybrid III drawing is somewhat higher than that of the AATD-50M when the H-points are aligned. An investigation into this concern led to the finding that the Hybrid III eye height had been based on an estimate of driver eye height relative to H-point height for a 50th percentile male using population eyellipse data (Roe 1975). The results are shown in Table 5–1 and indicate that, for a 24-degree seatback angle (the average seatback angle used in the AATD anthropometric study),

TABLE 5–1

MEAN MALE EYE LOCATION ACCORDING TO SEATBACK ANGLE, REFERENCE TO H-POINT (Roe 1975)

Back Angle deg	X_e		Z_e	
	in	cm	in	cm
5	−7.61425	−19.3402	26.6125	67.5957
6	−7.04924	−17.9051	26.5612	67.4655
7	−6.49041	−16.4856	26.5067	67.3269
8	−5.93776	−15.0819	26.4488	67.1799
9	−5.39129	−13.6939	26.3875	67.0244
10	−4.851	−12.3215	26.323	66.8604
11	−4.31689	−10.9649	26.2551	66.6881
12	−3.78896	−9.62396	26.184	66.5073
13	−3.26721	−8.29871	26.1095	66.318
14	−2.75164	−6.98917	26.0316	66.1204
15	−2.24225	−5.69532	25.9505	65.9143
16	−1.73904	−4.41716	25.866	65.6997
17	−1.24201	−3.15471	25.7783	65.4768
18	−0.75116	−1.90795	25.6872	65.2454
19	−0.26649	−0.676885	25.5927	65.0056
20	0.212	0.53848	25.495	64.7573
21	0.68431	1.73815	25.3939	64.5006
22	1.15044	2.92212	25.2896	64.2355
23	1.61039	4.09039	25.1819	63.9619
24	2.06416	5.24297	25.0708	63.6799
25	2.51175	6.37984	24.9565	63.3895
26	2.95316	7.50103	24.8388	63.0907
27	3.38839	8.60651	24.7179	62.7834
28	3.81744	9.6963	24.5936	62.4676
29	4.24031	10.7704	24.4659	62.1435
30	4.657	11.8288	24.335	61.8109
31	5.06751	12.8715	24.2007	61.4699
32	5.47184	13.8985	24.0632	61.1204
33	5.8699	14.9098	23.9223	60.7625
34	6.26196	15.9054	23.778	60.3962
35	6.64775	16.8853	23.6305	60.0215
36	7.02735	17.8495	23.4796	59.6383
37	7.40079	18.798	23.3255	59.2467
38	7.76804	19.7308	23.168	58.8466
39	8.12911	20.6479	23.0071	58.4381
40	8.434	21.5494	22.843	58.0212
41	8.83271	22.4351	22.6755	57.5959
42	9.17524	23.3051	22.5048	57.1621
43	9.51159	24.1594	22.3307	56.7199
44	9.84176	24.9981	22.1532	56.2692
45	10.1658	25.821	21.9725	55.8101

the vertical eye-to-H-point distance is 637 mm (25.1 in) while the front-to-back distance is approximately 52 mm (2 in).

In the AATD-50M drawing, the vertical H-point-to-eye distance is exactly 636 mm (25 in) and, thus, in excellent agreement with the predicted distance for a 50th percentile male. This observation suggested that the AATD-50M drawing should be followed rather than the Hybrid III drawing with regard to the H-point-to-eye vertical distance. It was subsequently learned that the Hybrid III assembly drawings may not accurately reflect the dimensions of the actual Hybrid III dummy that should, in fact, be in good agreement with the AATD-50M drawing with respect to the H-point-to-eye vertical distance, if the goal of the 50th-percentile-male eye height was successfully achieved in the Hybrid III hardware.

The front-to-back H-point-to-eye distance in the AATD-50M drawing is about 100 mm (4.0 in), which is about 50 mm (2-in) greater (eye more rearward) than the distance for a 50th-percent-male base on the eyellipse data shown in Table 5–1 for a 24-degree seatback angle. An explanation for this difference is not apparent but, since the AATD-50M data were based on measurements for both eye location and an estimate for human H-point (see Robbins 1985a) from subjects seated in a normal, relaxed driving posture, it was decided to follow these data in the first prototype. Thus, in developing the architecture of the new thorax assembly, an attempt was made to follow the AATD-50M front and back contour lines rather than those of the Hybrid III.

5.2 RIBCAGE

After several iterations overlaying drawings of prototype designs on the AATD-50M drawing with skeletal rendering, and several iterations of acrylic and cardboard models of prototype thorax assemblies, an eight-rib configuration was established for the first hardware prototype. In the first acrylic model, a chest form was hand sculpted from a block of Styrofoam formed by gluing multiple layers of 25-mm-thick Styrofoam sheets together as shown in the top half of Figure 5–2. The model was used to determine layout patterns for the ribs that would allow for humanlike contouring of the ribcage without the stair-stepping effect that results from using straight strips of steel in a slanted rib model. While this effort was successful in the acrylic model shown in the bottom of Figure 5–2, and offered significant advantages to coupling and unitizing the ribcage, it was the general consensus of the project staff that fabrication of these patterned ribs would be expensive and that attachment of damping material would pose further difficulties and cost problems in manufacturing.

A decision was therefore made to fabricate the ribs for the first hardware Prototype-50M using standard 19-mm (0.75-in) wide, 1.6-mm (0.0625-in) thick strips of 1075 steel, and to vary the angle at the back of the spine to accommodate the desired rib angles. Figures 5–3a and 5–3b show a cardboard model developed at NHTSA and an acrylic model developed concurrently at UMTRI to assist in the design process. Figure 5–4 shows an overlay drawing of the initial slanted eight-rib ribcage on the AATD-50M side-view drawing.

As illustrated, the top rib attaches to the upper sternum and provides chest stiffness in this region. In the normal seated posture, it is oriented horizontally with the ATD, which allows it to fasten to the spine below the neck load cell and shoulder. The second rib is angled downward at three degrees, the next at six degrees, the fourth rib at nine degrees, and the four bottom ribs at ten degrees to the horizontal. As described in Section 5.4, the thoracic spine of this first prototype was segmented at approximately the level of T7/T8 on the AATD-50M so that the top four ribs attached to the upper thoracic spine and the bottom four ribs attached to the lower thoracic spine. The spacings of the ribs were adjusted appropriately to accommodate this configuration and, as illustrated, were larger at the front of the chest for the top four ribs than at the back due to the incrementally increasing rib angles.

Figures 5–5a through 5–5d show photographs of the first hardware Prototype-50M and illustrate the shape of the ribcage. The slopes of the new ribs represent a compromise between the Hybrid III ribs and human ribs in that the angles of the ribs increase from horizontal at the top rib to ten degrees downward slope for ribs four through eight. The top rib aligns approximately with rib two of the AATD-50M drawing at the front of the chest, while the bottom, or eighth, rib aligns with the front of rib ten. From the side view, the ribcage was shaped to follow the contour of the human ribcage as represented in the AATD-50M drawing. From the front view, the width of the ribcage widens from the top and narrowest rib to rib six. Also, the ribcage mimics the human geometry anteriorly near the midline so that the distances between the anterior ends of ribs two through four are constant with the sternum in between, while the distances between the anterior ends increase from rib five through rib eight to form the abdominal cavity, which is unprotected by the ribcage in the human. The distance between the anterior ends of the first rib is less than for ribs two through four since this rib attaches to the top portion of the sternum (see Section 5.3 below).

The ribcage of the second and current Prototype-50M is very similar to that of the first prototype except for the removal of the bottom or eighth rib due to its close proximity to the pelvis and consequent modifications in spacing and orientation of the ribs. Figures 5–6a and 5–6b show front- and side-view drawings of the current Prototype-50M assembly and illustrate the planar contours of this seven-rib thorax. The top or first rib remained horizontal in the normal seated position and the angles of the next three ribs increase from three to nine degrees as in the first prototype. The nine-degree angle was maintained for the lower three ribs, however, instead of changing to ten degrees.

Some reshaping of the ribs was also done for the second prototype. Figure 5–7 shows an overlay of the seven ribs as viewed from the top, where each rib is shown in its respective plane. In the first prototype, the contour of the ribs had been modified from those of the Hybrid III ribs, which are flat on the sides and have relatively small radii at the corners of the hoops. An attempt had been made in the first prototype to increase these radii to make the rib hoops more elliptical and humanlike but, in the second prototype, these radii were reduced, especially at the back of the ribcage, to provide maximum space for the chest displacement transducers. At the lower ribcage, the front-to-back depths of the rib hoops were also increased to reduce the possibility of interference with the ASIS of the pelvic bone and to provide maximum space and stroke distance for the lower ribcage response and instrumentation. In addition, the contours of the rib hoops were adjusted from those of the first prototype to distribute the stair-stepping between adjacent ribs, and especially between ribs four and five across the thoracic spine articulation, to facilitate implementation of ribcage coupling. As shown in Figure 5–8, the ends of the steel ribs were twisted prior to heat treating to provide a smooth surface to attach the bib.

5.3 STERNUM AND RIBCAGE COUPLING

Throughout the development process, various designs for the sternum were examined and tested. Because of concerns that the top of the sternum might bottom against the upper spine due to the reduced space for compression available in this region, and that this would restrict further compression of the chest at the levels of the mid and lower sternum if the sternum were made from a single rigid piece, it was decided to separate the sternum into top and bottom segments hinged together by the urethane bib. In this way, the bottom of the sternum would be free to continue to pivot and move inward should bottoming occur at the top of the sternum. This feature was found to be particularly important during calibration testing with a 152-mm (6-in) diameter rigid loading plate where it is necessary to place the top edge of the loading plate below the edge of the upper sternum in order not to limit chest displacement due to bottoming of the upper sternum on the upper thoracic spine.

Figure 5–9 shows the upper and lower segments of the current version of the sternum while Figure 5–10 shows a drawing of the upper portion that is made of mild steel and is designed for attachment of the clavicle rod ends (see Section 5.5.3). Originally, the lower part of the sternum was made of aluminum but this was also changed to mild steel to increase sternal mass. Because of reported problems with the Hybrid III sternum rotating ninety degrees on the bib hinges under certain types of loading conditions, the bottom portion of the new sternum was made narrower and more humanlike in its dimensions in an attempt to reduce the tendency and/or consequences of this rotation. In the second prototype, the lower sternum is made from a 6-mm (0.236-in) thick piece of steel cut to approximately 38 mm (1.5 in) by 115 mm (4.5 in) and is slightly bent to follow the anterior contour of the chest.

In a modification of the sternum, the top segment was divided into left and right halves in an attempt to provide additional compliance and a greater degree of independence between the two shoulders. This three-piece sternum was subsequently judged to provide too much decoupling and instability, however, and the single-piece upper sternum was retained.

Throughout the process of testing the first prototype thorax, various modifications were made to the manner in which ribcage coupling was accomplished at the front of the chest. In the first prototype, two layers of durometer-90 Shore A urethane were cut to follow the shape of the anterior ribcage and were fastened to the sternum and rib ends using buttonhead screws, washers, and nuts. One modification to the coupling at the front of the ribcage involved the use of two (i.e., inside and outside) steel plates for the lower sternum with the inner plate sandwiched between two layers of urethane bib. The concept is illustrated in Figure 5–11, which also shows how the ends of the ribs were fitted with wedges of urethane material so that a softer, more compressible Sorbothane material could be installed between adjacent rib ends. It had been hoped that the more substantial coupling at the front of the chest offered by this construction would increase the stability of the ribcage at the flexible thoracic spine, but little effect was achieved and this approach was not implemented in the second prototype.

Additional coupling up and down the ends of the ribs on each side was achieved by connecting the rib ends with thin strips of spring steel. Originally, these strips were placed over the outer layer of urethane, but permanent deformation and failure of the material was noted in the initial series of belt-restrained sled tests. An attempt to place these strips between two layers of urethane, as shown in Figure 5–12, also resulted in plastic deformation of the steel and these bands were therefore not included in the final version of the second prototype.

5.4 SPINE

5.4.1 Thoracic Spine of the First Prototype-50M

From the outset, flexibility in the thoracic spine was considered important to the overall biofidelity and kinematics of the new thorax system, although it soon became clear that including this feature might have a significant influence on system performance and impose additional constraints on chest deflection measurement hardware. Numerous approaches to implementing a single flexible link near the middle of the thoracic spine at about T7/T8 were examined, but the spine for the first prototype utilized the rubber spine from a standard Hybrid-II-type, six-year-old dummy since it was immediately available. Figures 5–13a through 5–13d show photographs of the thoracic spine for the first prototype, including the six-year-rubber spine and the upper and lower thoracic spine segments. In its original configuration, the end plates molded into the six-year-old rubber spine were simply bolted to the steel plates welded inside each thoracic spine segment. To reduce the length of rubber column contributing to bending and thereby effectively stiffen the six-year-old spine,

the ends of the rubber cylinder were captured in steel "cups" placed between the rubber segment and the spine mounting plates.

The rigid upper- and lower-spine segments of the first prototype were designed with rectangular cross sections, although consideration was given to using a T-shaped spine if this appeared to offer advantages with regard to placement of instrumentation. (The idea of using a T-shaped spine was a primary consideration for a thorax design based on internal fluid-filled response elements.) The upper spine segment was comprised of two side plates with two steel plates welded inside at specified angles for mounting the neck bracket or lower neck load cell and the six-year-old rubber spine. The front of the upper spine was left open for access to fasteners and the back was enclosed with a stair-step plate with the steps positioned and angled for mounting of the four upper ribs at the angles described in Section 5.2. The shoulder pivot blocks (described in the following section) were bolted to the front-top corners of the upper spine segment.

The lower thoracic spine of the first prototype was of similar construction but also included a mounting plate for the triaxial chest accelerometer block at the top-front of the spine segment (not shown in figures), which is close to the AATD-50M thorax center-of-gravity. As in the upper thoracic spine segment, the back consists of stair-step plates for mounting the four lower ribs at the specified angles. In this first prototype, the lower thoracic spine segment also provided space for the Hybrid III T12 load cell just below the thoracic spine articulation mounting plate.

5.4.2 Spine of the Second Prototype-50M

After conducting pendulum tests with the first Prototype-50M, incorporating the thoracic spine described in the previous section, it was determined that the modified rubber six-year-old spine was too flexible, particularly during initial positioning of the dummy. It was found that the static torque due to the dummy components above the rubber segment was sufficient to flex the rubber spine significantly forward of the design seated posture. In addition, it was determined that the length of spine taken up by this articulation would present significant problems in terms of allowing space for mounting of chest deflection transducers. As a result of these concerns, a shorter rubber segment was molded for the second prototype and the angles of the mounting plates in the upper and lower thoracic spine segments were adjusted to compensate for bending during static preload so that the dummy would achieve the desired pretest seated posture.

Figure 5–14 shows the molded rubber segments for both the thoracic flexible link and the new lumbar spine that was required to interface the new thoracic spine with the pelvis. Both pieces are molded with durometer-70 Shore A natural rubber and with steel end plates for attaching to the rigid segments of the spine. In addition, bilateral steel cables were incorporated into the assemblies to provide durability and lateral stability.

Figure 5–15a shows a drawing of the complete spine of the second and current Prototype-50M, while Figure 5–15b shows front- and side-view photographs of this spine assembly. Compared to the spine of Hybrid III, the new spine has a more natural and continuous curvature from the pelvis to the top of the neck. In order to prevent possible interaction of the upper sternum with the neck, the Hybrid III cantilevered neck bracket/load cell is replaced with a new component that fastens directly above and in line with the upper thoracic spine segment. The Hybrid III neck is also positioned directly on top of this neck bracket or load cell and is angled forward at approximately nine degrees to achieve the same head position as in Hybrid III. However, in order to maintain the same head orientation, it was necessary to modify (i.e., bevel) the head nodding block at the top of the Hybrid III spine.

The upper thoracic spine segment is essentially the same as in the first prototype with small changes in the locations and angles of the back of the spine to accommodate small changes in the design of the ribcage. The smaller molded rubber element has been moved up, however, so that it corresponds approximately to the level of T7 in the human. This was done primarily to increase the length of the lower thoracic spine segment to allow all chest deflection instrumentation to be mounted to it. Note also that the lower thoracic spine segment is reduced in depth to allow the joy sticks of the DGSP units (see Section 4.5) to rotate inward as far as possible and the stair-step plate at the back provides for only the three lower ribs of the seven-rib thorax used in the second prototype.

Modifications to the lumbar spine were necessary to connect between the Hybrid III pelvic block and the new location and design of the lower thoracic spine, which was rearward of the current Hybrid III spine relative to the pelvis. The lumbar spine for the first prototype used the straight rubber spine from the 5th-percentile-female dummy. However, for the lumbar spine in the second and current prototype, a special mold was made to fabricate the stiffer segment shown in Figure 5–14. This consists of steel plates molded into the ends of a block of durometer-70 Shore A natural rubber with holes provided for two bilaterally positioned steel cables. Because of the need to install gimbals and potentiometers inside the lower thoracic spine segment, it was necessary to eliminate the T12 load cell from the second prototype. This was partially compensated for, however, by changing the configuration of the lumbar load cell located at the top of the pelvic ballast block to make it a six-axis load cell instead of a five-axis load cell as is currently used in Hybrid III.

5.5 DESIGN OF SHOULDERS AND COMPONENTS

5.5.1 Overall Design Goals Re Human Shoulder Function

For a belt-restrained occupant involved in a frontal crash, an effective restraint system will allow the shoulder to take a significant proportion of the restraint load so that a minimal amount of force and energy will be transferred to the chest and abdomen. As indicated in Figure 5–16, there is concern that the proportionate sharing of load by the thorax and shoulder may be significantly different for two- and three-point belt systems where the kinematics of the body are likely to be significantly different. With the two-point shoulder-belt/knee-bolster system, the lower torso will tend to translate forward, thereby reducing the forward movement of the shoulder (i.e., flexion of the hip and torso), causing greater loading on the lower ribcage. With an effective three-point lap-/shoulder-belt system, the pelvis will be restrained sooner causing the torso to flex forward, resulting in a beneficial increase in load taken by the shoulder complex.

What is not clearly understood is how the compliance and mobility of the shoulder complex and its interaction and coupling with the chest (i.e., the ribcage) influence the proportion of load and deflection experienced at the chest versus the shoulder by an ATD. In the absence of such information, it must be concluded that biofidelity in shoulder kinematics, mass distribution, and coupling to the chest are important in order for the crash dummy to represent the human appropriately with regard to these kinematic and restraint interaction issues.

As noted in Section 2.1.7 of this report, the Hybrid III shoulder has been designed for high durability, but is not very humanlike with regard to mobility and performance under impact loading. In fact, high-speed films of 48 km/h (30 mph) belted cadaver tests and belted dummy tests conducted in the mid-1970s at UMTRI (then HSRI) for General Motors (Melvin et al. 1975, Alem et al. 1976, 1977, 1978) demonstrate that, even under the asymmetric loading imposed by a diagonal shoulder belt, both shoulders of the Hybrid III dummy move relatively little and very symmetrically with respect to the spine while, under identical restraint geometry, the shoulders of the cadaver move significantly forward and

upward, but quite asymmetrically. It can be expected that the living, tensed human will respond somewhere between these two extremes.

Unfortunately, data that quantitatively describe the kinematics of the different shoulder components and their effective mass properties during crash loading conditions do not exist. In the absence of such data, the shoulder design must be based on an understanding of the mobility and range of motion of the shoulder complex and its components under voluntary movements. The most descriptive information on voluntary shoulder movement and mobility was obtained and described by Dempster (1965). As shown in Figure 5–17, the shoulder consists of three skeletal components or links—the scapula, the clavicle, and the humerus. To understand the movement of the shoulder, it is necessary to understand the manner in which these structures connect and interface with each other and the thoracic ribcage. The key elements are the following.

- The clavicle pivots in three dimensions at its connection with the lateral superior corner of the sternum (sternoclavicular articulation) as illustrated in Figure 5–18.

- The scapula slides along the posterior ribcage mediolaterally as well as in the superior-inferior direction. In its lateral region, it connects with the lateral end of the clavicle to form the claviscapular articulation, and with the humerus where it forms the glenoid fossa on which the head of the humerus rides. In a general sense, the scapula slides on the posterior ribcage with the clavicle acting as a "radius arm" pivoting about the sternoclavicular joint.

- The movement of the scapula has significance in that it allows the lateral end of the clavicle to move and allows the reorientation of the glenoid fossa.

- The head of the humerus rotates within the glenoid fossa (i.e., the glenohumeral joint) and pivots about an eccentric pivot at the head-fossa interface (i.e., not at the center of the humeral head), which contributes to additional fore/aft movement of the shoulder.

The net result of the shoulder linkage geometry and the allowed range of sliding and rotating movements of the different interfaces and articulations is a wide and complex range of arm movement patterns and ranges of motion as shown in Figure 5–19. In a crash dummy, it is probably unnecessary and prohibitive—from cost, durability, and performance perspectives—to simulate the complete shoulder structure and its full mobility. Rather, the shoulder movements most critical to dummy/restraint-system performance are considered the first priority. For this project, the critical kinematics are those required for biofidelic performance under *frontal* impact testing conditions. It was also considered important, however, to provide some compliance or movement for lateral loading that may occur during contact with the vehicle door during frontal impacts into a 30-degree-oblique barrier.

5.5.2 Evolution of Shoulder Design

Assuming that a shoulder belt has its primary interaction with the shoulder through the clavicle, a critical question is with regard to the extent and nature of clavicle movement during shoulder belt loading. A review of high-speed films of belted cadaver sled tests did not offer much additional insight into this question since it was impossible to distinguish between movement of the shoulder due to rotation of the humerus in the glenoid fossa and movement of the shoulder due to rotation of the clavicle (and sliding of the scapula) about the sternoclavicular joint. Intuitively, one would expect the clavicles to rotate forward due to inertial loading of the arms on the scapula, and for the shoulder on one side to be pushed rearward by direct loading of the shoulder belt. During a given crash test, a combination of both forward and rearward movements of the clavicle on the shoulder belt side may occur

depending on the timing of these different forces on the shoulder complex and the location of the shoulder belt on the clavicle (i.e., medial versus lateral positioning).

Based on the above analysis, it was concluded that the new shoulder design should include a claviclelike structure articulating at, and connecting to, the top of the sternum, and that both forward and rearward pivoting of the clavicle about the sternoclavicular articulation should be provided. Upward movement of the shoulder complex (from the initial pretest condition) was considered of secondary importance, to be included in the design at this time only if it could be easily accomplished without additional sacrifice in cost and durability. While downward mobility of the shoulder did not seem important, some downward compliance was considered desirable since it would serve to reduce stresses in the structure. In addition, some degree of lateral compliance was considered important, primarily to prevent damage to the shoulder structures during impact with door components during frontal tests into a 30-degree-oblique barrier.

In the process of designing a dummy shoulder to achieve these goals, a review of other dummy shoulder designs was conducted. Of the dummy shoulders examined, those of the Ogle/MIRA dummy shown in Figures 5–20a and 5–20b had the greatest appeal. In this design, a shoulder beam is attached to the spine by means of a ball and socket joint surrounded by rubber disks to provide compliance and limit range of motion with soft "stops." A scapulalike structure slides in a slot machined into this beam and a claviclelike component connects between the distal end of the scapula and the sternum by means of spherical rod ends.

While this design was attractive from the point of view that it mimics the human shoulder kinematics reasonably well (i.e., sliding scapula, clavicle pivoting at sternum, etc.), it lacks stability in the initial position and is suspected to be mechanically noisy and lacking in durability. An effort was therefore made to design and develop a prototype shoulder using a modified version of the Ogle/MIRA shoulder in which the ball joint at the spine is replaced with a simple pin joint to prevent downward movement of the shoulder and undesirable mechanical interaction with the ribcage. A satisfactory solution to the design of the sliding mechanism could not be found that would provide the support and stability needed, and a number of alternative design approaches to the shoulder were subsequently considered. These included a design based on modifying the Hybrid III shoulder to increase front/back range-of-motion (i.e., increasing the mobility at the clavicle/shoulder pivot joint) and designs based on flexible steel ribs or rubber columns.

With regard to modifying the Hybrid III shoulder, a review of belted cadaver sled tests indicated the importance of providing compliance and compression of the sternoclavicular articulation relative to the spine (i.e., in belted cadaver runs the shoulder belt "digs in" significantly at this region). While living, tensed humans may not demonstrate this phenomenon as dramatically as the cadaver, provision for greater compression and compliance at the sternoclavicular joint than provided in Hybrid III was nonetheless considered to be an important factor in the shoulder/thorax system. Because of this, it was necessary to either remove or move the elevation "box" on the front of the Hybrid III thoracic spine by which the shoulder attaches to the spine and is provided with limited up/down mobility.

Figure 5–21 shows top and front sketches of a significantly modified Hybrid III shoulder design in which the Hybrid III shoulder-elevation mechanism has been moved to the side of the spine. The front/back pivot of the Hybrid III shoulder was maintained as close to the spine as possible, but the mobility of this articulation was increased significantly over that provided in the Hybrid III shoulder. In the sketch shown, a second pivot is provided on the arm clevis mounting bracket to simulate the eccentric rotation of the humerus in the glenoid fossa. The illustration does not show a clavicle which, in this design, was envisioned to be a rigid shelf extending from the top of the center shoulder piece (i.e.,

between the two front/back pivots) with a compliant section extending inward and downward in front at the ribs and sternum, but not attaching to the latter.

Consideration was also given to changing the arm/shoulder clevis to a ball-and-socket joint in order to accomplish the eccentric movement (i.e., the hunching) that occurs in the human by eccentric rotation of the glenoid fossa. Such a mechanism would replace the outer pivot and arm clevis, but was considered to present problems controlling initial positioning and joint resistance (i.e., friction).

A second modification of this design, which provided for mounting of the clavicle or clavicle "shelf" to the shoulder through a load cell, was also considered. However, the geometric requirements for implementing the load cell necessitated unreasonable compromises in the basic shoulder design and the idea of incorporating load measurement capability in the shoulder was subsequently set aside in the present effort.

Another design for the shoulder that was considered is illustrated in Figure 5–22. In this approach a 50- to 75-mm (2- to 3-in) wide steel rib forms the basic shoulder support structure, and is also intended to provide for, and limit, shoulder front/back mobility under inertial and direct loading. This design does not provide for up/down mobility of the shoulder but, in theory, would allow the clavicle to connect between the distal end of the curved shoulder rib and the sternum without the need for sliding parts. Pivoting of the clavicle at the sternum could take place if the shoulder rib straightens or bends, resulting in an effective extension or compression of this shoulder link (i.e., to simulate sliding of the scapula). The shoulder rib, it was argued, could be designed to wrap around and behind the ribcage, thereby eliminating the potential for ribcage/shoulder interaction.

Subsequent to building an acrylic model of this shoulder design, shown in Figure 5–23, calculations of force, stress, and excursion relationships were made and suggested serious problems with this approach. It was found, for example, that the forces required to straighten out a shoulder rib capable of supporting the arm weight and resisting the inertial forces from the arms with desired range-of-motion limits, would impose significant inward forces on the sternum. Furthermore, these calculations revealed that stresses could exceed material yield levels in the shoulder rib unless a double-rib design was implemented, which would diminish the space advantage of the single-rib approach, while still not resolving the problem of high inward forces at the sternum.

5.5.3 Final Shoulder Design

Upon further examination of the shoulder rib design concept, it was realized that the problem of forces at the sternum could be reduced by attaching the arm clevis mounting bracket to the main shoulder rib by a simple pivot joint. That is, instead of depending on the supporting rib to straighten out during forward movement of the shoulder, the mounting bracket for the arm clevis would pivot, thereby extending the effective length of the linkage between the spine and the clavicle. In essence, the three-bar shoulder linkage (spine to clavicle, clavicle to sternum, and clavicle to spine) would be replaced with a four-bar linkage (spine to clevis mount, clevis mount to clavicle, clavicle to sternum, and sternum to spine). However, this change alone does not eliminate the problem of exceeding yield stresses in the shoulder rib, nor does it deal with the issues of elastic bending (and resulting oscillations) and high initial stiffness of the shoulder (i.e., there is essentially no low resistance, normal range-of-motion as in the human shoulder).

With a desire to keep a thorax design that improves representation of the upper ribcage over that offered by Hybrid III, evaluation and study of the acrylic model with shoulder ribs led to a decision to replace the shoulder rib with shoulder support "beams" mounted to each side of the spine by means of pivot blocks. As with the modified version of the shoulder-rib approach, the arm clevis mounting brackets would also pivot in pin joints

located at the ends of the shoulder beams, thereby maintaining the four-bar linkage concept needed to allow the desired clavicle rotation.

Figure 5–24 shows top- and front-view drawings of this shoulder design, which was chosen for use in the final prototype. In order to minimize the rotation required between the clevis mounting bracket and the shoulder support, and to reduce the potential for interaction of this bracket with the ribcage, the inboard pivot point was mounted as far forward on the spine box as possible and the main shoulder support beam was angled rearward in the initial position. Also, the pivot just inboard of the arm clevis (i.e., pivot for simulating eccentric movement of the arm) was eliminated to simplify and stabilize the design.

Figure 5–25 shows a top view of the shoulder bushing blocks attached to the top of the thoracic spine and the rubber stops used to limit and control the shoulder range-of-motion. A steel "finger" extends down from the rear of the main shoulder support on each side into the gap between the two rubber blocks. Rearward range-of-motion is limited by the smaller rubber block attached to the spine while forward range-of-motion is controlled by the L-shaped rubber block, which is attached to the shoulder bushing block.

While this shoulder design does not directly include lateral compliance, the rearward mobility and initial rearward angulation of the main shoulder supports provide for some "give" and energy absorption during contact of the shoulder with the door structure in frontal-oblique barrier tests. As with the shoulder rib design, this approach allows the upper thoracic ribs to be included since the main shoulder supports bridge over the upper ribs and the arm clevis mounting bracket hangs lateral to the two upper ribs. Figure 5–26 shows this shoulder concept implemented in the acrylic model.

5.5.4 Estimates of Peak Shoulder Belt Loads

In order to determine the size and material requirements for the components of this shoulder design, particularly with regard to the design of the main pivot blocks at the spine box where the highest torques were expected, computer simulations of a belted Hybrid III dummy using the MVMA-2D Crash Victim were examined. Figure 5–27 illustrates the general model configuration for the shoulder belt. In one run, a two-point shoulder belt with a knee bolster was simulated with the angle of the upper shoulder belt at about 27 degrees to the horizontal (angle θ in Figure 5–27) during the onset of belt loading. The impact conditions for this run involved a velocity change of 54 km/h (33.6 mph) and a peak deceleration of 24 Gs. For the second run, a three-point belt was simulated with an upper shoulder belt angle of about 24 degrees to the horizontal at the onset of belt loading. In this test, the impact conditions were those of a 65 km/h (40.8 mph) velocity change and a 37.7 G peak deceleration.

For the 65 km/h (40.6 mph) three-point-belt run, the peak downward load on the shoulder was 4137 N (930 lb), while for the 54 km/h (33.6 mph) two-point-belt run, the peak downward force was 5115 N or 1150 lb (6825 N and 11394 N for 54 km/h and 65 km/h, respectively). The downward force was considered to be the most important with regard to the pivot strength requirements since no compliance or movement was provided in this direction in the current design.

Using a peak downward load of 5115 N (1150 lb) and assuming that the shaft for the main shoulder pivot would be free to rotate (i.e., there would be no torsion in the shaft itself), a 19-mm (0.75-in) diameter shaft was determined to offer a sufficient safety margin if a high-strength alloy, heat-treated steel was used. It was also determined that a high-quality bushing could withstand the side loads and offer a smoother, quieter, less bulky, and less costly solution to the main shoulder pivot at the spine than ball or roller bearings.

5.5.5 Instrumentation for Shoulder Loads

As noted in the description of design goals listed in Section 2.1, it was originally desired to provide for measurement of belt loads on the shoulder as a way of comparing the performance of different restraint systems. As previously noted, the requirements for installing a two-axis load cell on a version of the modified Hybrid III shoulder were explored with R.A. Denton, Inc., but preliminary design efforts suggested the need for substantial modifications and compromise in the shoulder design, and efforts to incorporate shoulder load measurements were discontinued.

In the final shoulder design with a clavicle made from cylindrical stock, consideration was given to installing two-axis load cells at both ends of each clavicle. The concept is illustrated in Figure 5–28, which shows a cover over the load cell so that forces can be sensed for the full length of the clavicle. An analysis by R.A. Denton, Inc. indicated that the required diameter of the load cell was about 19 mm (0.75 in), thereby requiring a clavicle diameter, including load-cell cover, of about 25 mm (1 in) or greater. This was considered impractical for the current design and resulted in a decision to drop further consideration of shoulder load measurement in the current effort, while emphasizing the development of a fimctional, durable, and kinematically improved shoulder system.

However, as a carry-over from the interest in shoulder load measurement, R.A. Denton, Inc. proceeded to develop the prototype two-axis strain-gage clavicle load cell shown in Figure 5–29 using the machined shafts of rod-end bearings at the ends of the clavicles. The sum of the shear loads at each rod end would, in theory, represent the force applied to each clavicle. While the system requires testing and evaluation, there is some concern about the durability of the machined, 8-mm (0.313-in) diameter shafts, especially if the limits of rod-end movement are reached during shoulder movement. Also, in preliminary sled runs of a prototype chest (see Section 6), the shoulder belt was observed to move onto the sternum and did not stay between the ends of the clavicle. In this situation, the loads measured by the rod-end load cells would not represent the total load on the shoulder.

5.6 PELVIS

Although the pelvis was not included in the original project scope, it was necessary to implement preliminary modifications to this component to accommodate the new ribcage and abdomen. As noted previously and shown in Figure 5–1, the anterior-superior iliac spines (ASISs) of the Hybrid III pelvic bone are higher and more forward than those of the AATD-50M when the H-points of both are aligned. Since this higher pelvic bone interferes with the lower ribcage of the Prototype-50M, the pelvic crests of the Hybrid III bone were cut down about 25 mm (1 in) and back about 25 mm to match the AATD-50M drawings, which are in good agreement with the dimensions of the average male pelvis developed by Reynolds et al. (1981). Figure 5–30 compares the Hybrid III pelvic bone to the modified pelvic bone for which the contours of the ASIS were also reshaped (i.e., indented below the ASIS) to provide anatomical similarity to the human pelvis.

The Prototype-50M pelvis was molded with the modified pelvic bone positioned in the Hybrid III pelvic mold approximately 25 mm forward of its usual position. This had the effect of moving the back line of the pelvis approximately 25 mm rearward to improve its position relative to the spine of the new thorax assembly. While this process extended the length of the thigh portion of the pelvic mold, the distance from H-point to the knee remained the same as in Hybrid III. As shown in Figure 5–31, the skin and flesh (i.e., urethane foam) at the front of the Hybrid III pelvis have been cut away between the left and right ASISs to provide for placement of the frangible abdomen insert described below. Also, the vinyl skin has been cut down above the crest of the pelvic bone to reduce interference with the ribcage.

5.7 ABDOMEN

It had been hoped that the pursuit of fluid-based, internal response elements, described in Volume 2 of this report, would lead to a solution for a biofidelic and injury-sensing abdomen. However, when the decision was made in favor of a highly modified, damped-rib approach, an alternative solution to the abdomen was needed. While it is believed that a fluid- or fluid/gas-based abdomen will offer the best long-term solution to this dummy component, the current project has used a modified version of the GM frangible abdomen (Rouhana et al. 1989, 1990) as an interim solution.

The most significant modification to the design of the insert used in Hybrid III was the change from a five-point design to a two-point design as shown in Figures 5–32a and 5–32b. This change was necessitated by the more humanlike ribcage geometry and the desire to measure the motion of the lower ribs with instrumentation connecting between the ends of the sixth rib and the spine.

The new frangible abdomen consists of a two-point Styrofoam insert and a support bracket that installs between the lumbar spine and the pelvic ballast block. The biofidelity of the Styrofoam insert is assured by designing it with humanlike force-deflection properties using the corridors developed by Rouhana et al. (1989) as shown in Figure 5–33. Tests were performed with standard belt webbing positioned about 12 mm (0.47 in) below the top surface of the insert. As seen, the corridor is met by the two-point insert, although its apparent stiffness decreases after 60 mm (2.4 in) of deflection.

Figure 5–34a shows the abdomen support bracket installed between the pelvic block and the lumbar spine, while Figure 5–34b shows the frangible abdomen installed in the new pelvis assembly. By removing the abdomen flesh of the Hybrid III pelvis, more humanlike and independent inward deflection of the abdomen is allowed. This design change is considered important if realistic interaction of the lap belt with the pelvic bone is to be achieved with more humanlike geometry and girth of the abdomen and location and size of the pelvic bone. In the latest version of the Prototype-50M, the frangible insert is held in place against the reaction plate by a long screw through a wedge of hard urethane positioned at the bottom of the "V" between the two Styrofoam points, and by a steel "finger" extending out from the support bracket into a cutout in the insert.

5.8 INSTRUMENTATION

5.8.1 Chest Deflection Instrumentation

While evaluation of both the double-gimballed linear potentiometer and the double-gimballed string potentiometer (DGSP) with telescoping joy stick showed both systems to perform well (see Sections 4.5 and 4.6), upon fitting the two systems inside the dummy chest, the DGSP was found to offer a small but significant advantage in stroke length. It was also felt that this transducer had greater durability and a decision was therefore made to build and install four of these units in the second Prototype-50M for measuring chest displacements at the sternum and lower ribcage.

Figure 5–35 shows different views of the dummy chest and spine with these units installed. The two top units are attached to the upper part of the lower thoracic spine segment on each side just below the rubber articulation, while the bottom two units are attached to the bottom of the lower thoracic spine. The collapsing joy sticks for the two sternal transducers are connected to the ends of rib three on each side of the sternum by means of small universal joints, while the lower units are attached to the ends of rib six in a similar manner. The up/down gimbals are housed in the spine as are the rotary potentiometers that measure the up/down rotations. The rotary potentiometer for each yoke gimbal is attached to the pivot on one side of the yoke and measures the left/right movement

of the ribcage point as an Euler angle whose output must be interpreted in terms of the rotation and position of the in-spine gimbal for that unit.

Because of the new geometry of the ribcage and spine, and the articulation of the thoracic spine, it was necessary to reevaluate the definition of sternal compression. Also a definition for compression at the lower ribcage was needed. In order to perform the necessary calculations from the digitized output of the DGSPs during a crash test, a subroutine called DEFLECT was developed to compute compressive, lateral, and up/down motion of the ribcage at each of the four measurement sites. Volume 3 of this report provides a listing of the Fortran program, as well as a detailed description of the procedures and algorithm used for calculating the desired chest deflections.

The calculations require information on the initial position of each of the joy sticks relative to a spinal axis system defined, as shown in Figure 5–36, where the Z-axis is along the length of the lower thoracic spine in the midsagittal plane, the X-axis is perpendicular to the Z-axis in the midsagittal plane, and the Y-axis is perpendicular to the plane of the X and Z-axes. The positive directions are chosen to define a right-hand coordinate system so that X is positive toward the front of the dummy, Y is positive toward the left, and Z is positive up.

With this convention, downward rotation of each in-spine gimbal is positive and leftward rotation of the yoke gimbals is positive. Because the meaning of the output of the gimbal in the yoke, in terms of displacements within the spinal axis system, is dependent on the angular rotation and position of the yoke about the in-spine gimbal, it is necessary to use Euler-angle analysis to compute the ribcage deflections. To simplify the input of initial positions of the joy sticks and definitions for the compressive axes, projected angles (i.e., angles projected onto the X-Z and X-Y planes) are required by the program and are subsequently converted by DEFLECT to the appropriate Euler angles (see Volume 3).

Since the front of the dummy's sternum is vertical in a standard pendulum calibration test, it was decided that the direction of compression at the sternum should be defined perpendicular to this surface, which is also the direction of the impactor and the direction of chest compression defined in the Kroell et al. tests (1974). As illustrated in Figure 5–36, the long axis of the lower thoracic spine is nearly parallel to the sternal surface, and therefore the X-axis of the lower spine coordinate system is currently considered to be the direction of the compression axis for the sternum. In the chest deflection algorithm, DEFLECT, sternal compression is computed in the direction of the spinal X-axis, but deflections are also calculated in any other axis system that the user wishes to define.

For the lower ribcage, there is currently no precedent for a compression direction and the direction of the X-axis of the spinal coordinate system seems inappropriate. Thus, while the computer algorithm calculates deflections in the spinal-axis system for the transducers at the lower ribcage, it also computes deflections in an alternate compression axis system. Currently, this alternate system is defined with the compression axis angled upward at 15 degrees (front to back) to the spinal X-axis and inward (from rib to spine) at 18 degrees to the spinal X-axis. These projected angles can, however, be changed by the dummy user if a different definition of lower ribcage compression is desired.

5.8.2 Other Instrumentation

In addition to the chest deflection instrumentation, the new thorax assembly includes provision for a new lower neck six-axis load cell, a six-axis lumbar load cell, triaxial chest (i.e., spine) accelerometers located at the thorax center-of-gravity, and angular velocity sensors attached to the upper and lower thoracic spine segments and the pelvis. The latter measurements are provided by three magnetohydrodynamic angular motion sensors (MHD AMS) developed by Applied Technology Associates, Inc. (Laughlin 1989) that are mounted on

the sides of the spinal segments and the side of the pelvic block and provide kinematic information of relative rotation at the flexible lumbar and thoracic spine segments.

5.9 ANTHROPOMETRY AND ASSEMBLY OF THE SECOND AND CURRENT PROTOTYPE-50M

As noted in Section 5.1 and Figure 5–4, the spine of the first prototype was designed to follow the AATD-50M drawing as nearly as possible and the ribcage was designed to match the skeletal drawing. However, even after making the modifications to the Hybrid III pelvis noted in Section 5.6, the spine and ribcage appeared to fit too far rearward so that the lower-front margin of the ribcage was behind the ASISs and the thoracic spine was too far behind the back of the pelvis (see Figure 5–5c). As a result, it was decided to modify the posture somewhat from the AATD-50M drawings until a total redesign of the Hybrid III pelvis and buttock could be accomplished in a future study.

This modification consisted primarily of tilting the new lumbar spine forward about six degrees from its orientation in the first prototype. In addition, and as previously noted, the depths of the lower ribs were increased approximately 13 mm (0.5 in) to improve the spatial relationship between the front of the ribcage and the ASISs of the pelvis, and to improve agreement with the cartilaginous portion of the lower ribcage in the AATD-50M drawing.

Figure 5–37 is an overlay of the second prototype with the AATD-50M side-view drawing and shows this modified anthropometry. Figures 5–38a through 5–38c show photographs of the second and current Prototype-50M assembly including the shoulders, ribcage, spine, pelvis, and abdomen. The bib of this prototype is made of three layers of urethane, where the middle layer is lead-filled to provide additional mass. Only the top layer of urethane extends up and over the clavicles and shoulders and around the back of the neck where the two halves are connected and fastened to the upper thoracic spine, to prevent the shoulder belt from digging into the gap between the neck and the main shoulder supports. In addition, as shown in Figure 5–39, a urethane piece has been designed and molded to fit on the front of the upper thoracic spine and to extend up into the space between the shoulder supports and the neck load cell to further reduce the tendency for the shoulder belt becoming caught in this gap.

A chest jacket, sewn from material made of 4.8-mm-thick (0.1875 in) neoprene rubber between two layers of Lycra has been patterned and fabricated to fit snugly over the ribcage. A 19-mm (0.75-in) thick Ensolite pad has been shaped and beveled at the edges and top to fit over the urethane bib and is inserted into a pocket sewn into the inside of the chest jacket. In order to improve interaction of the shoulder belt with the dummy's clavicles, the top edge of the padding has been cut and beveled below the clavicles. The chest jacket has been designed to extend over the pelvis in order to help retain the abdomen, but is equipped with Velcro fasteners around the legs to allow access to the frangible insert without the need to completely remove the chest jacket.

Two lead ballasts are attached to the lower thoracic spine and are needed to lower the thorax center-of-gravity to the desired level near the bottom edge of the thoracic articulation. Figure 5–40a through 5–40c show the ballast in front that is triangulated and padded at the forward surface. This component provides protection for the instrumentation inside of the spine, as well as over-stroke protection for the DGSP instrumentation units. A padded steel bar attached crosswise to the top of this ballast also helps to limit chest compression in this region. The lead ballast at the back provides protection and strain relief for the instrumentation cables that exit through a hole in the back of the lower thoracic spine.

A late modification to the second Prototype-50M assembly was the fabrication and attachment of a weighted pad to the inside of the sternum. Currently, this mass is attached

by means of a wire attached laterally around the sternum and a wide rubber band that wraps around the sternum and pad longitudinally and attaches to the upper sternum at both ends by means of the screws that fasten the bib to the upper sternum. As indicated in Section 6.7, addition of this compliant mass improved the pendulum response of the Prototype-50M by helping to maintain a more constant force plateau during impact loading.

Other features included in the latest version of the Prototype-50M ribcage assembly include heavy-duty rib "helpers" or stiffeners behind the ribs at the spine and Teflon-surfaced steel shelves under the top or first rib. The rib helpers are shown in Figures 5–35 and 5–38c, which show that the top four stiffeners are curved to follow the shape of the ribs and thereby further minimize rib deflection at the spine. Figure 5–41 shows the steel shelves that are bolted to the upper thoracic spine so that the Teflon surface is in contact with the bottom of the first rib. Installation of these shelves was found to provide a useful reduction in the downward motion of the whole ribcage through the connection of ribs two through seven to the top rib by means of the triple-layered bib. The shelves do, however, continue to permit some downward ribcage displacement.

Finally, Figures 5–42 through 5–45 show two alternate versions of the prototype abdomen. Figure 5–42 shows a soft urethane abdomen inside a three-piece mold fabricated from a clay model sculpted into the second Prototype-50M abdominal cavity. The model was made with the abdomen support bracket for the frangible abdomen in place so that the back side of the urethane abdomen fits snugly against it and under the inferior-anterior margin of the ribcage. Figure 5–43 shows the soft abdomen installed in the second Prototype-50M. As indicated in Figure 5–44, a wood die of the frangible *Styrofoam* insert was made and can be placed inside the mold when the soft urethane abdomen is made to provide a cavity for the frangible insert. While the combined soft/frangible abdomen shown in Figure 5–45 has not been evaluated under dynamic testing, it is designed to fill out the abdominal cavity when using the frangible abdomen inserts and will hopefully provide additional support for the ribcage and assist in retaining the frangible abdomen in place.

5.10 MASS DISTRIBUTION AND CENTER OF GRAVITY

Table 5–2 compares the segment masses of the second and current Prototype-50M to the segment masses of Hybrid III and the AATD-50M as described by Robbins (1985a) and Melvin et al. (1988a). At this time, the only differences between the masses of Hybrid III and the Prototype-50M are in the thorax and abdomen/pelvis components. The mass of the Prototype-50M thorax, including shoulders and thoracic spine, is 4.5 kg greater than the mass of the Hybrid III thorax. However, the mass of the pelvis/abdomen of the Prototype-50M, including the lumbar spine, is 3.8 kg less than that of Hybrid III.

It can also be noted, however, that the mass of the Prototype-50M thorax is very close to that of the AATD-50M and that the mass of the pelvis/abdomen of the AATD-50M is about 9.1 kg less than that of Hybrid III and about 5.4 kg less than that of the Prototype-50M. This latter difference (i.e., between the Prototype-50M and the AATD-50M) is due to differences in the distribution of thigh mass.

For Hybrid III and the Prototype-50M, the total thigh mass is about 12.2 kg, whereas the mass of the thighs for the AATD-50M is greater by 5.8 kg at 18 kg. The greater thigh mass in the AATD-50M is due to the use of hip segmentation planes defined by McConville et al. (1980) that run from the crotch through the anterior-superior iliac spine of the pelvis as shown in Figure 5–46, and the assignment of mass below these planes to the thighs (i.e., the upper legs). In Hybrid III, the dummy thighs are segmented perpendicular to the long axis of the femurs below the level of the crotch and the thigh mass above this segmentation plane has apparently, and perhaps inappropriately, been assigned to the pelvis.

TABLE 5–2

SEGMENT MASSES FOR
PROTOTYPE-50M, HYBRID III, AND AATD-50M
(Robbins 1985a, Melvin et al. 1988b)

Body Part	Segment Mass (kg)		
	Hybrid III	Prototype-50M	AATD-50M
Head	4.54	4.54	4.54
Neck	1.54	1.54	1.06
Thorax	17.23	21.68	21.86
Pelvis/Abdomen	23.09	19.32	13.90
Arms	8.54	8.54	8.18
Thighs	12.18	12.18	18.00
Legs	9.36	9.36	9.91
TOTAL	76.48	77.16	77.46

Overall, then, the thoracic and pelvis masses of the Prototype-50M agree well with the AATD-50M, except for differences in distribution of mass between the pelvis and the thighs. At this time, the center of gravity (CG) of the Prototype-50M has only been roughly estimated, since additional changes to the design may be forthcoming. The CG is located within 25 mm of (above) the desired CG specified on the AATD-50M drawings, which is also the approximate location for the chest accelerometers attached to the lower thoracic spine.

5.11 FIGURES

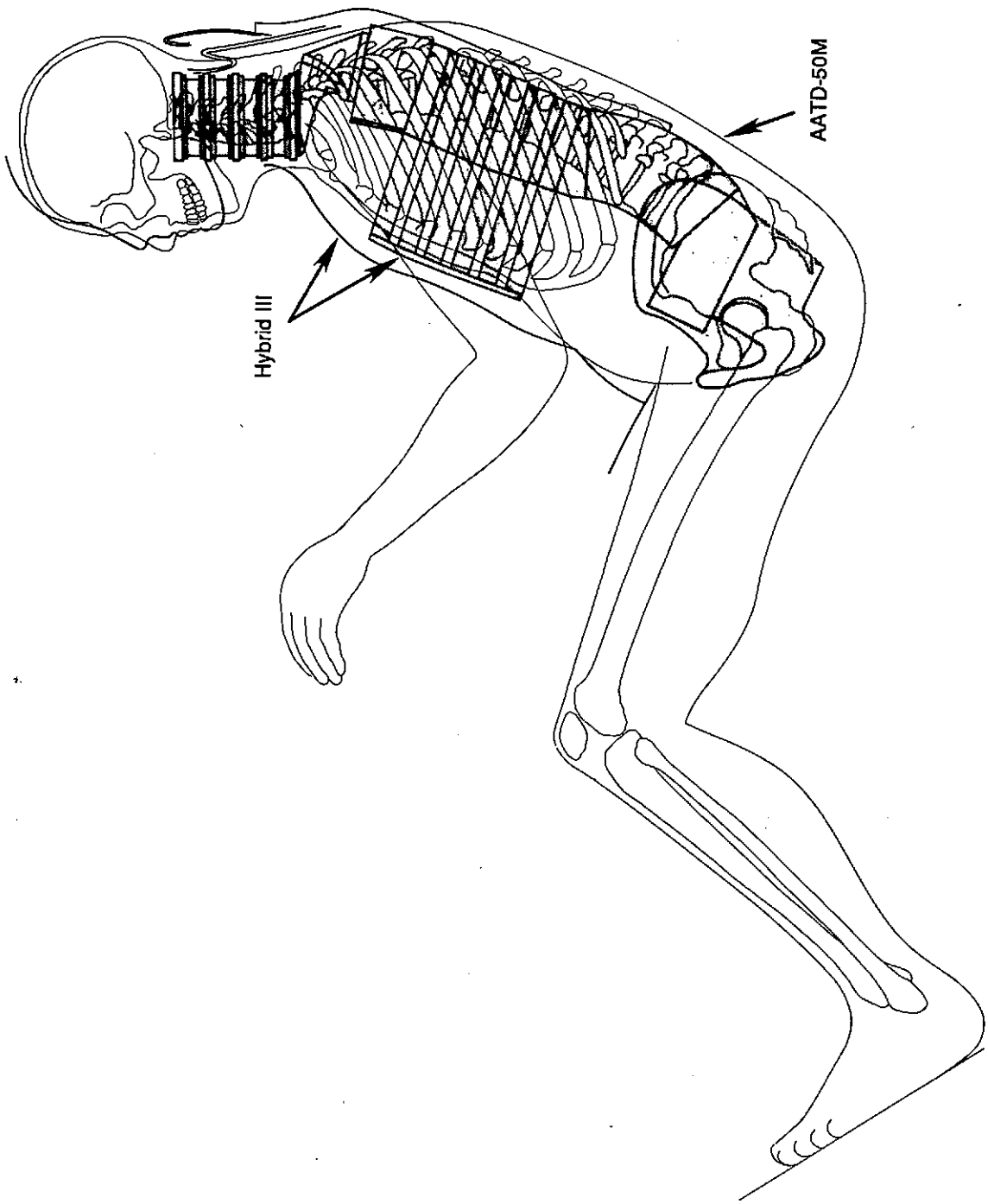

FIGURE 5–1. Hybrid III (shaded) overlay on AATD-50M side-view drawing with skeletal rendering.

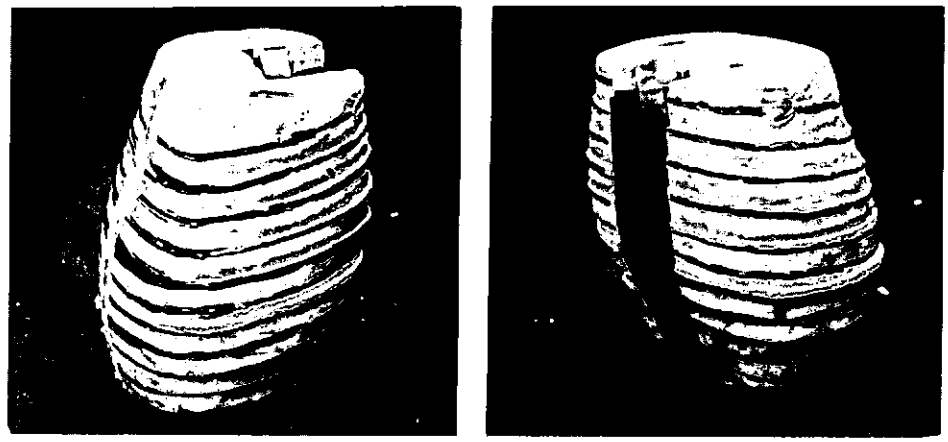

(a) Styrofoam form for rib contouring.

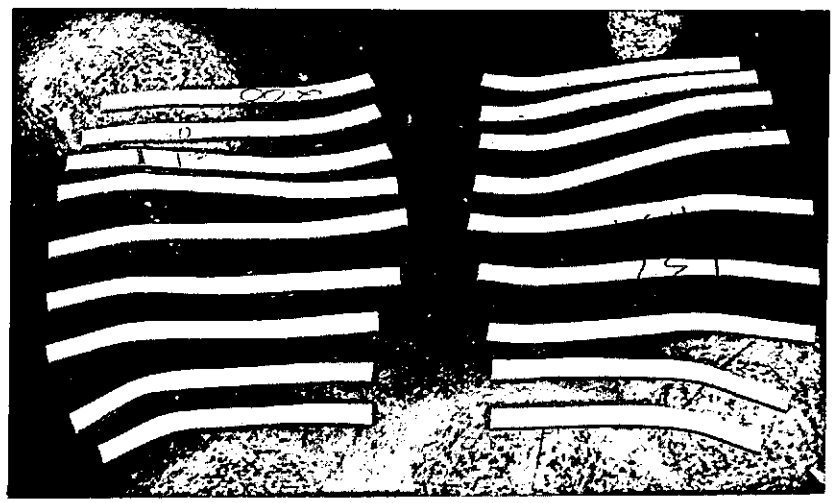

(b) Cut patterns of ribs.

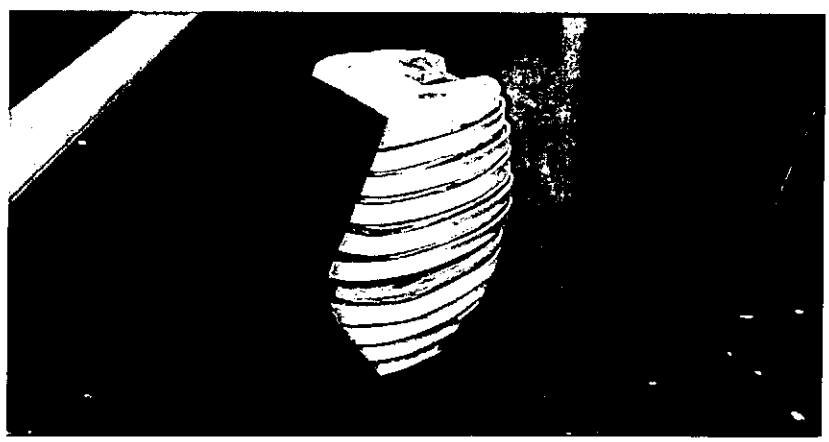

(c) Ribs fitted to Styrofoam form.

FIGURE 5–2. Styrofoam model (top) used to determine rib patterns (center) for contour ribcage (bottom).

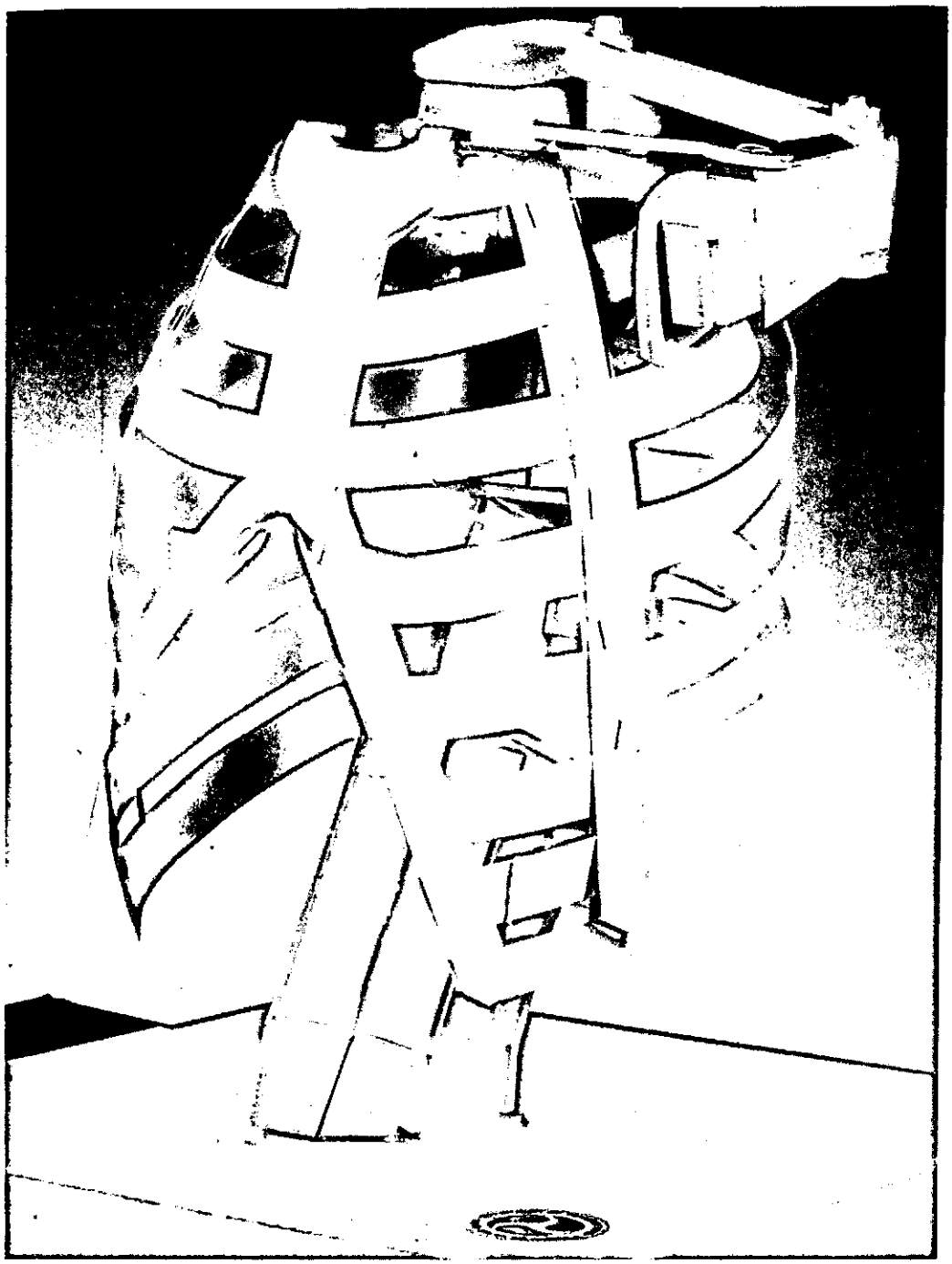

FIGURE 5–3a. Oblique view of cardboard model of eight-rib thorax assembly.

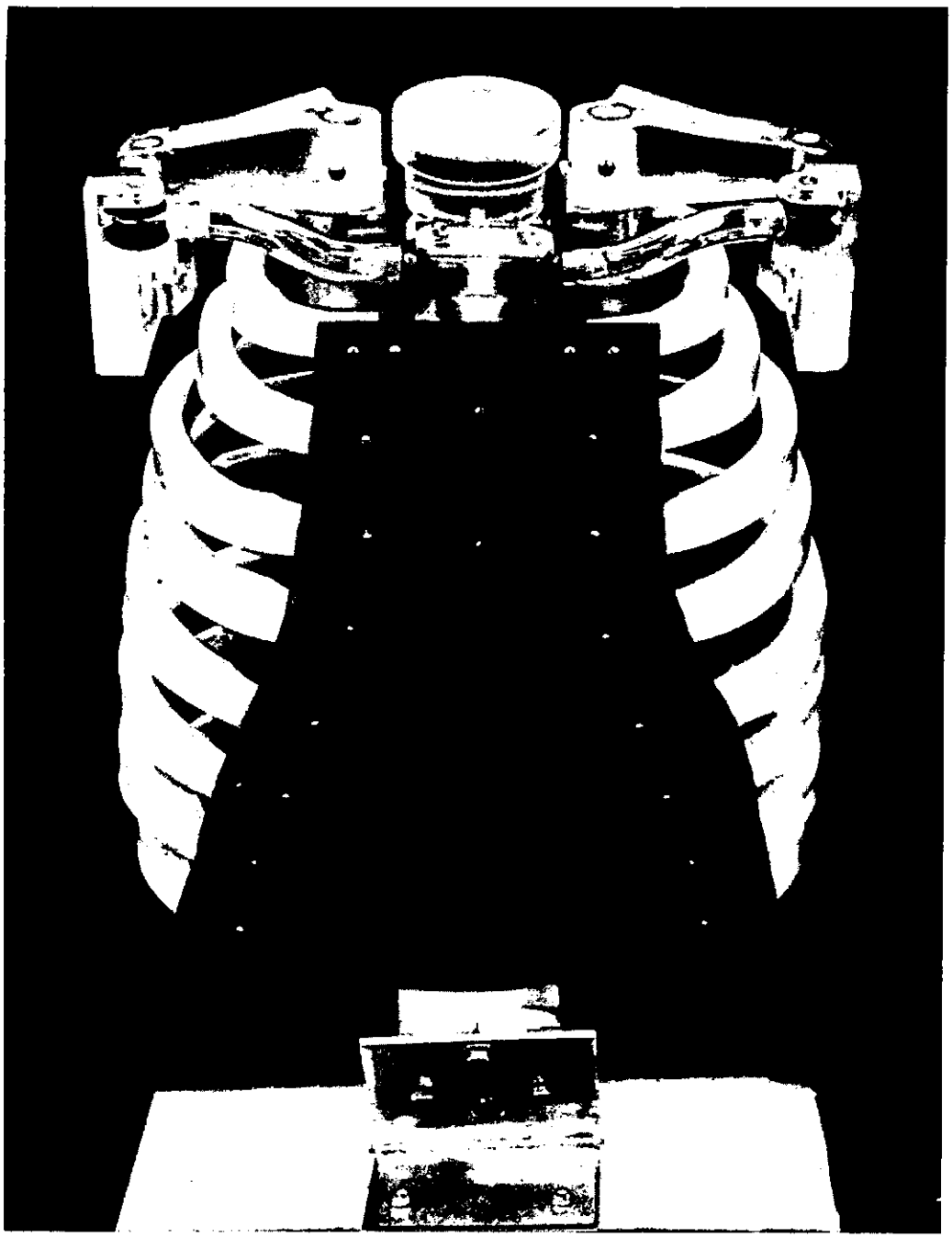

FIGURE 5–3b. Front view of acrylic model of eight-rib thorax assembly.

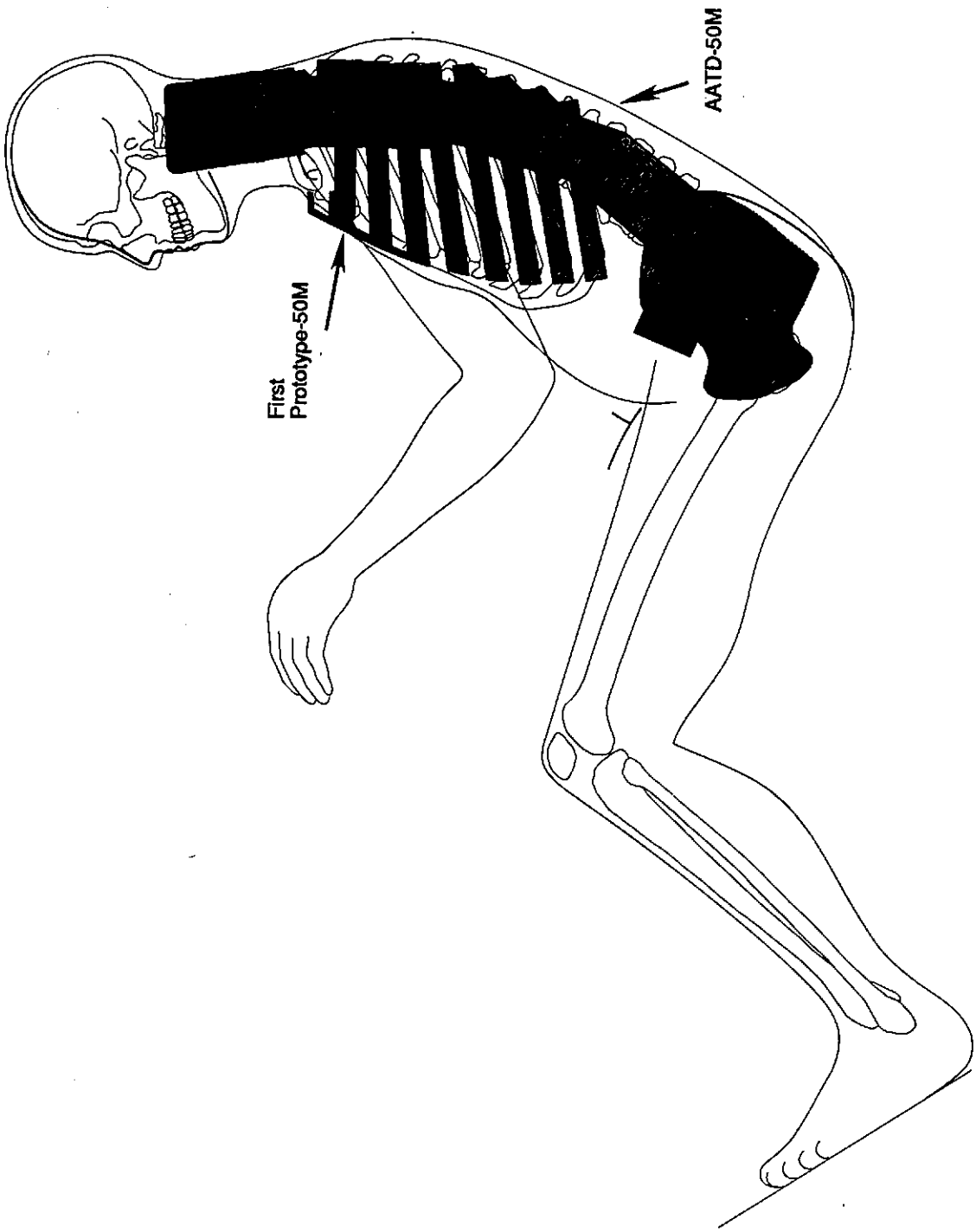

FIGURE 5–4. Overlay of First Prototype-50M on AATD-50M side-view drawing with skeletal rendering.

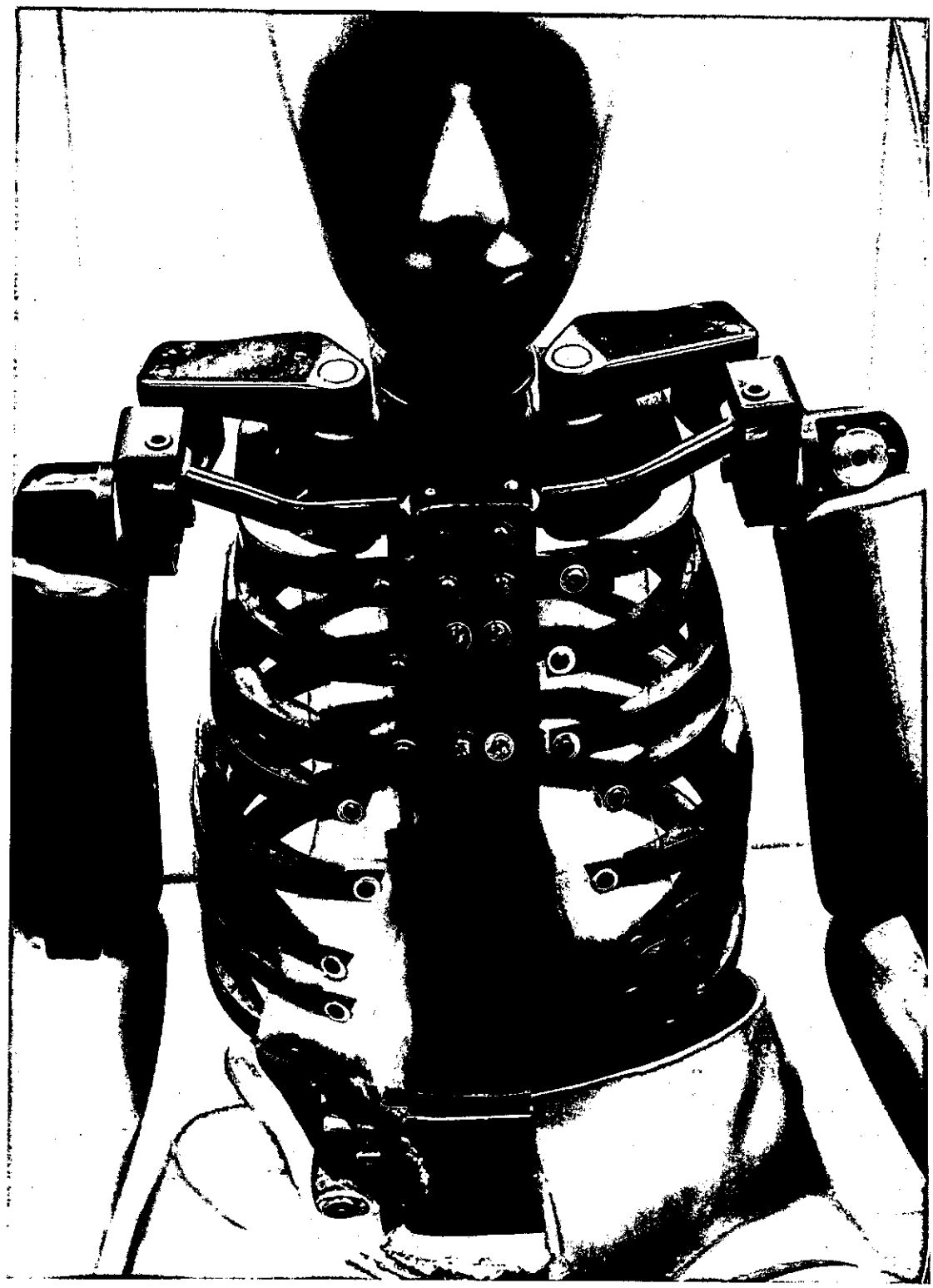

FIGURE 5–5a. Front view of First Prototype-50M with eight-rib ribcage.

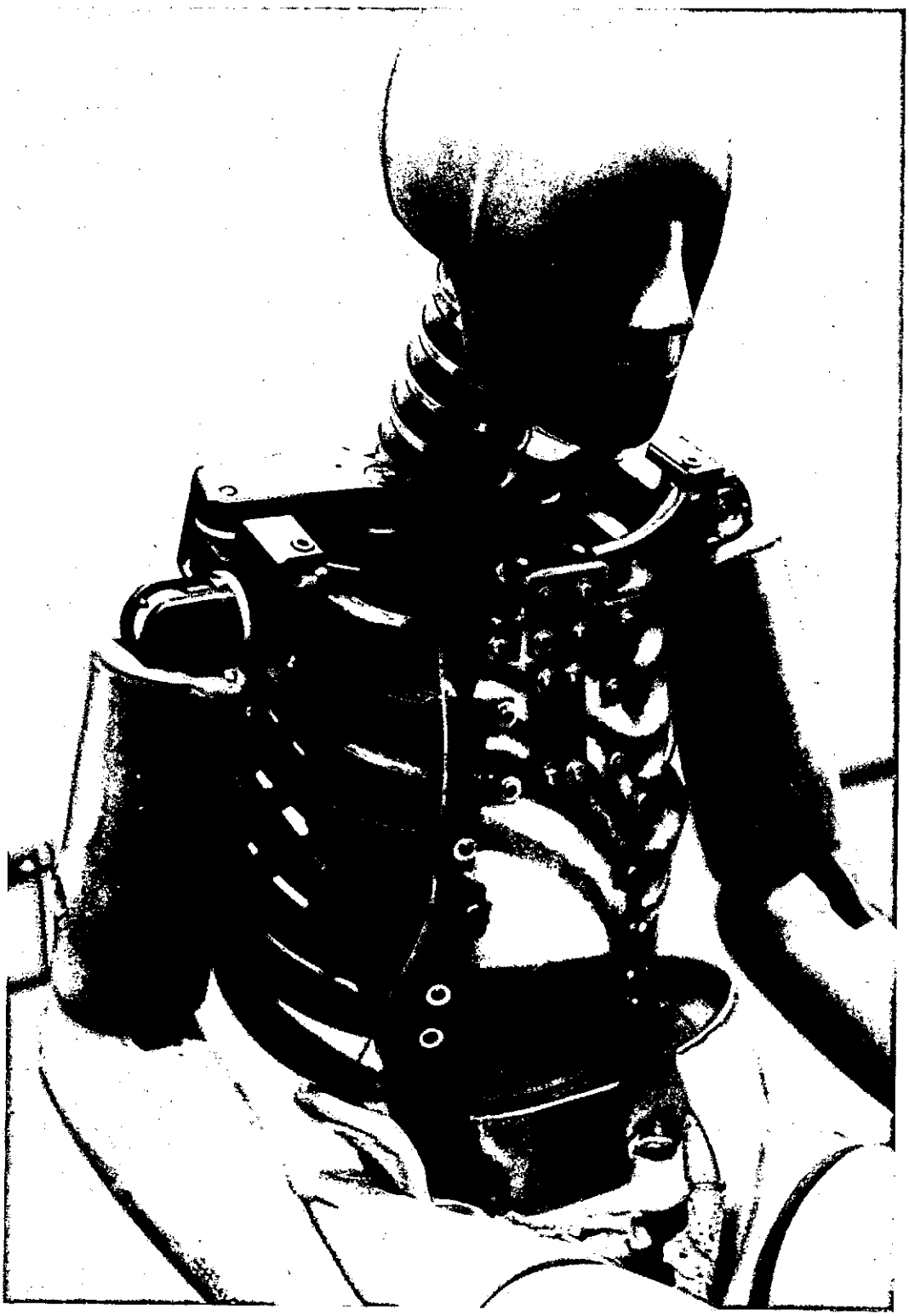

FIGURE 5–5b. Front oblique view of First Prototype-50M.

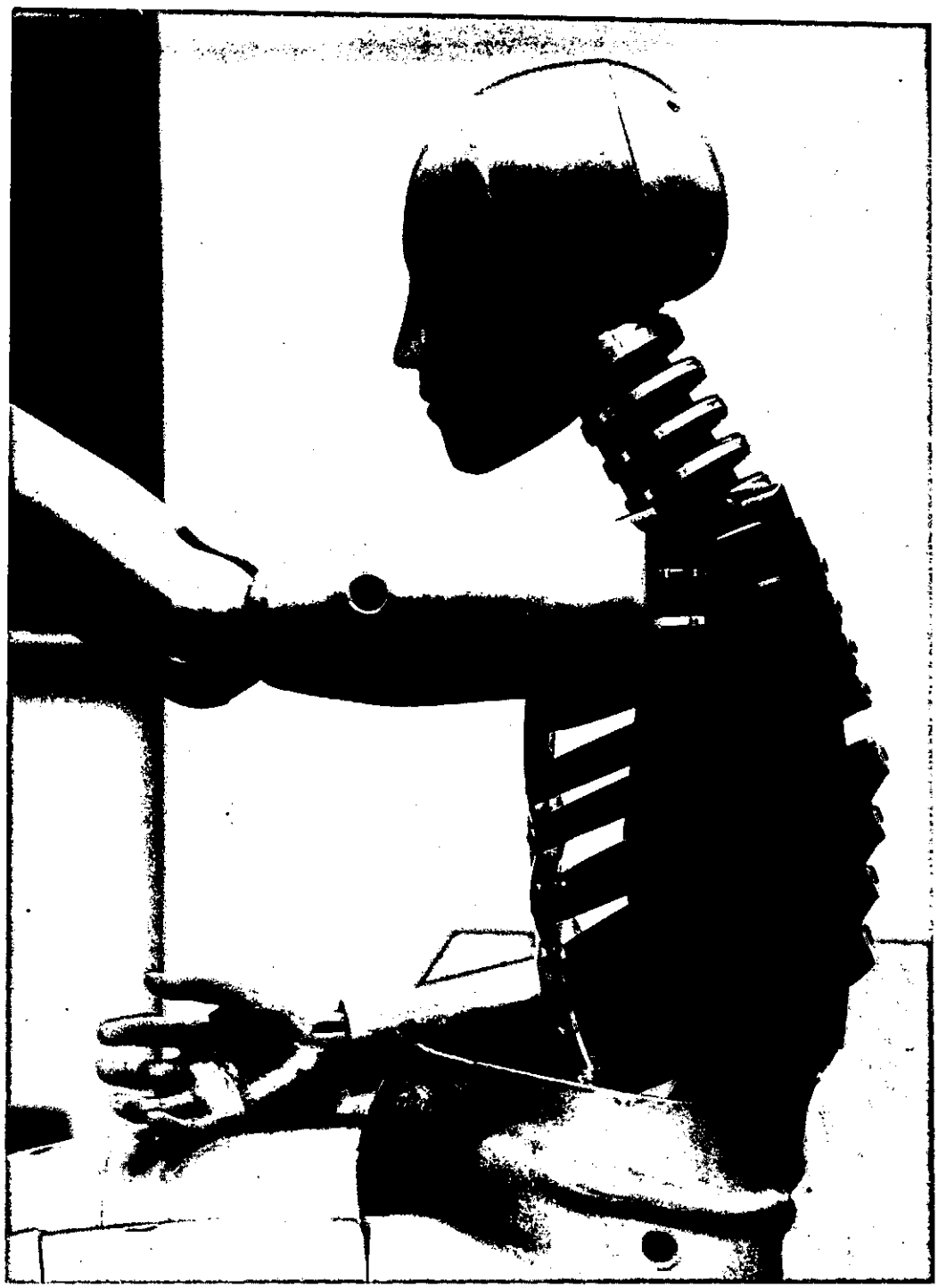

FIGURE 5–5c. Side view of First Prototype-50M.

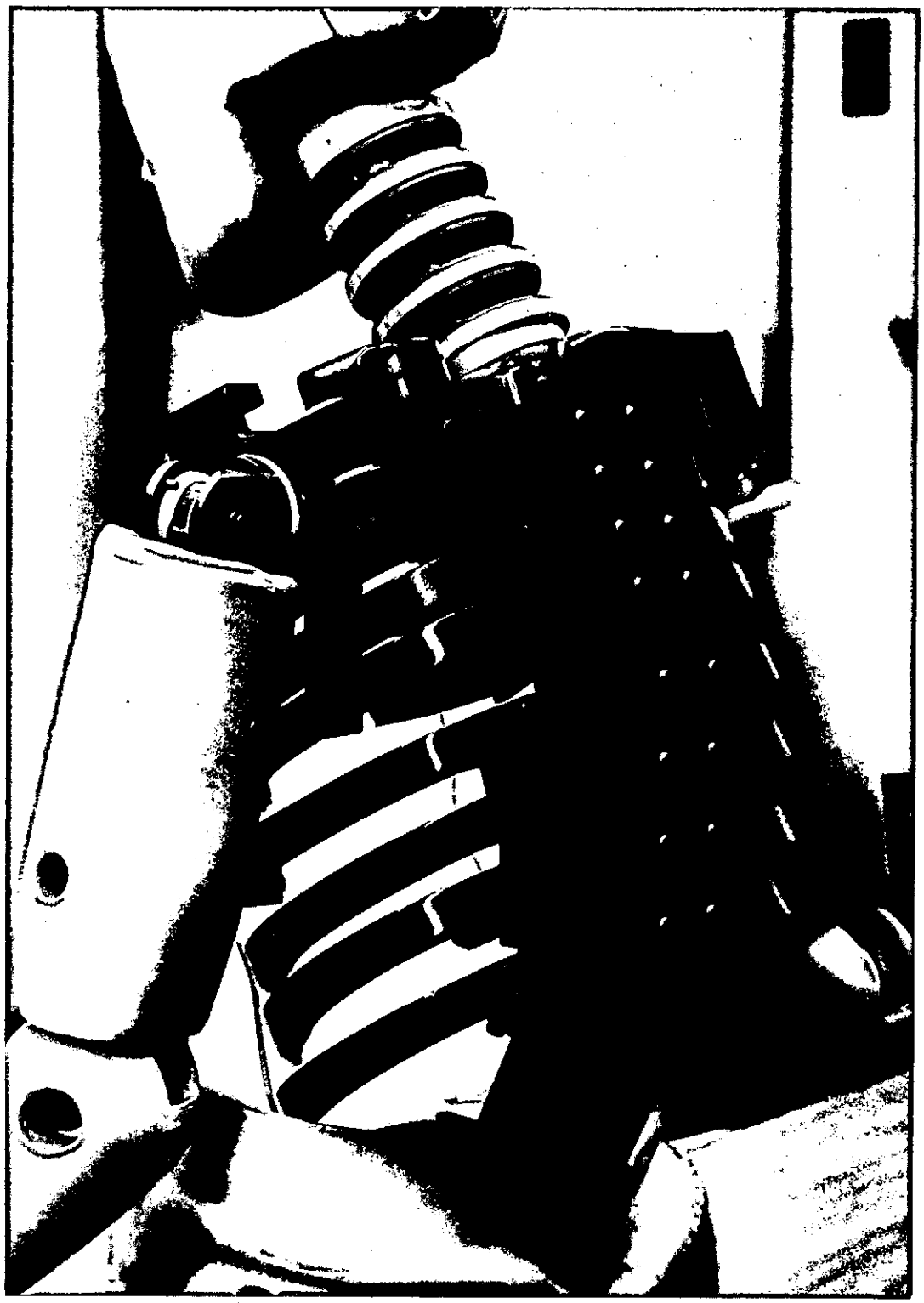

FIGURE 5–5d. Rear oblique view of First Prototype-50M.

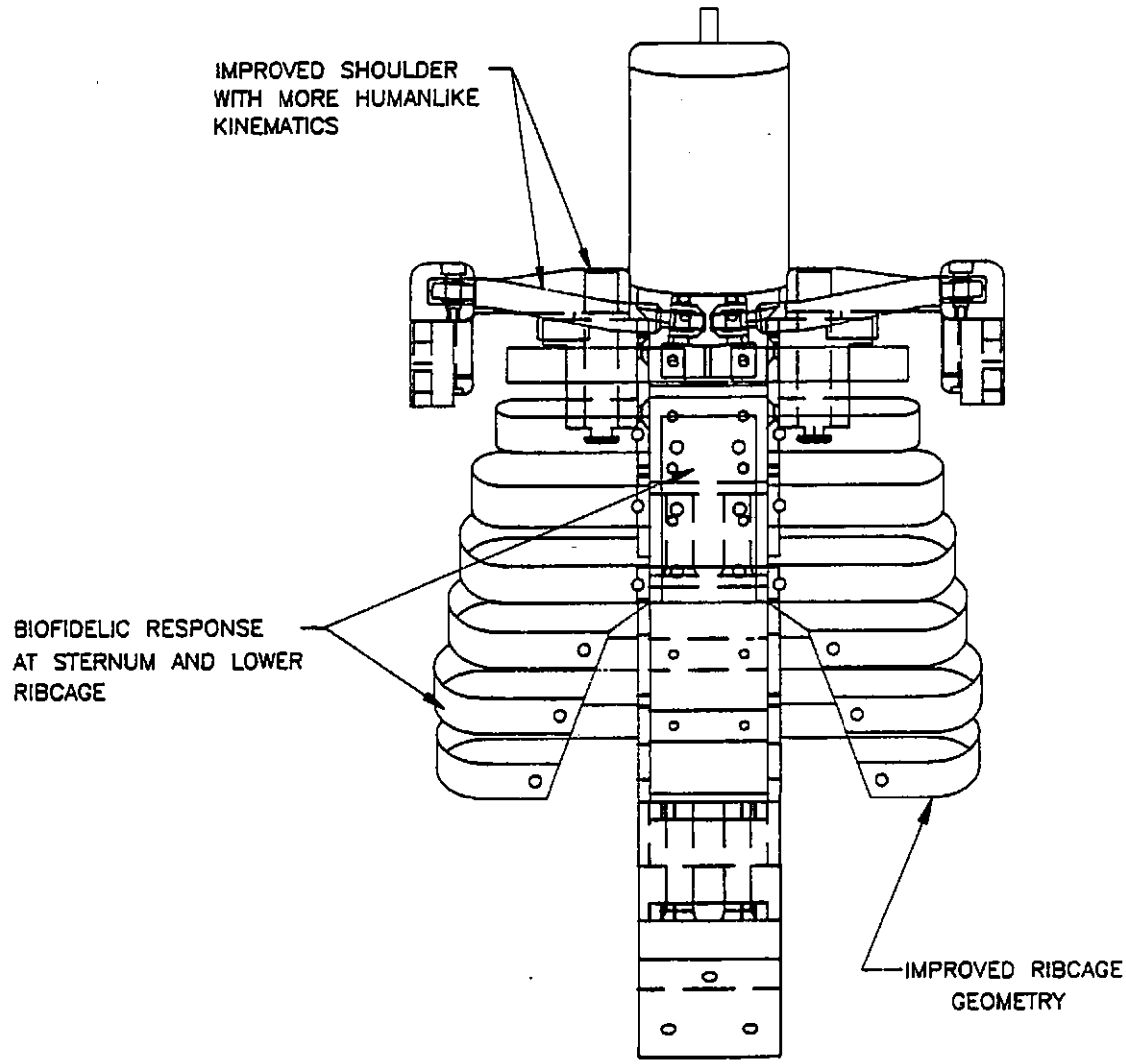

FIGURE 5–6a. Front-view drawing of final prototype thorax assembly (abdomen not included).

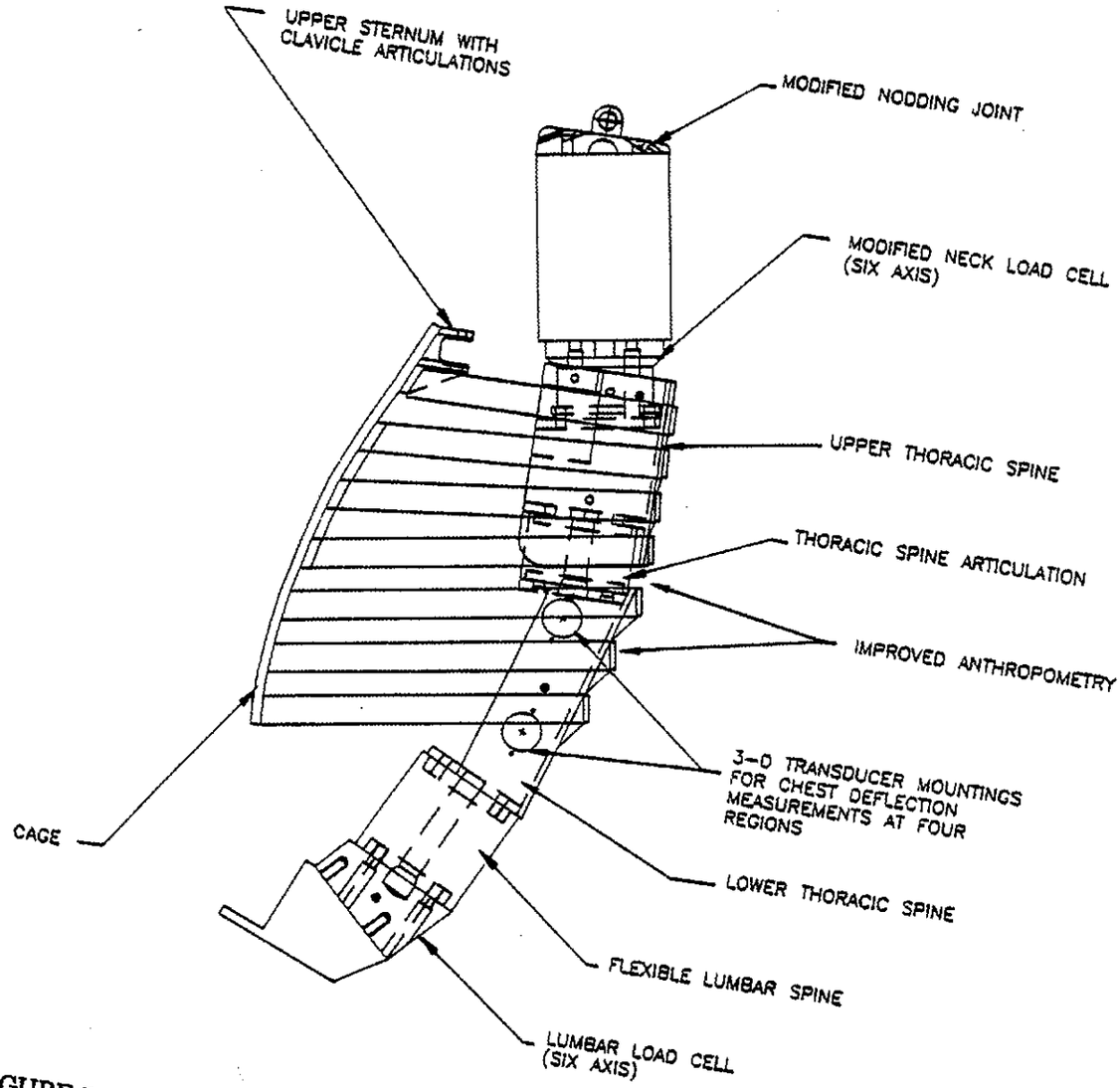

FIGURE 5–6b. Side-view drawing of final prototype assembly (shoulder omitted for clarity).

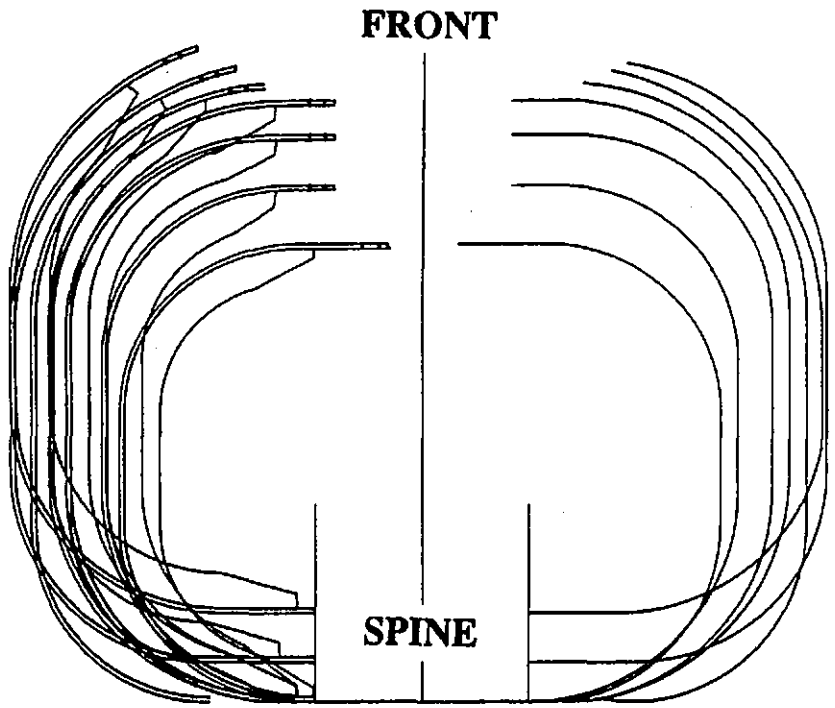

FIGURE 5–7. Overlay of rib contours for Second Prototype-50M. Each rib is shown in its own plane.

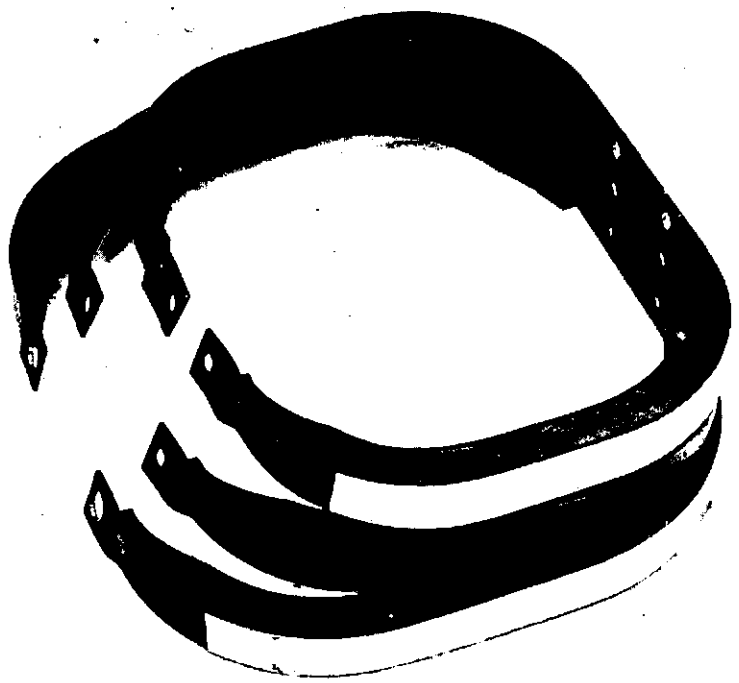

FIGURE 5–8. Top three ribs showing twisted tips for attachment of bib.

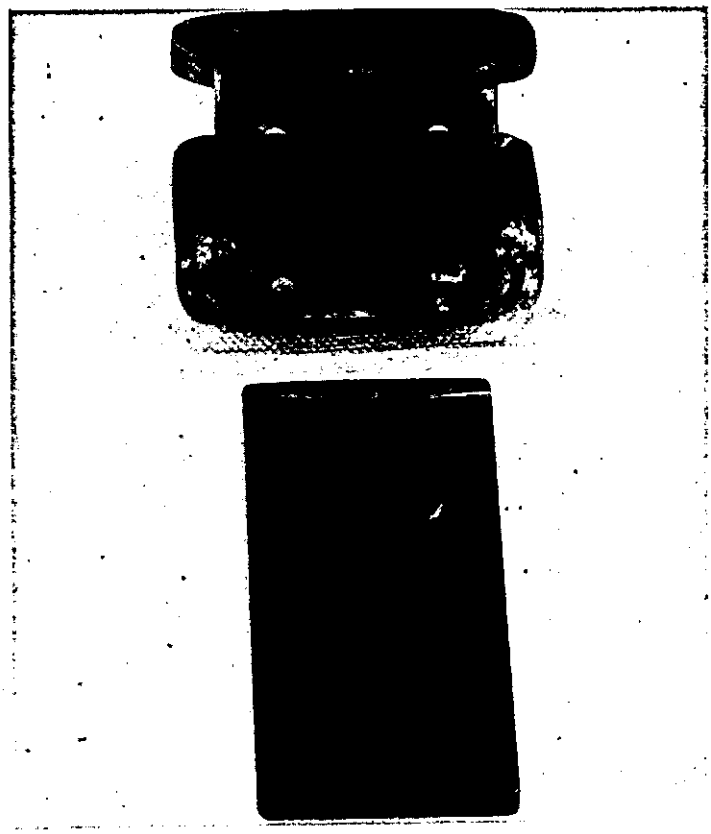

FIGURE 5–9. Upper and lower segments of sternum used in Second Prototype-50M.

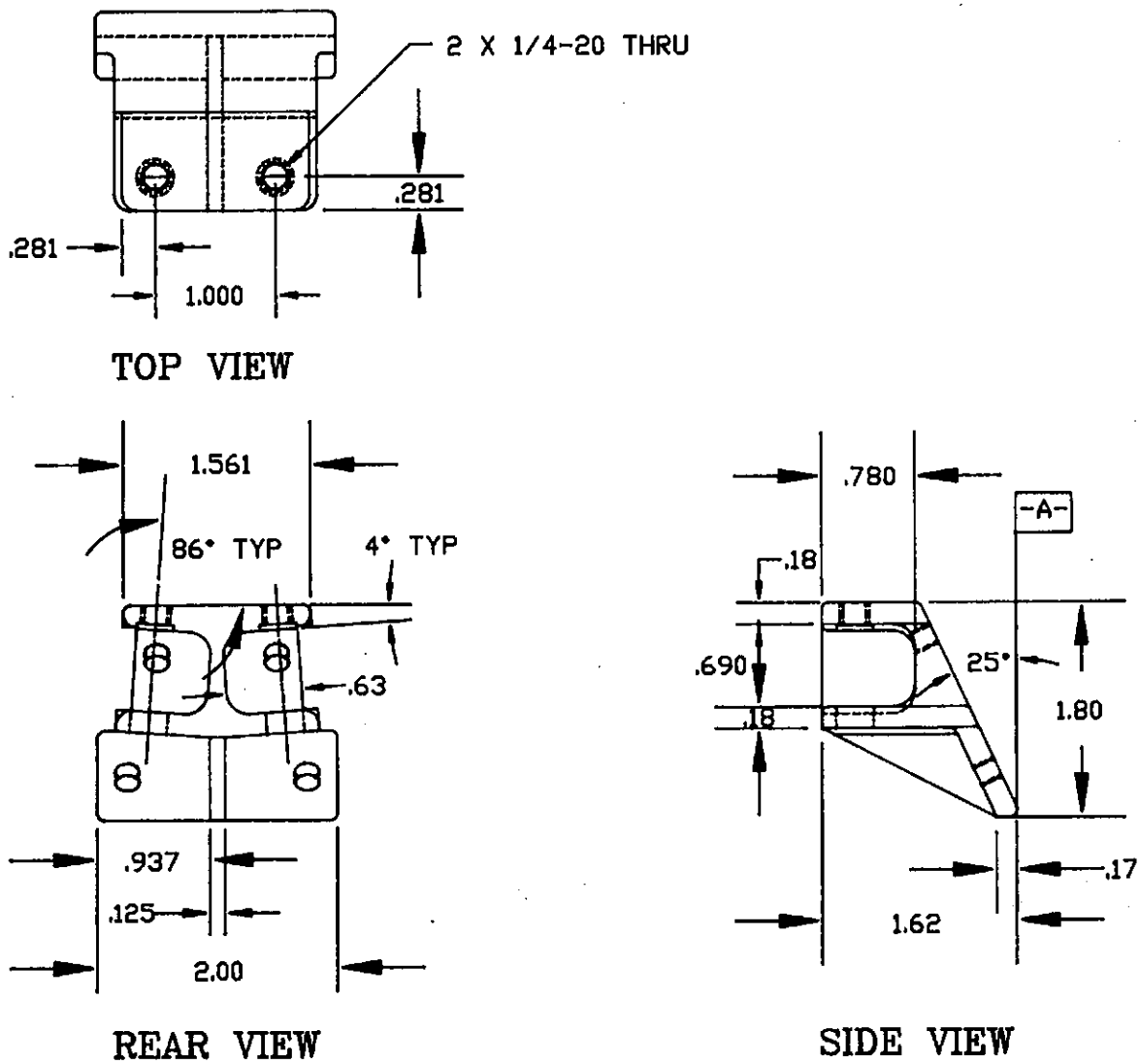

FIGURE 5–10. Rear-, top-, and side-view drawings of upper sternum.

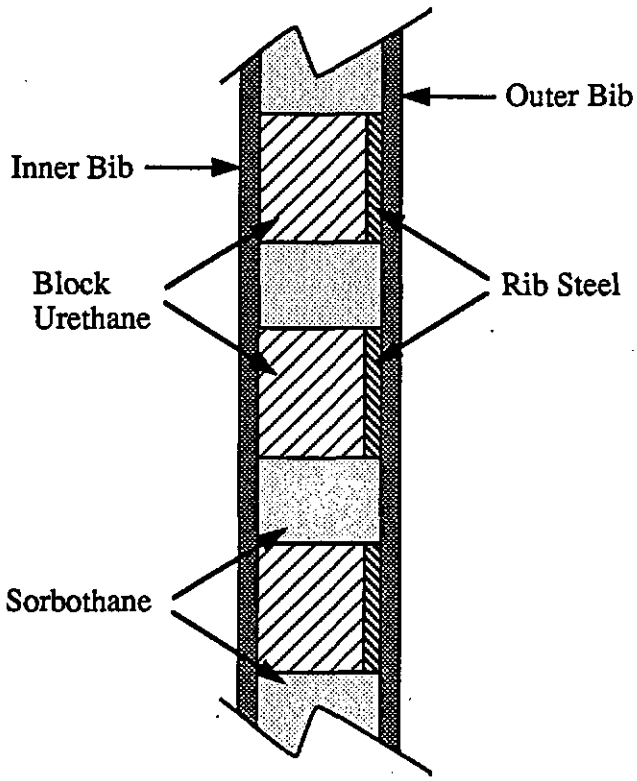

FIGURE 5–11. Cross-section drawing of ribcage just lateral to sternum showing modified rib coupling with alternating urethane and Sorbothane blocks sandwiched between inner and outer urethane bibs.

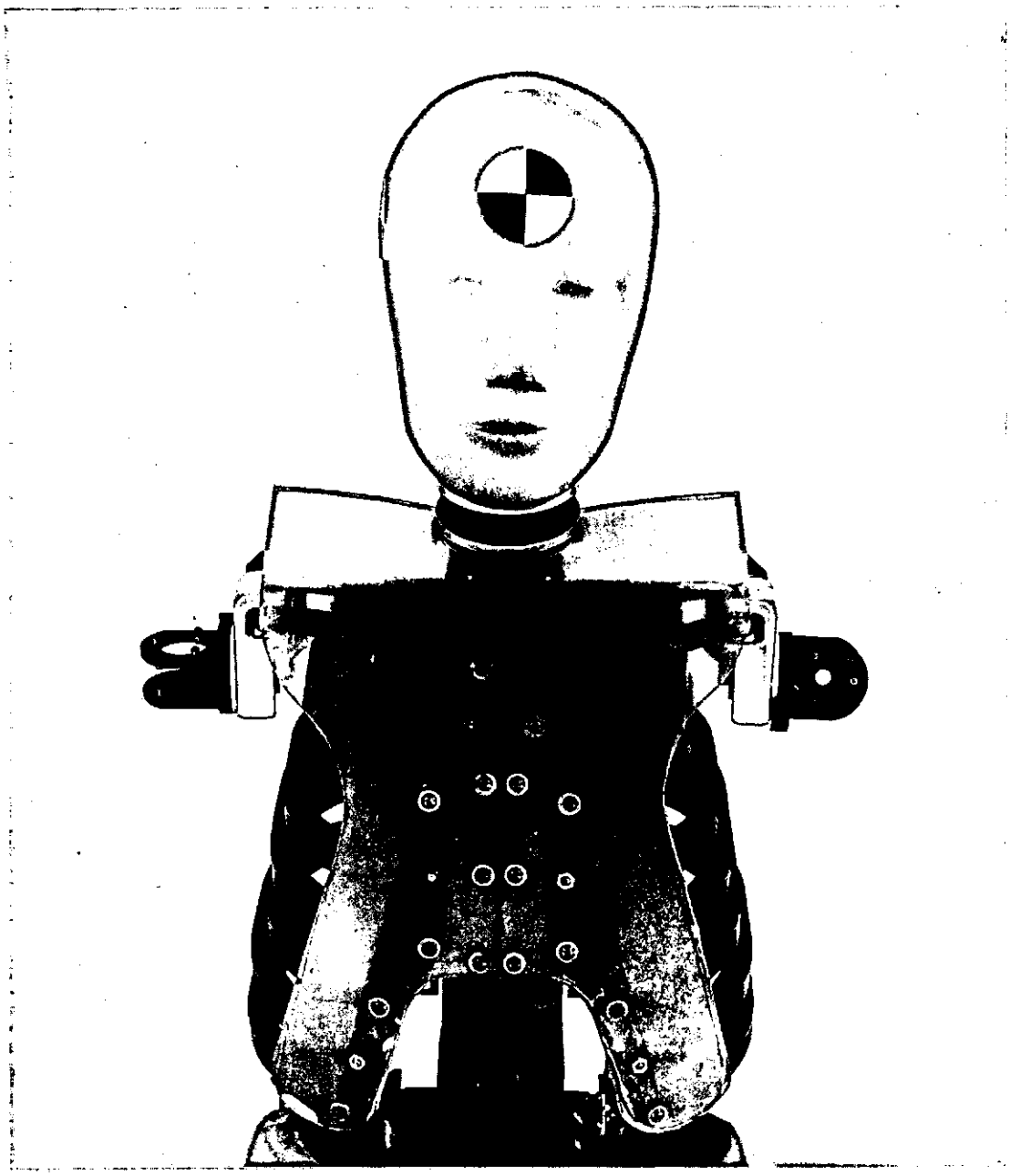

FIGURE 5–12. Front view of Second Prototype-50M showing spring steel sandwiched between bib material on both sides of the anterior ribcage.

FIGURE 5–13a. Thoracic spine articulation for First Prototype-50M using 6-year-old rubber spine.

FIGURE 5–13b. Thoracic spine articulation for First Prototype-50M with upper and lower thoracic spine segments.

FIGURE 5–13c. Thoracic spine assembly of First Prototype-50M.

FIGURE 5–13d. Front view of First Prototype-50M thoracic spine assembly with shoulder mounting blocks attached to upper spine segment.

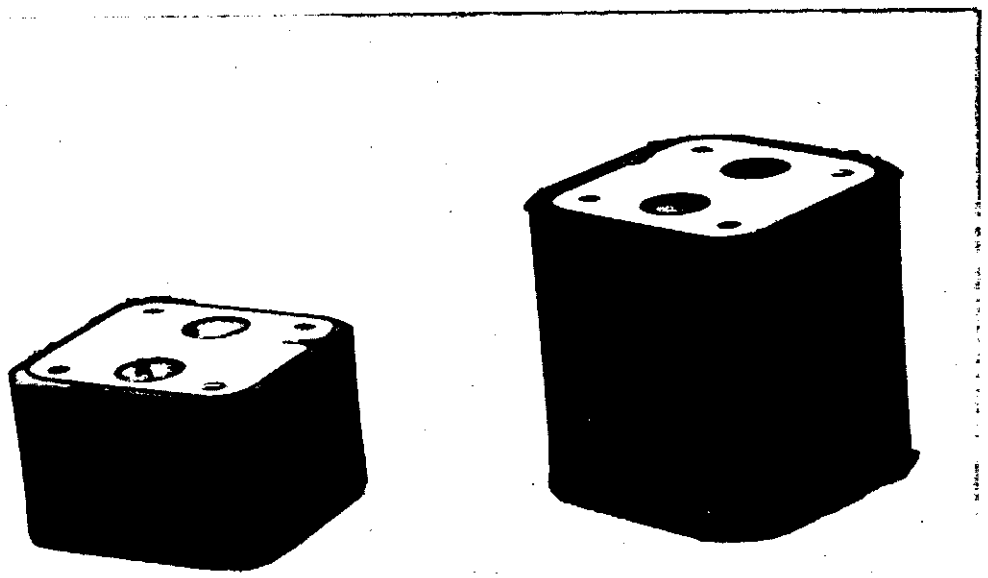

FIGURE 5–14. Molded rubber pieces with steel end plates for the thoracic (left) and lumbar (right) articulation of the Second Prototype-50M.

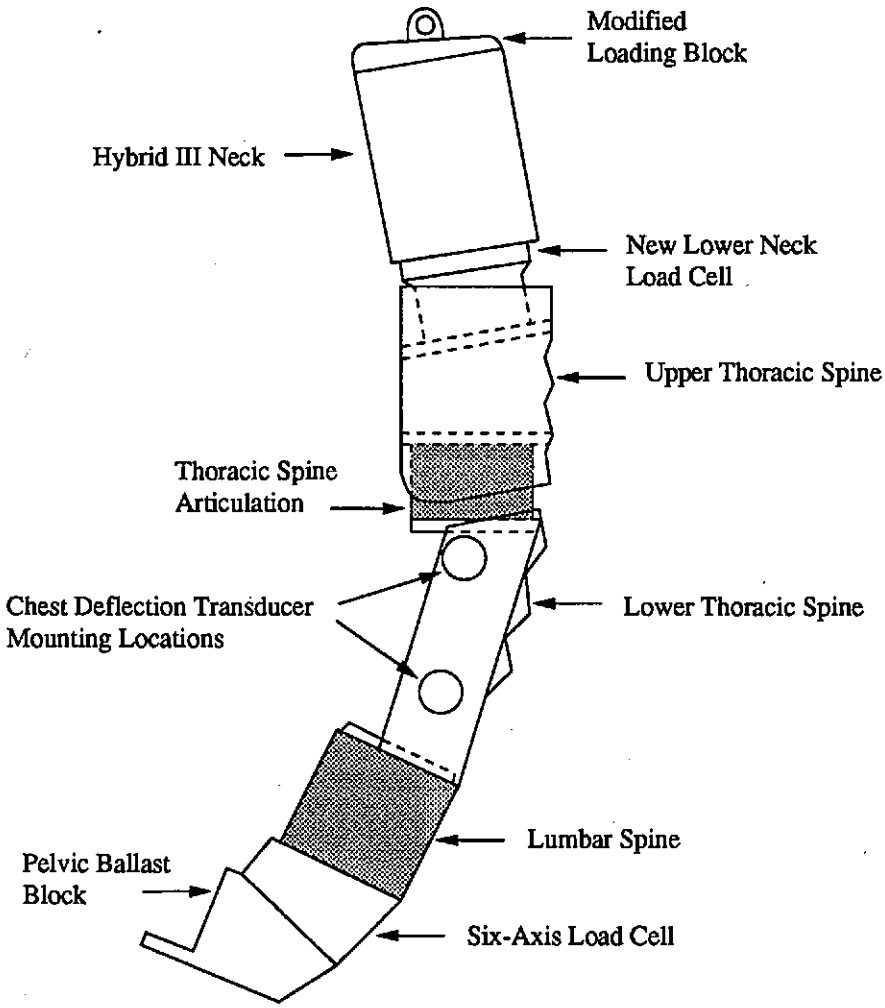

FIGURE 5–15a. Side-view drawing of spine for Second Prototype-50M.

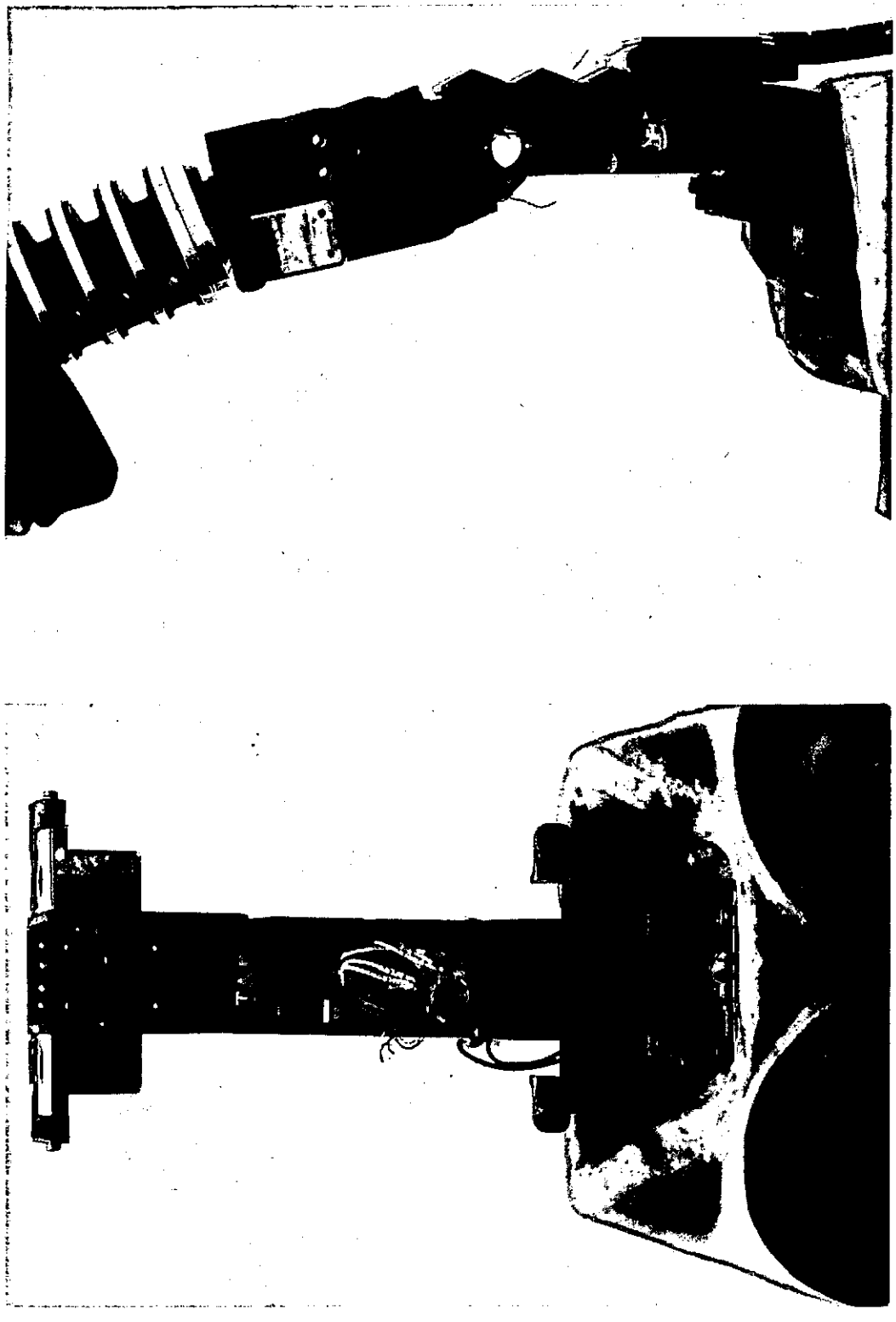

FIGURE 5–15b. Front- and side-view photographs of spine assembly for Second Prototype-50M.

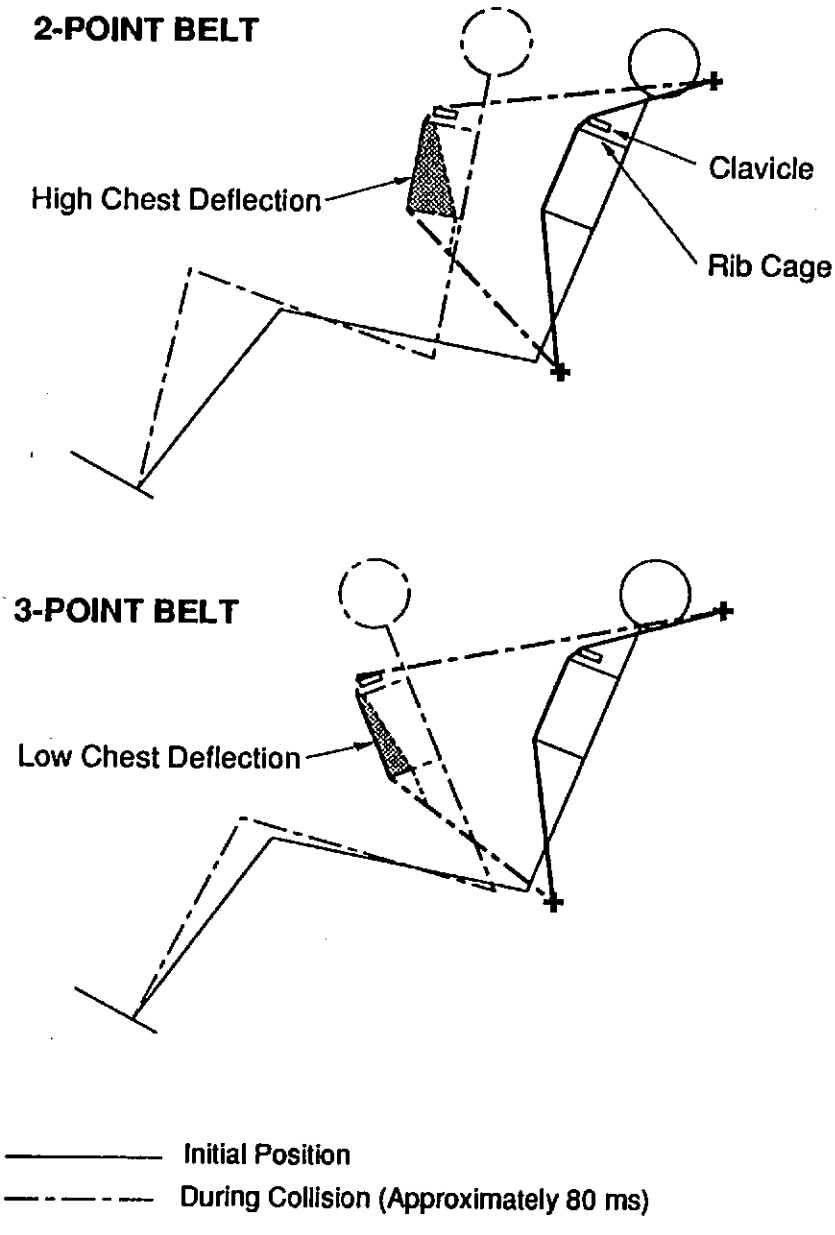

FIGURE 5–16. Kinematic response to two- and three-point belts (Backaitis 1987).

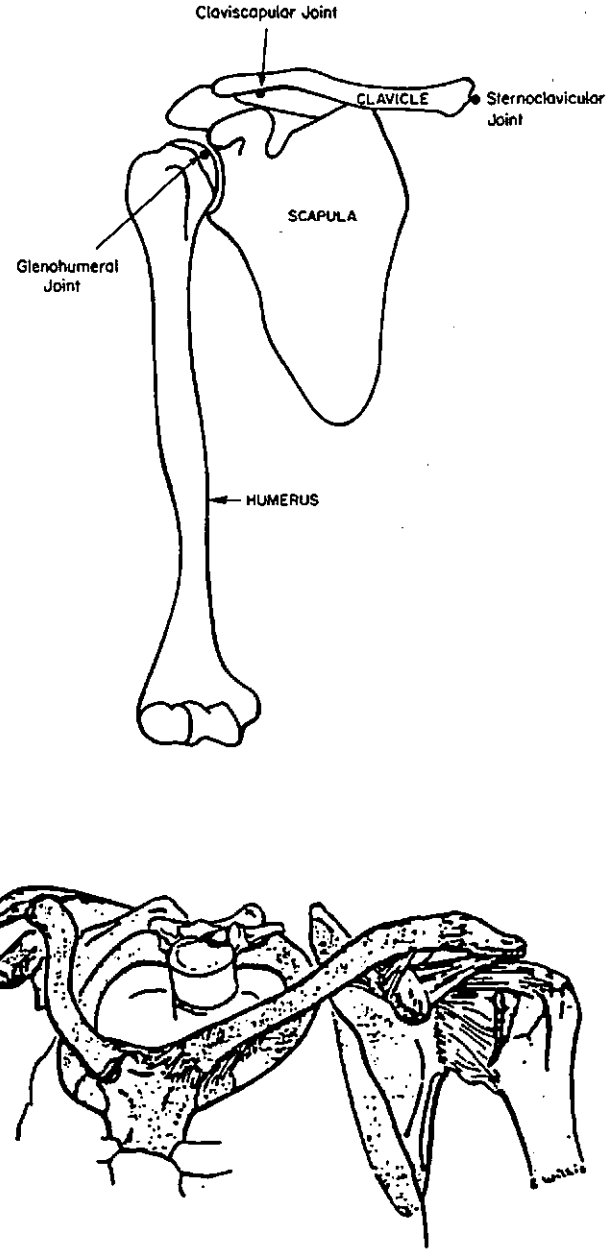

FIGURE 5–17. Components of shoulder including clavicle, scapula, and humerus bones (from Robbins 1985a and Dempster 1965).

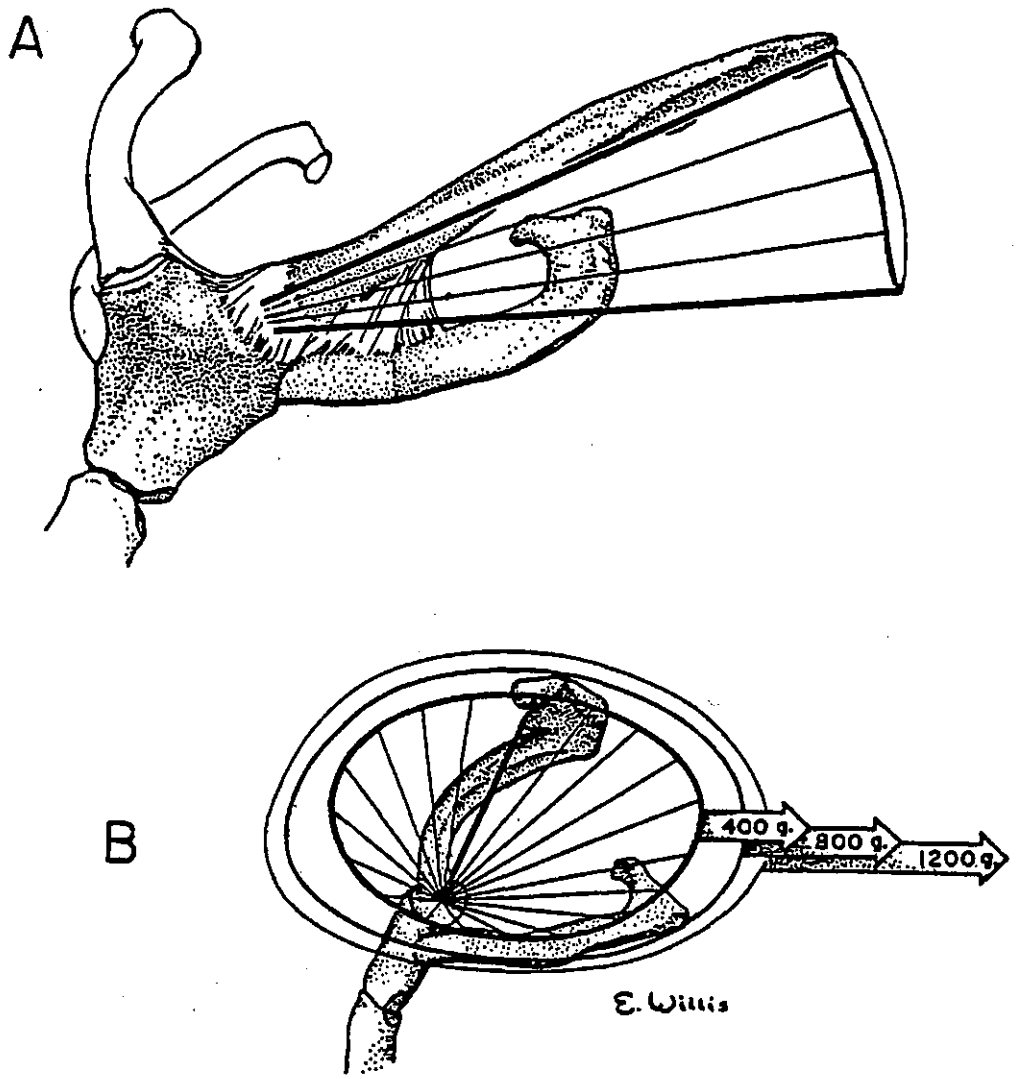

FIGURE 5–18. A: Joint sinus of sternoclavicular joint; view is parallel to resting position of the clavicle. B: Side view, looking into sternoclavicular joint sinus. The three ellipses represent increasing sinus size with increased levels of displacing force (Dempster 1965).

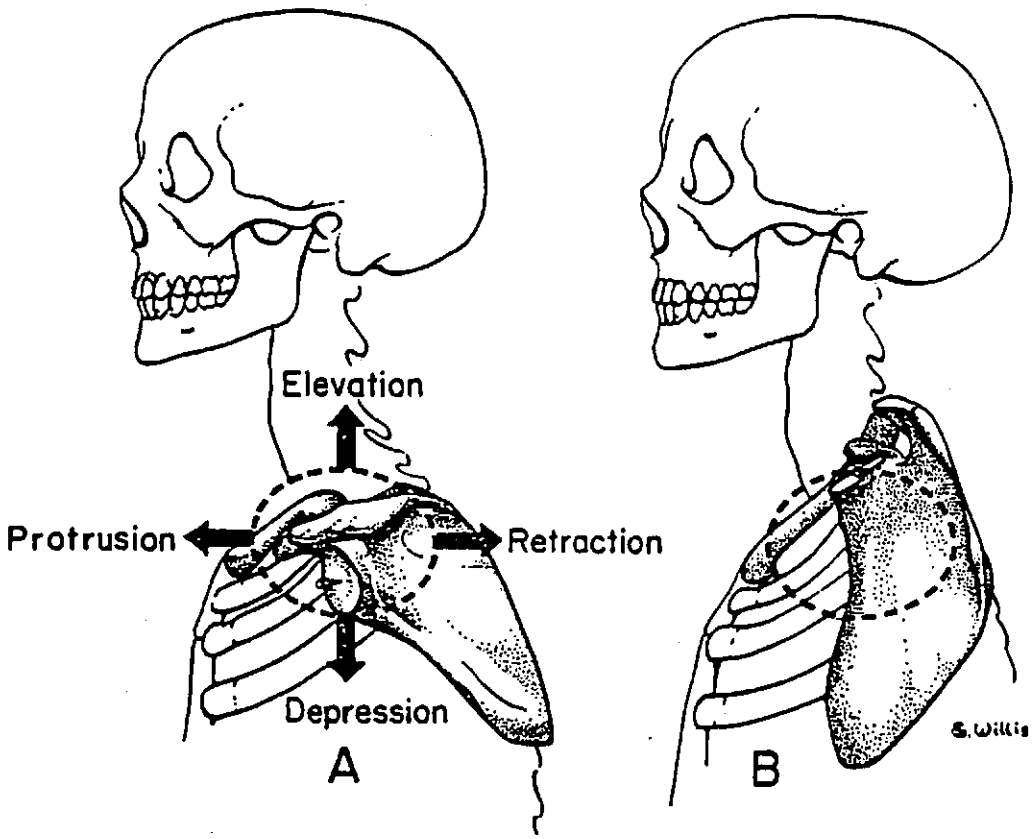

FIGURE 5–19. A: Left shoulder girdle of a skeleton-ligament preparation. The end of the pin at the glenoid fossa represents the mean center of the glenohumeral joint. Its maximum range of motion, without rotation of the shoulder girdle, is depicted by the dashed ellipse. B: The shoulder girdle at its highest position with the glenoid fossa and scaula rotated. Clavicle is rotated upward, elevated, and retracted; the scapula is flexed, medially rotated and adducted (Dempster 1965).

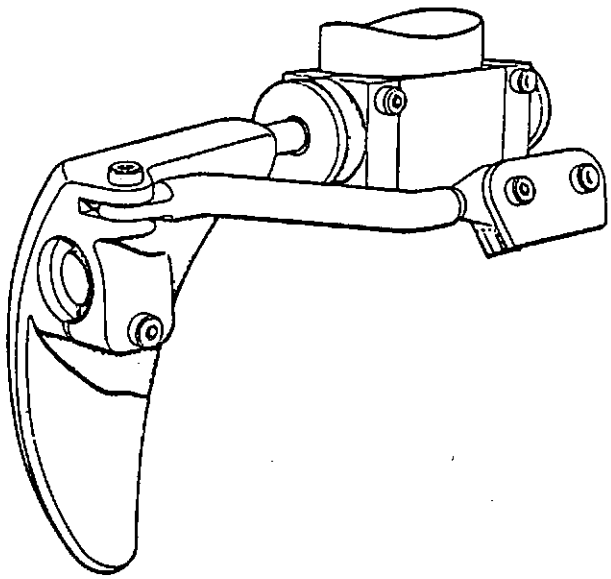

FIGURE 5–20a. Drawing of shoulder of Ogle/MIRA dummy (Warner 1974).

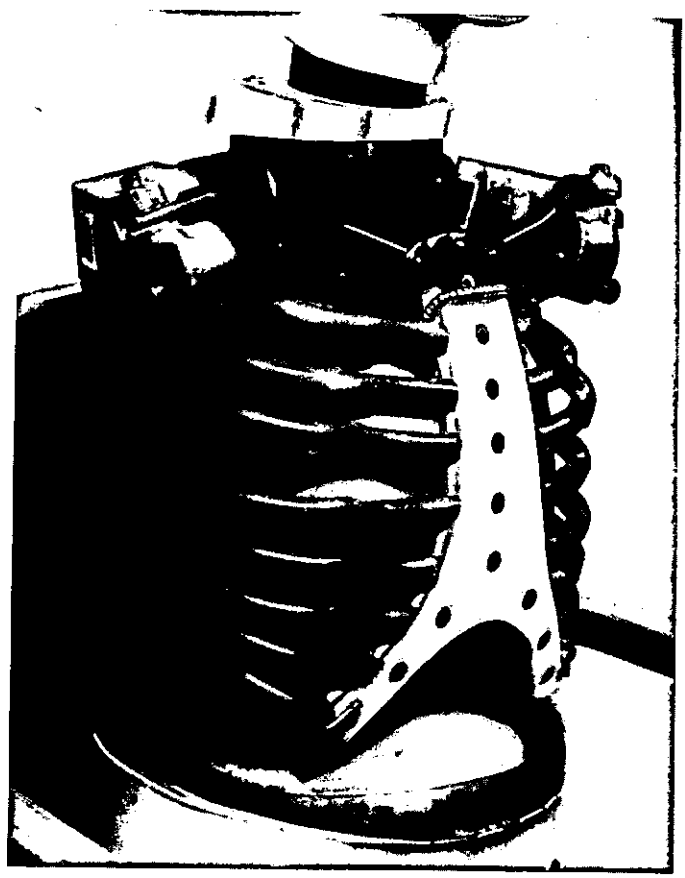

FIGURE 5–20b. Shoulders and ribcage of the Ogle/MIRA dummy.

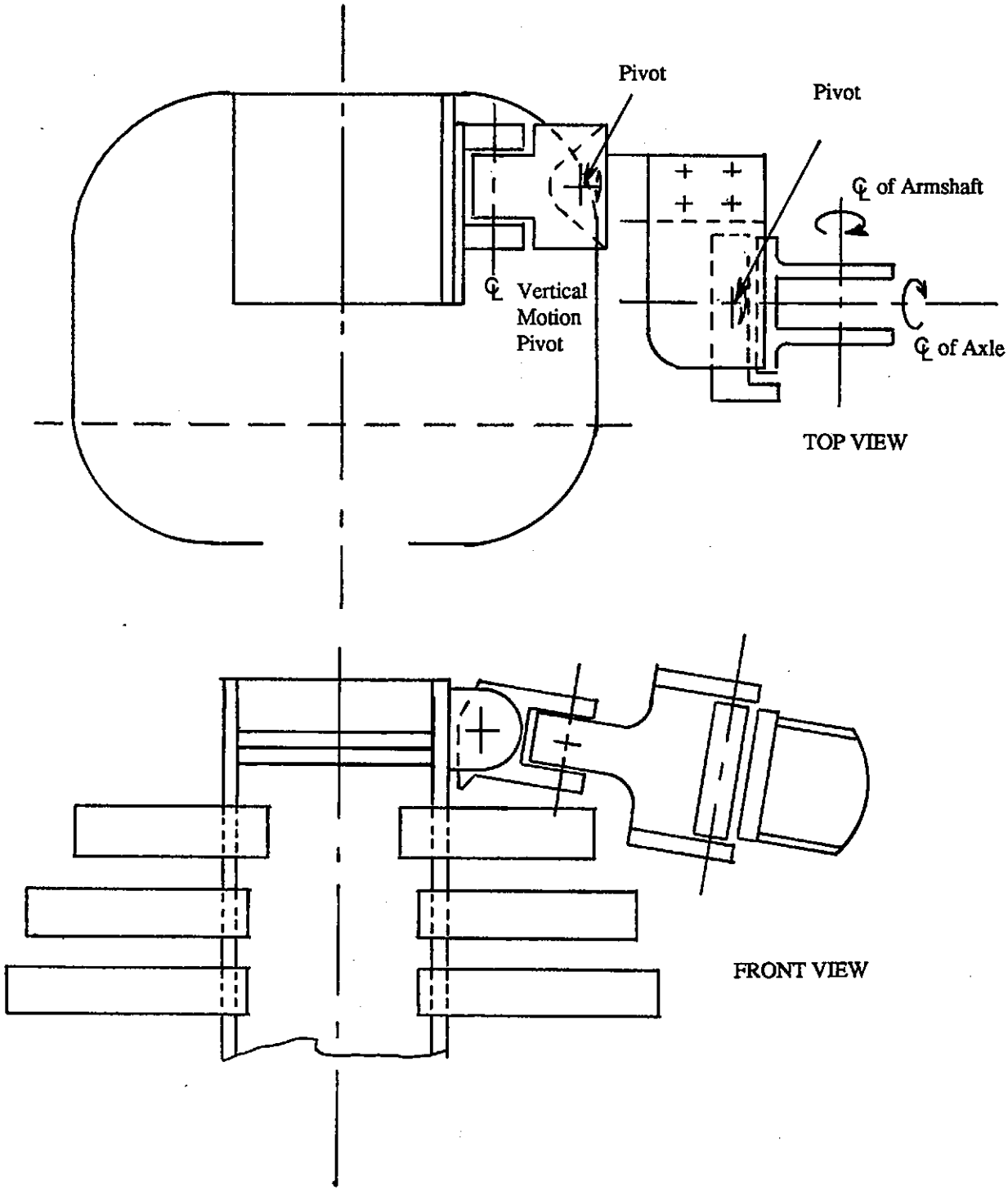

FIGURE 5–21. Top- and front-view sketches of modified Hybrid III shoulder with elevation/ attachment mechanism attached to side of spine and increased mobility in main clavicle pivot.

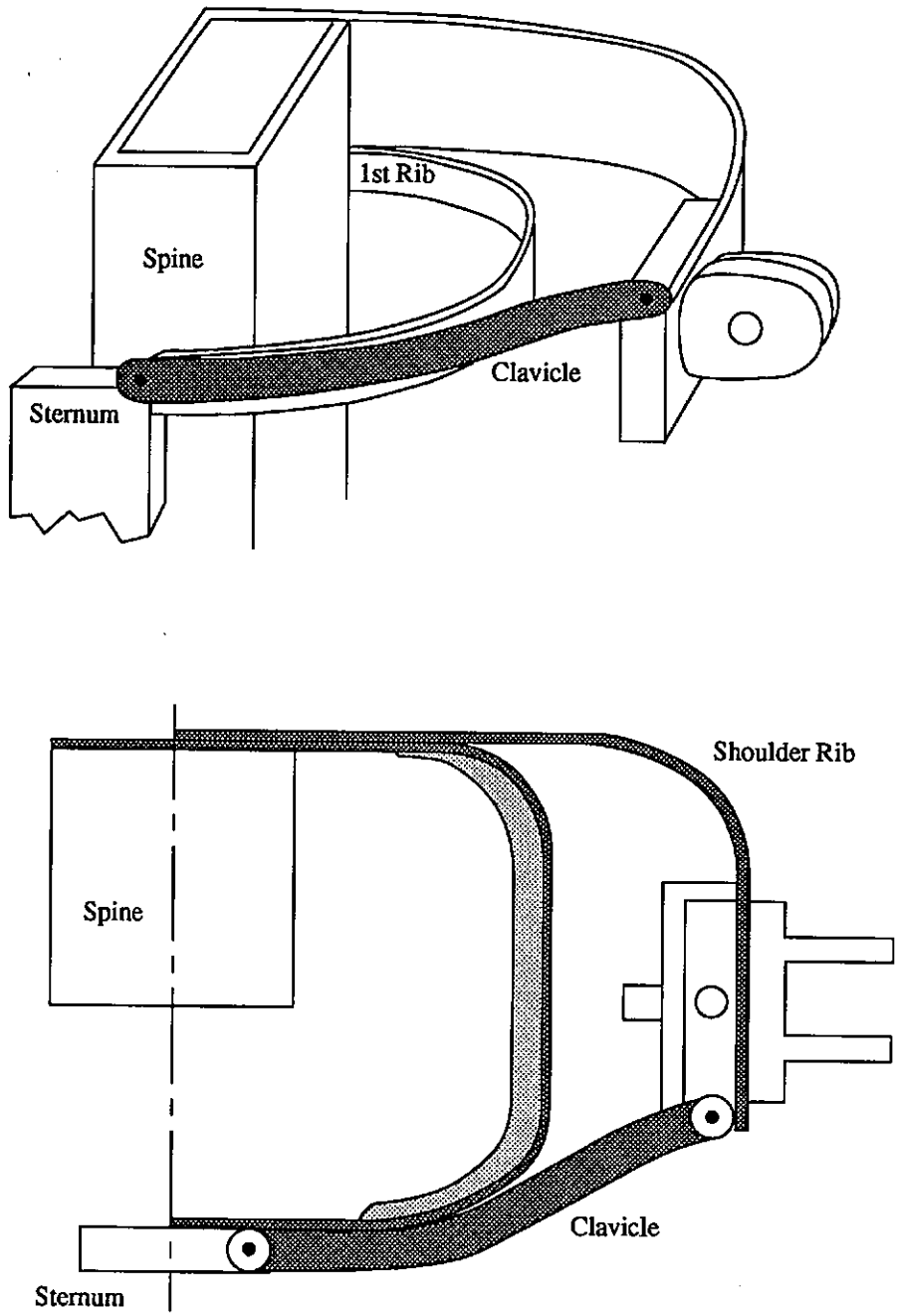

FIGURE 5–22. Sketch of alternative shoulder design using steel rib for main shoulder support and front/back mobility.

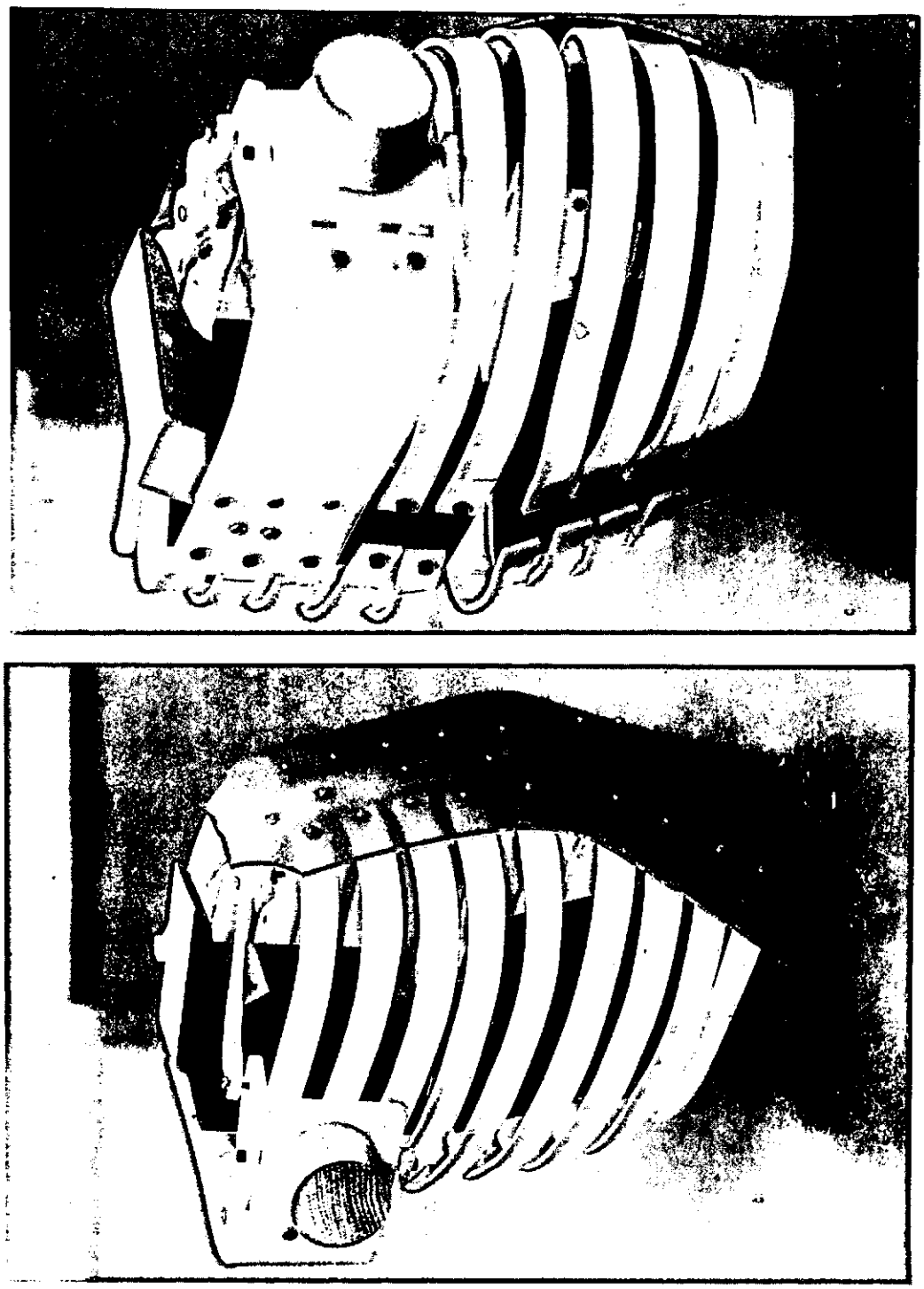

FIGURE 5–23. Acrylic model of shoulder rib design.

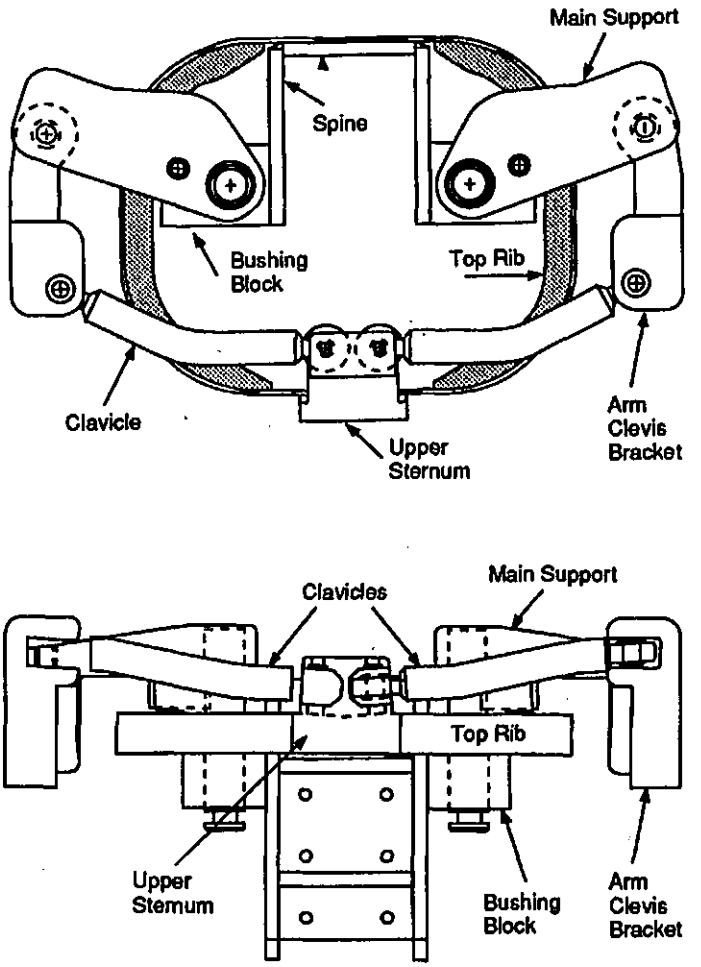

FIGURE 5–24. Top- and front-view drawings of final shoulder design concept used in First and Second Prototype-50M.

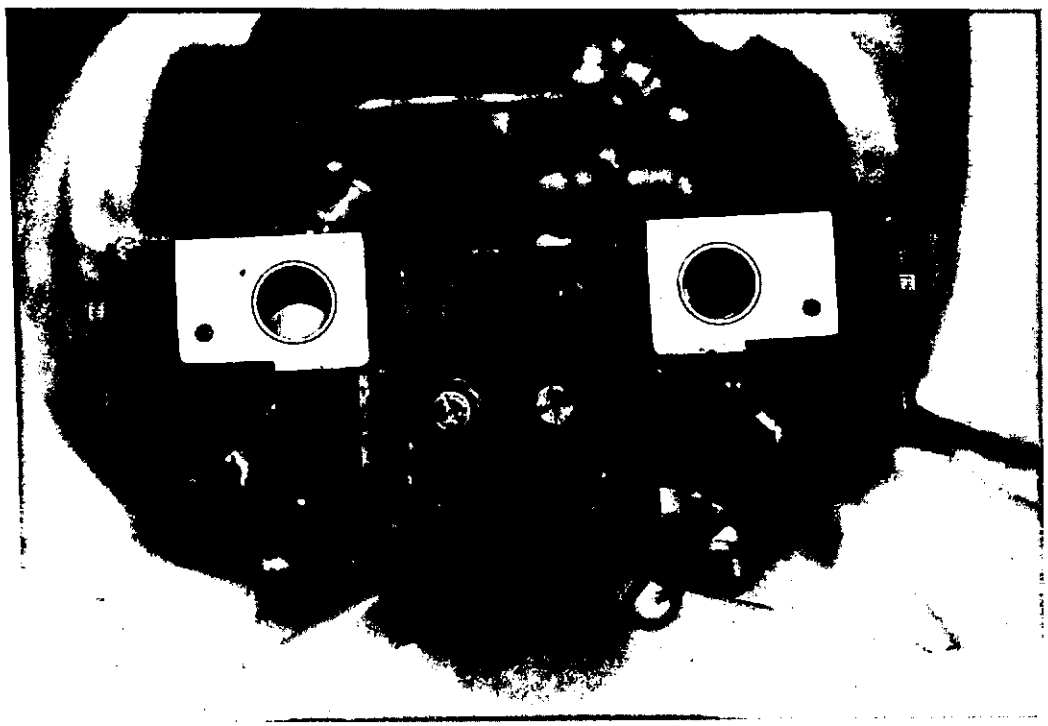

FIGURE 5–25. Top view of shoulder bushing blocks and rubber stops used to limit and control shoulder front/back range-of-motion.

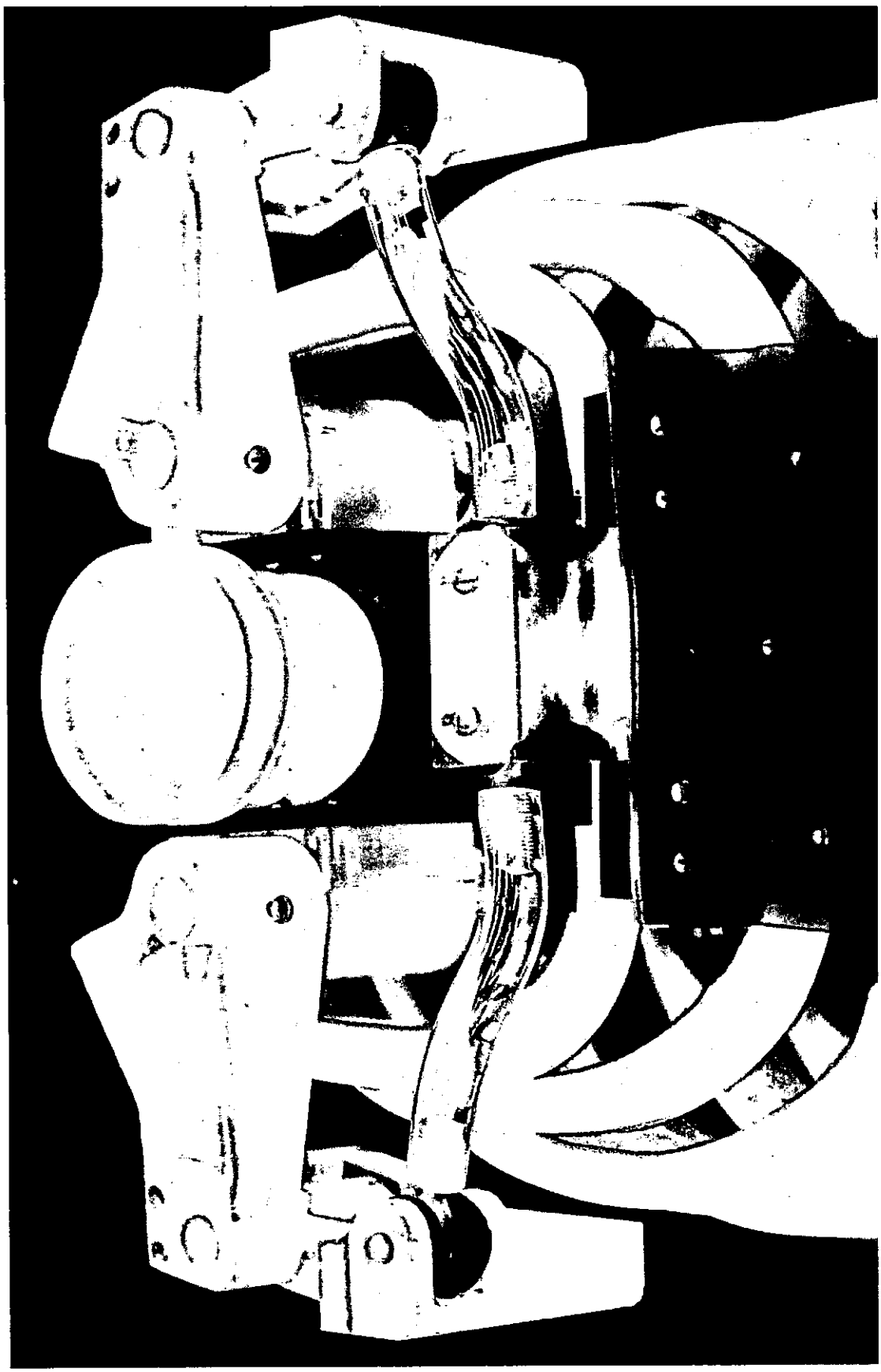

FIGURE 5–26. Acrylic model of final shoulder design.

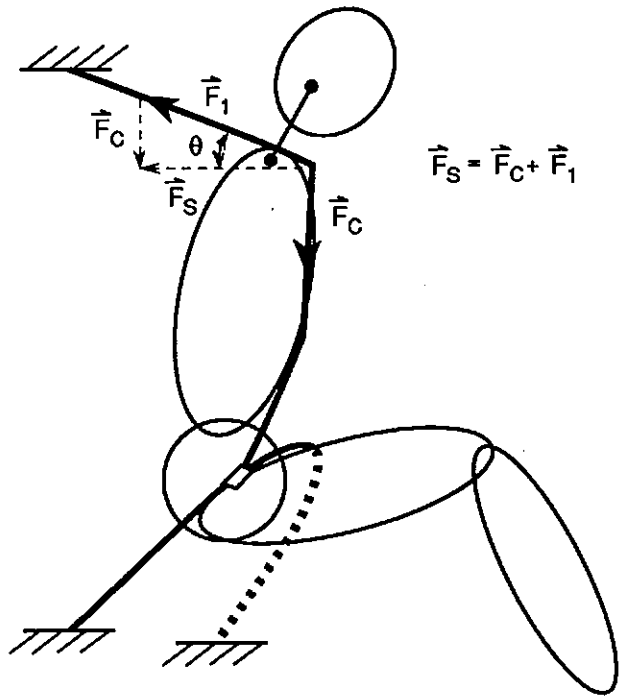

FIGURE 5–27. Configuration of MVMA-2D model for simulation of best Hybrid III sled runs.

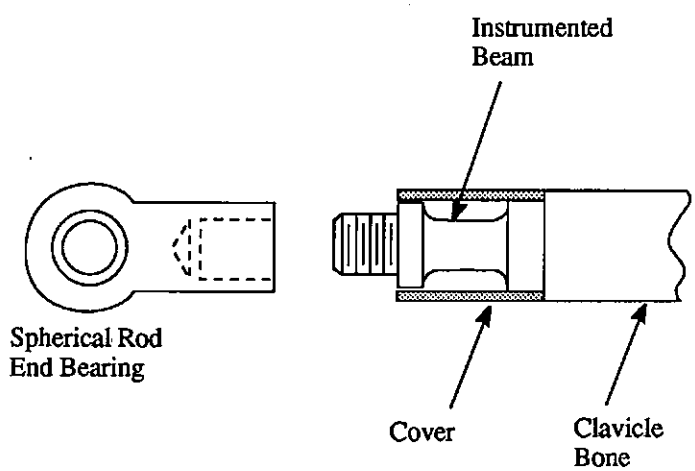

FIGURE 5–28. Clavicle force-transducer concept.

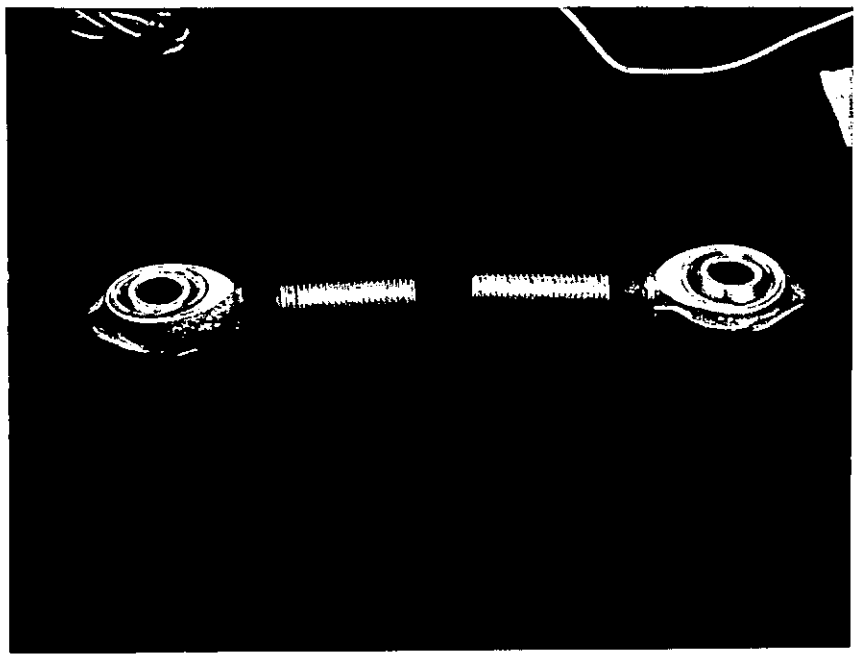

FIGURE 5–29. Prototype of instrumented rod-end shafts for measurement of clavicle loads.

Front view

Side view

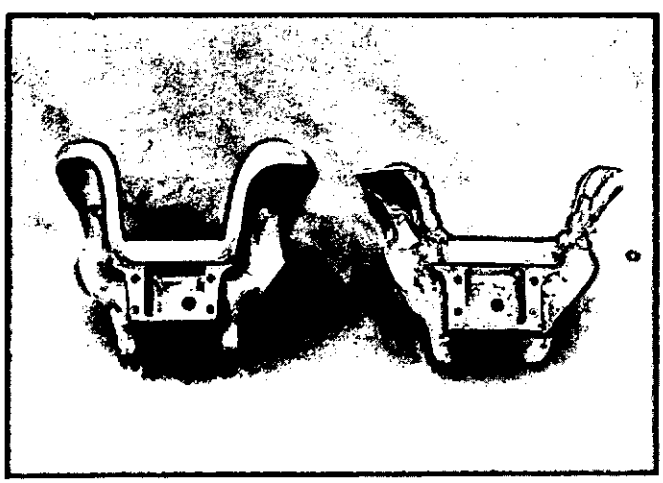

Rear view

FIGURE 5–30. Comparison of Hybrid III pelvic bone (left) to modified pelvic bone (right).

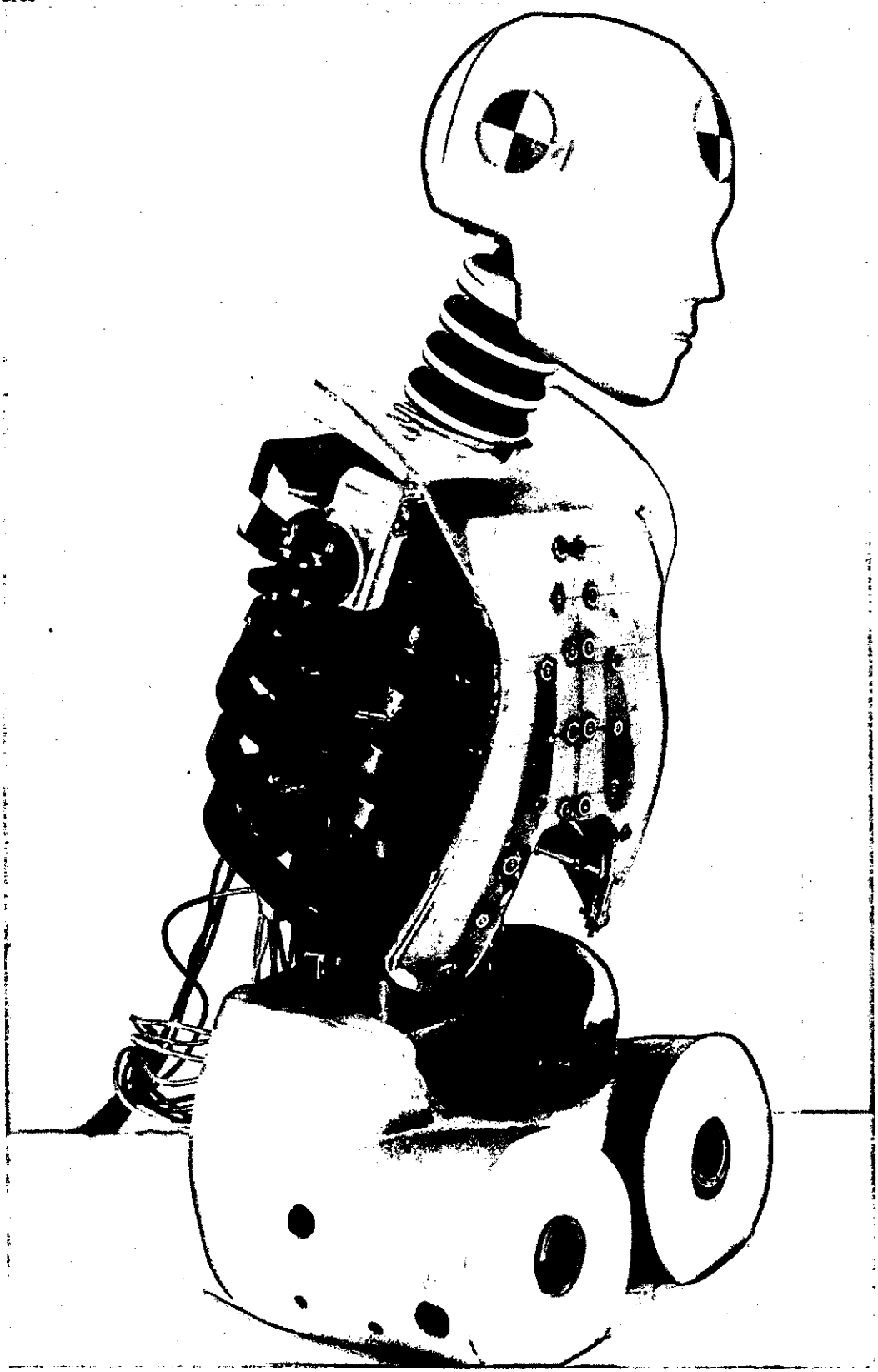

FIGURE 5–31. Second Prototype-50M showing modified pelvis assembly with skin and flesh cut away between left and right ASISs.

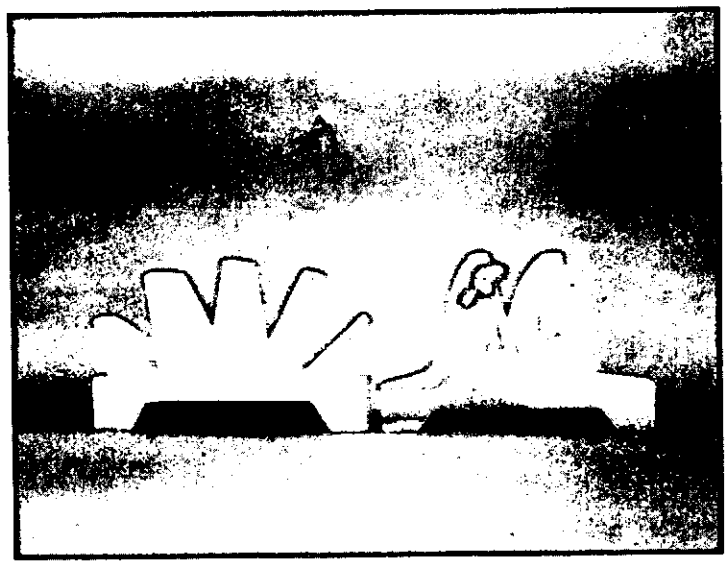

FIGURE 5–32a. Photograph of side-by-side comparison of five–point and two–point Styrofoam inserts.

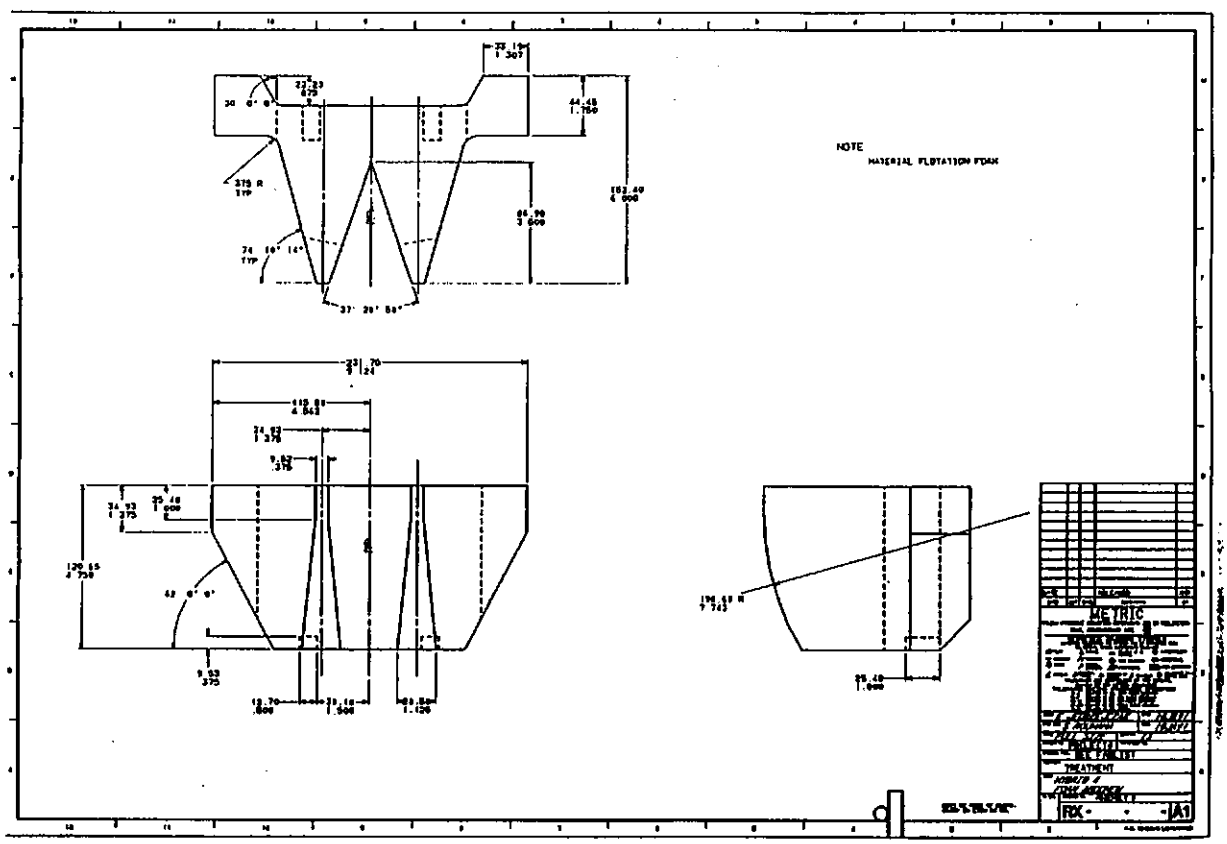

FIGURE 5–32b. Drawing of modified Styrofoam abdominal insert.

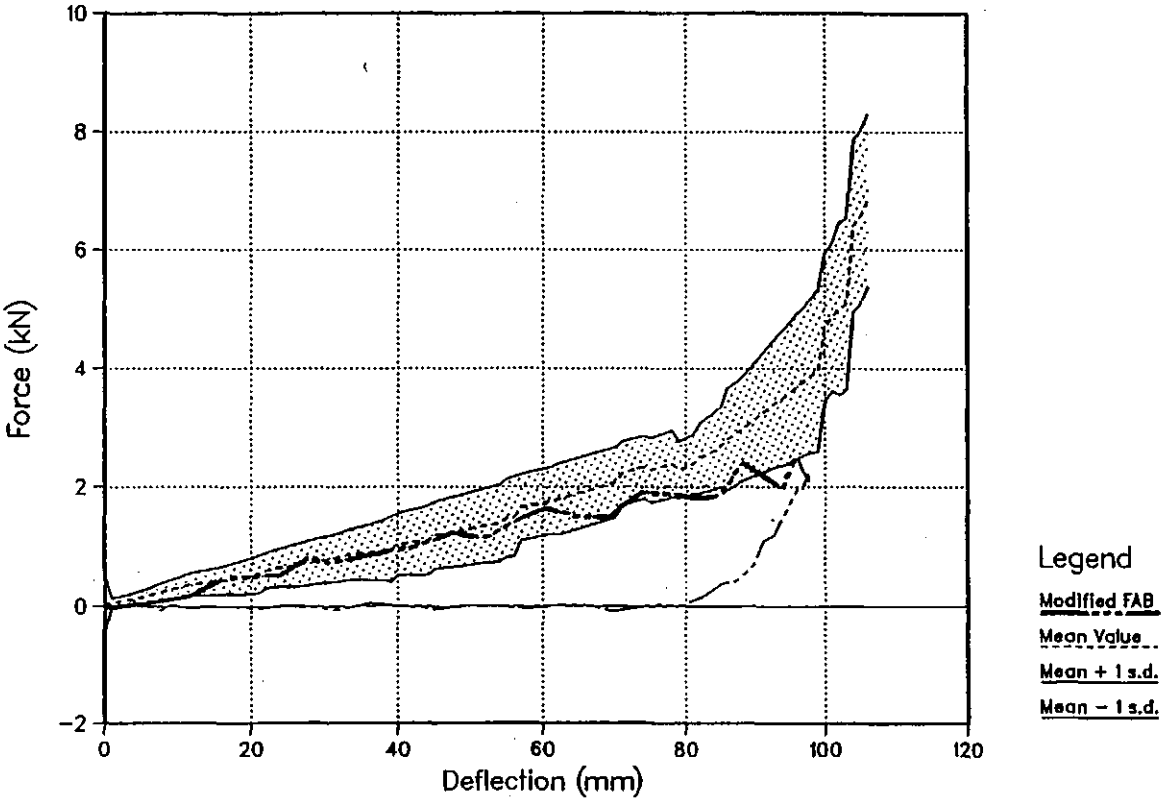

FIGURE 5–33. Comparison of belt-loading F-δ response of modified two-point Styrofoam insert with performance corridors.

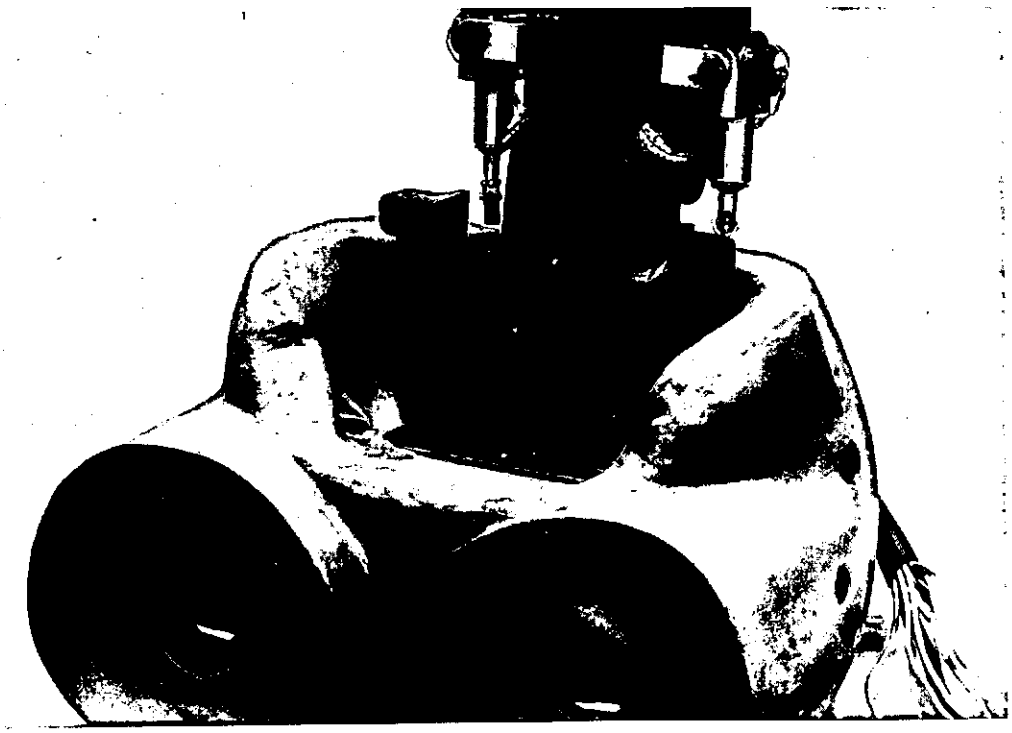

FIGURE 5–34a. View of abdomen support bracket installed between pelvic block and lumbar spine.

FIGURE 5–34b. Two-point frangible abdomen installed in Second Prototype-50M pelvis. Note urethane wedge at bottom of "v" that holds insert against reaction plate. Chest jacket provides for access to insert.

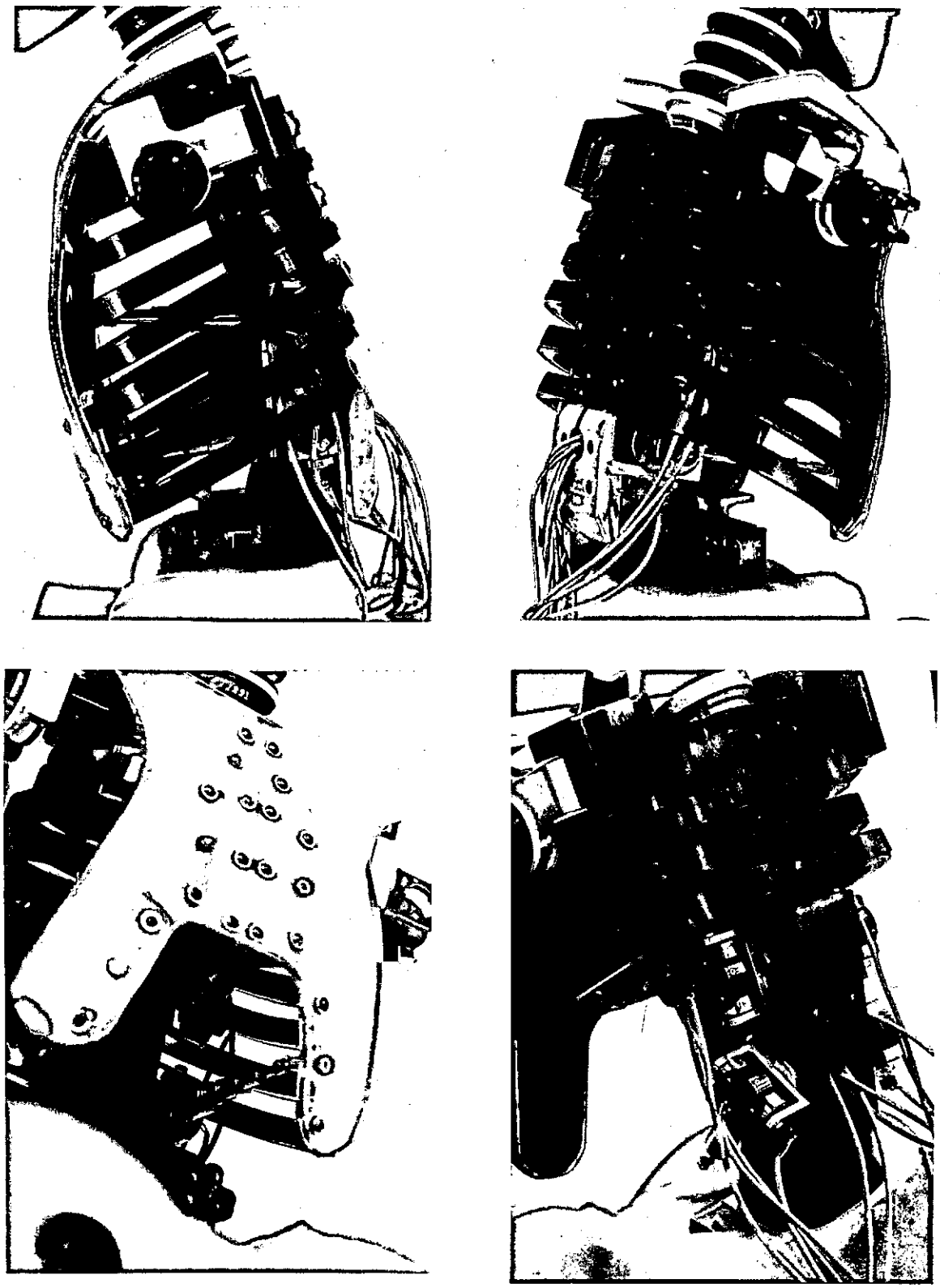

FIGURE 5–35. Views of Second Prototype-50M chest showing DGSP chest-deflection transducers installed on lower thoracic spine and connecting to third and sixth ribs.

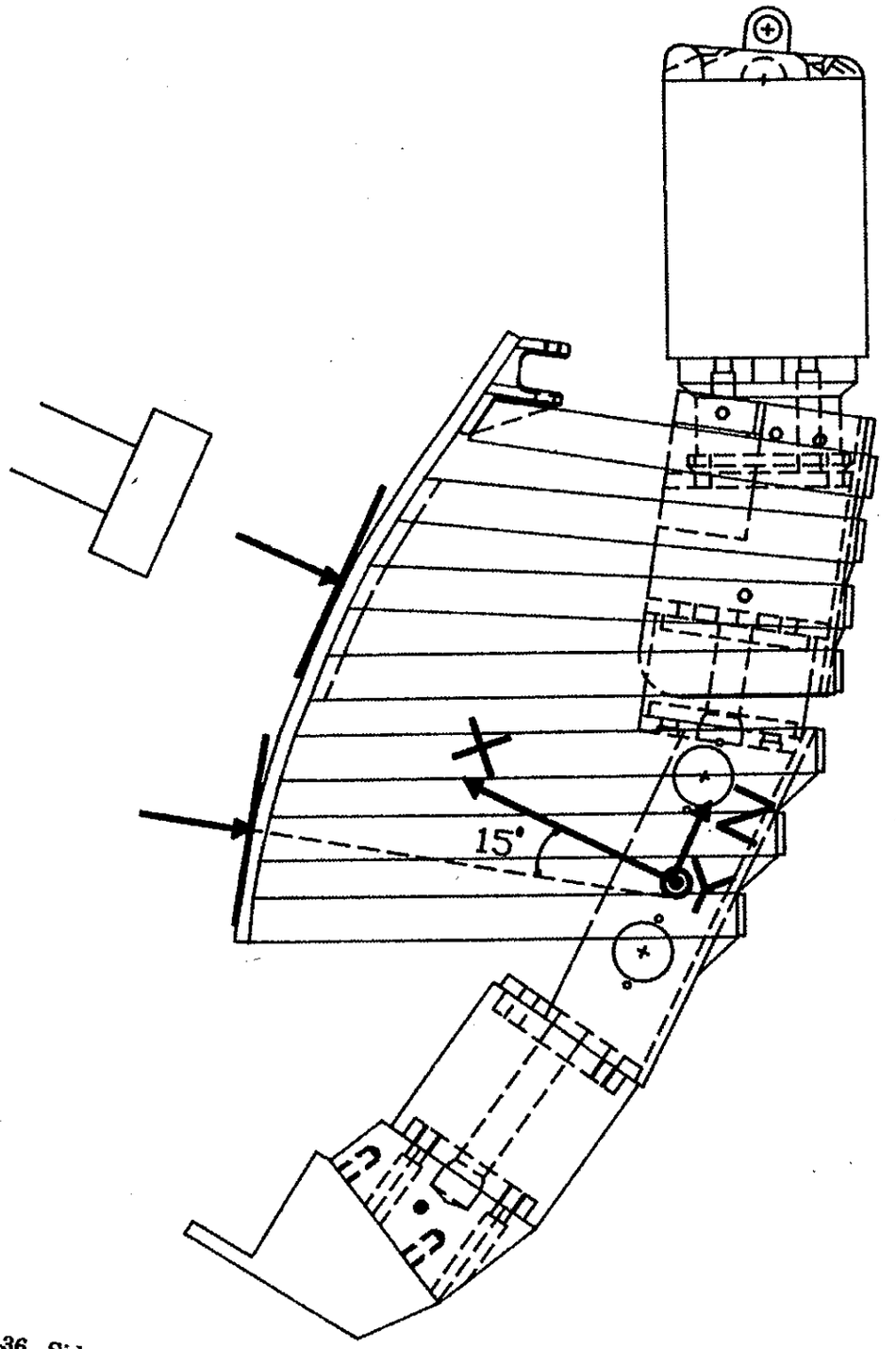

FIGURE 5–36. Side-view drawing of Second Prototype-50M assembly showing lower thoracic spine coordinate system and direction of sternal and lower ribcage compression axes.

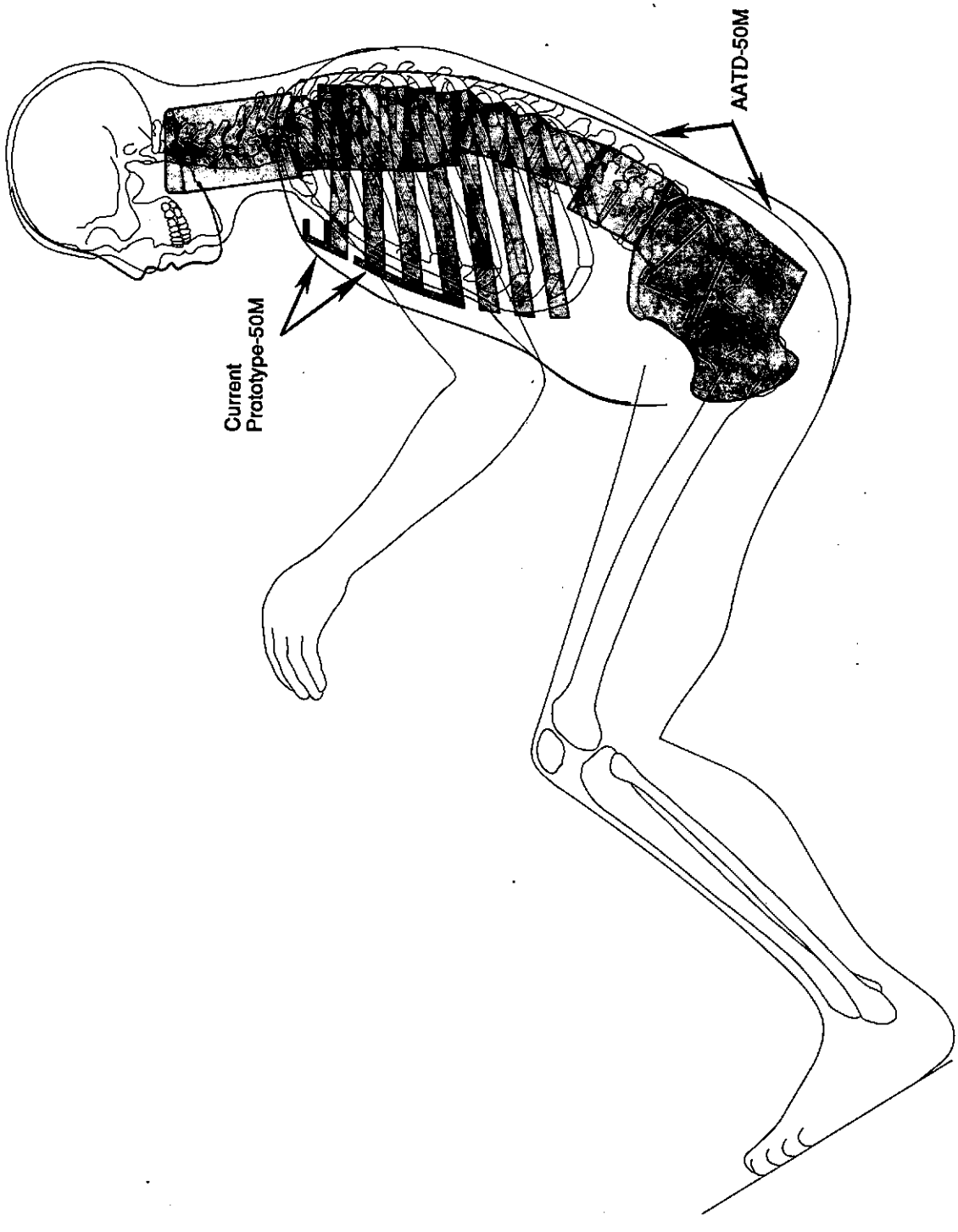

FIGURE 5–37. Overlay of the Second Prototype-50M with the AATD-50M side-view drawing.

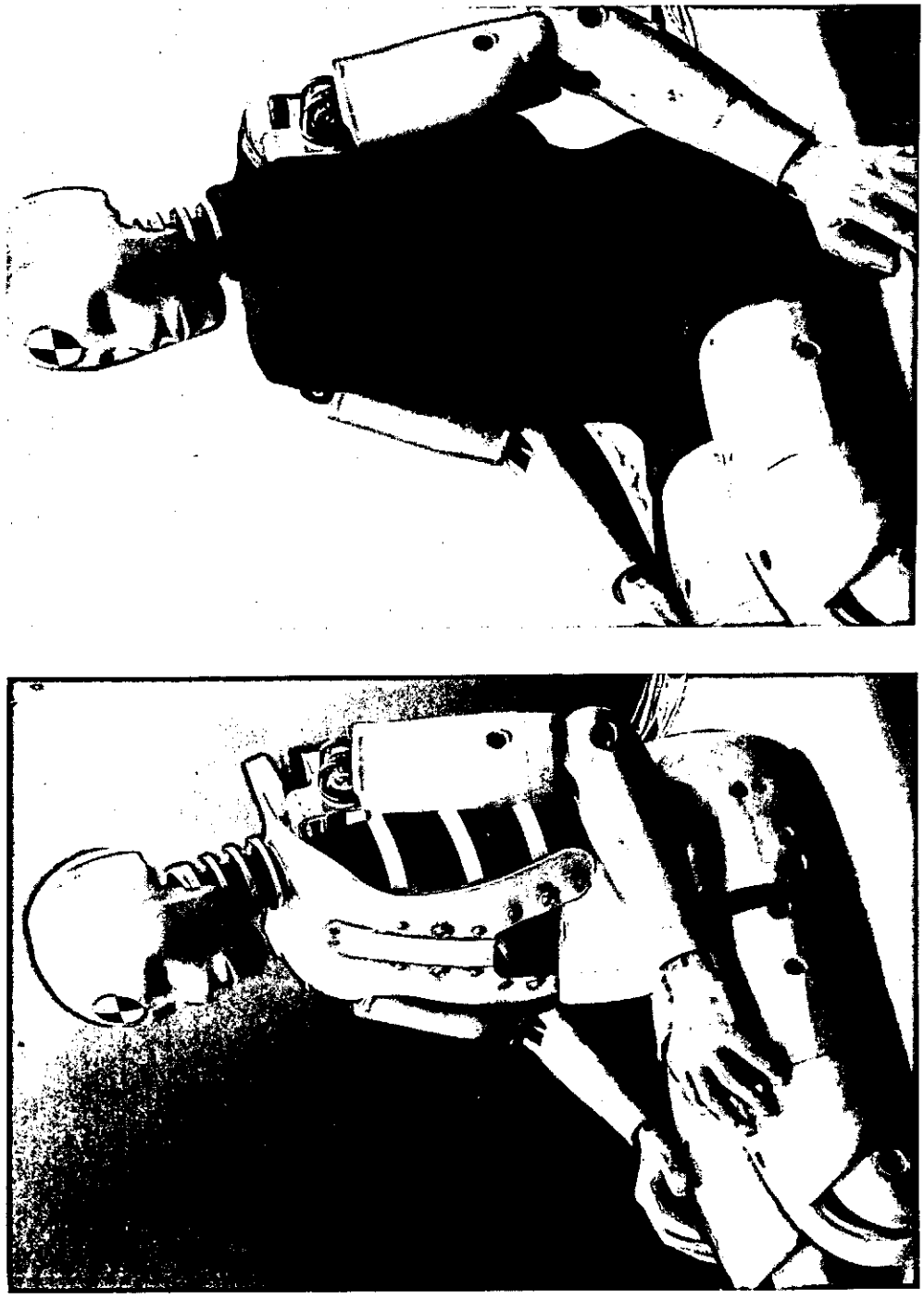

FIGURE 5–38a. Photographs of the Second Prototype-50M assembly.

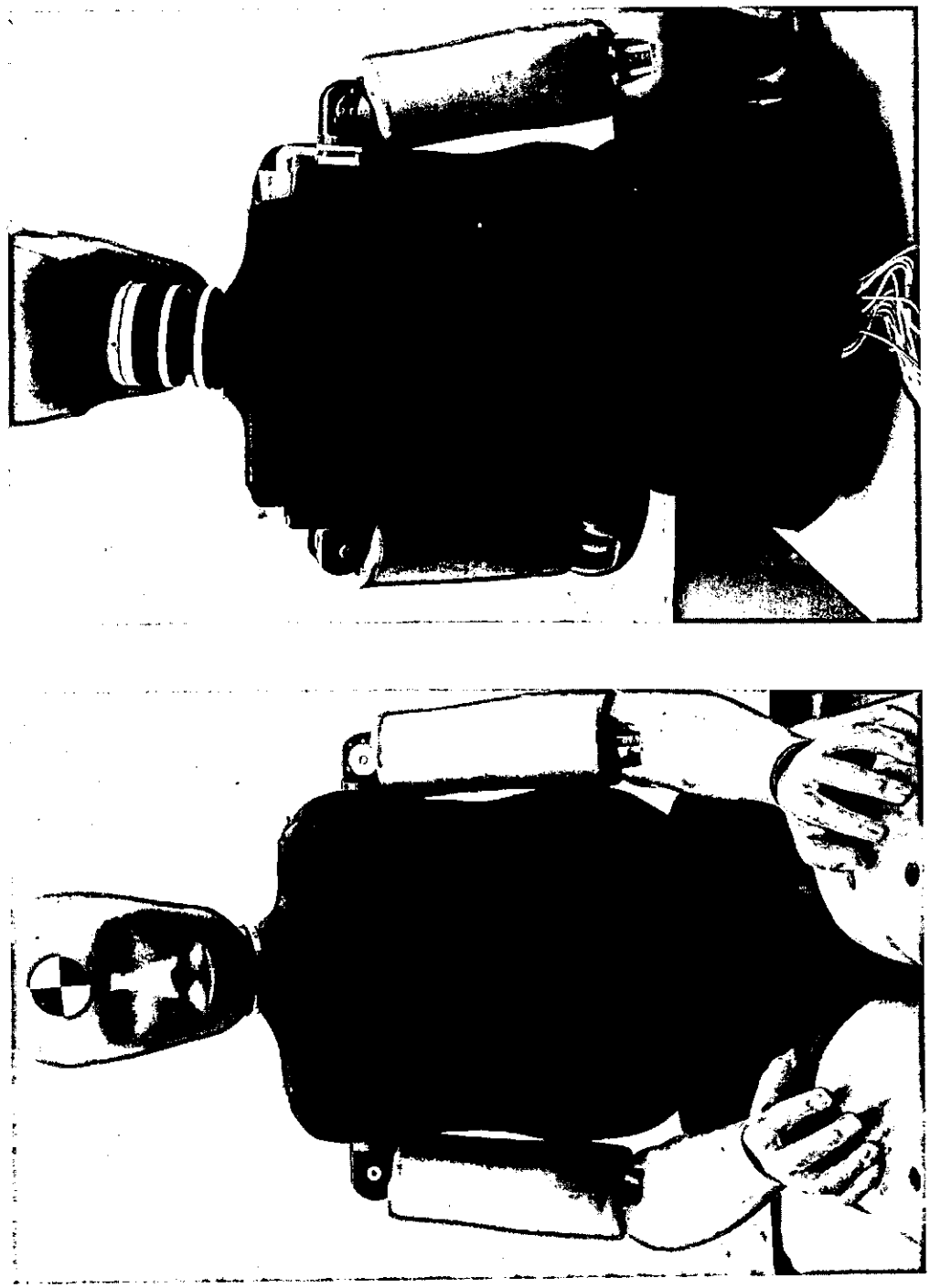

FIGURE 5–38b. Photographs of the Second Prototype-50M assembly.

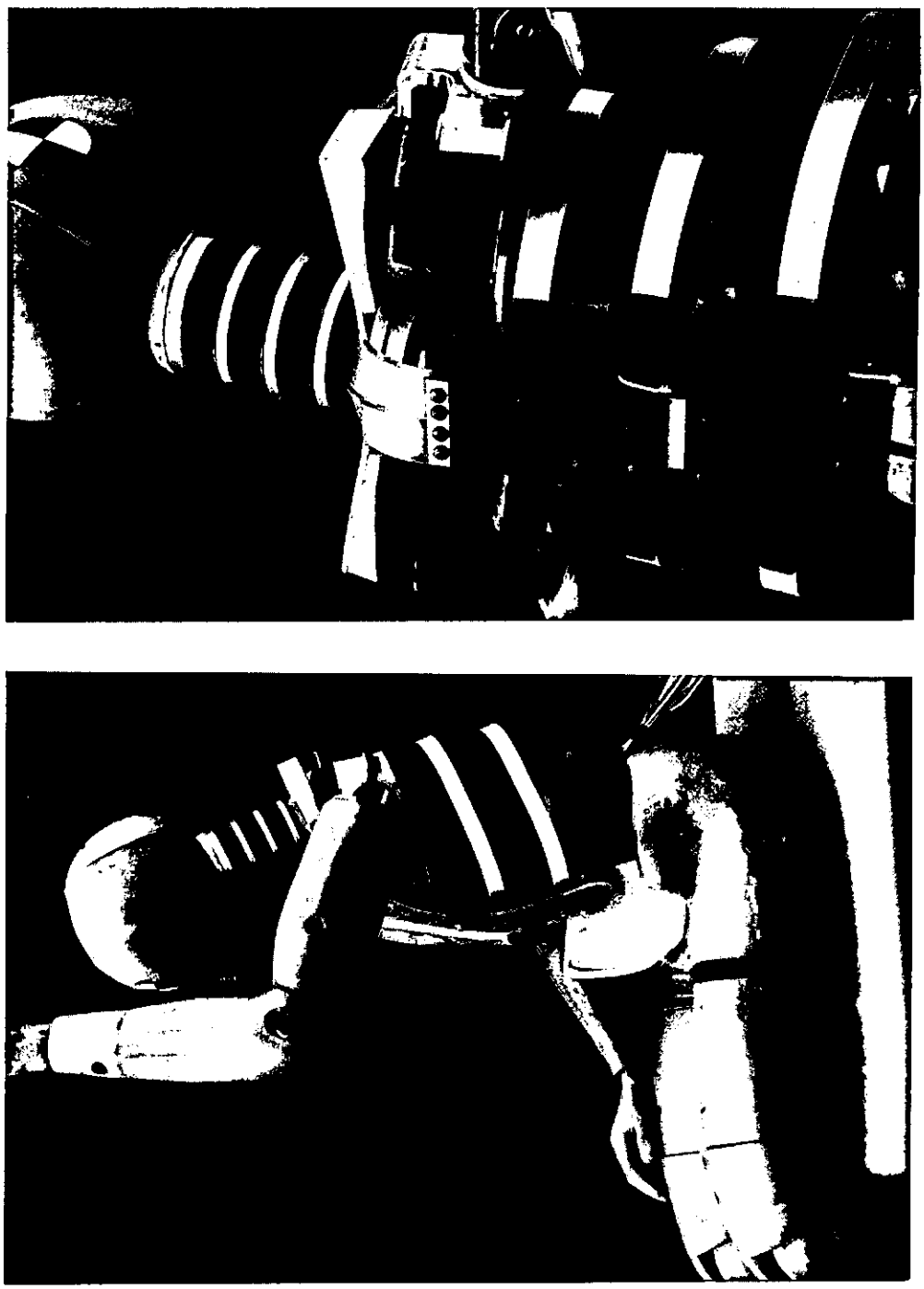

FIGURE 5–38c. Photographs of the Second Prototype-50M assembly.

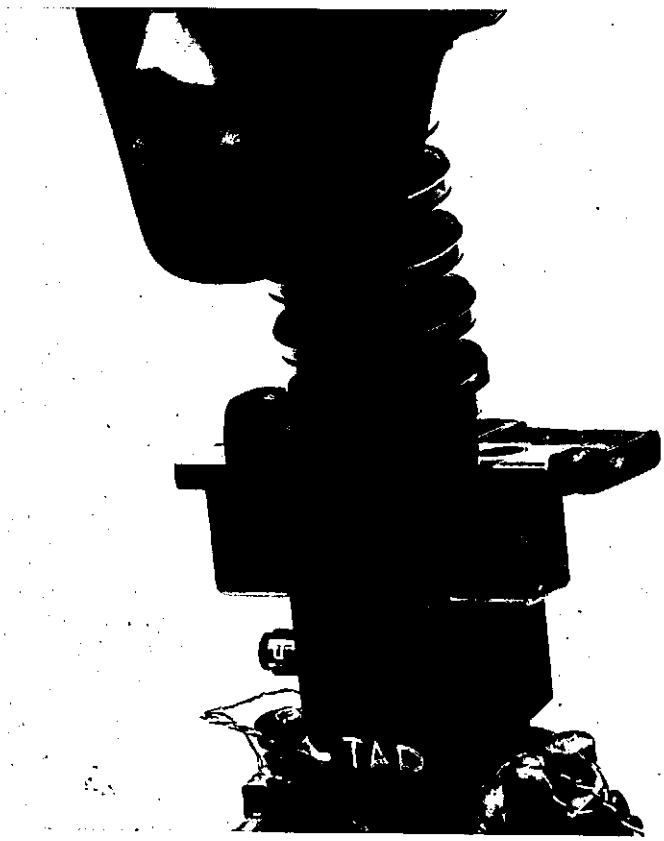

FIGURE 5–39. View of upper thoracic spine showing molded urethane piece designed to reduce shoulder-belt intrusion into the neck/shoulder gap.

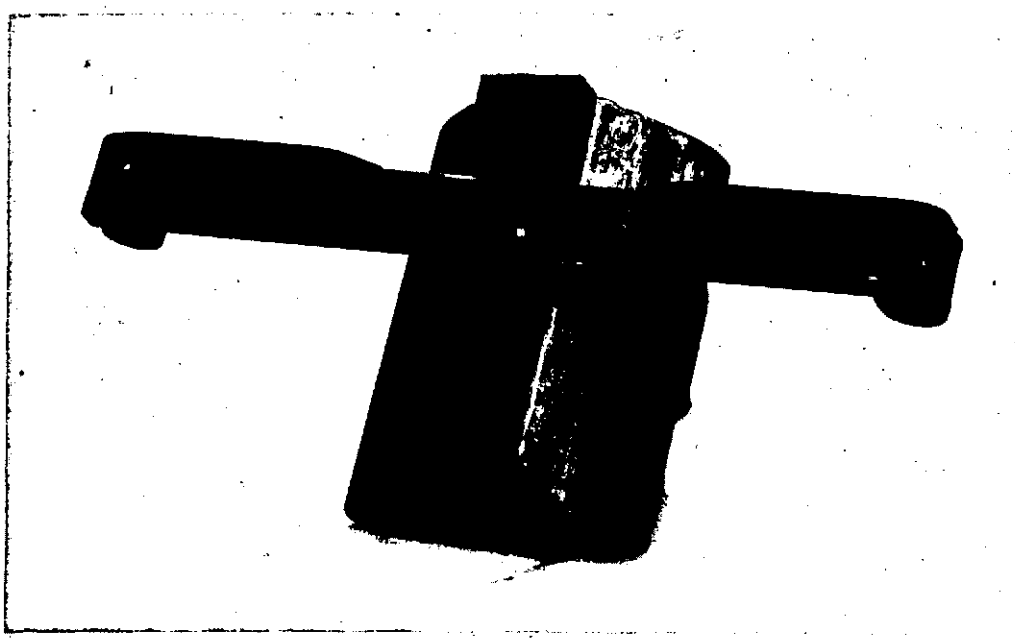

FIGURE 5–40a. Triangular lead ballast and padded cross bar designed for overload protection in front of lower thoracic spine.

FIGURE 5–40b. Side view of ballast and cross bar installed in front of lower thoracic spine.

FIGURE 5–40c. Closeup of ballast and padded cross bar in front of spine box.

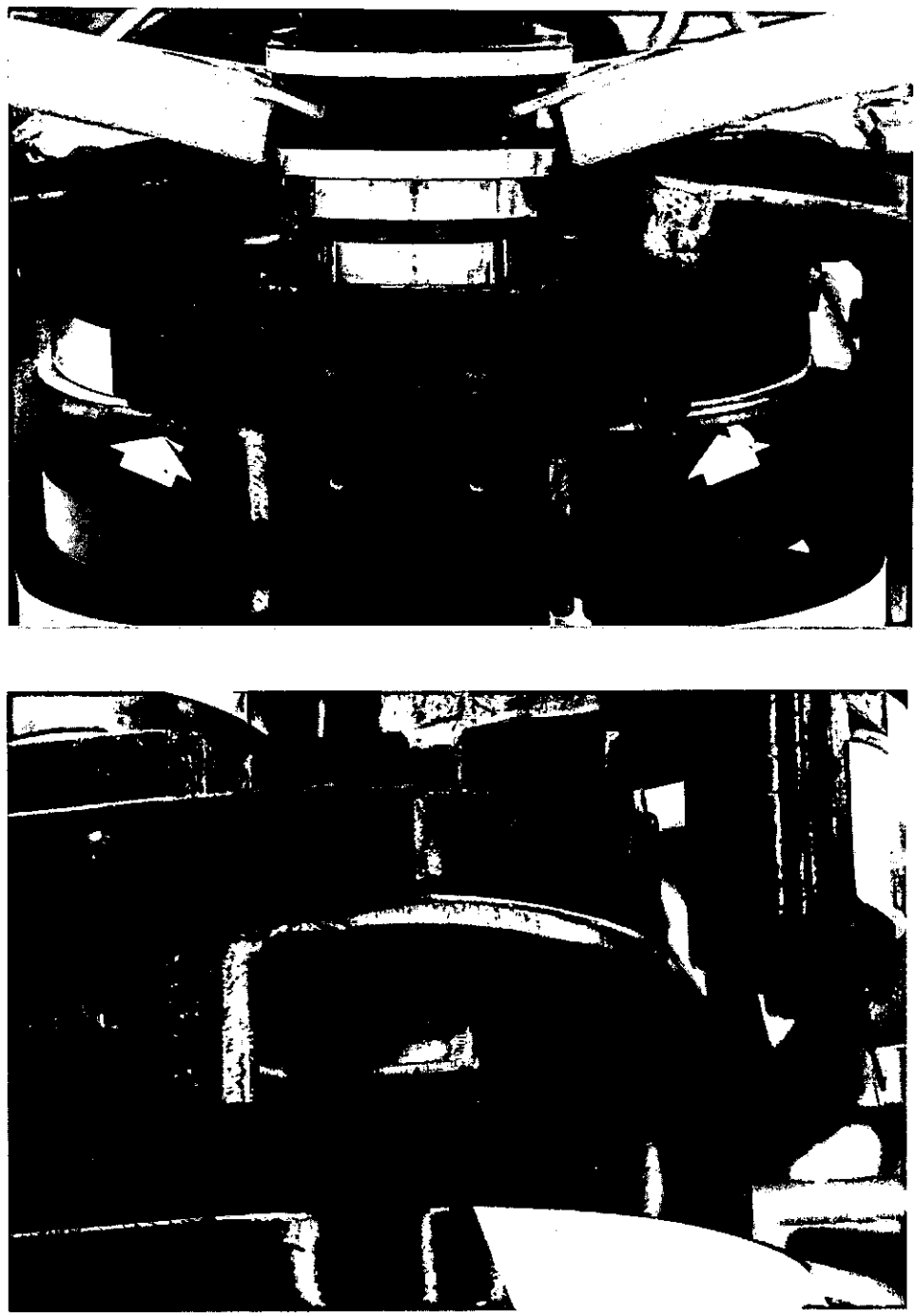

FIGURE 5–41. Photographs of Teflon-covered steel shelves under the top rib of the Second Prototype-50M ribcage.

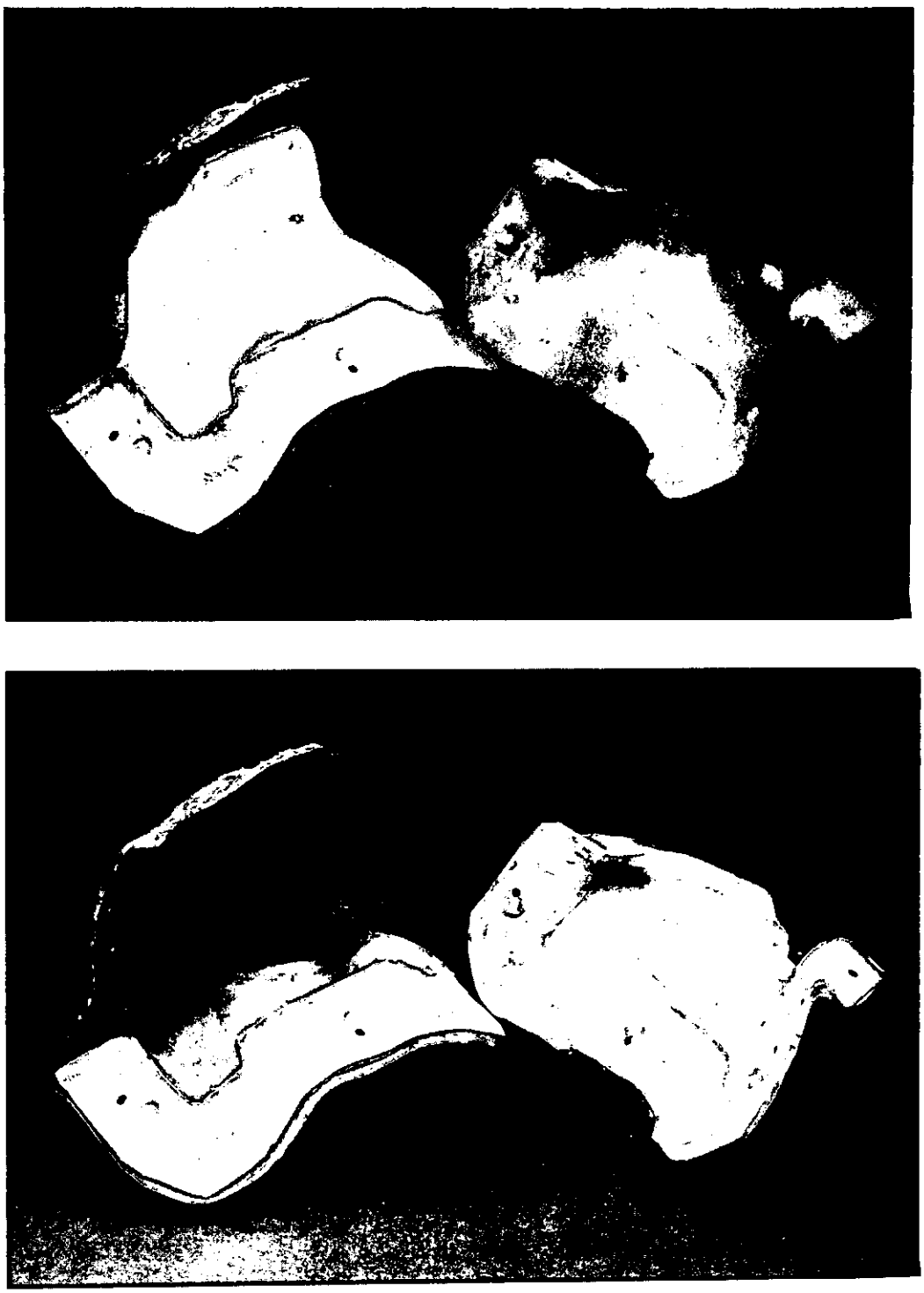

FIGURE 5–42. Three-piece fiberglass abdomen mold at top shown with soft urethane abdomen at bottom.

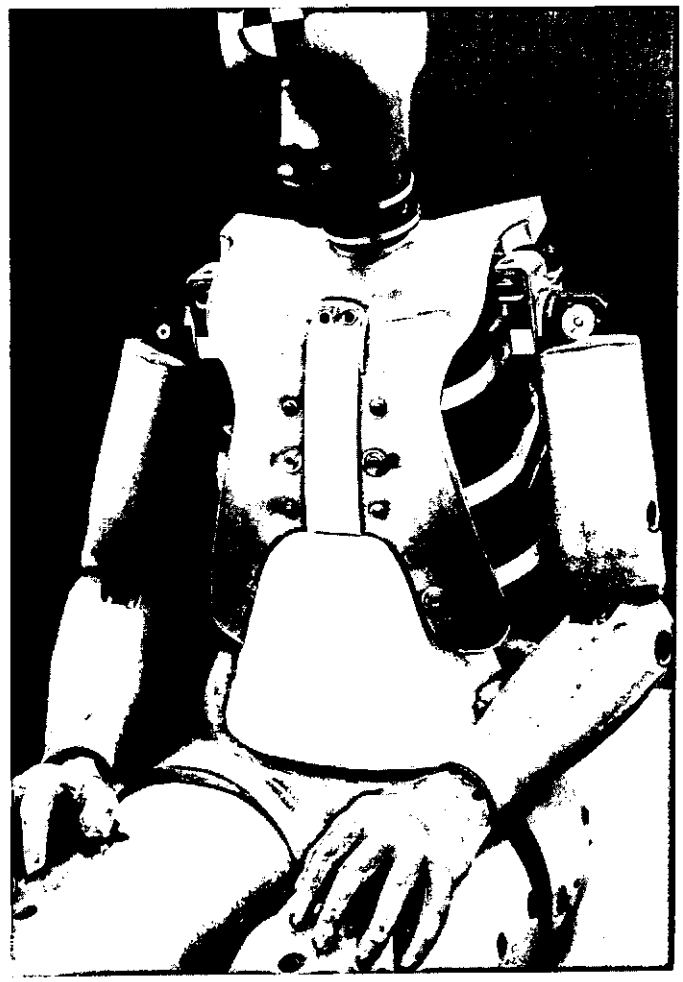

FIGURE 5–43. Soft urethane abdomen installed in Second Prototype-50M.

FIGURE 5–44. Wood die of frangible abdomen installed in mold.

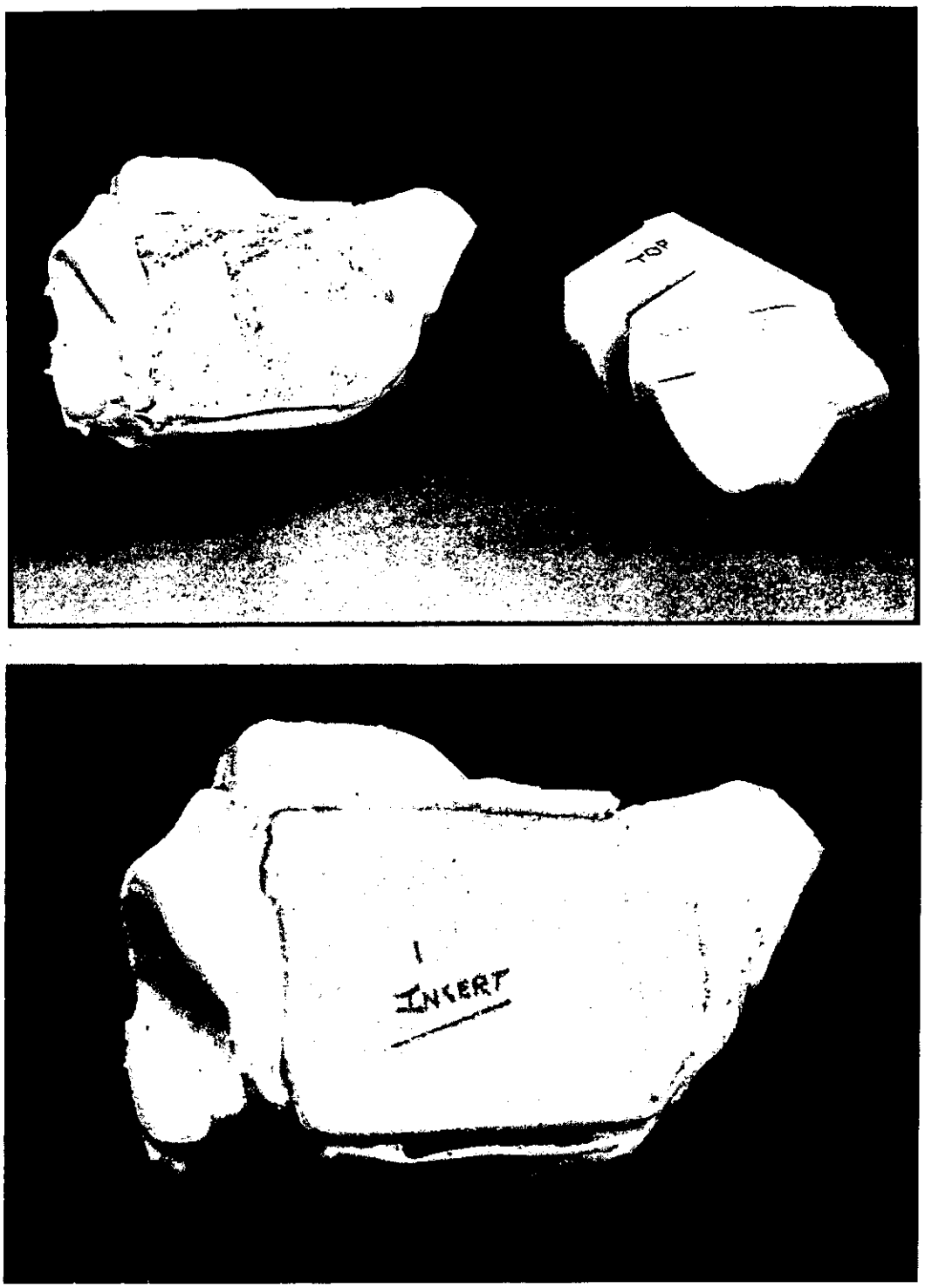

FIGURE 5–45. Soft urethane abdomen with cavity and Styrofoam insert.

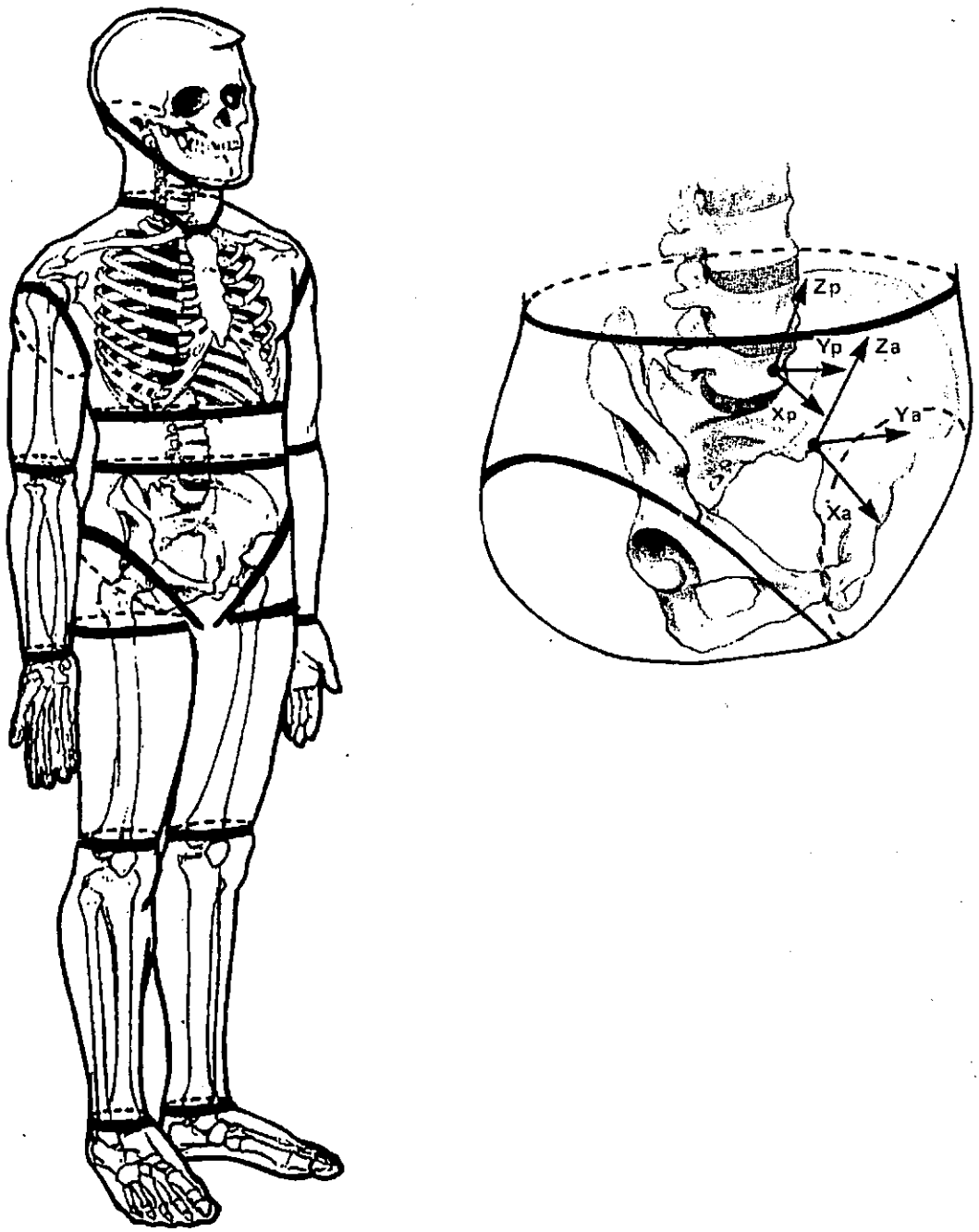

FIGURE 5–46. Body and pelvic segmentation planes used by McConville et al. (1980).

6. TESTING AND PERFORMANCE OF THE FIRST AND SECOND PROTOTYPE-50M THORAX ASSEMBLIES

6.1 OVERVIEW

During the course of the design and development process, the thorax assemblies described in Section 5 underwent extensive testing and performance evaluations relative to the specifications outlined by Schneider et al. (1990) and summarized in Section 2 and Appendix A of this report. Testing was conducted on both the first and second (i.e., current) Prototype-50M assemblies and with various hardware modifications that were implemented, in an attempt to fine-tune the response. These tests included quasi-static loading of the thorax with both 152-mm (6-in) diameter and 50-mm by 100-mm (2-in by 4-in) rigid loading plates, pendulum impact testing to the sternal and lower ribcage areas, and impact sled testing with three-point restraint systems. This section describes these tests and the performance of the prototype systems in comparison to the targeted specifications.

6.2 QUASI-STATIC LOADING OF THE FIRST PROTOTYPE-50M THORAX

Prior to dynamic testing of the first prototype ribcage, a series of quasi-static loading tests was carried out using the UMTRI Instron facility. Tests were conducted using both a 152-mm-diameter (6-in) rigid loading plate as used by Lobdell et al. (1973) on cadavers, and with the 50-mm by 100-mm (2-in by 4-in) rigid loading plate used by Cavanaugh (in Schneider et al. 1990).

6.2.1 Loading with 152-mm (6-in) Diameter Plate

Figures 6–1a through 6–1c show the first Prototype-50M ribcage undergoing quasi-static loading with the 152-mm (6-in) diameter plate. These tests were conducted at the upper and and midsternum on the midline and at the lower ribcage approximately 75 mm (3 in) lateral to the midline without padding in place. Tests were conducted for both 25 and 50 mm (1 and 2 in) strokes of the Instron head, which were also used as the measure of chest compression or deflection in these tests. Initial tests were conducted without steel bands coupling the ribs up and down on each side of the sternum, but a final test was conducted with two 3.8-mm (0.015-in) thick strips of spring steel fastened to the top layer of urethane bib on each side.

Figure 6–2 shows the results of these initial tests. The stiffness at the mid/lower sternum was affected very little by the presence of the coupling bands and was significantly greater than the stiffness of tensed humans from the Lobdell et al. (1973) study. It is also noted that the stiffness of the upper sternum was lower than the stiffness of the mid/lower sternum. The obvious reason is the reduction in the number of ribs that are directly loaded by the 152-mm (6-in) diameter plate, but the result is the opposite of that desired for human biofidelity. The stiffness for the lower ribcage is similar to that of the tensed-human corridor.

6.2.2 Loading with 50-mm by 100-mm (2-in by 4-in) Plate

Prior to conducting quasi-static loading tests with the 50-mm by 100-mm (2-in by 4-in) loading plate, the eighth or bottom rib was removed from the assembly after problems with pelvic interaction were observed. In part, these problems were due to the geometry of the Hybrid III pelvis, but comparison of the AATD-50M ribcage drawings with other anatomical photographs, skeletons, and drawings suggested that the tenth rib in the AATD-50M drawing (Schneider et al. 1985) may be somewhat low. In any case, removal of the bottom rib seemed to be the most expedient solution to this problem.

Figures 6–3a and 6–3b show the forces recorded for 25 mm (1 in) and 50 mm (2 in) of Instron stroke at different regions of the ribcage and for coupling with different thicknesses of spring-steel bands. These results are summarized in Table 6–1.

TABLE 6–1

RIBCAGE STIFFNESS VALUES (N/mm) OBTAINED FOR 50-MM BY 100-MM RIGID-PLATE LOADING OF DIFFERENT REGIONS OF THE PROTOTYPE RIBCAGE AND WITH DIFFERENT THICKNESSES OF STEEL-BAND COUPLING THE RIBS FROM TOP TO BOTTOM ON EACH SIDE OF THE STERNUM

Position	NO STEEL		0.01 STEEL		0.02 STEEL		0.025 STEEL	
	25-mm Defl.	50-mm Defl.	25-mm Defl.	50-mm Defl.	25-mm Defl.	50-mm Defl.	25-mm Defl.	25-mm Defl.
Upper Sternum	15.8	16.2	15.8	17.5	21.0	18.8	21.0	21.0
Mid Sternum	24.5	25.0	28.0	28.5	28.0	28.9	31.5	29.8
Lower Sternum	19.3	21.5	21.0	22.8	24.5	25.4	24.5	25.4
Top Ribs	22.8	25.0	23.6	26.3	24.5	28.9	29.8	30.6
Mid Ribs	17.5	21.5	20.1	23.6	23.6	26.3	22.8	27.1
Lower Ribs	15.8	14.0	14.0	18.0	15.8	16.6	19.3	21.9

As with the 152-mm (6-in) diameter plate, the stiffness values are lower for the upper sternum than for the mid and lower sternum and are lowest for the lower ribcage. The thickness of the coupling band has an effect on stiffness, but not on the relative differences in stiffness between the different regions. At the midsternum, the stiffness ranges from about 24.5 N/mm (140 lb/in) without steel-band coupling to about 31.5 N/mm (180 lb/in) for coupling with 0.635-mm (0.025-in) thick steel bands. At the lower ribcage, the stiffness ranges from about 14.0 N/mm (80 lb/in) to about 19.3 N/mm (110 lb/in).

6.3 PENDULUM TESTING OF THE FIRST PROTOTYPE-50M THORAX

6.3.1 Calibration of UMTRI Pendulum Test Results

Because of concerns during fixed-back pendulum tests of the thin-steel Hybrid III chest (see Section 3.4.2), with regard to the amount of energy represented in the force-deflection loading curves compared to the amount of energy delivered to the chest, it was

desired to compare the results obtained with the UMTRI pendulum to results obtained at other labs prior to conducting tests of the prototype chest. In order to do this, a new set of standard Hybrid III ribs was obtained and installed in the Hybrid III dummy. The impactor mass on the UMTRI pendulum was changed from 13.6 kg (30 lb) to 23 kg (51.5 lb) to match the Kroell et al. (1974) unrestrained test conditions and the chest was impacted at nominal impact velocities of 4.3 m/s and 6.7 m/s. The results are shown in Figures 6–4a and 6–4b.

For comparison, Hybrid III calibration test results were also obtained from First Technology Safety Systems, Inc. (FTSS) for tests conducted at 6.7 m/s. Figure 6–5 compares the results from the UMTRI test facility to those from FTSS, which include one test conducted several years ago using a chest with the old (i.e., Lord) damping material. The other test is for a Hybrid III calibration conducted at the FTSS calibration laboratory at Wayne State University. While it would have been most ideal to conduct tests at different laboratories using the same ATD chest, the results obtained on the UMTRI pendulum were considered to be in good agreement with those from other facilities and confirmed the validity of the results from the UMTRI test facility.

Differences between the force-deflection curves noted in Figure 6–5 may be attributed to differences in the damping material and the absence of a chest jacket in the UMTRI test. It should also be noted that the velocity for the UMTRI test was somewhat low at 6.3 m/s and that the UMTRI force level is based on a load cell that was not inertially compensated. For the 23-kg (51.5-lb) impactor mass used, it is estimated that the force shown is approximately four percent lower than actual.

6.3.2 Tests of First Prototype-50M Chest

With confidence in the validity of results from the UMTRI pendulum, the first Prototype-50M chest/spine/shoulder system was installed in a Hybrid III dummy with a single Space Age Controls, Inc. (SAC) string potentiometer mounted near the bottom of the upper thoracic spine segment on one side and with the cable attached to a small aluminum block bolted to the ends of the third and fourth ribs. As shown in Figure 6–6, the dummy's pelvic/buttock region was clothed with cotton undergarments to reduce sliding friction and was positioned on the aluminum test platform with legs extended and toes pushed rearward to form the smallest ankle angle (i.e., leg-to-foot angle) possible.

The results of initial tests at 4.3 and 6.7 m/s are shown in Figures 6–7a and 6–7b. As previously noted, the bottom rib (eighth rib) of the prototype was removed prior to conducting these tests. While, in each case, the force and deflection reach the specified corridors by the end of the stroke (which, along with meeting hysteresis criteria is sufficient for current certification), it is seen that the early force levels are too low and that the desired plateau is not achieved. Results are better for the higher velocity test, but the first priority was to tune for the low-velocity response.

Also, at both levels, but especially at 4.3 m/s, there is insufficient energy in the loading portion of the force-deflection curves. While these tests were conducted without the chest jacket, so that motion of the ribs could be filmed and studied, it was considered doubtful that addition of the chest jacket mass would be sufficient to increase and sustain the early force at the desired level. A review of high-speed films indicated that some downward deflection of the ribcage occurred during impact loading. This downward motion no doubt contributed to the low force values and low loading energies, since the deflection measured by a single string potentiometer does not account for energy involved in downward ribcage motion.

Subsequent to examination of these initial test results, additional pendulum tests were conducted with various modifications to the first prototype in an attempt to improve the force-deflection response at the sternum. These tests and their results are discussed in the following sections.

6.3.2.1 Addition of Sternal Mass. In an attempt to improve the early phase of the force-deflection response using mass effects, a sandwich of three lead sheets interspaced with soft sponge was taped to the front of the sternum. The sternum in these tests was a three-piece unit, described in Section 5.3, consisting of a two-piece steel upper sternum hinged with soft rubber and a one-piece aluminum, lower-sternum segment. These sternal pieces were hinged together with a double layer of urethane bib and two strips of 0.381-mm (0.015-in) thick spring steel that coupled the rib ends up and down.

Figure 6–8a shows the results at 4.3 m/s with the lead "sandwich" distributed-mass system added to the front of the chest. It is seen that there is a distinct improvement in the force level early in the impact, as well as a reduction in force near the end of the stroke. The net effect is an improved plateau but, overall, the force-deflection curve is still low in both force and deflection. Again, the total loading energy is only 79 N·m (703 in·lb) compared to a desired energy of about 135 N·m (1200 in·lb) for this impactor mass and velocity.

Figure 6–8b shows results with the distributed mass up front for an impact velocity of 6.7 m/s. In this case, the extra mass improves the front end of the force-deflection curve (compared with Figure 6–7b). Both the force and deflection barely reach the corridors, however, and overall the loading energy is again too low at 212 N·m (1876 in·lb) compared to a desired 305 N·m (2700 in·lb).

Note again that, in these force-deflection plots, the force used is the total force measured by the load cell and is three to four percent lower due to inertial effects. More importantly, the deflection was the internal deflection measured by a string potentiometer attached between the upper thoracic spine segment and two ribs, which are also attached to the upper spine. The deflection measured did not, therefore, include the deflection of padding or distributed-mass elements in front of the ribcage, nor does it account for downward chest displacement, which was observed in high-speed films of these tests.

6.3.2.2 Rigid versus Flexible Spine. Because flexion of the thoracic spine was observed in high-speed films to contribute to downward deflection of the top four ribs which, in turn, was considered to be a contributing factor to the low values of absorbed energy based on deflection measurement from the single string potentiometer, it was desired to determine the effect of replacing the flexible thoracic segment with a rigid component. This was accomplished by replacing the six-year-old rubber spine by an equivalent-length cylinder made of solid aluminum. Results for tests with the rigid thoracic spine are shown in Figures 6–9a and 6–9b and can be compared to results shown in Figure 6–7a and 6–7b with the flexible thoracic spine in place. The primary effect of the flexible-spine element is to reduce both the peak force and the peak deflection. There is little effect, however, on the early phase of the curve. The loading energy is also increased from 85.8 N·m to 101.0 N·m (759.4 in·lb to 894 in·lb) at 4.3 m/s and from 212.5 N·m to 250.3 N·m (1880.8 in·lb to 2215.4 in·lb) at 6.7 m/s.

6.3.2.3 Rigid versus Mobile Shoulder. It was also desired to determine the effect of the greater mobility of the new shoulder in the prototype system compared to the rigid shoulder of the Hybrid III dummy. To study this, the two main shoulder supports that pivot at the spine were pinned to their mounting/pivot blocks. Comparing Figures 6–10a and 6–10b with Figures 6–7a and 6–7b shows that the primary effects of increased shoulder mobility are to decrease peak force and increase peak deflection. The effect on the early part of the force-deflection or force-time plot is relatively minor.

6.3.2.4 Dummy Positioning and Sternal Coupling. During these pendulum tests, it became evident that, due to the more flexible (than in Hybrid III) lumbar spine segment, as well as the new flexible thoracic spine segment, the prototype dummy lacked the postural stability needed to establish and hold the initial seated position and posture without external support. As previously noted, the mass of the upper dummy components produced a bending moment on the flexible-spine elements that rotated the upper thoracic spine relative to the

lower thoracic spine, making it impossible to achieve the desired seating posture without the application of external force above the thoracic articulation. In each pendulum test described in this section of the report, the pelvic angle was adjusted to enable orientation of the sternum parallel to the impactor surface (i.e., to be vertical), but the initial relative orientation between the upper and lower spine segments, and between the lower spine and the pelvis, was incorrect due to static deformation in the flexible elements.

While, under dynamic loading, the thoracic and lumbar spines did not appear to be overly flexible, improvement of the static stability of the spine for forward and lateral flexion was needed. Initial efforts to improve the static stability involved the addition of ribcage coupling at the front of the chest as discussed in Section 5.3. These modifications were also accompanied by changes to the sternum implemented to improve the impact response through mass effects.

A cross section of the sternal region of the modified ribcage was previously described and is illustrated in Figure 5–10. Urethane blocks were attached inside the undamped free ends of the steel ribs to provide a reaction surface for blocks of softer Sorbothane that were wedged in the spaces between the ribs. These alternating blocks of urethane and Sorbothane were sandwiched between two layers of urethane bib and fastened by means of machine screws through the ends of the ribs. The upper sternum was replaced by a single steel plate and the lower sternum, previously made from aluminum, was replaced with two steel plates—one outside the outer bib and one between the two urethane bibs. In addition to these heavier and wider sternal pieces, a multiple-layer, flexible-lead fabric (from a radiological apron) was folded and taped to the front of the chest to increase the effective sternal mass. The total mass of these two sternal pieces and lead fabric was over 1.4 kg (3 lb) compared to less than 0.23 kg (0.5 lb) for the lower aluminum sternal piece used previously.

Figures 6–11a and 6–11b show the results for impact tests with this modified chest. As indicated, the additional sternal mass had the effect of raising the force to the desired level in approximately the desired force-time corridor, but this force was not sustained. Rather, the force dipped below the corridor in each case, before rising into (4.3 m/s), or above (6.7 m/s), the force corridor at the end of the stroke. As noted previously, the peak deflections were still too low, as were the loading energies.

For the 6.7-m/s test, the force increased sharply at the end of deflection. This bottoming was found to be due to contact of two sternal screws with the cover plate protecting the AP spinal accelerometer. It was also noted that these two screws moved downward about 38 mm (1.5 in), as well as inward, for this contact to take place. The limit of 50 mm (2 in) of deflection for this test was partially a result of under-representation of deflection measured by the string potentiometer for this combined AP and downward movement. The more extensive ribcage coupling had little apparent influence on either the pretest positioning or the impact response.

6.3.2.5 Further Tests with Distributed Masses. In order to pursue improvement of the force-deflection response characteristics using mass elements, a decision was made to build and test a distributed-mass module that would attach to the front of the sternum. The potential for achieving improved response with distributed mass was supported by results from a lumped parameter model of the chest and by results from previous tests with the "lead sandwich" described above. The test results using the heavier sternum showed improved performance with additional sternal mass, but indicated a need to distribute the mass so that the effect would be sustained over a larger displacement of the chest.

Figures 6–12a and 6–12b illustrate the distributed-mass module that was fabricated for these tests and show the unit positioned on the dummy chest. The module consisted of an aluminum housing of approximately 1.2 kg (2.5 lb) and three steel disks of approximately 0.45 kg (1 lb) each that were free to slide inside the housing on a shaft. The purpose of the

housing structure was to transmit the impact energy directly to the ribcage via the foam padding so that ribcage deflection would not be dependent on displacement of the mass elements. The back side of the housing was fitted with a 152-mm (6-in) diameter aluminum plate so that the surface contacting the chest was essentially the same as the impactor surface. Initially, the steel disks were separated by lightweight foam but these were later removed to allow free sliding of the disks during impact. The assembly was supported in front of the chest by a rope to prevent the additional mass from pulling the ribcage downward, and was taped to the chest to maintain contact with the sternum prior to impact.

In addition to adding this distributed-mass element to the front of the dummy chest, aluminum blocks were fabricated to fill the gaps between the ribs and ends of the rib helpers as shown in Figure 6–13. This was done in an attempt to reduce rib bending at the spine and thereby increase damping during initial deflections. Also, the sternum and ribcage coupling in front were again modified—the blocks of urethane and Sorbothane were removed, two layers of urethane bib were used to couple the ribs at the front, and the lower sternum was made from a single piece of 6.3-mm (0.25-in) thick steel with a mass of approximately 0.27 kg (0.6 lb).

Figures 6–14a through 6–14c show test results for various conditions of this distributed-mass module with the rib-helper blocks in place. The dummy platform was raised up slightly from previous tests in order to ensure that the top of the 152-mm (6-in) impactor plate was below the urethane gap separating the upper and lower sternal parts (i.e., the center of the impactor was aimed at about the 3rd/4th prototype rib interspace). In previous tests it was noted that the top edge of this plate may have overlapped the top of the sternum due to the sagging posture of the dummy. Since it had been observed that the top of the sternum was bottoming out on the spine at about 50 mm (2 in) of AP deflection, it was hypothesized that this may have contributed to the limited deflections achieved at the midsternum. In order for the sternal hinge to allow the mid and lower sternum to deflect inward further than the upper sternum, it is necessary that the rigid impactor surface contact below this hinge. As will be seen in the following results, however, this change in impact location did little to improve the peak deflections measured by the single string potentiometer.

The results in Figures 6–14a and 6–14b are for the complete distributed-mass assembly in place with a 25-mm-thick (1-in-thick), Hybrid III pad in front of the module. As had been predicted, the force increased to, or just above, the desired plateau level in approximately the desired amount of time and deflection, and this level was maintained. However, the peak deflection was further reduced as was the force at peak deflection.

Figure 6–14c shows results at 6.7 m/s with only the 1.1-kg (2.5-lb) aluminum housing in place (i.e., without the three steel disks). Comparing Figures 6–14b and 6–14c, the positive effect of the distributed-mass module on maintaining the force level after the initial inertial force peak is evident, but a practical method for implementing this distributed-mass effect inside a dummy chest is not so obvious.

6.3.2.6 Addition of Sorbothane Block Behind Upper Sternum. From the high-speed films of three-point belted sled tests (see Section 6.5), it was observed that the top of the sternum and clavicles bottomed on the spine from the shoulder belt loading. While results of additional quasi-static loading with the 50-mm by 100-mm (2-in by 4-in) plate (see Section 6.4) indicated that the quasi-static stiffness of the upper sternum was greater in the prototype than in a cadaver (but maybe not greater than in a living human), the sled test results suggested a need to increase the compression stiffness at the upper sternum. To do this, a block of soft Sorbothane was fastened to an aluminum plate and placed in front of the upper thoracic spine behind the upper sternum.

Pendulum test results with this Sorbothane block in place are shown in Figures 6–15a and 6–15b. The force-deflection responses were similar to earlier findings without the Sorbothane block although deflections were further reduced.

6.3.2.7 Response at Lower Ribcage. Several impact tests were conducted at the lower ribcage about 75 mm (3 in) from the midline (i.e., centered at about R5-R6 of the prototype). For these tests, the dummy was raised up by means of spacers placed under the dummy's pelvis. It was also angled at about fifteen degrees to the direction of impact so that the impactor was centered on the anterior-lateral surface of the lower ribcage and toward the spine. To measure deflection in these tests, a second string potentiometer was installed on the side of the lower spine segment with the cable angled downward and slightly outward to attach to the end of the sixth rib.

Figure 6–16a shows the lower-ribcage response at 4.3 m/s when a 25-mm (1-in) thick Hybrid III Ensolite pad was placed in front of the lower ribcage. While the response is lacking in initial mass effects, it shows a much greater deflection than for the sternal region and is within the corridor described in Appendix A of this report. Figure 6–16b shows the response when the 1.1-kg (2.5-lb) aluminum housing plus 25-mm (1-in) thick pad was positioned in front of the lower ribcage. The effect of this additional mass is clearly evident. Figure 6–16c shows the response at 6.7 m/s with this aluminum housing in place.

Interestingly, the peak deflection was less at 6.7 m/s than at 4.3 m/s. The sharp rise in force at the end of the stroke indicates that the ribcage bottomed on the spine, which was also evident upon inspection of the lumbar spine bracket. It is curious, however, that this occurred only at the higher velocity. Figures 6–16d and 6–16e show responses at the two velocities when the three 1.4-kg (1-lb) masses were added to the module. The positive effect of these distributed-mass elements in maintaining the force level is clearly evident.

6.3.2.8 Further Studies of Padding Effects. Figures 6–17a through 6–17c show test results for impacts to the sternal region with the distributed-mass unit in place and for different thicknesses of padding. The role of padding in reducing the initial force due to inertia is clearly evident, but the padding appears to have relatively little effect on the peak internal deflection.

6.3.2.9 Effect of String Potentiometer Location and Orientation. As has been previously noted, the peak deflections measured by the single string potentiometer mounted near the bottom of the upper thoracic spine with the cable attached to the end of rib three were consistently low compared to the specified corridors at both 4.3 and 6.7 m/s. Because of the downward movement of the ribcage during the pendulum tests, it was suspected that at least part of the reason for these low deflections was that the string or cable, which is nearly horizontal in the pretest condition, lengthens as the front of the ribcage moves downward.

In order to further investigate the effects of this measurement deficiency, several tests were conducted with the string potentiometer mounted to the lower thoracic spine so that the cable was initially angled upward toward its attachment to the third rib. In this configuration, the cable of the string potentiometer not only does not lengthen for downward movement of the ribcage, but it includes some of this downward movement in the measured deflection (i.e., the extended cable length now shortens as a result of downward movement).

Figures 6–18a through 6–18d compare force-deflection results obtained for these two configurations of string potentiometer mounting and orientation at 4.3 and 6.7 m/s. For the results in Figures 6–18a and 6–18c, the string potentiometer was mounted to the upper thoracic spine as in previous tests. For the results for Figures 6–18b and 6–18d, the string potentiometer was mounted to the lower thoracic spine. The differences in peak deflections are striking, with the deflections from the string potentiometer mounted to the lower spine reaching well within the corridors, while the deflections from the string potentiometer mounted to the upper spine continue to fall well short of the corridors.

In general, the force-deflection plots generated with the string potentiometer mounted to the lower spine are much improved with regard to the specified response corridors and the computed loading energies are much closer to the desired and expected levels. For example, at 4.3 m/s, the computed loading energy is 67.3 N·m (596 lb·in) for the string potentiometer mounted to the upper spine and is 132.1 N·m (1169 lb·in) for the string potentiometer mounted to the lower spine. Similarly, for tests at 6.7 m/s, the computed loading energies are 167.3 N·m (1480 lb·in) and 288.7 N·m (2555.3 lb·in) for the two conditions, respectively.

6.4 ADDITIONAL QUASI-STATIC LOADING TESTS OF THE FIRST PROTOTYPE-50M

A series of additional quasi-static loading tests was carried out with the 50-mm by 100-mm (2-in by 4-in) loading plate to obtain further information on regional ribcage stiffness values and ribcage coupling, and to examine the effect of the Sorbothane placed between the sternum and spine on stiffness in this region. The prototype design conditions used for these tests included the two-piece steel sternum and two layers of urethane bib coupling the ribcage and sternal pieces at the front. In addition, the rib-helper blocks described above were in place, as was the Sorbothane block for selected tests.

The tests were conducted using the UMTRI Instron facility and the loading plate was positioned at each of three locations—upper sternum, lower sternum, and fourth rib about 75 mm (3 in) lateral to the midline. For upper and lower sternal loading, the top of the loading plate was placed even with the top or bottom of the sternum. For fourth-rib loading, the center of the loading plate was placed at the desired loading site. In all cases, the loading plate was oriented with the narrow (i.e., 50-mm or 2-in-wide) edges facing up and down on the chest.

In each loading configuration, the deflection at several other rib sites was determined by measuring the height of a point on each selected ribcage location before and during peak loading, using a manual height gage. These measurement sites and the results obtained are shown in Tables 6–2 through 6–6. Table 6–2 indicates that the Sorbothane block behind the upper sternum dramatically increased the quasi-static stiffness in this region but changed the stiffness elsewhere relatively little. In Tables 6–2 through 6–6, the deflections have been normalized so that the 25-mm (1-in) deflection at the loaded site is indicated by 1.0. The numbers in parentheses indicate the target corridors based on analysis of data from Cavanaugh et al. (1988) adjusted for muscle tension as described in Appendix A. The degree of rib coupling compares favorably with desired results and was affected very little by the addition of the Sorbothane block.

6.5 THREE-POINT BELTED SLED TESTS WITH THE FIRST PROTOTYPE-50M

In order to obtain a preliminary understanding of the prototype chest performance and durability under belt-restraint loading, two sled tests were conducted without dummy instrumentation. The setups for both tests used the same bucket-type vehicle seat, but the geometries of the three-point restraint systems were quite different in the two tests. Pre-test photos are illustrated in Figures 6–19a through 6–19d. Both tests were conducted for nominal sled pulse conditions of 48 km/h (30 mph) and with a 20 G average plateau level for the relatively rectangular deceleration pulse of the UMTRI sled. The sled deceleration pulses for the two tests are illustrated in Figure 6–20.

In the first test, the inboard belt-anchor point was located somewhat forward so that the angle of the lap belt was greater than 45 degrees to the horizontal. While this belt angle minimized the tendency of the dummy to submarine, it allowed the dummy's pelvis to slide forward a significant distance before engaging with the restraint system. In the second test,

TABLE 6–2

QUASI-STATIC STIFFNESS VALUES OF PROTOTYPE RIBCAGE WHEN LOADED IN AP DIRECTION TO 25-MM DEFLECTION WITH 50-MM by 100-MM RIGID PLATE

Location of Rigid Plate	STIFFNESS			
	Prototype Chest		Cadaver	
	lb/in	N/mm	lb/in	N/mm
With Sorbothane Block Behind Upper Sternum				
Upper Sternum	200–250	35–44	63	11
Lower Sternum	120	21	35	6.1
Fourth Rib Lateral to Midline	120	21	31*	5.4*
Without Sorbothane Block				
Upper Sternum	140	25	63	11
Lower Sternum	140	25	35	6.1
Fourth Rib Lateral to Midline	117	21	31	5.4

*Fifth Rib.

the anchor points were adjusted more rearward to ensure that the lower torso of the dummy was effectively restrained, thereby causing the dummy torso to flex forward and engage the shoulder belt sooner. In both tests, side-, top-, and front-view high-speed films were taken at 1000 frames per second. In order to view the action of the shoulders and ribcage, a chest jacket and padding were not used.

Figures 6–21a through 6–21d show Polaroid time-sequence photographs of these sled tests, while Figures 6–22a through 6–22f show post-test photographs. Study of the high-speed films from these tests indicated that the kinematics of the prototype shoulder was more humanlike than the Hybrid III shoulder but also that the proximal end of the clavicle (i.e., sternal end) was too easily and quickly bottoming on the spine. In the first sled test, a three-piece sternum was used and may have been partially responsible for this "caving" in of the upper sternum. In the second test, the two-piece sternum was used but the inboard clavicle rod-end broke on the loaded side, thereby contributing to the apparent weakness of the upper chest.

It will be noted from the time-sequence photographs and post-test photos of the second sled test that the dummy's head came off during the test. This was later determined to have been caused by a weak point on the modified nodding block due to machining required to correct the head orientation for the new neck angle (i.e., nine degrees forward). This problem was easily corrected in the second prototype.

6.6 QUASI-STATIC LOADING OF THE SECOND PROTOTYPE-50M

To evaluate the second Prototype-50M ribcage with regard to quasi-static loading stiffness and ribcage coupling, compression tests were conducted using both the 152–mm (6–in) diameter and 50-mm by 100-mm (2-in by 4-in) rigid loading plates. Figure 6–23 shows the setup for these tests in the UMTRI Instron facility.

TABLE 6-3
Relative Deflections Measured for Loading of Upper Sternum with Sorbothane Block Behind Upper Sternum*

TRIAL 1

Right 2nd Rib .59 (.6-.8)	Upper Sternum 1.0	Left 2nd Rib .53 (.5-.7)
Right 4th Rib .32 (.3-.5)	Mid Sternum (Not Measured)	Left 4th Rib .34 (.2-.4)
Right 7th Rib .15 (.1-.3)	Lower Sternum (Not Measured)	Left 7th Rib .21 (.1-.3)

TRIAL 2

Right 2nd Rib .59 (.6-.8)	Upper Sternum 1.0	Left 2nd Rib .64 (.5-.7)
Right 4th Rib .31 (.3-.5)	Mid Sternum (Not Measured)	Left 4th Rib .37 (.2-.4)
Right 7th Rib .13 (.1-.3)	Lower Sternum (Not Measured)	Left 7th Rib .20 (.1-.3)

TABLE 6-4
Relative Deflection Measured for Loading of Lower Sternum with Sorbothane Block Behind Upper Sternum*

Right 2nd Rib .15 (.2-.4)	Upper Sternum (Not Measured)	Left 2nd Rib .18 (.2-.4)
Right 4th Rib .39 (.5-.7)	Mid Sternum (Not Measured)	Left 4th Rib .66 (.4-.6)
Right 7th Rib .23 (.4-.6)	Lower Sternum 1.0	Left 7th Rib .22 (.4-.6)

* Numbers in parentheses correspond to results from Cavanaugh tests on cadavers compiled and adjusted as described in Appendix A.

TABLE 6-5
Relative Deflections Measured for Loading of Left Fourth Rib
Approximately 75 mm (3 in) Lateral to Centerline with
Sorbothane Block Behind Upper Sternum*

Right 2nd Rib .03 (.0-.2)	Upper Sternum (Not Measured)	Left 2nd Rib .12 (.1-.3)
Right 4th Rib .10 (.1-.3)	Mid Sternum (Not Measured)	Left 4th Rib 1.0
Right 7th Rib .09 (.1-.3)	Lower Sternum (Not Measured)	Left 7th Rib .4 (.5-.7)

* Numbers in parentheses correspond to results from Cavanaugh tests on cadavers compiled and adjusted by Neathery.

TABLE 6-6
Relative Deflections Measured for Loading of Upper Sternum
without Sorbothane Block*

Right 2nd Rib .59 (.6-.8)	Upper Sternum 1.0	Left 2nd Rib .57 (.5-.7)
Right 4th Rib .30 (.3-.5)	Mid Sternum (Not Measured)	Left 4th Rib .33 (.2-.4)
Right 7th Rib .1 (.1-.3)	Lower Sternum (Not Measured)	Left 7th Rib .14 (.1-.3)

* Numbers in parentheses correspond to results from Cavanaugh tests on cadavers compiled and adjusted as described in Appendix A.

For tests with the 152-mm-diameter plate, compression loads were applied to achieve peak deflections of 25 mm (1 in) and 50 mm (2 in) at the midsternum, upper sternum, and lower ribcage about 75 mm (3 in) lateral to the midline. Also, tests were conducted with and without padding in place and with and without the steel shelves supporting the first rib.

For tests with the rectangular loading plate, compression loads were applied to the unpadded ribcage to achieve a peak deflection of 25 mm at the regions of the upper, mid, and lower sternum, the level of the third dummy rib lateral to the midline, and the level of the sixth dummy rib lateral to the midline. For the latter two tests, the loading plate was oriented and locked tangent to the undeflected surface of the ribcage in these regions, but the deflections were applied in the AP direction. For all tests to the sternum and upper ribcage, the rectangular loading plate was oriented lengthwise with the dummy spine.

In each case, the dummy was supported at the back of the spine so that flexion of the spine would not occur during loading, and the chest was positioned so that the sternum was horizontal and parallel to the loading plate. Peak deflection at the loaded site was measured externally using the peak stroke of the Instron table, as well as internally using a string potentiometer installed in the dummy chest with the cable attached to the rib in the loaded region. For tests without padding, the two measures were found to provide similar results and the Instron stroke was generally used to compute stiffness values. For loading with the rectangular plate, peak deflections were maintained while deflections were measured at several other locations using a manual height gage. These readings were compared with measurements taken at the same locations prior to loading to determine the relative deflections occurring at the unloaded sites.

6.6.1 Results for 152-mm-Diameter Rigid Plate

Figure 6–24 compares the quasi-static stiffness values obtained with the 152-mm-diameter loading plate without padding and without the steel shelves to results obtained from the first Prototype-50M, the Hybrid III unpadded ribcage, and tensed human volunteers (Lobdell et al. 1973). As expected, the results for the two prototypes are very similar with stiffness values for the second Prototype-50M ranging from about 24 N/mm (140 lb/in) at the lower ribcage to about 39 N/mm (220 lb/in) at the midsternum. As with the first prototype, the stiffness at the sternum is higher than for the tensed human but is significantly lower than for Hybrid III.

Figure 6–25 shows stiffness values for the second Prototype-50M for loading at the midsternum region with the 152-mm-diameter plate for conditions with and without padding and with and without the steel shelves under the first rib, and compares these results to similar test conditions for Hybrid III and to results for the tensed human. It should be noted that these tests were conducted several months after the results shown in Figure 6–24 were obtained and after several pendulum tests, which may explain why a lower stiffness (33 N/mm versus 39 N/mm) was obtained for the case with no padding.

The effect of the shelves under the first rib is to increase the effective AP stiffness, although the stiffness is still closer to the tensed human corridor than for Hybrid III. As expected, the stiffness values calculated using external deflection with padding are always the lowest. In terms of dummy testing and injury criteria, the stiffness calculated using internal deflection for loading with padding is probably the most meaningful and it is seen that this stiffness for the second Prototype-50M with shelves is about 37.3 N/mm (213 lb/in), which is close to the upper bound of the tensed human corridor. The reason that the internal stiffness for tests with padding is consistently lower than the stiffness measured without padding is not obvious, but may be due to the use of internal string pots for the tests with padding and Instron stroke distance for tests without padding, and effects of rib curvature on the string potentiometer readings.

6.6.2 Results for 50-mm by 100-mm Rigid Plate

Figure 6–26 shows the stiffness values for different regions of the Prototype-50M chest obtained with the rectangular loading plate and compares these values to results from similar tests performed on the unpadded Hybrid III ribcage and unembalmed cadavers (Cavanaugh et al. 1988). An attempt to adjust the cadaver stiffness values for muscle tension by using a factor of 3.4, which is the ratio of tensed to relaxed chest stiffness reported by Lobdell et al. (1973) for a 152-mm-diameter loading plate on human volunteers, resulted in a higher sternal stiffness for the smaller, rectangular loading plate. This was considered to be an unreasonable result and so no adjustment factor has been applied at this time.

Comparing the results for the second Prototype-50M with those for Hybrid III, it is seen that the stiffness at the sternal region of the prototype for this loading plate is only slightly less than that of Hybrid III, and that, in both cases, the stiffness at the upper sternum is somewhat less than the stiffness at the midsternum. Most important, however, is the difference in stiffness at the lower portions of the ribcages lateral to the midline. For Hybrid III, this stiffness is significantly greater than that of the sternal region while, for the Prototype-50M, this stiffness is significantly lower, which is in better agreement with the relative stiffness values measured in cadavers.

While the actual stiffness values obtained by Cavanaugh from tests on cadavers are low compared to what would be expected for tensed humans, the relative deflections at the various regions of the chest for loading at one region have been considered to provide a preliminary target for coupling stiffness of the ribcage, after a small adjustment for muscle tension and variability. Figures 6–27a through 6–27c compare the relative deflections at different regions of the ribcage for loading with the rectangular plate at five different sites with the desired deflection ranges developed from the cadaver data as described in Appendix A. In each of the plots, the boxes at the center represent the upper-, mid-, and lower-sternal regions while the boxes at the sides represent the lateral upper, mid, and lower ribcage at the levels of dummy ribs 2, 4, and 6. In each box, the amount of deflection measured during quasi-static testing of the prototype ribcage is plotted as a shaded bar, where the results have been normalized so that a deflection of 25 mm is plotted as 1.0. The brackets show the target deflection range based on the adjusted cadaver results. As shown, there is generally good agreement between the achieved deflections and the desired deflections for loading at the different sites, although improvements in both the coupling specifications and the performance of the prototype could be realized.

6.7 PENDULUM TESTS OF THE SECOND PROTOTYPE-50M

A series of pendulum impact tests was conducted with the second Prototype-50M described in Section 5.8.1. Kroell-type tests were conducted at the midsternum for nominal velocities of 4.3 m/s and 6.7 m/s and to the lower ribcage at 4.3 m/s. For the latter tests, the dummy was angled approximately fifteen degrees to the AP direction and positioned (i.e., tilted backward from the standard calibration position) so that the face of the impactor was approximately tangent to the surface of the chest in this region. Figure 6–28 shows the dummy positioning used for sternal and lower ribcage pendulum tests.

Force on the impactor was measured by a Denton load cell installed at the end of the impactor and the output signal was compensated for mass effects. Three-dimensional displacements were measured by the DGSP in the respective impact region (i.e., the right sternal DGSP for sternal impacts and the left- or right-lower DGSP for the lower ribcage impacts). Analog output signals from the transducers were recorded on magnetic tape and subsequently sampled at 10,000 Hz and digitally filtered at channel class 180 (–4dB at 300 Hz). The filtered data were then used in the program DEFLECT to compute chest

compression and lateral and up/down displacements in the spinal and alternate axis systems described in Section 5.8.1 and Volume 3.

Figures 6–29a and 6–29b show the force-deflection plots obtained at the sternum for representative tests at nominal impact velocities of 4.3 m/s and 6.7 m/s, respectively. In both cases, the response follows the specified corridor indicated by the shaded area. Figure 6–30 compares these force-deflection responses for the Prototype-50M with results from similar tests obtained in tests at First Technology Safety Systems for a Hybrid III chest meeting current specifications. As indicated, the response of the Prototype-50M chest is comparable to that of Hybrid III at 6.7 m/s in meeting the desired corridor and is significantly better than that of Hybrid III at 4.3 m/s, especially with regard to peak chest compression.

Figures 6–31a and 6–31b show force-time and displacement-time plots for these same tests where the RL and IS displacements are computed for the spinal axis system in the subroutine DEFLECT. As one would expect, there is relatively little lateral displacement of the chest for these AP sternal impacts, but there is approximately 20 mm (0.79 in) of downward movement of the sternum.

Figure 6–32 shows force-deflection plots for 4.3-m/s pendulum impacts to the right- and left-lower ribcage along with the preliminary target corridor for this region based on pendulum tests reported by Viano (1989) as described in Appendix A. In these plots, the deflections are those computed by DEFLECT using the filtered output signals from the DGSP in the impact region for the alternate compression axis that has been defined for these tests to be angled downward 15 degrees and outward 18 degrees from the spinal X-axis (see Section 5.8.1). In both cases, the response follows the corridor for approximately 20 mm, but the force exceeds the corridor beyond 25 mm of deflection.

Figures 6–33a through 6–33c show force-time and displacement-time histories for these tests, where the displacement-time histories are given along the spinal system axes, as well as along the alternate system axes. In the spinal axis system, the RL displacement for the impact to the right-lower ribcage is to the left, as expected, and that the IS displacement is upward. Similarly, for the impact to the left-lower ribcage, the RL displacement is to the right, as expected, and the IS displacement is very small and negligible. In the alternate axis system, the peak inward compressions are seen to be slightly larger than those computed for the spinal axis system (i.e., peak compressions are larger than peak deflections). This is as expected since the alternate compression axis was chosen to be in line with the impactor direction.

For impact to the right-lower ribcage, the RL and IS displacements in the alternate axis system (i.e., TWIST and LIFT) are in the left and upward directions, respectively, but are much smaller than those for the spinal axis system. For impact to the left-lower ribcage, the RL displacement in the alternate axis system (TWIST) is to the right, but is much smaller than the RL displacement in the spinal axis system. Also, the up/down displacement (LIFT) is downward for this impact, whereas it was negligible in the spinal axis system. These differences between displacements in the spinal and alternate axis systems are in agreement with expected differences and suggest that the impact to the right-lower ribcage was closely in line with the defined alternate compression axis for this region. The impact to the left-lower ribcage appears to have been aligned more closely with the alternate compression axis in the RL direction, but more closely with the spinal X-axis in the IS direction, indicating, perhaps, that the dummy was not tilted backward far enough in this test.

6.8 SLED TESTS OF THE SECOND PROTOTYPE-50M

Several 30-mph, 20-G sled tests were conducted of the second Prototype-50M thorax assembly installed in in the Hybrid III dummy using a standard automotive bucket seat and a three-point belt restraint system. Figures 6–34a through 6–34d show pretest photos for the last two tests conducted, SX9104 and SX9105. Instrumentation for these tests included the four DGSP chest displacement assemblies, three chest accelerometers located at the top of the lower thoracic spine, three angular velocity sensors attached to the upper and lower thoracic spine and pelvis, respectively, and belt load cells.

The dummy's neck was wrapped with soft padding and tape for both tests to provide a more realistic neck circumference and to assist in keeping the shoulder belt from sliding inappropriately far to the right side of the dummy. Also, in test SX9105, a block of padding made from Ensolite and Sorbothane was wedged between the upper sternum and the urethane guard at the front of the upper thoracic spine in an effort to stiffen the compliance in this region. Also, in both tests the modified frangible abdomen was installed and held in place as described in Section 5.7.

The first eight plots of Appendix B show the filtered (at channel class 180) time traces of test instrumentation including the sled deceleration profiles for these two tests, while Figures 6–35a and 6–35b show side-view, time-sequence photographs of these tests. The chest deflection signals were processed in the subroutine DEFLECT to produce three-dimensional displacements in the spinal and alternate (for lower ribcage) axis systems. Printouts of these results are shown in the remaining plots of Appendix B.

Figures 6–36a and 6–36b show composite plots of the AP, RL, and IS displacements measured by the four DGSP units for the two sled tests where, for purposes of comparison, all displacements are given in the spinal axis system. It is interesting to note the differences in displacements at the different regions of the chest.

In test SX9104, the compression (i.e., deflection) at the right sternum is significantly greater than that at the left sternum due to routing of the shoulder belt to the right side of the chest. Inward deflection at the left sternum is quite small. The inward displacement of the right-lower ribcage is comparable in magnitude to that of the right sternum and the displacement at the left-lower ribcage is outward.

RL displacements for test SX9104 are primarily leftward and are greatest for the right sternal area where maximum AP compression occurred. IS displacements are primarily upward and are largest for the lower ribcage. The only exception is at the left sternal region, which shows downward movement after an initial upward movement.

Similar results are seen for test SX9105, although the inward deflection for the right sternum is smaller than in test SX9104 and is only slightly larger than for the left sternum. It is suspected that this reduced deflection at the sternum may be a result of the Ensolite/ Sorbothane pad placed between the sternum and the spine. The greatest inward deflection was obtained at the right-lower ribcage, and the left-lower ribcage again showed an outward displacement. The RL and IS displacements are again primarily toward the left and upward, although the left sternal region again shows a downward movement after an initial upward movement.

Figures 6–37a and 6–37b show post-test photographs from these tests and, in particular, show the condition of the frangible abdomen that remained in place in both cases. Note that the manner in which the Styrofoam has been penetrated by the lap belt is different in the two cases as illustrated in Figure 6–37b. In test SX9104, the top of the Styrofoam has been damaged, possibly indicating that the lap belt slid above the ASISs of the pelvis. In test SX9105, the lap belt clearly penetrated the Styrofoam below the ASISs, indicating that lap-belt submarining did not occur. Other damage to the frangible abdomen

appears to have resulted from interaction with the lower ribcage due to flexion at the lumbar and thoracic spine articulations. It is also significant that the dummy sustained no damage during these sled tests and that all instrumentation was still functioning and intact after the tests.

6.9 FIGURES

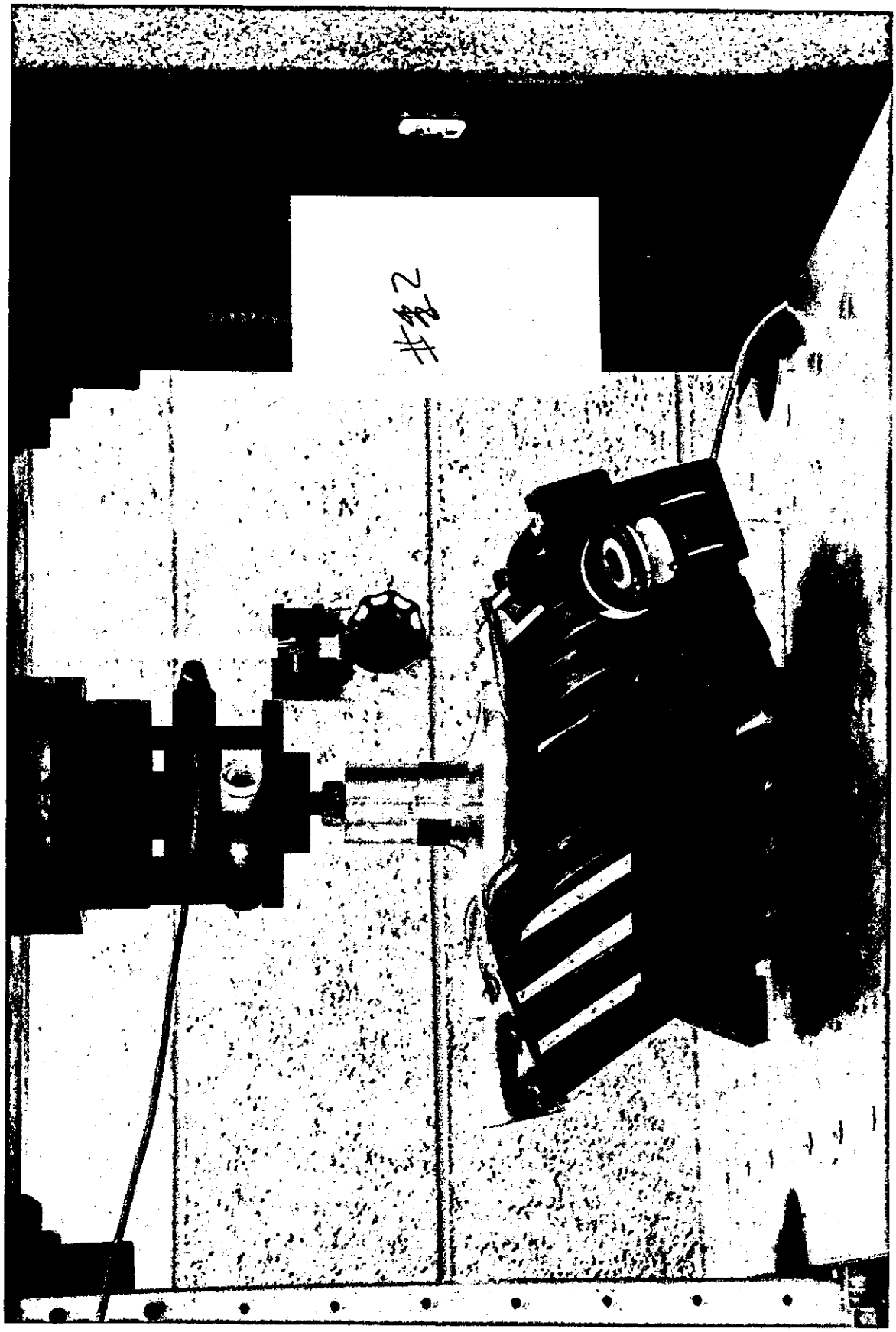

FIGURE 6–1a. Quasi-static loading of First Prototype-50M ribcage with 152-mm (6-in) diameter rigid plate located at midsternum.

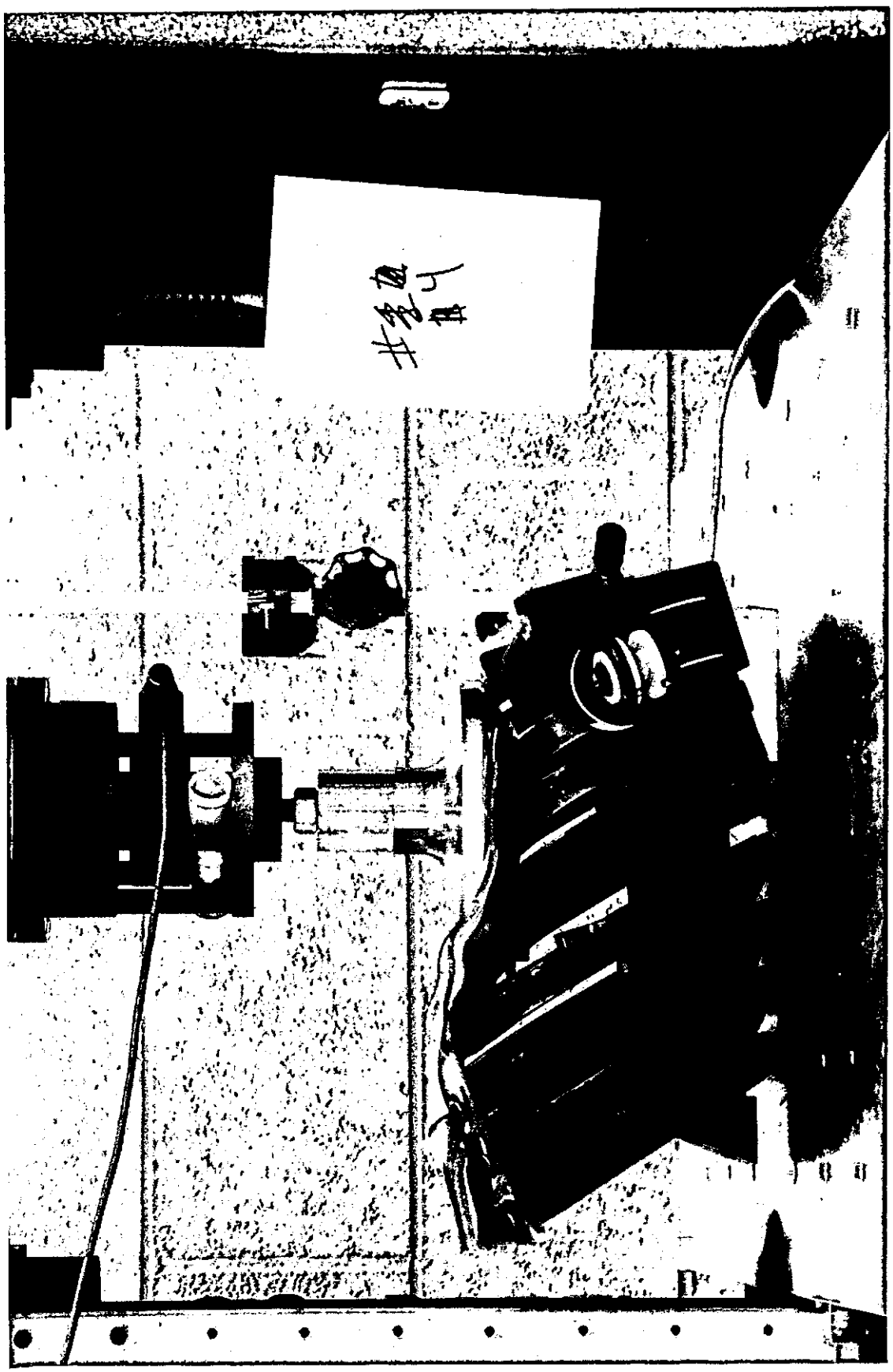

FIGURE 6–1b. Quasi-static loading of First Prototype-50M ribcage with 152-mm (6-in) diameter rigid plate located at upper sternum.

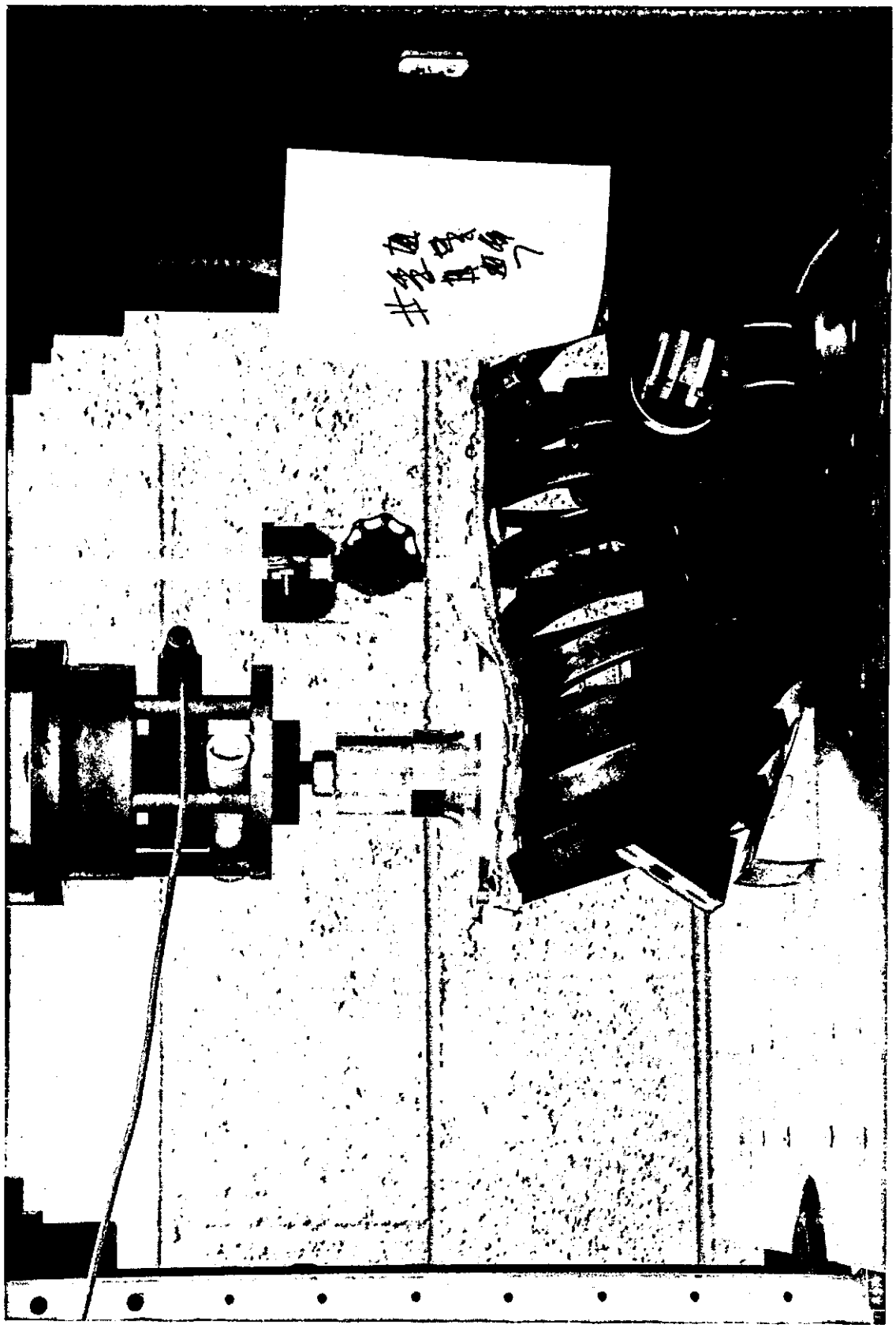

FIGURE 6–1c. Quasi-static loading of First Prototype-50M ribcage with 152-mm (6-in) diameter rigid plate located at lower ribcage lateral to midline.

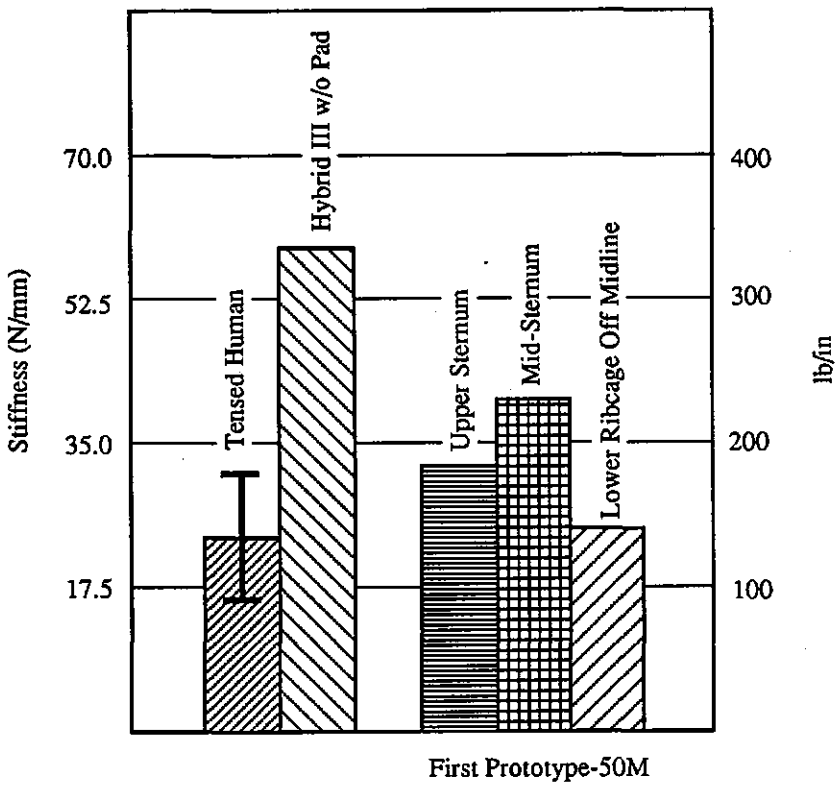

FIGURE 6–2. Comparison of quasi-static loading stiffness values using 152-mm (6-in) diameter rigid plate on tensed humans, Hybrid III ribcage without padding and jacket, and First Prototype-50M ribcage.

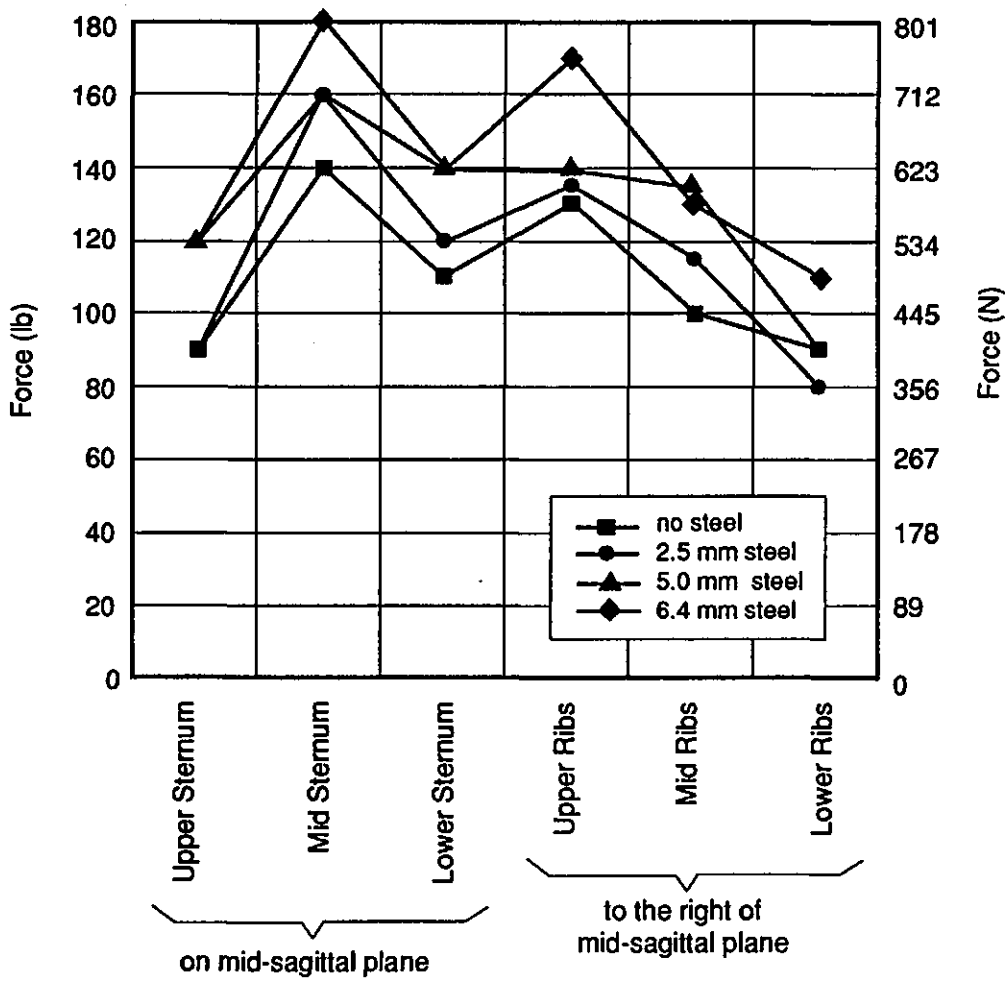

FIGURE 6–3a. Force levels obtained for loading of First Prototype-50M ribcage minus eighth rib to 25-mm (1-in) deflection using a 50-mm by 100-mm (2-in by 4-in) loading plate and different thicknesses of spring steel coupling the rib ends from top to bottom on each side of sternum.

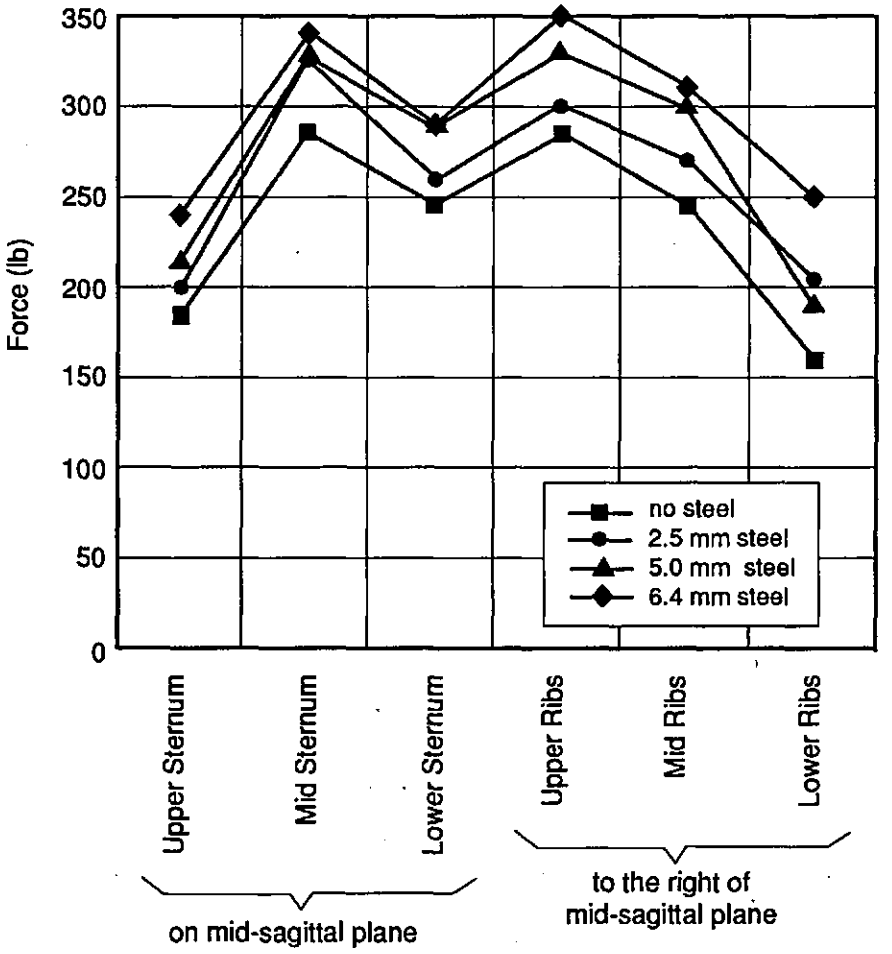

FIGURE 6–3b. Force levels obtained for loading of First Prototype-50M ribcage minus eighth rib to 50-mm (2-in) deflection using a 50-mm by 100-mm (2-in by 4-in) loading plate and different thicknesses of spring-steel coupling the rib ends *from top to bottom* on each side of sternum.

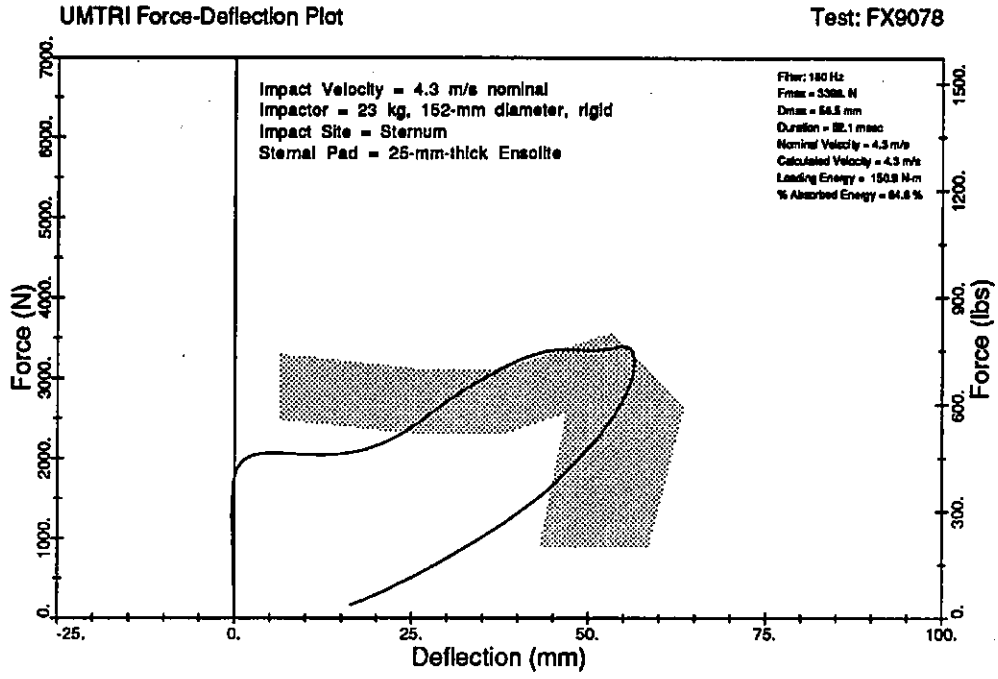

FIGURE 6–4a. F-δ response for 4.3-m/s pendulum test of Hybrid III chest installed in dummy.

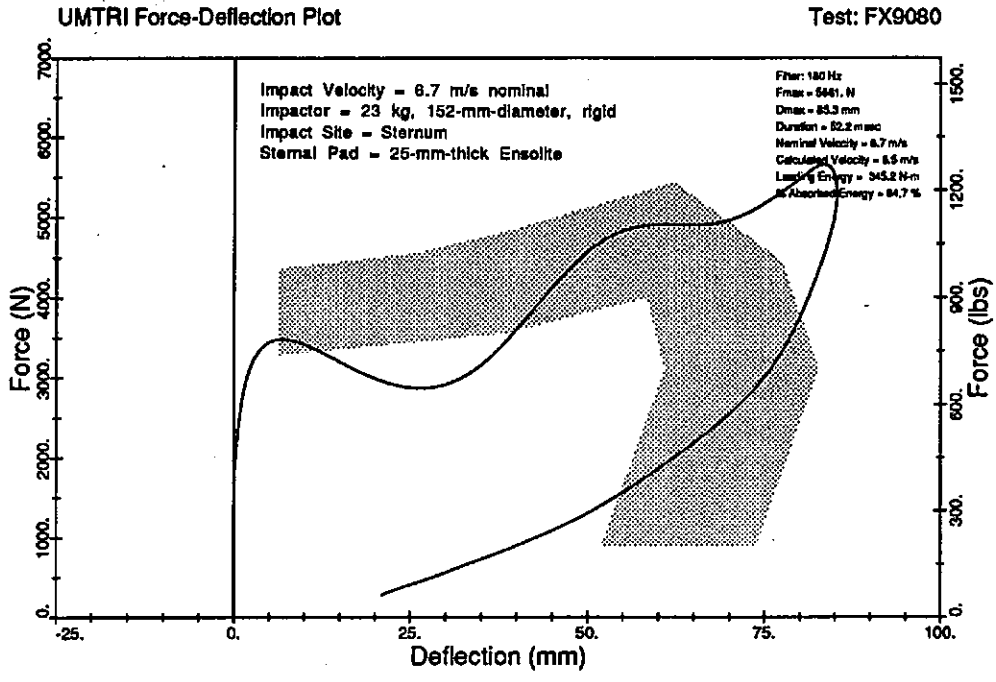

FIGURE 6–4b. F-δ response for 6.7-m/s pendulum test of Hybrid III chest installed in dummy.

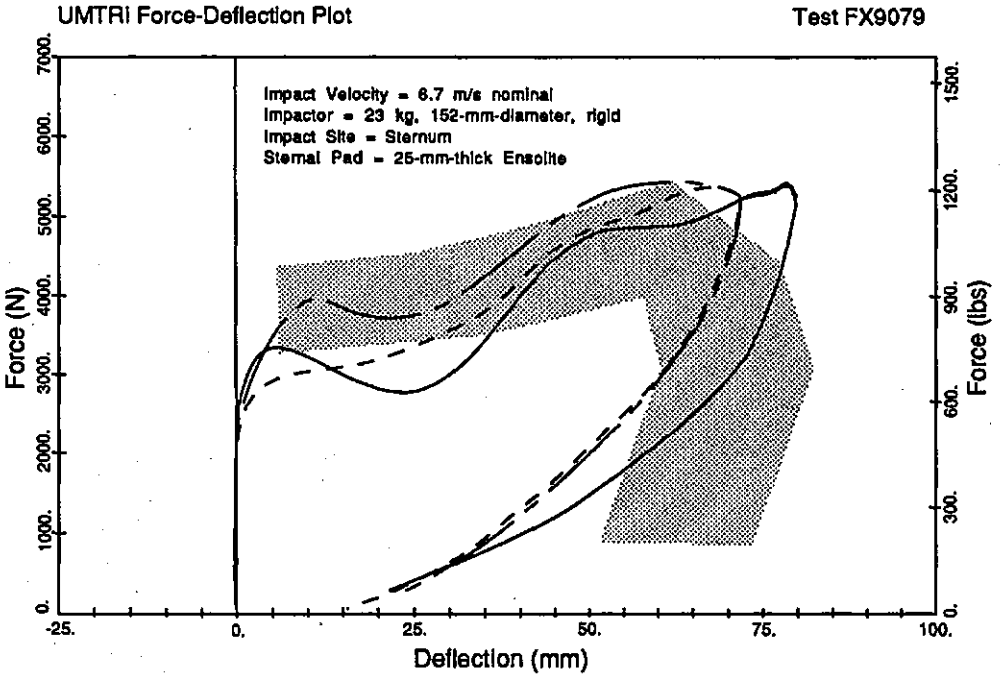

FIGURE 6–5. Comparison of F-δ responses for 6.7-m/s pendulum tests of in-dummy Hybrid III chests tested at UMTRI (solid line), First Technology Safety Systems (dashed line), and SRL (long-short dashed line).

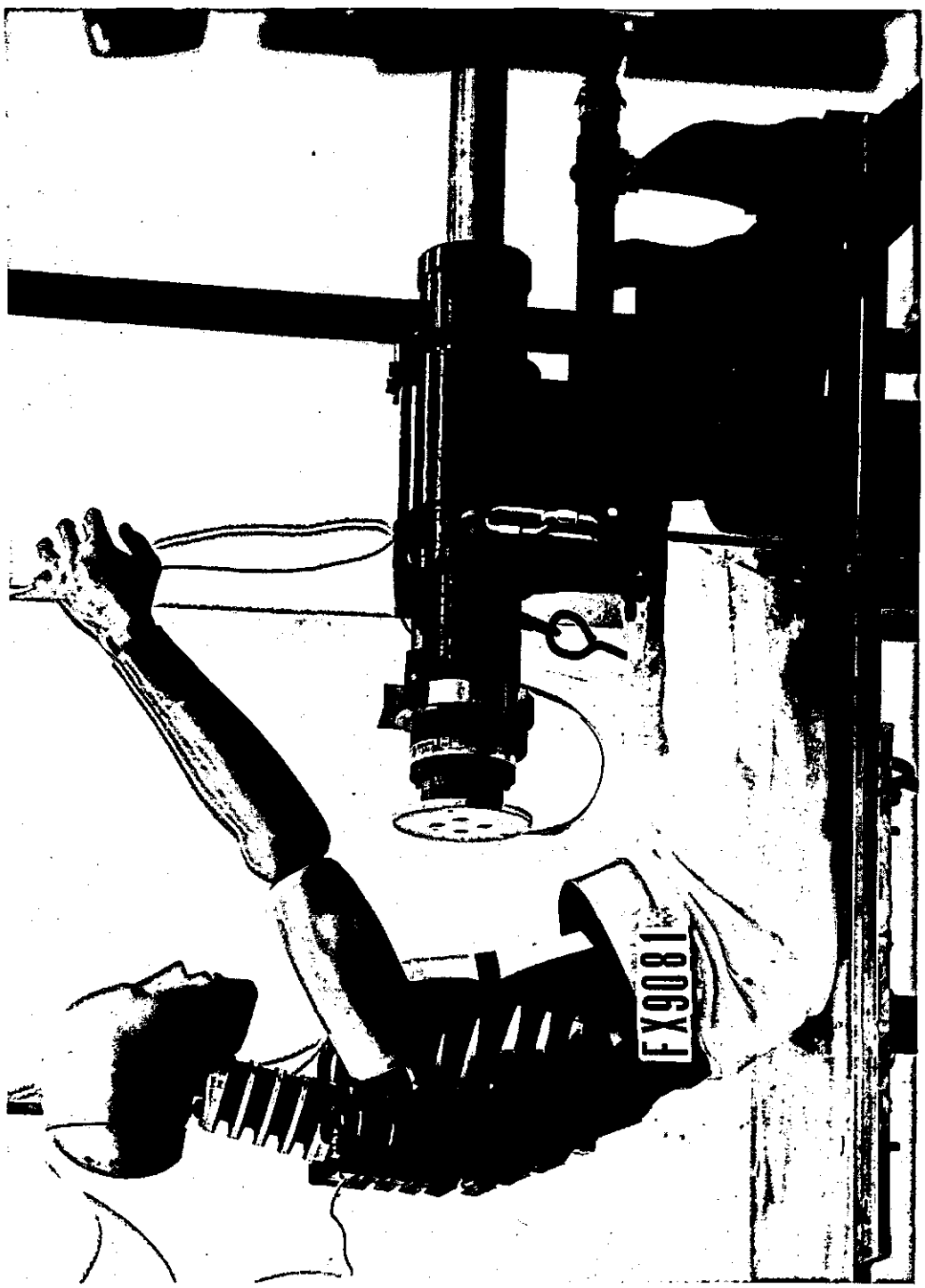

FIGURE 6–6. Pendulum testing of First Prototype-50M thorax assembly installed in Hybrid III dummy. Note that the bottom, or eighth rib, has been removed.

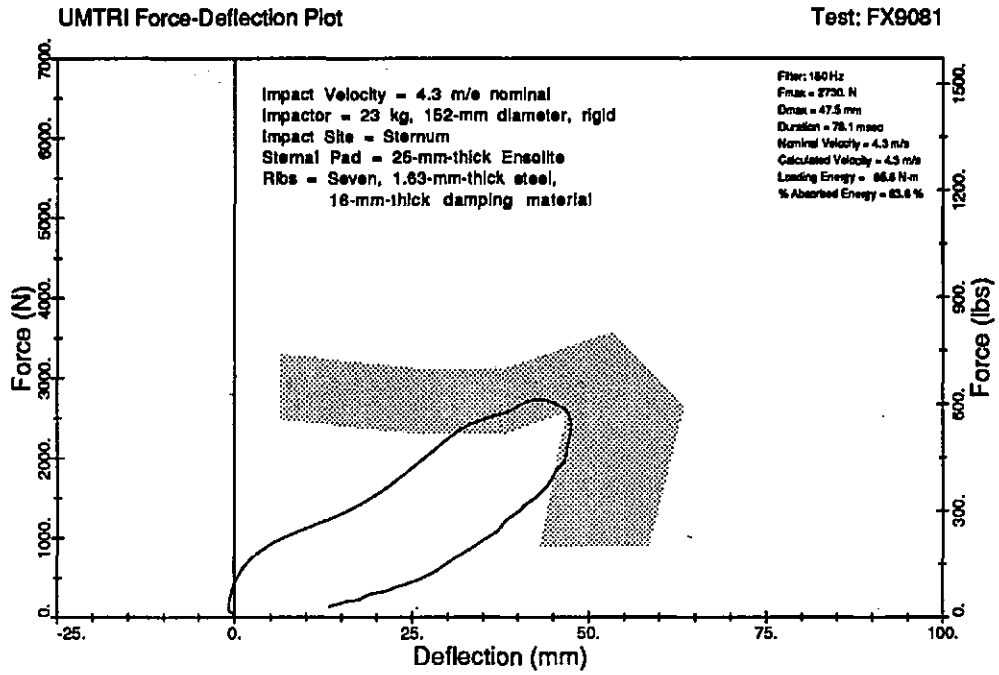

FIGURE 6–7a. F-δ response for 4.3-m/s pendulum test of First Prototype-50M chest installed in dummy.

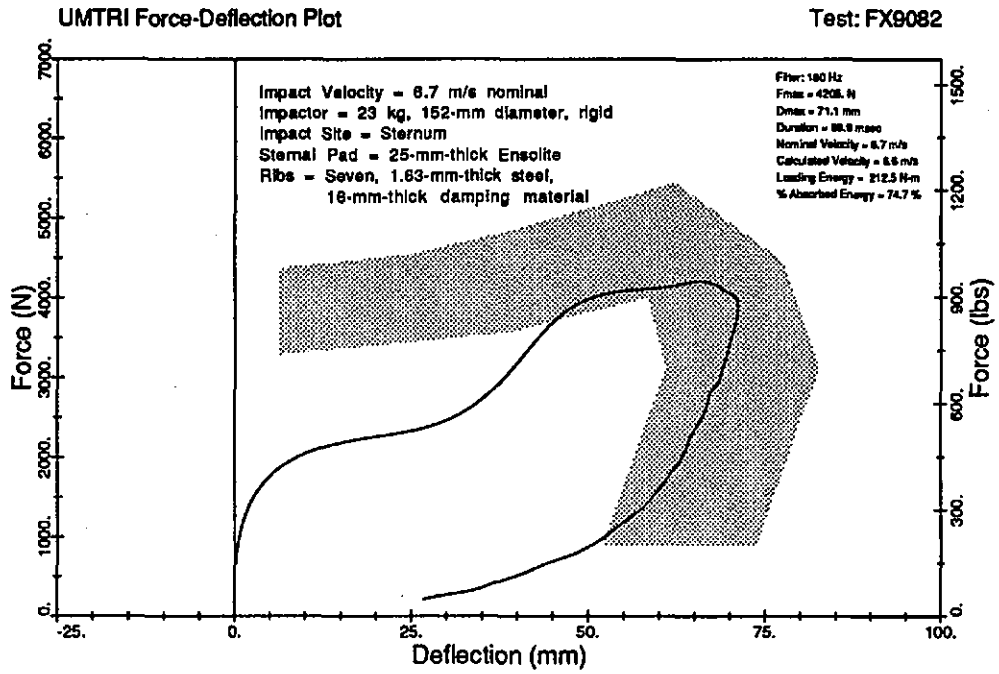

FIGURE 6–7b. F-δ response for 6.7-m/s pendulum test of First Prototype-50M chest installed in dummy.

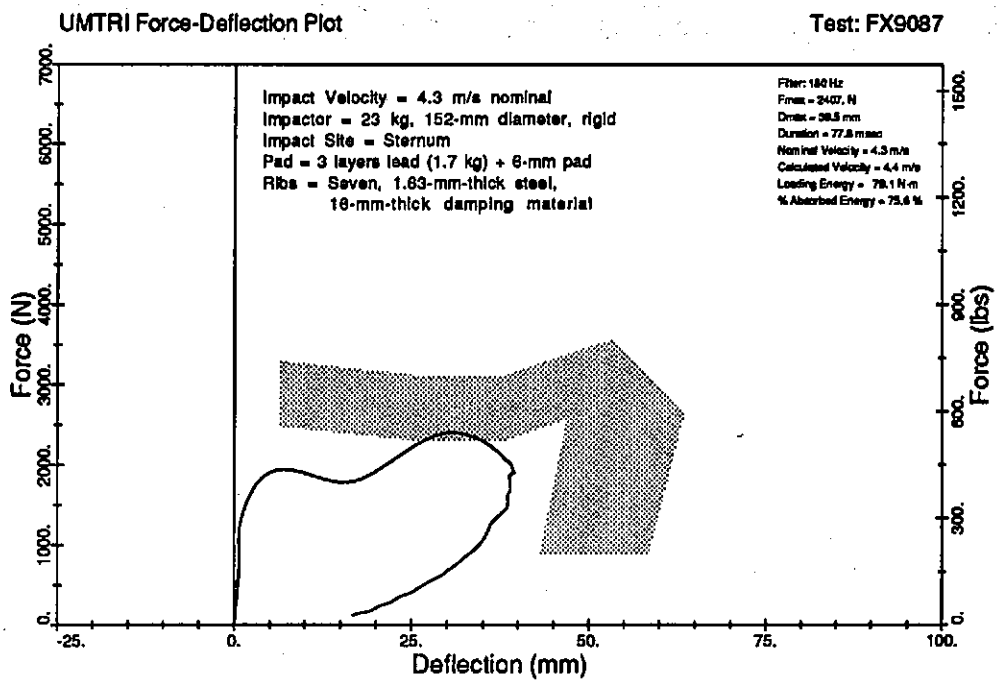

FIGURE 6–8a. F-δ response for 4.3-m/s pendulum test of First Prototype-50M chest installed in dummy with three layers of lead sheeting (total mass=1.7 kg or 3.7 lb) and 6-mm (0.24-in) thick pad over sternum.

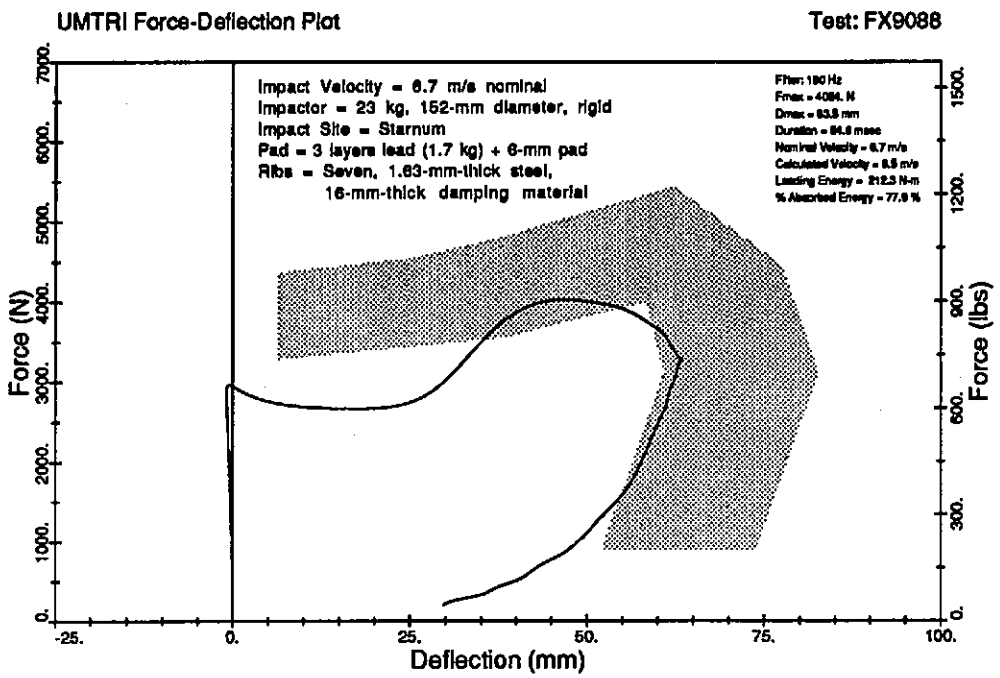

FIGURE 6–8b. F-δ response for 6.7-m/s pendulum test of First Prototype-50M chest installed in dummy with three layers of lead sheeting (total mass=1.7 kg or 3.7 lb) and 6-mm (0.24-in) thick pad over sternum

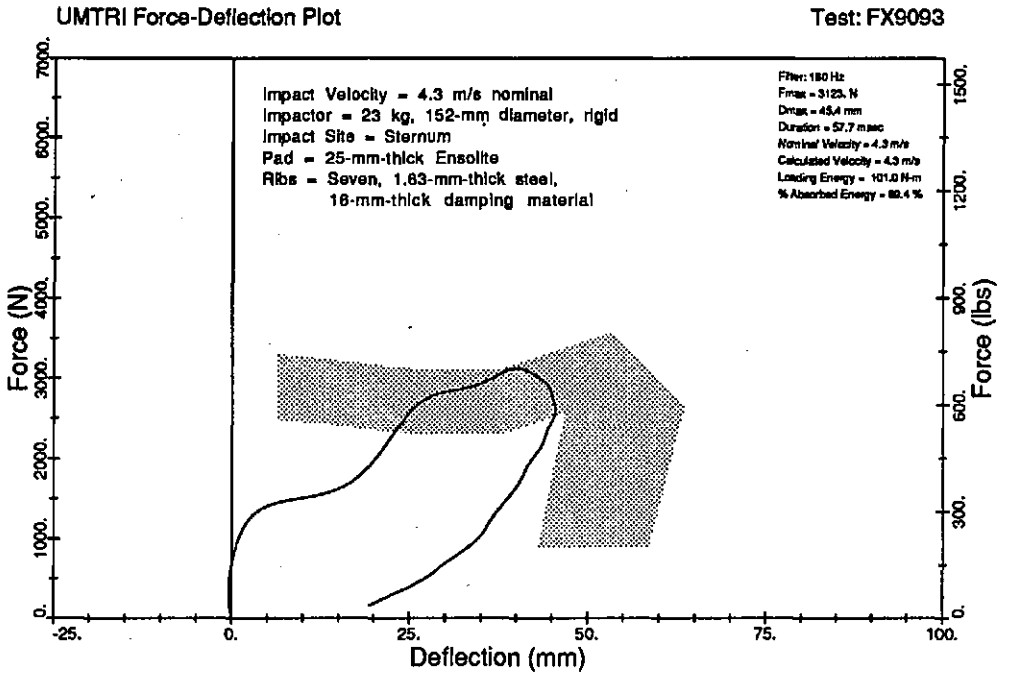

FIGURE 6–9a. F-δ response for 4.3-m/s pendulum test of First Prototype-50M chest installed in dummy with *rigid thoracic spine*.

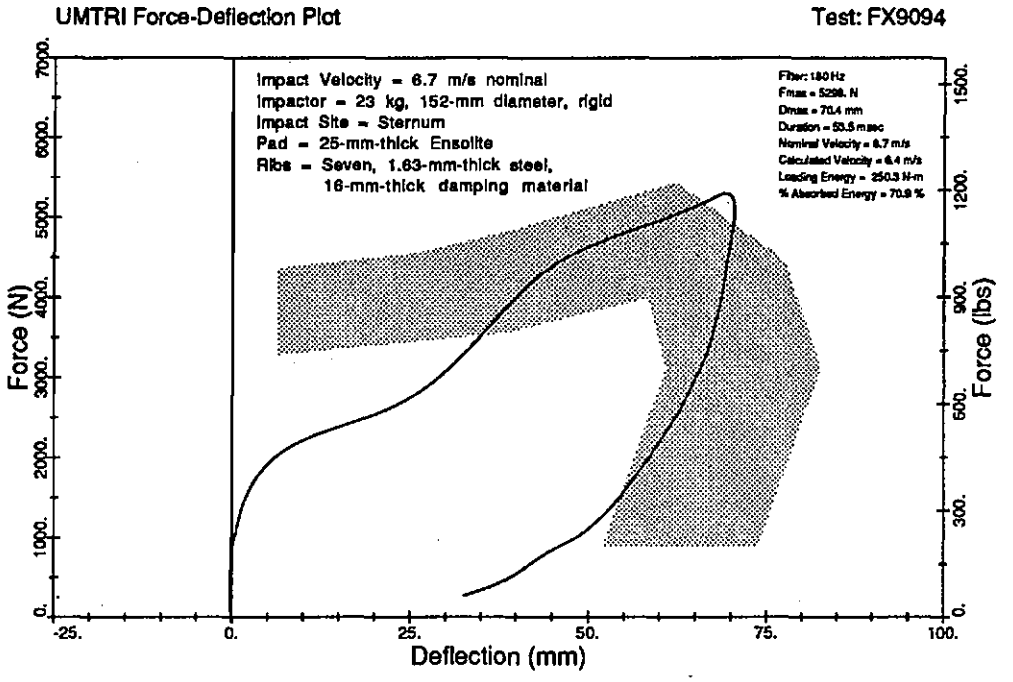

FIGURE 6–9b. F-δ response for 6.7-m/s pendulum test of First Prototype-50M chest installed in dummy with *rigid thoracic spine*.

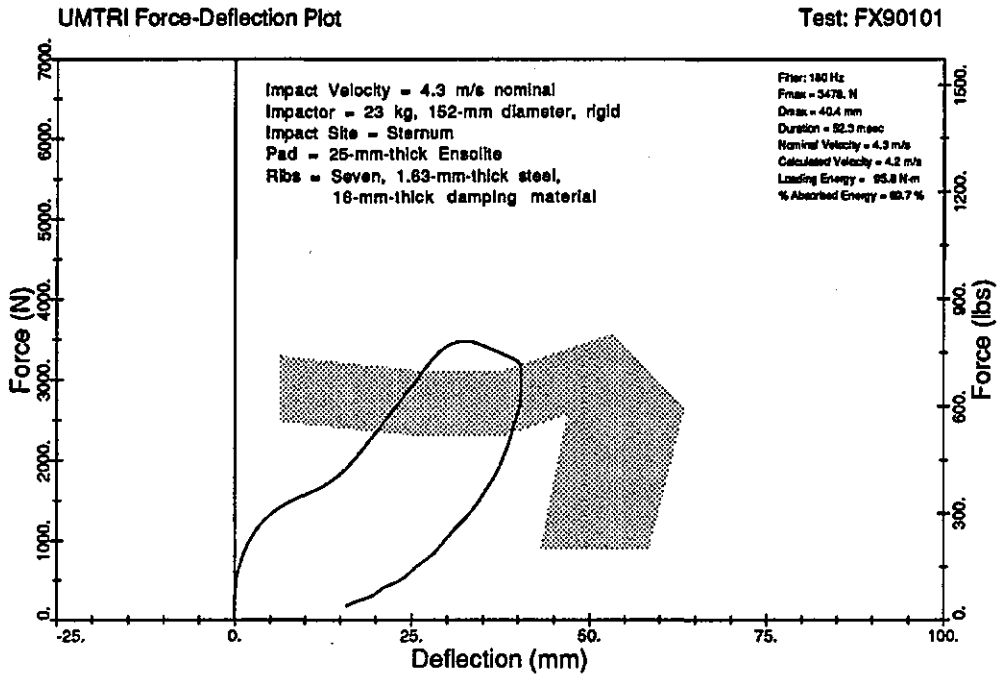

FIGURE 6–10a. F-δ response for 4.3-m/s pendulum test of First Prototype-50M chest installed in dummy with *shoulders pinned.*

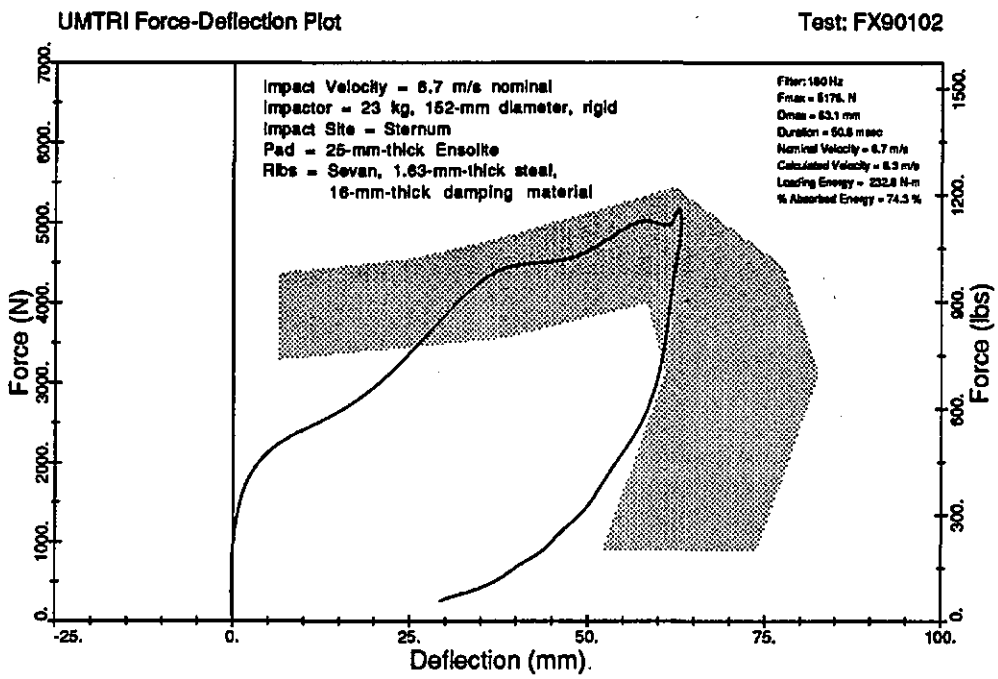

FIGURE 6–10b. F-δ response for 6.7-m/s pendulum test of First Prototype-50M chest installed in dummy with *shoulders pinned.*

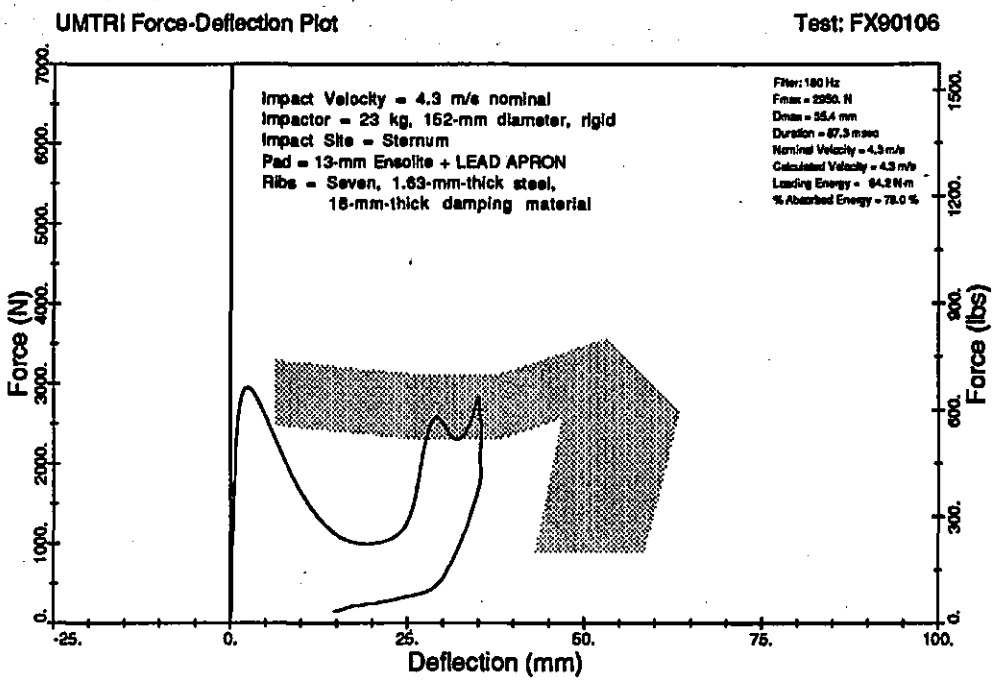

FIGURE 6–11a. F-δ response for 4.3-m/s pendulum test of First Prototype-50M chest installed in dummy with *modified sternum and ribcage coupling plus lead apron.*

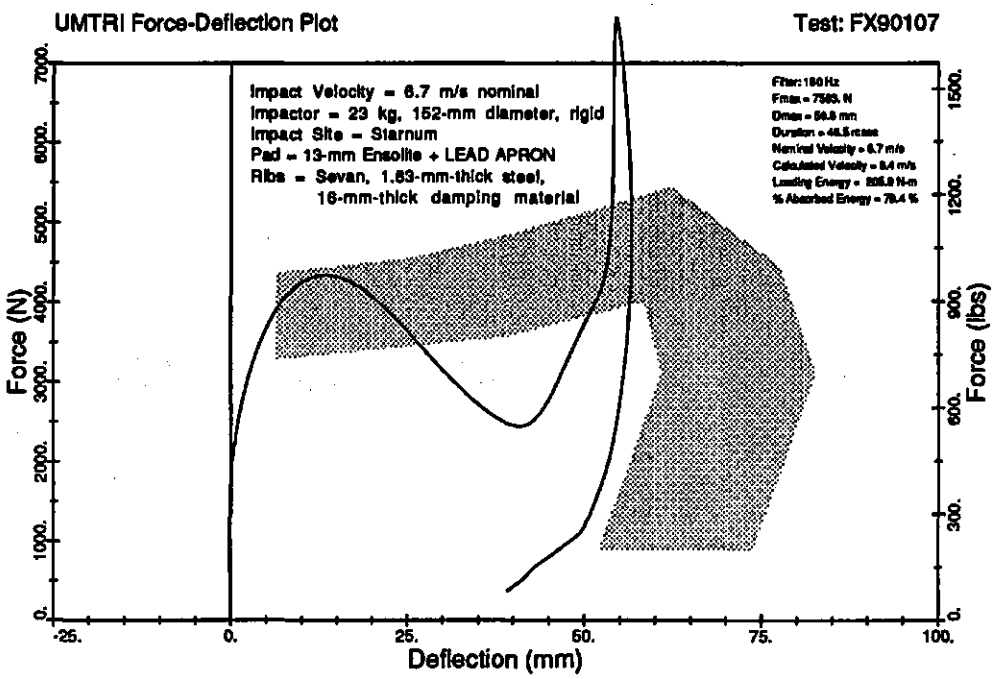

FIGURE 6–11b. F-δ response for 6.7-m/s pendulum test of First Prototype-50M chest installed in dummy with *modified sternum and ribcage coupling plus lead apron.*

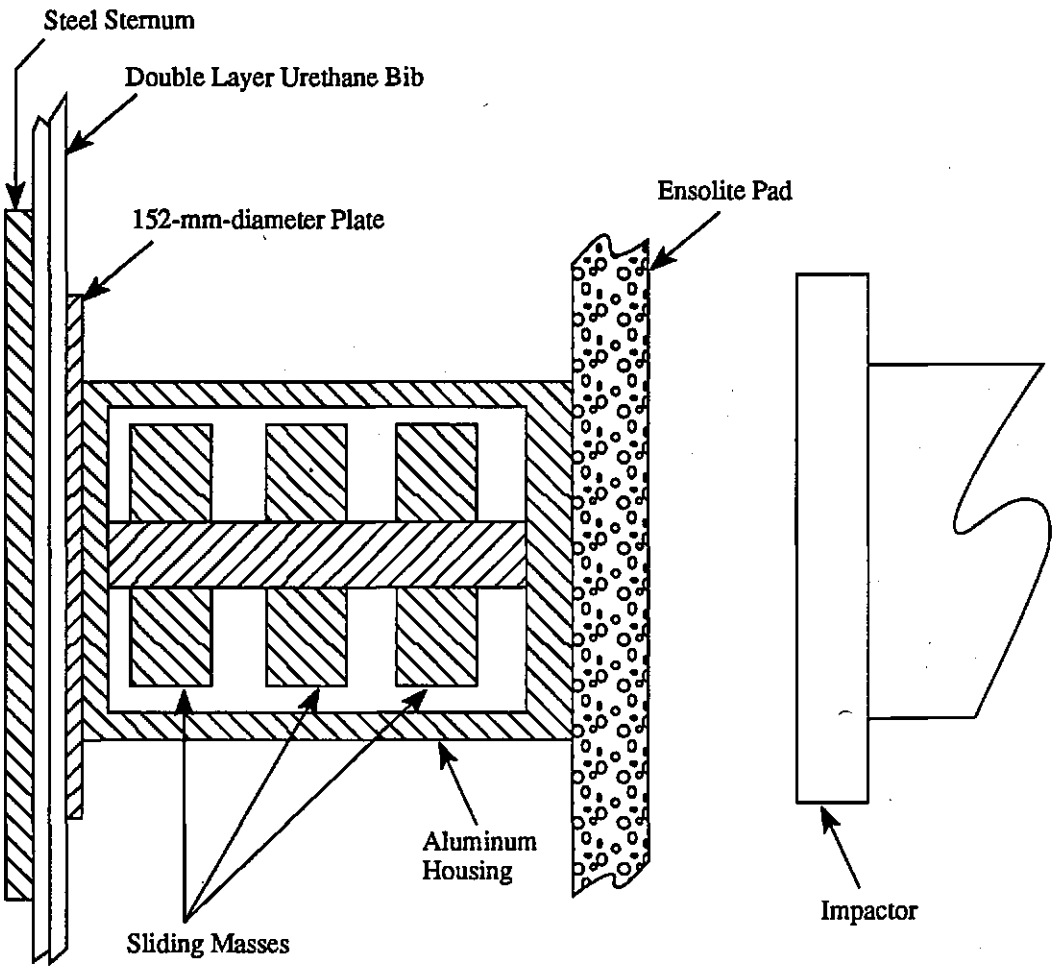

FIGURE 6–12a. Sketch of distributed-mass module added to front of First Prototype-50M chest.

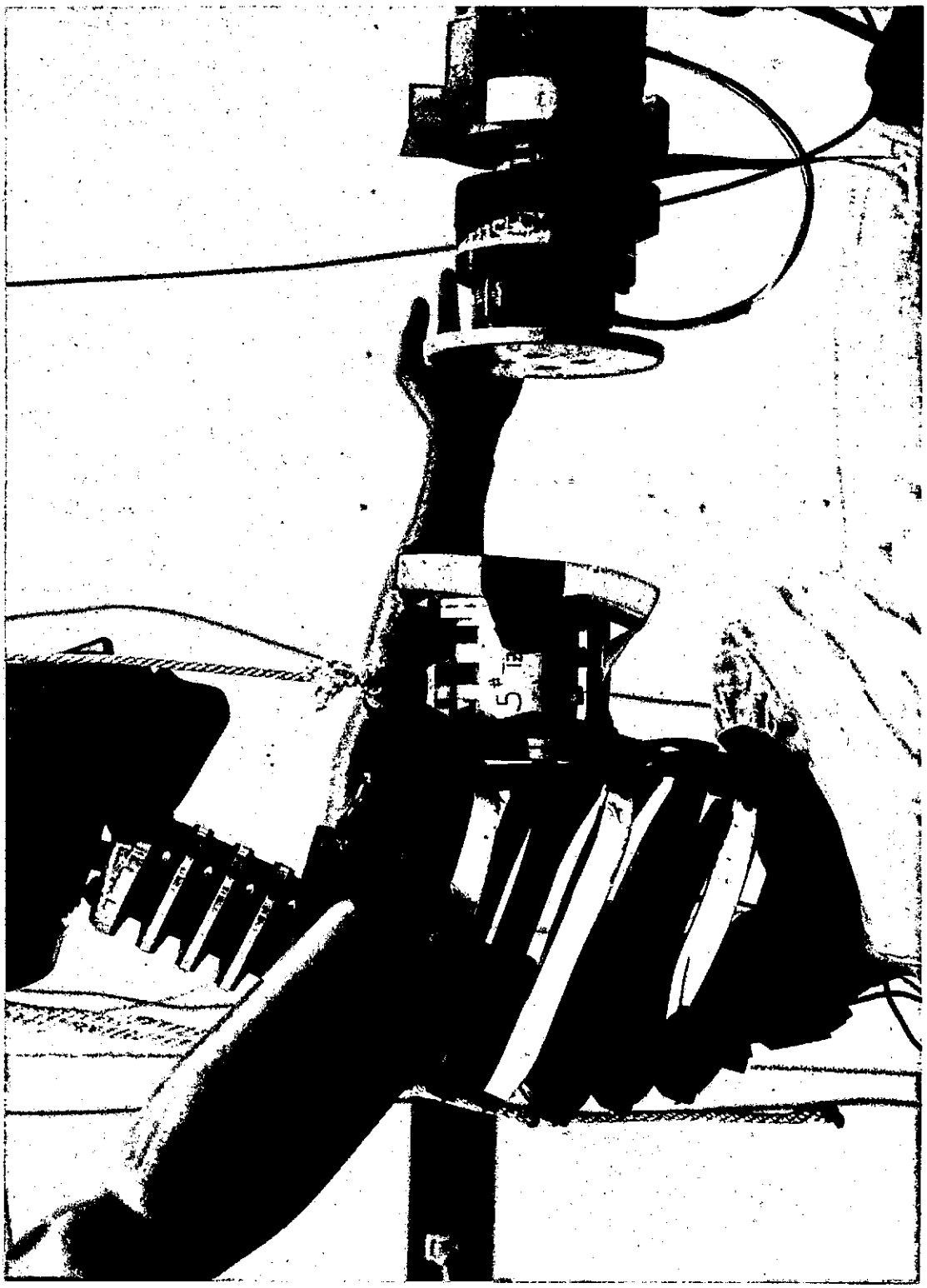

FIGURE 6–12b. Distributed-mass module attached to sternal region of First Prototype-50M chest.

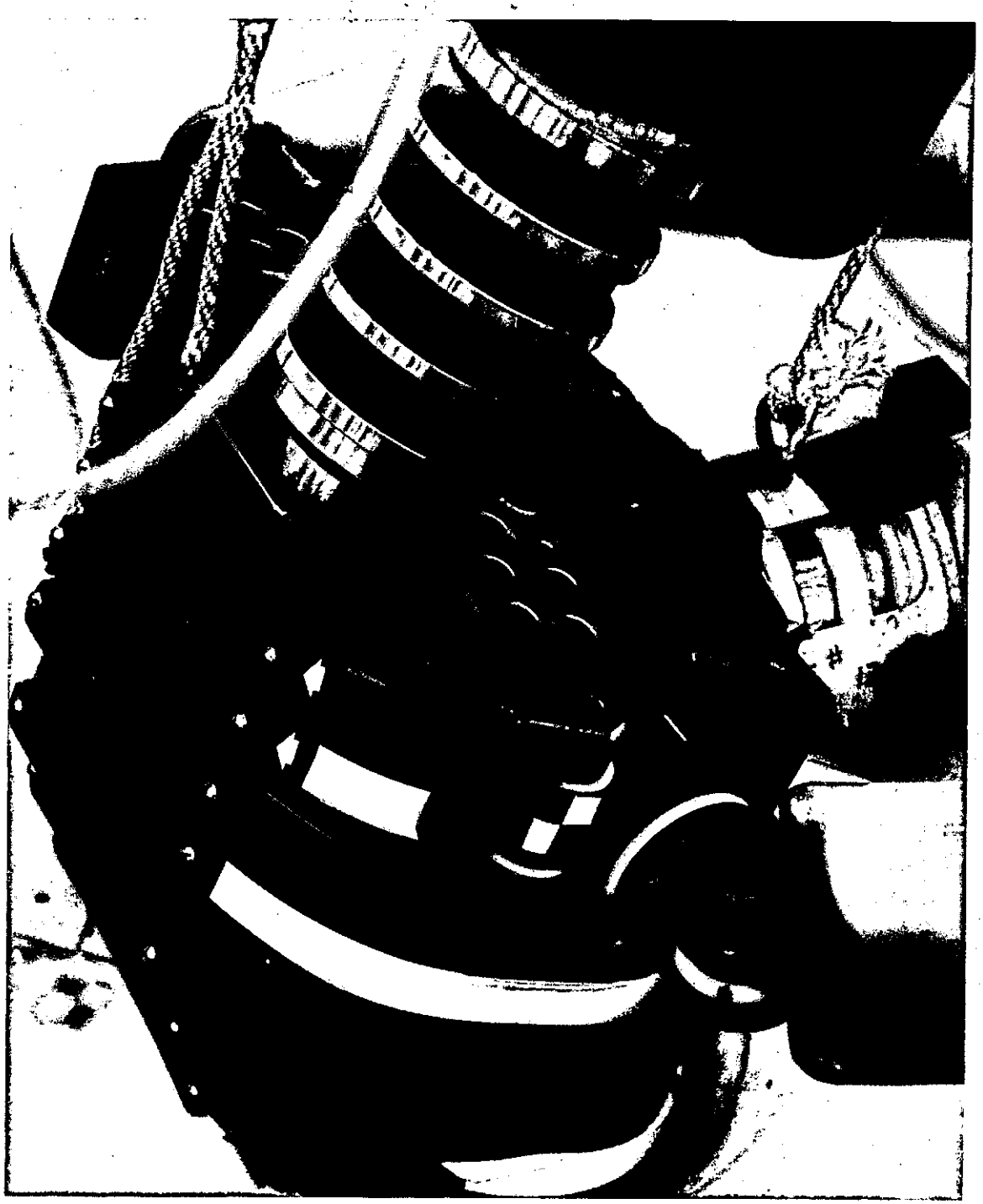

FIGURE 6–13. View of First Prototype-50M chest showing aluminum wedges between ribs and rib helpers to reduce rib bending at spine.

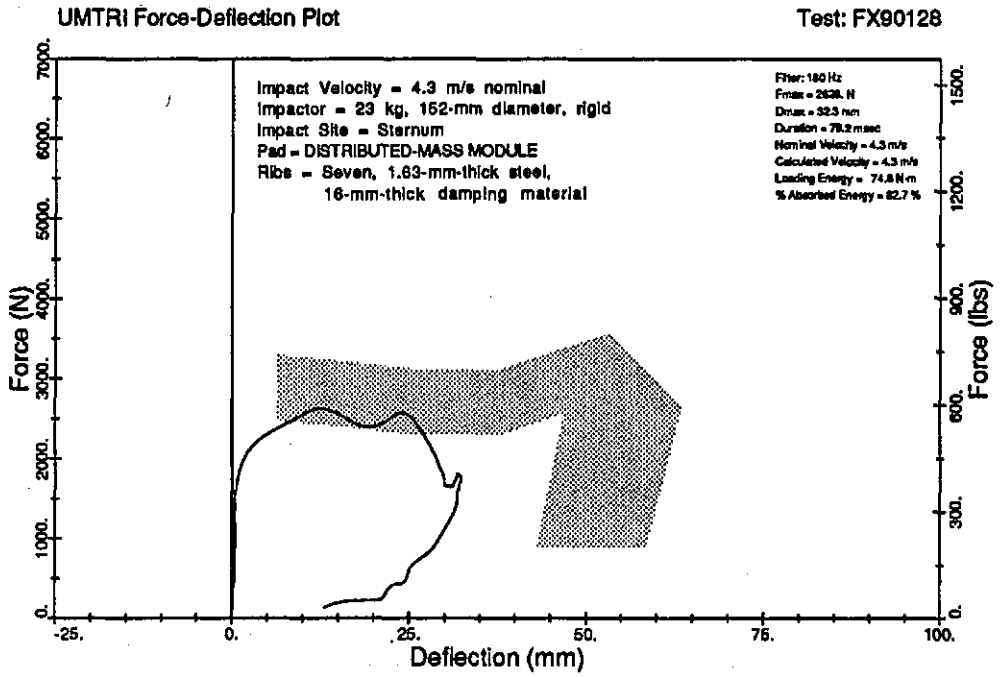

FIGURE 6–14a. F-δ response for 4.3-m/s pendulum test of First Prototype-50M chest installed in dummy with *distributed-mass module attached to front of sternum*.

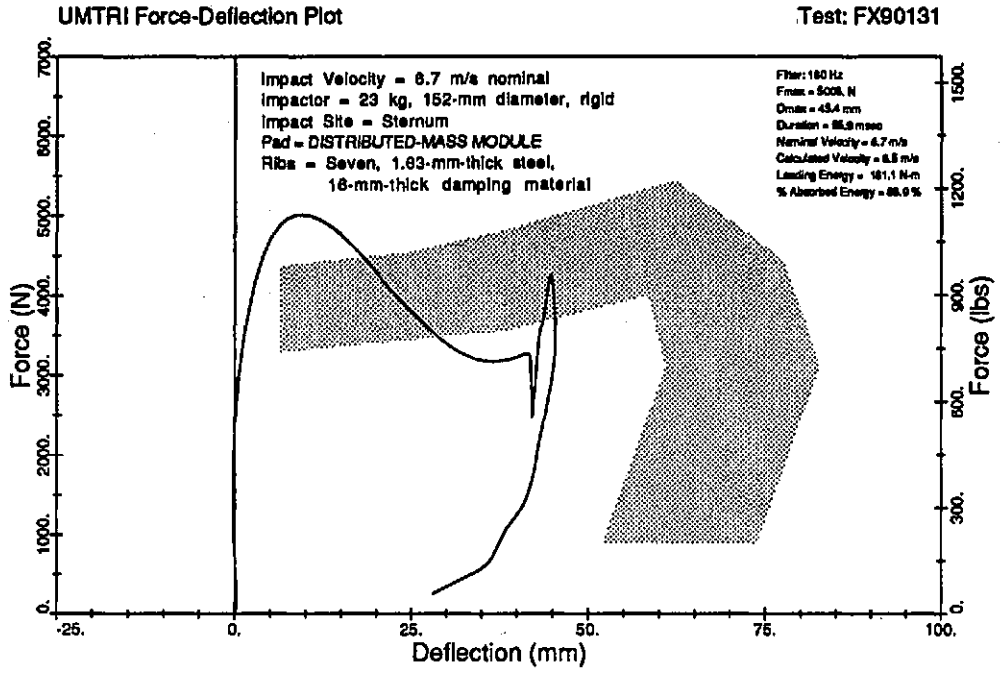

FIGURE 6–14b. F-δ response for 6.7-m/s pendulum test of First Prototype-50M chest installed in dummy with *distributed-mass module attached to front of sternum*.

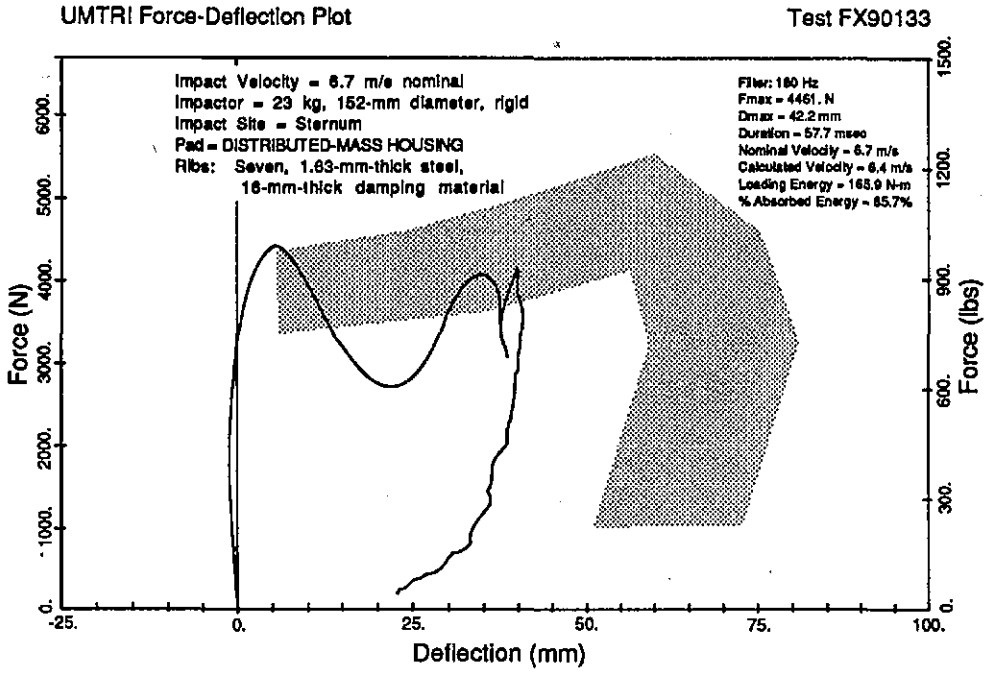

FIGURE 6–14c. F-δ response for 6.7-m/s pendulum test of First Prototype-50M chest installed in dummy with *housing of distributed-mass module attached to front of sternum.*

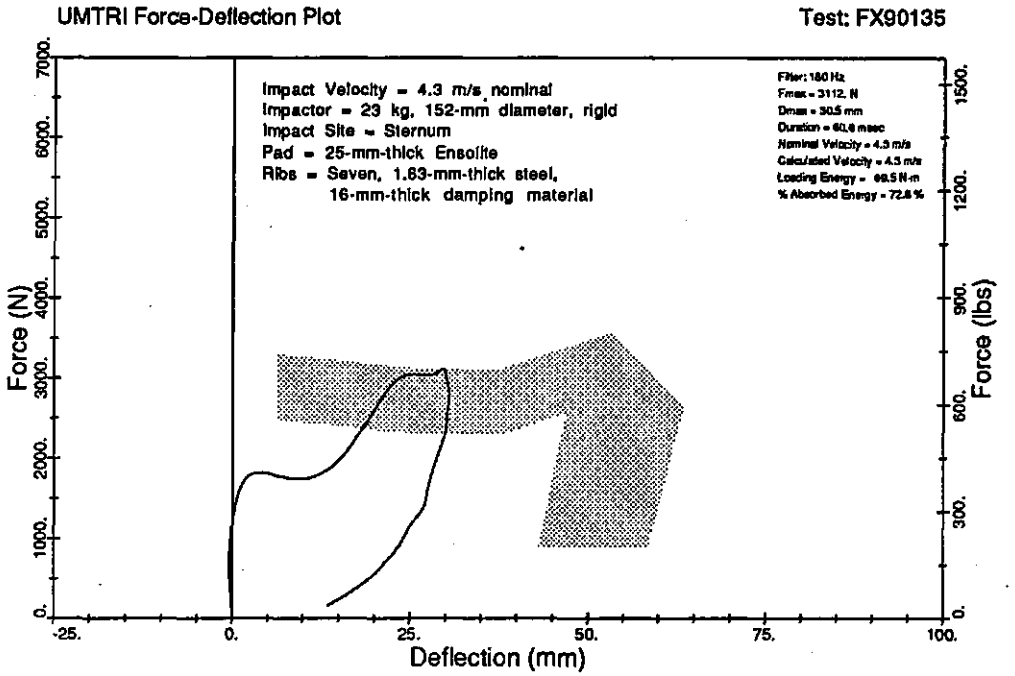

FIGURE 6–15a. F-δ response for 4.3-m/s pendulum test of First Prototype-50M chest installed in dummy with *Sorbothane block between upper sternum and spine*.

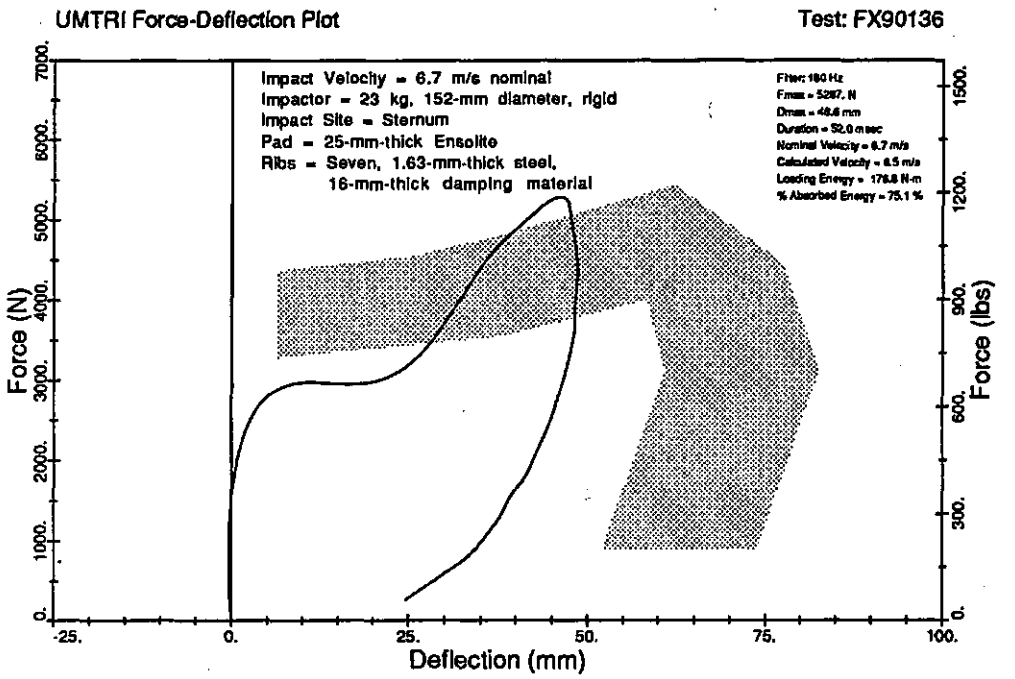

FIGURE 6–15b. F-δ response for 6.7-m/s pendulum test of First Prototype-50M chest installed in dummy with *Sorbothane block between upper sternum and spine*.

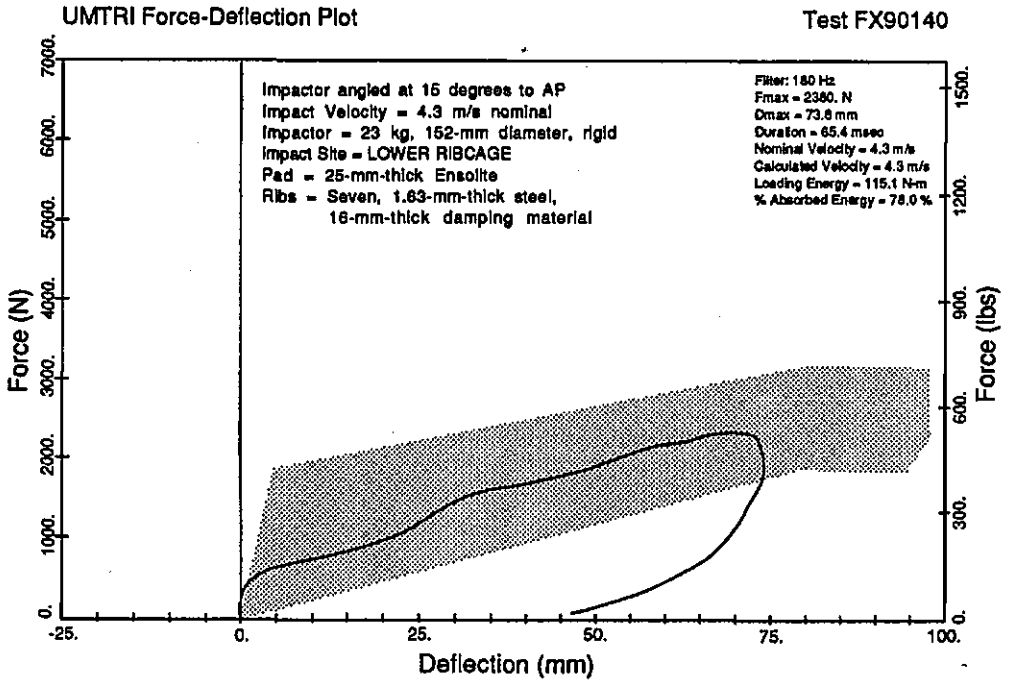

FIGURE 6–16a. F-δ response for 4.3-m/s pendulum test of First Prototype-50M chest installed in dummy with impact to *lower ribcage*.

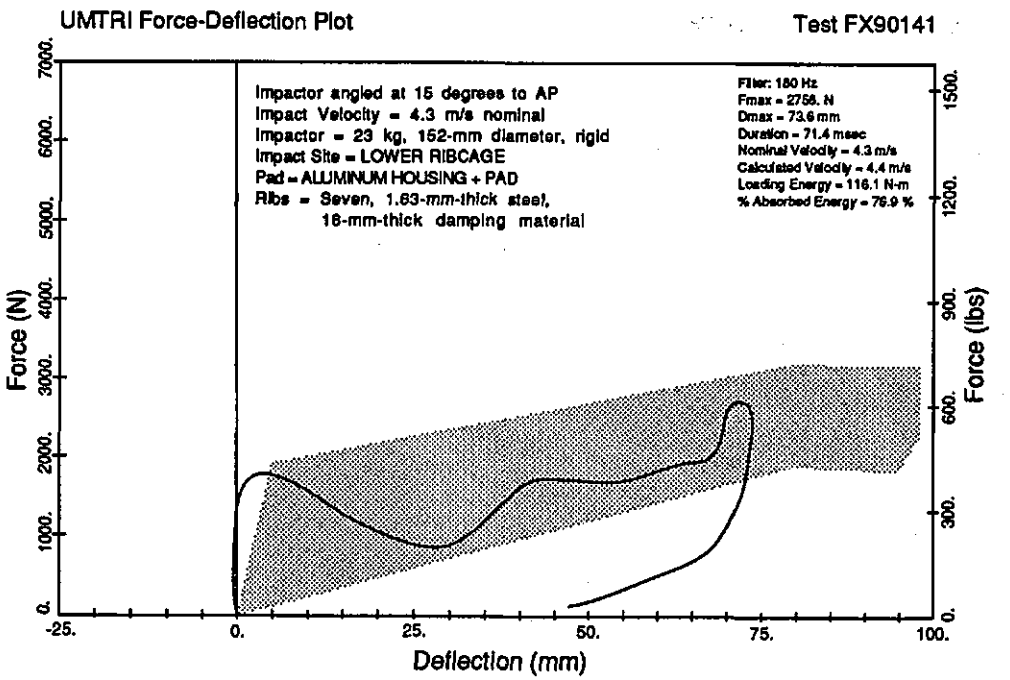

FIGURE 6–16b. F-δ response for 4.3-m/s pendulum test of First Prototype-50M chest installed in dummy with impact to *lower ribcage with 1-kg aluminum housing of distributed-mass module* in front of ribs

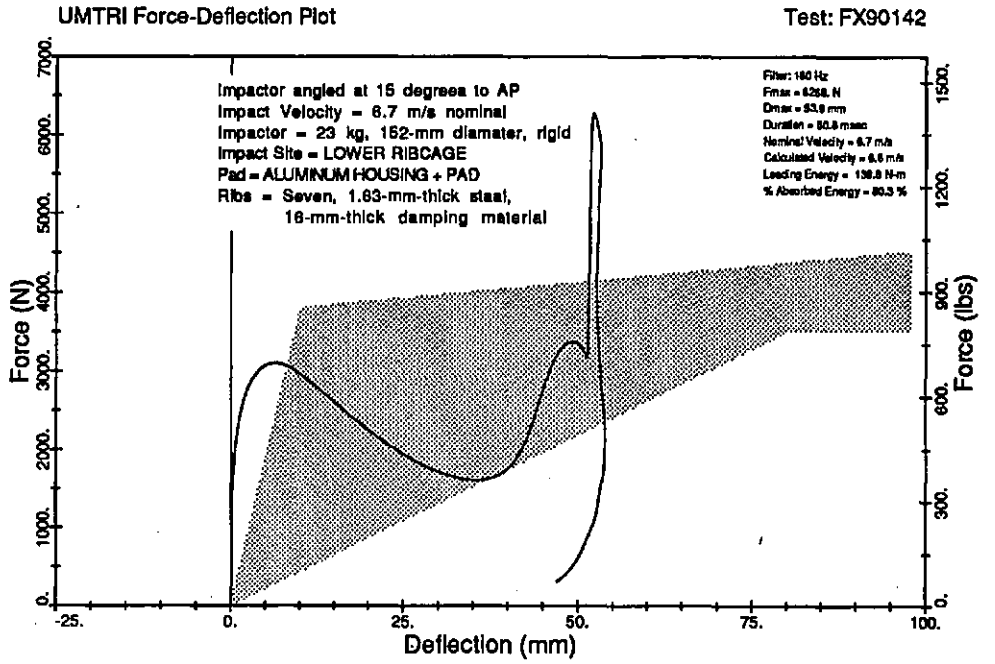

FIGURE 6–16c. F-δ response for 6.7-m/s pendulum test of First Prototype-50M chest installed in dummy with impact to *lower ribcage with 1-kg aluminum housing of distributed-mass module* in front of ribs.

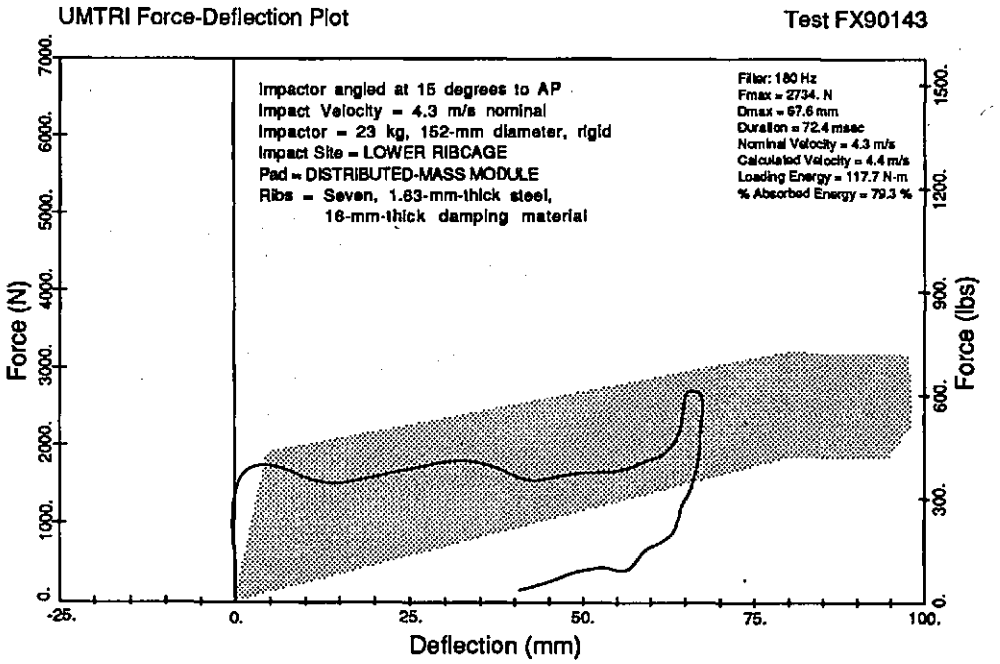

FIGURE 6–16d. F-δ response for 4.3-m/s pendulum test of First Prototype-50M chest installed in dummy with impact to *lower ribcage with distributed-mass module* in front of ribs.

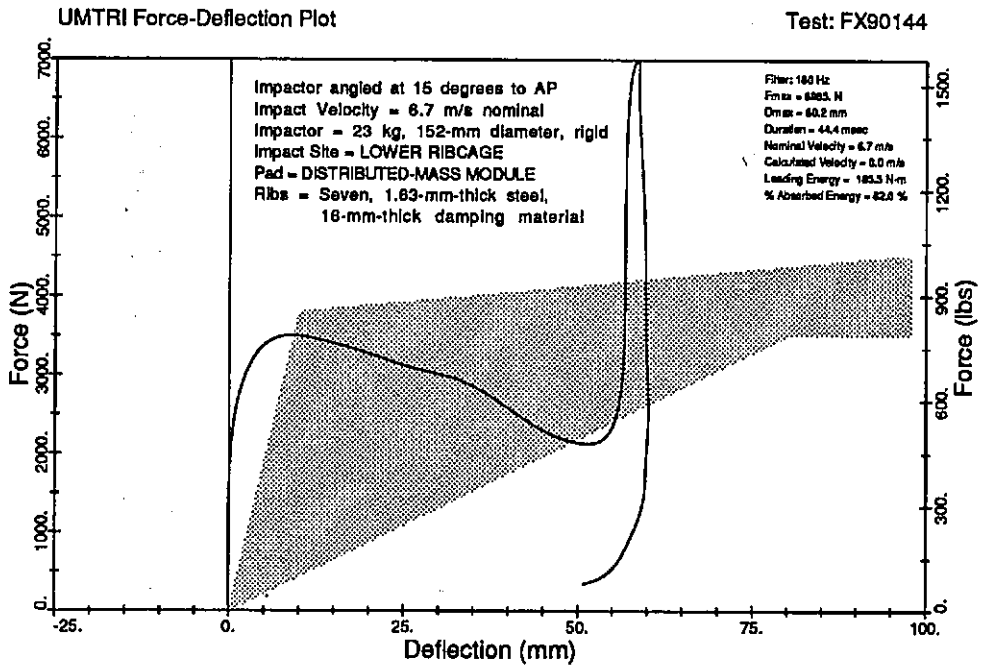

FIGURE 6–16e. F-δ response for 6.7-m/s pendulum of First Prototype-50M chest installed in dummy with impact to *lower ribcage with distributed-mass module* in front of ribs.

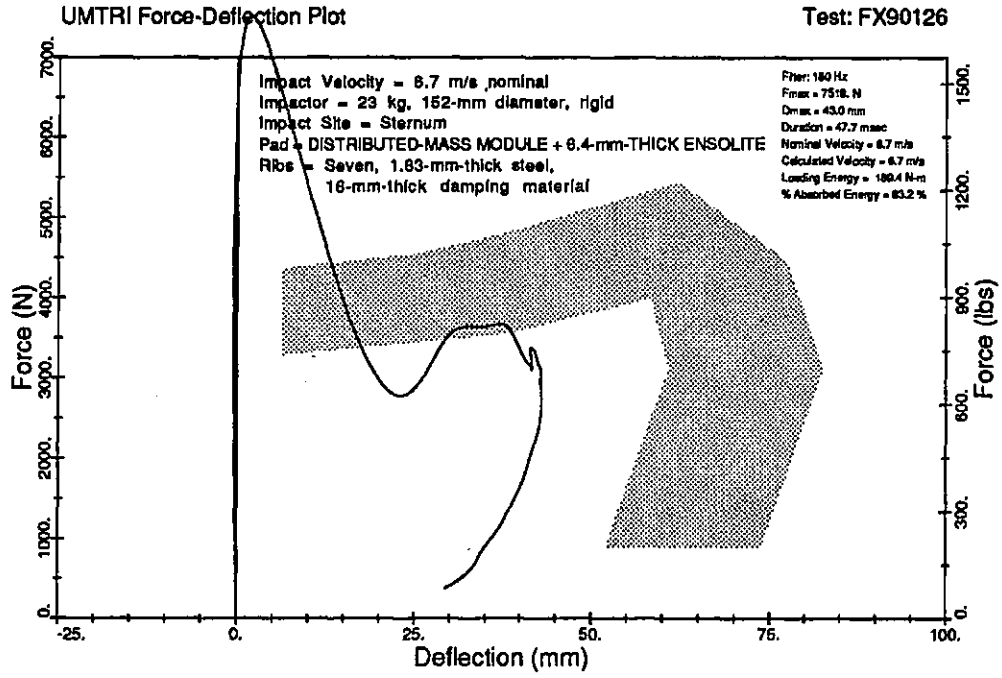

FIGURE 6–17a. F-δ response for 6.7-m/s pendulum test of First Prototype-50M chest installed in dummy with *distributed-mass module* and 6.4-mm (0.25-in) thick pad) in front of sternum.

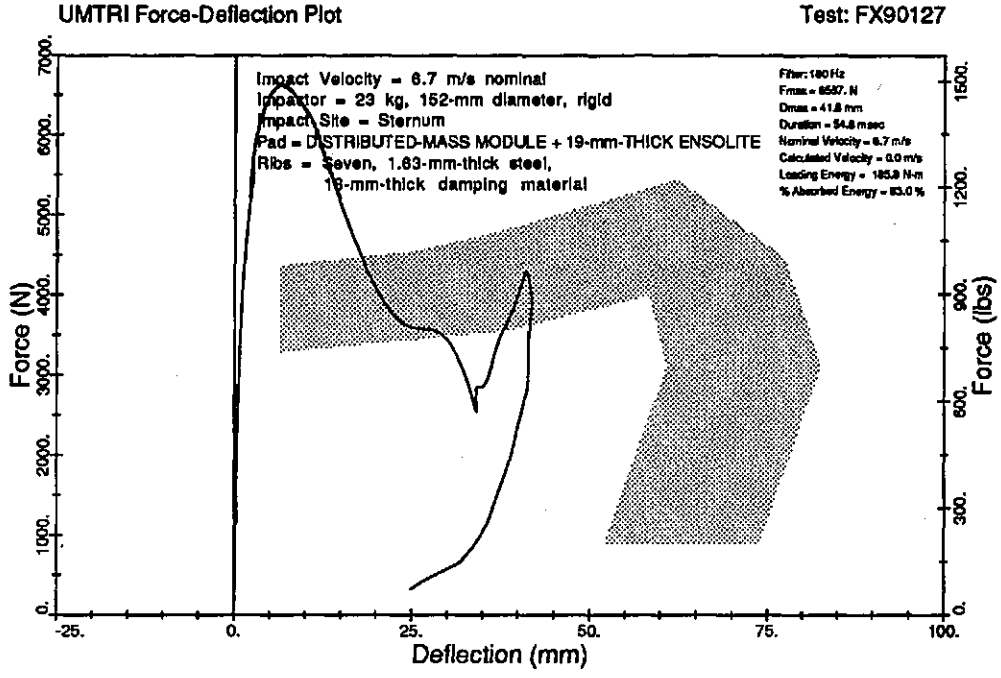

FIGURE 6–17b. F-δ response for 6.7-m/s pendulum test of First Prototype-50M chest installed in dummy with *distributed-mass module* and 19-mm (0.75-in) thick pad) in front of sternum.

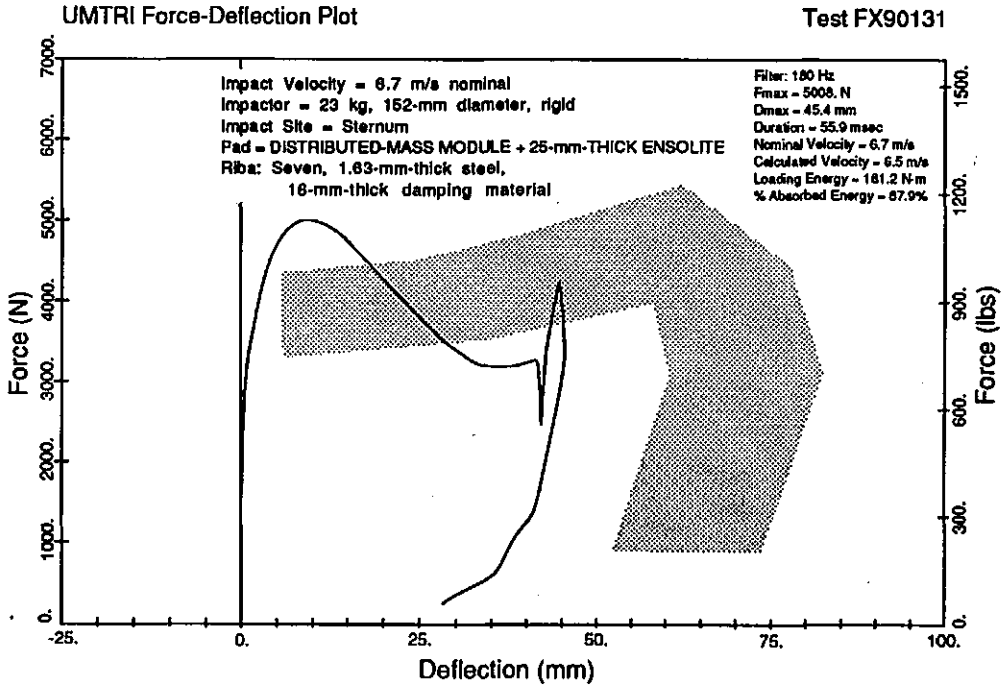

FIGURE 6–17c. F-δ response for 6.7-m/s pendulum test of First Prototype-50M chest installed in dummy with *distributed-mass module* and 25-mm (1-in) thick pad) in front of sternum.

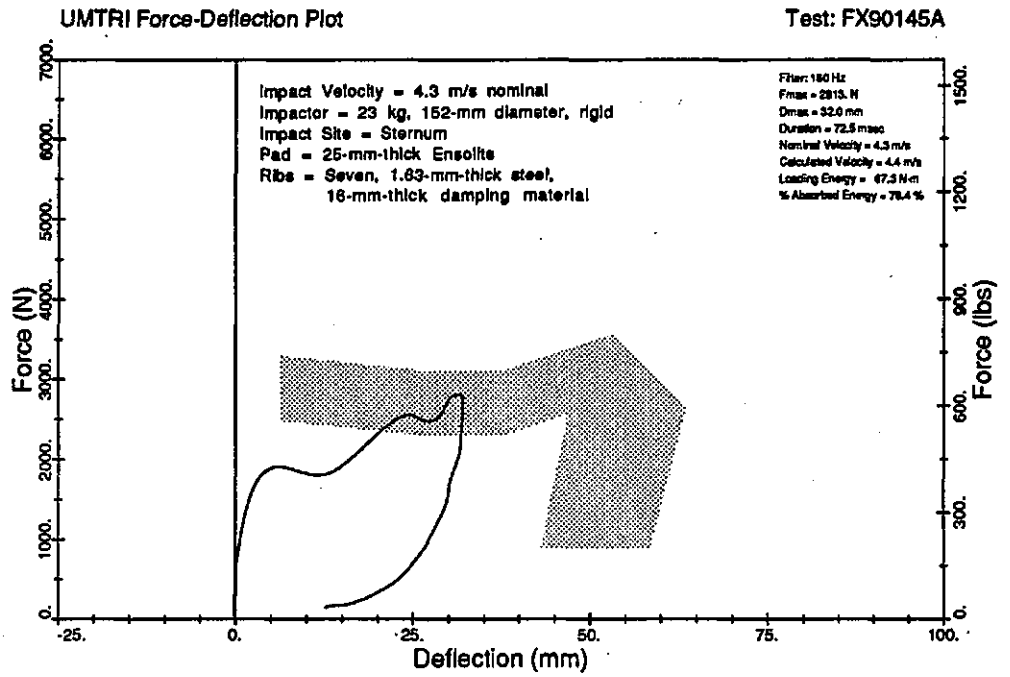

FIGURE 6–18a. F-δ response for 4.3-m/s pendulum test of First Prototype-50M chest installed in dummy using *string potentiometer mounted to **upper** thoracic spine for deflection*.

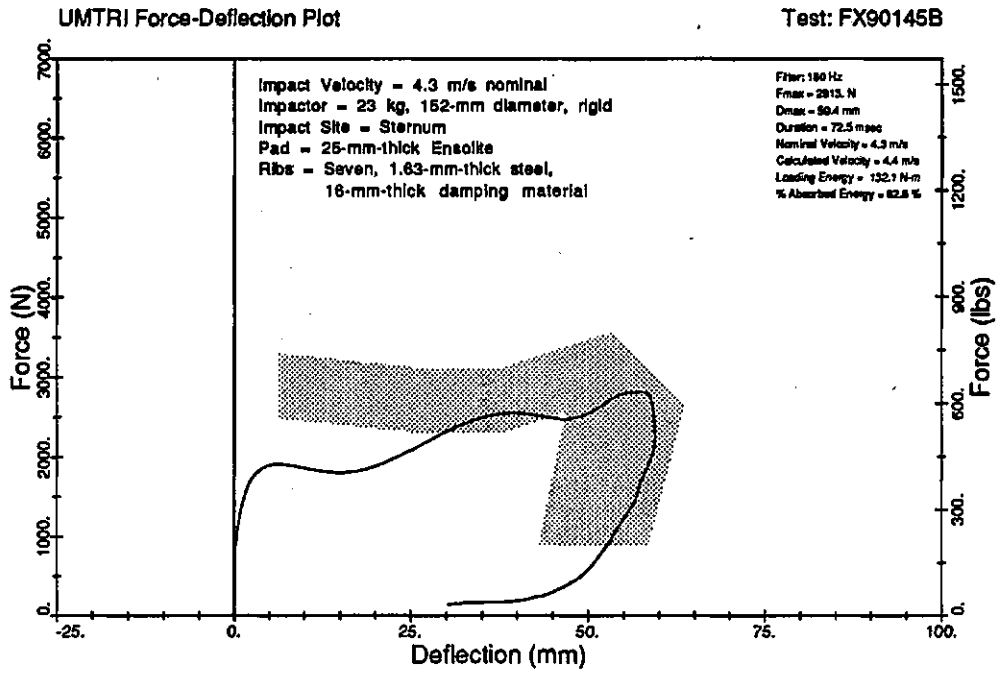

FIGURE 6–18b. F-δ response for 4.3-m/s pendulum test of First Prototype-50M chest installed in dummy using *string potentiometer mounted to **lower** thoracic spine for deflection*.

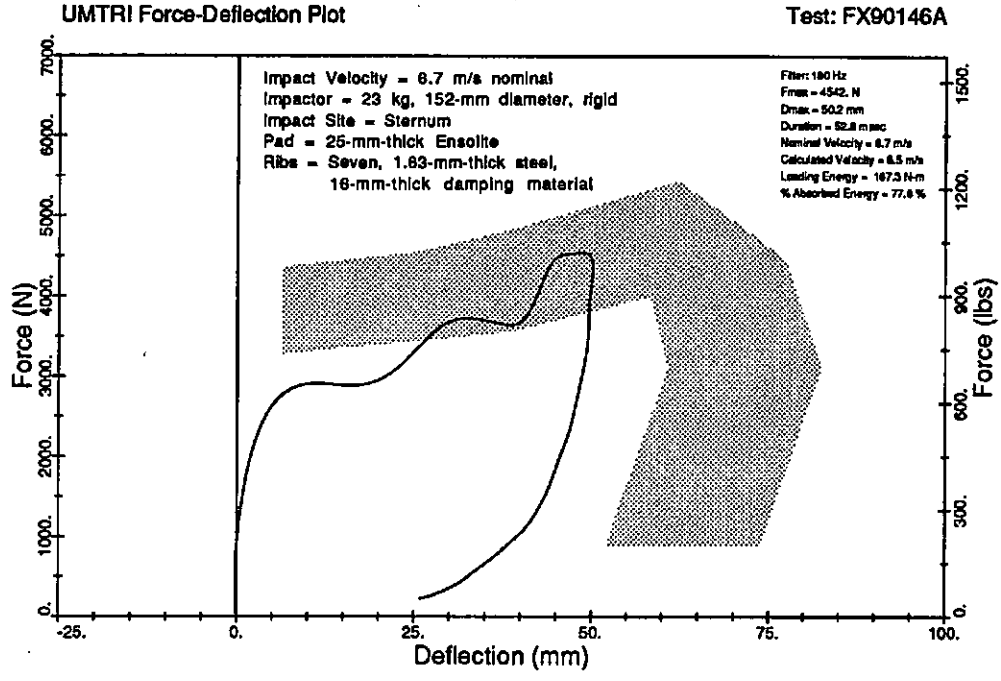

FIGURE 6–18c. F-δ response for 6.7-m/s pendulum test of First Prototype-50M chest installed in dummy using *string potentiometer mounted to* ***upper*** *thoracic spine for deflection.*

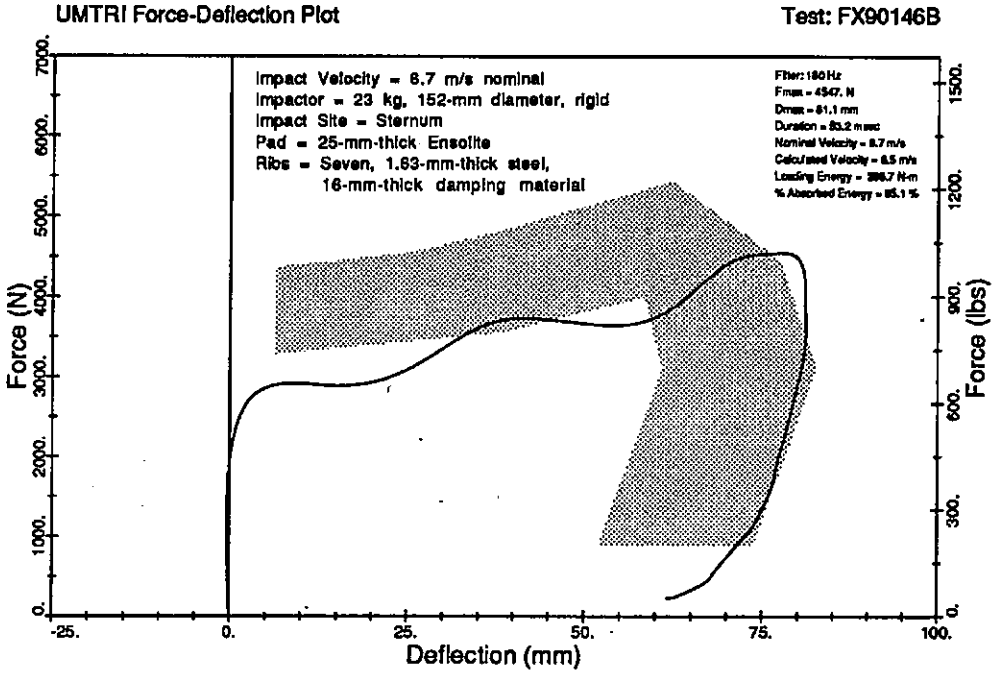

FIGURE 6–18d. F-δ response for 6.7-m/s pendulum test of First Prototype-50M chest installed in dummy using *string potentiometer mounted to* ***lower*** *thoracic spine for deflection.*

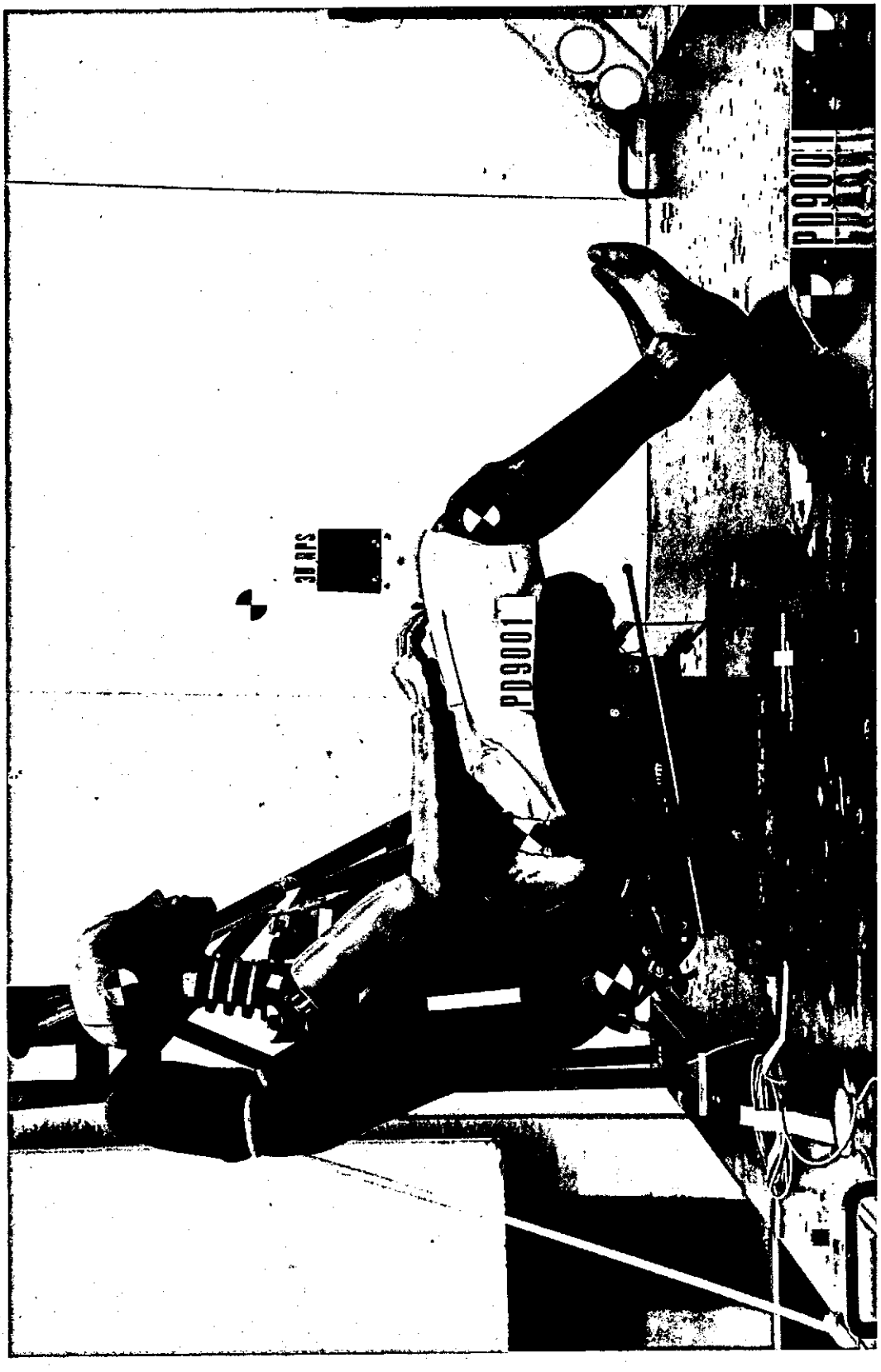

FIGURE 6–19a. Side view of sled test setup of First Prototype-50M dummy with forward position of right lap-belt anchor point.

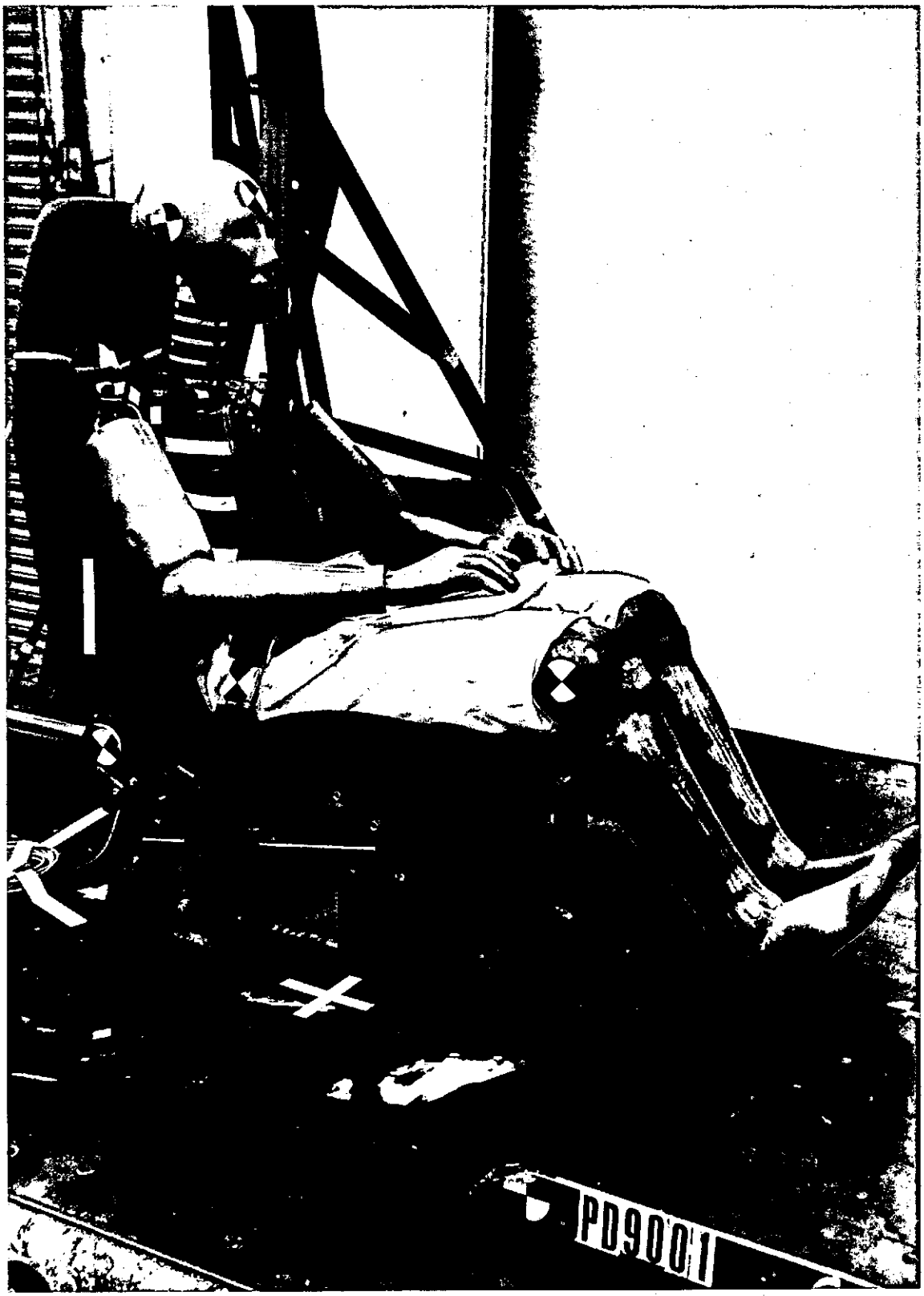

FIGURE 6–19b. Oblique view of sled test setup of First Prototype-50M dummy with forward position of right lap-belt anchor point.

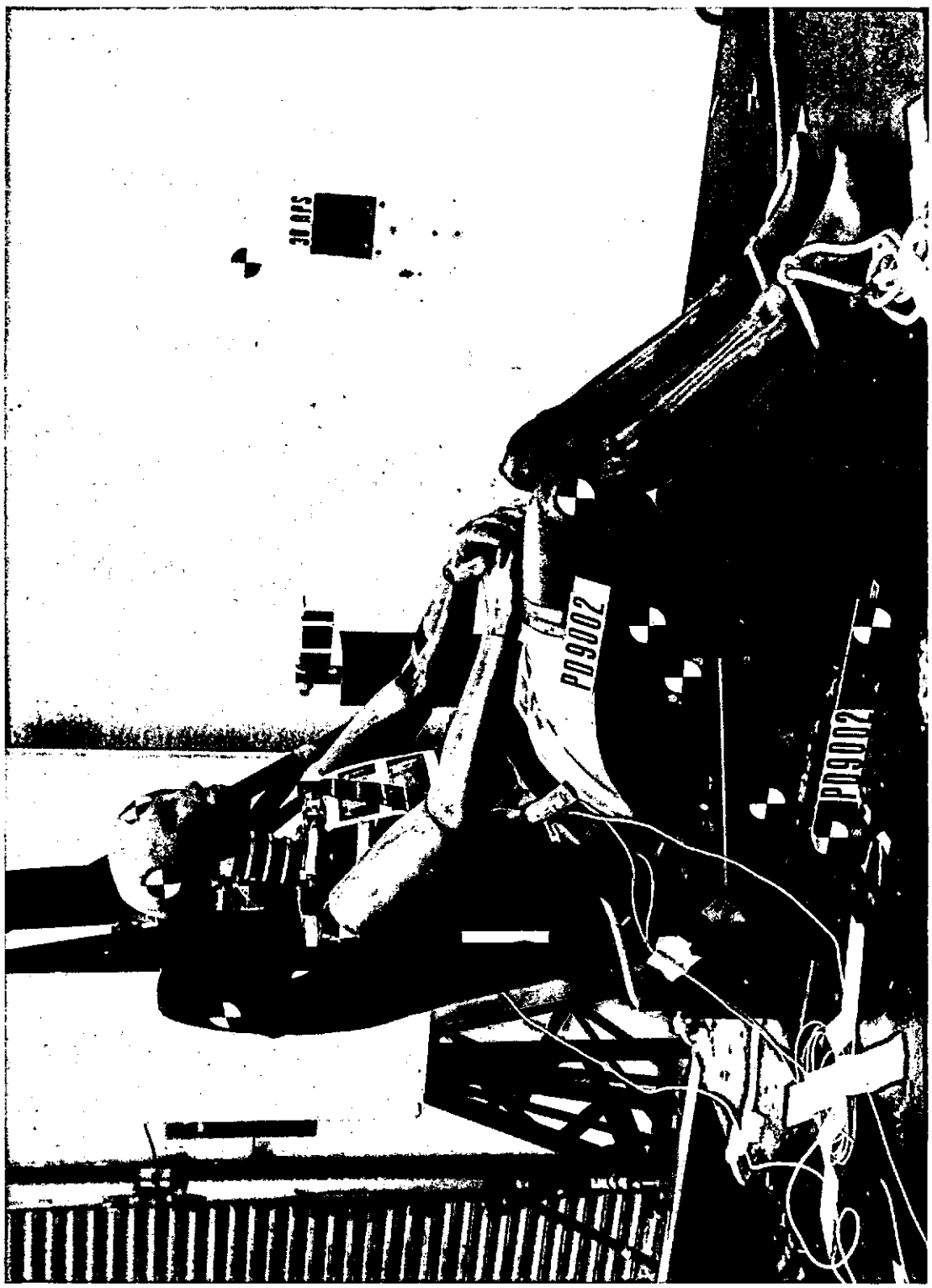

FIGURE 6–19c. Side view of sled test setup of First Prototype-50M dummy with more rearward position of right lap-belt anchor point.

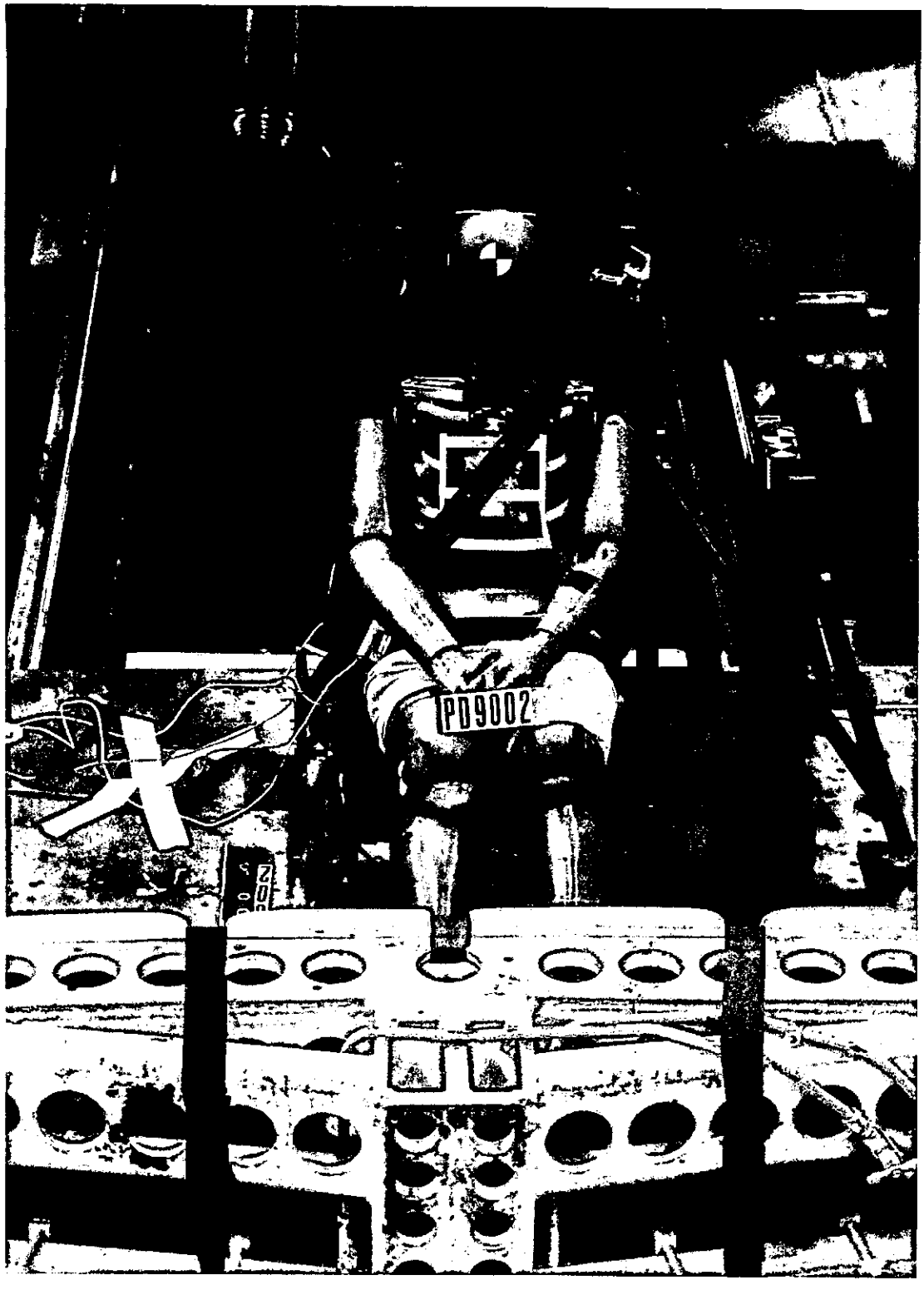

FIGURE 6–19d. Front view of sled test setup of First Prototype-50M dummy with more rearward position of right lap-belt anchor point.

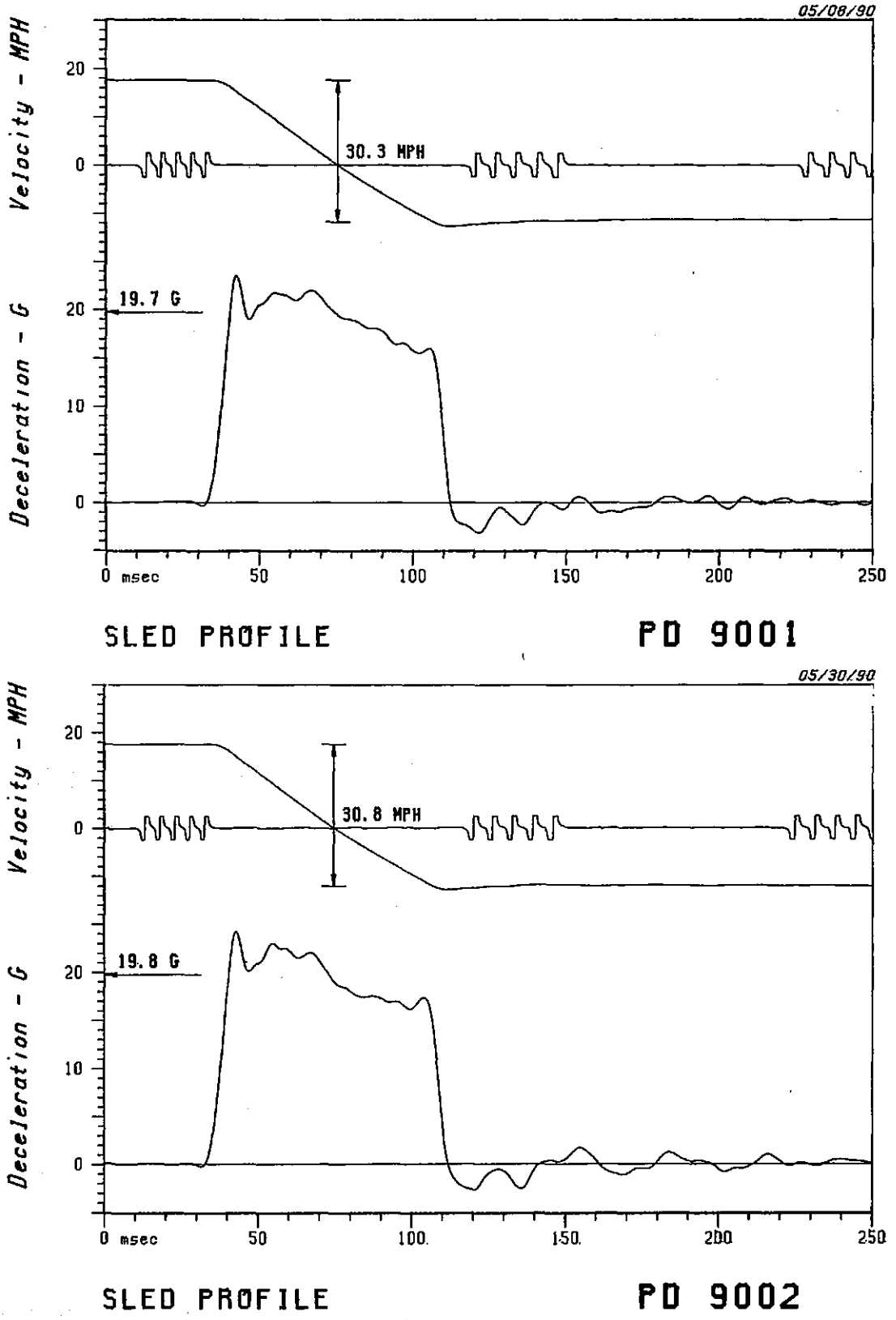

FIGURE 6–20. Sled deceleration and velocity time histories for preliminary sled test of the First Prototype-50M.

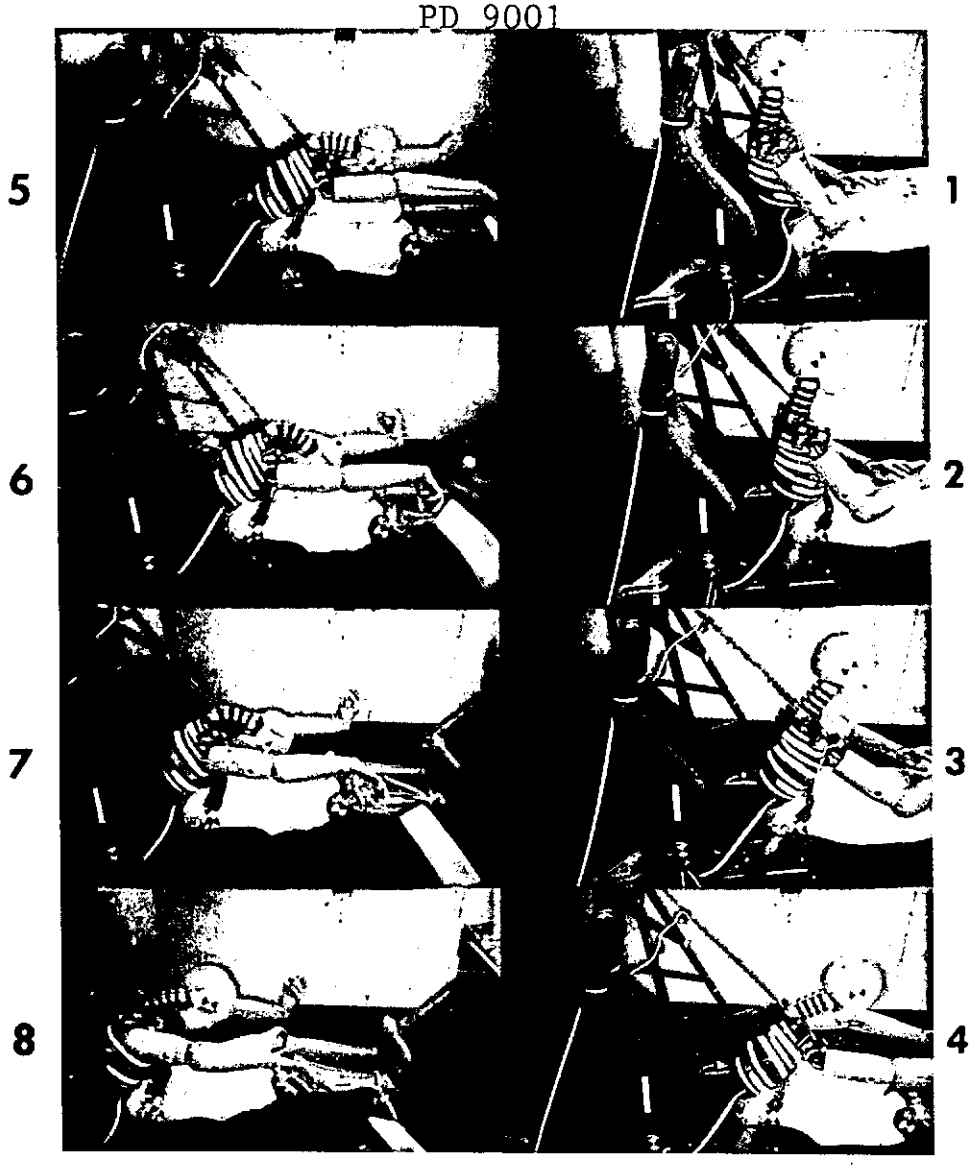

FIGURE 6–21a. Side-view, time-sequence photograph of Test PD9001.

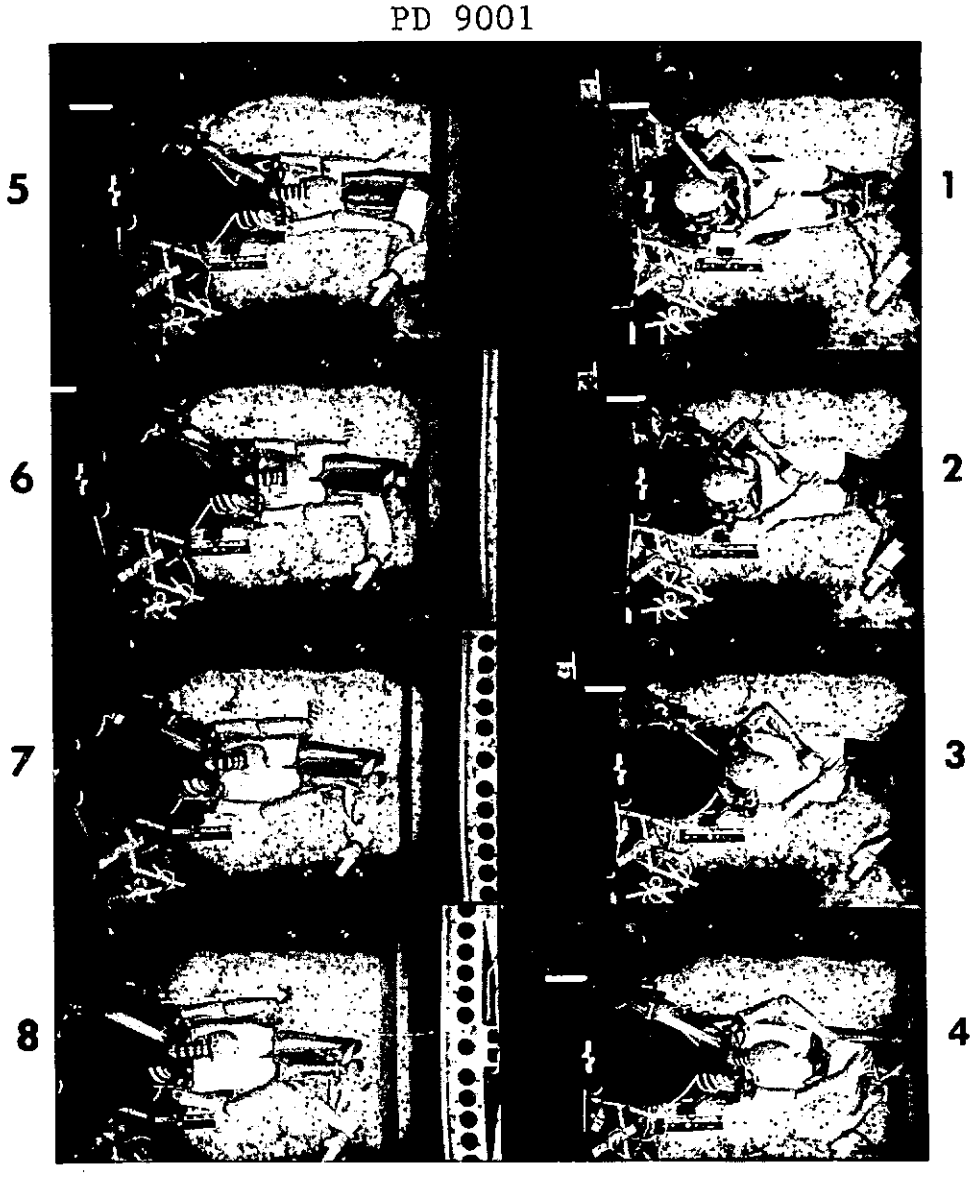

FIGURE 6–21b. Top-view, time-sequence photograph of Test PD9001.

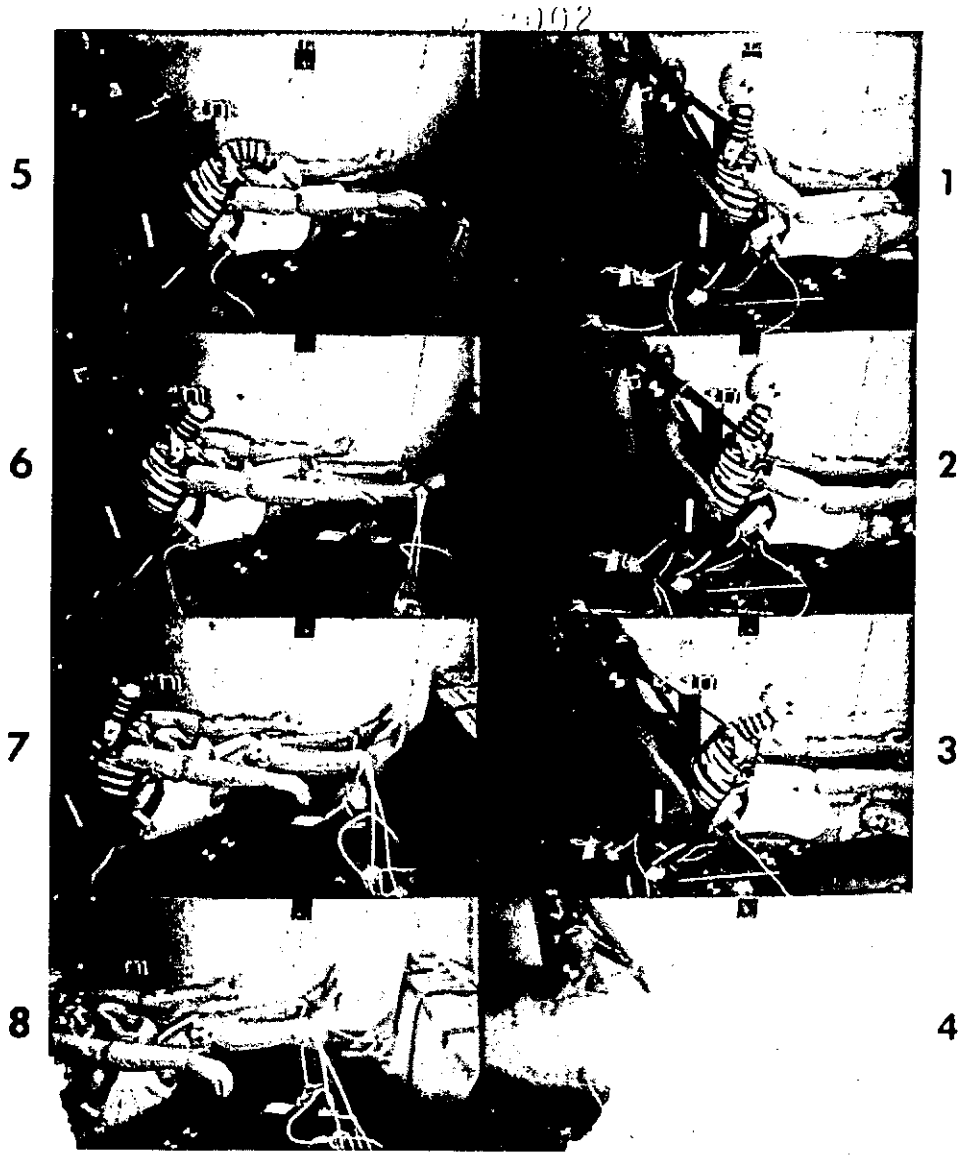

FIGURE 6–21c. Side-view, time-sequence photograph of Test PD9002.

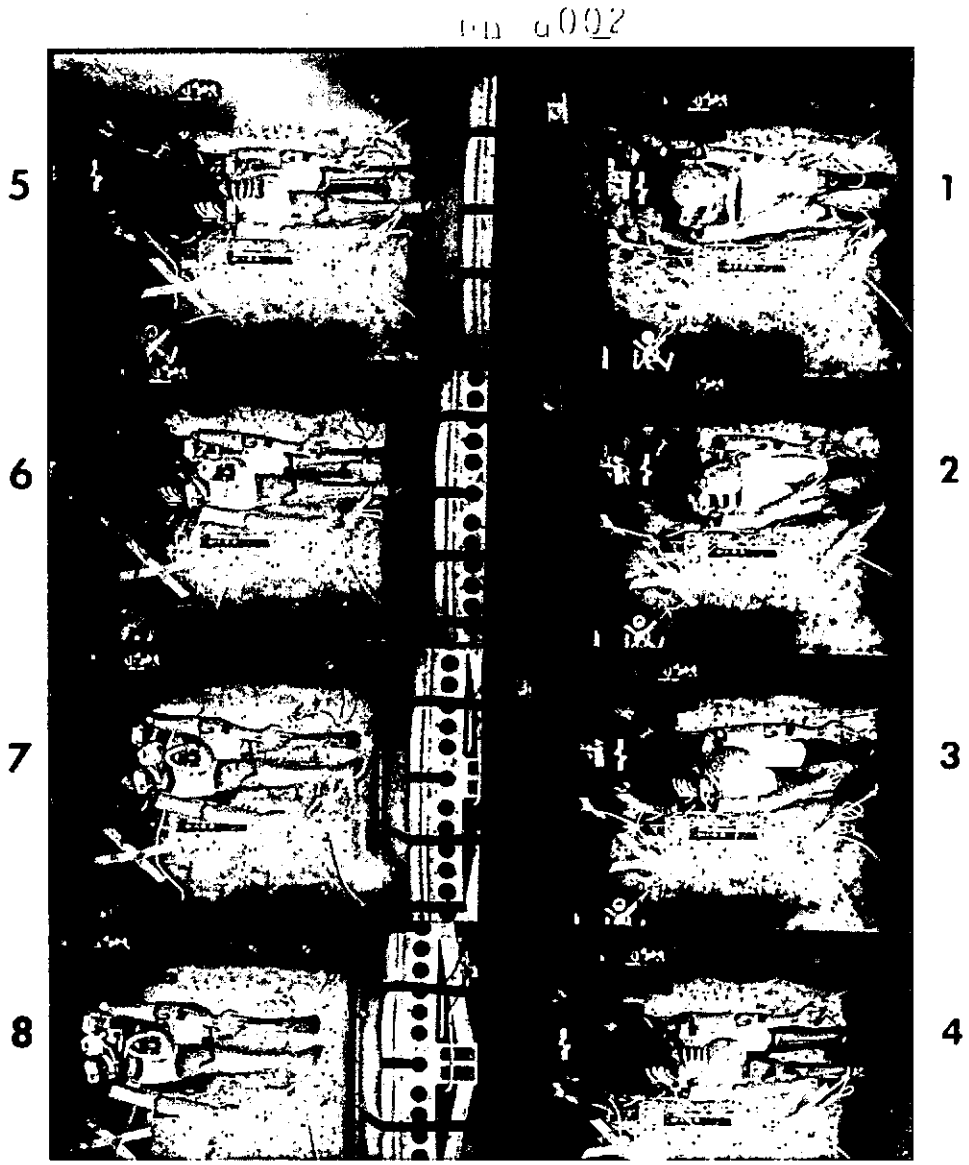

FIGURE 6–21d. Top-view, time-sequence photograph of Test PD9002.

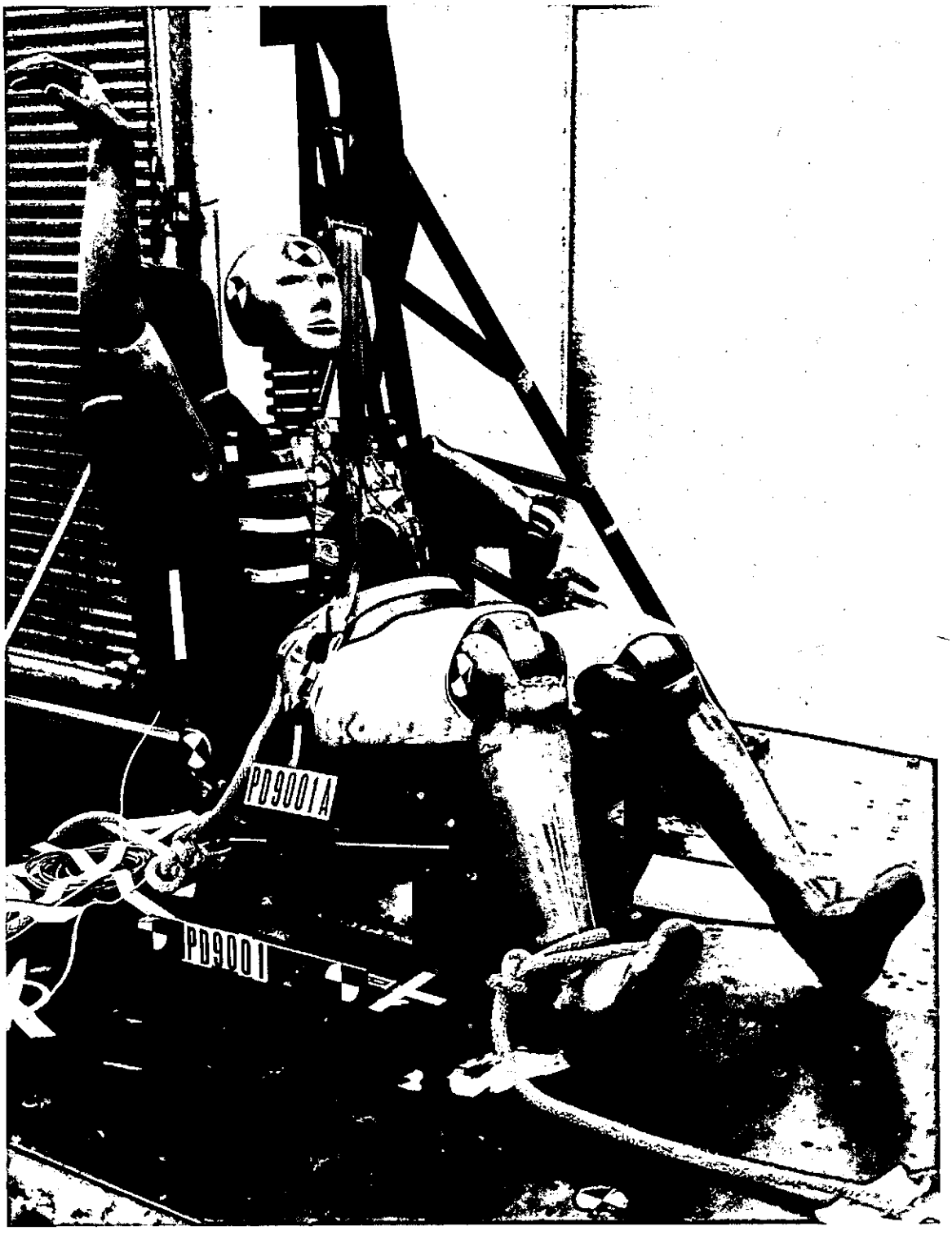

FIGURE 6–22a. Post-test photo of sled test PD9001.

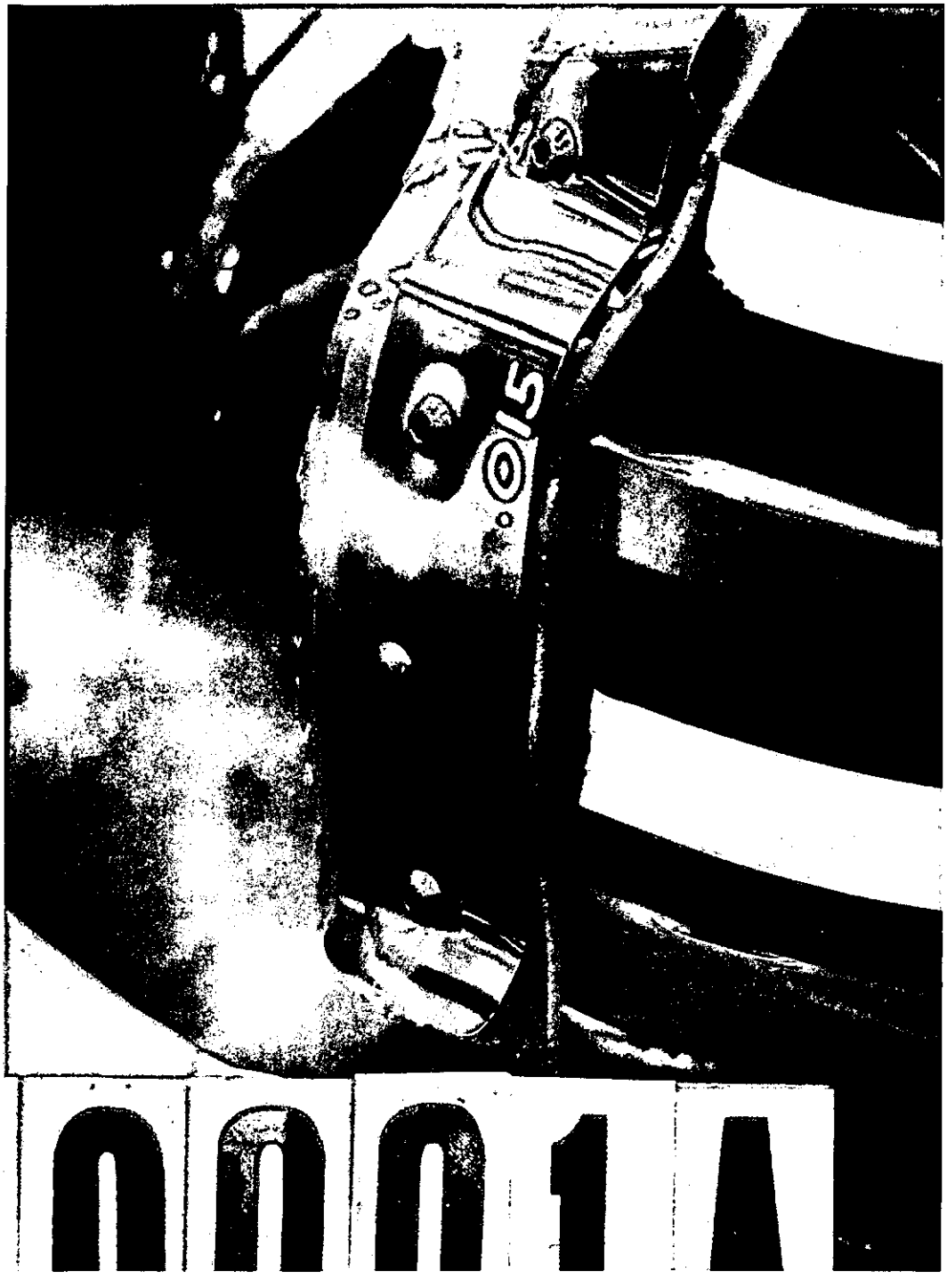

FIGURE 6–22b. Post-test photo of spring-steel band coupling ribcage following sled test PD9001. Note permanent deformation in material.

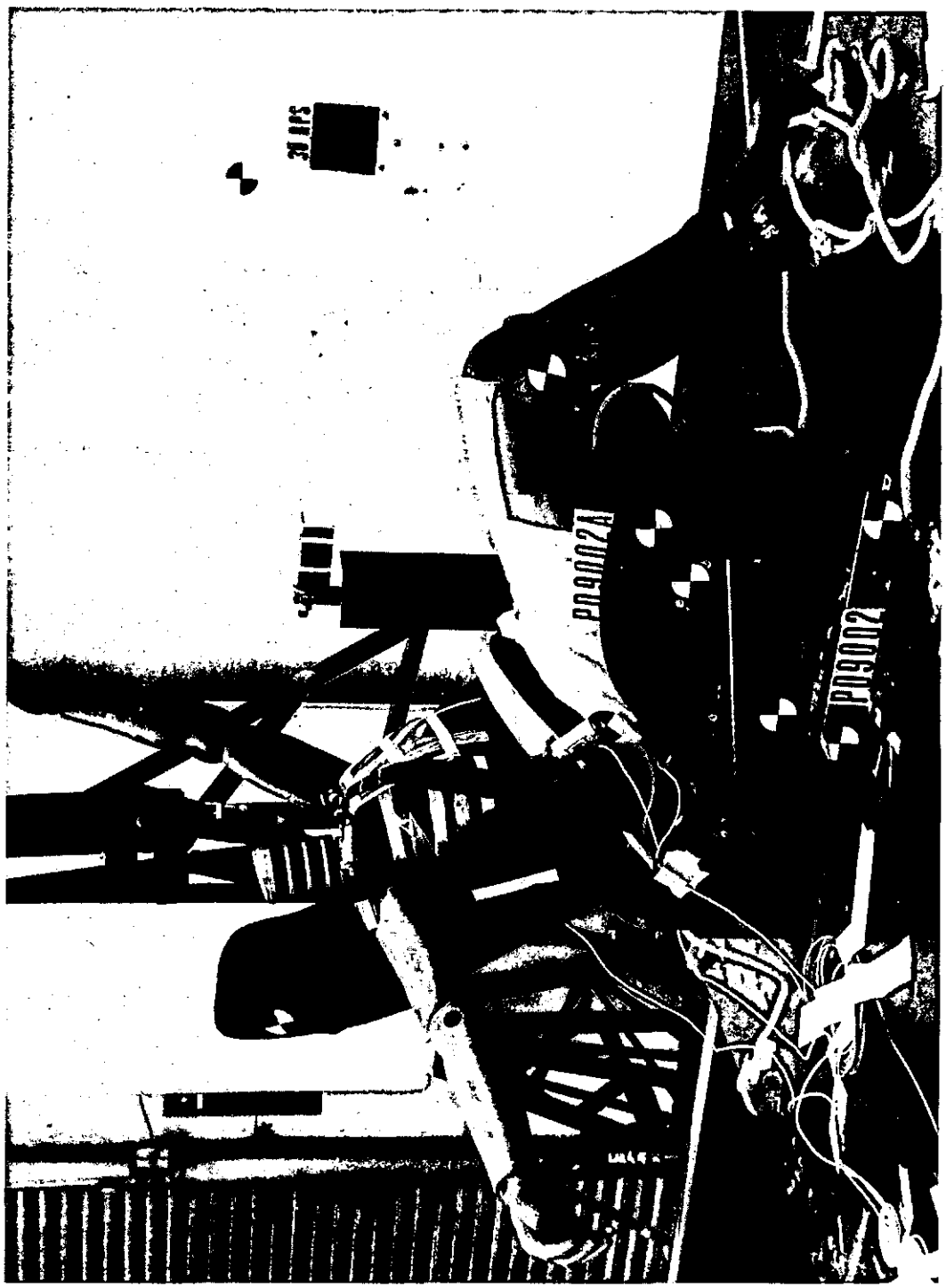

FIGURE 6–22c. Post-test photo of sled test PD9002.

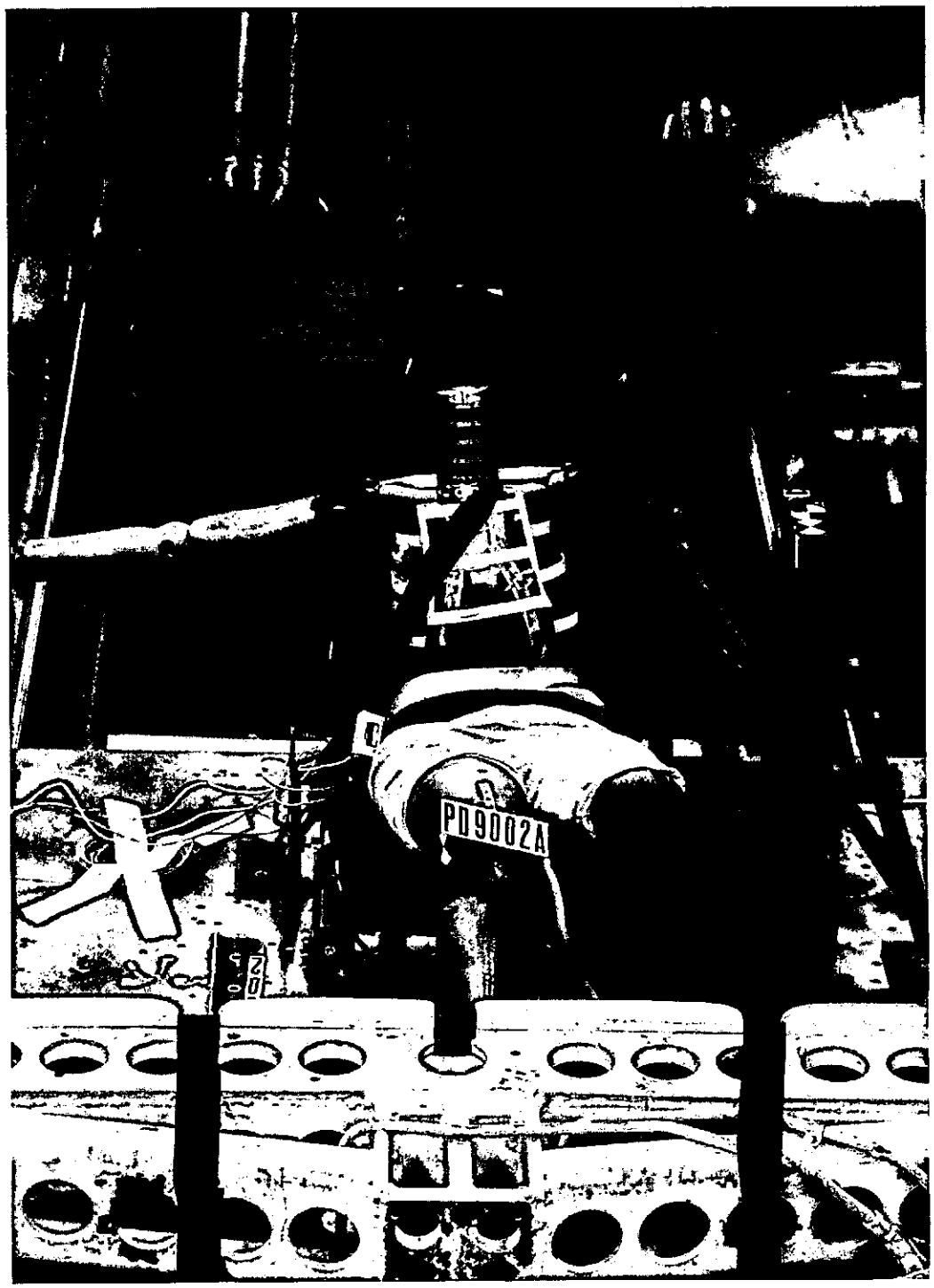

FIGURE 6–22d. Post-test photo of sled test PD9002.

FIGURE 6–22e. Close-up photo of shoulder/clavicle region of prototype chest after sled test PD9002. Note broken rod end on proximal end of left clavicle and shoulder belt buried between shoulder and neck.

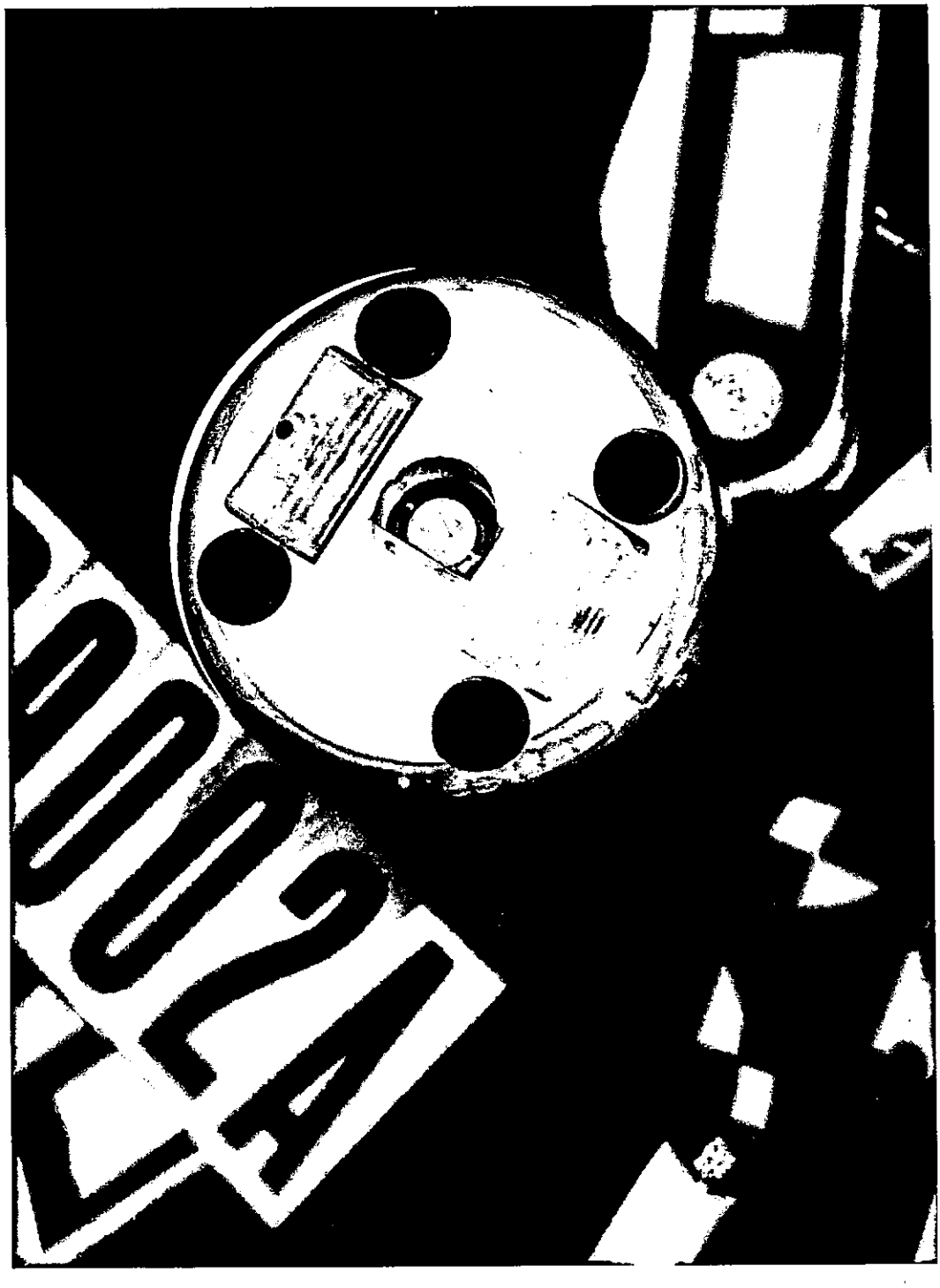

FIGURE 6–22f. Close-up photo of neck nodding block after sled test PD9002 showing failure at center that resulted in released dummy head.

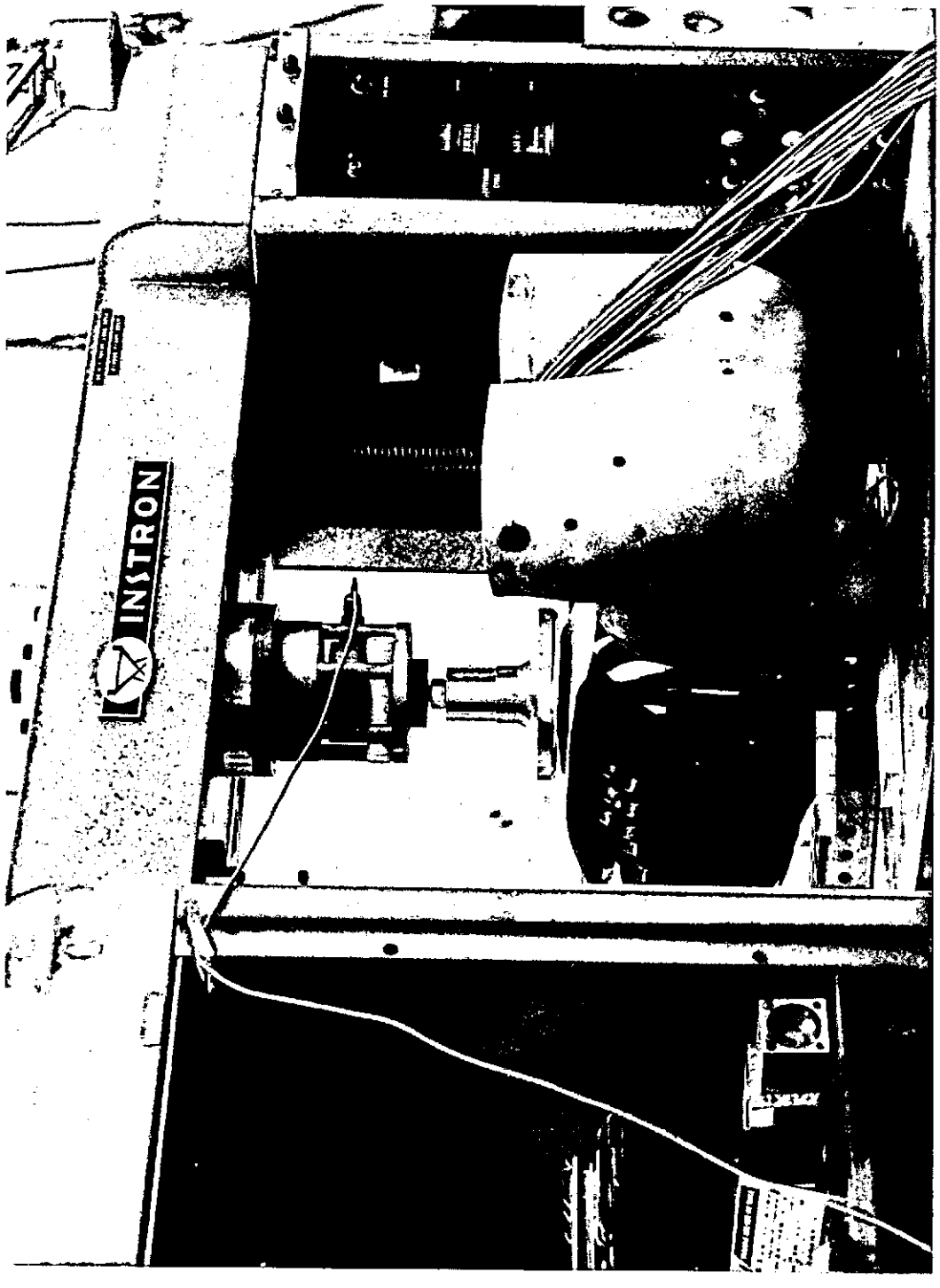

FIGURE 6–23. Setup for quasi-static compression loading of the Second Prototype-50M using a 152-mm (6-in) diameter rigid plate.

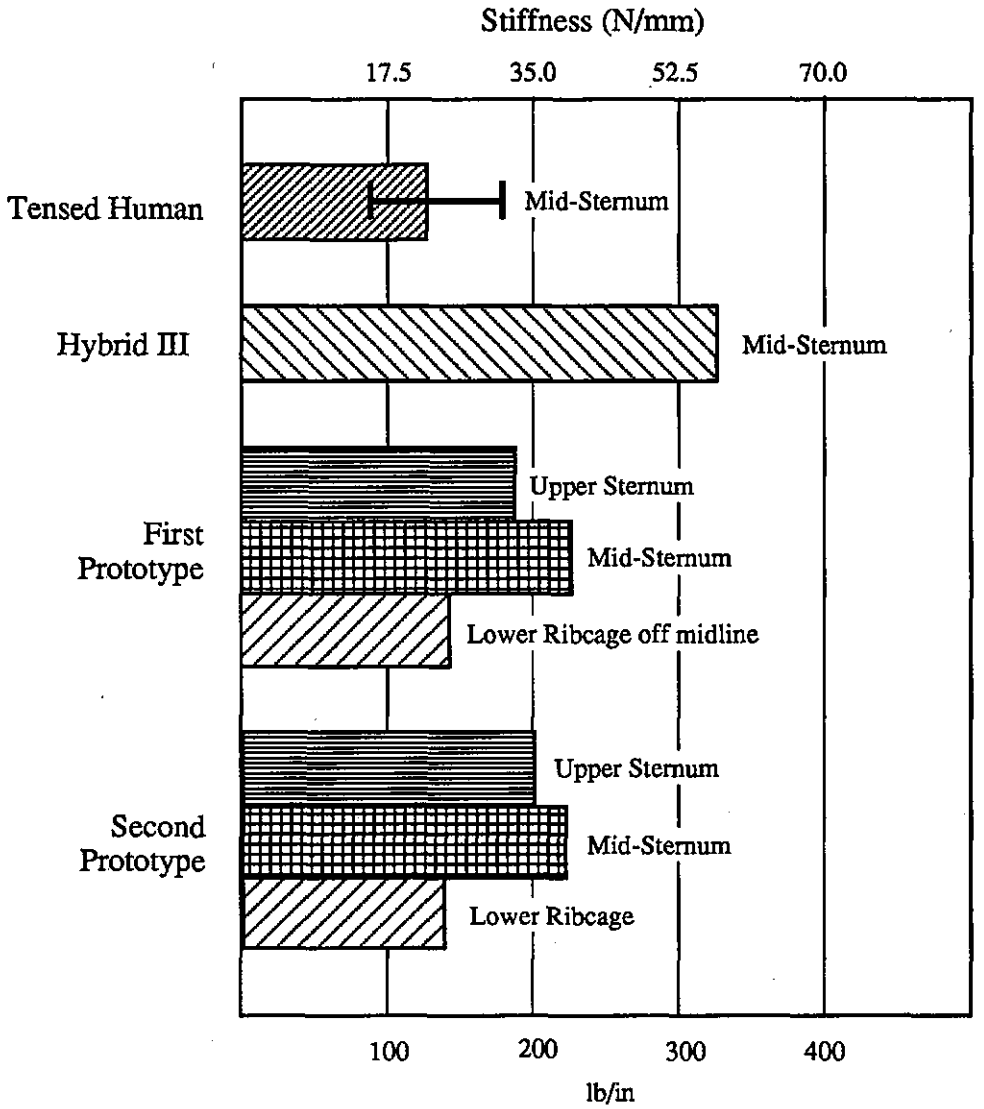

FIGURE 6–24. Comparison of quasi-static stiffness values of the Second Prototype-50M using the 152-mm (6-in) diameter loading plate without padding and without the steel shelves to results obtained from the First Prototype-50, the Hybrid III unpadded ribcage, and Lobdell et al. (1973) human volunteer tests.

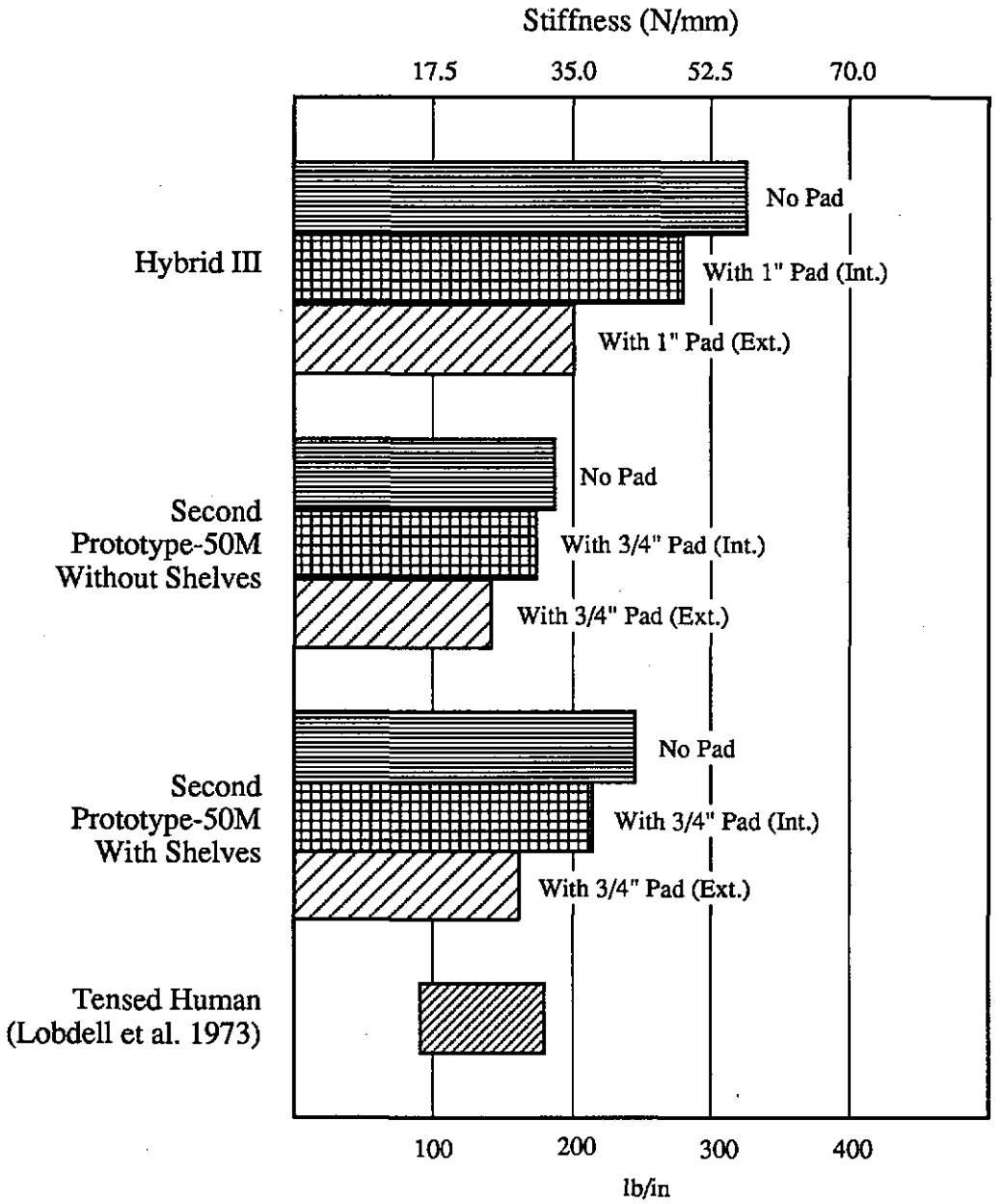

FIGURE 6–25. Comparison of quasi-static stiffness values of the Second Prototype-50M using the 152-mm (6-in) diameter loading plate with and without padding and with and without the steel shelves under the first rib to results obtained from Hybrid III and Lobdell et al. (1973) tensed volunteer tests.

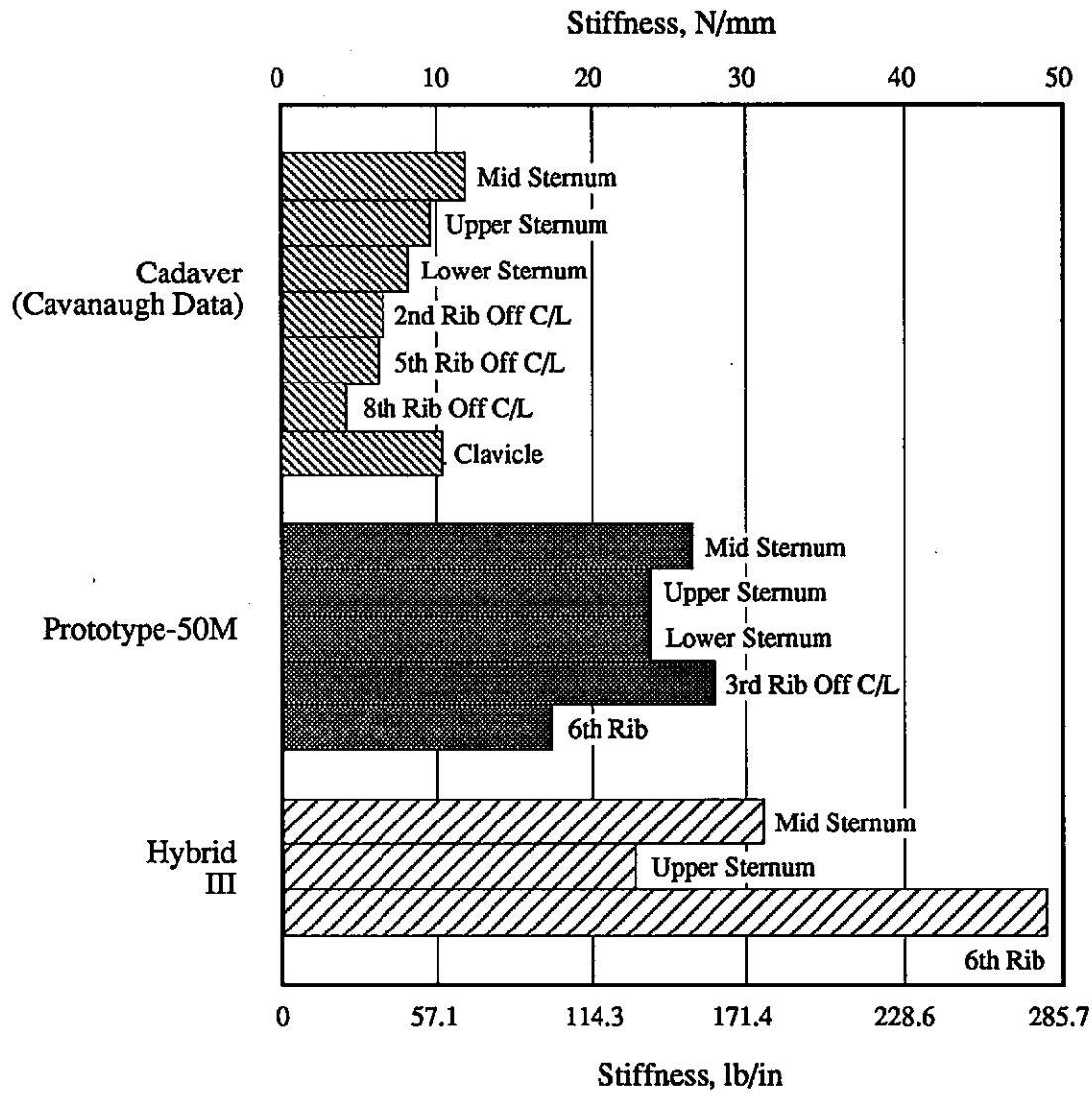

FIGURE 6–26. Comparison of regional quasi-static stiffness values of the Second Prototype-50M using the 50-mm by 100-mm (2-in by 4-in) rigid loading plate to results from similar tests performed on the unpadded Hybrid III ribcage and unembalmed cadavers (Cavanaugh et al. 1988).

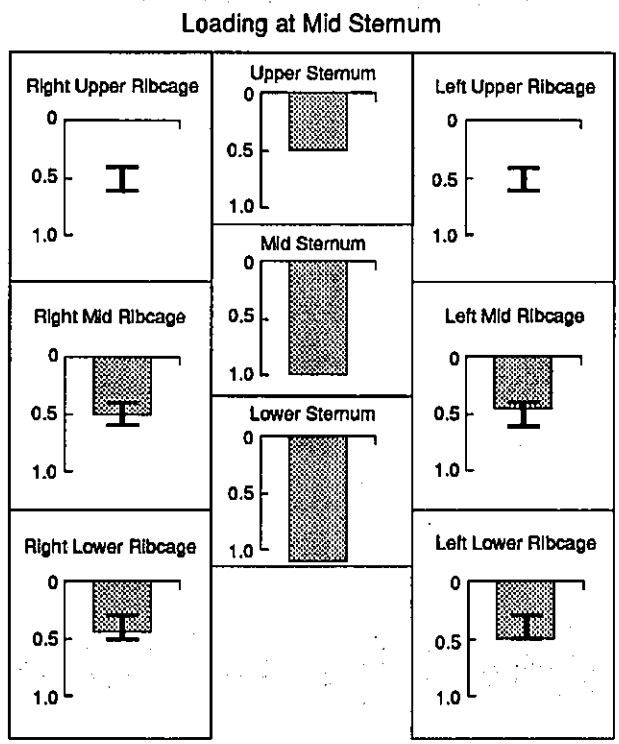

FIGURE 6–27a. Relative normalized deflections at different regions of the ribcage for loading at the midsternum with a 50-mm by 100-mm (2-in by 4-in) rigid plate.

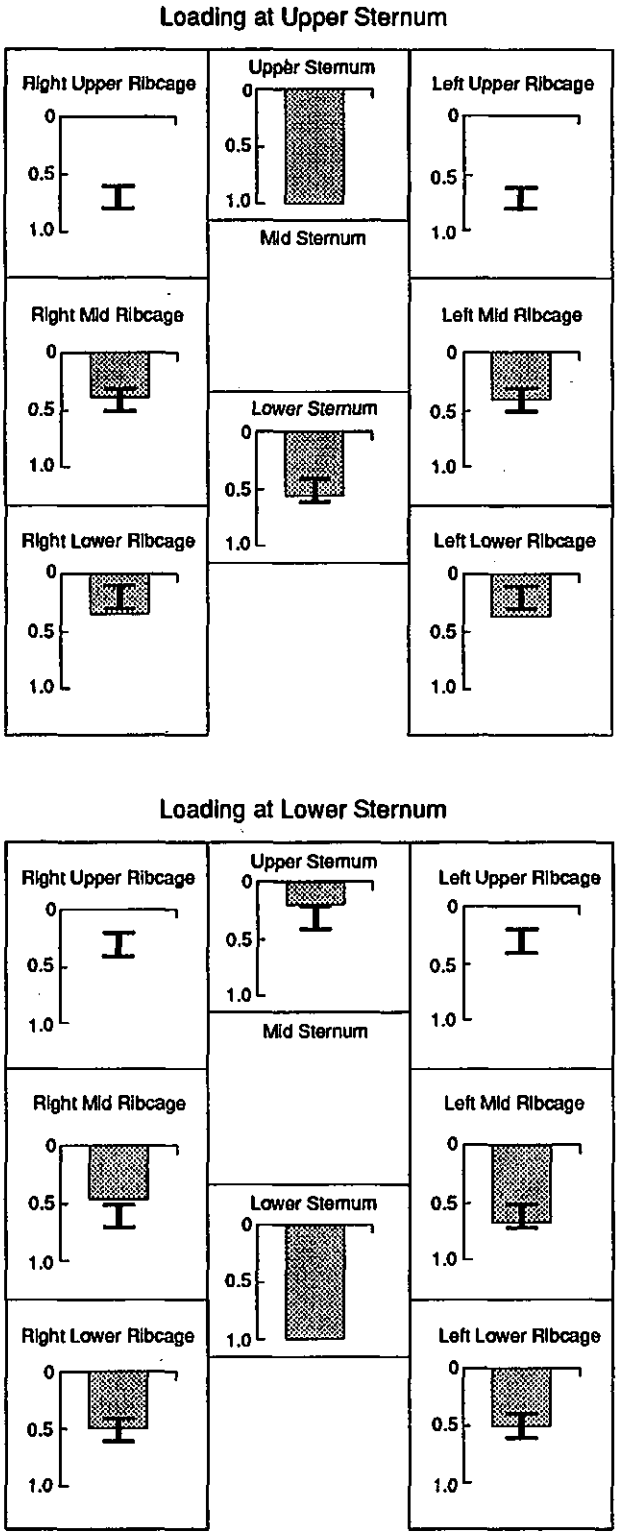

FIGURE 6–27b. Relative normalized deflections at different regions of the ribcage for loading at the upper and lower sternum with a 50-mm by 100-mm (2-in by 4-in) rigid plate.

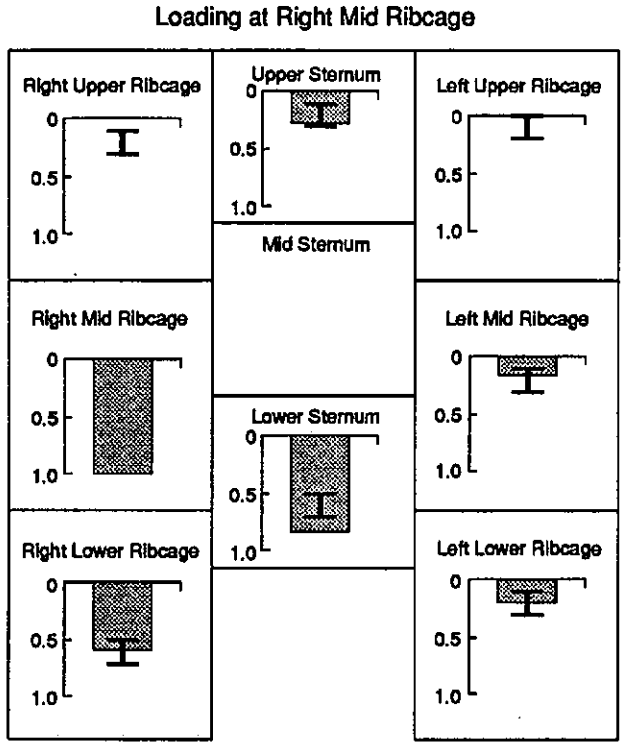

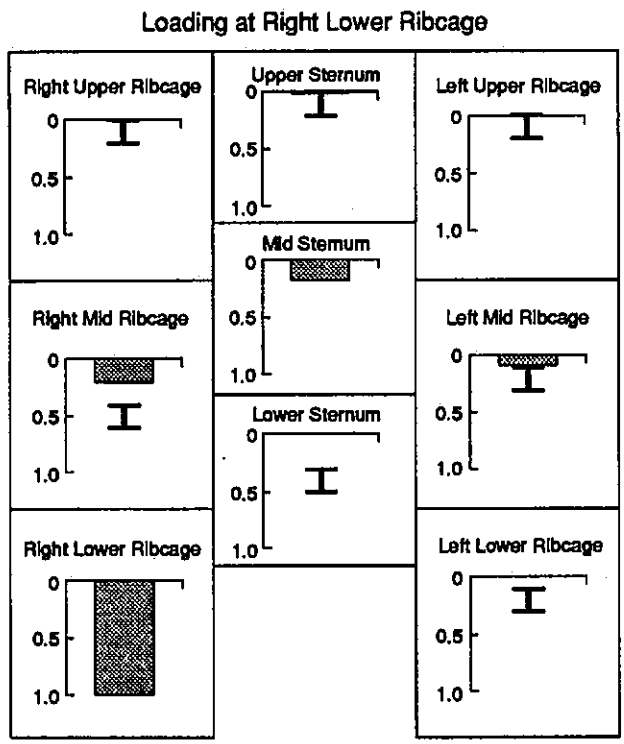

FIGURE 6–27c. Relative normalized deflections at different regions of the ribcage for loading at the right-mid and right-lower ribcage with a 50-mm by 100-mm (2-in by 4-in) rigid plate.

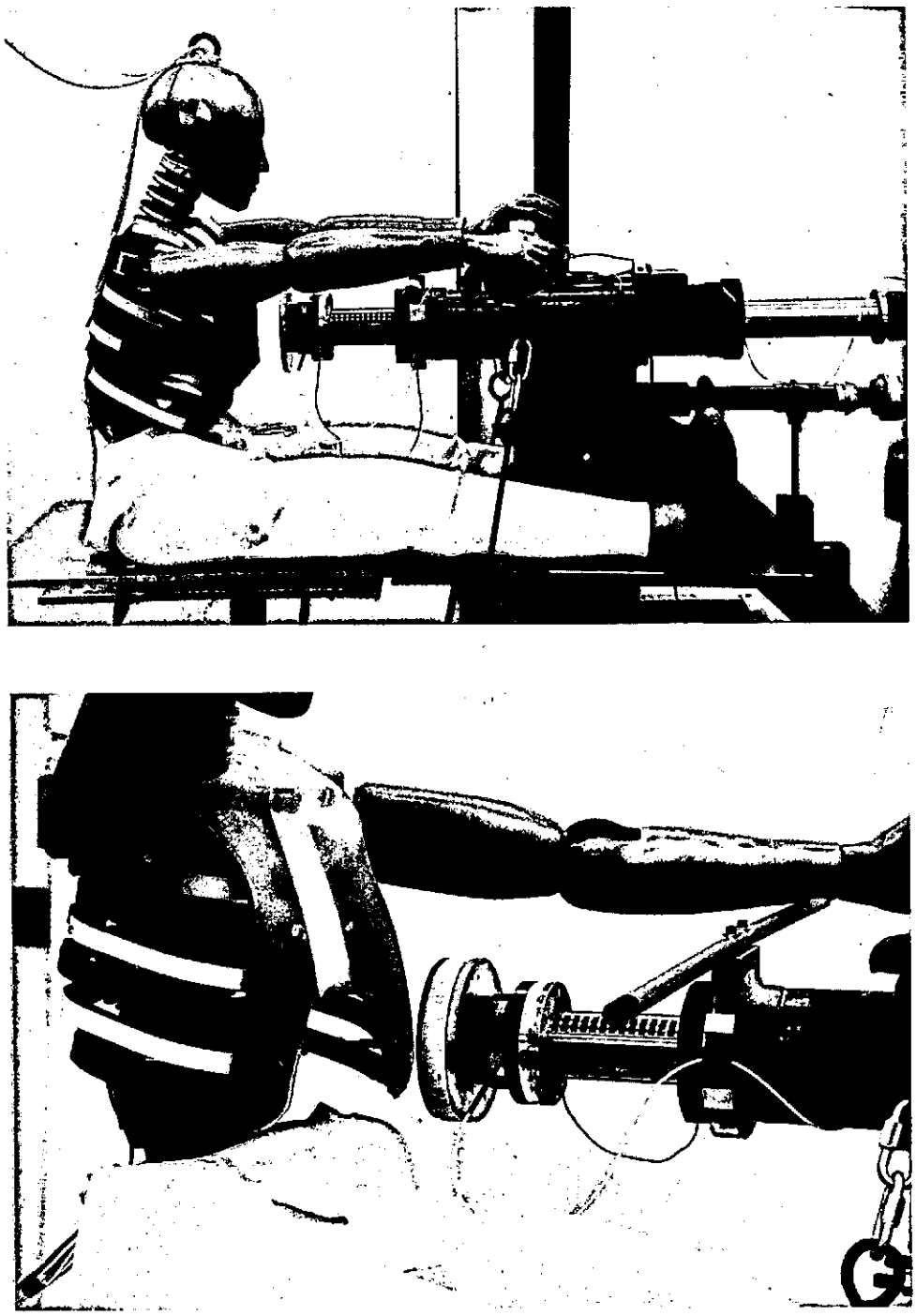

FIGURE 6–28. The Second Prototype-50M positioned on the UMTRI pendulum for sternal (top) and lower-ribcage (bottom) impact tests.

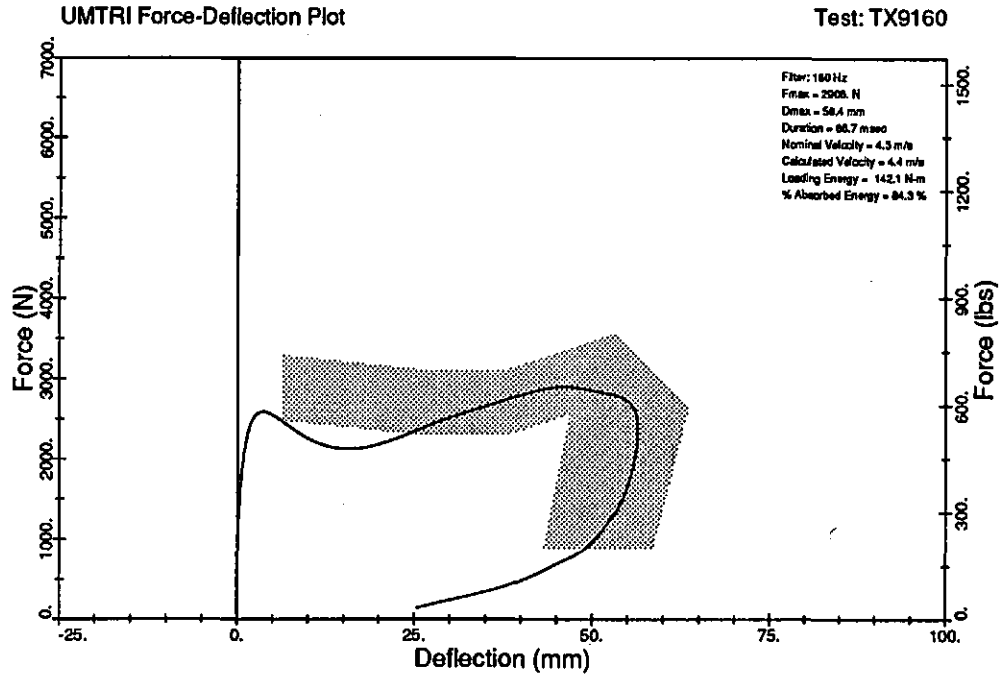

FIGURE 6–29a. F-δ plot from 4.3-m/s Kroell-type pendulum tests at the *sternal region* of the Second Prototype-50M. Deflection is computed by DEFLECT from output of right-sternal DGSP. Impactor mass=23 kg (51.5 lb).

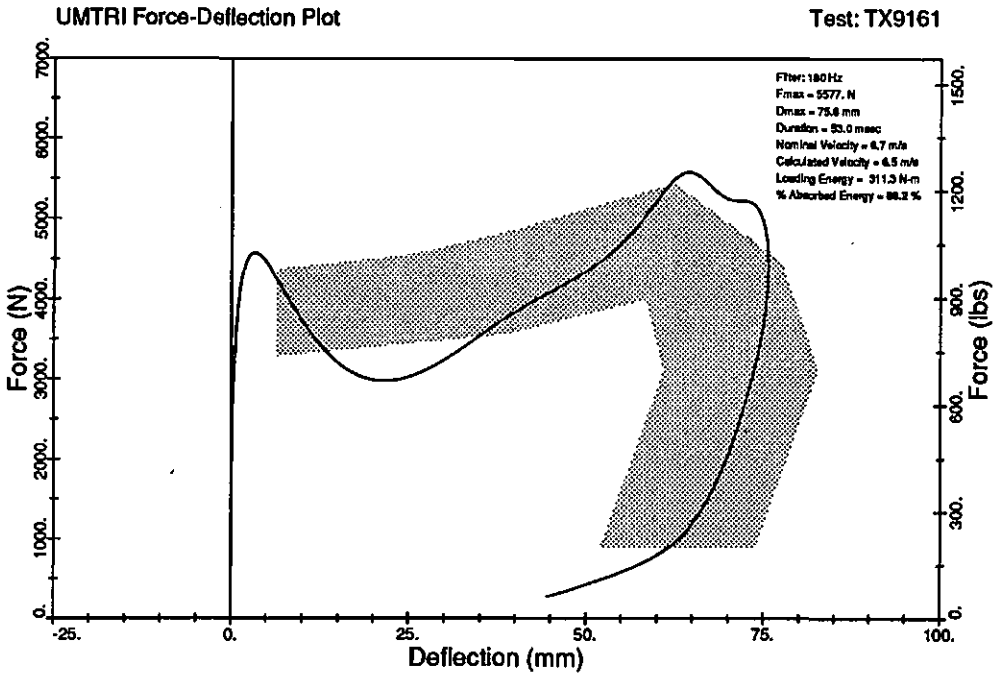

FIGURE 6–29b. F-δ plot from 6.7-m/s Kroell-type pendulum tests at the *sternal region* of the Second Prototype-50M. Deflection is computed by DEFLECT from output of right-sternal DGSP. Impactor mass=23 kg (51.5 lb).

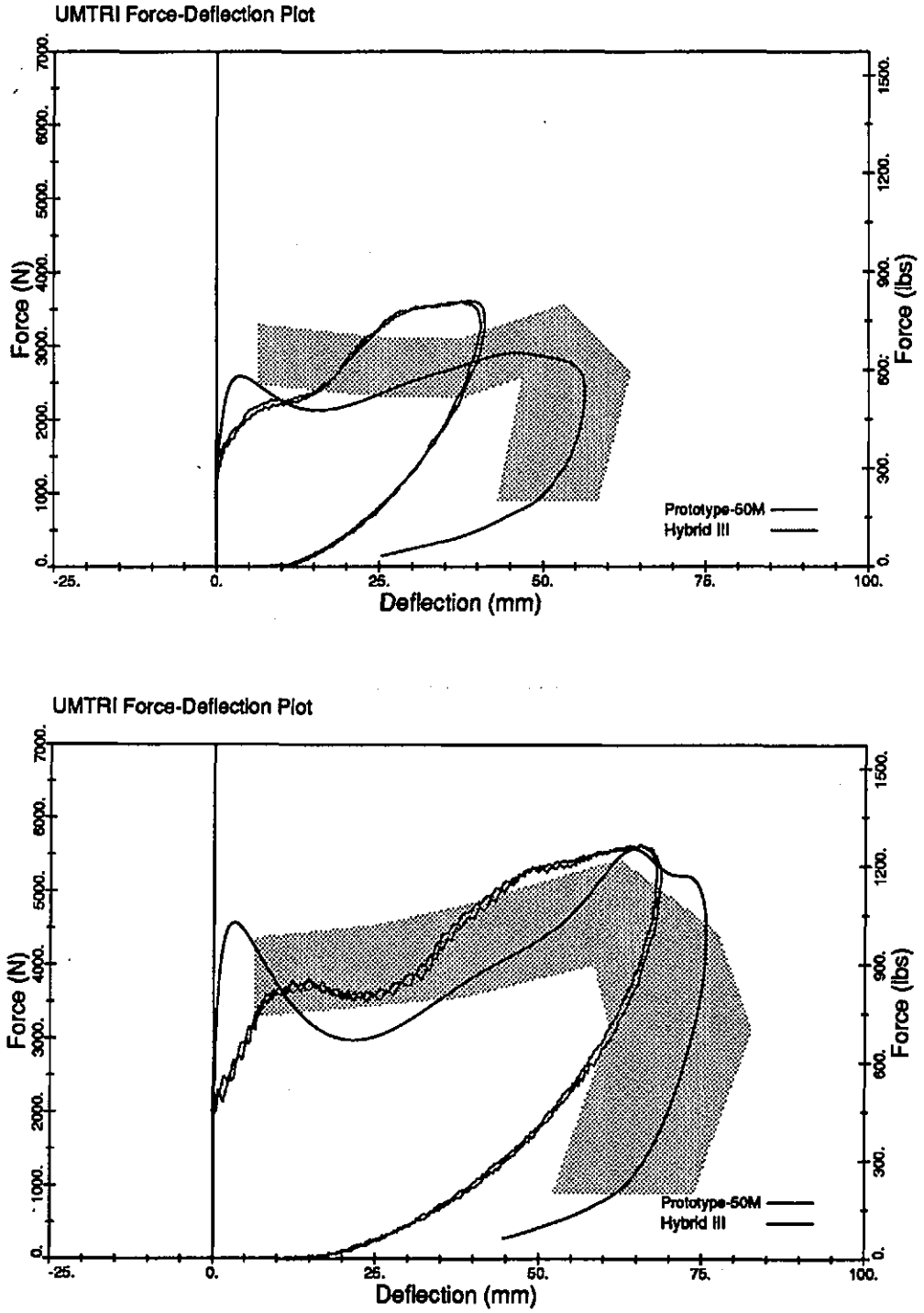

FIGURE 6–30. Comparison of F-δ plots from Hybrid III (dotted lines) with F-δ plot from the Second Prototype-50M (solid line) for Kroell-type pendulum tests to the *sternum* at 4.3 m/s (top) and 6.7 m/s (bottom). Impactor mass=23 kg (51.5 lb)

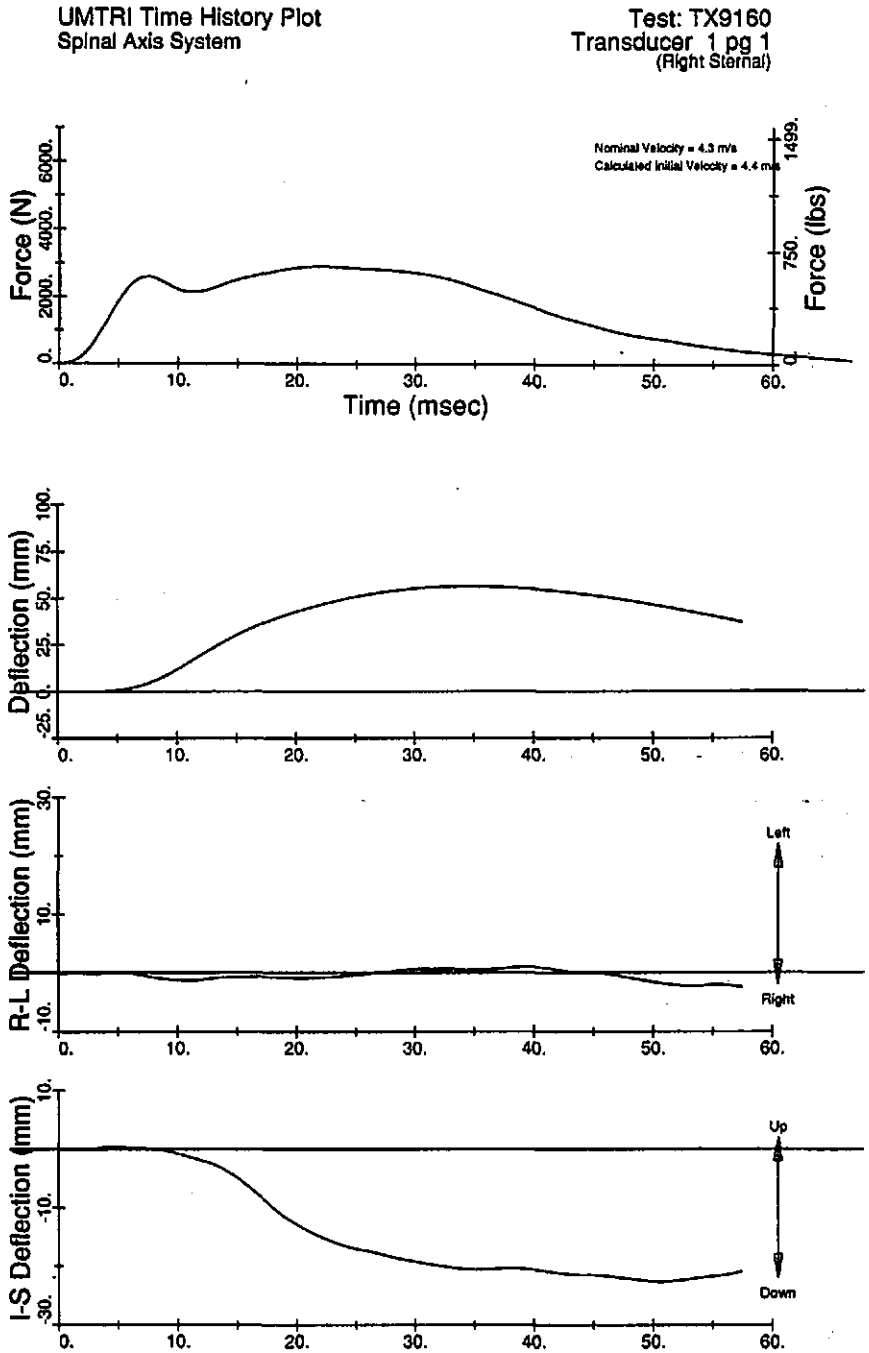

FIGURE 6–31a. Time traces for 4.3-m/s pendulum impact test to the *sternal region* of the Second Prototype-50M. Deflection is inward compression along the spinal X-axis computed by DEFLECT. RL and IS deflections are along Y and Z-axes, respectively.

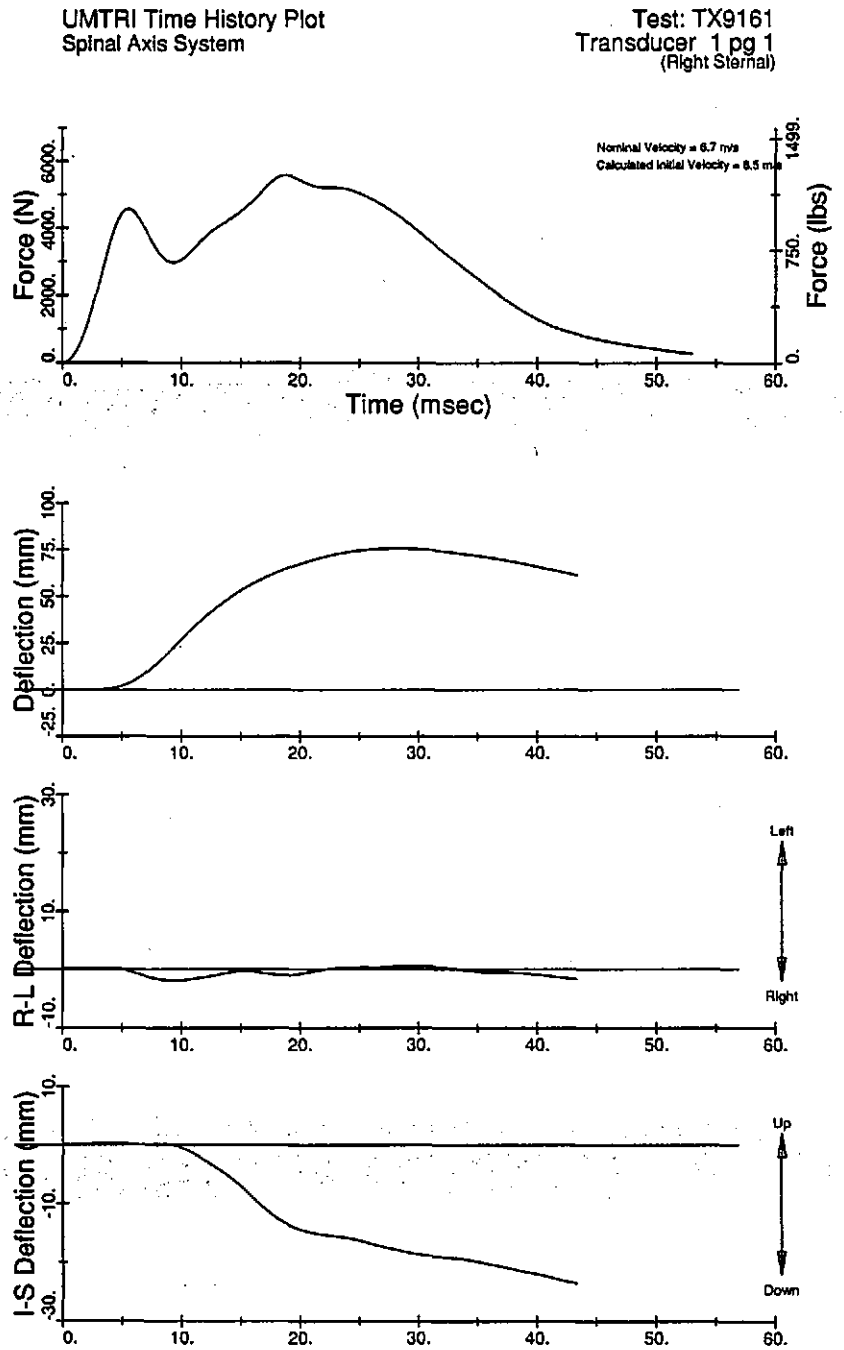

FIGURE 6–31b. Time traces for 6.7-m/s pendulum impact test to the *sternal region* of the Second Prototype-50M. Deflection is inward compression along the spinal X-axis computed by DEFLECT. RL and IS deflections are along Y and Z-axes, respectively.

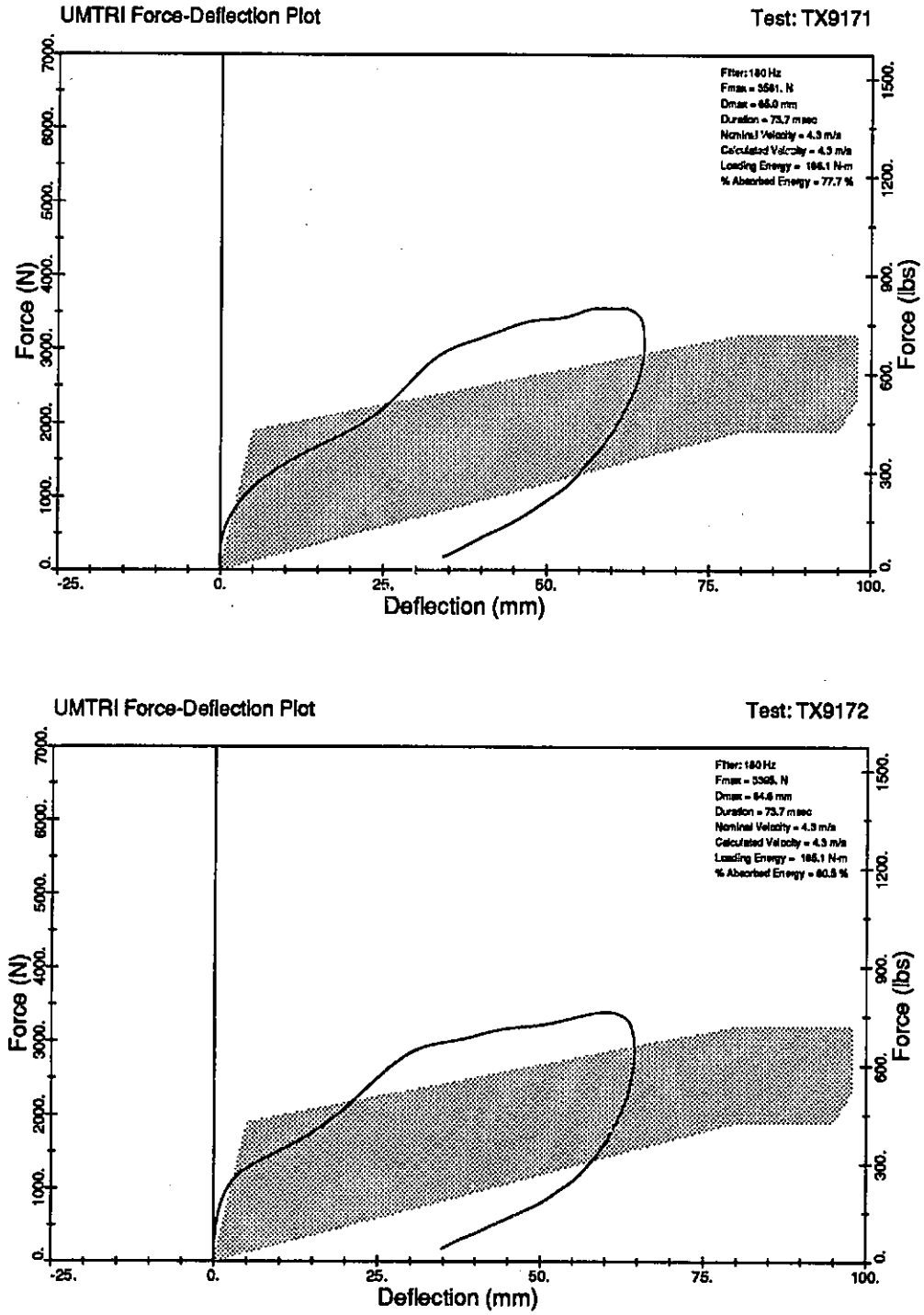

FIGURE 6–32. F-δ plots for Kroell-type pendulum impacts to the *left-lower* (top) and *right-lower* (bottom) *ribcage* of the Second Prototype-50M at a nominal impact velocity of 4.3 m/s. Shaded area shows preliminary corridor for this region as described in Appendix A. Deflection used in plot is inward compression along the alternate axis system computed by DEFLECT. Impactor mass=23 kg (51.5 lb).

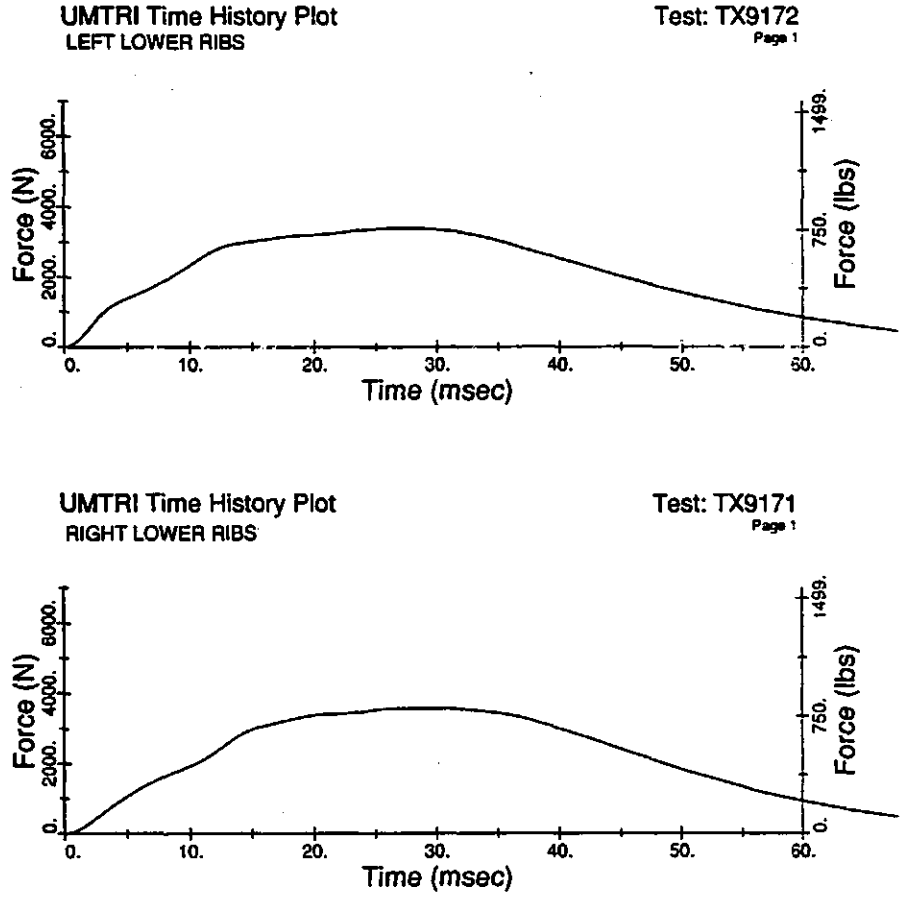

FIGURE 6–33a. Force-time traces from 4.3-m/s impacts to the *left-lower* (top) and *right-lower* (bottom) *ribcage* of the Second Prototype-50M.

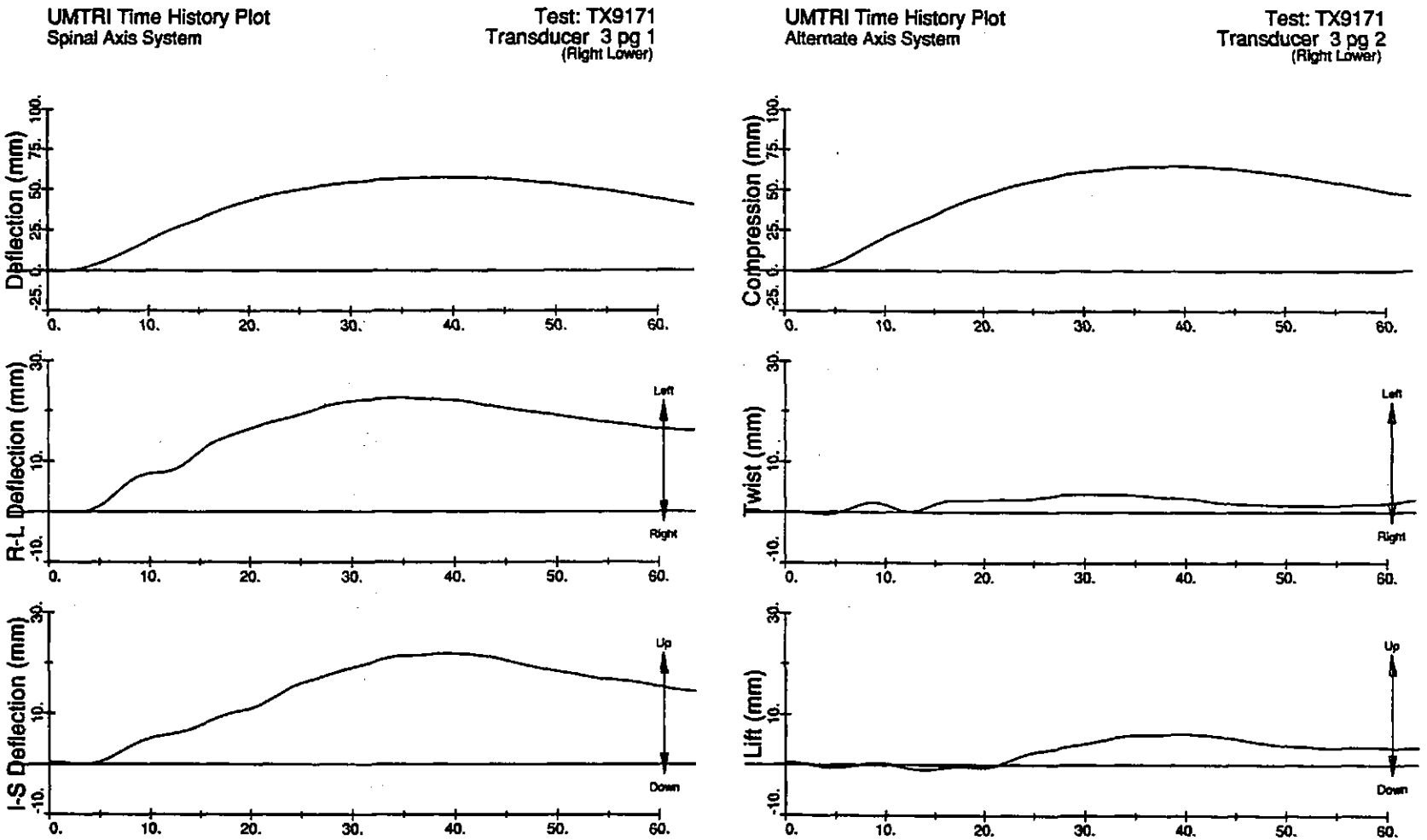

FIGURE 6–33b. Displacement-time traces for 4.3-m/s pendulum impacts to the *right-lower ribcage* of the Second Prototype-50M. Plots on the left are for displacements along the spinal axes while plots on the right are for displacements in the alternate coordinate system.

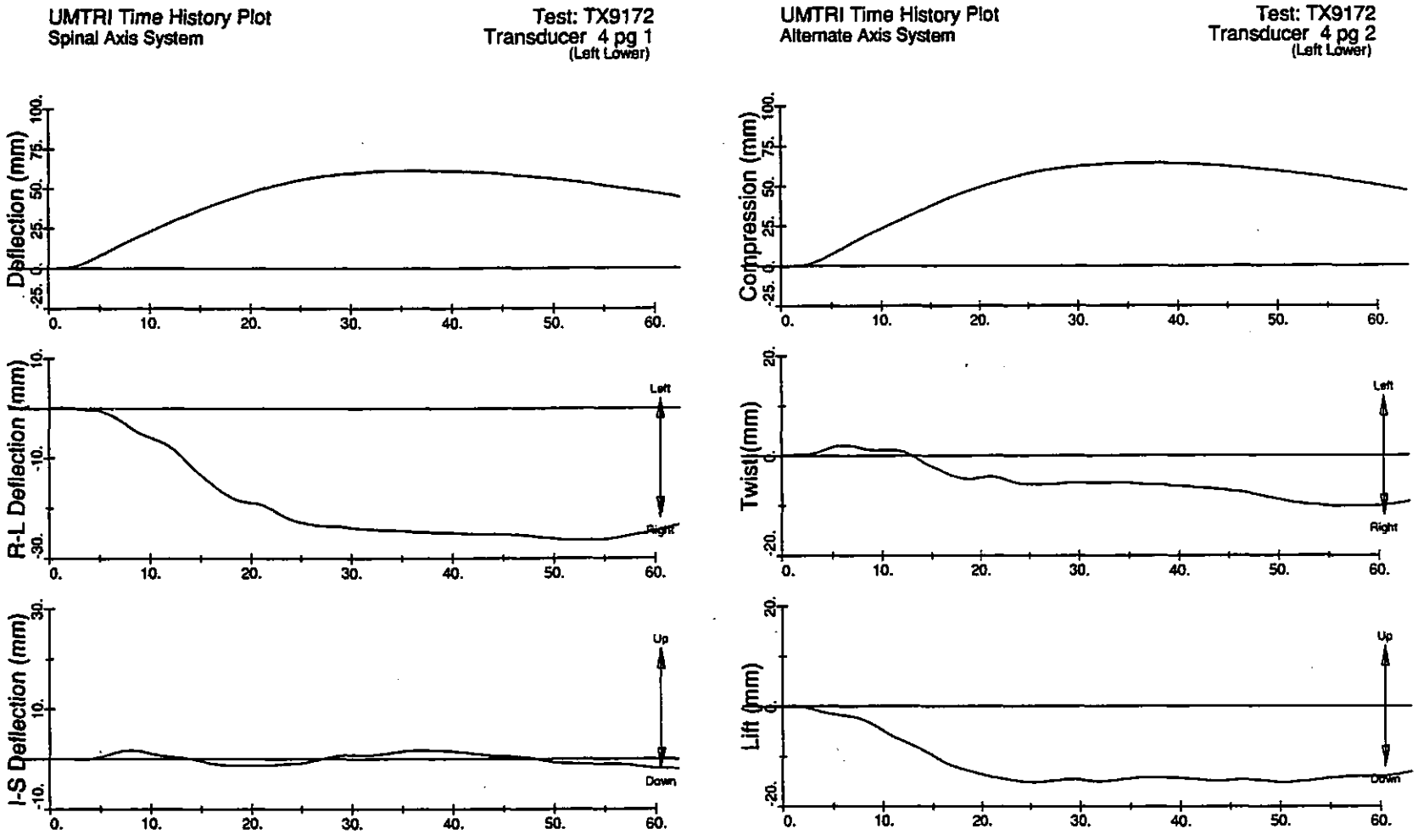

FIGURE 6–33c. Displacement-time traces for 4.3-m/s pendulum impacts to the *left-lower ribcage* of the Second Prototype-50M. Plots on the left are for displacements along the spinal axes while plots on the right are for displacements in the alternate coordinate system.

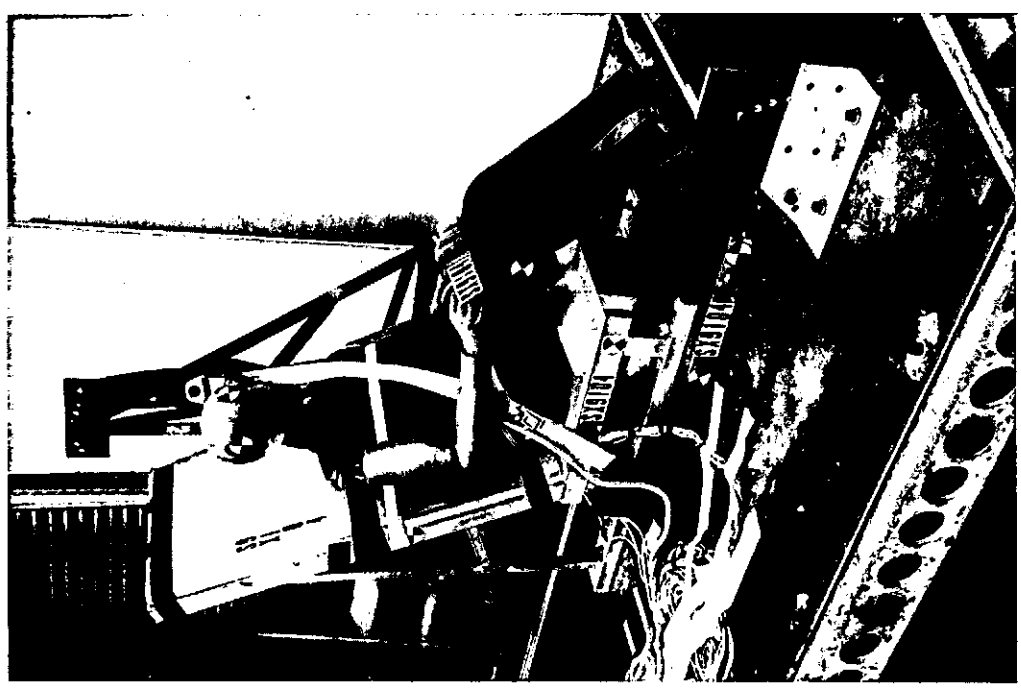

FIGURE 6–34a. Pretest photos for sled test SX9104.

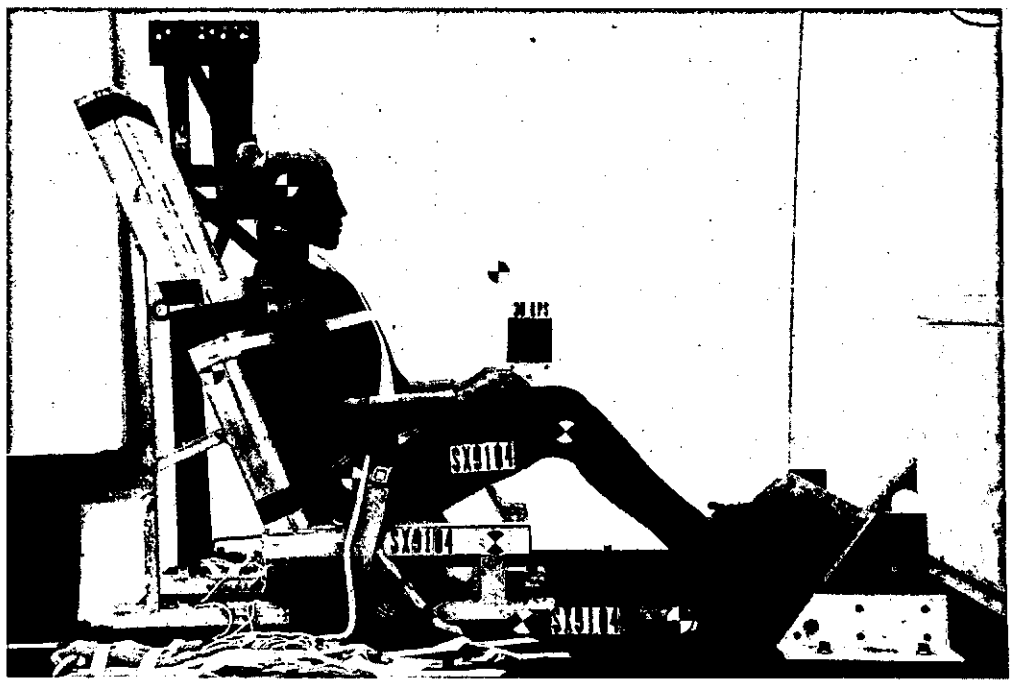

FIGURE 6–34b. Pretest photos for sled test SX9104.

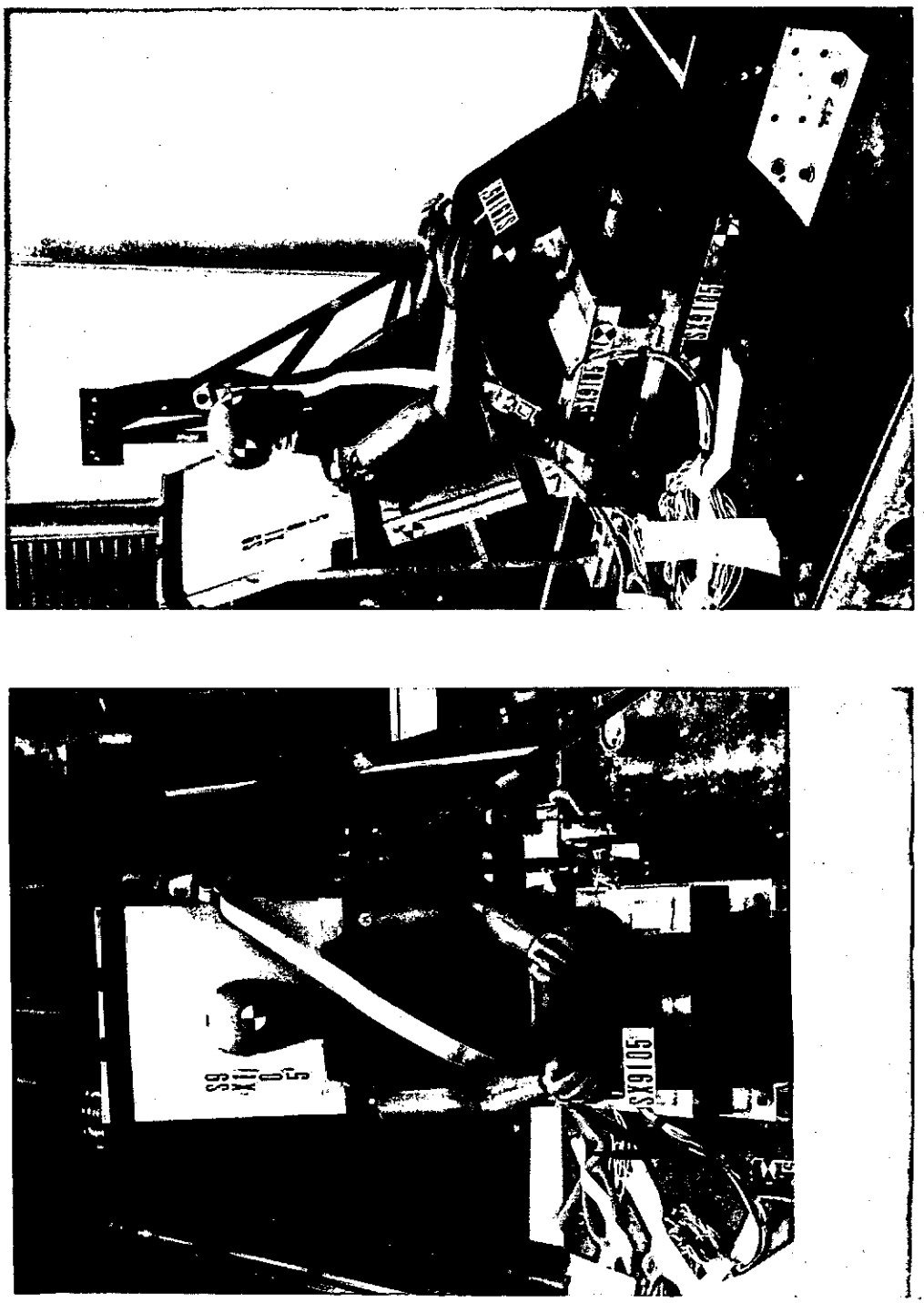

FIGURE 6–34c. Pretest photos for sled test SX9105.

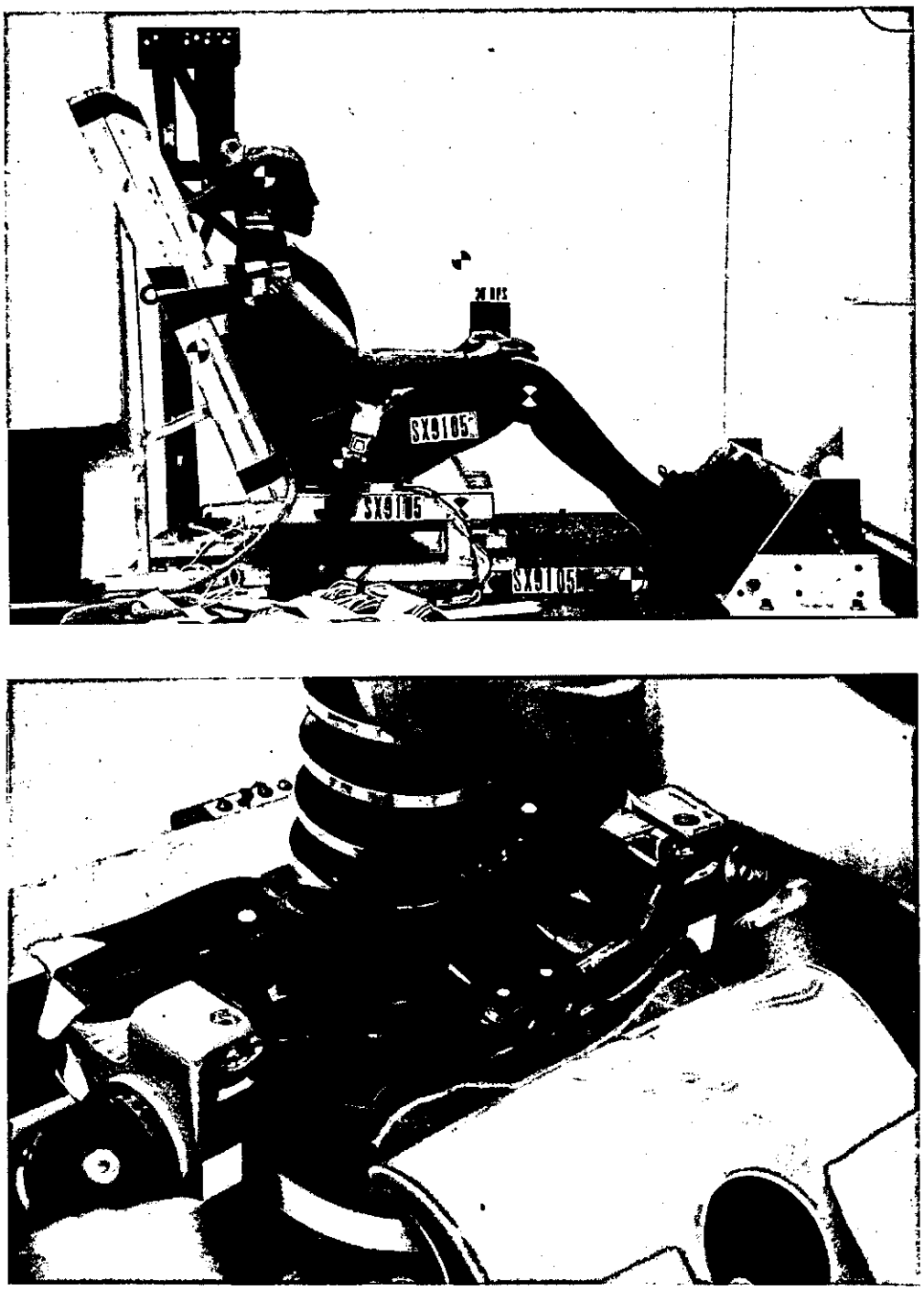

FIGURE 6–34d. Pretest photos for sled test SX9105.

FIGURE 6–35a. Side-view, time-sequence photograph of sled test SX9104.

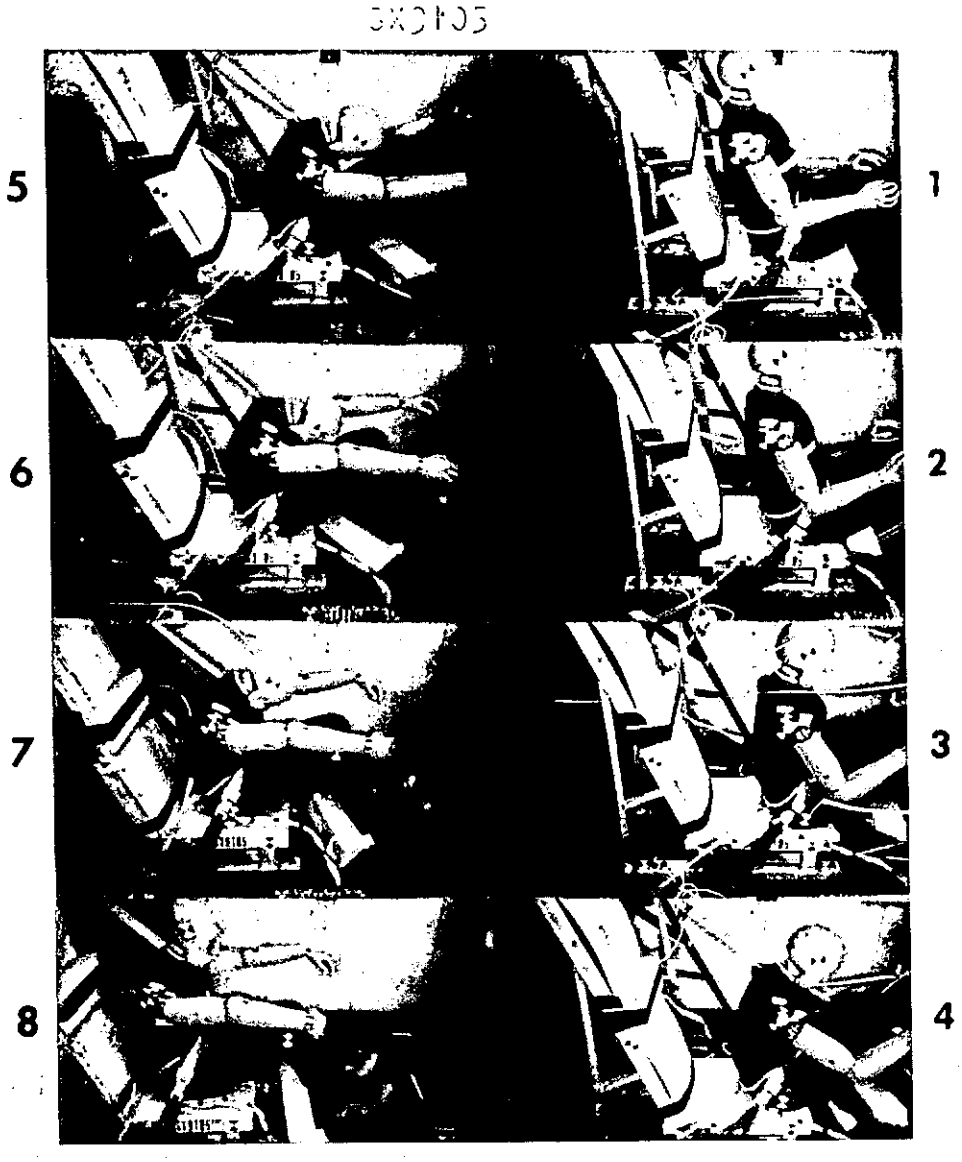

FIGURE 6–35b. Side-view, time-sequence photograph of sled test SX9105.

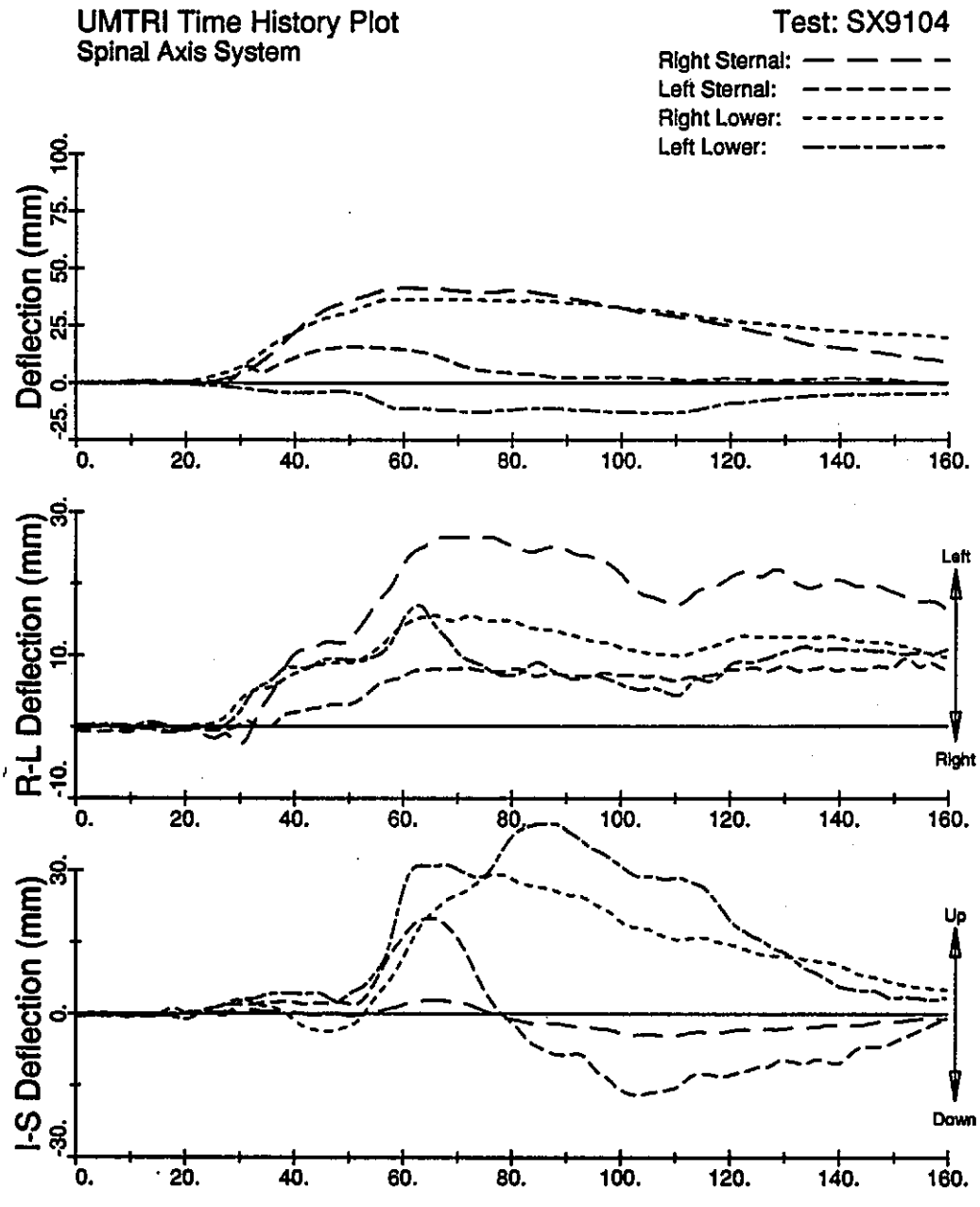

FIGURE 6–36a. Composite plot for chest displacements in spinal coordinate system computed by DEFLECT from DGSP outputs during sled test SX9104.

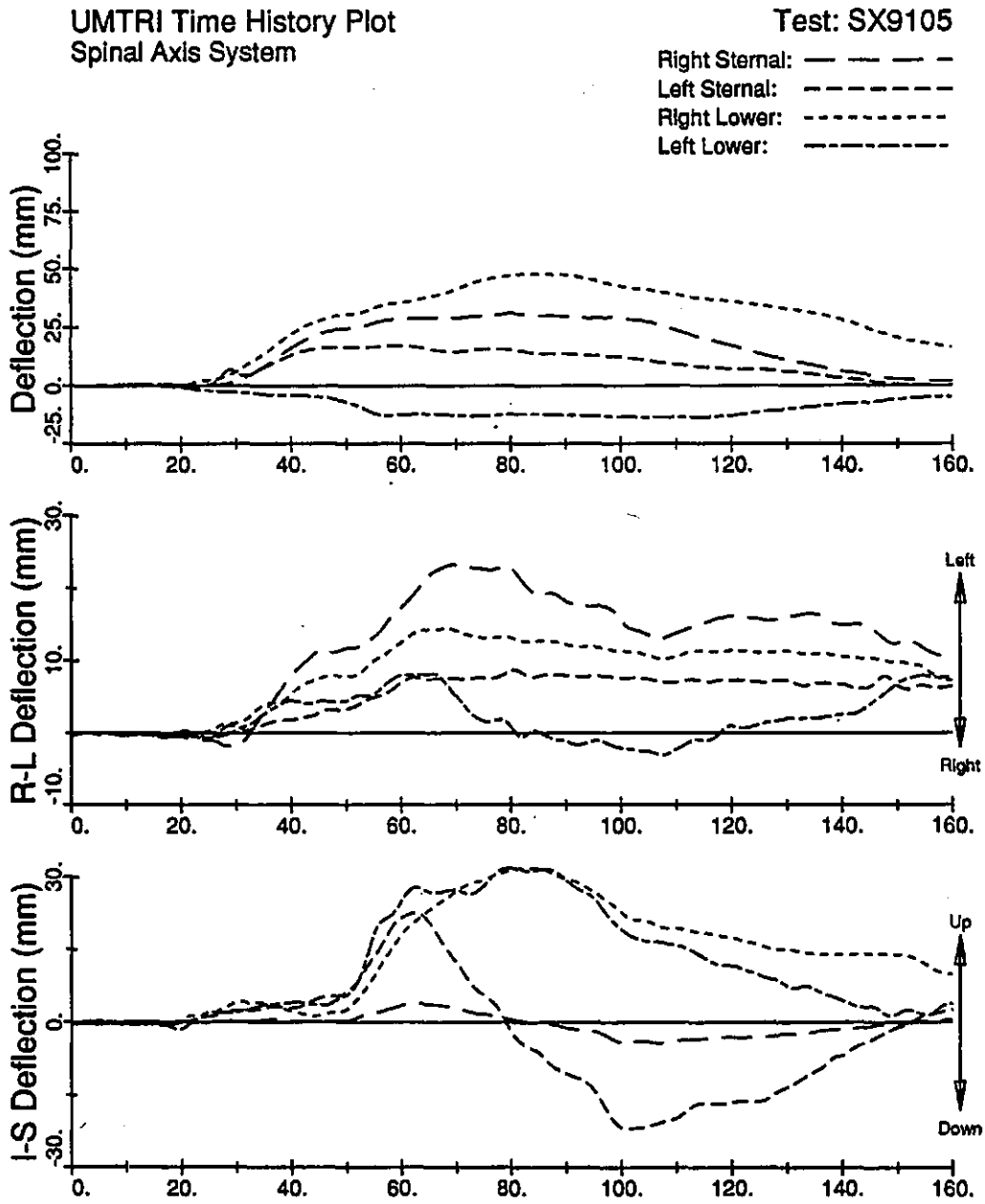

FIGURE 6–36b. Composite plot for chest displacements in spinal coordinate system computed by DEFLECT from DGSP outputs during sled test SX9105.

FIGURE 6–37a. Post-test photos from sled tests SX9104 and SX9105.

FIGURE 6–37b. Post-test photos from sled tests SX9104 and SX9105.

7. SUMMARY AND FINAL COMMENTS

Anthropomorphic test dummies or ATDs are injury-assessment tools used to evaluate the level of occupant protection offered by vehicles and their restraint systems in crash environments. Paradoxically, crash dummies are designed to respond like humans under injury-producing dynamic loading, but without being injured (i.e., damaged). To be a useful tool for both research and regulatory applications, an ATD must also produce results that are repeatable for the same test conditions. These goals of repeatability and durability present a constant challenge in the effort to upgrade the biofidelity and injury-sensing capability of crash dummies.

In spite of significant advances in the design and performance of ATDs over the past three decades, they are, at best, simplified analogs of the exceedingly complex human occupant, and represent a limited sampling of size, response, and injury tolerance characteristics of the population of motor vehicle occupants. They are, however, necessary and valuable tools in vehicle safety testing, and as knowledge of injury mechanisms, human tolerance, and human response to impact loading increases, improvements in ATD design, both in terms of more humanlike response and greater injury-sensing capability, must be sought.

A primary concern for crash testing of today's vehicles equipped with various designs and geometries of passive and active restraint systems is the ability of a crash dummy to provide realistic response and injury assessment for both concentrated and distributed types of loading. This three-volume report describes a research and development project to upgrade the Hybrid III crash dummy toward improved assessment of restraint-system effectiveness through more humanlike interaction of the dummy's chest and abdomen with restraint systems and steering wheels, and improved assessment of injuries to these body regions from belt, airbag, and steering-wheel loading.

The activities and developments described in this report represent a coordinated effort by a number of experts in dummy design, testing, and impact biomechanics toward improving the state of the art of ATD design. The goals were set high and some compromises to these goals have, temporarily, been necessary. It is believed, however, that the achievements attained have advanced the direction of ATD design and design philosophy.

A prototype thorax system has been developed for frontal crash dummies that represents a significant enhancement with regard to assessment of injuries to the thoracic region during frontal impacts in restrained and unrestrained environments. The essential features of this new thorax assembly include:

- improved anthropometry based on the AATD-50M specifications;
- a new ribcage with more humanlike geometry, including representation of the lower ribs over the regions of the liver and spleen, and more humanlike response to quasi-static and low-velocity impacts;
- a new spine with more humanlike curvature from the pelvis to the neck and a flexible link in the thoracic spine;
- new shoulders with increased front/back mobility and clavicles connecting between the sternum and the lateral aspect of the shoulders;

- a two-piece sternum with compliance between the upper sternum and the upper thoracic spine;
- a modified version of the GM frangible abdomen to provide biofidelity for lap-belt loading and to monitor intrusion due to lap-belt submarining;
- a pelvis with modified Hybrid III pelvic bone and preliminary design changes to accommodate the new ribcage and abdomen;
- an enhanced chest deflection instrumentation system that measures three-dimensional displacements of the chest at four potential injury sites, including the left and right midsternum and the left- and right-lower ribcage;
- provision for a six-axis pelvic/lumbar load cell to quantify forces and moments at the spine due to restraint and vehicle component interactions.

In addition, the neck mounting bracket, lumbar spine, and pelvis of Hybrid III have been modified to accommodate the new thorax system and associated anthropometry.

The Prototype-50M thorax has been designed using a slanted, damped-steel-rib model and with lower stiffness to quasi-static and low-velocity loading than that in Hybrid III. The first priority in thorax biofidelity at the sternum was for impact velocities of 4.3 m/s, and test results indicate excellent fit of the Prototype-50M sternal response to the low-velocity corridors. The new thorax also demonstrates more humanlike response characteristics to quasi-static loading conditions than that of the Hybrid III.

Results from a limited number of belt-restrained sled tests conducted at 30-mph, 20-G are positive with regard to both durability and performance. It is expected that some upgrading of the current Prototype-50M will take place as a result of further testing and evaluation and in conjunction with the continuation of the NHTSA's advanced dummy development program. In particular, refinements to the geometry and anthropometry of the Prototype-50M ribcage and thorax will be possible as further improvements in the pelvis/abdomen design are made and as reductions in the size of the chest deflection instrumentation are realized. Also, the application of composite material technology to the improved design and manufacture of the ribcage should be sought.

APPENDIX A

UPDATE OF PERFORMANCE SPECIFICATIONS

APPENDIX A

UPDATE OF PERFORMANCE SPECIFICATIONS

In *Design Requirements and Specifications: Thorax-Abdomen Development Task* by Schneider et al. (1990), preliminary results from pendulum tests to the mid and lower ribcages of unembalmed cadavers at 60 degrees to the anterior-posterior (AP) direction and to the abdomen in the AP direction about 75 mm (3 in) below the xiphoid process were described, based on a personal communication with General Motors research staff who sponsored the tests. In addition, Appendix B of this document described and reported on tests conducted by Cavanaugh in which quasi-static loading of the denuded ribcage of unembalmed cadavers was performed using a 50-mm by 100-mm (2-in by 4-in) rigid loading plate applied to different regions while monitoring deflection at several regions of the ribcage. In both instances, however, the data were not analyzed to develop performance corridors for crash dummies that are intended to represent the living and tensed motor-vehicle occupant.

Further analyses of these data have since been completed toward the development of preliminary corridors for the impact response of the lower ribcage and the relative stiffness and coupling of the chest under quasi-static loading. These results are presented in this appendix and are used in Section 6 of the report for comparison with the performance of the Prototype-50M test dummy.

A.1 PENDULUM RESPONSE OF THE LOWER RIBCAGE

Since development of the design requirements and specifications by Schneider et al. (1990), Viano (1989) has reported on response data for Kroell et al. (1971, 1974) type of impacts to the abdomen at 60 degrees from the AP direction and 75 mm (3-in) below the xiphoid process using a 23.4-kg (51.5-lb) mass at velocities of 4.3, 6.7, and 9.5 m/s. As shown in Figure A-1, corridors were given but were not adjusted for muscle-tensing effects, as had been done by Neathery (1974) for the Kroell et al. (1971, 1974) midsternal response corridors. In addition to these impacts, similar tests were conducted at 75 mm below the xiphoid process but in the AP direction. Table A-1 summarizes the peak force and peak deflection results from these tests which have not yet been reported in the literature. (The values shown in the table were obtained through personal communication with GM research staff.) As indicated, there were two tests near 4.3 m/s and two near 6.7 m/s. However, one of the latter tests showed a peak force that is 65 percent greater than the other with a spike at the end of penetration, and was rejected from the current analysis.

To develop the preliminary low-velocity corridor for impacts to the lower ribcage, which were considered to be approximately 30 degrees to the AP direction, the averaged maximum force and maximum penetration values from the central (i.e., AP) and lateral (i.e., 60 degrees to AP) impact sites were scaled to a velocity of 4.3 m/s using procedures developed by Mertz (1984). These values were then averaged to obtain a force of 2.00 kN (450 lb) and a penetration of 114 mm (4.5 in) for the 30-degree position. Ratios for scaling Viano's corridors for tests at 60 degrees to frontal were obtained by dividing these values by his corridor averages. This yielded scale factors of 0.830 and 1.056, which were applied, respectively, to the force and penetration break points on the corridors. In addition, the force levels were increased by 0.67 kN (150 lb) to adjust for muscle tension effects and the

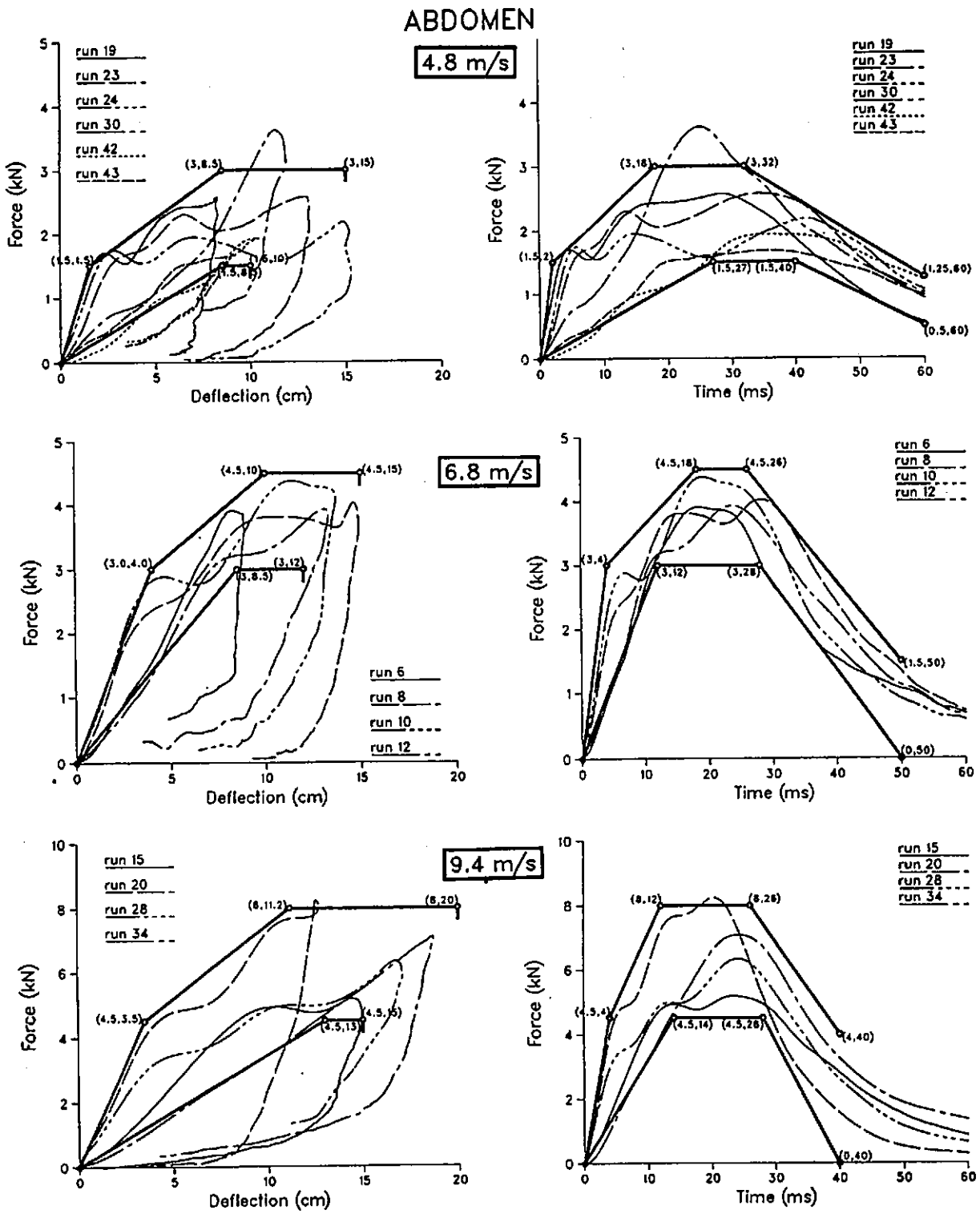

FIGURE A-1. Corridors for force-deflection and force-time responses for blunt lateral abdomen impacts at three severities (Viano 1989).

TABLE A-1

PRELIMINARY RESULTS FROM GM/WSU KROELL IMPACT TESTS
7.5 CM (3 IN) BELOW THE XIPHOID PROCESS
ON THE MIDLINE (Viano, May 1989)

Test No.	Impact Velocity	Peak Force	Peak Deflection	Outside Dimension	Percent Deflection
49	4.3 m/s	1.99 kN	11.0 cm	29.4 cm	37.2%
53	4.5 m/s	1.75 kN	15.6 cm	35.5 cm	43.9%
56	6.7 m/s	5.60 kN	9.5 cm	24.7 cm	38.3%
59	6.7 m/s	3.40 kN	12.9 cm	26.4 cm	48.8%

values rounded. Figure A-2 shows the resulting corridor for 4.3 m/s for total penetration or external chest deflection.

A similar procedure was used to develop the external-deflection corridor at 6.7 m/s shown in Figure A-3. When compared to the 4.3-m/s corridor of Figure A-2, it was found that the lower-speed corridor had a steeper slope. Given that data from only one test were used for the central impact, and the expectation that stiffness should increase with velocity, the slope of the lower-speed corridor has also been applied to the higher-speed corridor until further data suggest a better value. This is indicated by the dashed line in Figure A-3.

For crash dummies, where chest deflections are measured internally, corridors for skeletal deflection are more useful. In the absence of other data, the 12.5-mm (0.5-in) adjustment in total deflection used by Neathery (1974) in developing the response corridors at midsternum was applied to the lower-ribcage response corridors in Figures A-2 and A-3 (actually used 10 mm rather than 12.5 mm). Figures A-4 and A-5 show the adjusted 30-degree corridors that provide preliminary internal or skeletal response corridors for the lower ribcage and that are used in Section 6 of this volume for comparison with the impact response of the Prototype-50M in this region.

A.2 LOCALIZED QUASI-STATIC STIFFNESS

As noted and described in the design requirements and specifications document (Schneider et al. 1990), Cavanaugh conducted quasi-static loading tests on the denuded ribcage of unembalmed cadavers using a 50-mm by 100-mm (2-in by 4-in) rigid pad that was pushed into the anterior of the thorax to a distance of 25-mm (1-in) while force and deflection were recorded at the loaded site and AP deflections were recorded at seven other locations on the ribcage as well. These loading and deflection measurement sites are shown in Figure A-6.

Table A-2 shows the stiffness values reported by Cavanaugh at 25 mm (1 in) of deflection at six locations for three different cadavers along with the average values. To provide stiffness values for the tensed human, a muscle-tensing adjustment factor was needed. In the absence of other data, an attempt to determine this factor was made using results from the tensed and relaxed volunteer quasi-static loading tests with a larger 152-mm-diameter (6-in) plate reported by Lobdell et al. (1973). In these data, the chest stiffness increases from 7.0 N/mm (40 lb/in) for relaxed volunteers to 23.6 N/mm (135 lb/in) for tensed subjects, for a factor of 3.4. Table A-3 shows the results obtained by applying this factor to the average values in Table A-2. The ranges of stiffness values indicated in each case were obtained by bracketing the adjusted average by plus/minus 5 N/mm (29 lb/in).

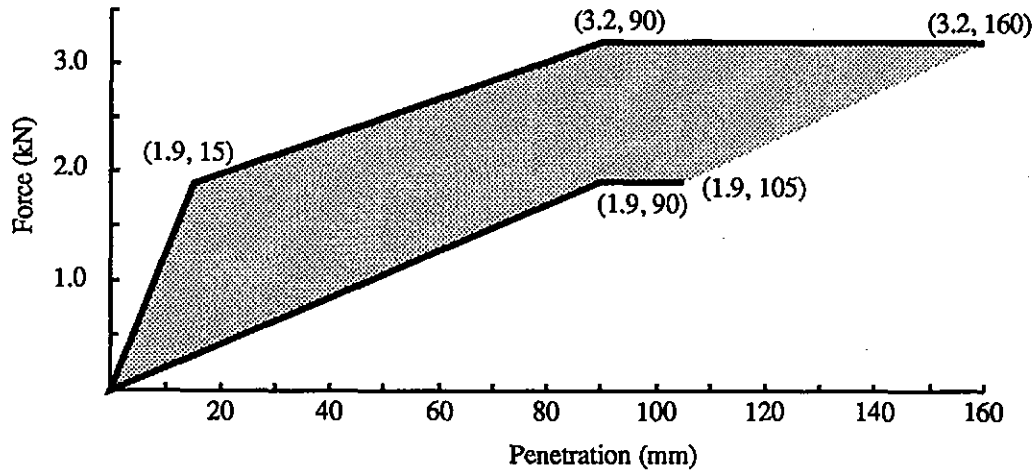

FIGURE A-2. Tensed response corridor for 23.4-kg blunt impactor at 4.3 m/s at 75 mm (3 in) below xiphoid level, 30° off center.

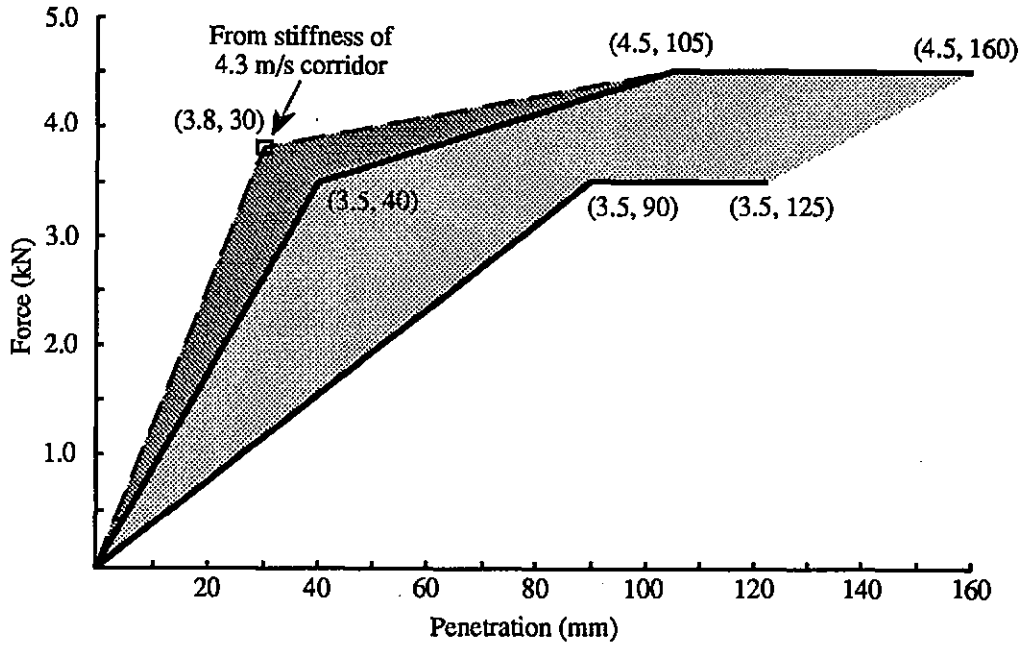

FIGURE A-3. Tensed response corridor for 23.4-kg blunt impactor at 6.7 m/s at 75 mm (3 in) below xiphoid level, 30° off center.

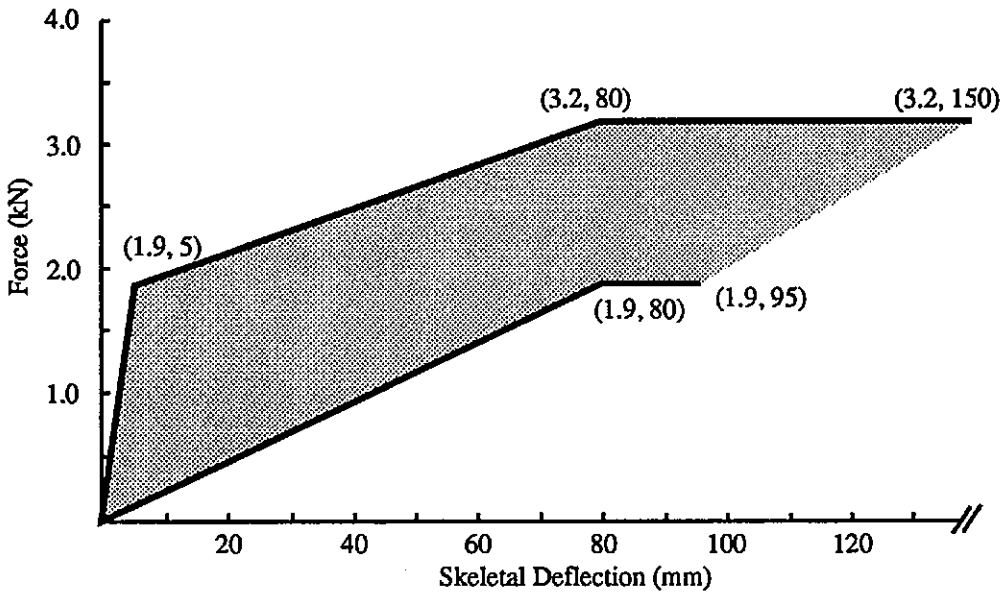

FIGURE A-4. Adjusted 30° corridor for 23.4-kg blunt impactor at 4.3 m/s at 75 mm (3-in) below xiphoid level.

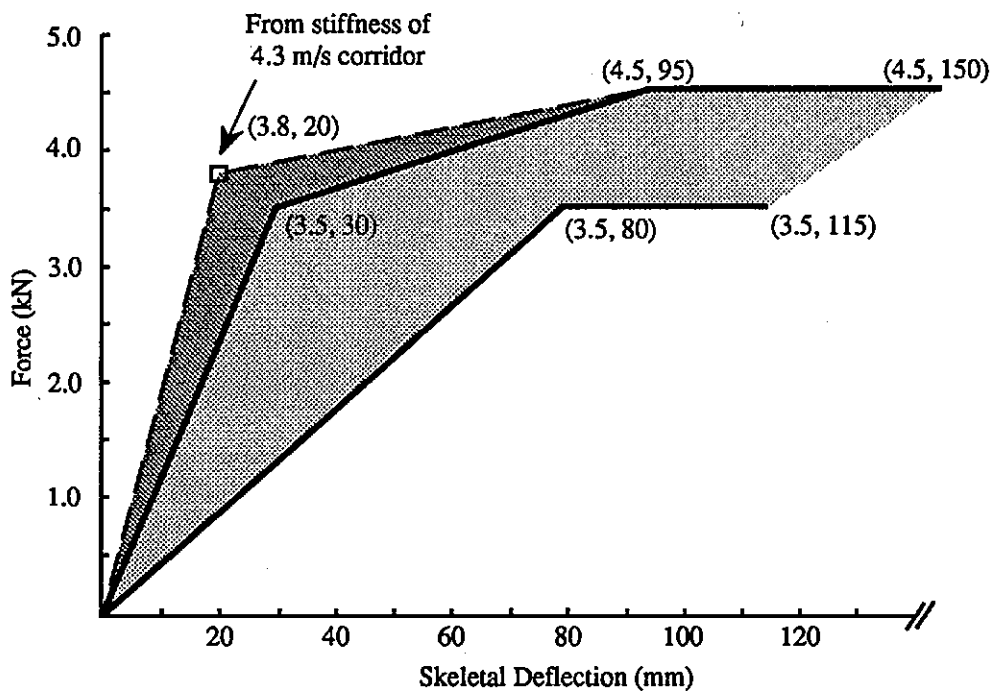

FIGURE A-5. Adjusted 30° corridor for 23.4 kg blunt impactor at 6.7 m/s at 75 mm (3 in) below xiphoid level.

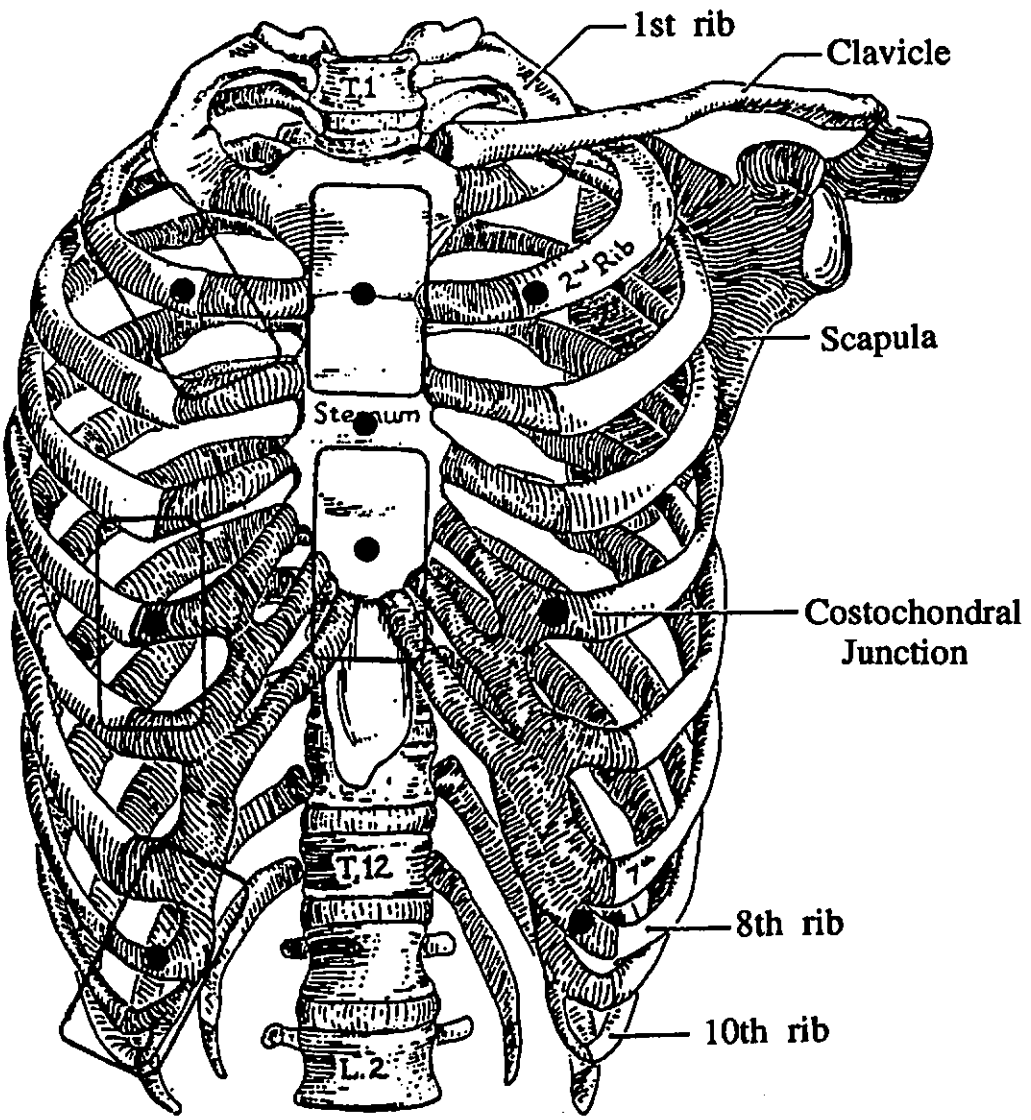

FIGURE A-6. Regions of loading and deflection measured used by Cavanaugh et al. (1988) in quasi-static tests with 50-mm by 100-mm (2-in by 4-in) rigid loading plate.

TABLE A-2

QUASI-STATIC STIFFNESS VALUES AT 25 MM DEFLECTION OBTAINED BY CAVANAUGH USING A 50-MM by 100-MM (2-IN BY 4-IN) RIGID LOADING PLATE

Cadaver No.	Sternum						Ribcage—Left Side					
	Top		Middle		Bottom		Second		Fifth		Eighth	
	N/mm	lb/in	N/mm	lb/in	N/mm	lb/in	N/mm	lb/in	N/mm	lb/in	N/mm	lb/in
1	12.3	70	10.6	61	11.4	65	7.3	42	8.4	48	5.2	30
2	11.4	65	10.6	61	5.9	34	5.6	32	5.4	31	3.4	19
3	11.7	67	8.6	51	7.4	42	7.0	40	5.1	29	3.9	22
Mean	11.8	67	9.93	57	8.23	47	6.63	38	6.33	36	4.17	24
S.D.	0.67	4	0.94	5	2.32	13	0.74	4	1.49	9	0.76	4

TABLE A-3

AVERAGE CADAVER STIFFNESS VALUES FOR TABLE A-2 MULTIPLIED BY 3.4 TO ADJUST FOR MUSCLE TENSION EFFECTS

Region	N/mm	lb/in	Region	N/mm	lb/in
STERNUM			LEFT SIDE		
Top	40	228	Second Rib	22	126
Range	35–45	200–257	Range	17–27	97–154
Middle	34	194	Fifth Rib	22	126
Range	29–39	166–223	Range	17–27	97–154
Bottom	28	160	Eighth Rib	14	80
Range	23–33	131–188	Range	9–19	51–108

An obvious problem with these results is that the adjusted midsternum stiffness value for the 50-mm by 100-mm (2-in by 4-in) loading plate of 34 N/mm (194 lb/in) is greater than the average tensed-human stiffness value of 23.6 N/mm (135 lb/in) reported by Lobdell et al. (1973) for a larger 152-mm (6-in) diameter plate. This inconsistency between the adjusted midsternum results from the Cavanaugh study and the midsternum results from volunteer subjects could be due to a number of factors, including differences in the manner of back or spine support in the two studies. However, it could also be the case that the muscle-tensing factor for the larger loading plate is not appropriate for the smaller loading plate. Since further data are needed to resolve this question, it is recommended that the values provided in Table A-3 not be used in dummy design at this time.

In the meantime, some benefit from the adjusted Cavanaugh data can be realized by using the measures of *relative* stiffness values that they provide. Table A-4 shows the results obtained by dividing the adjusted stiffness value at each location by the adjusted stiffness value at the sternum. The result suggests, for example, that the quasi-static

stiffness at the upper sternum should be 18 percent greater than at midsternum, and that the stiffness at the lower ribcage should be only about 41 percent of that at the midsternum. It should be noted that these values, as well as those in Tables A-2 and A-3, are based on skeletal deflections and should only be applied to the unpadded ribcage (i.e., to internal deflection measures) of crash dummies.

TABLE A-4
RELATIVE REGIONAL STIFFNESS VALUES BASED ON QUASI-STATIC LOADING WITH A 50-MM BY 100-MM (2-IN BY 4-IN) RIGID PLATE

Sternum			Ribcage—Left Side		
Top	Middle	Bottom	Second	Fifth	Eighth
1.18	1.00	0.82	0.64	0.64	0.41

A.3 QUASI-STATIC THORAX COUPLING

In addition to obtaining estimates for the relative stiffness values at different regions of the chest from the Cavanaugh data, the deflections measured at these different regions during loading of one region can be used to provide preliminary guidelines for interregional quasi-static stiffness coupling of the ribcage. Figure A-7 summarizes the average relative deflection results measured on three cadavers, where the data have been normalized so that 25 mm (1-in) of deflection at the loaded site is indicated by a "10" and the measured deflections elsewhere are proportioned accordingly. Also, in cases of sternal loading to cadavers where the average deflection values for the left and right sides were different, the larger of the two average deflection values was used for both sides to provide response symmetry for dummy design. To provide a tolerance range and account for muscle-tensing effects, a plus 5-mm (0.2-in) envelope was added to the original deflection data. The scaled relative deflection results are shown in Figure A-8 and provide a preliminary basis for evaluating ribcage coupling of the Prototype-50M dummy chest until additional data become available.

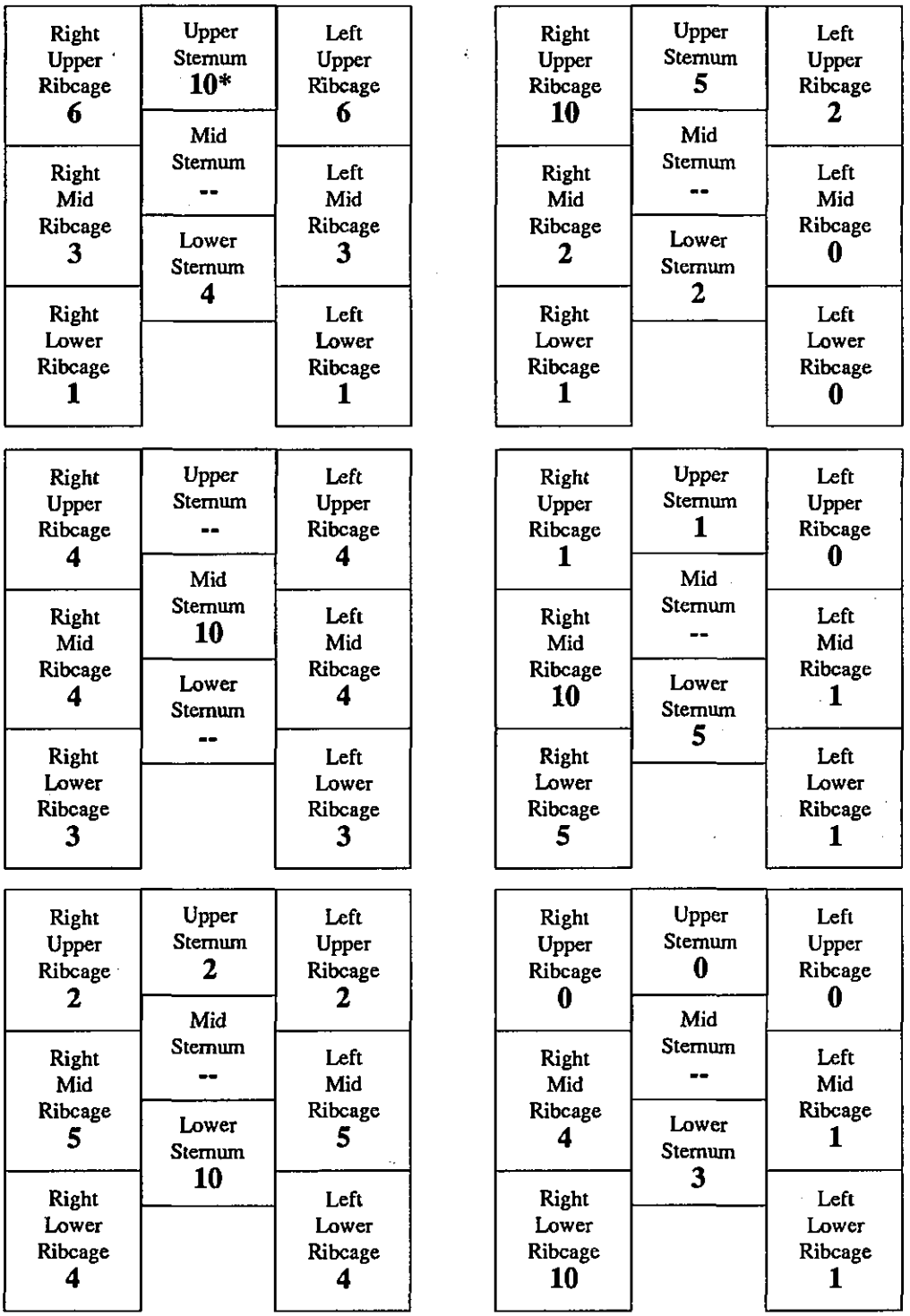

* 10 represents 25 mm deflection at the point of loading. The remaining values are the scaled deflections of these points.

FIGURE A-7. Average normalized relative deflections of cadaver ribcage during quasi-static loading with 50-mm by 100-mm (2-in by 4-in) rigid plate to 25 mm (1 in) at region indicated by "10."

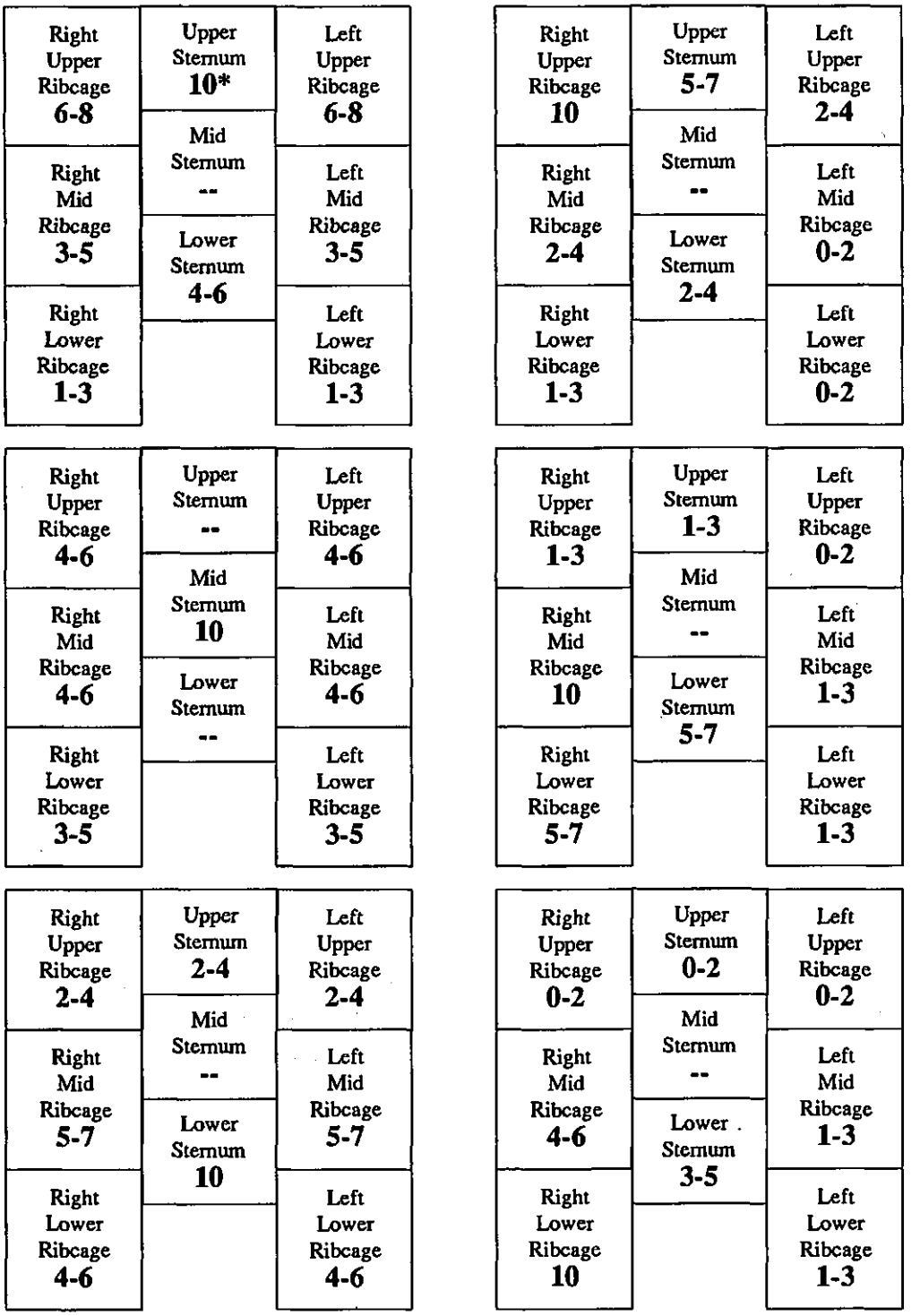

* 10 represents 25 mm deflection at the point of loading. The remaining values are the scaled deflection range at these points.

FIGURE A-8. Recommended normalized thorax coupling response for quasi-static loading with a 50-mm by 100-mm (2-in by 4-in) rigid plate at regions indicated by "10."

APPENDIX B

TIME TRACES OF FILTERED TEST SIGNALS AND DISPLACEMENTS COMPUTED BY "DEFLECT" FOR THREE-POINT-BELTED SLED TESTS OF SECOND PROTOTYPE-50M

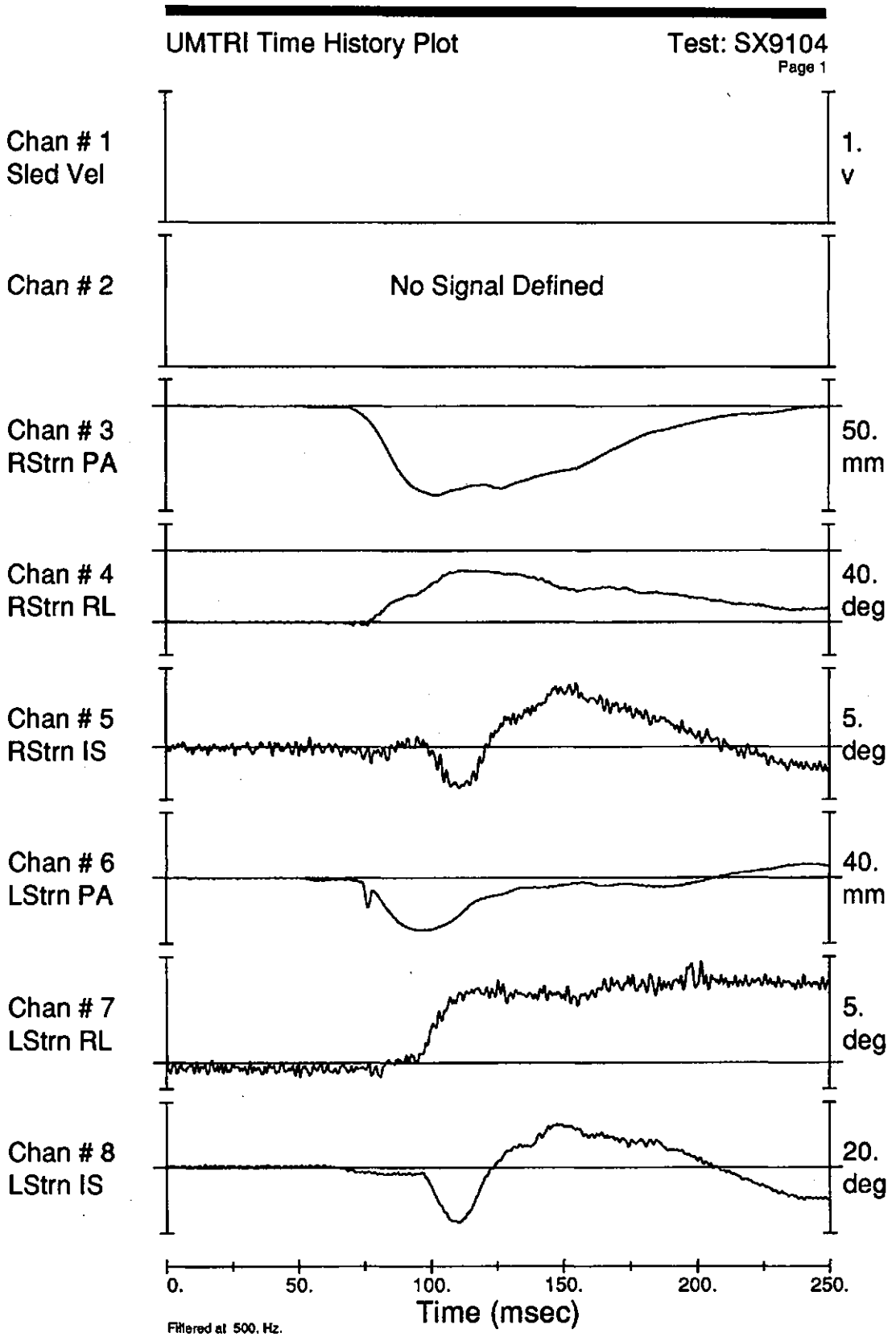
UMTRI Time History Plot
Test: SX9104
Page 1
Chan # 1
Sled Vel
1.
v
Chan # 2
No Signal Defined
Chan # 3
RStrn PA
50.
mm
Chan # 4
RStrn RL
40.
deg
Chan # 5
RStrn IS
5.
deg
Chan # 6
LStrn PA
40.
mm
Chan # 7
LStrn RL
5.
deg
Chan # 8
LStrn IS
20.
deg
0.
50.
100.
150.
200.
250.
Time (msec)
Filtered at 500. Hz.

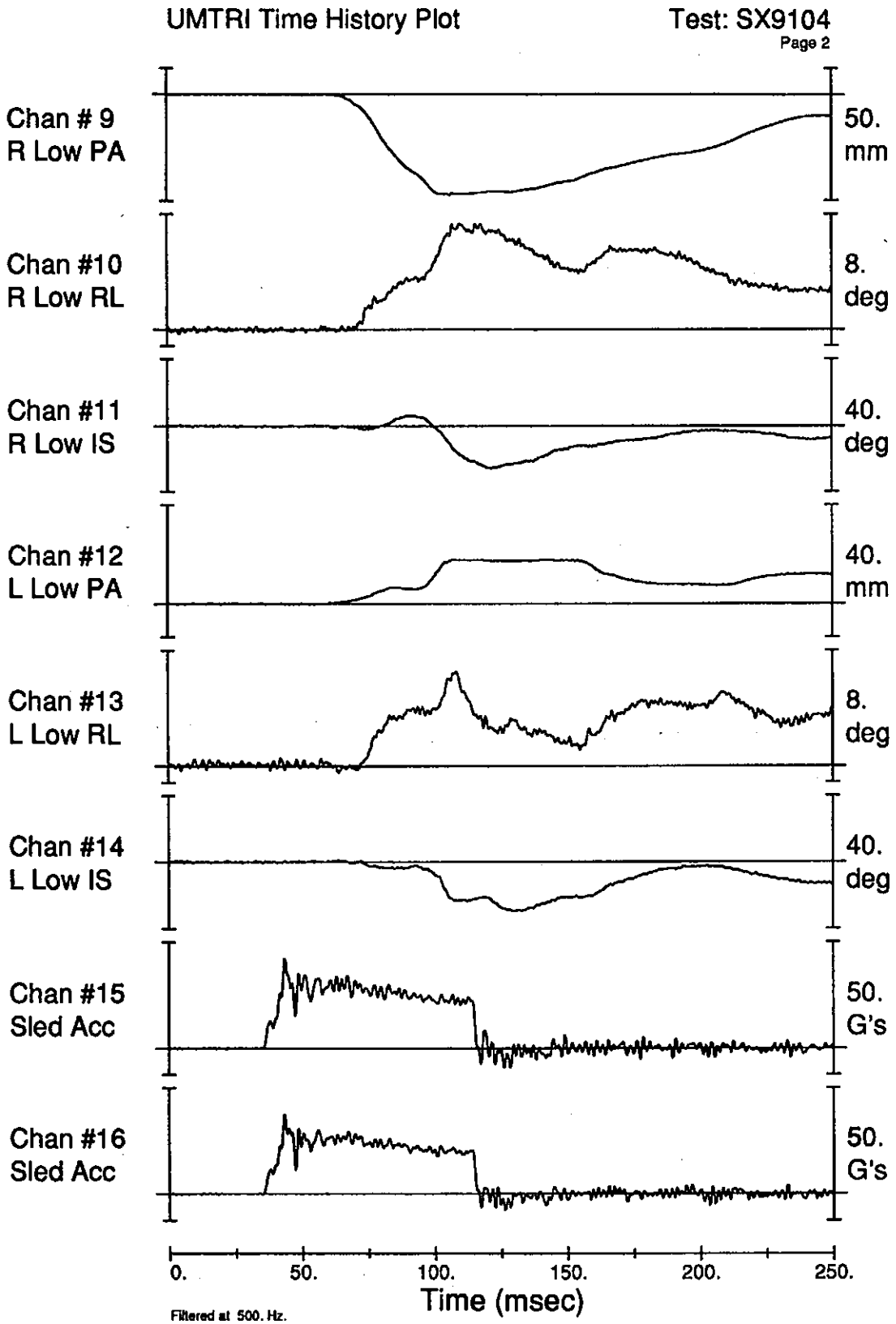
UMTRI Time History Plot
Test: SX9104
Page 2
Chan # 9
R Low PA
50.
mm
Chan #10
R Low RL
8.
deg
Chan #11
R Low IS
40.
deg
Chan #12
L Low PA
40.
mm
Chan #13
L Low RL
8.
deg
Chan #14
L Low IS
40.
deg
Chan #15
Sled Acc
50.
G's
Chan #16
Sled Acc
50.
G's
0.
50.
100.
150.
200.
250.
Time (msec)
Filtered at 500. Hz.

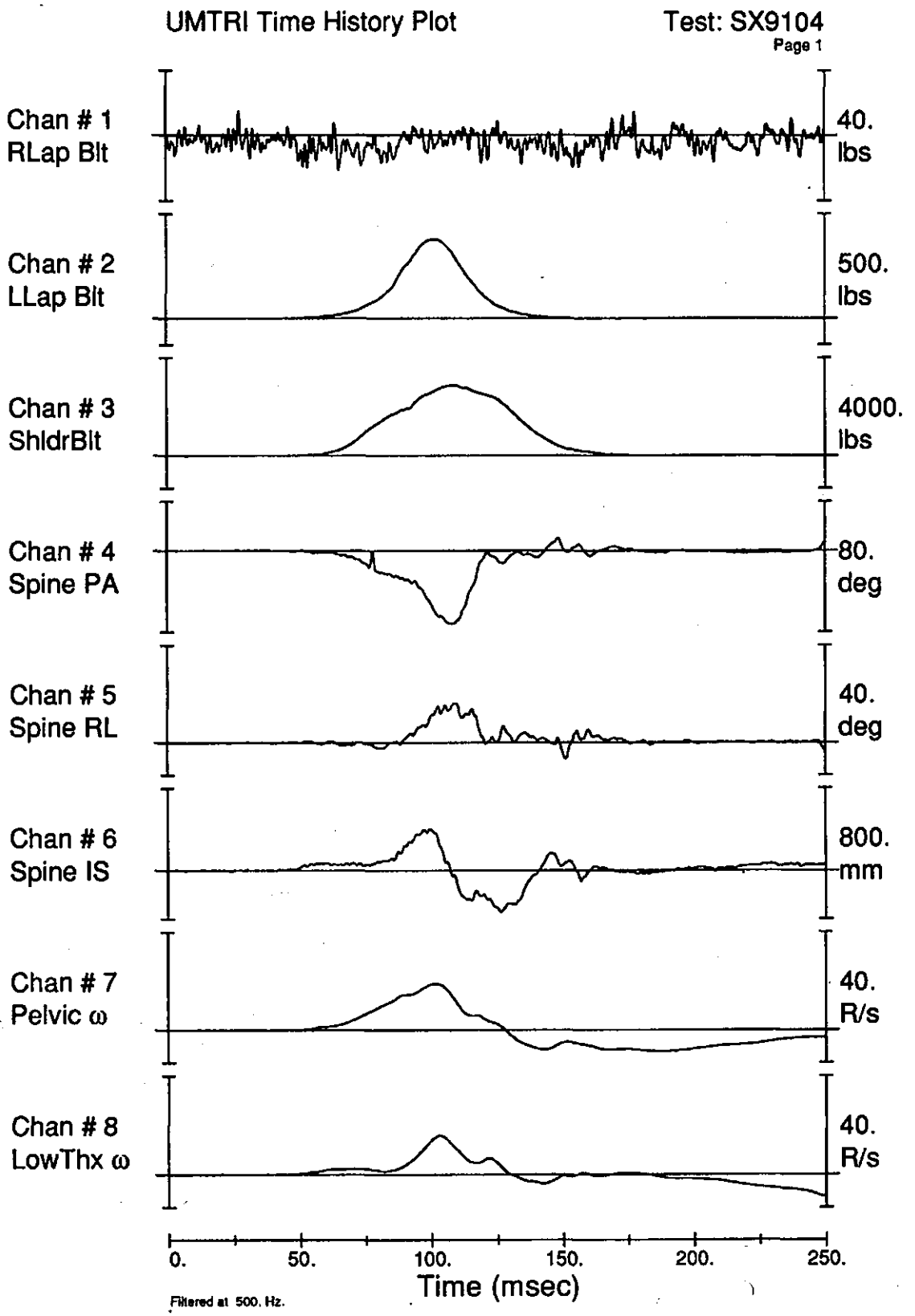
UMTRI Time History Plot
Test: SX9104
Page 1
Chan # 1
RLap Blt
40.
lbs
Chan # 2
LLap Blt
500.
lbs
Chan # 3
ShldrBlt
4000.
lbs
Chan # 4
Spine PA
80.
deg
Chan # 5
Spine RL
40.
deg
Chan # 6
Spine IS
800.
mm
Chan # 7
Pelvic ω
40.
R/s
Chan # 8
LowThx ω
40.
R/s
0.
50.
100.
150.
200.
250.
Time (msec)
Filtered at 500. Hz.

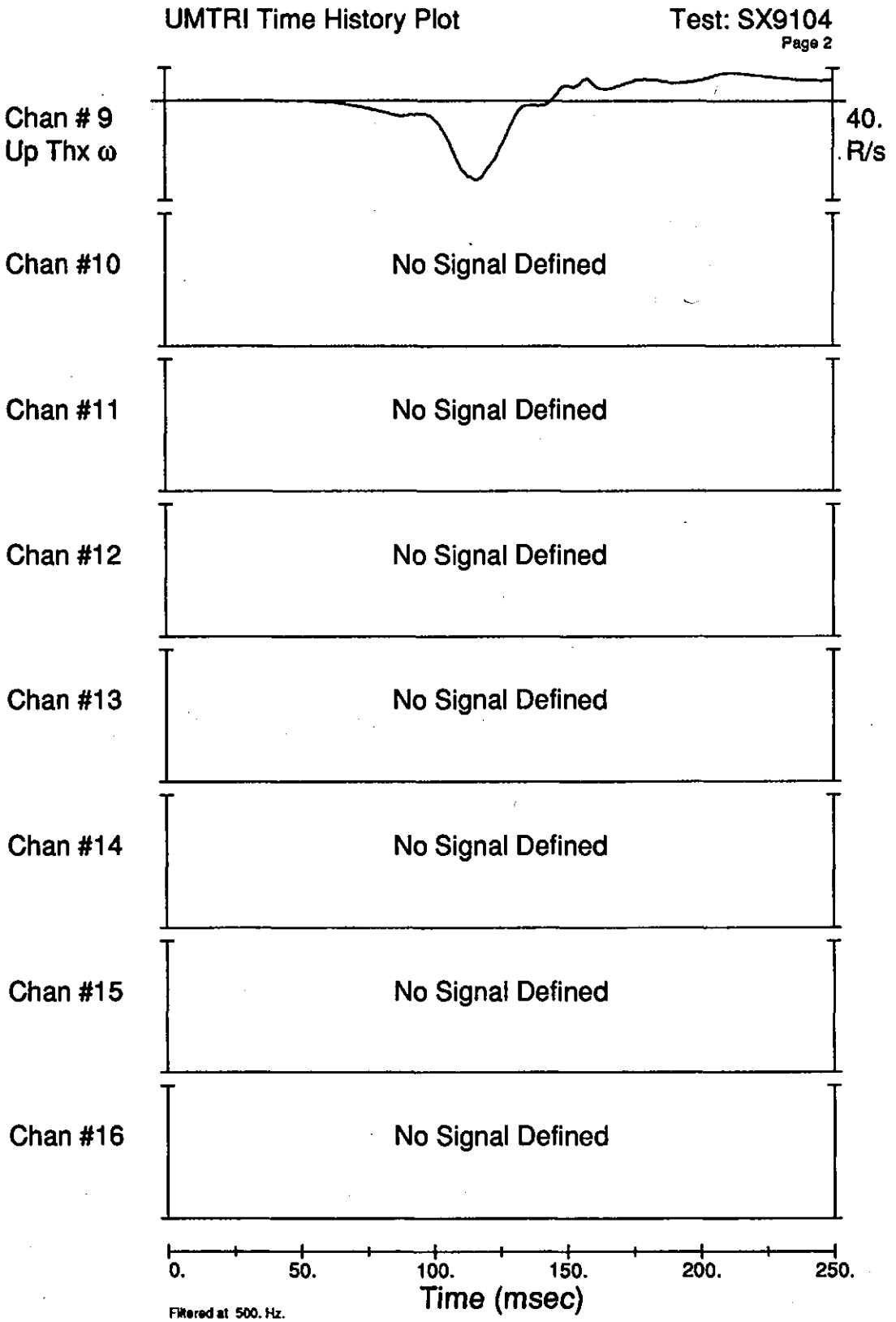
UMTRI Time History Plot
Test: SX9104
Page 2
Chan # 9
Up Thx ω
40.
R/s
Chan #10
No Signal Defined
Chan #11
No Signal Defined
Chan #12
No Signal Defined
Chan #13
No Signal Defined
Chan #14
No Signal Defined
Chan #15
No Signal Defined
Chan #16
No Signal Defined
0.
50.
100.
150.
200.
250.
Time (msec)
Filtered at 500. Hz.

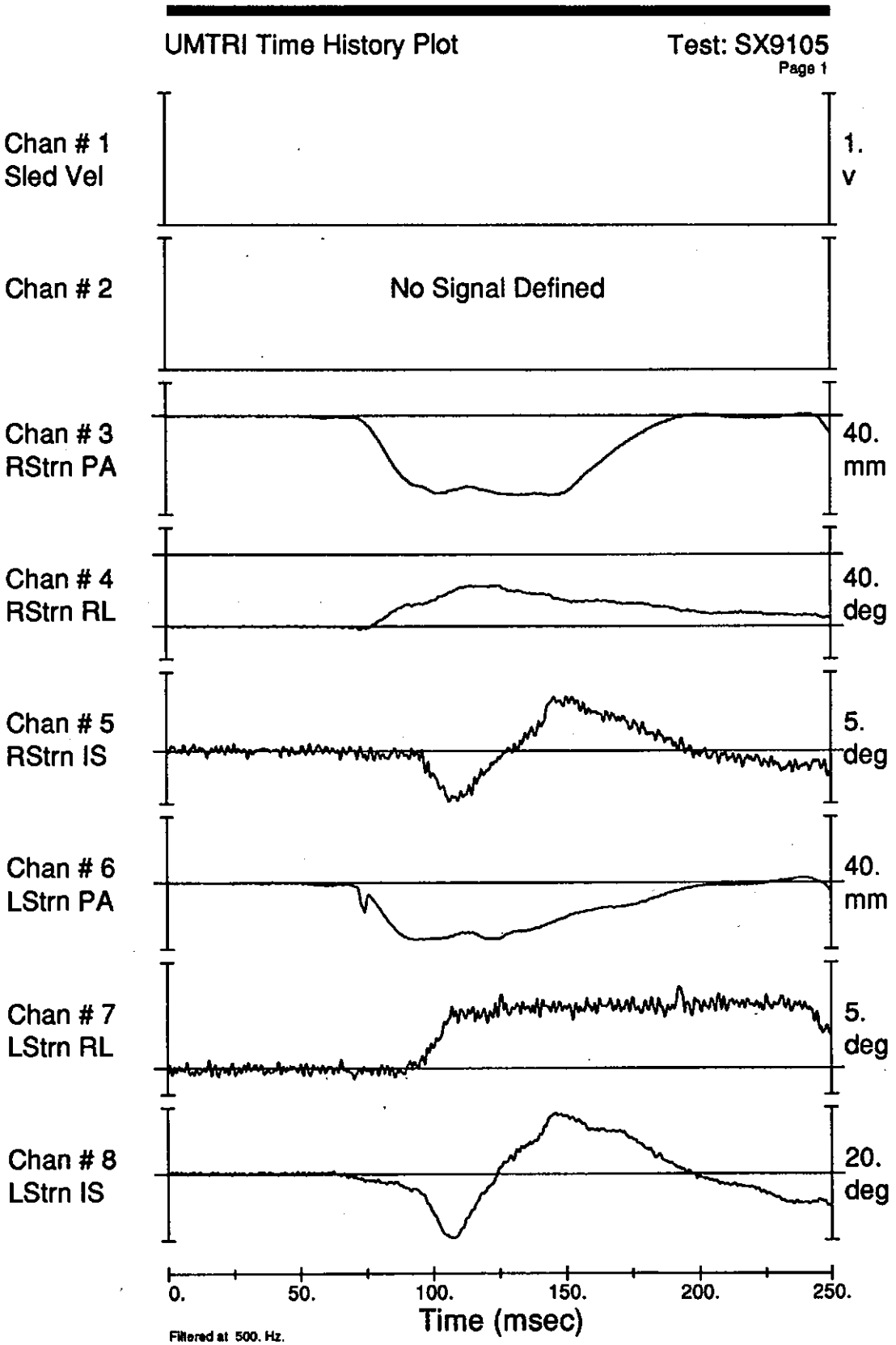
UMTRI Time History Plot
Test: SX9105
Page 1
Chan # 1
Sled Vel
1.
v
Chan # 2
No Signal Defined
Chan # 3
RStrn PA
40.
mm
Chan # 4
RStrn RL
40.
deg
Chan # 5
RStrn IS
5.
deg
Chan # 6
LStrn PA
40.
mm
Chan # 7
LStrn RL
5.
deg
Chan # 8
LStrn IS
20.
deg
0.
50.
100.
150.
200.
250.
Time (msec)
Filtered at 500. Hz.

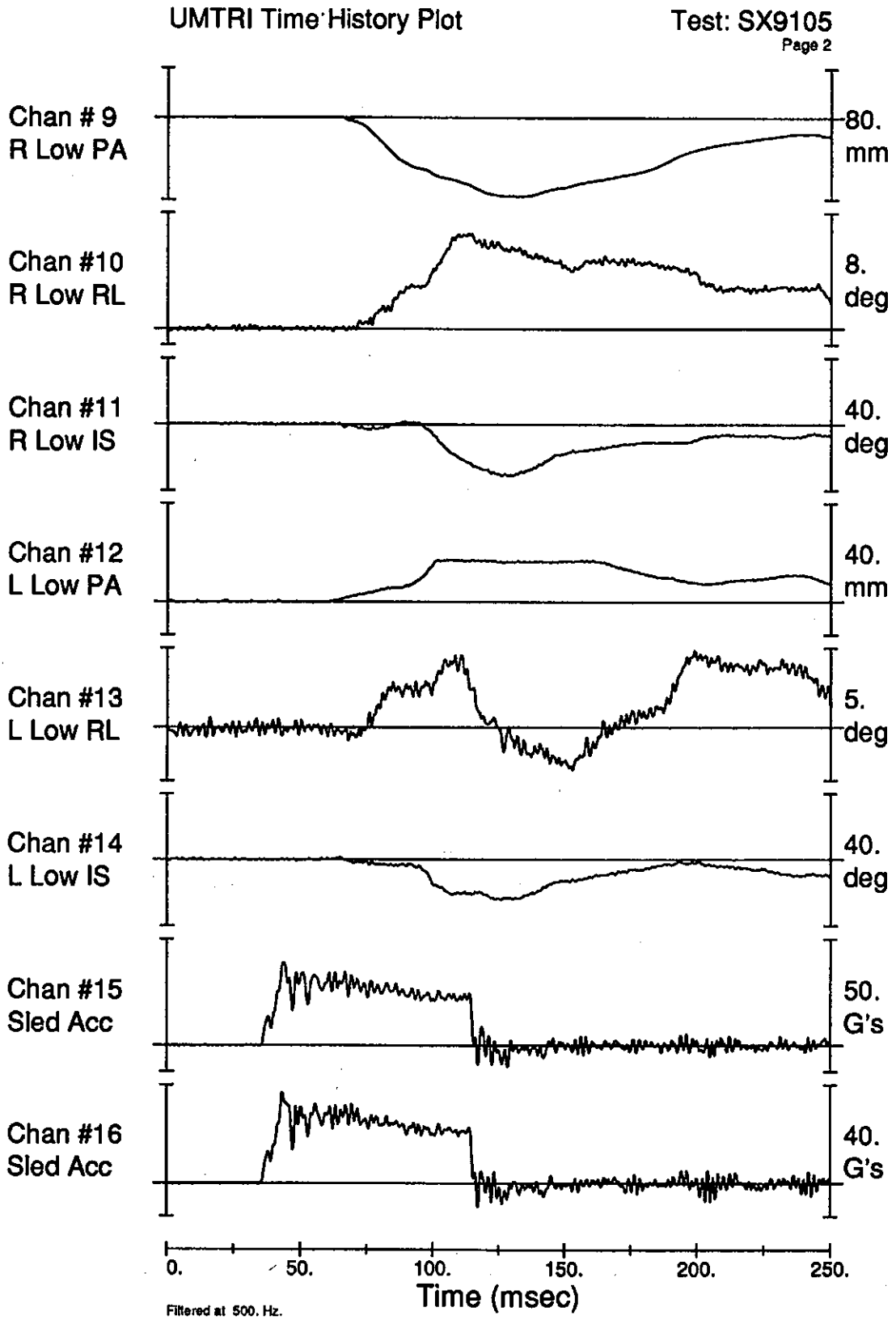
UMTRI Time History Plot
Test: SX9105
Page 2
Chan # 9
R Low PA
80.
mm
Chan #10
R Low RL
8.
deg
Chan #11
R Low IS
40.
deg
Chan #12
L Low PA
40.
mm
Chan #13
L Low RL
5.
deg
Chan #14
L Low IS
40.
deg
Chan #15
Sled Acc
50.
G's
Chan #16
Sled Acc
40.
G's
0.
50.
100.
150.
200.
250.
Time (msec)
Filtered at 500. Hz.

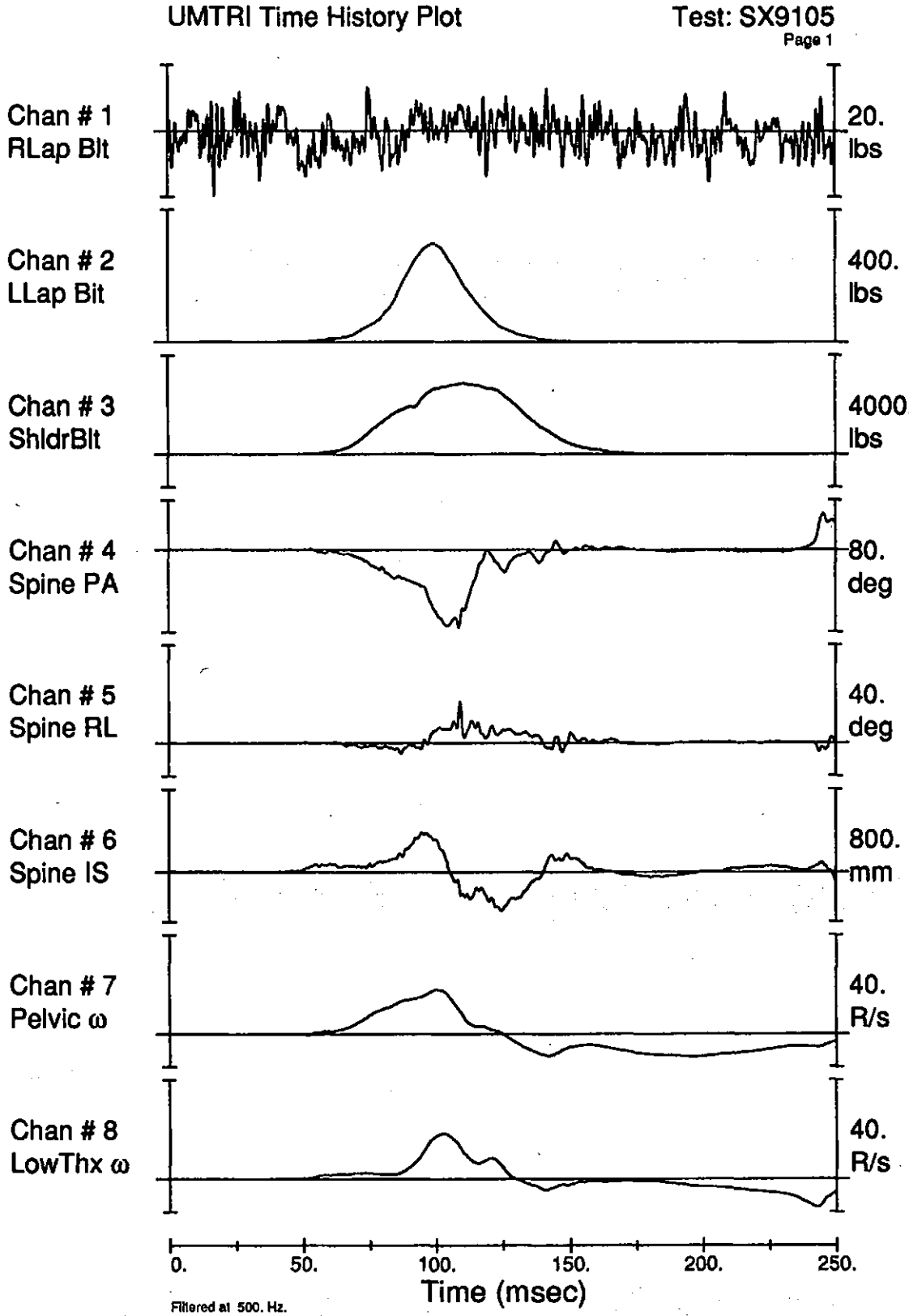
UMTRI Time History Plot
Test: SX9105
Page 1
Chan # 1
RLap Blt
20.
lbs
Chan # 2
LLap Bit
400.
lbs
Chan # 3
ShldrBlt
4000.
lbs
Chan # 4
Spine PA
80.
deg
Chan # 5
Spine RL
40.
deg
Chan # 6
Spine IS
800.
mm
Chan # 7
Pelvic ω
40.
R/s
Chan # 8
LowThx ω
40.
R/s
0.
50.
100.
150.
200.
250.
Time (msec)
Filtered at 500. Hz.

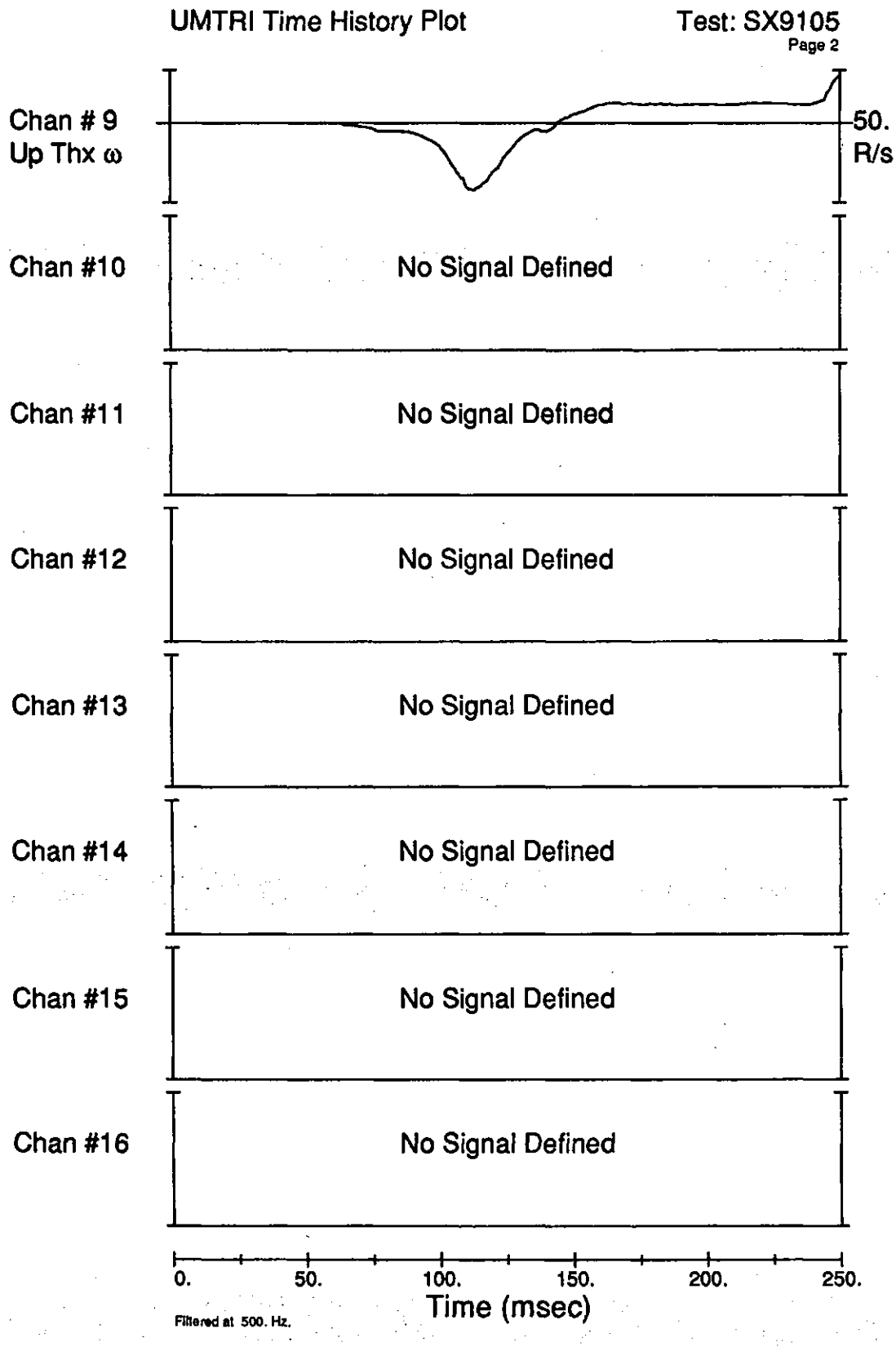
UMTRI Time History Plot
Test: SX9105
Page 2
Chan # 9
Up Thx ω
50.
R/s
Chan #10
No Signal Defined
Chan #11
No Signal Defined
Chan #12
No Signal Defined
Chan #13
No Signal Defined
Chan #14
No Signal Defined
Chan #15
No Signal Defined
Chan #16
No Signal Defined
0.
50.
100.
150.
200.
250.
Time (msec)
Filtered at 500. Hz.

UMTRI Time History Plot
Spinal Axis System

Test: SX9104
Transducer 1 pg 1
(Right Sternal)

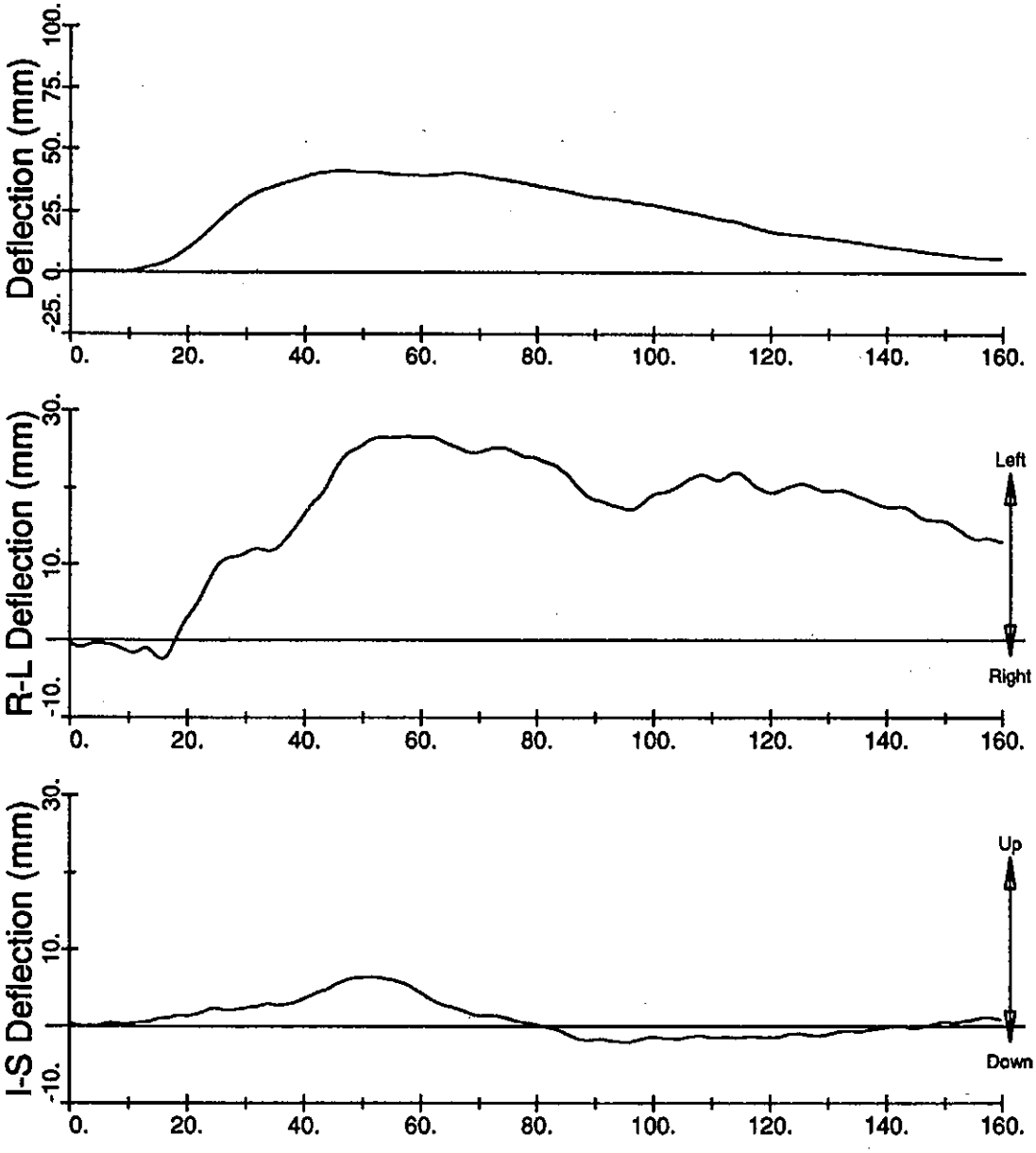

UMTRI Time History Plot
Spinal Axis System

Test: SX9104
Transducer 2 pg 1
(Left Sternal)

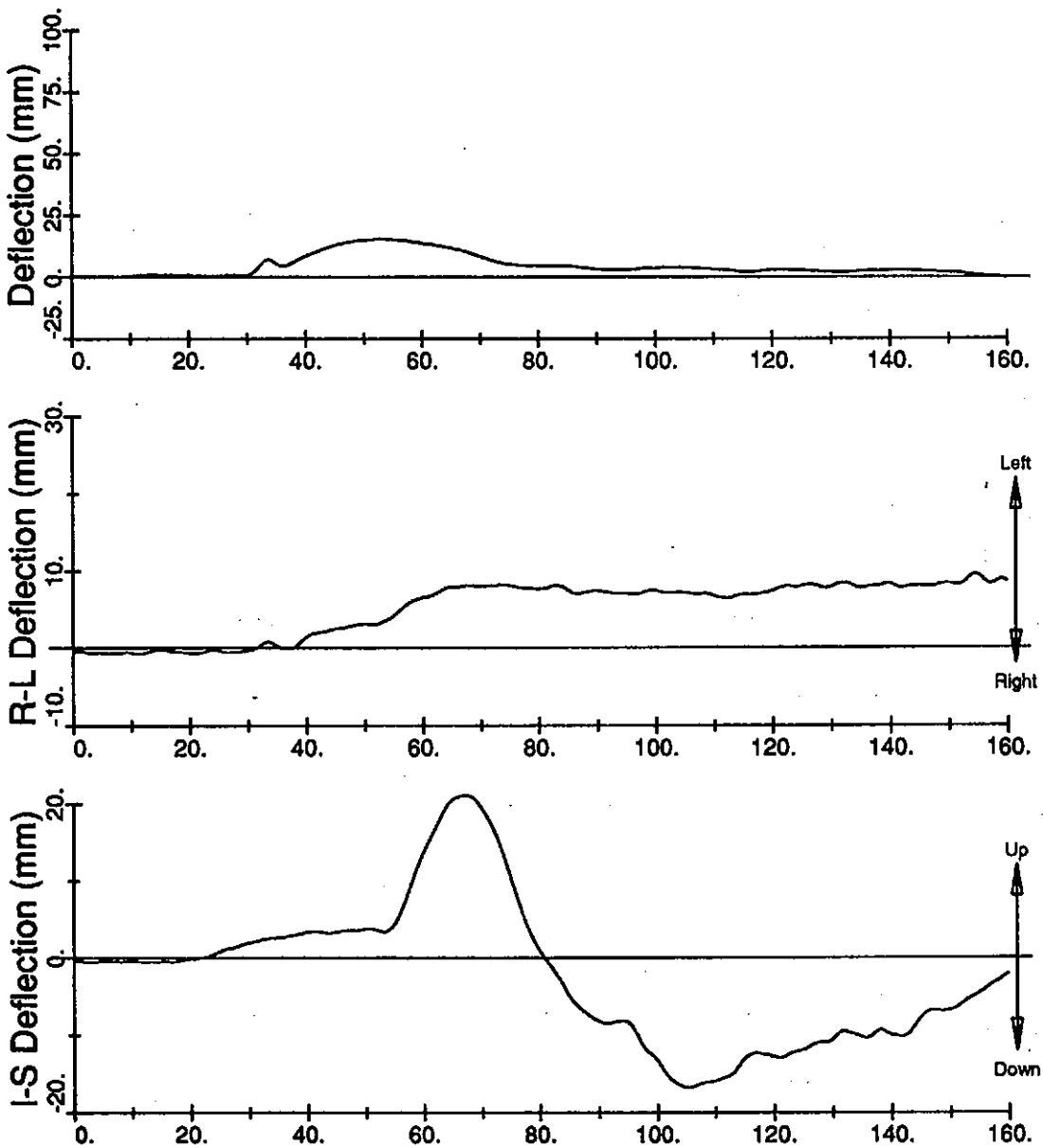

UMTRI Time History Plot
Spinal Axis System

Test: SX9104
Transducer 3 pg 1
(Right Lower)

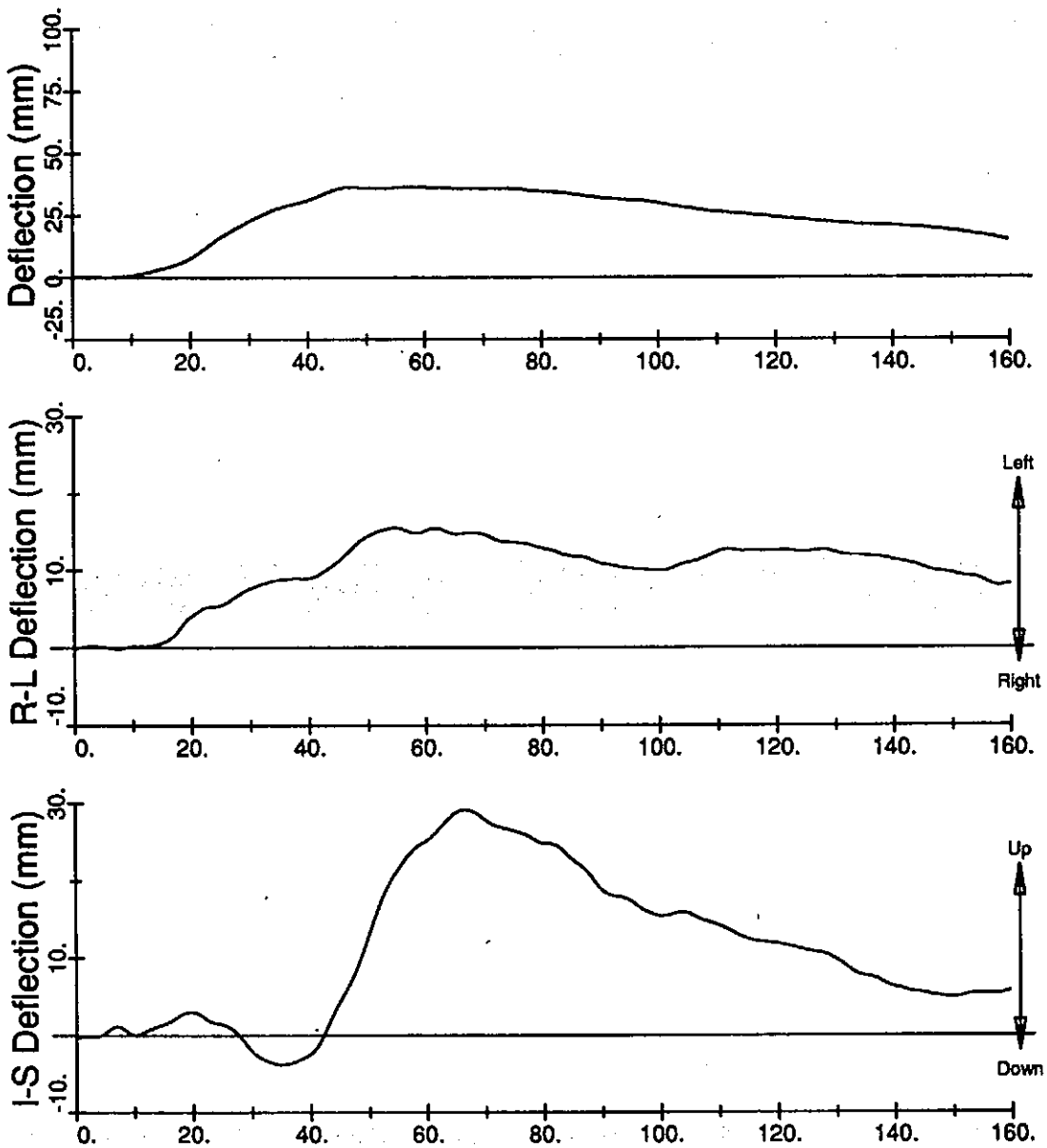

UMTRI Time History Plot
Alternate Axis System

Test: SX9104
Transducer 3 pg 2
(Right Lower)

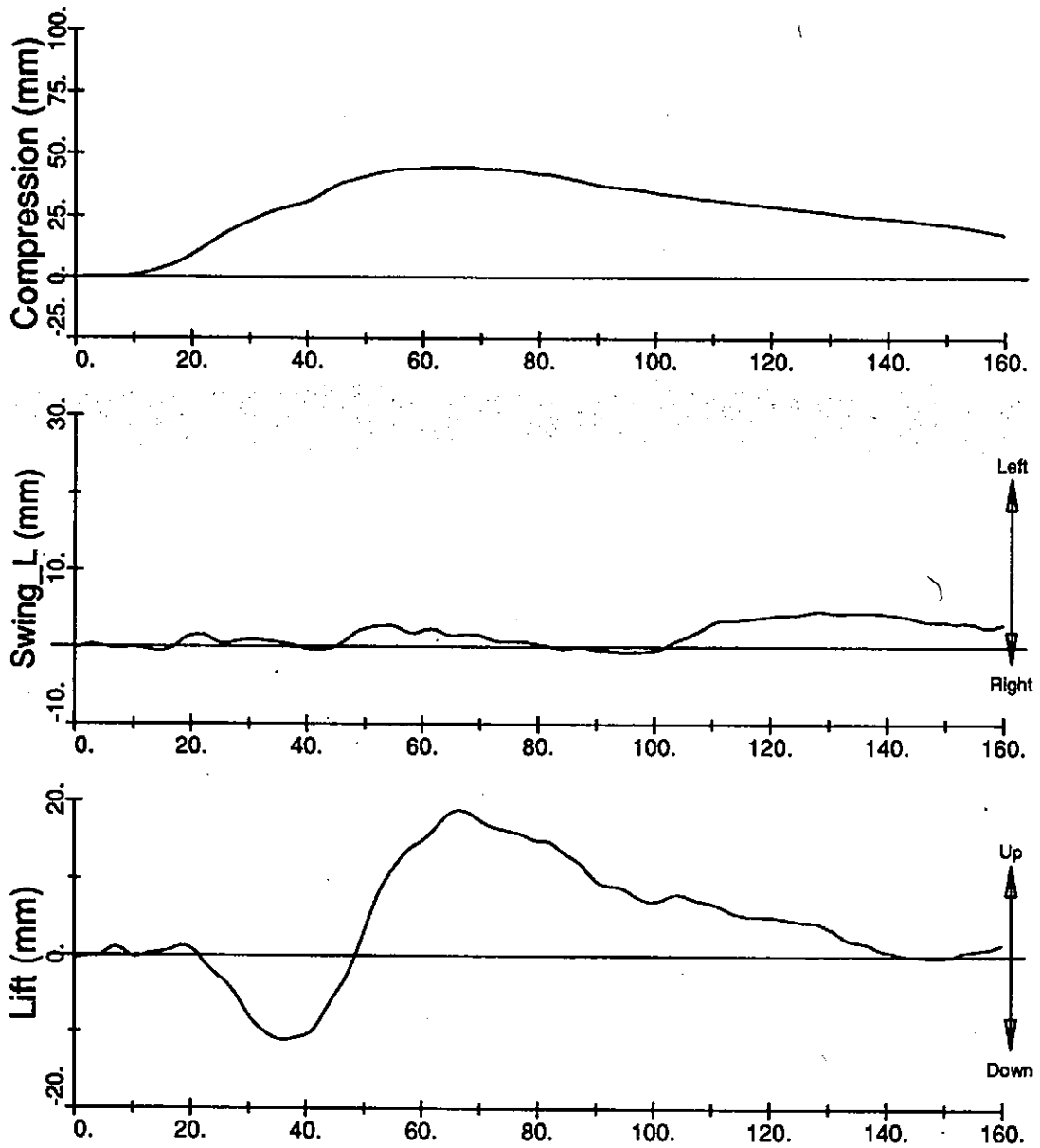

UMTRI Time History Plot
Spinal Axis System

Test: SX9104
Transducer 4 pg 1
(Left Lower)

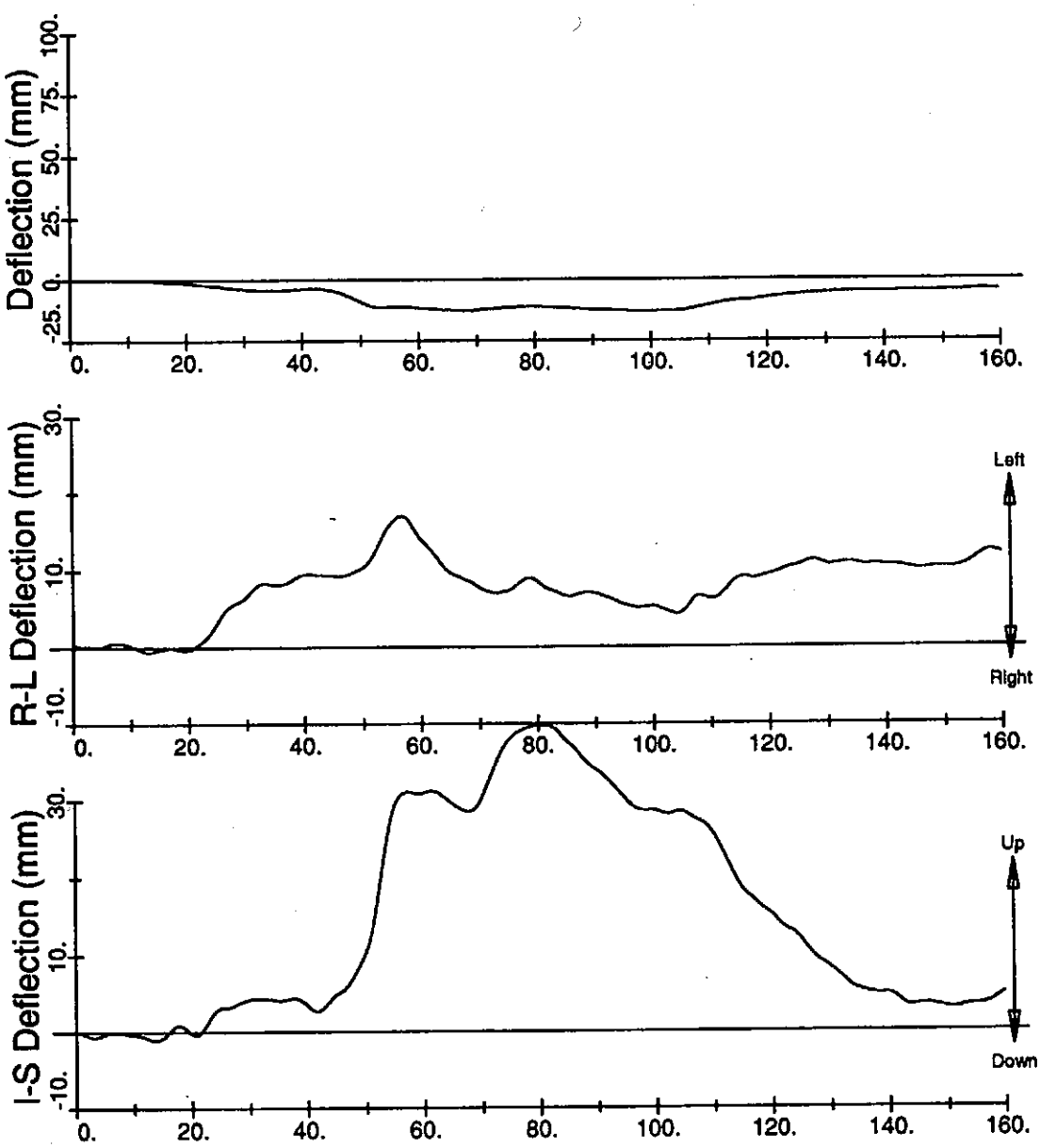

UMTRI Time History Plot
Alternate Axis System

Test: SX9104
Transducer 4 pg 2
(Left Lower)

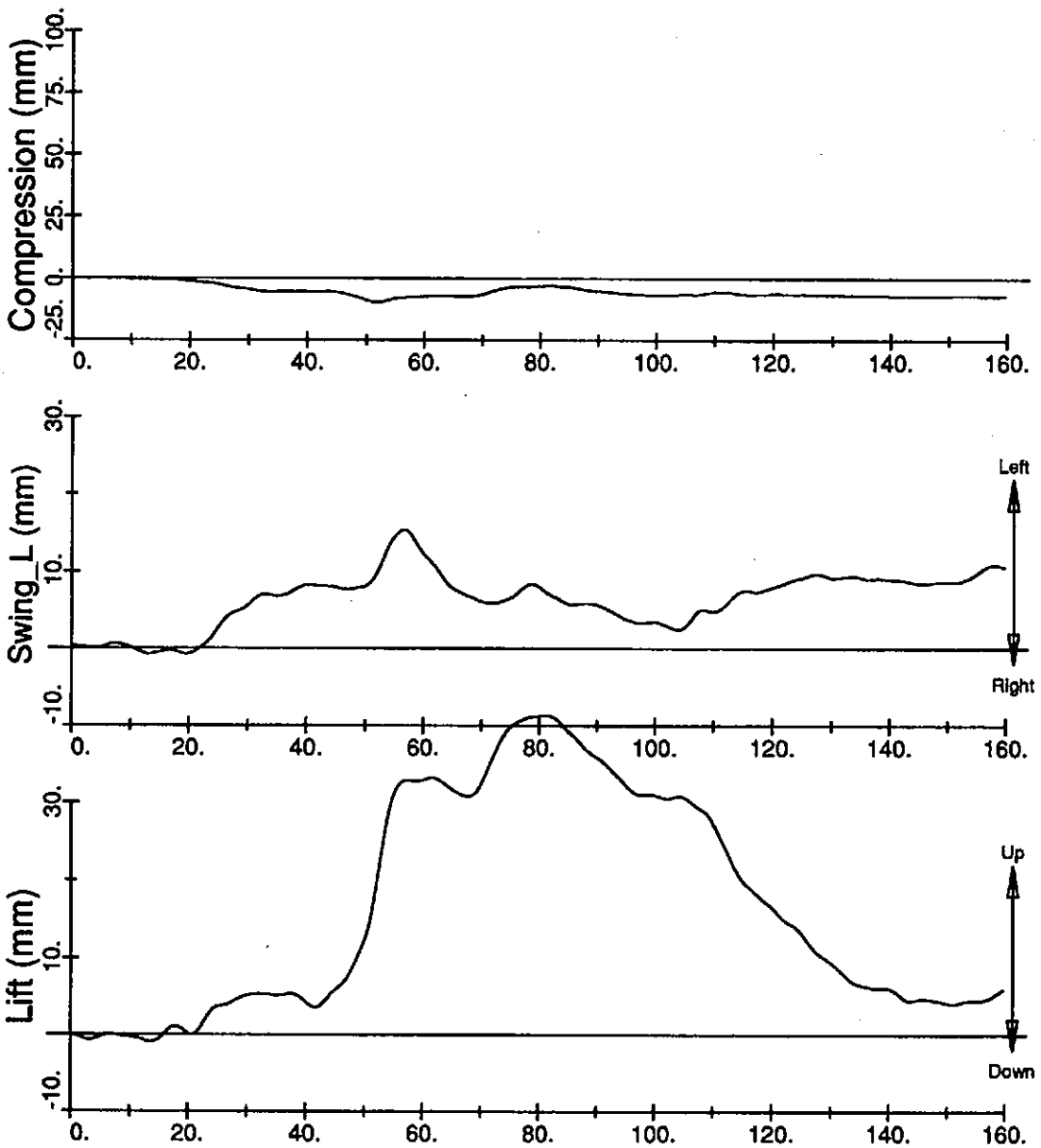

UMTRI Time History Plot
Spinal Axis System

Test: SX9105
Transducer 1 pg 1
(Right Sternal)

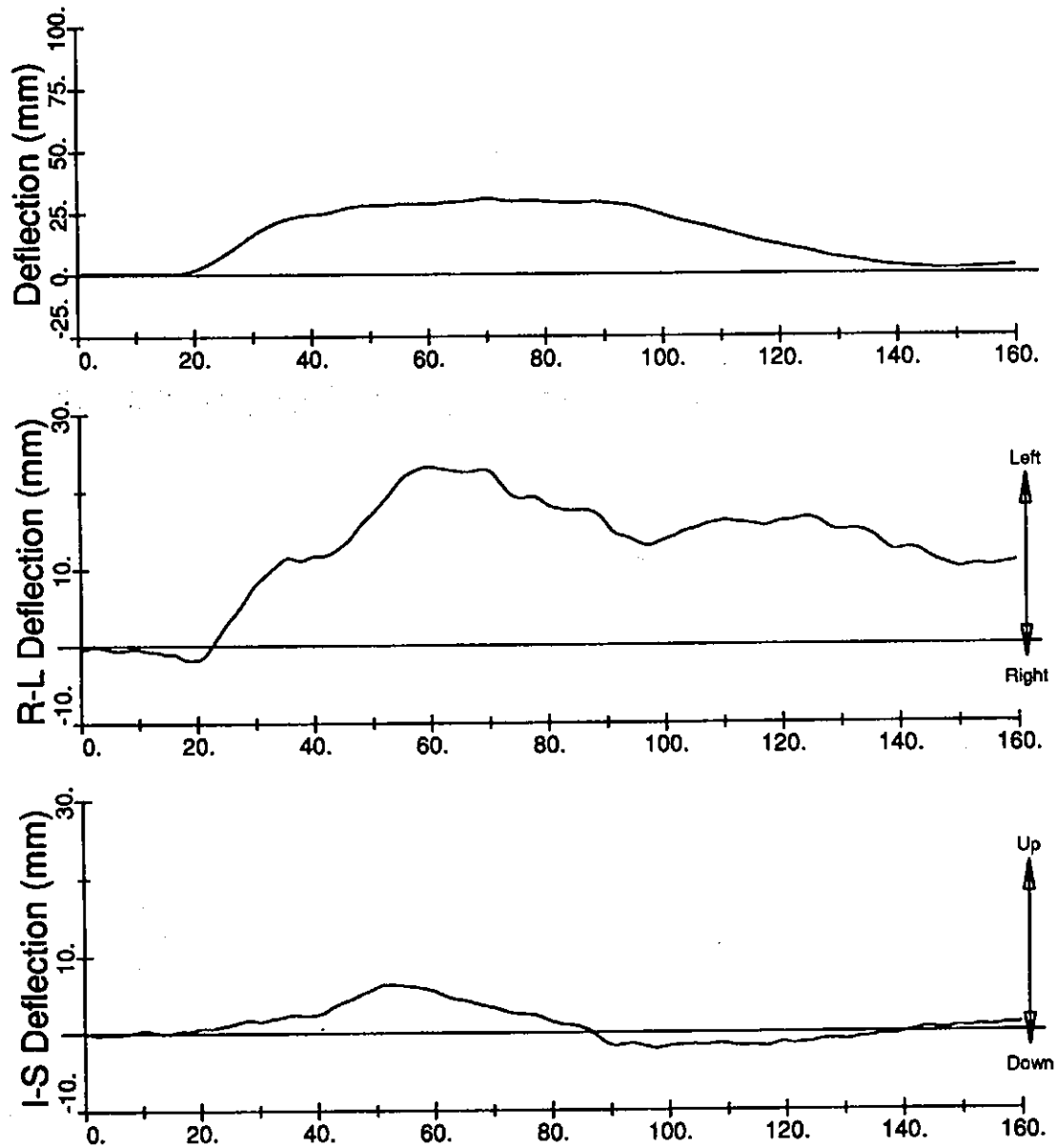

UMTRI Time History Plot
Spinal Axis System

Test: SX9105
Transducer 2 pg 1
(Left Sternal)

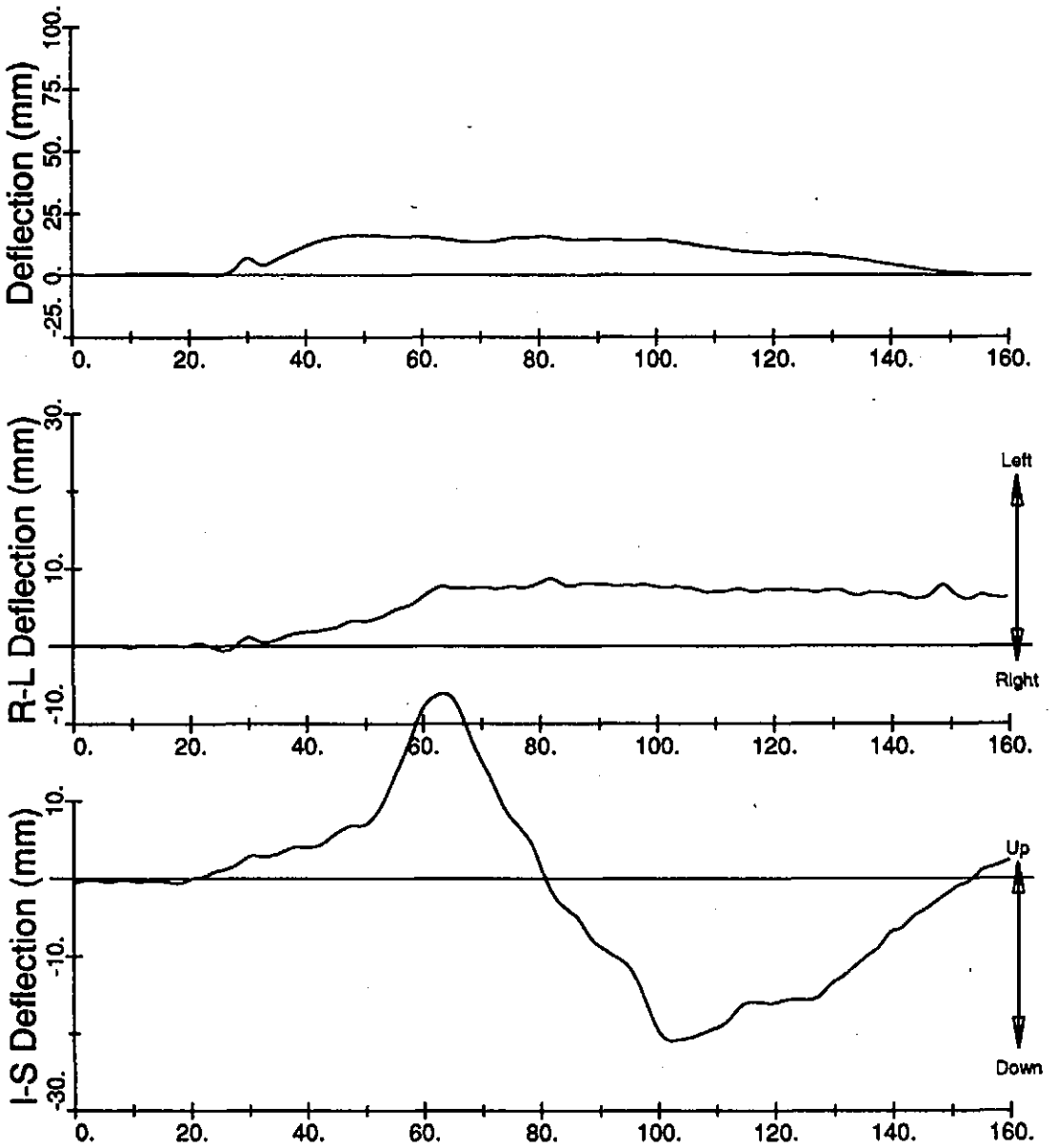

UMTRI Time History Plot
Spinal Axis System

Test: SX9105
Transducer 3 pg 1
(Right Lower)

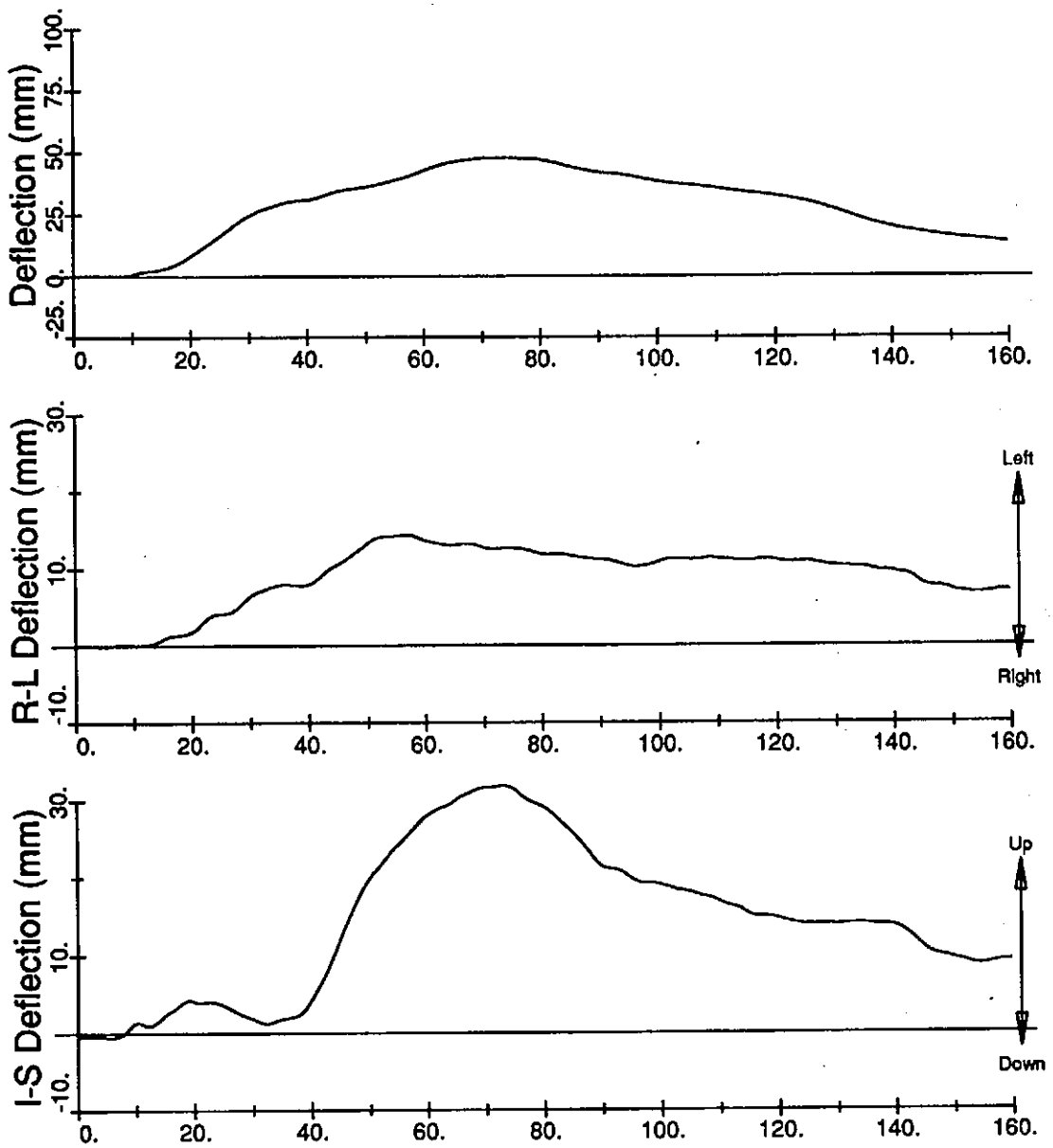

UMTRI Time History Plot
Alternate Axis System

Test: SX9105
Transducer 3 pg 2
(Right Lower)

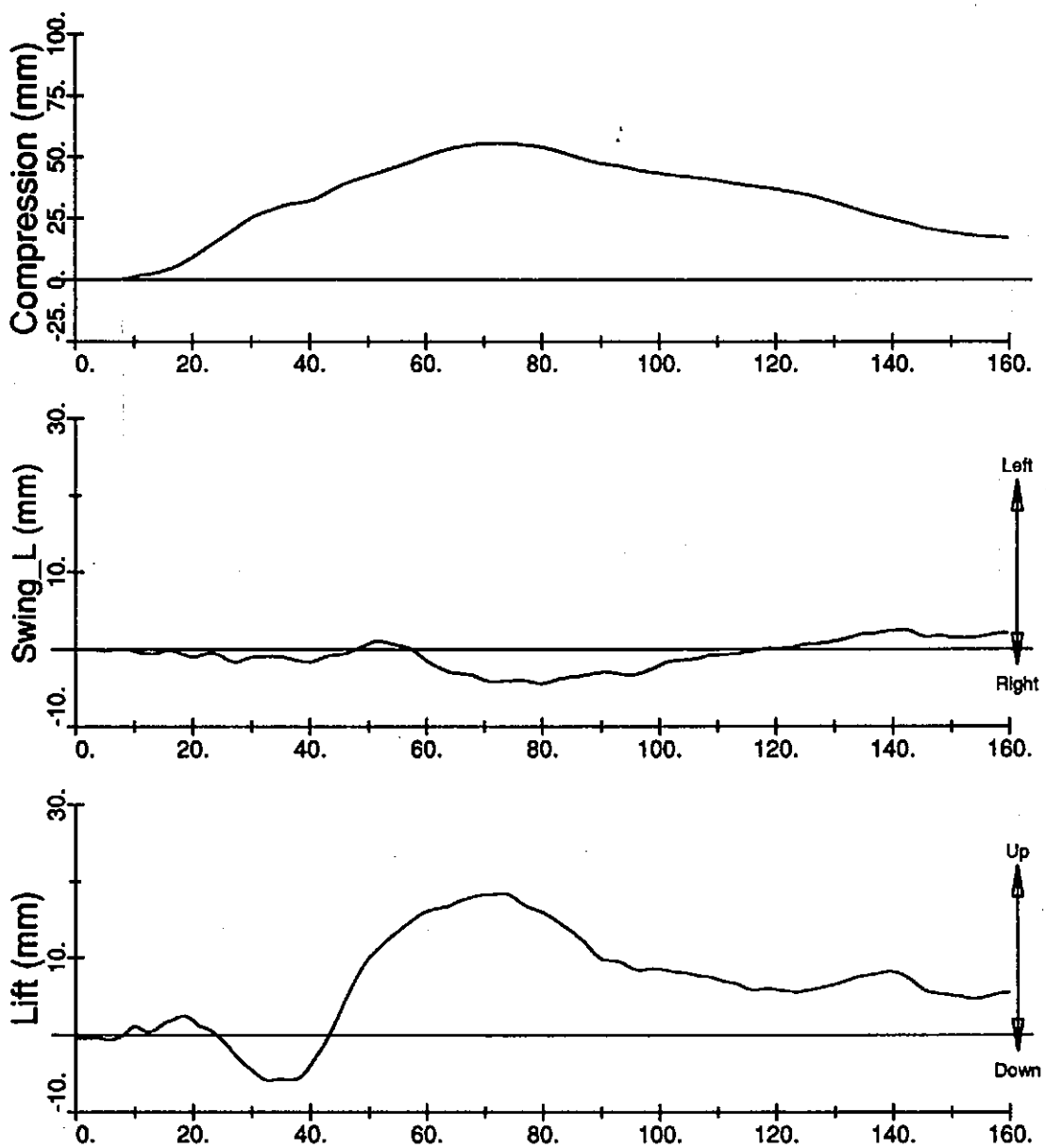

UMTRI Time History Plot
Spinal Axis System

Test: SX9105
Transducer 4 pg 1
(Left Lower)

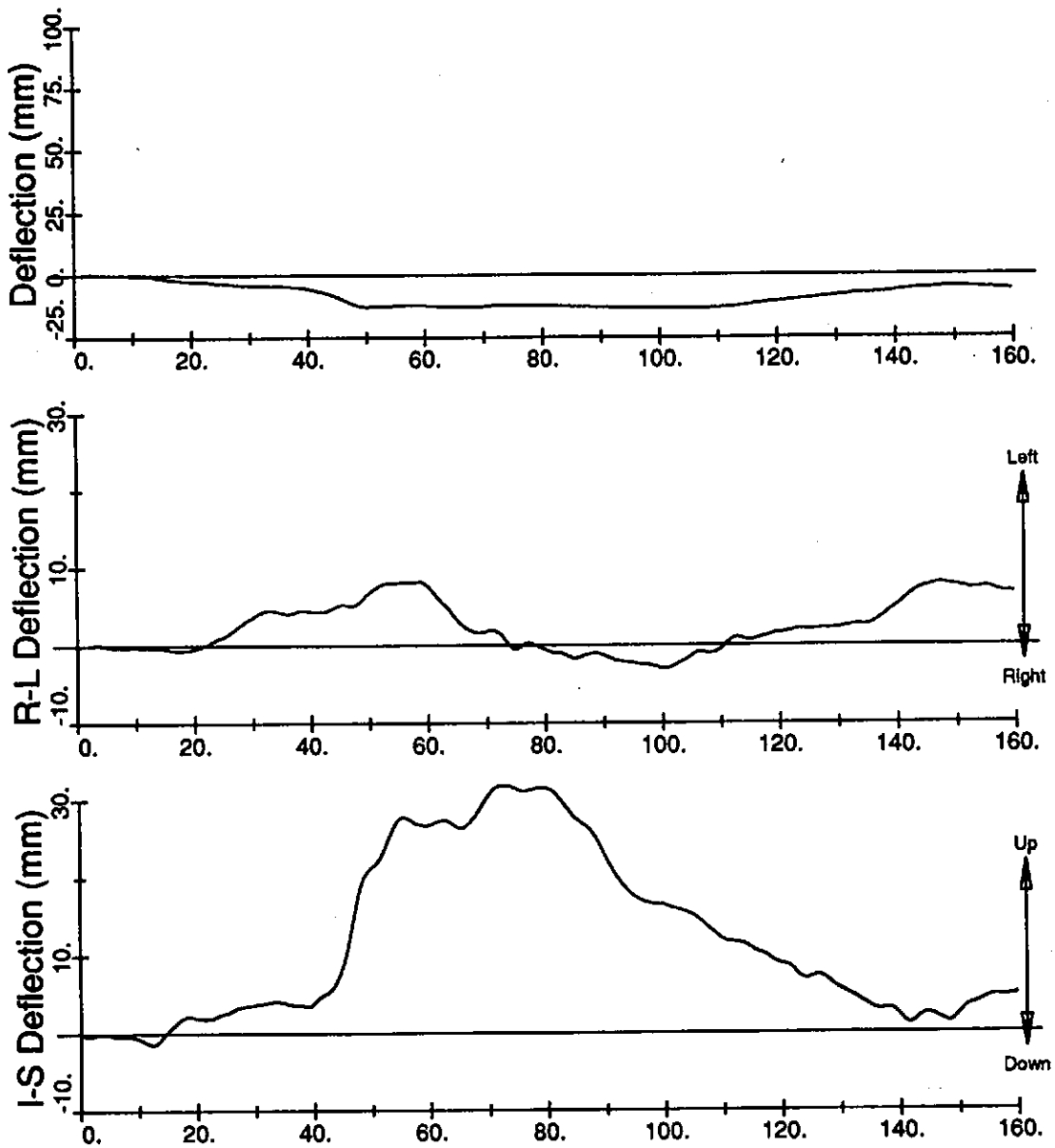

UMTRI Time History Plot
Alternate Axis System

Test: SX9105
Transducer 4 pg 2
(Left Lower)

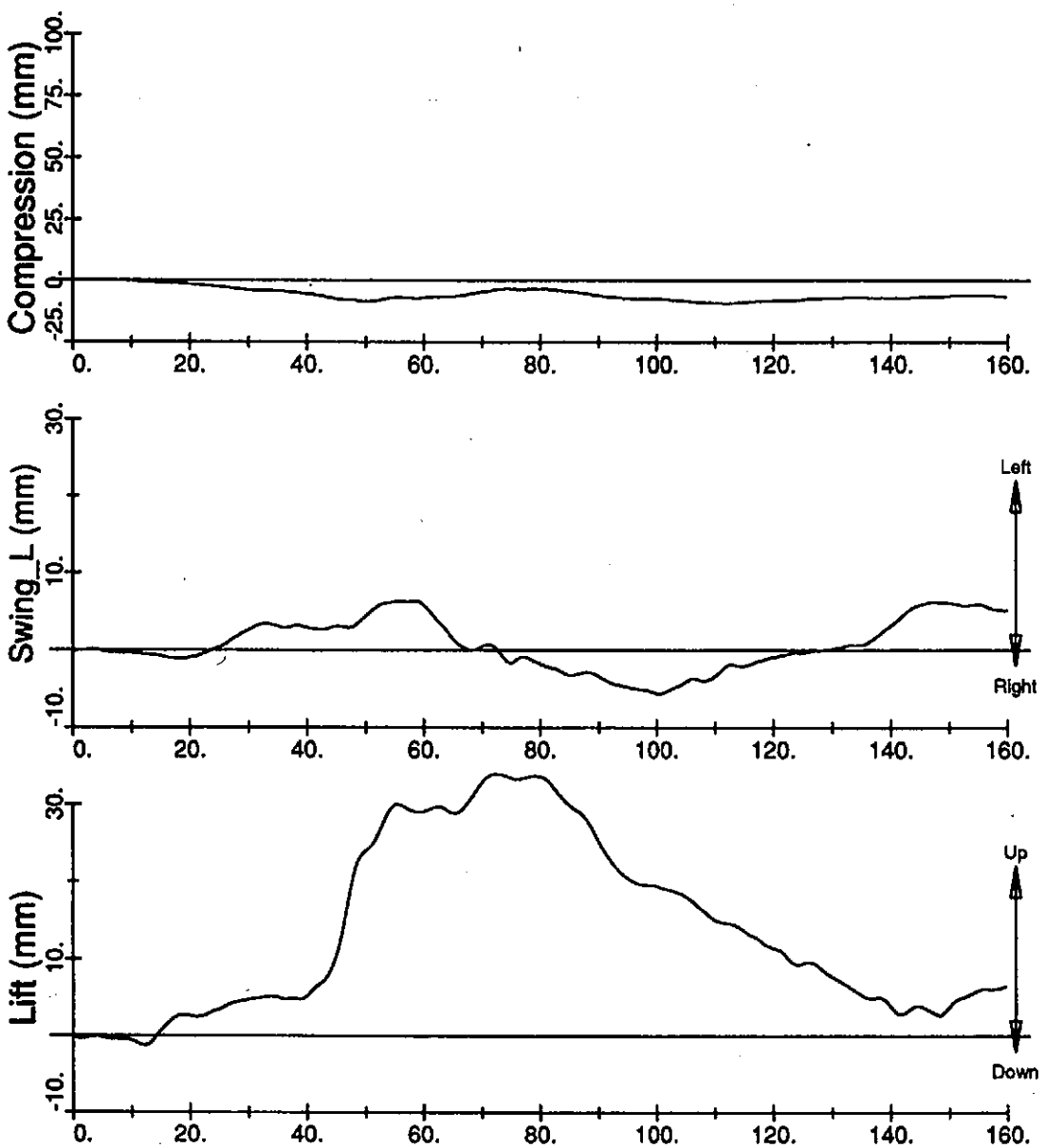

REFERENCES

Alem, N.M.; Benson, J.B.; and Melvin, J.W. (1976) *Whole body response research program—Second year final report*. Report no. UM-HSRI-76–3. Highway Safety Research Institute, The University of Michigan, Ann Arbor.

Alem, N.M.; Benson, J.B.; and Melvin, J.W. (1977) *Whole body response of the Hybrid III anthropomorphic test device*. Final report no. UM-HSRI-77–10. Highway Safety Research Institute, The University of Michigan, Ann Arbor.

Alem, N.M.; Melvin, J.W.; Bowman, B.M.; and Benson, J.B. (1978) *Whole body response research program*. Final report no. UM-HSRI-77–39–1. Highway Safety Research Institute, The University of Michigan, Ann Arbor.

Alem, N.M.; Benson, J.B.; Holstein, G.L.; and Melvin, J.W. (1978) *Whole body response research program—Appendix A: Methodology*. Final report no. UM-HSRI-77–39–2. Highway Safety Research Institute, The University of Michigan, Ann Arbor.

Alem, N.M.; Benson, J.B.; and Tann, T.A. (1978) *Whole body response research program—Appendix B: Raw data*. Final report no. UM-HSRI-77–39–3. Highway Safety Research Institute, The University of Michigan, Ann Arbor.

Alem, N.M. (1978) *Whole body response research program—Appendix C: Processed data*. Final report no. UM-HSRI-77–39–4. Highway Safety Research Institute, The University of Michigan, Ann Arbor.

Arendt, R.H.; Segal, D.J.; and Cheng, R. (1988) *Review of anthropomorphic test device instrumentation, data processing and certification procedures*. AATD Task C Final Report (1984) in DOT-HS-807–224. U.S. Department of Transportation, National Highway Traffic Safety Administration, Washington, D.C.

Backaitis, S.H. (1987) Unpublished SAE handout information.

Biokinetics & Associates Ltd. (1985) *Finalization of an improved ATD Thorax: Activity Report IB4.2B*. Document no. R85–15C. Prepared under contract no. OSV84–00162 to Road and Motor Vehicle Safety Branch, Transport Canada. Biokinetics & Associates Ltd., Ottawa, Ontario.

Carsten, O.; and O'Day, J. (1988) *Injury priority analysis*. AATD Task A Final Report (1984) in DOT-HS-807–224. U.S. Department of Transportation, National Highway Traffic Safety Administration, Washington, D.C.

Cavanaugh, J.M.; Jepsen, K.; and King, A.I. (1988) Quasi-static frontal loading to the thorax of cadavers and Hybrid III dummy. In *Human Subjects for Biomechanical Research, 16th Annual International Workshop*, pp. 3–20. Atlanta, Georgia.

Cesari, D.; and Bouquet, R. (1990) Behaviour of human surrogates thorax under belt loading. *Proc. 34th Stapp Car Crash Conference*, pp. 73–82. Society of Automotive Engineers, Warrendale, Pa.

Church, A.H. (1963) *Mechanical vibration*, 2nd ed. John Wiley and Sons, New York.

Dansereau, J.; and Stokes, I.A.F. (1988) Measurements of the three-dimensional shape of the rib cage. *Journal of Biomechanics*, 21:11, 893–901.

Davis Engineering Ltd. (1985) *Documentation of ATD thorax design and fabrication modifications*. Prepared under DE contract 84-104 for Biokinetics & Associates Ltd. Davis Engineering Ltd., Ottawa, Ontario.

Dempster, W.T. (1965) Mechanisms of shoulder movement. *Archives of Physical Medicine and Rehabilitation*, 46:49–70.

Foster, J.K.; Kortge, J.O.; and Wolanin, M.J. (1977) Hybrid III: A biomechanically-based crash test dummy. *Proc. 21st Stapp Car Crash Conference*, pp. 975-1014. Society of Automotive Engineers, Warrendale, Pa.

Haffner, M. (1987) Trauma assessment device development program: Thorax-abdomen development task. Preliminary goals and design requirements statement. Contract communication. National Highway Traffic Safety Administration, U.S. Department of Transportation, Washington, D.C.

Kallieris, D. (1987) Correspondence to Rolf Eppinger, U.S. Department of Transportation, National Highway Traffic Safety Administration, Biomechanics Branch, Washington, D.C.

Kroell, C.K.; Schneider, D.C.; and Nahum, A.M. (1971) Impact tolerance and response to the human thorax. *Proc. 15th Stapp Car Crash Conference*, pp. 84–134. Society of Automotive Engineers, Warrendale, Pa.

Kroell, C.K.; Schneider, D.C.; and Nahum, A.M. (1974) Impact tolerance and response to the human thorax II. *Proc. 18th Stapp Car Crash Conference*, pp. 383–457. Society of Automotive Engineers, Warrendale, Pa.

Laughlin, D.R. (1989) A magnetohydrodynamic angular motion sensor for anthropomorphic test device instrumentation. *Proc. 33rd Stapp Car Crash Conference*, pp. 43–78. Society of Automotive Engineers, Warrendale, Pa.

Lobdell, T.E.; Kroell, C.K.; Schneider, D.C.; Hering, W.E.; and Nahum, A.M. (1973) Impact response of the human thorax. In *Human Impact Response Measurement and Simulation*, pp. 201–245. Edited by W.F. King and H.J. Mertz. Plenum Press, New York.

L'Abbe, R.J.; Dainty, D.A.; and Newman, J.A. (1982) An experimental analysis of thoracic deflection response to belt loading. *Seventh International IRCOBI Conference on the Biomechanics of Impacts*, pp. 184–194. Bron, France.

Malliaris, A.C.; Hitchcock, R.; and Hedlund, J. (1982) A search for priorities in crash protection. *Crash Protection, SAE SP-513*, pp. 1–33. Society of Automotive Engineers, Warrendale, Pa.

Matsuoka, F.; Kumagai, K.; and Takahashi, H. (1989) *Problem and improvement of Hybrid III dummy rib cage features*. Report no. 89–4A-0–009. Toyota Motor Corporation.

McConville, J.T.; Churchill, T.D.; Kaleps, I.; Clauser, C.E.; and Cuzzi, J. (1980) *Anthropometric relationships of body and body segment moments of inertia*. AMRL-TR-80–119. Aerospace Medical Research Laboratory, Wright-Patterson AFB, Ohio.

Melvin, J.W. (1988) *The engineering design, development, testing, and evaluation of an advanced anthropometric test device. Phase 1: Concept definition,* (1985). In report no. DOT-HS-807–224. U.S. Department of Transportation, National Highway Traffic Safety Administration, Washington, D.C.

Melvin, J.W.; and Weber, K., eds. (1988) *Review of biomechanical impact response and injury in the automotive environment.* Phase I Task B Final Report (1985) in DOT-HS-807–224. U.S. Department of Transportation, National Highway Traffic Safety Administration, Washington, D.C.

Melvin, J.W.; Benson, J.B.; and Alem, N.M. (1975) *Whole body response research program—First year final report.* Report no. UM-HSRI-BI-75–1. Highway Safety Research Institute, The University of Michigan, Ann Arbor.

Melvin, J.W.; King, A.I.; and Alem, N.M. (1988a) *AATD system technical characteristics, design concepts, and trauma assessment criteria.* AATD Task E-F Final Report (1985) in DOT-HS-807–224. U.S. Department of Transportation, National Highway Traffic Safety Administration, Washington, D.C.

Melvin, J.W.; Robbins, D.H.; Weber, K.; Campbell, K.L.; and Smrcka, J. (1988b) *Review of dummy design and use.* AATD Task D Final Report (1985) in DOT-HS-807–224. U.S. Department of Transportation, National Highway Traffic Safety Admin istration, Washington, D.C.

Mertz, H.J. (1984) *A procedure for normalizing impact response data.* SAE paper no. 840884. Society of Automotive Engineers, Warrendale, Pa.

Neathery, R.F. (1974) Analysis of chest impact response data and scaled performance recommendations. *Proc. 18th Stapp Car Crash Conference*, pp. 459–493. Society of Automotive Engineers, Warrendale, Pa.

Patrick, L.M. (1981) Impact force-deflection of the human thorax. *Proc. 25th Stapp Car Crash Conference*, pp. 471–496. Society of Automotive Engineers, Warrendale, Pa.

Reynolds, H.M.; Snow, C.C.; and Young, J.W. (1981) *Spatial geometry of the human pelvis.* Memorandum report no. AAC-119–81–5. Civil Aeromedical Institute, Federal Aviation Administration, Oklahoma City.

Robbins, D.H. (1985a) *Anthropometric specifications for mid-sized male dummy, Volume 2.* Final report no. DOT-HS-806–716. U.S. Department of Transportation, National Highway Traffic Safety Administration, Washington, D.C.

Robbins, D.H. (1985b) *Anthropometric specifications for small female and large male dummies, Volume 3.* Final report no. DOT-HS-806–717. U.S. Department of Transportation, National Highway Traffic Safety Administration, Washington, D.C.

Roe, R.W. (1975) *Describing the driver's workspace: Eye, head, knee, and seat positions.* SAE paper no. 750356. Society of Automotive Engineers, Warrendale, Pa.

Rouhana, S.W.; Jedrzejczak, E.A.; and McCleary, J.D. (1990) Assessing submarining and abdominal injury risk in the Hybrid III family of dummies: Part II—Development of the small female Frangible Abdomen. *Proc. 34th Stapp Car Crash Conference*, pp. 145–174. Society of Automotive Engineers, Warrendale, Pa.

Rouhana, S.W.; Viano, D.C.; Jedrzejczak, E.A.; and McCleary, J.D. (1989) Assessing submarining and abdominal injury risk in the Hybrid III family of dummies. In *Proc. 33rd Stapp Car Crash Conference*, pp. 257–280. Society of Automotive Engineers, Warrendale, Pa.

Schneider, L.W.; Robbins, D.H.; Pflug, M.A.; and Snyder, R.G. (1985) *Development of anthropometrically based design specifications for an advanced adult anthropomorphic dummy family, Volume 1.* Final report no. DOT-HS-806–715. U.S. Department of Transportation, National Highway Traffic Safety Administration, Washington, D.C.

Schneider, L.W.; King, A.I.; and Beebe, M.S. (1990). *Design requirements and specifications: Thorax-abdomen development task. Trauma assessment device development program.* Interim report no. DOT-HS-807–511. U.S. Department of Transportation, National Highway Traffic Safety Administration, Washington, D.C.

Schneider, L.W.; Ricci, L.L.; King, A.I.; Neathery, R.F.; and Beebe, M.S. (1993) *Design and development of an advanced ATD thorax system for frontal crash environments, Volume 2: Exploration of alternative design approaches.* Final report on NHTSA Contract No. DTNH22–83-C-07005. U.S. Department of Transportation, National Highway Traffic Safety Administration, Washington, D.C.

Viano, D.C. (1989) Biomechanical responses and injuries in blunt lateral impact. *Proc. 33rd Stapp Car Crash Conference*, pp. 113–142. Society of Automotive Engineers, Warrendale, Pa.

Viano, D.C. (May 1989) Personal communication to L.W. Schneider, UMTRI.

DOT HS 808 138
July 1994
NRD-10